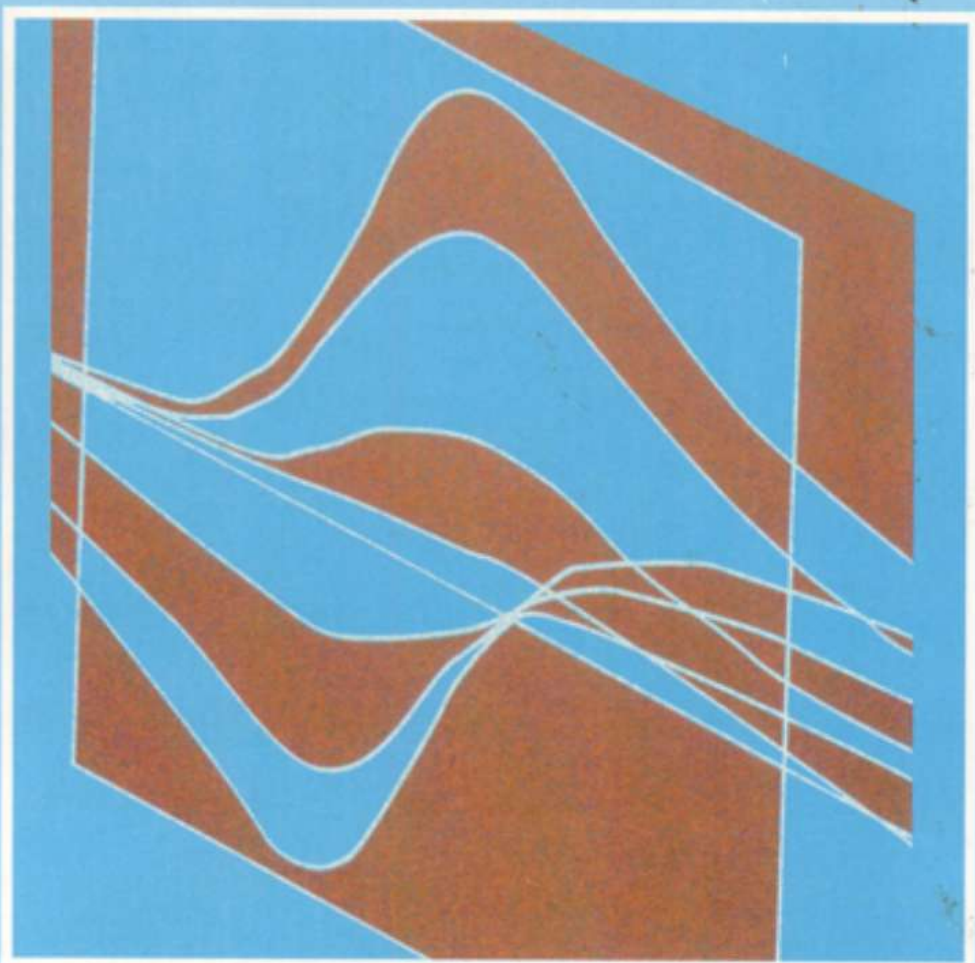


HORWOOD PUBLISHING
CHEMICAL SCIENCE SERIES

INSTRUMENTAL METHODS IN ELECTROCHEMISTRY

*Southampton Electrochemistry Group,
University of Southampton*



INSTRUMENTAL METHODS IN ELECTROCHEMISTRY

Talking of education, people have now a-days (said he) got a strange opinion that every thing should be taught by lectures. Now, I cannot see that lectures can do so much good as reading the books from which the lectures are taken. I know nothing that can be best taught by lectures, except where experiments are to be shewn. You may teach chymestry by lectures. – You might teach making of shoes by lectures!

James Boswell: *Life of Samuel Johnson, 1766*
(1709–1784)

INSTRUMENTAL METHODS IN ELECTROCHEMISTRY

Southampton Electrochemistry Group

PROFESSOR D. PLETCHER, Department of Chemistry, Southampton University

DR R. GREFF, Department of Chemistry, Southampton University

DR R. PEAT, now AEA Industrial Technology Division, Harwell

PROFESSOR L. M. PETER, now Department of Chemistry, University of Bath

DR J. ROBINSON, now Department of Physics, University of Warwick



Oxford Cambridge Philadelphia New Delhi

Published by Woodhead Publishing Limited,
80 High Street, Sawston, Cambridge CB22 3HJ
www.woodheadpublishing.com

Woodhead Publishing, 1518 Walnut Street, Suite 1100, Philadelphia,
PA 19102-3406, USA

Woodhead Publishing India Private Limited, G-2, Vardaan House, 7/28 Ansari Road,
Daryaganj, New Delhi – 110002, India
www.woodheadpublishingindia.com

First published by Ellis Horwood Limited, 1985
Reprinted 1990, 1993
Republished by Horwood Publishing 2001
Reprinted by Woodhead Publishing Limited, 2011

© Horwood Publishing Limited, 2001; © Woodhead Publishing Limited, 2010
The authors have asserted their moral rights

This book contains information obtained from authentic and highly regarded sources.
Reprinted material is quoted with permission, and sources are indicated. Reasonable
efforts have been made to publish reliable data and information, but the authors and
the publisher cannot assume responsibility for the validity of all materials. Neither the
authors nor the publisher, nor anyone else associated with this publication, shall be
liable for any loss, damage or liability directly or indirectly caused or alleged to be
caused by this book.

Neither this book nor any part may be reproduced or transmitted in any form or by
any means, electronic or mechanical, including photocopying, microfilming and
recording, or by any information storage or retrieval system, without permission in
writing from Woodhead Publishing Limited.

The consent of Woodhead Publishing Limited does not extend to copying for
general distribution, for promotion, for creating new works, or for resale. Specific
permission must be obtained in writing from Woodhead Publishing Limited for such
copying.

Trademark notice: Product or corporate names may be trademarks or registered
trademarks, and are used only for identification and explanation, without intent to
infringe.

British Library Cataloguing in Publication Data
A catalogue record for this book is available from the British Library

ISBN 978-1-898563-80-8

Contents

Preface	7
List of symbols	9
1 Introduction to the fundamental concepts of electrochemistry	15
2 Steady state and potential step techniques	42
3 Electron transfer	76
4 Convective diffusion systems – the rotating disc and ring-disc electrodes	113
5 The electrical double layer	149
6 Potential sweep techniques and cyclic voltammetry	178
7 Electrocatalysis	229
8 A.C. techniques	251
9 ElectrocrySTALLISATION	283
10 Spectroelectrochemistry	317
11 The design of electrochemical experiments	356
APPENDIX	
Mathematical methods for the development of a theory for electrochemical experiments	388
Index	439

Preface

The idea for this book arose from a one-week residential postgraduate course entitled 'Advanced Instrumental Methods in Electrode Kinetics' which has been organised almost yearly since 1969 by the Electrochemistry Group at Southampton University. Our experience with this course persuaded us of the need for a book which treats not only the fundamental concepts of electrode reactions, but also covers the methodology and practical application of the many versatile electrochemical techniques now available. The book is pitched at the senior undergraduate and postgraduate level, and it should also benefit physical chemists and engineers in industry or research who wish to have an up-to-date survey of the wider uses of electrochemical techniques. The organisation of the book reflects the structure of the course in which successive lectures cover alternately fundamentals and techniques, but all the chapters have been completely rewritten so as to bring them up to date and to extend them to include many advanced topics and illustrative examples. Thus, the book goes well beyond the original content of the course lectures. Much of the additional material was chosen as the result of discussions with course participants over the years, either in the laboratory or in the more convivial atmosphere of the bar. Each chapter is essentially self-contained for those who wish to select a specialised topic of particular interest, but cross-references between chapters and many literature references are included.

The writing of a book of this kind must always cause the authors to take stock and reflect on progress in their field. In the present case, that progress has been systematically documented and emphasised by the successive revisions and updating of the lecture notes and experiments. While the basic principles have remained largely unchanged, modern instrumentation and data-handling tech-

niques have simplified the experiments and their analysis. Improvements in the way experiments are carried out and the emergence of a range of *in situ* spectroscopic techniques have greatly increased our ability to unravel complex reaction mechanisms. Overall, electrochemical techniques have become so powerful that their field of applications now spreads throughout chemistry and related sciences. The last fifteen years represent an exciting and critical period in the development of electrochemistry. The authors hope that this is reflected in their book.

The present authors would like to thank those many current and former colleagues who have contributed to earlier versions of the lecture notes and thereby influenced the content of this book; it is proper to mention here the names of such valued colleagues as Martin Fleischmann, Graham Hills, Alan Bewick, Gamini Gunawardena, Bob Jansson, and David Schiffrin. Because, however, we decided to rewrite completely and extend substantially the lecture notes to form this book, responsibility for the content and presentation, as well as for errors, must lie entirely with us. Without the expert manuscript preparation of Kate Welfare, this book would never have reached the printers, and to her we are especially grateful. The preparation of the illustrations was carried out with great patience and skill by Laurie Dykes. Finally, we express our thanks for the forbearance of our families who have encouraged us and tolerated the many hours that we have spent with pen in hand.

List of symbols

Regrettably, the symbols used in the electrochemical literature remain far from uniform. Hence the symbols used in this book are listed below as an aid to the reader. In general, when selecting symbols we have tried to conform to the IUPAC convention (see ref. 1 in Chapter 1); in a few instances there is an obvious clash between the convention and present practice, and in some of these cases, after a struggle with our consciences, we have come down on the side of current practice.

It will be seen that the list is long; even so, symbols used only in one place in the book, and there clearly defined, have been omitted. It will also be found that symbols appear in some places in the text with an additional subscript or superscript in order to emphasise a point. Again this is clearly explained in the text, and we hope the reader is aided and not confused! Finally, it will be seen below that some symbols have several different meanings. This is unfortunate but unavoidable, and in all cases the different usages are well separated in the text and conform to common usage. The units in brackets indicate those used throughout the book except where specifically stated.

a	radius of ion (cm)
a_i	activity of the species i (mol cm^{-3})
A	geometric area of electrode (cm^2) <i>or</i> rate constant for nucleation (s^{-1}) <i>or</i> gain of amplifier
$A(\lambda)$	absorbance at the wavelength λ (dimensionless)
c_i	concentration of species i (mol cm^{-3})

10 List of symbols

c_i^∞	concentration of species i in the bulk solution (mol cm^{-3})
c_i^σ	concentration of species i at the electrode surface, i.e. $x = 0$ (mol cm^{-3})
C	capacitance (F cm^{-2})
C_{dl}	double layer capacitance (F cm^{-2})
C^d	capacitance of diffuse layer (F cm^{-2})
C^i	capacitance of inner layer (F cm^{-2})
C_s	pseudo-capacitance (F cm^{-2})
d	diameter of the tip of the Luggin capillary (cm)
D	diffusion coefficient ($\text{cm}^2 \text{s}^{-1}$)
e	charge on the electron (C)
E	potential vs a reference electrode (V)
E_e	equilibrium (or reversible potential) (V).
	Sometimes superscripted A or C to denote anode or cathode respectively
E_e^S	standard potential (V)
E_{CELL}	difference between cathode and anode potentials (V)
E_i	initial potential e.g. for a sweep experiment (V)
E_p	peak potential, sometimes superscripted A or C to denote anodic or cathodic process respectively (V)
$E_{p/2}$	half peak potential. Superscripts A and C as above (V)
$E_{1/2}$	half wave potential (V)
E_{FB}	flat band potential (V)
E	phasor potential (V)
ΔE	amplitude of a modulated potential e.g. in an ac experiment (V)
E_i	energy of a species i (J mol^{-1})
E_F	Fermi energy (eV)
f	frequency, either revolutions per s of a rotating disc electrode or cycles per s of an ac modulation (s^{-1})
f'	frequency of a rotating disc in r.p.m.
F	the Faraday (C mol^{-1})
$F(t)$	convoluted current ($\text{A s}^{1/2}$)
F_L	limiting value of convoluted current ($\text{A s}^{1/2}$)
g	coefficient in Frumkin isotherm (dimensionless)
ΔG_i	free energy change (J mol^{-1} of species i)
ΔG_{ADS}	free energy of adsorption (J mol^{-1})
ΔG^\ddagger	free energy of activation (J mol^{-1})
$\overline{\Delta G}^\ddagger$	free energy of activation for the forward electron transfer process (J mol^{-1})
$\overleftarrow{\Delta G}^\ddagger$	free energy of activation for the back electron transfer process (J mol^{-1})
${}^\ominus \Delta G^\ddagger$	standard free energy of activation for the electron transfer reaction (at the equilibrium potential) (J mol^{-1})
ΔG_c	critical free energy for phase growth (J mol^{-1})
h	thickness of a monolayer deposit (cm) or Planck constant (J s)
ΔH	enthalpy of reaction (J mol^{-1})

i	current (A)
i_0	exchange current (A)
i_D	current at rotating disc electrode (A)
i_R	current at ring electrode (A)
$(i_R)_{SH}$	current at ring electrode when shielded by the disc (A)
i_p	peak current (A). Superscripts A and C indicate anodic and cathodic processes respectively
I	current density (A cm^{-2})
I_0	exchange current density (A cm^{-2})
\overline{I}	partial cathodic current density (A cm^{-2})
\overline{I}	partial anodic current density (A cm^{-2})
I_p	peak current density (A cm^{-2}). Superscripts A and C denote anodic and cathodic processes respectively
I_L	limiting (plateau) current density (A cm^{-2})
I_D	diffusion limited current density (A cm^{-2})
$I_{t=0}$	current density obtained by extrapolation to $t = 0$ (A cm^{-2})
I_{dl}	current density due to double layer charging (A cm^{-2})
I_m	current at maximum in an $I - t$ transient (A cm^{-2})
\mathbf{i}	vector current density (A cm^{-2})
J_i	flux of species i ($\text{mol cm}^{-2} \text{s}^{-1}$)
k	rate constant for a chemical reaction (generally s^{-1})
	Various subscripts depending on type mechanism
k_B	Boltzmann constant (J K^{-1})
k^\ominus	standard rate constant for an electron transfer couple (cm s^{-1})
\overleftarrow{k}	rate constant for cathodic process (cm s^{-1})
\overleftarrow{k}	rate constant for anodic process (cm s^{-1})
\overrightarrow{k}_0	rate constant for cathodic process at 0V vs reference electrode (cm s^{-1})
\overleftarrow{k}_0	rate constant for anodic process at 0V vs reference electrode (cm s^{-1})
K	equilibrium constant
L	length of a plate or electrode (cm)
l	thickness of thin layer cell (cm)
m	moles of electroactive species in electrolysis cell (mol)
M	molecular wt (g mol^{-1})
	or integration constant
	or flow rate of mercury (g s^{-1})
n	number of electrons involved in overall electrode reaction (dimensionless)
n_α	number of electrons involved before and including the rate determining step (dimensionless)
n_i	number concentration of species i (cm^{-3})
	or refractive index of phase i (dimensionless)
n_o	bulk electron density (cm^{-3})
n_s	surface electron density (cm^{-3})
N	collection efficiency of RRDE (dimensionless)

N_0	number of sites where nucleation can occur (cm^{-2})
$N(t)$	number of nuclei at time t (cm^{-2})
p	partial pressure (N m^{-2})
P	pressure (N m^{-2})
q	charge (C)
Q	charge density (C cm^{-2})
r	coordinate in spherical or cylindrical coordinates (cm)
r_0	radius of a disc or sphere (cm)
r_1, r_2, r_3	dimensions of rotating ring disc electrode (cm)
r_c	critical radius for spontaneous growth of a nucleus (cm)
R	gas constant ($\text{J K}^{-1} \text{mol}^{-1}$) or resistance (Ω) or reflectivity (dimensionless)
ΔR	change in reflectivity due to a modulation (dimensionless)
R_u	uncompensated resistance between reference electrode probe and working electrode (Ω)
R_{ct}	charge transfer resistance ($\Omega \text{ cm}^2$)
Re	Reynolds number (dimensionless)
s	variable of Laplace transform (s^{-1})
S	entropy ($\text{J mol}^{-1} \text{K}^{-1}$) or surface area of growing nucleus (cm^2)
Sc	Schmidt number (dimensionless)
Sh	Sherwood number (dimensionless)
t	time from commencement of experiment (s)
t_L	constant in equation for chronocoulometry (s)
t_m	time to maximum in I - t transient (s)
T	temperature (K)
V	cell voltage or applied voltage (V) or solution flow rate subscripted zero in situations where it varies to indicate initial flow rate or x, y, z , or r, θ, z etc. to indicate direction of flow (cm s^{-1}) or solution volume (cm^3)
\bar{V}	molar volume ($\text{cm}^3 \text{mol}^{-1}$)
V_{iR}	voltage drop due to uncompensated resistance (V)
x	distance perpendicular to the electrode surface (cm)
x_o	half space between steps on growing surface (cm)
X	capacitive reactance (Ω)
Y	admittance (Ω^{-1})
z	distance perpendicular to the surface of a rotating disc (cm)
z_i	charge number on ion i
Z	impedance (Ω) or pre-exponential factor (as corresponding rate constant)
Z_w	Warburg impedance (Ω)
Z'	real component of impedance (Ω)
Z''	imaginary component of impedance (Ω)
α	transfer coefficient. Subscripts A and C indicate anodic and cathodic processes respectively (dimensionless)

γ	surface tension (J cm^{-2}) or ratio c_A^∞/c_P^∞ in redox catalysis (dimensionless)
Γ_i	surface excess of species i (mol cm^{-2})
δ	diffusion layer thickness (cm) or reaction length (cm)
ϵ_i	relative permittivity of phase i (dimensionless)
$\hat{\epsilon}$	complex optical constant for phase i (dimensionless)
ϵ_0	permittivity of free space (F cm^{-1})
$\epsilon(\lambda)$	molar absorbance at wavelength λ ($\text{mol}^{-1} \text{cm}^2$)
η	overpotential, $E-E_e$ (V). Subscripts A and C indicate anode and cathode respectively
θ	angular coordinate of rotating disc or fractional surface coverage or angle of incidence
λ	wavelength of light (nm) or reorganisation energy (J mol^{-1} or eV)
μ	viscosity (centipoise)
μ_i	chemical potential of species i (J mol^{-1})
$\tilde{\mu}_i$	electrochemical potential of species i (J mol^{-1}). Superscript indicates phase
μ_i^Θ	standard chemical potential of species i (J mol^{-1})
ν	potential scan rate (V s^{-1}) or kinematic viscosity ($\text{cm}^2 \text{s}^{-1}$)
π	surface pressure (N m^{-2})
ρ	density (g cm^{-3}) or charge density (C cm^{-2})
σ	surface excess charge density (C cm^{-2}). Superscript indicates phase or Warburg coefficient ($\Omega \text{s}^{-1/2}$)
τ	transition time (s)
ϕ	electrical (Galvani) potential of phase (V). Superscript indicates phase or phase shift in ac experiment (dimensionless)
$\Delta\phi_{SC}$	potential drop in semiconductor (V)
ω	angular rotation rate of disc (s^{-1}) or angular frequency of ac excitation (s^{-1})
$\Delta\omega$	amplitude in modulation of ω (s^{-1})

Sign convention

The IUPAC convention is followed. Thus anodic currents are positive and cathodic currents are negative, while moving to more positive potentials corresponds to increasing the driving force for an oxidation, or moving to more negative potentials corresponds to increasing the driving force for reduction.

1

Introduction to the fundamental concepts of electrochemistry

This book was initially prepared as lecture notes for an electrochemistry course which has been presented regularly in Southampton and elsewhere during the past fifteen years. The course seeks to develop an understanding of electrochemical experiments and to illustrate the applications of electrochemical methods to, for example, the study of redox couples, homogeneous chemical reactions, and surface science. In many studies, several of the techniques will be equally applicable, but there are situations where one technique has a unique advantage and hence the course also seeks to discuss the selection of method and the design of experiments to aid the solution of both chemical and technological problems.

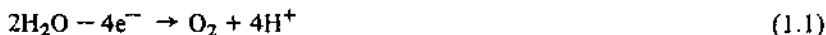
It will be shown that the methods are, in general, based on very similar principles. Commonly the need is to carry out an experiment so as to separate the effects on the measurements of the kinetics of electron transfer or a coupled chemical reaction from those which arise from mass transport of species to and from the electrode surface. Thus it is important to understand how the measurement of current as a function of time in potential step methods, of potential scan rate in cyclic voltammetry, of frequency in ac methods, or of rotation rate in experiments with a rotating disc electrode, can be used to isolate pure kinetic information. A grasp of the fundamentals of electrochemistry and an understanding of the theoretical background to the methods is extremely helpful to the experimental electrochemist for another reason — although often disguised by our use of the literature, e.g. of equations or dimensionless plots, the conclusions from electrochemical experiments always come from a comparison of the experimental data with a theoretical response, derived from a mathematical description of the experiment and the solution of the resulting equations. Hence

it is, at least, essential to be certain that the conditions for the experiment are appropriate to the results taken from the literature. Furthermore, the reliable employment of electrochemical techniques requires an appreciation of the way in which the electrode and cell should be designed, the way in which the equipment operates, and the ways in which the procedure for carrying out the experiment can determine the quality of the data.

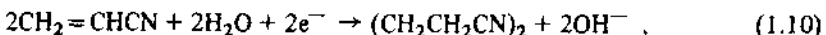
Hence the structure of this book quite deliberately follows that of the course. The theoretical background to electrochemistry and the discussion of electrochemical techniques are developed as parallel themes. The general principles of instrumentation and experiment design are introduced in later chapters, while those readers interested in the mathematical and computational techniques used in electrochemistry are directed to the appendix. The purpose of this first chapter is to give an overview of electrochemistry and to summarise those important equations and ideas which will be used repeatedly throughout the book and which will also be more fully justified in later chapters.

1.1 ELECTRODE REACTIONS AND CELL CHEMISTRY

An electrode reaction is a heterogeneous chemical process involving the transfer of electrons to or from a surface, generally a metal or a semiconductor. The electrode reaction may be an anodic process whereby a species is oxidised by the loss of electrons to the electrode, e.g.

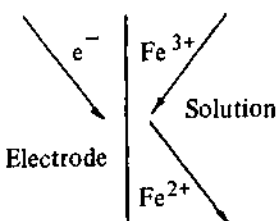


By convention [1], the current density, I , for an anodic process is a positive quantity. Conversely, the charge transfer may be a cathodic reaction in which a species is reduced by the gain of electrons from the electrode, e.g.

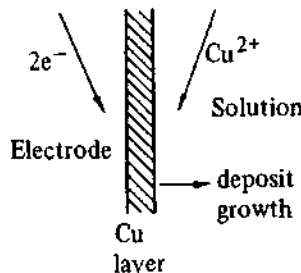
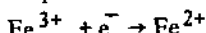


and the current density for a cathodic process is a negative quantity. The diversity of electrode reactions can already be seen from Equations (1.1)-(1.10): the electroactive species may be organic or inorganic, neutral or charged, a species

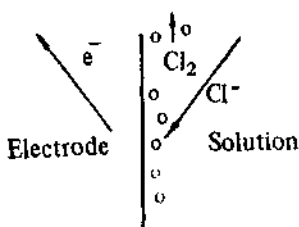
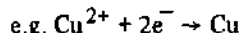
dissolved in solution, the solvent itself, a film on the electrode surface, or, indeed, the electrode material itself. Moreover, the product may be dissolved in solution, a gas, or a new phase on the electrode surface. The many types of electrode reactions are also illustrated pictorially in Fig. 1.1.



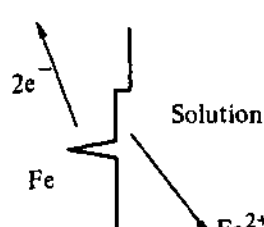
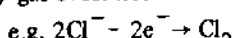
(a) simple electron transfer



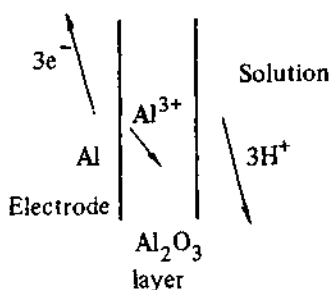
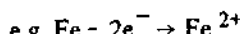
(b) metal deposition



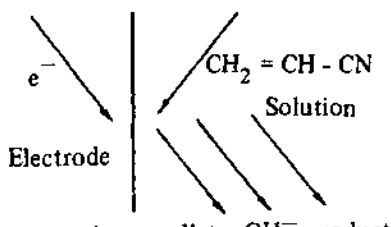
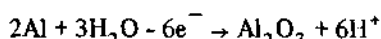
(c) gas evolution



(d) corrosion



(e) oxide film formation



(f) electron transfer with coupled chemistry

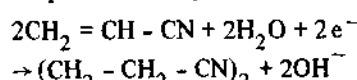


Fig. 1.1 – Schematic view of some types of electrode reactions met in applied and fundamental electrochemistry.

Electrolysis is only possible in a cell with both an anode and a cathode, and, because of the need to maintain an overall charge balance, the amount of reduction at the cathode and oxidation at the anode must be equal. The total chemical change is found by adding the two individual electrode reactions; for example, the chemical change in a chlor-alkali membrane or diaphragm cell is obtained by adding Equations (1.3) and (1.8), i.e.



Moreover, when electrolysis occurs, in addition to electron transfer at the anode and cathode surfaces, ions must pass through the solution between the electrodes and electrons through the wires externally interconnecting the two electrodes (in order to maintain electrical neutrality at all points in the system). Hence the current through the external circuit, i , given by

$$i = AI \quad (1.12)$$

(when A is the electrode area and I the current density), is a convenient measure of the rate of the cell reaction, and the charge, q , passed during a period, t , indicates the total amount of chemical reaction which can have taken place: indeed, the charge required to convert m moles of starting material to product in an electrode reaction involving the transfer of n electrons/molecule is readily calculated using Faraday's law

$$q = \int_0^t idt = mnF . \quad (1.13)$$

When the two electrodes of a cell are interconnected by an external circuit, however, the cell reaction will only occur spontaneously if the free energy change associated with the net cell reaction is negative. This is not the case in a cell for the production of chlorine and caustic soda, i.e. the free energy of reaction (1.11) is positive, and for reaction (1.11) to occur it will be necessary to supply energy by applying a potential between the two electrodes. This potential must certainly be greater than the difference between the reversible potentials of the cathode and anode in the cell, ($E_e^C - E_e^A$), calculated from

$$\Delta G = -nF(E_e^C - E_e^A) \quad (1.14)$$

where ΔG is the free energy change associated with the overall cell reaction under the electrolysis conditions.

Even if the conditions are such that the reaction is thermodynamically favourable (either the overall cell reaction has a negative free energy or we are applying the thermodynamic driving force via an externally applied potential), the rate of electrolysis (i.e. the current density, I) will depend on the kinetics of the two electrode reactions. We shall see later that it is commonly essential to have an overpotential, η , to increase the rate at which an electrode reaction occurs. Also for ions to move through the electrolyte in the cell, energy must be supplied. Hence the total cell voltage, V , required to bring about chemical change by electrolysis is given by

$$V = E_e^C - E_e^A - |\eta_A| - |\eta_C| - iR \quad (1.15)$$

where R is the resistance of the electrolyte solution between the electrodes. This equation is at the heart of applied electrochemistry since in all cells the overpotentials and the iR term represent energy inefficiencies which we must seek to minimise.

The potential drop term, iR , also explains the way in which laboratory investigations are carried out. If a two electrode cell were used, the plot of I versus V would tell us little about the electron transfer processes in the cell, since both the overpotentials and the iR term vary with the current and in quite different ways. Hence it is normal to design the cell so that an $I-E$ response is characteristic of the processes at only one of the electrodes. This is achieved by introducing a third electrode, the reference electrode, into the cell. This electrode is placed inside a Luggin probe, the tip of which is positioned very close to the working electrode surface. The potential of the working electrode is controlled versus the reference electrode, using a feedback circuit or potentiostat. The principle of a potentiostat is shown in Fig. 1.2, and more complete circuits are discussed in Chapter 11; the operational amplifier is the key component of the potentiostat, and the feedback circuit drives the current between the working and secondary electrodes while ensuring that none passes through the reference electrode circuit. Hence the contribution of iR drop to the measured potential is minimised; there remains a relatively small iR drop (commonly negligible) because the tip of the Luggin capillary cannot be placed right on the electrode surface. Also the working electrode should be much smaller than the counter electrode so that no serious polarisation of the latter can occur, and therefore the characteristics of the counter electrode reaction do not contribute to the response of the cell.

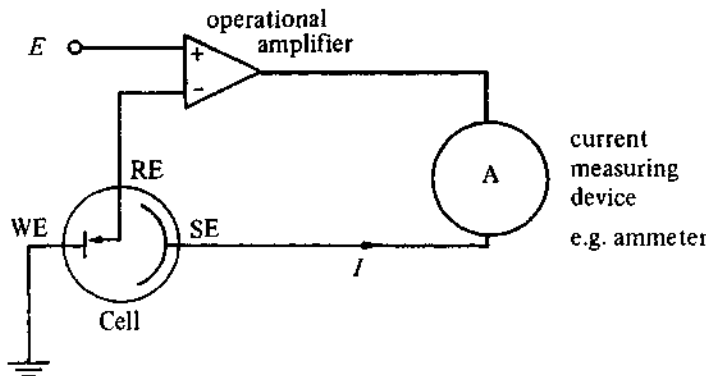


Fig. 1.2 ~ The principle of a potentiostat.

1.2 THE NATURE OF ELECTRODE REACTIONS

Perhaps the simplest electrode reaction is one which interconverts at an inert surface, two species, O and R, which are completely stable and soluble in the electrolysis medium containing an excess of an electrolyte which is electro-inactive.



Even in this case, however, the electrode reaction is a sequence of more basic steps; to maintain a current it is essential to supply reactant to the electrode surface and also to remove the product, as well as for the electron transfer reaction at the surface to occur. Hence, for example, in experimental conditions where O is reduced to R, the electrode reaction must have three steps:

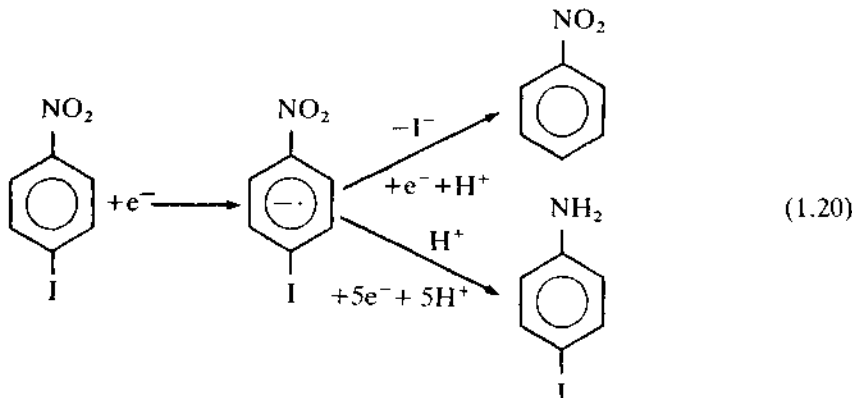


and since the rate of reduction, and hence cathodic current, is determined by the rate of the overall sequence, it must be dependent on the rate of the slowest step. Thus to understand the characteristics of such an electrode reaction, we need to know about both mass transport and electron transfer.

An examination of Reactions (1.1)-(1.10) at the beginning of this chapter quickly shows that electrode reactions are commonly not that simple. They can involve multiple electron transfers, and at least three additional types of basic steps also occur.

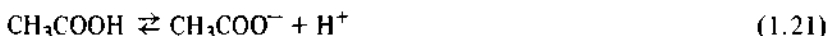
(a) Coupled chemical reactions

The species formed by electron transfer may not be stable in the electrolysis medium: it may only be an intermediate which undergoes chemical change to form the observed product. In favourable conditions there may be a single reaction pathway leading to one product, but with organic intermediates it is common for there to be competitive reactions leading to a mixture of products, e.g. in the reduction of *p*-iodonitrobenzene in aqueous acid, the anion radical initially formed can either lose iodide ion or protonate, leading to different final products.



In general, the chemical reaction may be a homogeneous process occurring as the product of electron transfer (R in the case of a reduction) is transported away from the surface, or a heterogeneous process occurring while the species R is adsorbed on the surface. Reaction (1.10) is another example where such following chemical reactions are important; the initial electron transfer produces the anion radical of acrylonitrile, and to form adiponitrile, a dimerisation, two protonations, and a further electron transfer must take place.

Less frequently it is found that the electroactive species is not the major species in bulk solution but is only formed by a chemical process, i.e. the electrode reaction is disturbing an equilibrium in homogeneous solution. An example is the reduction of acetic acid to hydrogen which proceeds via dissociation prior to electron transfer:



If the dissociation reaction is slow compared to the transport of acetic acid to the cathode surface, it will limit the current density for the evolution of hydrogen.

(b) Adsorption

Sequence (1.17)–(1.19) assumes that electron transfer occurs at the electrode surface but without specific interaction between the surface and either O or R . This may not be the case, and for the reaction to proceed it may be necessary for reactants, intermediates, or products to be adsorbed on the electrode.

Moreover, adsorption has other important roles in electrochemical technology. In electrocatalysis, adsorption of intermediates is a key step since their presence on the surface provides alternative lower energy pathways (see Chapter 7). Also, adsorption of species not directly involved in the electron transfer process is used to modify electrode reactions, to change the product, to modify the structure of metal deposits, and to slow down electron transfer reactions (as in corrosion inhibition).

(c) Phase formation

The electrode reaction may involve the formation of a new phase (e.g. the electrodeposition of metals in plating, refining and winning or bubble formation when the product is a gas) or the transformation of one solid phase to another (e.g. Reaction (1.9)). The formation of a new phase is itself a multistep process requiring both nucleation and subsequent growth. Moreover, growth of an electrodeposited metal layer may involve both diffusion of metal adatoms (resulting from reduction of metal ions in solution) across the surface and incorporation of the adatoms into the lattice at an appropriate site.

Since electrode reactions commonly involve the transfer of several electrons, the complications (a)–(c) can occur sandwiched between, as well as preceding or following, electron transfer. Thus, for example, Reaction (1.9) is likely to involve electron transfer, diffusion, chemical reactions (protonation and hydration

equilibria as well as sulphation), phase transformation, and adsorbed intermediates! In this book, however, we shall take the approach of considering each fundamental type of process in turn, in particular seeking to define (i) its consequences on our theoretical view of electrode processes, and (ii) how to recognise when it is important in influencing experimental data.

1.3 ELECTRON TRANSFER

We shall discuss the electrode reaction



occurring in the cell shown schematically in Fig. 1.3. It contains two electrodes, a small and inert working electrode (WE) and a large platinum electrode which will act both as the counter and reference electrode. Both are in aqueous acid (1 mol dm^{-3}) but are separated by a glass frit. Hydrogen gas is bubbled over the surface of the platinum so that this electrode is effectively a normal hydrogen electrode (NHE) whose potential is, by convention, taken to be zero. The solution in the working electrode compartment is deoxygenated and contains low concentrations, c_O^∞ and c_R^∞ , of the electroactive species O and R respectively. The relative areas of the two electrodes are chosen so that the NHE is never polarised

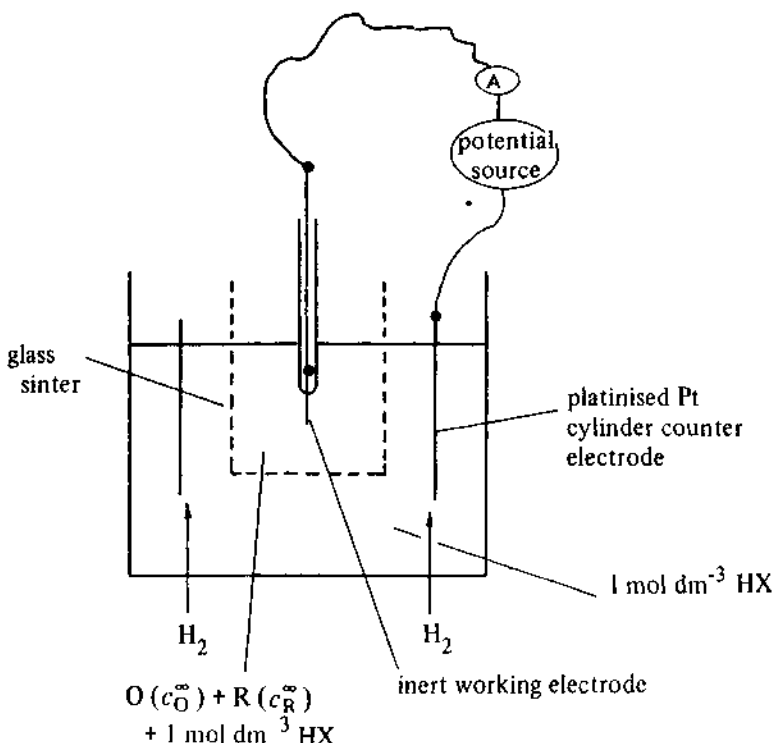


Fig. 1.3 – Schematic cell used in the development of the equations describing the thermodynamics and kinetics of the electron transfer process.

(its potential remains at zero even when current is passed). Hence the characteristics of the cell are determined solely by the behaviour at the WE. Moreover, low concentrations of O and R are used, so that the iR drop through the solution between the electrodes is never significant.

As with any chemical process, it is necessary to consider both the thermodynamics and kinetics of the electron transfer process. If the cell potential is monitored while allowing no current to flow through the cell, the potential of the working electrode will eventually reach a steady state value indicating that the cell is in equilibrium. The potential of the WE is then given by the Nernst equation

$$E_e = E_e^\ominus + \frac{RT}{nF} \ln \frac{c_O^g}{c_R^g} \quad (1.24)$$

where the equilibrium (or reversible) potential, E_e , is related to the standard potential of the couple O/R, E_e^\ominus , and the surface concentrations of O and R, c_O^g and c_R^g (it is assumed that the activity coefficients of O and R are unity so that concentrations rather than activities may be used in the Nernst equation). Clearly the standard potential is the particular equilibrium potential when the surface concentrations of O and R are equal. In the experiment outlined above, no current has passed through the cell, and hence no chemical change can have occurred; the surface concentrations must therefore be equal to the bulk concentrations, c_O^∞ and c_R^∞ , prepared for the experiments. Hence we may write

$$E_{\text{CELL}} = E_{\text{WE}} - E_{\text{NHE}} = E_{\text{WE}} - 0$$

or

$$E_{\text{CELL}} = E_e^\ominus + \frac{RT}{nF} \ln \frac{c_O^\infty}{c_R^\infty} \quad (1.25)$$

While no net current is flowing and there is no overall chemical change in the cell, there must be a dynamic equilibrium at the surface of the WE, i.e. the reduction of O and the oxidation of R are both occurring, but the processes are of equal rate

$$-\vec{I} = \vec{I} = I_o \quad (1.26)$$

where I_o is an important kinetic characteristic of an electron transfer process known as the exchange current density, and \vec{I} and \vec{I} are the partial current densities for the forward and back reactions. The negative sign reflects our sign convention that a cathodic current is negative.

If the potential of the WE is made more negative than the equilibrium potential determined by the bulk concentrations of O and R, equilibrium can only be reestablished when the surface concentrations of O and R have taken up the new values demanded by the Nernst equation, Equation (1.24), at the applied potential. This will require current to flow through the electrode/solution interface. In fact, a decrease in the ratio c_O^g/c_R^g is necessary, and this

can only be brought about by the conversion of O to R by the passage of a cathodic current. Conversely, if the potential of the WE is made more positive than E_e , an anodic current should be observed.

These simple predictions about the $I-E$ behaviour of the cell in Fig. 1.3 are based only on thermodynamics. In fact, the magnitude of the current flowing at any potential will also depend on the kinetics of electron transfer. At any potential the measured current density is given by

$$I = \vec{I} + \hat{I} \quad (1.27)$$

(where \vec{I} is negative) and these partial current densities are each only dependent on a rate constant and the concentration of the electroactive species at the site of electron transfer, the electrode surface, i.e.

$$\vec{I} = -nFk_c^g_O \quad \text{and} \quad \hat{I} = nFk_c^g_R . \quad (1.28)$$

The rate constants, however, have a particular property; they vary with the applied electrode potential (in other words, the potential difference at the electrode surface during electron transfer), and invariably it is found experimentally that the rate constants vary with potential according to equations of the form

$$\vec{k} = \vec{k}_0 \exp\left(-\frac{\alpha_C nF}{RT} E\right) \quad \text{and} \quad \hat{k} = \hat{k}_0 \exp\left(\frac{\alpha_A nF}{RT} E\right) \quad (1.29)$$

where α_A and α_C are constants (between 0 and 1 and generally approximately 0.5) known as the transfer coefficients for the anodic and cathodic reactions respectively. For a simple electron transfer reaction $\alpha_A + \alpha_C = 1$, so that one transfer coefficient may be eliminated from any equation.

Algebraic manipulation of Equations (1.27)–(1.29), defining the overpotential as the deviation of the potential from the equilibrium value, i.e.

$$\eta = E - E_e \quad (1.30)$$

and noting the definition of the exchange current density, $I_0 = -\vec{I} = \hat{I}$ at $\eta = 0$, leads to the Butler–Volmer equation

$$I = I_0 \left[\exp\left(\frac{\alpha_A nF}{RT} \eta\right) - \exp\left(-\frac{\alpha_C nF}{RT} \eta\right) \right] . \quad (1.31)$$

This must be regarded as the fundamental equation of electrode kinetics, and it shows the way in which current density varies with exchange current density, overpotential, and the transfer coefficients. In the laboratory it is, however, more common to use one of the three limiting forms of Equation (1.31). The first two apply at high overpotentials. At high positive overpotentials $|\hat{I}| \gg |\vec{I}|$, and the second term may be ignored; the anodic current density is then given by

$$\log I = \log I_0 + \frac{\alpha_A nF}{2.3RT} \eta . \quad (1.32)$$

Conversely, at high negative overpotentials $|\vec{I}| \gg |\vec{J}|$ and the cathodic current density is given by

$$\log -I = \log I_o - \frac{\alpha_C nF}{2.3RT} \eta \quad (1.33)$$

The third limiting form applies at very low values of η where $\eta \ll (RT/\alpha_C nF)$ and $\eta \ll (RT/\alpha_A nF)$. The two exponential terms of Equation (1.31) may then be expanded as series, and ignoring quadratic and higher order terms leads to the simple equation

$$I = I_o \frac{nF}{RT} \eta \quad (1.34)$$

Equations (1.32) and (1.33) are known as the Tafel equations and are the basis of a simple method of determining the exchange current density and a transfer coefficient, see Fig. 1.4. While these two parameters characterise totally the kinetics of an electrode reaction, the exchange current density varies with the

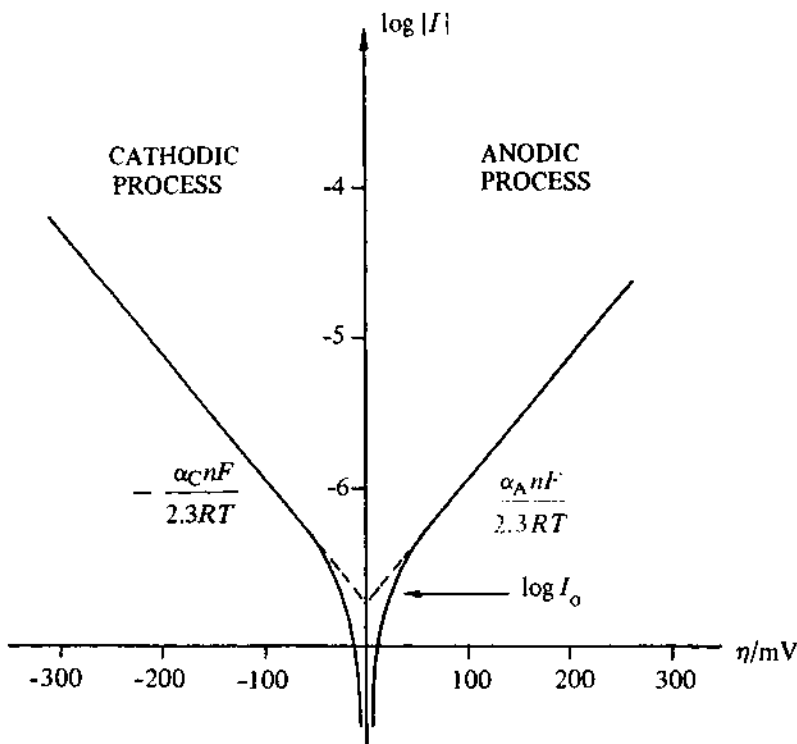


Fig. 1.4 – Experimental determination of the kinetic constants, I_o and α , using the Tafel equations. Note the deviations from linearity at low η where the limiting form of the Butler-Volmer equation is no longer appropriate.

concentration of both O and R at the surface. Hence it is often better to quote the standard rate constant defined by

$$k^\ominus = \frac{I_0}{nF(c_O)^\alpha A(c_R)^\alpha C} \quad (1.35)$$

since this is a kinetic parameter which is independent of the concentration of O and R. k^\ominus is also the value of the rate constant for electron transfer at the standard potential, E_e^\ominus . Thus the I-E characteristic is completely specified by k^\ominus and a transfer coefficient.

1.4 MASS TRANSPORT

In general, in electrochemical systems, it is necessary to consider three modes of mass transport; namely,

(a) *Diffusion*

Diffusion is the movement of a species down a concentration gradient, and it must occur whenever there is a chemical change at a surface. An electrode reaction converts starting material to product ($O \rightarrow R$), and hence close to the electrode surface there is always a boundary layer (up to 10^{-2} cm thick) in which the concentrations of O and R are a function of distance from the electrode surface. The concentration of O is lower at the surface than in the bulk, while the opposite is the case for R, and hence O will diffuse towards and R away from the electrode.

(b) *Migration*

Migration is the movement of charged species due to a potential gradient, and it is the mechanism by which charge passes through the electrolyte; the current of electrons through the external circuit must be balanced by the passage of ions through the solution between the electrodes (both cations to the cathode and anions to the anode). It is, however, not necessarily an important form of mass transport for the electroactive species even if it is charged. The forces leading to migration are purely electrostatic, and hence the charge can be carried by any ionic species in the solution. As a result, if the electrolysis is carried out with a large excess of an inert electrolyte in the solution, this carries most of the charge, and little of the electroactive species is transported by migration.

(c) *Convection*

Convection is the movement of a species due to mechanical forces. It can be eliminated, at least on a short timescale (it is difficult to eliminate natural convection arising from density differences on a longer time, i.e. >10 s) by carrying out the electrolysis in a thermostat in the absence of stirring or vibration. In industrial practice it is much more common to stir or agitate the electrolyte or to flow the electrolyte through the cell. These are all forms of forced convection and, when present, they have a very large influence on the current density.

The investigation of the mechanism and kinetics of electrode processes is normally undertaken with solutions containing a large excess of base electrolyte (i.e. the migration of electroactive species is unimportant), and two types of experiment are common:

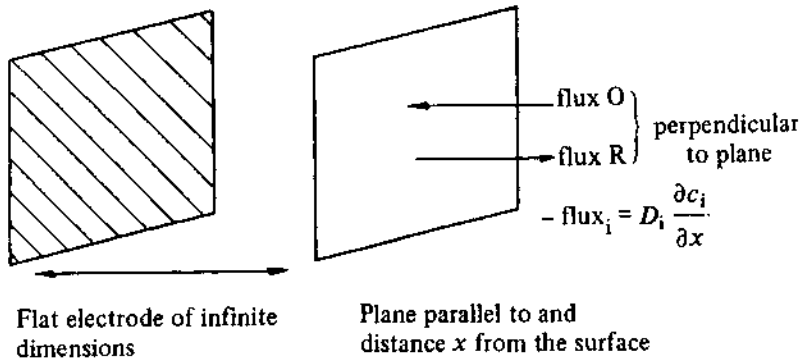
- (i) using unstirred solutions
- (ii) using a form of forced convection which may be described exactly. By far the most important system is the rotating disc electrode.

In both, the experiment is carried out so that we may assume that mass transport in only one dimension, that perpendicular to the electrode surface, is important.

1.4.1 Linear diffusion to a plane electrode

In unstirred solution and in the presence of a base electrolyte, diffusion is the only form of mass transport for the electroactive species which need be con-

(a)



(b)

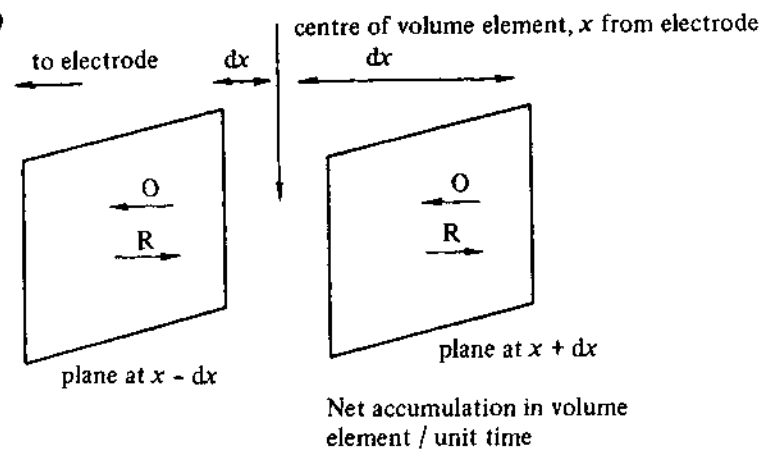


Fig. 1.5 – Model for linear diffusion to a plane electrode for the electrode reaction $O + ne^- \rightarrow R$. (a) Fick's 1st law, (b) Fick's 2nd law.

sidered. The simplest model is that of linear diffusion to a plane electrode; it is assumed that the electrode is perfectly flat and of infinite dimensions, so that concentration variations can only occur perpendicular to the electrode surface. Diffusion may then be characterised by Fick's laws in a one dimensional form, see Fig. 1.5.

Fick's first law states that the flux of any species, i , through a plane parallel to the electrode surface is given by

$$\text{Flux} = -D_i \frac{dc_i}{dx}, \quad (1.36)$$

where D_i is the diffusion coefficient and typically has the value $10^{-5} \text{ cm}^2 \text{ s}^{-1}$. The second law describes the change in concentration of i with time due to diffusion. At a point at the centre of an element of solution bounded by two planes parallel to the electrode the concentration will change because diffusion is occurring both into and out of the element. This leads to the equation (see Appendix)

$$\frac{\partial c_i}{\partial t} = D_i \frac{\partial^2 c_i}{\partial x^2}. \quad (1.37)$$

Integration of Equation (1.37) with initial and boundary conditions appropriate to the particular experiment is the basis of the theory of instrumental methods

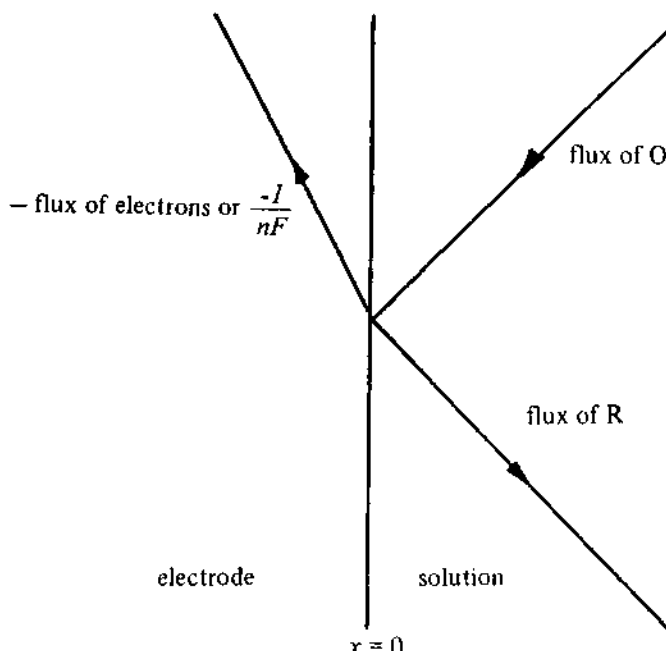


Fig. 1.6 – The flux balance at the electrode surface drawn for the reaction $\text{O} + ne^- \rightarrow \text{R}$.

such as chronopotentiometry, chronoamperometry, and cyclic voltammetry. The first law applied at the electrode surface, $x = 0$, is used to relate the current to the chemical change at the electrode by equating the flux of O or R with the flux of electrons, see Fig. 1.6, where

$$\frac{I}{nF} = -D_O \left(\frac{\partial c_O}{\partial x} \right)_{x=0}$$

or

$$\frac{I}{nF} = D_R \left(\frac{\partial c_R}{\partial x} \right)_{x=0} . \quad (1.38)$$

The zone close to the electrode surface where the concentrations of O and R are different from those in the bulk is known as the diffusion layer. In most experiments its thickness increases with time until it reaches a steady state value, approximately 10^{-2} cm thick, as natural convection stirring the bulk solution becomes important. It takes of the order of 10 s for this boundary layer to form. This also means that for the first 10 s of any experiment, the concentration changes close to the electrode are the result of only diffusion. Thereafter the effects of natural convection must be taken into account.

The graphs which show the dependence of concentration on distance from the electrode surface are known as concentration profiles. The concentration profiles are the complete solutions to Equation (1.37), $c_i = f(x, t)$, but many experiments may be understood from a qualitative consideration of the way in which concentration profiles develop with time and vary with experimental parameters. For example, Fig. 1.7 shows the time development of the concentration profiles for O and R during an experiment carried out with a solution initially containing O but no R and in which the electrode potential is stepped at $t = 0$ in such a way as to cause the surface concentration of O to change instantaneously from c_O^∞ to zero, i.e. the potential is stepped from a value well positive to the standard potential of the couple to one well negative of E_e^Θ . At short times the concentration of O will only have changed from its initial value, c_O^∞ , at points very close to the electrode surface, and the concentration profile will consequently be steep. With increasing time, diffusion (the physical process which seeks to minimise differences in concentration) will cause the concentration profiles to relax towards their steady state by extending into solution and becoming less steep. Since the current is a simple function of the flux of O at the electrode surface, Equation (1.38), we can also see that it will decrease with time, Figure 1.8. As indicated above, to obtain a more detailed knowledge of the transient we must solve the equation

$$\frac{\partial c_O}{\partial t} = D_O \frac{\partial^2 c_O}{\partial x^2} \quad (1.37)$$

with the initial and boundary conditions which describe this particular potential step experiment, i.e.

at $t = 0$ and for all $x, c_O = c_O^\infty$
 and for $t > 0$, at $x = 0, c_O^g = 0$
 and at $x = \infty, c_O = c_O^\infty$. (1.39)

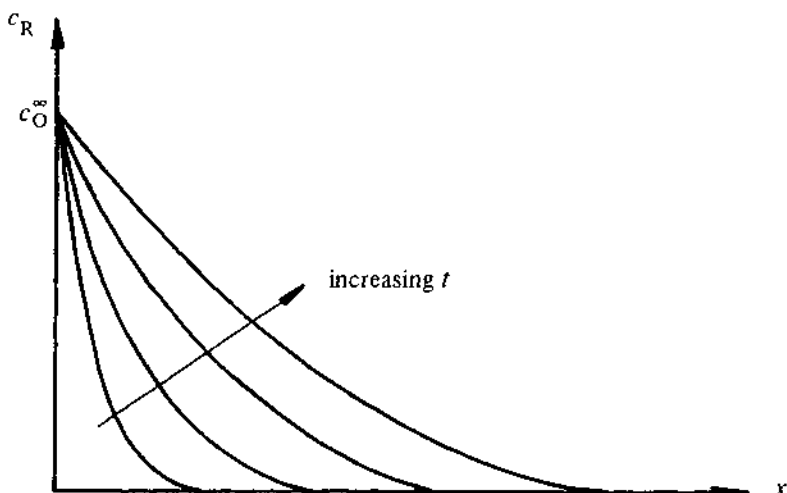
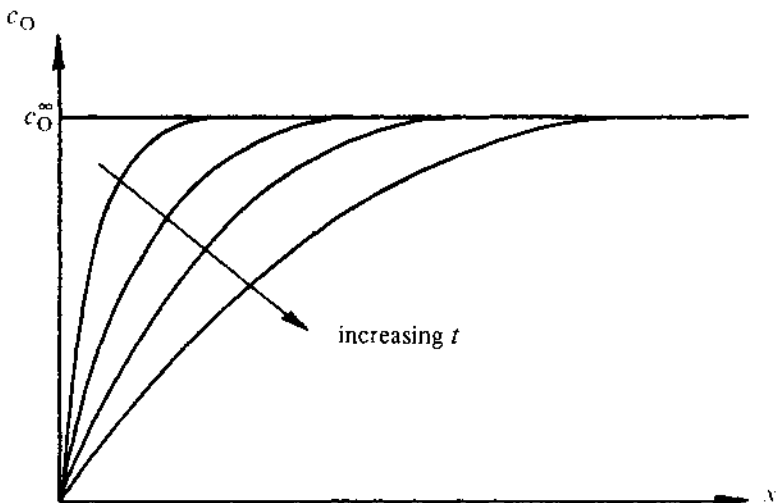


Fig. 1.7 - The time evolution of the concentration profiles for the reaction $O + ne^- \rightarrow R$ at a potential where the process is diffusion controlled; i.e. for $t > 0, c_O = 0$ at $x = 0$. Initially $c_O = c_O^\infty$ and $c_R = 0$ at all x .

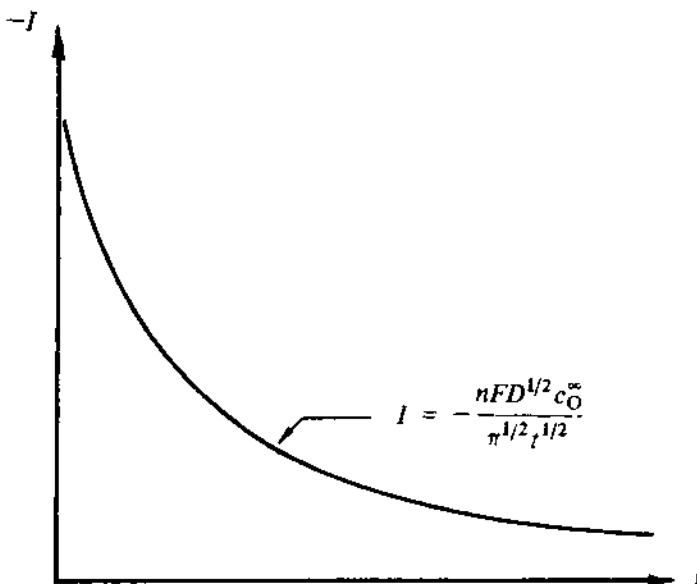


Fig. 1.8 – Current-time response to the potential step experiment described in the legend to Fig. 1.7.

The mathematical procedure to solve the Equations (1.37) and (1.39) is described in the appendix, and it leads to the exact form of the I - t transient, i.e.

$$I = -\frac{nFD^{1/2}c_O^\infty}{\pi^{1/2}t^{1/2}} \quad . \quad (1.40)$$

This equation is an example of an equation taken from the literature and used to compare theory and experiment. It has been frequently used to confirm the potential range where an electrode reaction is diffusion controlled and also to estimate values of diffusion coefficients. It was stressed earlier than when taking an equation from the literature it is important to ensure that the experimental conditions are appropriate to the model used in developing the equation. In this case it would be essential to work (a) with a large excess of base electrolyte in the solution, (b) with a solution which is unstirred, and, ideally, it should be thermostatted, (c) only on a timescale less than 10 s (note also that below 1 ms, the data will be adversely affected by a charging current, see later), and (d) sufficient time must be left after each experiment for the concentration profile for O to be restored to the correct initial condition, i.e. $c_O = c_O^\infty$ at all x , before a further experiment is attempted.

On the other hand it should be noted that Equation (1.40) has been derived from a model which assumes linear diffusion to a planar electrode. In the laboratory we cannot use electrodes that are flat on a molecular level or of infinite

dimensions. Indeed disc, drop, or wire electrodes are most commonly used, and these are made from real materials which cannot be perfectly polished. Fortunately this is not important, and it may be shown analytically that, provided the electrodes are of reasonable size, and for timescales below 10 s the much more complex equations required to take into account three-dimensional geometry lead to the same equation (again, see Appendix). Moreover, this is a general observation, and the theory for most electrochemical experiments can be safely developed using the one dimensional model.

1.4.2 The rotating disc electrode

A rotating disc acts as a pump, pulling solution up to the disc and throwing it out across the shroud, see Fig. 1.9; hence in experiments with a rotating disc electrode, concentration changes will arise due to both diffusion and convection.

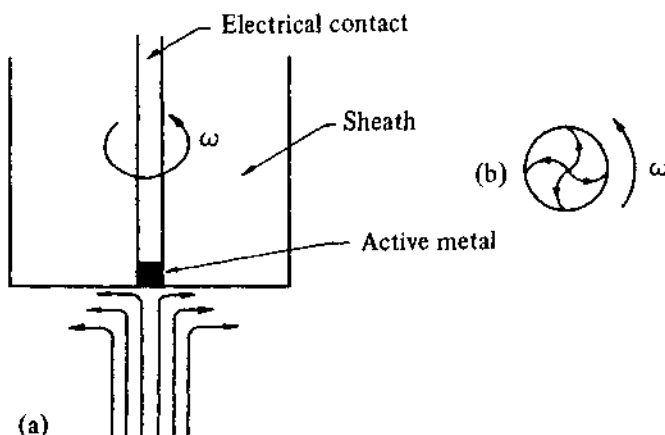


Fig. 1.9 – Convective flow resulting from the rotation of a disc electrode. Stream lines: (a) side view (b) from below the disc.

If the radius of the disc is small compared to that of shroud, we can assume that access of the solution to all the electrode surface is uniform, and again write an expression in one dimension:

$$\frac{\partial c_i}{\partial t} = D_i \frac{\partial^2 c_i}{\partial x^2} - V_x \frac{\partial c_i}{\partial x}, \quad \text{diffusion convection} \quad (1.41)$$

where V_x is the velocity of solution movement perpendicular to the disc. A solution of this problem depends on knowing the relationship between V_x and x and other parameters, particularly the rotation rate of the disc, ω . The relationship

$$V_x \propto \omega^{3/2} x^2 \quad (1.42)$$

was deduced for small x from a consideration of the fluid mechanics by Levich [2]. Equation (1.42) shows that V_x , and hence the importance of convection in the system, increases as the square of the distance from the electrode surface. Hence close to the surface, convection will not be an important form of mass transport, and it is therefore possible and certainly convenient for our understanding of the experiment to define a boundary layer, thickness δ , inside which diffusion is the only significant form of mass transport. Outside this boundary layer, convection is strong enough to maintain the concentrations of all species uniform and at their bulk values. Using this concept, the steady state concentration profiles for a solution of O and R are shown in Fig. 1.10. With a rotating disc electrode, the diffusion layer thickness is determined by the rotation rate of the disc, the layer becoming thinner with increasing rotation rate. The c_i vs x plots inside the boundary layer must in the steady state be effectively linear,[†] because any other concentration profile would lead, at some points in space, to an increased flux and hence to diffusion and further changes in profile. The steady state current will be given by

$$\begin{aligned} I &= -nFD \left(\frac{dc_O}{dx} \right)_{x=0} \\ &= nFD \frac{c_O^\infty - c_O^\infty}{\delta} . \end{aligned} \quad (1.43)$$

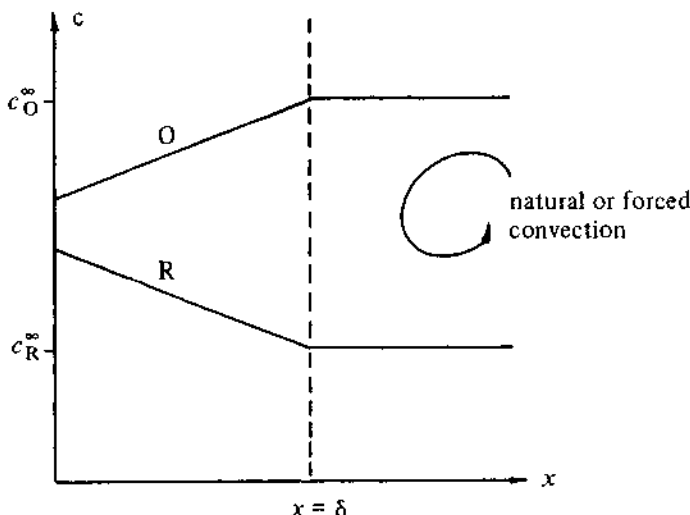


Fig. 1.10 – Steady state concentration profiles for the process $O + ne^- \rightarrow R$. Solution contains $c_O^\infty = 3c_R^\infty$.

[†] This model is slightly oversimplified because at $x = \delta$ there cannot be a sudden transition from pure diffusion to pure convection. Nor can the concentration profile be as shown; there must be a gradual change from a linear profile to a constant value, see Chapter 4.

The surface concentration c_O^∞ is, of course, a function of potential, but the 'diffusion limited current density' or 'limiting current density' corresponds to the maximum flux, i.e. to potentials where $c_O^\infty = 0$. Therefore

$$I_L = -\frac{nFDc_O^\infty}{\delta}. \quad (1.44)$$

It is now possible to understand the complete steady state $I-E$ characteristic sketched in Fig. 1.11. As the potential is made more negative than the equilibrium value, the reduction of $O \rightarrow R$ will commence and then increase in rate as the overpotential becomes larger, causing the surface concentration, c_O^∞ , to decrease.

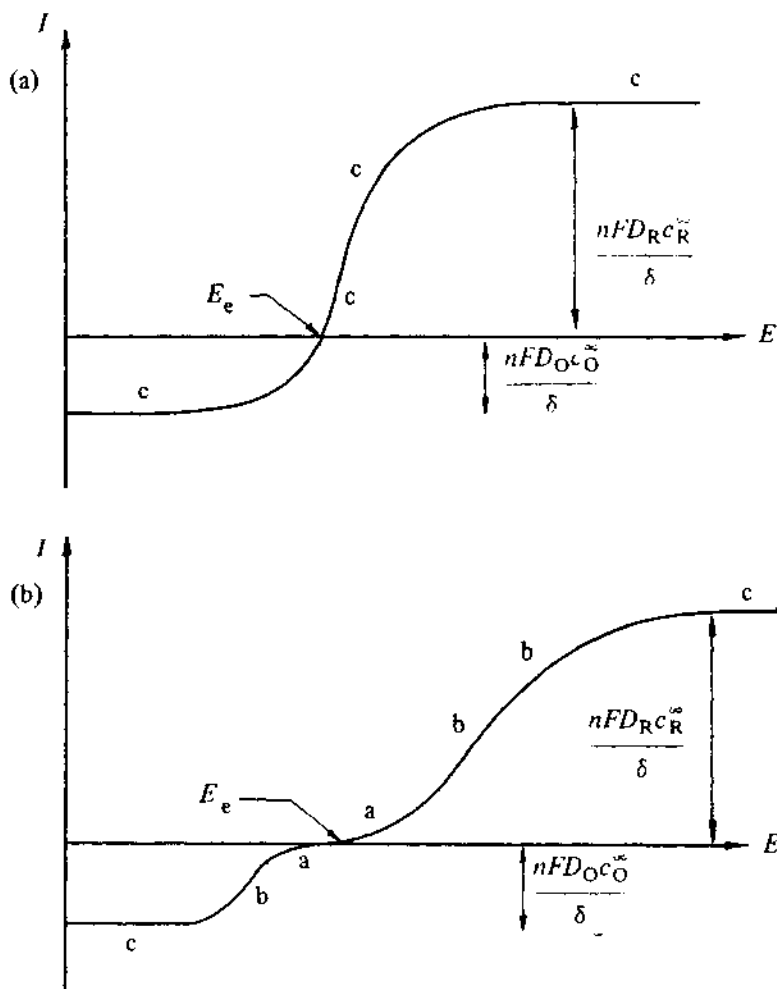


Fig. 1.11 – Complete $I-E$ curves over a wide range of overpotentials for a reaction $O + ne^- \rightleftharpoons R$ when the solution contains $c_R^\infty = 3c_O^\infty$. (a) Reversible electron transfer (b) irreversible electron transfer. a: Pure electron transfer control b: mixed control c: mass transfer control.

Eventually the surface concentration of O will approach zero, and mass transport will become the rate determining step in the sequence making up the overall electrode reaction, see Equation (1.17)-(1.19). The current will then plateau at the value given by Equation (1.44). A similar argument applies to the oxidation reaction, although in the example shown in Fig. 1.11 the oxidation plateau current is three times the reduction plateau current because of the ratio of bulk concentrations used. Similar mass transport limitations arise even in unstirred solution, but the value of δ is ill-defined. A much more detailed discussion of the rotating disc electrode is to be found in Chapter 4.

1.5 THE INTERACTION OF ELECTRON TRANSFER AND MASS TRANSPORT

Until the previous paragraph, the electron transfer and mass transport steps in the sequence (1.17)-(1.19) for the simple electrode reaction have been considered in isolation, although it was recognised that the rate of the former increases with overpotential, Equations (1.31)-(1.34), while the maximum rate of the mass transport step depends only on the bulk concentration of the electroactive species and the mass transport regime, Equation (1.44).

Now, it is important to see how the processes interact in many experiments. Steady state $I-E$ curves such as those in Fig. 1.11 have three distinct zones, and these are labelled (a)-(c) on this figure. The region (a) corresponds to a current density less than a few per cent of the limiting current density. Since the current density is low, the extent of the resulting chemical change at the electrode surface is small, and hence the surface concentrations of O and R are not significantly different from the bulk concentrations (e.g. for a reaction $O \xrightarrow{+e^-} R$, $c_O^S > 0.95 c_O^\infty$). Mass transport conditions will hence have a negligible effect on the surface concentrations or the experimental current; it is under these conditions that the current is solely determined by the rate of electron transfer and Equations (1.31)-(1.34) apply. This may sound a restricted region, but since small currents may be measured precisely, it is common for a Tafel slope to be observed over three orders of magnitude of current. Certainly, Tafel slopes which extend over less than one order of magnitude should be interpreted with caution. The other limiting situation, that labelled (c), corresponds to overpotentials where electron transfer is very fast and mass transport the sole rate determining step. Now the surface concentration of electroactive species will be effectively zero (i.e. as soon as the species reaches the surface, it undergoes electron transfer). The measured current is independent of overpotential, but is very sensitive to any changes in stirring or agitation.

Region (b) corresponds to the intermediate situation where there is mixed control of the current by the mass and electron transfer steps. It should be emphasised that the mixed control region corresponds to much of the rising part of the $I-E$ curve. The surface concentration of electroactive species, O, will fall in the range $0.05 c_O^\infty < c_O^S < 0.95 c_O^\infty$, so that mass transport is essential to maintain the surface concentration constant, and it is also sensitive to overpotential. To understand this region the sequence



must be considered, and two types of behaviour are observed depending on the relative rates of the two steps. Firstly if both \vec{k} and \vec{k} are large, the rates of the Reactions (1.46) will be fast compared to (1.45), and (1.46) will appear to be in equilibrium. Conversely, if \vec{k} and \vec{k} are not both large, (1.46) cannot remain in equilibrium. In the former case we are dealing with a surface process in equilibrium and surface concentrations can be calculated using thermodynamic arguments, in fact, the Nernst equation, (1.24). Such electrode reactions are termed by electrochemists *reversible*. In the latter case, the surface concentrations must be estimated using the kinetic Equations (1.31)-(1.33), and the process is termed *irreversible*. Quite different I - E curves result from reversible and irreversible electrode reactions, and both are shown in Fig. 1.11. The difference arises because in the irreversible case an overpotential is required to drive both the oxidation and reduction processes. Fig. 1.12 shows a Tafel plot

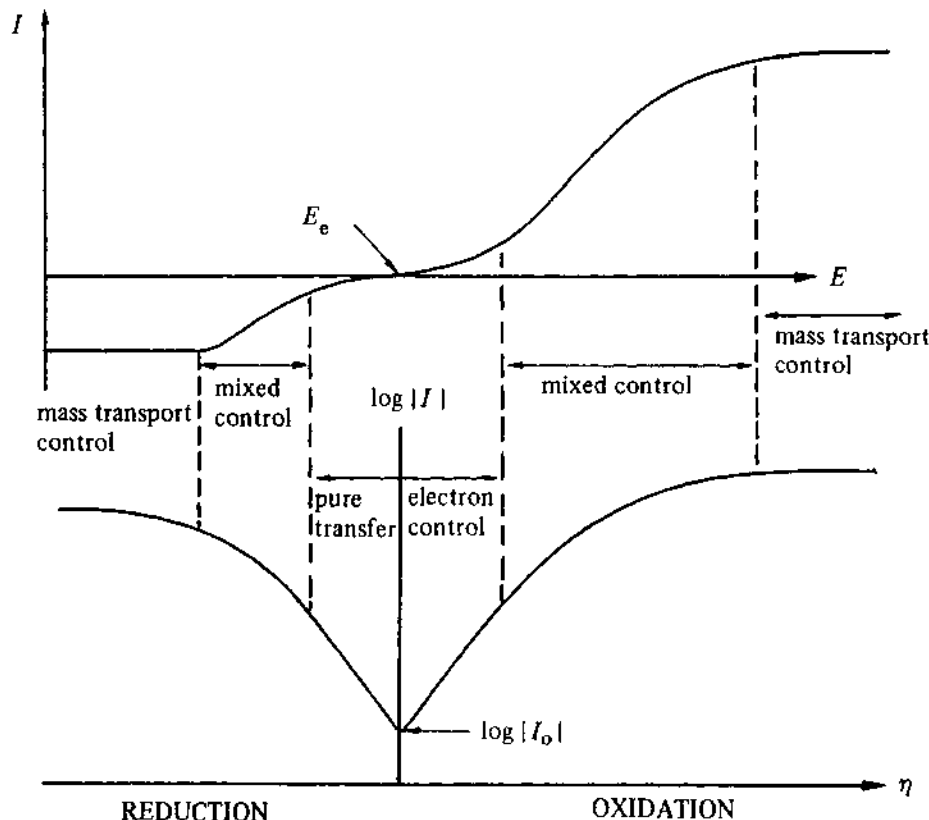


Fig. 1.12 – I - E and corresponding $\log I$ - E characteristics for an irreversible electron transfer reaction. Solution as in Fig. 1.11.

for the experimental data of Fig. 1.11(b); it differs from the $\log I - \eta$ plots earlier in the chapter because the overpotential range is greatly extended to regions where mass transport as well as electron transfer is important in determining the current. The figure stresses that only in region (a) is the $\log I - \eta$ relationship linear. In the region of mixed control, the $\log I - \eta$ plot is curved, while in region (c), mass transport control, $\log I$ is independent of η .

In practice, the situation is more complex, since as has already been implied, e.g. Equation (1.40), and will be discussed many times later, our design of the experiment can greatly influence the rate of mass transport. Thus, for example, the rate of rotation of a disc electrode or the timescale of measurement of current following a potential step will greatly influence the rate of mass transport. Hence the experiment carried out may determine whether an electrode reaction appears reversible or irreversible. Furthermore, the rate of mass transport may change during the experiment; for example, in a potential step experiment, the rate of mass transport will fall with time, and then the reaction may change from irreversible to reversible during the experiment. We shall also see later that it is a general principle of experiments to study the kinetics of fast redox couples, that one deliberately increases the rate of mass transport; commonly the current will be measured as a function of the mass transport conditions, and then an extrapolation procedure will be used to obtain the current under conditions of infinite mass transport. This extrapolated current must be purely electron transfer controlled.

Clearly, whether an electrode reaction appears reversible or irreversible depends both on the kinetics of electron transfer (i.e. the standard rate constant k^\ominus for Reaction (1.46)) and the mass transport conditions. As a guide, however, it is found that for a steady state experiment in unstirred solution,

$k^\ominus > 2 \times 10^{-2} \text{ cm s}^{-1}$ leads to a reversible $I-E$ curve

$k^\ominus < 5 \times 10^{-3} \text{ cm s}^{-1}$ leads to an irreversible $I-E$ curve .

1.6 COUPLED CHEMICAL REACTIONS

The response recorded in many electrochemical experiments is extensively changed by the chemical reactivity of the product of electron transfer. Indeed, the study of chemical reactions of intermediates either adsorbed on the surface or free in the solution close to the electrode surface has become a major application of several techniques, e.g. cyclic voltammetry, rotating ring disc electrodes, spectroelectrochemistry, and double potential step.

In most studies, one of the reactants in the chemical reaction is produced by electron transfer at the electrode surface, and loss of reactant with time is monitored either spectroscopically or electrochemically following a change in potential of the working electrode or using a second electrode held at an appropriate potential. From the point of view of electrochemistry such systems are known as following chemical reactions, i.e.



and analysis of data from suitable experiments allows the elucidation of the order of the reaction with respect to both A and R and the determination of the rate constant, k .

It is also possible to design systems where a chemical step determines the concentration of the electroactive species, and in such cases the current for the electrode process can be a direct measure of the rate of the chemical reaction. Such systems are known as preceding chemical reactions, i.e.



The study of homogeneous and heterogeneous chemical reactions will be covered in each of the chapters describing the techniques.

1.7 ADSORPTION

Adsorption is the formation of some type of bond between the adsorbate and the electrode surface. The interaction may be merely electrostatic (e.g. the adsorption of cations or anions on a surface of opposite charge) or charge-dipole in nature (e.g. the adsorption of amines, thiourea, or benzene) or due to the formation of a covalent bond. Moreover, one sees great variations in the strength of the bonding and the reversibility of the adsorption process. Electrode reactions are most strongly affected when the adsorbate is the electroactive species, a reaction intermediate, or the product, but the adsorption of species apparently not directly involved in the electrode process can also change the rate of electron transfer and indeed the final product.

There are many examples where either a neutral or charged species is adsorbed essentially unchanged and reversibly onto the electrode surface. The extent of adsorption is usually expressed as a surface coverage, θ , i.e. the fraction of the surface covered by adsorbate. Such adsorption must be considered as a competition both between all species in the system for sites on the electrode surface and between the electrode surface and the solution medium for each species. Hence θ will depend on the solvent, electrolyte, adsorbate structure and concentration and the concentration of any other species in the system as well as the nature of the electrode. Moreover, the surface coverage will change, sometimes sharply, with the electrode potential. This is because at each potential the electrode will have a characteristic surface charge and this charge will lead to the organisation of ions within molecular dimensions of the surface, i.e. the formation of a double layer. If the electrode is positively charged it will promote adsorption of anions, while a negatively charged surface will enhance cation adsorption. In addition, the charge on the electrode can interact with dipoles in solution leading to their adsorption and orientation at the surface. Neutral molecule adsorption occurs most strongly where competition from charged species is at a minimum, and this is when the electrode is uncharged. The electrode is uncharged at the potential of zero charge.

The coverage by an adsorbate is related to its concentration in solution by an isotherm. There are several isotherms which differ in the extent and method

of taking into account lateral interactions between adjacent adsorbed species. For example, the Langmuir isotherm assumes that the free energy of adsorption is independent of coverage, i.e. there are no lateral interactions

$$\frac{\theta}{1-\theta} = c^\infty \exp(-\Delta G_{\text{ADS}}^\ominus / RT) , \quad (1.51)$$

while the Frumkin isotherm assumes that the free energy of adsorption increases linearly with coverage, i.e.

$$\Delta G_{\text{ADS}} = \Delta G_{\text{ADS}}^\ominus + g\theta \quad (1.52)$$

leading to the isotherm

$$\frac{\theta}{1-\theta} \exp \frac{g\theta}{RT} = c^\infty \exp(-\Delta G_{\text{ADS}}^\ominus / RT) . \quad (1.53)$$

Such isotherms are usually deduced from the measurement of capacitance (as a function of c^∞ and E), see Chapter 5.

The adsorption of an electroinactive species can affect the kinetics of a redox couple in solution, most commonly by reducing its rate. The model for this inhibition can envisage either that (a) there is a reduction in electrode area active for electron transfer or (b) the electron transfer must occur over a greater distance (see Chapter 5). In a few cases adsorption has, however, been shown to catalyse electron transfer, e.g. adsorbed thiocyanate accelerates the reduction of Eu^{III} to Eu^{II}, and such behaviour can be explained if the adsorbed species can act as a ligand [3]. More extreme are the examples where adsorption of a species causes a change in the product of the electrode reaction. Here examples include tetraalkylammonium ions in the reduction of acrylonitrile changing the product from propionitrile to adiponitrile [4], and triphenylphosphine oxide in the reduction of oxygen causing superoxide ion rather than hydrogen peroxide as the final product in an aqueous solution [5]. In both examples the adsorbate prevents protonation of an intermediate presumably by forming a aprotic layer at the surface.

When the electroactive species is itself adsorbed, it makes electron transfer more difficult, while adsorption of the product will make electron transfer easier, in each case by a potential $-\Delta G_{\text{ADS}}/nF$. Such adsorption processes are readily seen on $I-E$ curves under non-steady state conditions.

Adsorption of intermediates whether formed by electron transfer, e.g.



or by predissociation of a bond in the electroactive species, e.g.



are very important in electrocatalysis. Particularly, reactions of the type illustrated by (1.55) are quite irreversible, and coverages cannot be described by isotherms. Indeed, the presence of such adsorbed species has generally been inferred from

kinetic analysis, although recent efforts have produced some direct spectroscopic evidence. Chapter 7, on electrocatalysis, will discuss such processes in more detail.

1.8 PHASE FORMATION

Many of the electrode reactions studied in electrochemistry involve the formation of a new phase. This may be a metal resulting from the reduction of an ion in solution, an oxide formed by corrosion or by oxidation of a solution species (e.g. PbO_2 from a $\text{Pb}(\text{NO}_3)_2$ bath), other metal salts from oxidation of an electrode (e.g. PbSO_4 from lead or AgCl from silver), or by the oxidation or reduction of another phase (e.g. PbSO_4 from the reduction of PbO_2).

Such electrode reactions frequently have a unique feature; namely, the I - E characteristics before and after the formation of the new phase are quite different. For example, the I - E curves for a solution of copper ions at an inert electrode (e.g. carbon) and at the same electrode covered with a thin layer of copper will be totally different, the latter being similar to a bulk copper cathode. Similarly, the I - E curve for a recharging lead/acid positive electrode will change dramatically once the lead sulphate layer contains microscopic centres of lead dioxide. This feature arises because the formation of a new phase requires nucleation, a process which only occurs with difficulty and in electrochemistry generally takes place at the cost of a substantial overpotential.

While nucleation phenomena are important in electrochemistry, it must be recognised that for most of the phase formation process, the nuclei will exist and the main reaction is expansion of the new lattice as the deposit thickens. Hence we need to think about two distinct situations: (i) the initial growth where a very thin layer or small centres of the deposit are created by nucleation and start to grow, and (ii) the subsequent growth to a macrophase.

If one considers the deposition of a metal onto an inert substrate, e.g. Ag onto C, the very first step has to be the collecting together of silver adatoms to form nuclei of the metal phase. As stated above, this will frequently require a large overpotential and will anyway be a relatively slow process; moreover, until the nuclei are created, almost no current for the reaction $\text{M}^{n+} + n\text{e}^- \rightarrow \text{M}$ can be observed. On the other hand, once the nuclei have been formed they grow readily. Since the rate of growth of each centre is proportional to its surface area, and in many cases the number of nuclei will also increase with time, the current will increase with time at constant potential. This behaviour leads to very characteristic responses in electrochemical experiments, e.g. rising I - t transients from potential step experiments, and quantitative analysis of the curves can furnish detailed information concerning the mechanism and kinetics of both the nucleation and growth processes.

Once the centres overlap to give a continuous layer of metal, the nature of the expansion process changes. Thereafter one is dealing solely with the reduction of metal ions to adatoms which must then be incorporated into the expanding lattice of the metal. The current will commonly be constant at

constant potential during this stage, but the form of the deposit will depend strongly on the relative rates of formation of adatoms, their diffusion across the surface, and their incorporation into the lattice. Phase formation is considered further in Chapter 9.

REFERENCES

- [1] Reports on the IUPAC Convention on Electrochemistry, *Electrochim. Acta* 27 (1982), 629, and *Pure and Applied Chemistry* 37 (1974) 503 and 51 (1979) 1159.
- [2] B. Levich, *Physicochemical hydrodynamics*, Prentice Hall, 1962.
- [3] M. J. Weaver & F. C. Anson, *J. Electroanal. Chem.* 65 (1975) 711, 737, and 759.
- [4] I. E. Gillet, *Chem. Ing. Techn.* 40 (1968) 573.
- [5] B. Kastening & G. Kazemifard, *Ber Bunsenges. Phys. Chem.* 74 (1970) 551.

Relevant reading

- (1) W. J. Albery, *Electrode processes*, Clarendon Press, 1975.
- (2) J. O'M Bockris & A. K. N. Reddy, *Modern electrochemistry – Volume 2*, Plenum Press, 1970.
- (3) A. J. Bard & L. R. Faulkner, *Electrochemical methods*, John Wiley and Sons, 1980.

2

Steady state and potential step techniques

As will now be clear from the first Chapter, electrochemical processes can be rather complex. In addition to the electron transfer step, coupled homogeneous chemical reactions are frequently involved and surface processes such as adsorption must often be considered. Also, since electrode reactions are heterogeneous by nature, mass transport always plays an important and frequently dominant role. A complete analysis of any electrochemical process therefore requires the identification of all the individual steps and, where possible, their quantification. Such a description requires at least the determination of the standard rate constant, k° , and the transfer coefficients, α_A and α_C , for the electron transfer step, or steps, the determination of the number of electrons involved and of the diffusion coefficients of the oxidised and reduced species (if they are soluble in either the solution or the electrode). It may also require the determination of the rate constants of coupled chemical reactions and of nucleation and growth processes, as well as the elucidation of adsorption isotherms. A complete description of this type is, however, only ever achieved for very simple systems, as it is generally only possible to obtain reliable quantitative data about the slowest step in the overall reaction scheme (or of two such steps if their rates are comparable).

A fairly wide range of techniques is now available to electrochemists to enable the determination of kinetic and thermodynamic data related to electrode processes. The application of these techniques is the subject of this and subsequent chapters. Throughout the emphasis will be placed on

- (a) developing diagnostic tests to be used in the elucidation of reaction mechanisms,

- (b) demonstrating how quantitative data for single reaction steps may be obtained.

2.1 STEADY STATE TECHNIQUES

Under steady state conditions electron transfer processes with k^\ominus values less than about $5 \times 10^{-3} \text{ cm s}^{-1}$ are regarded as irreversible, i.e. when current flows the electron transfer is insufficiently fast to maintain Nernstian equilibrium at the electrode surface. In such cases kinetic data can be obtained directly from steady state current-voltage measurements analysed on the basis of the Tafel equations (see Fig. 1.4). For a cathodic reaction

$$\log |I| = \log I_o - \frac{\alpha_C nF\eta}{2.3RT} \quad (2.1)$$

whilst for an anodic one

$$\log |I| = \log I_o + \frac{\alpha_A nF\eta}{2.3RT} \quad (2.2)$$

(|I| is written throughout most chapters on techniques since the current is negative if the process studied is a reduction and positive if it is an oxidation).

From these relationships which apply at large negative and positive overpotentials respectively, it can be clearly seen that the transfer coefficients, α_A and α_C , may be obtained from the gradients of a $\log |I|$ vs η plot whilst I_o may be obtained by extrapolation (see Fig. 1.4). The standard rate constant, k^\ominus , may then of course be obtained from the I_o value (see Equation (1.35)). The above equations only apply at high overpotentials (but not when mass transport has become significant). Therefore, in order to use data obtained at potentials close to the equilibrium value where both forward and back reactions are significant it is necessary to employ the complete Butler-Volmer equation. Rearrangement of this equation (Equation (1.31)) yields the following expression

$$\log \left| \frac{I}{\exp(nF\eta/RT) - 1} \right| = \log I_o - \frac{\alpha_C nF\eta}{2.3RT} \quad (2.3)$$

which may be used in a similar way to the Tafel equations to obtain α_C , I_o , and hence k^\ominus values (it is assumed that $\alpha_A + \alpha_C = 1$).

The type of analysis described above requires that both halves of the redox couple are stable and available (a known finite concentration of each must be present in solution to define an equilibrium potential), and that the equilibrium potential can either be measured, or calculated from the Nernst equation (i.e. the standard potential is known). This is often not the case, e.g. particularly in organic electrochemistry, one half of the redox couple may be unstable. However, Tafel type plots may still prove useful. Current-potential data are analysed using the Tafel equation in the form

$$\log |I| = A + BE \quad (2.4)$$

where A and B are both constants and E is the electrode potential with respect to any convenient reference electrode. Whilst α_C , α_A and k^\ominus may not be determined from such a plot, the value of the Tafel slope, B , may be useful in differentiating between possible reaction mechanisms. Further useful information may be obtained from $\log |I|$ vs $\log c$ plots at constant potentials, the slopes of which yield 'apparent' reaction orders. These values, which may be potential dependent, are again useful in mechanism assignment. Examples of this type of analysis are given in the chapter on electrocatalysis (Chapter 7).

For a simple electron transfer process, it is always possible, by applying a sufficiently high overpotential, to make the rate of the electron transfer step greater than the rate of mass transport. The current flowing in the cell will then reach a mass transport limited plateau value which will increase in magnitude if the solution is stirred, or the electrode is rotated or vibrated. On occasions, however, plateau currents are observed in steady state measurements which do not show this dependence on stirring and are also lower than typical mass transport limited values. This type of behaviour is indicative of the presence of a slow, rate determining, homogeneous reaction that precedes the electron transfer (see later). The rate constant for such a chemical step is then found from the simple relationship

$$|I| = nFkc_O^\infty \quad (2.5)$$

Experimentally, steady state data are recorded either (a) using a point by point method where the potential is changed manually at intervals and the current read after a defined period, e.g. 1 minute, or (b) using a very slow potential scan, $1-10\text{ mV s}^{-1}$, and displaying the current or (with a log amplifier) $\log I$ directly on a recorder. The technique requires only very simple instrumentation, but, because of its long timescale, it suffers more than other experiments from problems with trace impurities and slow changes in the electrode surface. A reasonable definition of 'steady state' is that the data are independent of the method of recording, at least over a range of variables. It should also be stressed that a reliable (and variable) stirring regime can aid reproducibility and give additional information and that the Tafel slopes should be regarded as meaningful only if the $\log I-E$ data are linear over at least a factor of 100-1000 in current density.

From the above discussion it will be seen that steady state techniques can only obtain kinetic data for slow processes. Faster reactions are studied by non-steady state techniques, but before discussing these, a steady state technique that is particularly useful in mechanism elucidation will be described.

2.2 CONTROLLED POTENTIAL BULK ELECTROLYSIS

Controlled potential bulk electrolysis or coulometry, as it is often called, is widely used to determine the overall number of electrons involved in an electrode process. It is also used to prepare a sufficient quantity of the reaction products to enable them to be identified by the application of conventional analytical techniques.

For the vast majority of techniques discussed in these chapters, the electrode area is chosen to be small compared with the solution volume. This means that bulk concentrations do not change appreciably during experiments. Controlled potential bulk electrolysis is an exception to this, a large electrode area to solution volume ratio being desirable. One special way in which very high ratios may be obtained is by using a thin layer cell in which a thin film of solution (typically 10^{-3} to 10^{-2} cm thick) is constrained between two parallel plates, one at least of which is the working electrode; secondary and reference electrodes are placed elsewhere. In such a cell exhaustive electrolysis typically occurs in less than a minute, which is considerably faster than in a more conventional cell. A further advantage of such systems is that if the cell is transparent, simultaneous optical spectroscopic measurements can also be made. Such applications are discussed in Chapter 10. Details of the design of thin layer cells and their application not only to coulometry but also to kinetic studies may be found in the literature [1, 2]; the remainder of this discussion here will be confined to the use of cells of more conventional design and capacity.

In the conventional bulk electrolysis experiment [3, 4] a divided cell is used in which the working electrode compartment is separated from the secondary electrode by means of a glass frit or ion-exchange membrane (see Chapter 11). The working electrode compartment, which should permit stirring, is then filled with a known volume of solution containing a known concentration of electro-active species. The potential of the working electrode is then fixed at a value determined on the basis of steady state or sweep voltammetry (usually a potential at which the reaction under investigation proceeds at a mass transport limited rate). The current, and its integral, the charge, are then monitored as a function of time, usually until the current drops to about 1% of its initial value. Samples for analysis are also sometimes removed at various stages of the electrolysis and at the end.

For a simple reaction of the type



assuming a constant rate of stirring (constant mass transfer coefficient) the current should fall exponentially as defined in Equation (2.7):

$$i(t) = i(0) \exp(-bt) \quad (2.7)$$

where $i(0)$ is the initial current at $t = 0$ and b is a constant related to the mass transfer coefficient and cell and electrode dimensions. For a simple reaction, therefore, $\log |i|$ should fall linearly with t . The charge passed as a function of time, $q(t)$, is given by

$$q(t) = \int_0^t idt \quad (2.8)$$

and therefore

$$q(t) = q(\infty)(1 - \exp(-bt)) \quad (2.9)$$

where $q(\infty)$ is the total charge consumed at the end of the experiment. It follows from Equations (2.7) and (2.8) that for a simple reaction $q(t)$ should vary linearly with $i(t)$, and $q(\infty)$ can be obtained by extrapolation to $i(t) = 0$. Any deviation from linear behaviour for either $\log |i|$ vs t or $q(t)$ vs $i(t)$ plots indicates that a more complex reaction scheme is operating, and mechanistic information about coupled homogeneous chemical reactions may be obtained from a detailed analysis of the results [3, 4]. A typical exhaustive electrolysis experiment takes up to about one hour, a timescale much longer than that of most other electrochemical techniques, and therefore this approach provides information about coupled reactions that are much slower than those that may be studied, for example, by cyclic voltammetry. The most significant piece of information that is obtained in the coulometric experiment, however, is the value of $q(\infty)$ (obtained either by exhaustive electrolysis or extrapolation of a linear $q(t)$ vs $i(t)$ plot) which is related to n , the number of electrons involved in the overall reaction, by the relationship

$$q(\infty) = nFcV \quad (2.10)$$

where c is the concentration of the electroactive species and V is the volume of solution in the working electrode compartment. The value of n is thus readily determined. It must be emphasised, however, that since the timescale of this experiment is long, the value of n obtained is sometimes different from that obtained for example by cyclic voltammetry or the use of a rotating disc electrode. Analysis of the reaction products will often help to explain these differences which imply the existence of coupled chemical reactions.

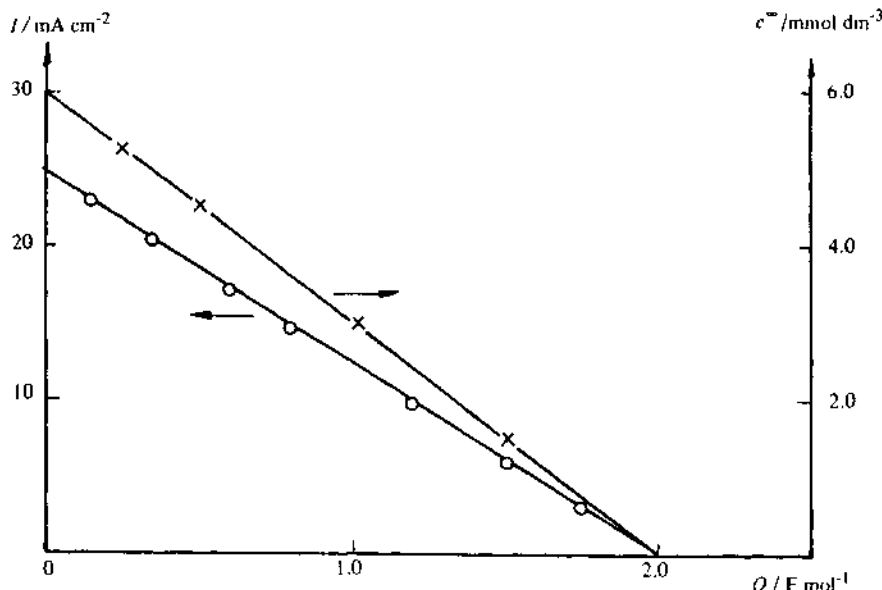


Fig. 2.1 - Analysis of data from a controlled potential electrolysis for the reduction of $\text{Mn}_2(\text{CO})_{10}$ in $\text{THF}/\text{Bu}_4\text{NBF}_4$ (0.2 mol dm^{-3}). The concentration of $\text{Mn}_2(\text{CO})_{10}$ was determined by UV spectrometry.

Finally, before leaving controlled potential electrolysis, it is worth noting that if there is an independent, e.g. spectroscopic, monitor of the concentration of the electroactive species, n values may also be obtained from

$$q(t) = nFV \Delta c \quad (2.11)$$

where Δc is the change in concentration up to time t . If the reaction mechanism is not simple it is, of course, possible that the value of n obtained will vary as the reaction proceeds. Fig. 2.1 shows an example of data treatment for a controlled potential electrolysis both by an i vs q and a c vs q plot.

2.3 TECHNIQUES FOR THE INVESTIGATION OF FAST ELECTRODE REACTIONS

For many electrode processes of interest, the rates of electron transfer, and of any coupled chemical reactions, are high compared with that of steady state mass transport. Therefore during any steady state experiment, Nernstian equilibrium is maintained at the electrode and no kinetic or mechanistic information may be obtained from current or potential measurements. Apart from in a few areas of study, most notably in the field of corrosion, steady state measurements are not therefore widely used by electrochemists. For the majority of electrode processes it is only possible to determine kinetic parameters if the Nernstian equilibrium is disturbed by increasing the rate of mass transport. In this way the process is forced into a mixed control region where the rates of mass transport and of the electrode reaction are comparable. The current, or potential, is then measured as a function of the rate of mass transport, and the data are, then either extrapolated or curve fitted to obtain the desired kinetic parameters. There are basically three different ways in which the rate of mass transport may be enhanced, and these are now discussed.

2.3.1 Hydrodynamic methods

In the first chapter we saw that under steady state conditions there is a thin layer next to an electrode (the Nernst diffusion layer) across which the concentration of electroactive species varies essentially linearly with distance from the electrode (constant concentration gradient). If the solution is agitated or the electrode is vibrated or rotated, the thickness of this layer decreases and the concentration gradient across it increases. Since the rate of mass transport of a species to an electrode is proportional to the concentration gradient at the electrode surface, this thinning of the diffusion layer leads to an increase in the rate of mass transport. It is this ability to vary the rate of mass transport by agitating the solution that forms the basis of hydrodynamic methods for the determination of electrode kinetics. Providing it is possible to increase the mass transport rate sufficiently to drive the electrode reaction into a mixed control regime, kinetic parameters may be obtained by recording current data over a wide range of mass transport rates and using an extrapolation or curve fitting procedure to obtain data corresponding to the hypothetical state where the rate of mass transport is infinite. This hypothetical current is then purely kinetically

determined, and kinetic parameters are readily evaluated. The principal requirement is that the mass transport rate can be varied in a known way. This is most commonly achieved by using a rotating disc electrode, and this will be discussed in detail in Chapter 4.

2.3.2 Transient techniques

There are in fact two slightly different types of non-steady state technique. In the first an instantaneous perturbation of the electrode potential, or current, is applied, and the system is monitored as it relaxes towards its new steady state; chronoamperometry and chronopotentiometry are typical examples of such techniques. In the second class of experiment a periodically varying perturbation of current or potential is applied to the system, and its response is measured as a function of the frequency of the perturbation; cyclic and a.c. voltammetry are examples of this type of approach. In both cases the rate of mass transport varies with the time (or frequency), and by obtaining data over a wide range of these variables and by using curve fitting procedures, kinetic parameters are obtainable. Pulse techniques will be discussed later in this chapter, whilst sweep methods are described in Chapter 6 and a.c. methods in Chapter 8.

2.3.3 Microelectrodes

In the first chapter we saw that the solution of Fick's 2nd Law for a potential step experiment at a planar electrode where an electrode reaction is diffusion controlled, gives rise to a current-time relationship of the form (see Appendix A.1.1.2 example 3).

$$|I| = \frac{nFD^{1/2}c_O^\infty}{\pi^{1/2}t^{1/2}} \quad (2.12)$$

the Cottrell equation. For a spherical electrode the solution becomes (see Appendix A 1.2.1, Example 7)

$$|I| = nFDc_O^\infty \left(\frac{1}{(\pi Dt)^{1/2}} + \frac{1}{r} \right) \quad (2.13)$$

where r is the electrode radius. At short times the first term predominates, and Equation (2.12) is a good approximation to the behaviour of the spherical electrode. On the other hand at long times, rather than approaching zero as at a planar electrode, the current at a spherical electrode remains finite and reaches a limiting value given by

$$|I| = \frac{nFDc_O^\infty}{r}, \quad (2.14)$$

i.e. in a spherical diffusion field the diffusive flux contains a steady state term that is inversely proportional to the electrode radius.

It can be shown that at a small disc or ring electrode (i.e. of a few micrometres radius) a diffusion field of this type exists, and that the steady state diffusive flux at these microelectrodes is such that kinetic investigations can be made of both

electron transfer and certain coupled homogeneous reactions. This technique has not yet been widely applied and will not be discussed here. Further details are, however, to be found in the original literature [5, 6].

The remainder of this chapter is concerned with the application of pulse techniques (both galvanostatic and potentiostatic) to the investigation of electrode kinetics.

2.4 POTENTIAL STEP TECHNIQUES

2.4.1 The investigation of the kinetics of heterogeneous reactions

In potential step experiments the potential of the working electrode is changed instantaneously, and either the current-time response or the charge-time response is recorded. These techniques are known respectively as chronoamperometry and chronocoulometry. First we will consider the type of chronoamperometric experiment that was briefly outlined in the first chapter.

2.4.1.1 Chronoamperometry

Let us assume an electrode reaction as described by Equation (2.15), and that initially only O is present in solution.



A potential-time profile as shown in Fig. 2.2 is then applied to the working electrode. E_1 is chosen such that no reduction of O, or indeed any other electrode reaction, occurs. Then at time $t = 0$ the potential is instantaneously changed to a new value E_2 , where the reduction of O occurs at a diffusion controlled rate.

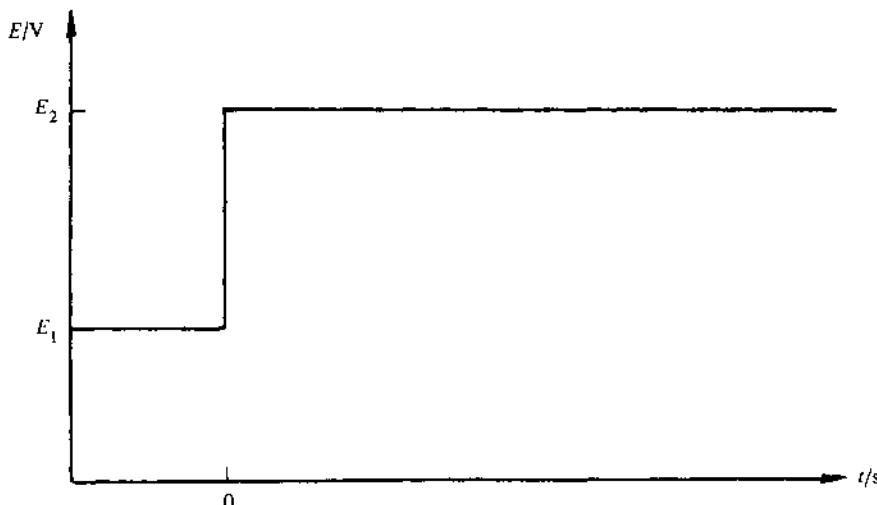


Fig. 2.2 .. The potential-time profile for a single potential step chronoamperometric experiment.

As was outlined in the first chapter, Fick's 2nd Law can then be solved with the appropriate boundary conditions, and for a planar electrode this solution is given by Equation (2.16), the Cottrell equation

$$|I| = \frac{nFD^{1/2}c_O^\infty}{\pi^{1/2}t^{1/2}} . \quad (2.16)$$

That is, the current falls as $t^{-1/2}$ as shown in Fig. 2.3 (curve a). A plot of I vs $t^{-1/2}$ should therefore be linear and should pass through the origin (this is frequently used as a test for diffusion control), and the diffusion coefficient of species O (typically $10^{-5}\text{ cm}^2\text{s}^{-1}$) can be found from the gradient of the straight line (or from the value of $It^{1/2}$ which should be independent of t). When applying these tests for diffusion control and evaluating diffusion coefficients it is very important that data are analysed over as wide a time range as possible, to ensure the reliability of results. The shortest time will be determined by the charging time of the cell (see later), but a few hundred microseconds is a good guide. The longest time is determined by the effects of natural convection, and even without taking special precautions a value of a few seconds should easily be possible. Hence data over the range 1 ms to 10 s can commonly be plotted.

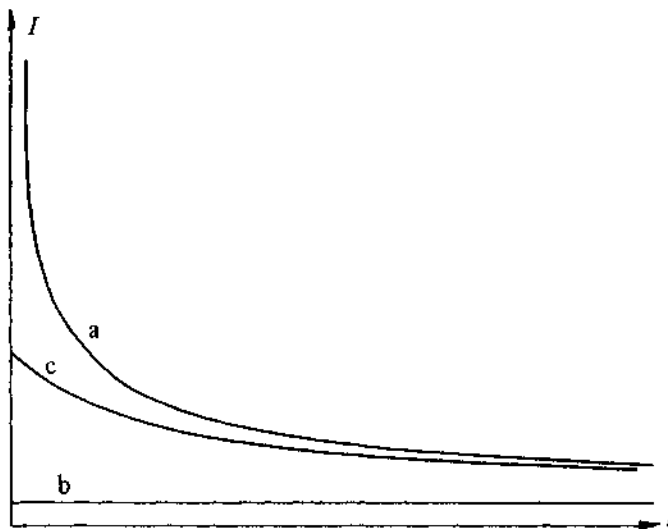


Fig. 2.3 - I - t responses for a potential step experiment. The potential E_2 is chosen so that a: the reaction is diffusion controlled, b: the reaction is kinetically controlled, and c: there is mixed control.

If the standard rate constant for the reaction described by Equation (2.15) is very small (or E_2 corresponds to a low overpotential for the reaction), a current-time transient of the type shown by curve b of Fig. 2.3 will be observed. This is because the surface concentration of O does not change significantly (<1%) due

to the imposition of the pulse, and therefore diffusion does not play a significant role in determining the rate. The measurement is essentially a steady state one, and may be analysed as outlined earlier. For the intermediate situation, where the rates of diffusion and electron transfer are comparable, the I vs t transient has the form shown by curve c of Fig. 2.3; the current falls with time but less steeply than for the diffusion controlled case. Under these conditions the system is said to exhibit mixed control.

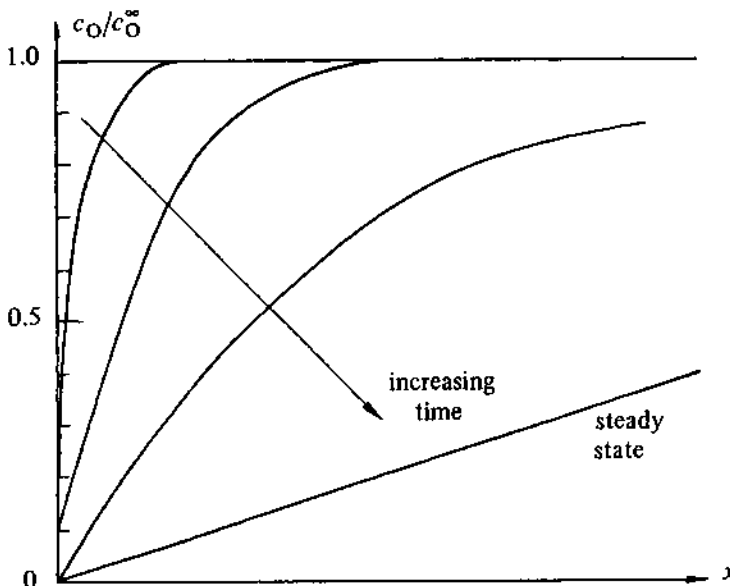


Fig. 2.4 – A schematic diagram of the time evolution of the concentration profiles for a species O undergoing reduction under conditions of mixed control.

The time evolution of the concentration profile for species O under mixed control is shown in Fig. 2.4. The flux of O at the surface is simply given by Fick's 1st Law, Equation (2.17)

$$J = -D(\partial c_O / \partial x)_{x=0} \quad (2.17)$$

and from Fig. 2.4 it can be seen that this flux is greatest at short times. Indeed at time $t = 0$, i.e. immediately after the potential step is applied, the flux would be infinite and therefore the current density at time $t = 0$ ($I_{t=0}$) would be kinetically controlled, and from its value the rate constant for the electrode reaction could be found. Unfortunately, for a number of reasons, the value of $I_{t=0}$ cannot be directly measured. These reasons are:

- (i) the rise-time of the potentiostat is not zero, i.e. it takes a finite time to reach the value E_2 when the pulse is applied;
- (ii) the current measuring system (e.g. oscilloscope) also has a finite rise-time;
- (iii) the presence of the double layer charging current.

This last point, which has been ignored until now, in fact imposes limitations on all transient techniques. Essentially, in addition to the faradaic current flowing in response to a potential perturbation, there is also a current due to the charging of the electrochemical double-layer capacitance (for more details see Chapter 5). In chronoamperometry this manifests itself as a sharp spike in the current at short times, which totally masks the faradaic current. The duration of the double layer charging spike depends upon the cell configuration, but might typically be a few hundred microseconds. Since $I_{t=0}$ cannot be measured directly it is necessary to resort to an extrapolation procedure to obtain its value, and whilst direct extrapolation of an I vs t transient is occasionally possible, a linear extrapolation is always preferable. In order to see how this should be done we must first solve Fick's 2nd Law for a potential step experiment under the conditions of mixed control. The differential equations to be solved are

$$\frac{\partial c_O}{\partial t} = D_O \frac{\partial^2 c_O}{\partial x^2} \quad (2.18)$$

$$\frac{\partial c_R}{\partial t} = D_R \frac{\partial^2 c_R}{\partial x^2}, \quad (2.19)$$

and for the case where both O and R are present in the solution prepared for the experiment, and the potential is stepped to negative overpotentials, these must be solved subject to the following initial and boundary conditions appropriate to mixed control.

$$\begin{aligned} t = 0, \quad x \geq 0 \quad & c_O = c_O^\infty, \quad c_R = c_R^\infty \\ t > 0, \quad x \rightarrow \infty \quad & c_O = c_O^\infty, \quad c_R = c_R^\infty \\ t > 0, \quad x = 0 \quad & -I/nF = D_O (\partial c_O / \partial x)_{x=0} \\ & = \vec{k}(c_O)_{x=0} - \vec{k}(c_R)_{x=0} \\ \text{and} \quad & D_O \left(\frac{\partial c_O}{\partial x} \right) + D_R \left(\frac{\partial c_R}{\partial x} \right) = 0 \end{aligned}$$

The solution by Laplace transform techniques is described in the Appendix (A 1.1.2 Example 4) and with the approximation that $D_R = D_O = D$ is given by

$$I = -nF\vec{k}c_O^\infty \exp \frac{(\vec{k} + \hat{k})^2 t}{D} \operatorname{erfc} \frac{(\vec{k} + \hat{k})t^{1/2}}{D^{1/2}}. \quad (2.20)$$

As discussed in the Appendix, Equation (2.20) has two limiting forms:

(i) at short times

$$I \approx -nF\vec{k}c_O^\infty \left(1 - 2 \frac{(\vec{k} + \vec{k})t^{1/2}}{\pi^{1/2} D^{1/2}} \right). \quad (2.21)$$

(ii) at long times

$$I \approx -\frac{nF\vec{k}c_O^\infty D^{1/2}}{\pi^{1/2}(\vec{k} + \vec{k})t^{1/2}} \quad (2.22)$$

and when \vec{k} is small compared to \vec{k} (i.e. at high cathodic overpotentials) Equation (2.22) further reduces to the Cottrell equation.

From Equation (2.21) it can be seen that at short times a plot of I vs $t^{1/2}$ should be a straight line of intercept $I_{t=0}$ given by

$$I_{t=0} = -nF\vec{k}c_O^\infty \quad (2.23)$$

from which the potential dependent rate constant \vec{k} can be obtained. From a consideration of the approximations made in deriving Equation (2.21) it can be shown that for typical values of rate constant and diffusion coefficient it is only a good approximation provided that

$$I/I_{t=0} > 0.8, \quad (2.24)$$

i.e. Equation (2.21) only applies at the top of the current-time transient. This imposes a limit on the rate of reaction that may be determined in this way; higher rates require measurements to be made at shorter times (the transients will be steeper), and eventually the measurements become affected by other factors such as double layer charging. Theoretically, with a well designed cell and an electrolyte solution of high conductivity it should be possible to determine rate constants less than about 0.1 cm s^{-1} [7, 8]. Fig. 2.5a shows a typical I vs $t^{1/2}$ plot.

Whilst being fairly simple to implement, the procedure described above is not ideal in that it ignores much of the available data. A technique for obtaining \vec{k} values from data obtained over a much wider time range is preferable. For the case where \vec{k} is much smaller than \vec{k} Equation (2.20) may be simplified to

$$I = -nF\vec{k}c_O^\infty \exp \frac{\vec{k}^2 t}{D} \operatorname{erfc} \frac{\vec{k}t^{1/2}}{D^{1/2}}. \quad (2.25)$$

Then dividing by the Cottrell equation (Equation (2.16)) we obtain

$$\frac{I}{I_d} = \pi^{1/2} \lambda \exp(\lambda^2) \operatorname{erfc}(\lambda) \quad (2.26)$$

where

$$\lambda = \frac{\vec{k}t^{1/2}}{D^{1/2}} \quad (2.27)$$

and I_d is the current in the absence of kinetic complications.

An analysis of experimental transient data based on the above equations can be made in the following manner. $It^{1/2}$ is first plotted as a function of $t^{1/2}$ as shown in Fig. 2.5b. The horizontal region at large values of $t^{1/2}$ corresponds

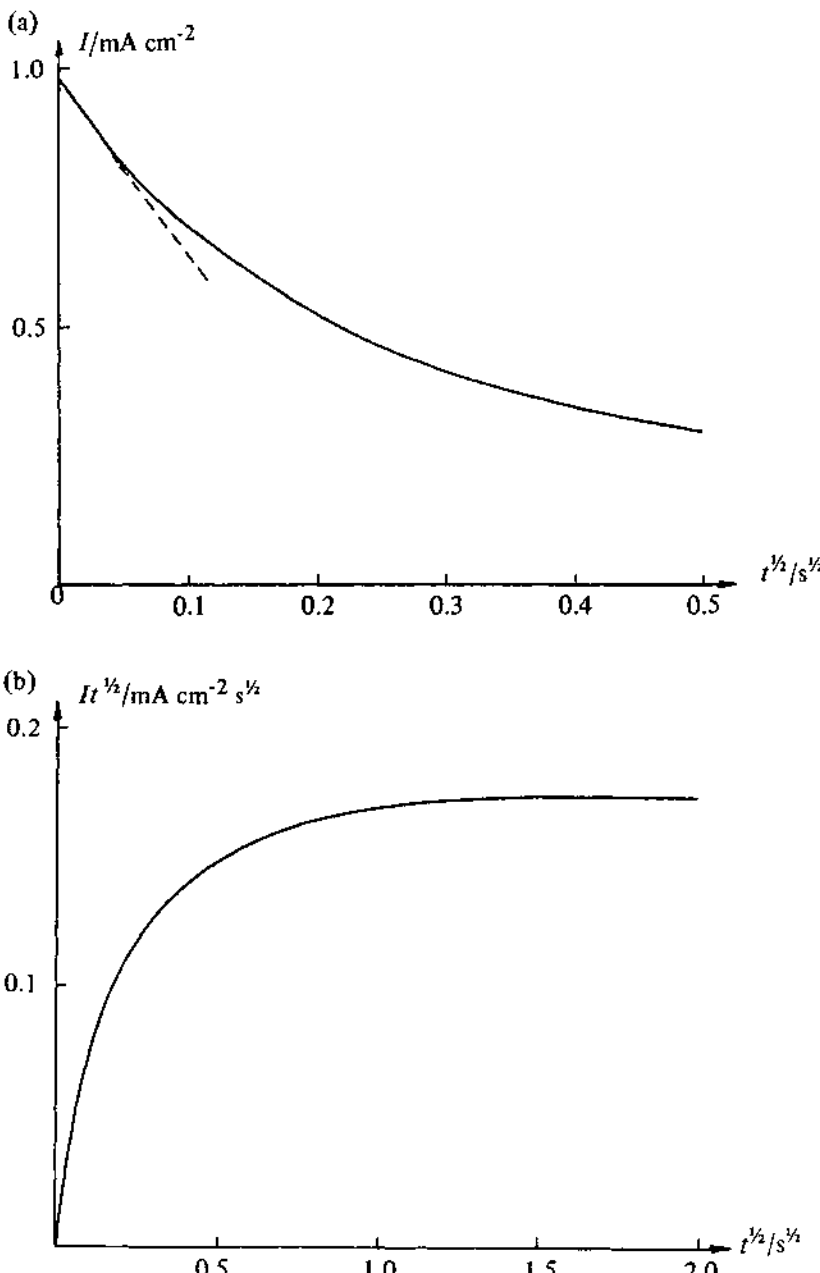


Fig. 2.5 - Analysis of I - t data from a chronoamperometric experiment corresponding to $\vec{k} = 10^{-2} \text{ cm s}^{-1}$, $D = 10^{-5} \text{ cm}^2 \text{ s}^{-1}$, and $c_O^\infty = 10^{-6} \text{ mol cm}^{-3}$. (a) I plotted as a function of $t^{1/2}$, (b) $It^{1/2}$ plotted as a function of $t^{1/2}$.

to the diffusion controlled region (I/I_D is a constant for a diffusion controlled process), whereas the short time data are affected by kinetics. From such a plot I/I_D values are calculated for a range of values of $t^{1/2}$ and using a working curve of the right-hand side of Equation (2.26) plotted as a function of λ it is possible to determine the values of λ corresponding to the various I/I_D values and hence to obtain \vec{k} from Equation (2.27). Provided the mechanistic assignment is correct, this should yield a unique \vec{k} value independent of time.

With the advent of cheap microcomputers with fast data acquisition systems an even better approach is now available. The current-time data obtained over a wide time range are acquired directly into the computer's memory, and are then fitted to Equation (2.20) using conventional curve fitting procedures to obtain values of \vec{k} and k .

Both the working curve and curve fitting methods described above are more sensitive to mechanistic complexities than the linear extrapolation procedure since they use data obtained over a wider time range. If practicable their use is therefore to be preferred.

With all determinations of reaction kinetics it is usual to perform experiments over a range of potentials, thus obtaining a range of potential dependent rate constants. In Chapter 3 (Equation (3.12)) it is shown that

$$\vec{k} = k^\ominus \exp -\frac{\alpha_C nF(E - E_e^\ominus)}{RT} \quad (2.28)$$

and

$$\hat{k} = k^\ominus \exp \frac{\alpha_A nF(E - E_e^\ominus)}{RT}, \quad (2.29)$$

or by taking logs

$$\log \vec{k} = \log k^\ominus - \frac{\alpha_C nF}{2.3RT} (E - E_e^\ominus) \quad (2.30)$$

and

$$\log \hat{k} = \log k^\ominus + \frac{\alpha_A nF}{2.3RT} (E - E_e^\ominus). \quad (2.31)$$

Plots of $\log \vec{k}$ or $\log \hat{k}$ as a function of E should therefore be linear, and from the gradient of these straight lines the values of the transfer coefficient α_A and α_C may be obtained. Also, provided E_e^\ominus is known, k^\ominus may be obtained by extrapolation. If $\log \vec{k}$ (or $\log \hat{k}$) is not a linear function of E it is probable that the reaction mechanism is more complex than had been assumed.

2.4.1.2 Chronocoulometry

In chronoamperometry, kinetic constants are obtained by analysis of current time data. It is often advantageous if the comparable chronocoulometric experiment is performed, i.e. the total charge (determined by the electronic integration of the current) is recorded as a function of time. A typical Q vs t transient is shown in Fig. 2.6a, whilst the mathematical form of the transient may be obtained by integration of the appropriate equation for I vs t . For mixed control and

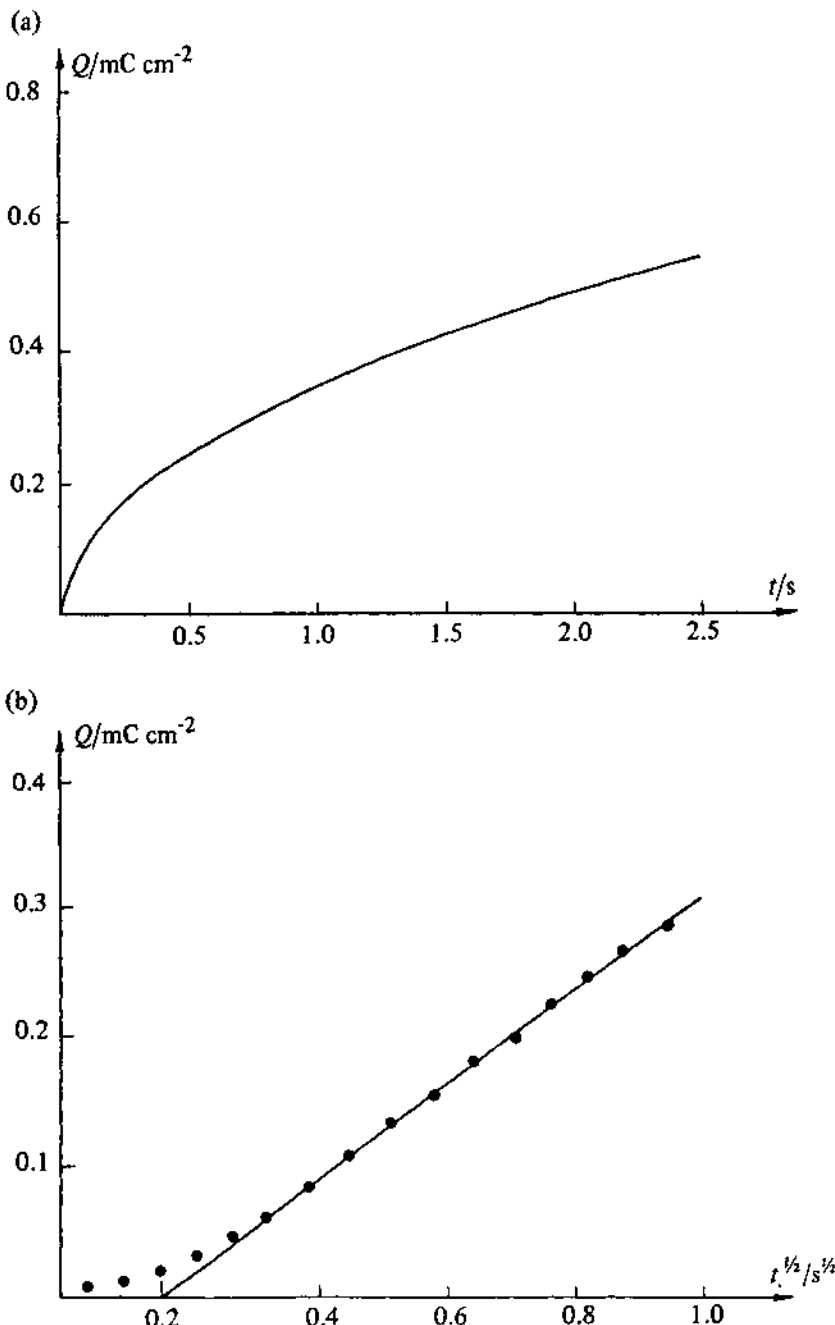


Fig. 2.6 – (a) Theoretical curve for $Q-t$ transient for reduction under conditions of mass transport control. $c^\infty = 1 \times 10^{-6} \text{ mol cm}^{-3}$, $D = 10^{-5} \text{ cm}^2 \text{ s}^{-1}$. (b) Q vs $t^{1/2}$ plot for a $2 \times 10^{-5} \text{ mol cm}^{-3}$ solution of Cd^{2+} in $1 \text{ mol dm}^{-3} \text{ Na}_2\text{SO}_4$ at a mercury electrode at an E_2 potential of -0.595 V vs SCE. (Reproduced with permission from J. H. Christie, G. Lauer, & R. A. Osteryoung, *J. Electroanal. Chem.*, 7 (1964), 80).

where the rate of the back reaction is negligible, integration of Equation (2.20) yields a rather complex relationship. However, it can be shown that if $|Q|$ is plotted as a function of $t^{1/2}$ the data asymptotes at long times to the straight line defined by

$$|Q| = \frac{4nF\vec{k}}{\pi} c_O^\infty (t_L^{1/2} t^{1/2} - t_L) \quad (2.32)$$

where $t_L^{1/2}$ is the intercept on the x -axis. Fig. 2.6b shows a typical example of a $|Q|$ vs $t^{1/2}$ plot. The value of \vec{k} is obtained from the slope and the value of t_L . As with chronoamperometry a full kinetic study would involve using \vec{k} values obtained for a range of potentials to determine k^Θ and α_C values from a Tafel type plot. As the value of \vec{k} increases, the value of t_L decreases until under the conditions of diffusion control no intercept is seen on the $t^{1/2}$ axis. Integration of the Cottrell equation (Equation (2.12)) then shows that Q will vary with $t^{1/2}$ according to the expression

$$|Q| = \frac{2nFD^{1/2}c_O^\infty t^{1/2}}{\pi^{1/2}} \quad (2.33)$$

and the value of D may be obtained from the gradient.

The advantage of chronocoulometry over chronoamperometry is that, since the charge is the integral of the current it retains at long times information about the value of the current at short times. The charge at very short times is still distorted by the double layer charging process, but its influence on the total charge rapidly becomes negligible. Hence, unlike Equation (2.22) Equation (2.32) is applicable over a very wide time range (perhaps 2000 times as long as the range for I vs $t^{1/2}$ plots) and only breaks down when natural convection begins to influence data, i.e. after several seconds. The value of \vec{k} can therefore be found from data obtained at quite long times. This permits rate constants perhaps an order of magnitude greater to be determined from charge, rather than current measurements [9, 10].

2.4.2 The determination of adsorption isotherms

Besides its use in the investigation of heterogeneous kinetics, chronocoulometry may be used to study the adsorption of electroactive species [11, 12, 13]. Let us consider a specific example, namely the halide induced adsorption of Pb^{2+} on a mercury electrode. A potential-time waveform of the type shown in Fig. 2.2 is used where E_1 is the potential at which the coverage of Pb^{2+} is desired, and E_2 is chosen such that the reduction of Pb^{2+} to $Pb(Hg)$ is diffusion controlled. The Q vs t transient is recorded, and Fig. 2.7 shows a typical result. Q is again plotted against $t^{1/2}$ and has the form shown in Fig. 2.8. The straight line corresponds to the diffusion controlled reduction of solution free Pb^{2+} , whilst the intercept on the Q axis is due to the instantaneous reduction of the adsorbed Pb^{2+} , and a small contribution from double layer charging. The magnitude of this latter contribution may be found either from a blank experiment (no Pb^{2+} present) as shown in Figs. 2.7 and 2.8 or, more accurately by drop expansion methods

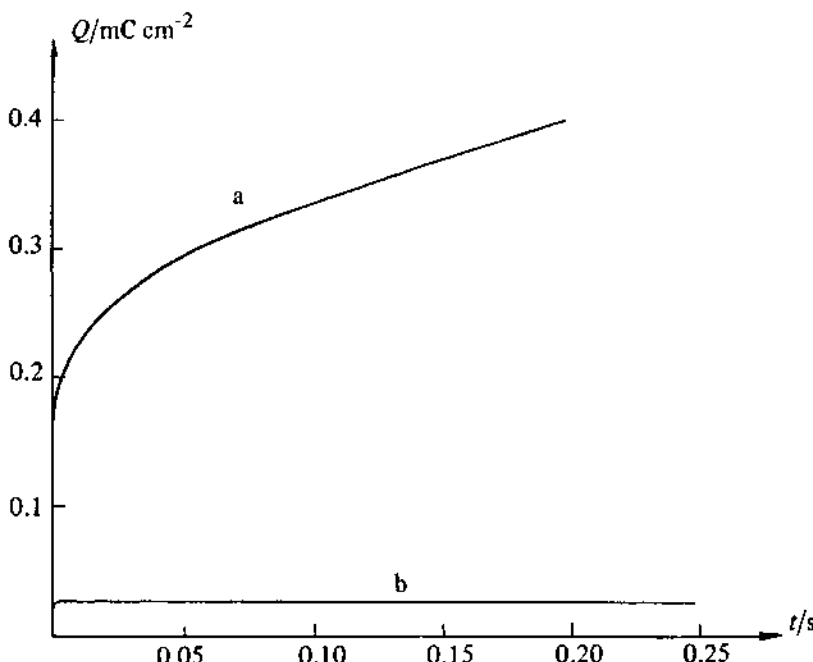


Fig. 2.7 – Q - t transient at a hanging mercury drop electrode for a potential step from -0.45 V to -0.70 V vs SCE in a solution of NaI ($1.0 \times 10^{-3}\text{ mol cm}^{-3}$), HClO_4 ($1 \times 10^{-5}\text{ mol cm}^{-3}$). Curve a $7 \times 10^{-7}\text{ mol cm}^{-3}$ Pb^{2+} present; curve b no Pb^{2+} present.

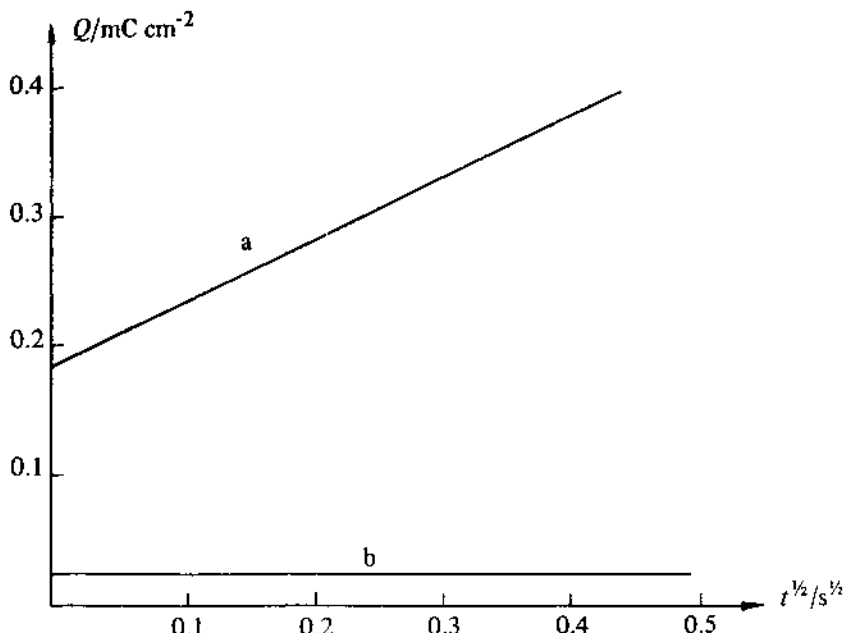


Fig. 2.8 – Q vs $t^{1/2}$ plot for the data of Fig. 2.7.

if the electrode is mercury or a mercury alloy [11] or double potential step chronoamperometry [12], and hence the value of the adsorbed charge density, or surface excess, is found.

2.4.3 The kinetics of coupled homogeneous reactions

Potential step techniques can be used to study a variety of types of coupled chemical reactions. With all these investigations it is necessary to consider the relative rates of all the individual steps involved, i.e. the diffusion steps, the electron transfers, and the chemical reactions. To simplify the analysis, the experimental conditions are nearly always chosen such that the electron transfer processes proceed at a diffusion controlled rate; it is then only necessary to consider the relative rates of mass transport and the chemical reactions.

Before discussing homogeneous reactions further, one point must be made which cannot be over-emphasised; whilst pulse techniques are very useful for determining the kinetics of this type of reaction, they can only be applied once the reaction mechanism has been definitely established by some other technique (e.g. cyclic voltammetry). Pulse techniques should not be used for mechanistic investigations, because most experiments lead to a falling transient and information is only obtained by a detailed mathematical analysis of its shape.

In view of the frequent occurrence in electrochemistry of certain reaction mechanisms involving coupled homogeneous reactions, a type of shorthand has been developed to describe them. In this shorthand the letter e refers to an electron transfer step, whilst the letter c refers to a homogeneous chemical reaction. Thus a ce reaction scheme implies a chemical step followed by an electron transfer. In all cases the electron transfer may be reversible, quasi-reversible, or irreversible, and the chemical steps may be reversible or irreversible and of first or higher order. The most commonly occurring reaction mechanisms are outlined below.

(a) Preceding chemical reaction (ce)



The species A is not electroactive in the potential range of interest but is in equilibrium with B which is.

(b) Following chemical reaction (ec)



The product of the electron transfer, B, reacts to produce C which is not electroactive in the potential region where A is reduced/oxidised.

(c) Catalytic reaction (ec')



This is a special case of the ec scheme where B reacts with the non-electroactive species Z to regenerate the reactant A.

(d) The ece reaction



In this case, contrary to the ec scheme, the product of the chemical step, C, is electroactive and usually more so than reactant A.

On consideration of the above scheme for the ece reaction it will be apparent that a homogeneous electron transfer between the species B and C is thermodynamically possible, and that the ece reaction is in fact a limiting case of the scheme



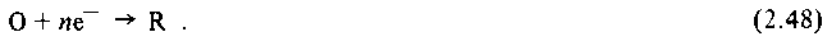
where Reaction (2.46) is unimportant. Two other limiting cases are

- (i) where Reaction (2.45) is unimportant and (2.44) is rate determining.
Designated disp 1;
- (ii) where Reaction (2.45) is unimportant and (2.46) is rate determining.
Designated disp 2.

Reactions proceeding by a disp 2 mechanism are easily recognised in view of their second order dependence (wrt B), but differentiation between disp 1 and ece schemes is difficult and has been the subject of much discussion. Which scheme is followed depends on the relative rates of the various steps, and under certain circumstances the reaction follows both routes. The differentiation between disp 1 and ece reactions is most readily achieved by optical techniques, and this will be discussed in Chapter 10, but it is also possible by double potential step chronoamperometry [14].

The application of pulse techniques to the determination of the kinetics of coupled homogeneous chemical reactions will now be discussed.

2.4.3.1 Preceding chemical reactions



Two limiting cases are apparent. If the chemical step is fast relative to the rate of mass transport, then the reaction will behave like a simple electron transfer process, and A will be reduced but via a mechanism where it is first converted to O. On the other hand, if Reaction (2.47) is slow, a steady state current controlled by the conversion of A to O will be observed in response to a potential step. (Note: in the extreme case where the reaction is very slow and no conversion of A to O occurs on the timescale of the experiment, then all that is observed is a diffusion controlled current due to the reduction of the low equilibrium concentration of O). The major region of interest is, of course, where the chemical step and mass transport are of comparable rate. To investigate reactions of this type it is again necessary to solve Fick's 2nd Law. For planar diffusion the equations to be solved are:

$$\frac{\partial c_A}{\partial t} = \frac{\partial^2 c_A}{\partial x^2} + k_{-1}(c_O - Kc_A) \quad (2.49)$$

$$\frac{\partial c_O}{\partial t} = D \frac{\partial^2 c_O}{\partial x^2} - k_{-1}(c_O - Kc_A) \quad (2.50)$$

where $K = k_1/k_{-1}$, the thermodynamic equilibrium constant, and $D_A = D_O = D$. The relevant initial and boundary conditions are

$$\begin{aligned} t = 0, \quad x > 0, \quad & c_O = c_O^\infty, \quad c_A = c_A^\infty, \quad c_O/c_A = K \\ t > 0, \quad x = \infty, \quad & c_O = c_O^\infty, \quad c_A = c_A^\infty, \quad c_O/c_A = K \\ t > 0, \quad x = 0, \quad & c_O = 0, \quad D(\partial c_A/\partial x)_{x=0} = 0 \\ & I = -nFD(\partial c_O/\partial x)_{x=0} \end{aligned}$$

The simplest representation of the solution to this equation is [15]

$$I/I_d = \pi^{1/2} b \exp(b^2) \operatorname{erfc}(b) \quad (2.51)$$

where $b = (Kk_1t)^{1/2}$ and I_d would be the diffusion controlled current density in the absence of kinetic complications. Since $I_d \propto t^{-1/2}$ (Cottrell Equation), Equation (2.51) can be written as

$$It^{1/2} = pb \exp(b^2) \operatorname{erfc}(b) \quad (2.52)$$

where p is a proportionality constant given by

$$p = nFD^{1/2}c_A^\infty \quad (2.53)$$

Chronoamperometric data are analysed by plotting $It^{1/2}$ as a function of $t^{1/2}$ over a wide range as shown in Fig. 2.9 (note the similarity to the determination of k values discussed earlier). The limiting value corresponds to the diffusion controlled region, whilst the non-horizontal region corresponds to mixed control. Kinetic data are obtained by fitting these data in the non-horizontal region to Equation (2.52) [16]. This produces a value of b from which $k_1 K$ is obtained. If K is known, then both k_1 and k_{-1} can be derived. First order rate constants as high as 10^6 s^{-1} and second order rates close to the diffusion controlled limit have been obtained in this way. Second order rates cannot of course be determined directly as outlined above. The reactions either have to be carried out under pseudo first order conditions, in which case the above analysis is valid, or kinetic data may be fitted to simulations.

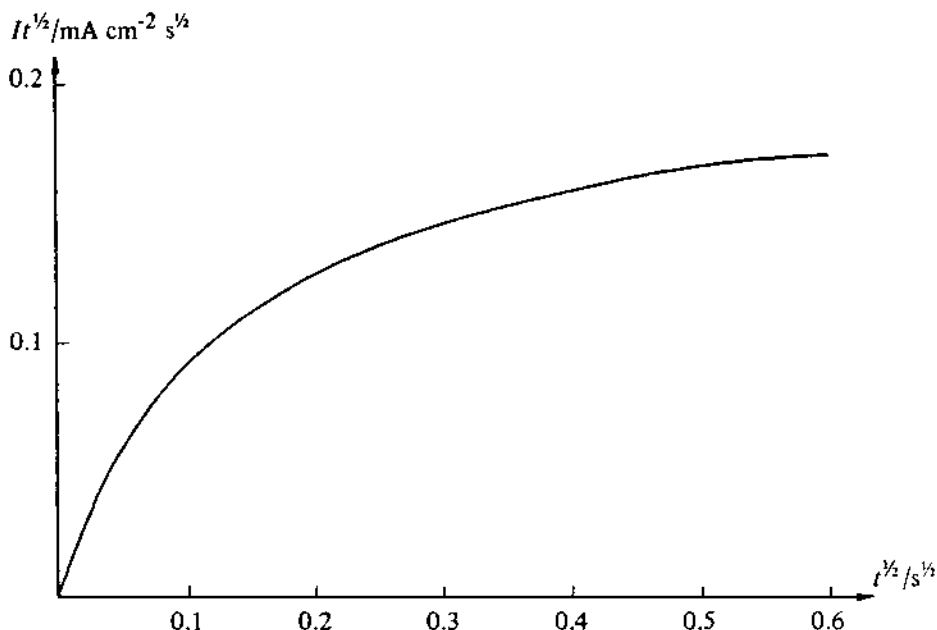


Fig. 2.9 – Plot of $It^{1/2}$ vs $t^{1/2}$ for ce system with $D = 10^{-5} \text{ cm}^2 \text{ s}^{-1}$, $c^\infty = 10^{-6} \text{ mol em}^{-3}$, $(k_1 K) = 25 \text{ s}^{-1}$.

Many ce processes are rather simpler than the one discussed above; the chemical step is irreversible and the equilibrium concentration of O is very low. For systems such as this it can be shown that, as for the slow electron transfer case, a plot of I vs $t^{1/2}$ should be a straight line at short times, and hence $I_{t=0}$, which is the purely kinetic current (mass transfer rate is infinite at $t = 0$) can readily be obtained by extrapolation. k_1 can then be found from Equation (2.54)

$$|I_{t=0}| = nFk_1c_A^\infty . \quad (2.54)$$

As previously discussed in respect of slow electron transfer (section 2.4.1.1), I only varies linearly with $t^{1/2}$ at very short times. This method thus suffers from similar limitations to those experienced when using the linear extrapolation procedure to determine k values; the determination of large k_1 values requires data to be analysed at shorter times where double layer currents are increasingly significant.

2.4.3.2 The ece mechanism

As we saw earlier in this chapter, the ece reaction is in fact a limiting case of a rather more complex reaction scheme. The arguments that apply are, however, similar for both ece and disproportionation mechanisms. Only the ece scheme will therefore be discussed in detail.

Let us consider the specific reaction scheme below where the standard potential for the second electron transfer is more positive than that for the first (Y is more readily reduced than O).



As before, it is useful to consider the limiting cases. When k is large compared to the rate of mass transport the reaction will behave as though it is an $(n_1 + n_2)$ electron transfer, as R will very rapidly convert to Y, which reduces further. Whereas when k is small, the reaction behaves as an n_1 electron transfer since within the timescale of the experiment R will not react to produce significant quantities of Y. As with many electrochemical techniques, it is useful to make a plot of some current function that is proportional to the number of electrons involved, as a function of time. For the ece scheme it can be shown [17] that

$$\left| \frac{I t^{1/2}}{c_O^\infty} \right| = \frac{FD^{1/2}}{\pi^{1/2}} (n_1 + n_2) (1 - \exp(-kt)) \quad (2.58)$$

A suitable current function plot is therefore $|I t^{1/2}/c_O^\infty|$ as a function of t or better $\log t$. Fig. 2.10 shows such a diagram for the above reaction scheme for the case where $n_1 = n_2$. Curve (a) corresponds to the situation when k is large, whilst curve (b) is for when it is small. For intermediate values of k (i.e. when the rate of reaction (2.56) and of diffusion of the intermediate Y away from the electrode are comparable) a plot of the type shown by curve (c) is to be expected. At short times the rate of mass transport is high and therefore large compared to k , R diffuses rapidly from the reaction layer before it has time to react, and therefore an apparently n_1 electron process is observed. At long times the rate of mass transport is lower, and R converts to Y, which remains near to the electrode and reduces further: hence an $(n_1 + n_2)$ process is seen. At intermediate times, apparent n values between n_1 and n_2 are found. The value of k may be found

by curve fitting of graphs such as curve (c) to Equation (2.59). For cases where the chemical step is not first order it is necessary to resort to fitting experimental results to simulated data in order to obtain k values (see Appendix).

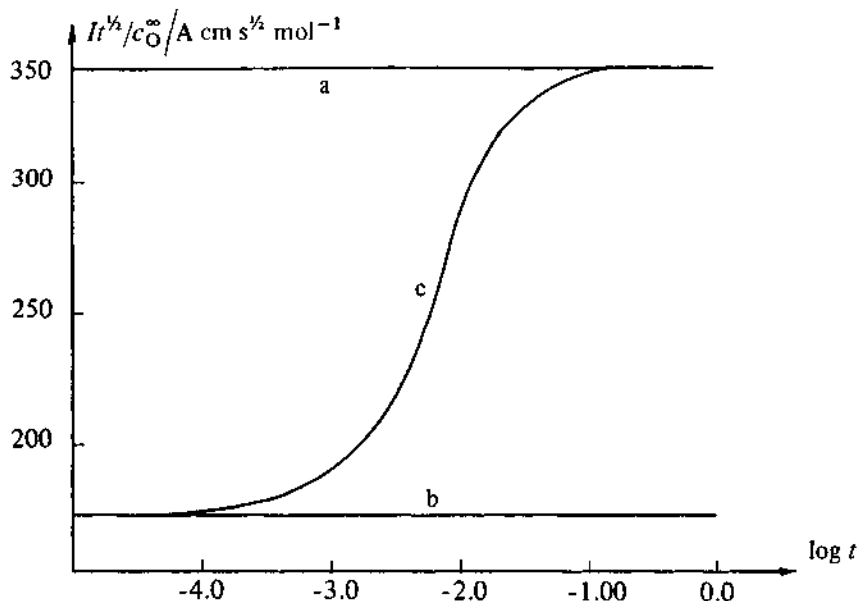


Fig. 2.10 – Current function plots for the ece mechanism (a) for a large value of k ; (b) for a small value of k , (c) for $k = 10^2 \text{ s}^{-1}$, $D = 10^{-5} \text{ cm}^2 \text{ s}^{-1}$. For all plots $c_O^{\infty} = 1 \times 10^{-6} \text{ mol cm}^{-3}$.

It was seen earlier that disp 1 is an alternative to the ece scheme. In this case the current function for $n_1 = 1$ is given by [18]

$$\left| \frac{I t^{1/2}}{c_O^{\infty}} \right| = \frac{FD^{1/2}}{\pi^{1/2}} \left(2 - \frac{1 - \exp(-2kt)}{2kt} \right). \quad (2.59)$$

The dependence of $I t^{1/2} / c_O^{\infty}$ on $\log t$ for the disp 1 mechanism (Equation (2.59)) and for the ece mechanism (Equation (2.58) with $n_1 = n_2 = 1$) is so similar that the two mechanisms cannot reliably be differentiated in this way. It is, however, possible by double potential step chronoamperometry [14].

2.4.3.3 Following chemical reactions

Whilst ec reactions as described by Equations (2.60) and (2.61) may sometimes be studied by single potential step methods, the double potential step technique is greatly preferred, i.e. a waveform of the type shown in Fig. 2.11 is applied to the working electrode.

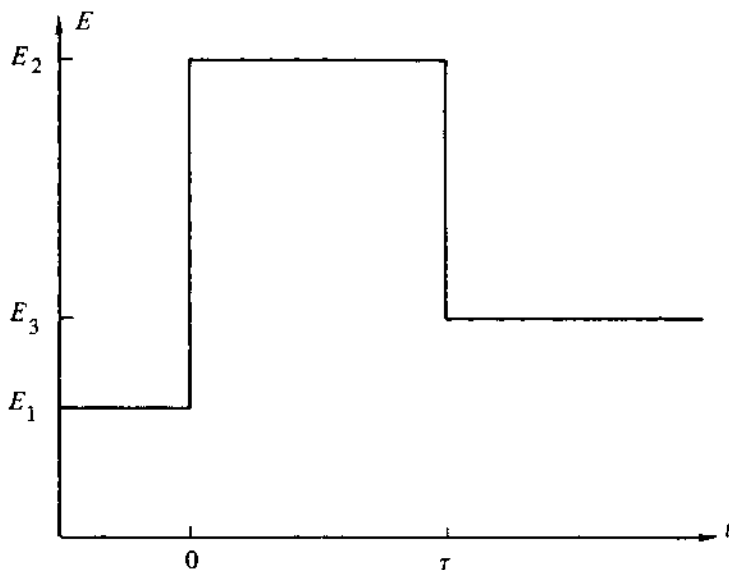


Fig. 2.11 – Potential-time profile for double potential step studies of ec systems.

The potential E_1 is chosen so that no reaction occurs ($I = 0$), then, at time $t = 0$ a pulse is made to a potential E_2 , where the reduction of O is diffusion controlled. After time τ at this potential it is stepped back to a value E_3 , where R is reoxidised, usually to O, again at a diffusion controlled rate. Thus the current that flows in response to the last pulse is used to monitor the amount of R present, the higher the value of k the less R there will be, and hence the lower the current observed. Fig. 2.12 shows the type of I vs t transient that is found, and it is most simply analysed in the following way which eliminates any dependence on the electrode area, solution concentration, or diffusion coefficients. The values of i_f and i_b , the currents on the forward and back pulses respectively, are determined for a range of values of t , as shown in Fig. 2.12. It can be shown that the ratio $-i_b/i_f$ is a rather complex function of k , t , and τ [19]. However, it is a fairly simple matter to obtain k values by comparison of the experimentally determined value of $-i_b/i_f$ with working curves of this ratio plotted as a function of $k\tau$. These curves are available for various values of the reduced time $(t - \tau)/\tau$, as shown in Fig. 2.13, and to ensure reliable values of k a wide range of values of this reduced variable should be investigated. Full details of this technique are to be found in the literature [19]. It should also be noted that the same information can be obtained from double potential step chronocoulometry. In this case it is the ratio q_b/q_f that is fitted to working curve values [20, 21].

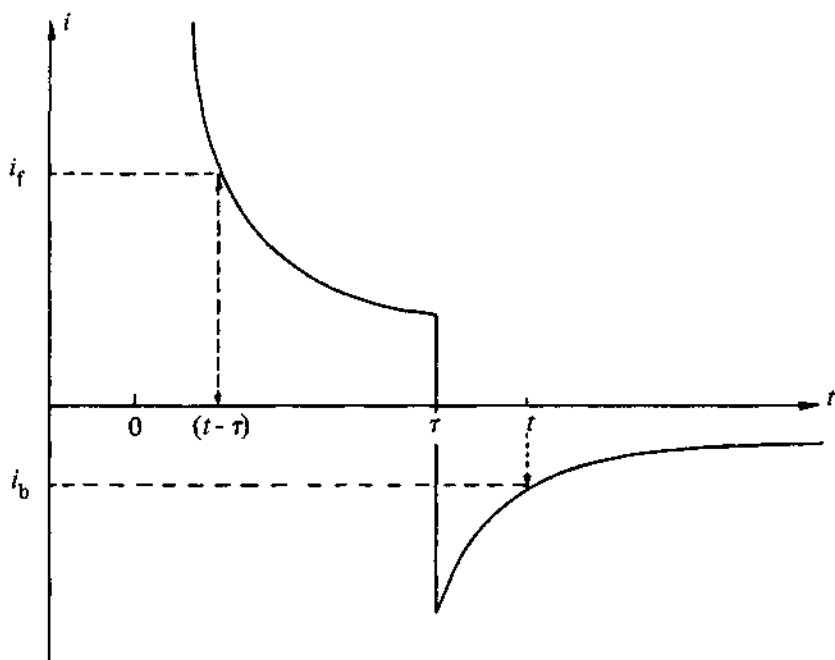


Fig. 2.12 – Schematic diagram showing the analysis of double potential step i - t data for an ec mechanism.

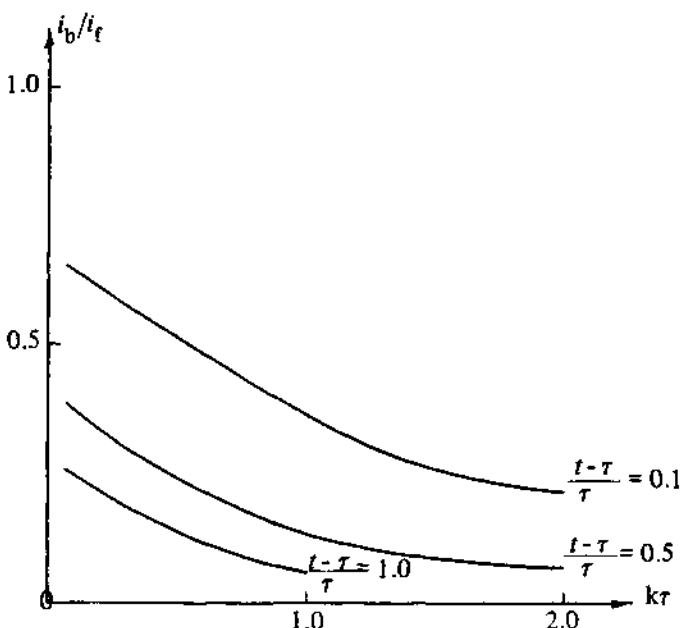


Fig. 2.13 – Working curves for the analysis of double potential step i - t transients for an ec mechanism. The curves are plotted for various values of the reduced time $(t - \tau)/\tau$.

2.4.4 Investigations of phase formation and adsorption

All the potential step studies considered so far have given rise to falling I vs t transients, and such transients are always found when both the reactant and product are soluble in solution and no adsorption is involved. There are, however, important areas of study where either the products or reactants are not soluble, e.g. metal deposition and corrosion. For such systems very different I vs t transients are observed, and these frequently contain a rising portion, as shown in Fig. 2.14, which is a clear indication of involvement of a nucleation step. Analysis of such plots generally involves treating I as a function of t^n , where n depends on the type of nucleation involved, the geometry of phase growth, and the rate determining step in phase formation. Such systems are discussed further in Chapter 9.

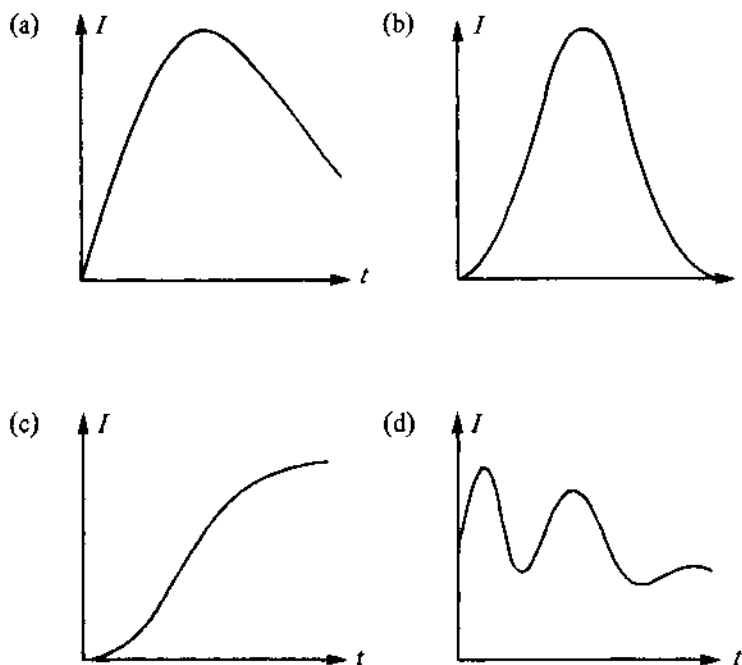


Fig. 2.14 – Schematic diagrams of I - t transients obtained for various types of phase formation process. (a) monolayer formation with instantaneous nucleation; (b) monolayer formation with progressive nucleation; (c) three-dimensional nucleation and growth process; (d) successive monolayer formation.

The shapes of chronoamperograms for systems involving adsorption are also rather different from those for solution free species. Fig. 2.15 shows the type of I vs t transient that might be obtained from a system where the electroactive species can adsorb at the electrode surface. It can be thought of as a combination of a phase formation type transient and a diffusion controlled one, i.e. the sum of a falling transient and a peak shaped response.

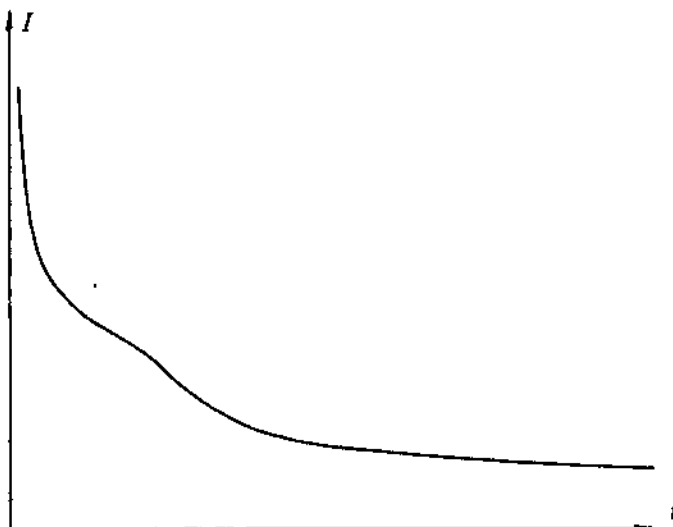


Fig. 2.15 – Schematic diagram of I - t transient for system involving product adsorption.

2.5 PULSE VOLTAMMETRY

The various pulse voltammetric methods (or pulse polarographic methods as they are called when applied to an Hg electrode) were developed largely to provide enhanced sensitivity in analytical applications as compared to classical polarography. Two techniques, differential and normal pulse polarography, dominate the field, and several commercial instruments designed to carry out these experiments are available. The potential-time waveforms applied to the electrode are shown in Figs. 2.16 and 2.17 for normal and differential pulse polarography respectively. In normal pulse polarography a fixed potential E_1 , at which no reaction occurs, is applied to the electrode, and then a short duration ($\sim 60\text{ms}$) pulse is applied and the current is recorded shortly before the potential is returned to E_1 . Since the current is measured well after the application of the pulse, the double layer charging current will have decayed essentially to zero and the current measured will be totally faradaic. After another period at the potential E_1 (usually a few seconds) the process is repeated with a slightly larger pulse, and this procedure is continued until the potential range of interest has been investigated. When used with a dropping mercury electrode the system is synchronised to the drop time; the pulse is applied late in the life of the drop, and as the potential returns to E_1 the drop is knocked off. The output of the normal pulse experiment looks essentially like that from a conventional polarographic or steady state measurement except that the values of the current are significantly increased (for analytical purposes the limit of detection is about 10^{-7} to $10^{-8}\text{ mol dm}^{-3}$). Normal pulse voltammetry is also a very good technique for determining diffusion coefficients. The plateau current density is given by

$$|I_L| = \frac{nFc^{\infty}D^{1/2}}{\pi^{1/2}t^{1/2}} , \quad (2.62)$$

i.e. the Cottrell equation, where t is the time after the application of the pulse when the current is measured.

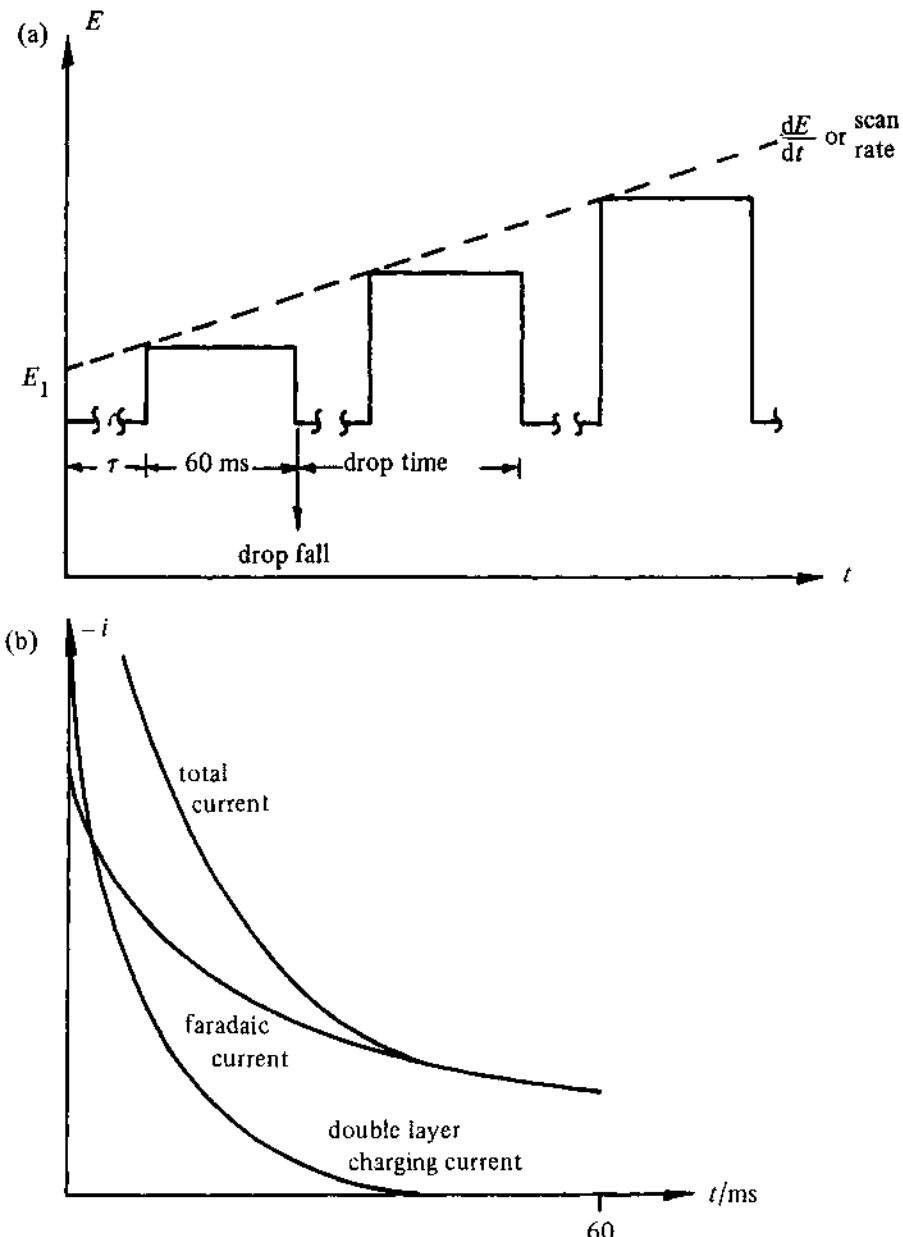


Fig. 2.16 – (a) The potential-time profile applied in normal pulse polarography, (b) a schematic diagram of the time dependence of the various components to the observed current.

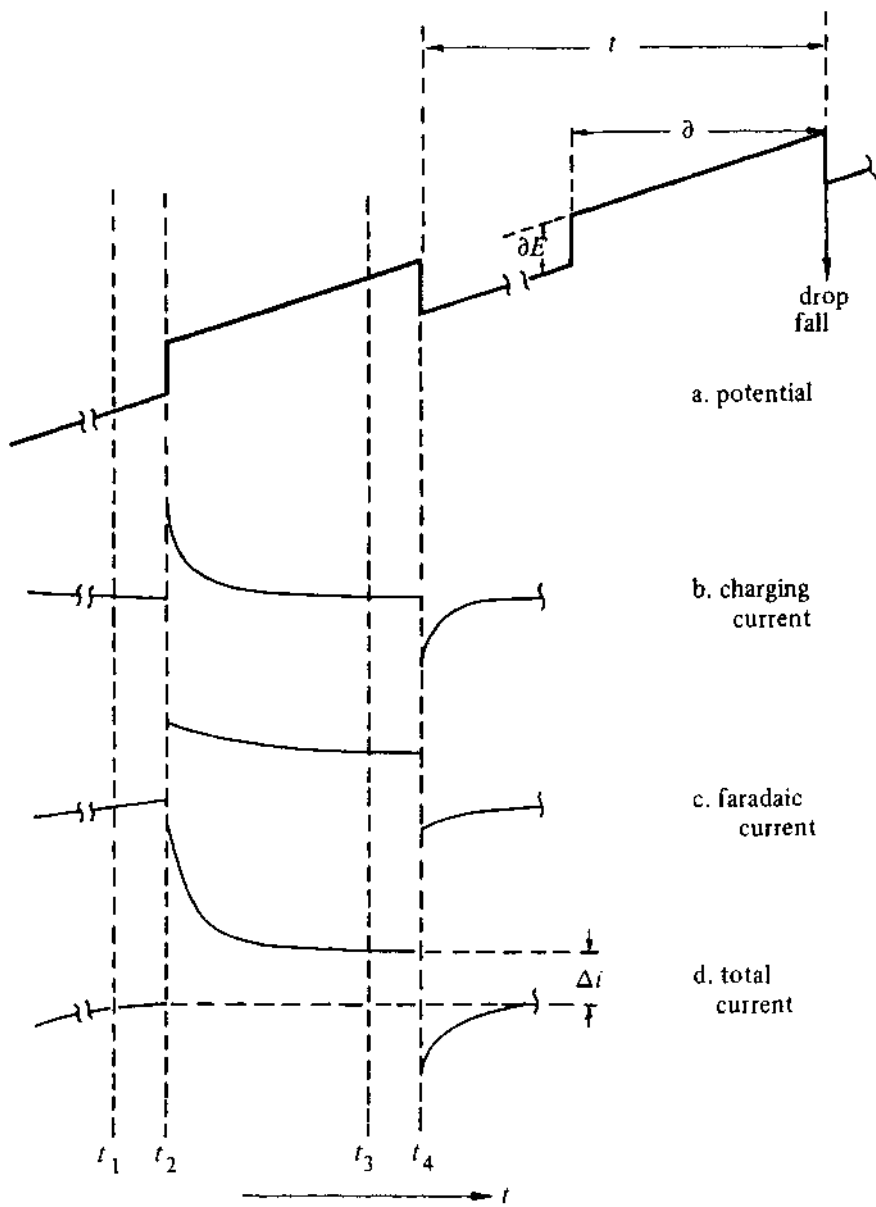
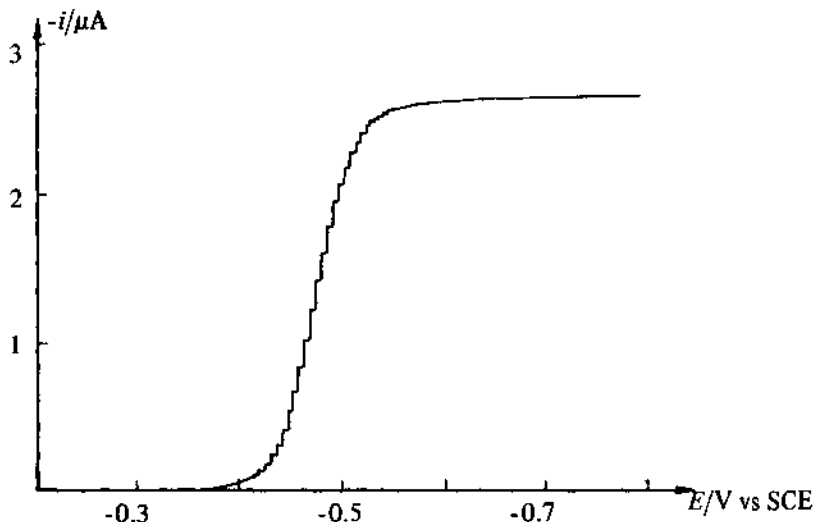


Fig. 2.17 . (a) The potential-time profile for differential pulse polarography. Also shown schematically, (b) the charging current-time dependence; (c) the Faradaic current-time dependence, and (d) the time-dependence of the total current.

Differential pulse voltammetry is rather similar except that now the pulse height is kept constant (typically a few tens of mV) and the base potential is swept slowly with time. The current shortly before the pulse is applied, and that at the end of the pulse are measured and the difference between these values as

a function of the potential is recorded. Differential pulse voltammograms are peaked shaped (essentially they are a differential of the conventional polarogram) and are thus well suited to analytical purposes. The limit of detection is about one order of magnitude lower than that of normal pulse voltammetry, i.e. 10^{-9} mol dm $^{-3}$. Fig. 2.18 shows typical normal and differential pulse voltammograms.

(a)



(b)

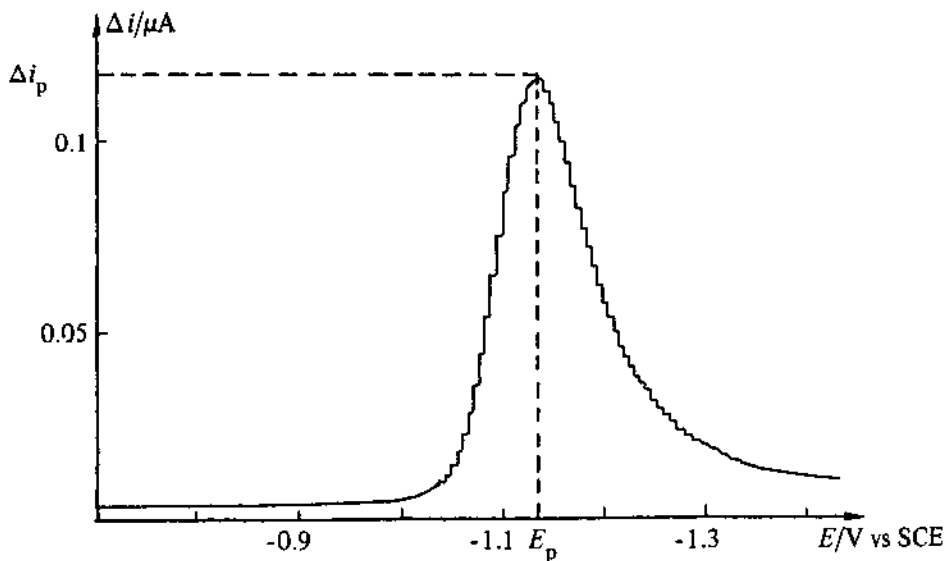


Fig. 2.18 - (a) Normal pulse polarogram of Pb^{2+} (10^{-4} mol dm $^{-3}$) in KNO_3 (0.1 mol dm $^{-3}$); (b) differential pulse polarography of Zn^{2+} (10^{-4} mol dm $^{-3}$) in KNO_3 (0.1 mol dm $^{-3}$), $\Delta E = 5$ mV.

Whilst these techniques are used almost entirely for analytical purposes [22, 23] their application to kinetic measurements has been described, and the theory for data analysis is available [24]. The major limitation is that with commercial instruments the current measurements are usually made about 50 ms after the application of the potential step. Such instruments are therefore only suitable for the study of relatively slow kinetics. More information on these techniques is available elsewhere [22, 23]. Recently a new pulse method has been developed, square wave voltammetry, which is again intended largely for analytical purposes. The potential-time waveform applied to the electrode is shown in Fig. 2.19, and pairs of current measurements are made on each period of the square wave. These are at time $p_1\tau$, late in the forward pulse and designated i_{forward} , and at $p_2\tau$, late in the reverse pulse and designated i_{reverse} . A square wave voltammogram is then a plot of i_{forward} , i_{reverse} , and $i_{\text{difference}}$ as a function of potential, and such a plot for a reversible system is shown in Fig. 2.20.

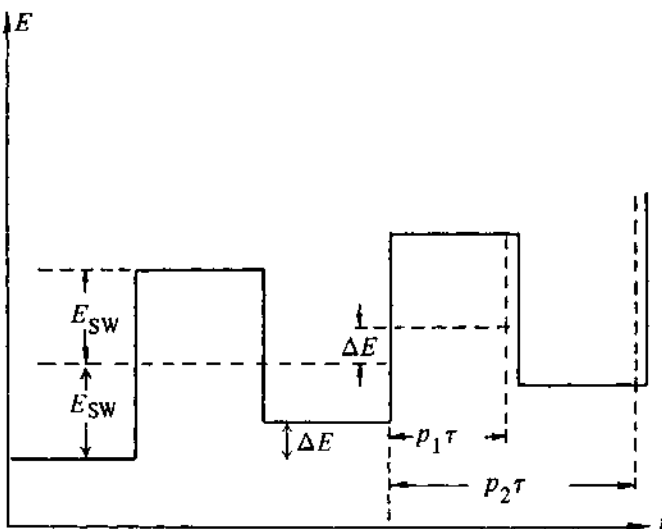


Fig. 2.19 – The potential-time waveform for square wave voltammetry.

There are a number of experimental variables including E_{SW} , which might typically be 50 mV, ΔE which might be 5 mV, and τ and the sweep rate which are of course related but might typically be 30 ms and a few hundred mV s^{-1} respectively. The suitability for analytical purposes is clearly seen from Fig. 2.20, but it has recently been shown [25, 26, 27] that square wave voltammetry is also eminently suitable for kinetic measurements (both of electron transfer rates and of rates of coupled chemical reactions), although as yet it not been widely applied. At present no commercial instrument is available for this technique, but it can easily be implemented on a computer based system.

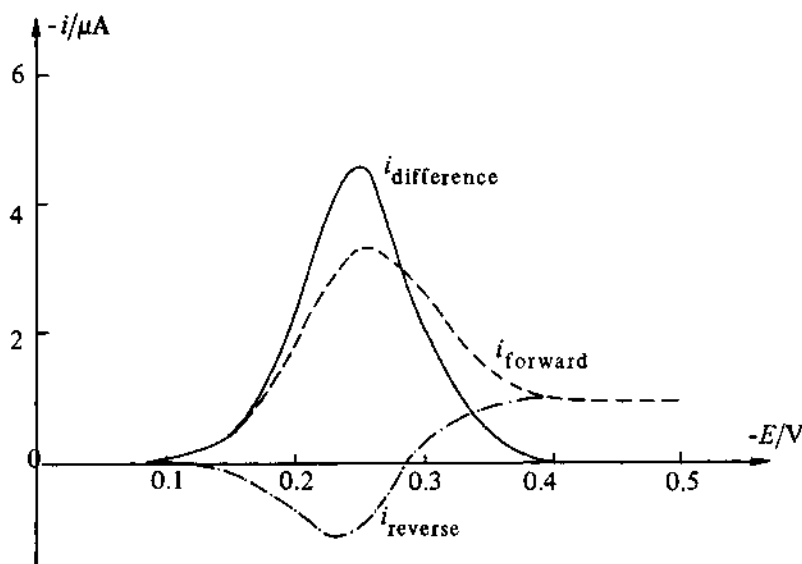


Fig. 2.20 — Square wave voltammograms for the reduction of ferric oxalate ($5.056 \times 10^{-4} \text{ mol dm}^{-3}$) in an oxalate buffer. $\tau = 33.3 \text{ ms}$, $p_1 = 0.499$, $p_2 = 0.999$, $E_{\text{SW}} = 30 \text{ mV}$, $\Delta E = 5 \text{ mV}$ (after ref. [26]).

2.6 CHRONOPOTENTIOMETRY

The galvanostatic experiment analogous to chronoamperometry is known as chronopotentiometry. In this type of experiment the current flowing in the cell is instantaneously stepped from zero to some finite value, i.e. the overall reaction rate is fixed, and the potential of the working electrode is then monitored as a function of time. The experiment is somewhat cheaper to carry out than chronoamperometry, as constant current devices are very easily made, but it is not very widely used by electrochemists for reasons which will become clear later.

For a simple reaction, as described by Equation (2.63), a chronopotentiogram will typically look like the plot in Fig. 2.21.



As the current pulse is applied there is an initial fairly sharp decrease in the potential as the double layer capacitance is charged, until a potential at which O is reduced to R is reached. There is then a fairly slow decrease in the potential, determined by the Nernst equation, until eventually the surface concentration of O reaches essentially zero. The flux of O to the surface is then no longer sufficient to maintain the applied current, and the electrode potential again falls more sharply, until a further electrode process occurs. The diffusion equations and initial and boundary conditions for this experiment are identical to those for the potential step experiment except that the current is now fixed, i.e. $(\partial c / \partial x)_{x=0}$ is a constant if only one reaction is occurring. The solution which is given in Equation (2.64) is known as the Sand equation.

$$|I\tau^{1/2}| = \frac{nFD_O^{1/2}\pi^{1/2}c_O^\infty}{2}, \quad (2.64)$$

where τ is the transition time as shown on Fig. 2.21. Thus the product $I\tau^{1/2}$ is independent of the applied current density, and proportional to c_O^∞ . This is used as a diagnostic test for a diffusion controlled process. The shape of the chronopotentiogram is given by Equation (2.65):

$$E = E_{\tau/4} + \frac{RT}{nF} \ln \frac{\tau^{1/2} - t^{1/2}}{t^{1/2}}. \quad (2.65)$$

The major problem associated with chronopotentiometric measurements is the determination of τ , owing to the double layer charging effects. In the absence of these effects the transition from one potential determining process to another would be essentially instantaneous, and τ could be easily determined. This is not, however, true of real experiments; the charging of the double layer requires a finite time as given by the solution of Equation (2.66):

$$\int_0^{\tau} \frac{I}{C_{dl}} dt = \Delta E. \quad (2.66)$$

Thus as shown on Fig. 2.21, τ measurements are imprecise. In view of this, whilst investigations of both heterogeneous and homogeneous kinetics are theoretically possible using chronopotentiometry, they are not frequently undertaken and are not recommended. Further details can be obtained from the literature [28-31].

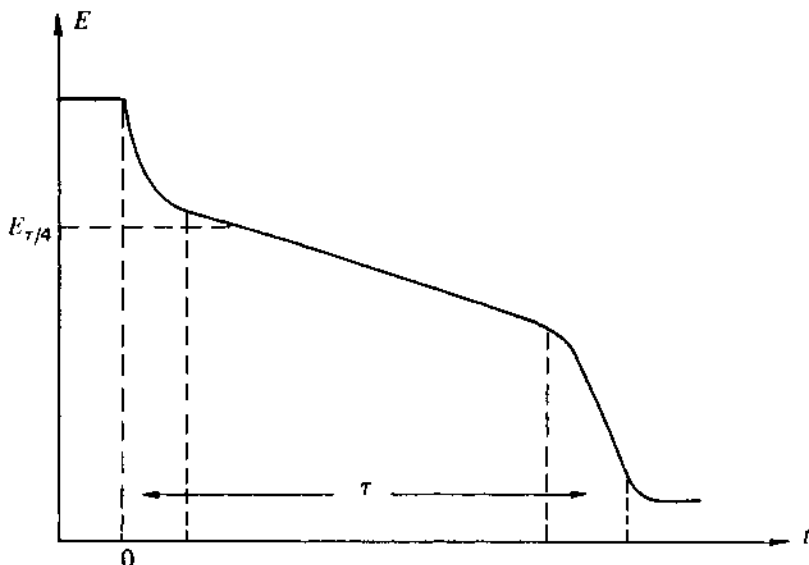


Fig. 2.21 – Schematic diagram of a chronopotentiogram for a reversible system.

REFERENCES

- [1] A. T. Hubbard, & F. C. Anson in *Electroanal Chem.*, A. J. Bard (Ed), Marcel Dekker, New York 4 (1970) 129.
- [2] A. T. Hubbard, *J. Electroanal. Chem.*, 22 (1969) 165.
- [3] L. Meites in *Techniques of chemistry*, A. Weissberger and B. W. Rossiter, (Eds.) Wiley-Interscience, New York 1971, Part Two A Vol. 1 Chapter IX.
- [4] A. J. Bard & K. S. V. Santhanam, *Electroanal. Chem.*, A. J. Bard (Ed), Marcel Dekker, New York 4 (1970) 215.
- [5] R. M. Wightman, *Anal. Chem.* 53 (1981) 1125A-1134A.
- [6] M. Fleischmann, F. Lassare, J. Robinson, & D. Swan, *J. Electroanal. Chem.*, 171 (1984) 97 and 115.
- [7] H. Gerischer & W. Vielstich, *Z. Physik. Chem. (Frankfurt)* 3 (1955) 16.
- [8] P. Delahay, *New instrumental methods in electrochemistry*, Wiley-Interscience, New York 1954, Chapter 4.
- [9] J. H. Christie, G. Lauer, & R. A. Osteryoung, *J. Electroanal. Chem.*, 7 (1964) 60.
- [10] J. H. Christie, G. Lauer, R. A. Osteryoung, & F. C. Anson, *Anal. Chem.*, 35 (1963) 1979.
- [11] F. C. Anson, *Anal. Chem.*, 38 (1966) 54.
- [12] J. H. Christie, R. A. Osteryoung, & F. C. Anson, *J. Electroanal. Chem.*, 13 (1967) 236.
- [13] M. J. Weaver & F. C. Anson, *J. Electroanal. Chem.*, 60 (1975) 19.
- [14] C. Amatore & J. M. Saveant, *J. Electroanal. Chem.*, 107 (1980) 353.
- [15] J. Koutecky & R. Brdicka, *Coll. Czech. Chem. Comm.* 12 (1947) 337.
- [16] P. Delahay & S. Oka, *J. Amer. Chem. Soc.*, 82, (1960) 329.
- [17] G. S. Alberts & I. Shain, *Anal. Chem.*, 35 (1963) 1859.
- [18] D. Evans, T. Rosanke and P. Jimenez, *J. Electroanal. Chem.*, 51 (1974) 449.
- [19] W. M. Schwarz & I. Shain, *J. Phys. Chem.*, 69 (1965) 30.
- [20] K. Holub, *J. Electroanal. Chem.*, 65 (1975) 193.
- [21] T. H. Ridgway, R. P. Van Duyne, & C. N. Reilley, *J. Electroanal. Chem.* 34 (1972) 267.
- [22] A. Bond, *Modern polarographic methods in analytical chemistry*, Marcel Dekker, New York 1980.
- [23] J. B. Flato, *Anal. Chem.*, 44 (1972) 75A.
- [24] K. B. Oldham & E. P. Parry, *Anal. Chem.*, 40 (1968) 65.
- [25] J. H. Christie, J. A. Turner, & R. A. Osteryoung, *Anal. Chem.*, 49 (1977) 1899.
- [26] J. A. Turner, J. H. Christie, M. Vukovic, & R. A. Osteryoung, *Anal. Chem.*, 49 (1977) 1904.
- [27] J. O'Dea, J. Osteryoung & R. A. Osteryoung, *Anal. Chem.*, 53 (1981) 695.
- [28] P. Delahay & T. Berzins, *J. Amer. Chem. Soc.*, 75 (1953) 2486.
- [29] T. Berzins & P. Delahay, *J. Amer. Chem. Soc.*, 77 (1955) 6448.
- [30] T. Berzins & P. Delahay, *J. Chem. Phys.*, 23 (1955) 972.
- [31] H. B. Herman & A. J. Bard, *Anal. Chem.*, 36 (1964) 510.

3

Electron transfer

Electrochemical reactions involve the transfer of electrons between an electronically conducting phase and localised energy levels on molecules or ions in an adjacent phase. In many cases, the reacting chemical species are present in an electrolyte solution, but interfacial charge transfer reactions can also involve solid ionic or covalent phases as well as ionic liquids (molten salts). Since the description of electron transfer should be applicable to a wide range of systems, it is useful to list some of the materials which can form part of the interface

<i>electrodes</i>	metals semiconductors insulators
<i>electrolytes</i>	aqueous electrolyte solutions non-aqueous electrolyte solutions polyelectrolytes molten salts solid electrolytes

In some special cases electron transfer may also occur between molecules or ions in adjacent phases, for example in membrane systems or at the interface between two immiscible liquids.

In this chapter, the transfer of electrons across the phase boundary is examined, and the kinetics of interfacial charge transfer are considered from empirical and fundamental points of view. The treatment is restricted largely to simple charge-transfer reactions since mechanistic complications are dealt with elsewhere in this book.

An electron in a solid sees the interface between the electrode and an electrolyte as an abrupt discontinuity in its environment. In a metal, for example, conduction band electrons are essentially delocalised, moving about freely in the regular periodic environment of the crystal lattice, whereas on the solution side of the interface the situation is quite different, since the electrons are localised on the orbitals of individual ionic or molecular species and conduction involves the migration of ions. At the same time, the absence of long range order in an electrolyte solution gives rise to an environment which is subject to random thermal fluctuations; ions are free to move, and they are surrounded by other ions and dipoles that are in constant thermal turmoil. As a consequence of these polarisation fluctuations, the electronic energy levels of a particular ion will change with time over a range of values determined by the interactions of the ion with its local environment, placing important restrictions on the probability of electron transfer to and from energy levels in the adjacent electrode.

Electron transfer processes are subject to the restrictions of the *Franck Condon principle* which implies that the probability of electron transfer will be greatest when the initial and final electronic states involved have the same energy. If the electronic states have different energies, electron transfer can only be accompanied by the simultaneous absorption or emission of thermal energy, reducing considerably the probability of such an event. Therefore, in order to gain even a qualitative insight into electrochemical electron transfer processes at the molecular level, we must attempt to develop a microscopic description of the interface which takes proper account of the fluctuation of energy levels in the electrolyte phase. This is clearly a difficult task, and progress towards a satisfactory theory of heterogeneous electron transfer has been slow. The structure of modern electrochemistry therefore remains surprisingly empirical; electrode kinetics is very largely based on semi-empirical equations developed many years ago by Tafel [1], Butler [2], and Erdey Gruz & Volmer [3]. For this reason, the discussion of the microscopic theory of electron transfer has been placed at the end of this chapter, and we begin instead with the empirical description of electron transfer kinetics which has been incorporated into the theory of electrode processes as a whole. Since several textbooks are available which give a full account of the formal development of electrode kinetics [4-10], only the most important results will be derived here.

3.1 AN EMPIRICAL DESCRIPTION OF ELECTRON TRANSFER

3.1.1 The situation at equilibrium

A simple electron exchange between ions in the electrolyte solution and an electrode can be written as



Here \vec{k} and \bar{k} are first order heterogeneous rate constants for the reduction and oxidation reactions respectively. The definition of equilibrium for such a system

can be based on either thermodynamics or kinetics. The kinetic definition of equilibrium is very straightforward: the net rate of chemical change in the reaction must be zero. In other words,

$$\vec{k}c_O^g = \vec{k}c_R^g , \quad (3.2)$$

where c_O^g and c_R^g are the concentrations of O and R at the electrode surface. If the concentrations of O and R are defined in units of mol cm^{-3} , then \vec{k} and \vec{k} are expressed in units of cm s^{-1} . Alternatively, equilibrium can be defined in terms of the current densities by the identity

$$I = \vec{I} + \vec{I} = 0 \quad (3.3)$$

where

$$\vec{I} = -nF\vec{k}c_O^g \quad (3.4a)$$

and

$$\vec{I} = nF\vec{k}c_R^g . \quad (3.4b)$$

Note that the current density, \vec{I} , for oxidation has a positive sign whereas \vec{I} , the current for the reduction process, has a negative sign. \vec{I} is referred to as the anodic partial current density and \vec{I} as the cathodic partial current density. The measured current density, I , is therefore made up from contributions of opposite sign from the anodic and cathodic processes as shown in Fig. 3.1.

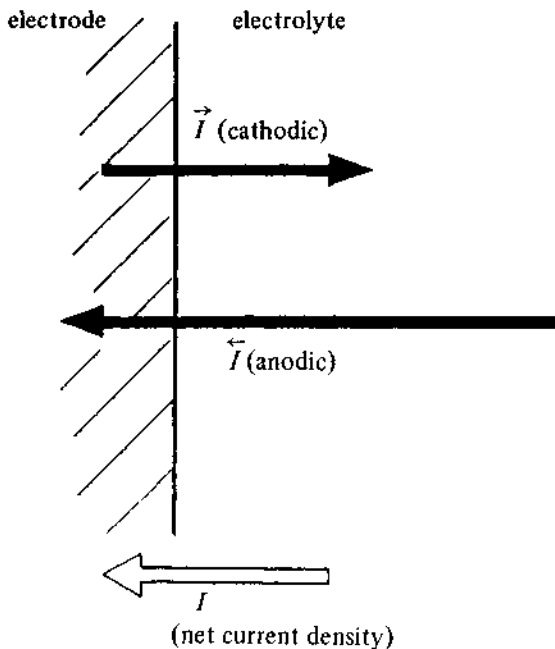


Fig. 3.1 Partial anodic (\vec{I}) and cathodic (\vec{I}) current densities and the resulting net current density, I , at an electrode (the length of the arrows represents the magnitudes of the current densities).

The net current at an electrode in contact with a solution containing O and R is exactly zero when the system is in thermodynamic equilibrium, and the Gibbs free energy change for the process shown in Equation (3.1) must be zero. Since the reactants and products are generally charged species, it is necessary to recognise that the Gibbs free energy of the components involved can be changed at constant composition by altering the electrical potential of the phases. The *electrochemical potential* of a species i is defined by the relationship

$$\bar{\mu}_i = \mu_i + z_i F \phi \quad (3.5)$$

where μ_i is the chemical potential of the species i, and the second term takes care of the free energy change brought about by altering the potential ϕ of the phase in which the species is situated ($z_i F$ corresponds to the charge *per mole* of i). ϕ is referred to as the *inner* (or *Galvani*) *potential* of the phase

At equilibrium, the electrochemical potential of the reactants and products must satisfy the identity

$$\mu_O^{\text{sol}} + n\bar{\mu}_e^M = \bar{\mu}_R^{\text{sol}} \quad (3.6)$$

which can be expanded using Equation (3.5) to give

$$\mu_O^{\text{sol}} + z_O F \phi^{\text{sol}} + n\mu_e^M - nF\phi_e^M = \mu_R^{\text{sol}} + z_R F \phi^{\text{sol}} \quad (3.7)$$

where the superscripts refer to the solution (sol) and electrode (M) phases. Since $z_O - z_R = n$, the number of electrons transferred in the reaction, it follows that the *equilibrium potential difference* across the electrode solution interface must be given by

$$\phi^M - \phi^{\text{sol}} = \frac{1}{nF} \{n\mu_e^M + \mu_O^{\text{sol}} - \mu_R^{\text{sol}}\} \quad (3.8)$$

The right-hand side of Equation (3.8) now contains only the chemical potentials of the species involved in the equilibrium, and it is convenient to express the dependence of these chemical potentials on the concentrations or activities of O and R. Since in general

$$\mu_i = \mu_i^\ominus + RT \ln a_i \quad (3.9)$$

where μ_i^\ominus is the standard chemical potential of species i and a_i is its activity, Equation (3.8) can be rearranged to give the potential difference in the form

$$\Delta\phi = \phi^M - \phi^{\text{sol}} = \Delta\phi^\ominus + \frac{RT}{nF} \ln (a_O/a_R) \quad (3.10)$$

where $\Delta\phi^\ominus$ is the value of $\Delta\phi$ under standard conditions when $a_O = a_R = 1$. In practice, $\Delta\phi$ cannot be measured directly; instead, the potential difference between the terminals of an electrochemical cell containing a second reference electrode (e.g. the hydrogen electrode) is accessible, so that Equation (3.10) is usually written as the more familiar *Nernst equation*:

$$E_e = E_e^\ominus + \frac{RT}{nF} \ln(a_O/a_R) \quad (3.11)$$

where E_e^\ominus is the *standard electrode potential*, and E_e is the equilibrium potential.

The same result should follow from the kinetic description of equilibrium. Here the key assumption concerns the potential dependence of \vec{k} and \vec{k} in Equation (3.1). This is usually written as

$$\vec{k} = k^\ominus \exp\left(-\frac{\alpha_C nF(E - E_e^\ominus)}{RT}\right) \quad (3.12a)$$

and

$$\vec{k} = k^\ominus \exp\left(\frac{\alpha_A nF(E - E_e^\ominus)}{RT}\right) \quad (3.12b)$$

where k^\ominus is the *standard rate constant* and α_A and α_C are the *anodic and cathodic transfer coefficients* respectively. These equations are essentially empirical, and it will be shown later in this chapter that their use implies the assumption that the free energy of activation of the electrode reaction depends *linearly* on electrode potential. For the moment, α_A and α_C are assumed to be constants which take values between 0 and 1; in fact $\alpha_A + \alpha_C = 1$, and it is commonly found that $\alpha_A = \alpha_C = 0.5$.

At the equilibrium potential E_e , the anodic and cathodic currents must sum to zero, Equation (3.3), and the magnitudes of the anodic and cathodic partial currents are identical to the exchange current density I_0 :

$$|\vec{I}| = |\vec{I}| = I_0 \quad \text{at} \quad E = E_e \quad (3.13)$$

The expressions for \vec{I} and \vec{I} can now be substituted from Equations (3.4) and (3.12), assuming $\alpha_A = 1 - \alpha_C$, to give

$$nFc_O^g k^\ominus \exp\left(-\frac{\alpha_C nF(E_e - E_e^\ominus)}{RT}\right) = nFc_R^g k^\ominus \exp\left(\frac{(1 - \alpha_C)nF(E_e - E_e^\ominus)}{RT}\right). \quad (3.14)$$

Rearrangement of Equation (3.14) leads to the expression

$$E_e = E_e^\ominus + \frac{RT}{nF} \ln \frac{c_O^\infty}{c_R^\infty}. \quad (3.15)$$

But since the system is at equilibrium $c_O^g = c_O^\infty$ and $c_R^g = c_R^\infty$, where c_O^∞ and c_R^∞ are the bulk concentrations of O and R. Equation (3.15) becomes identical to the Nernst equation (Equation (3.11)) if the concentration terms are replaced by activities, so that the thermodynamic and kinetic treatments are evidently consistent.

3.1.2 Departure from equilibrium

An understanding of electrochemical equilibrium is important, and for many years electrochemistry was regarded as part of thermodynamics (Bockris [11] has referred to this period as the 'Nernstian hiatus'). From the point of view of modern experimental electrochemistry, however, the non-equilibrium situation is more interesting. It is an experimental fact that the rate of an electron transfer reaction is sensitive to changes in electrode potential, and it is therefore convenient to choose the equilibrium potential as a reference point and then to define the *overpotential* η as

$$\eta = E - E_e . \quad (3.16)$$

Alternatively, the overpotential can be referred to the standard potential using the Nernst equation (assuming for simplicity that activities can be replaced by concentrations):

$$\eta = E - E_e^\ominus - \frac{RT}{nF} \ln (c_O^\infty / c_R^\infty) . \quad (3.17)$$

The exchange current density I_o can now be obtained by substitution of Equation (3.17) into (3.14):

$$I_o = |\vec{I}| = |\overset{\leftarrow}{I}| = nFk^\ominus (c_R^\infty)^{\alpha_C} (c_O^\infty)^{1-\alpha_C} . \quad (3.18)$$

The variation of I_o with the concentration of O and R can be expressed by the partial derivatives

$$\left(\frac{\partial \log I_o}{\partial \log c_R^\infty} \right)_{c_O^\infty} = \alpha_C \quad (3.19)$$

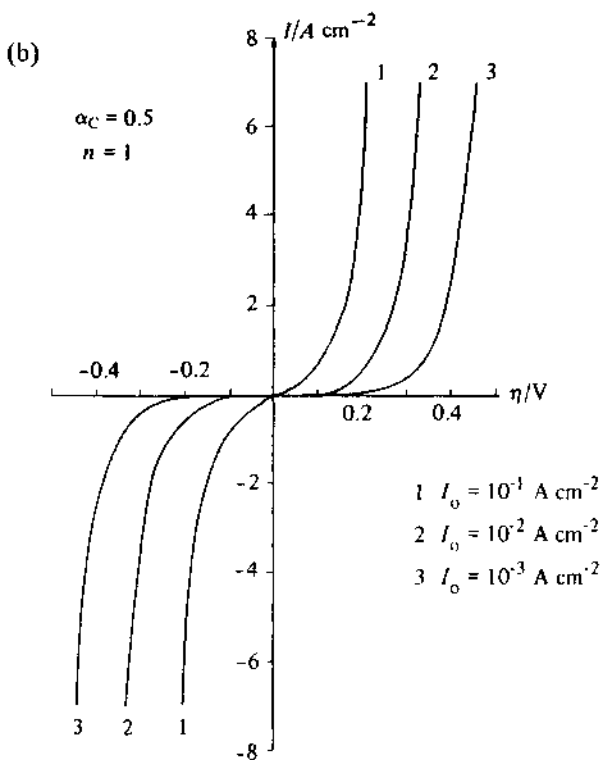
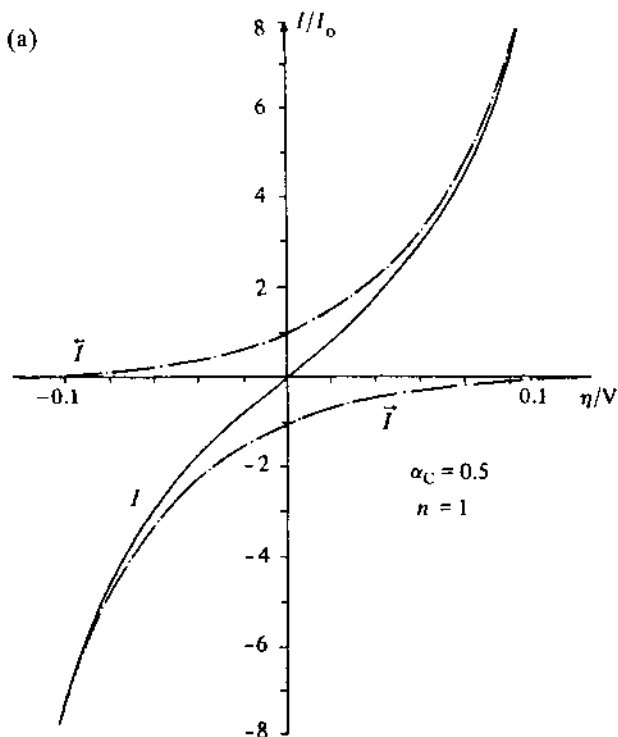
$$\left(\frac{\partial \log I_o}{\partial \log c_O^\infty} \right)_{c_R^\infty} = 1 - \alpha_C . \quad (3.20)$$

These expressions are particularly useful for the determination of the transfer coefficient α_C by small amplitude perturbation methods such as a.c. impedance.

The net current density can now be expressed in terms of the exchange current in the form

$$I = \vec{I} + \overset{\leftarrow}{I} = I_o \left[\exp \left(\frac{(1 - \alpha_C)nF\eta}{RT} \right) - \exp \left(- \frac{\alpha_C nF\eta}{RT} \right) \right] . \quad (3.21)$$

Equation (3.21) is known as the *Butler-Volmer equation*, and it forms the basis for the theoretical description of electrode processes. The terms in the square brackets represent the anodic (positive) and cathodic (negative) contributions to the net current, and I_o is a scaling factor that depends on the values of k^\ominus , c_O^∞ and c_R^∞ (Equation (3.18)). The symmetry of the current-potential



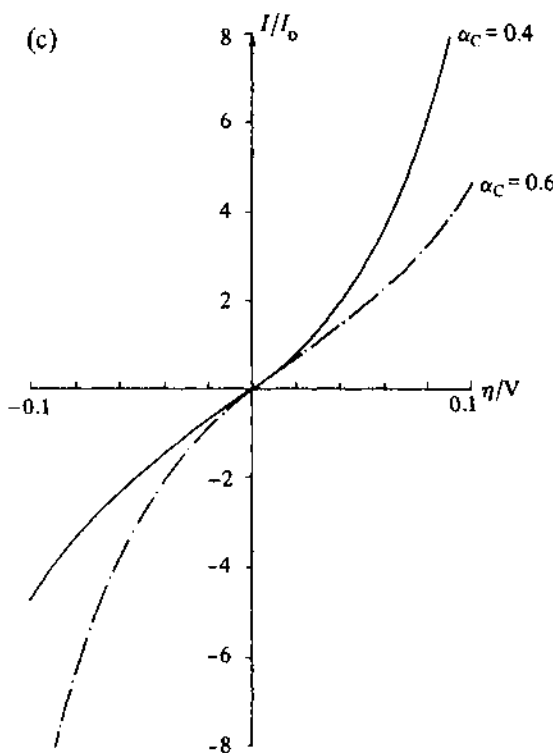


Fig. 3.2 – Current–voltage characteristics predicted by Equation (3.21). (a) shows the contributions from \bar{I} and \bar{I}_i ; (b) shows the scaling effect of I_0 ; (c) shows the effect of α_C on the symmetry of the curves.

curve depends on the value of the transfer coefficient α_C , and it is clear that symmetrical anodic and cathodic branches are obtained if $\alpha_C = 0.5$ when the graph of I vs η corresponds to a sinh function. The scaling effect of I_0 and the symmetry effect of α_C are illustrated in Fig. 3.2 which also shows the anodic and cathodic partial current densities \bar{I} and \bar{I}_i .

3.1.3 The link to experiments; limiting forms of the Butler–Volmer equation

For practical purposes, it is often convenient to consider the limiting behaviour of Equation (3.21) for small and large values of the arguments of the exponential terms. The exponential terms can be written as Taylor expansions, and for small values of the arguments $\alpha_C nF\eta/RT$ and $(1 - \alpha_C)nF\eta/RT$, the first two terms can be combined to give

$$I = \frac{I_0 nF\eta}{RT} \quad \text{for } \alpha_C nF\eta/RT \ll 1 . \quad (3.22)$$

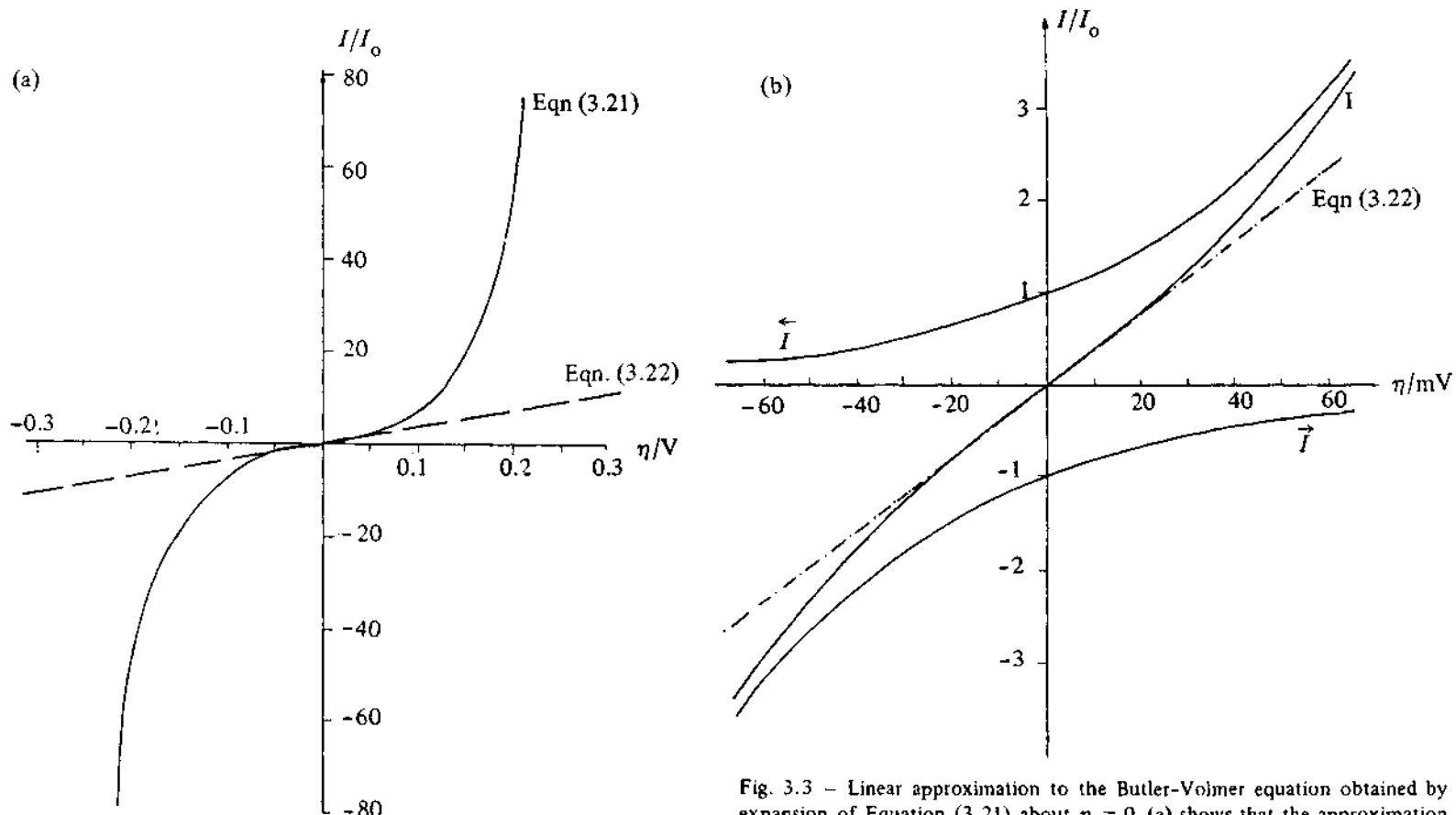


Fig. 3.3 – Linear approximation to the Butler-Volmer equation obtained by expansion of Equation (3.21) about $\eta = 0$. (a) shows that the approximation is only valid near $\eta = 0$, and (b) illustrates the approximation over the range $\eta = \pm 60\text{ mV}$.

This linear approximation to the Butler-Volmer equation is shown in Fig. 3.3. The *charge transfer resistance* R_{ct} is defined by rearranging Equation (3.22) by analogy with Ohm's law;

$$R_{ct} = RT/nFI_0 . \quad (3.23)$$

In practice, the linear approximation can be used for $|\eta| \leq 10/n$ mV when the error from the approximation is about 1% for $\alpha_C = 0.5$. If α_C differs significantly from 0.5, the errors involved should be calculated.

The linear approximation results in loss of direct information about the transfer coefficient α_C , and in small amplitude methods it is therefore necessary to measure I_o as a function of c_O^∞ and c_R^∞ in order to obtain α_C indirectly via Equations (3.19) and (3.20).

Fig. 3.2a shows that the curves for the net current density coincide with the partial current density curves at large positive or large negative overpotentials. Under these conditions, one or other of the exponential terms in the Butler-Volmer equation dominates, and the limiting relationships become

$$I \doteq \tilde{I} = -I_o \exp(-\alpha_C nF\eta/RT) \quad (3.24a)$$

for large negative overpotentials, and

$$I \doteq \tilde{I} = I_o \exp((1 - \alpha_C)nF\eta/RT) \quad (3.24b)$$

for large positive overpotentials. These relationships are often written in the form of the *Tafel equations*:

$$\eta = -\frac{2.3RT}{\alpha_C nF} \log |I| + \frac{2.3RT}{\alpha_C nF} \log I_o \quad (\eta < 0) \quad (3.25a)$$

$$\eta = \frac{2.3RT}{(1 - \alpha_C)nF} \log |I| + \frac{2.3RT}{(1 - \alpha_C)nF} \log I_o \quad (\eta > 0) \quad (3.25b)$$

where I is the net current density. The Tafel approximation is generally used for $|\eta| \geq 70/n$ mV.

The Tafel equations contain information about both the exchange current density, I_o , and the transfer coefficient, α_C . Plots of $\log |I|$ vs η are more commonly used than the true Tafel plots of η vs $\log |I|$, simply because η is now usually the controlled variable. Fig. 3.4 illustrates plots of this kind, and shows how I_o is obtained from the extrapolation of the data obtained in the limiting Tafel regions at high positive and negative values of η . The relationships between the slopes of the plots and the value of α_C are given by

$$\frac{d(\log |I|)}{d\eta} = -\frac{\alpha_C nF}{2.3RT} \quad (\eta < 0) \quad (3.26a)$$

$$\frac{d(\log |I|)}{d\eta} = \frac{(1 - \alpha_C)nF}{2.3RT} \quad (\eta > 0) \quad (3.26b)$$

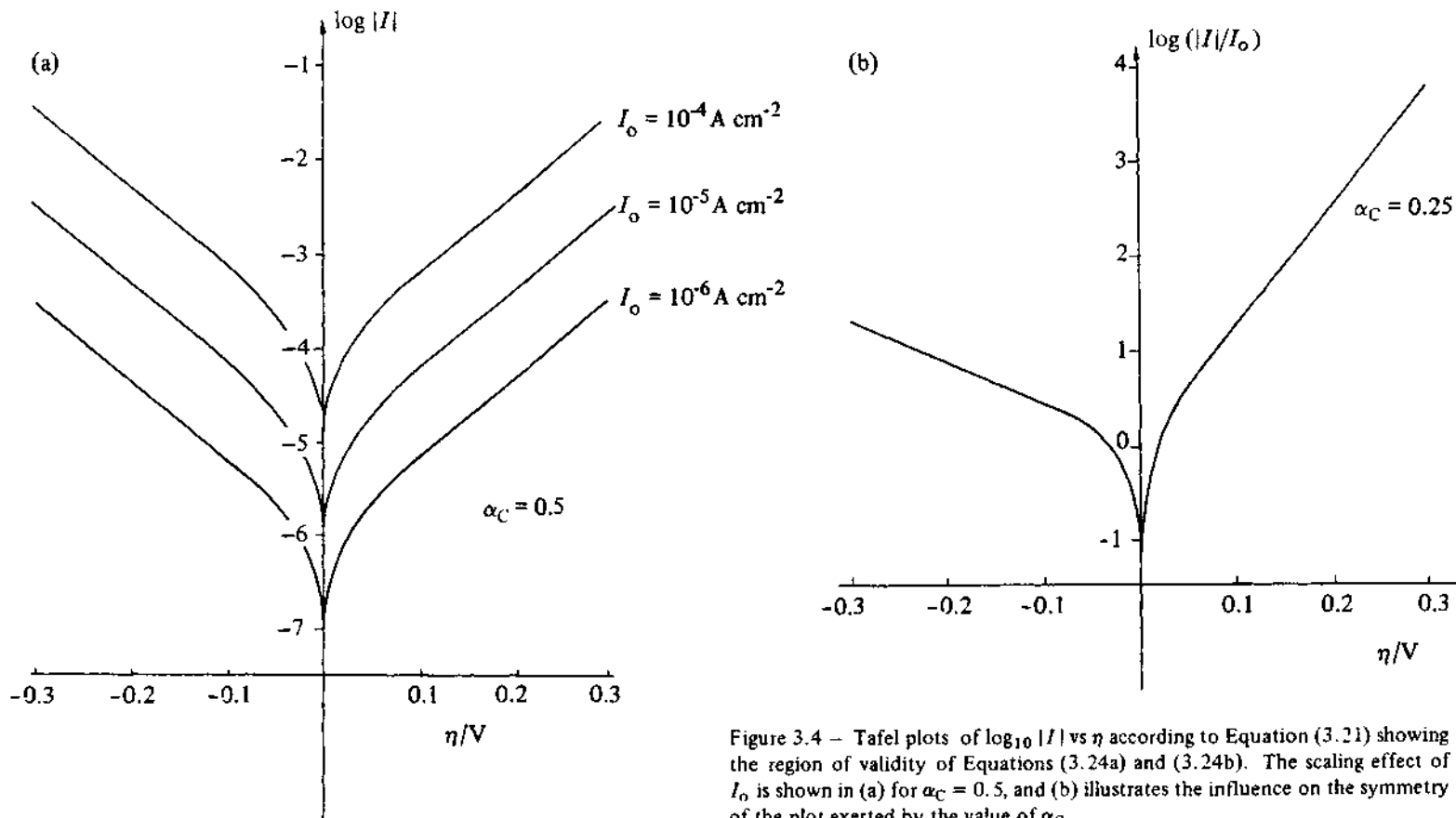


Figure 3.4 – Tafel plots of $\log_{10} |I|$ vs η according to Equation (3.21) showing the region of validity of Equations (3.24a) and (3.24b). The scaling effect of I_o is shown in (a) for $\alpha_C = 0.5$, and (b) illustrates the influence on the symmetry of the plot exerted by the value of α_C .

3.2 MORE FUNDAMENTAL MODELS OF ELECTRON TRANSFER

3.2.1 Why do changes in electrode potential affect \vec{k} and \bar{k} ?

Absolute rate theory

The generalised electron transfer reaction



can be represented with the help of the simplified free energy diagram shown in Fig. 3.5. The system must surmount an energy barrier in order for the electron transfer reaction to occur in either direction, and at equilibrium the rates of the forward and reverse transitions across the barrier must be equal. If the concentrations of O and R are the same, the equilibrium condition implies that the rate constants \vec{k} and \bar{k} are equal:

$$\vec{k} = \bar{k} = k^\ominus \quad (c_O^\infty = c_R^\infty, E = E_e^\ominus) . \quad (3.27)$$

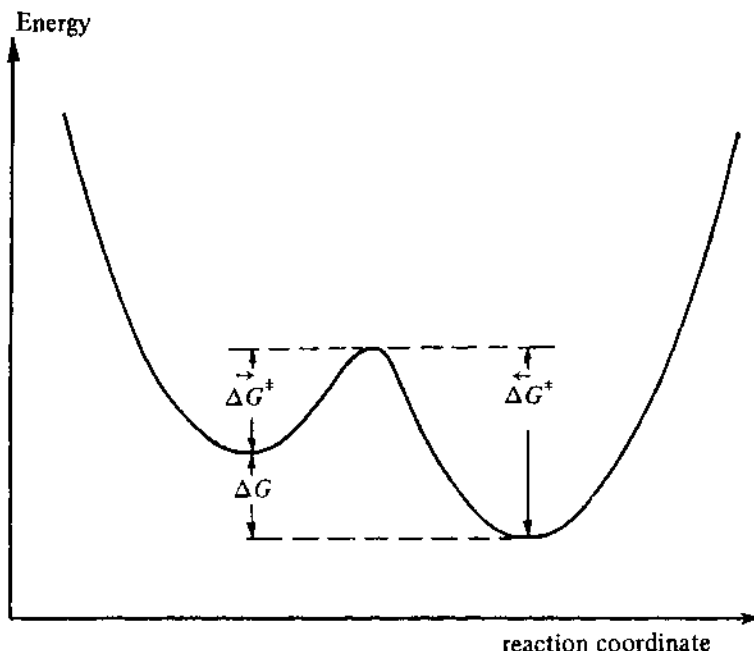


Fig. 3.5 - Simplified energy plot used to describe the course of an electrochemical reaction. The activation barriers for the forward and reverse reactions are related to the overall free energy change: $\Delta G = \Delta\tilde{G}^\ddagger - \Delta\tilde{G}^\ddagger$. In the case where $c_O^\infty = c_R^\infty$, the barrier is symmetrical at equilibrium (i.e. $\Delta\tilde{G}^\ddagger = \Delta\tilde{G}^\ddagger$).

The relationship between rate constants and activation energy can be derived from the absolute rate theory, and for a heterogeneous reaction the result is

$$k = \kappa Z \exp\left(-\frac{\Delta G^\ddagger}{RT}\right) \quad (3.28)$$

where κ is the transmission coefficient and Z is given by $k_B T \delta / \hbar$, where δ is a reaction length of the order of a molecular diameter. Z can also be interpreted as the upper limit to the heterogeneous rate constant set by the vibrations of the transition state, and for heterogeneous electron transfer reactions it is commonly taken to have a value of between 10^4 and 10^5 cm s^{-1} .

In the special case where $c_O^\infty = c_R^\infty$, the energy barrier must be symmetrical at equilibrium, i.e.

$$\vec{\Delta G}^\ddagger = \overleftarrow{\Delta G}^\ddagger = {}^\ominus \Delta G^\ddagger \quad (3.29)$$

where the arrows refer to the direction of the transition across the barrier in Fig. 3.5 and ${}^\ominus \Delta G^\ddagger$ is the standard free energy of activation when the system is at equilibrium at E_e^\ominus .

The free energies of activation $\vec{\Delta G}^\ddagger$ and $\overleftarrow{\Delta G}^\ddagger$ respond to changes of electrode potential because the free energy of the species involved is sensitive to the Galvani potential difference across the interface (Equation (3.5)). In fact, of course, the charge on O and R must differ by an amount equivalent to the number of electrons transferred multiplied by the charge of the electron, so that when the potential of the electrode is perturbed from the equilibrium value; the free energy curves for O and R move apart by an amount given by

$$\Delta G = nF(E - E_e^\ominus) \quad (3.30)$$

as shown in Fig. 3.6. As a consequence of this shift, the activation energies for the forward and reverse reactions are now different, and therefore the equilibrium must be perturbed. In the case shown in Fig. 3.6, $\vec{\Delta G}^\ddagger > \overleftarrow{\Delta G}^\ddagger$ and a net oxidation reaction occurs.

In order to calculate the rates of the forward and reverse reactions, it is necessary to make some assumptions about the shape of the free energy curves. If the system is treated by the simple harmonic oscillator approximation, the curves can be assumed to be identical parabolas, and it is easy to show by elementary geometry that $\vec{\Delta G}^\ddagger$ and $\overleftarrow{\Delta G}^\ddagger$ are related to the equilibrium barrier height ${}^\ominus \Delta G^\ddagger$ by the expressions

$$\vec{\Delta G}^\ddagger = {}^\ominus \Delta G^\ddagger + \frac{n^2 F^2 (E - E_e^\ominus)^2}{16 {}^\ominus \Delta G^\ddagger} + \frac{1}{2} nF(E - E_e^\ominus) \quad (3.31a)$$

and

$$\overleftarrow{\Delta G}^\ddagger = {}^\ominus \Delta G^\ddagger + \frac{n^2 F^2 (E - E_e^\ominus)^2}{16 {}^\ominus \Delta G^\ddagger} - \frac{1}{2} nF(E - E_e^\ominus) . \quad (3.31b)$$

The rate constants for the forward and reverse reactions are

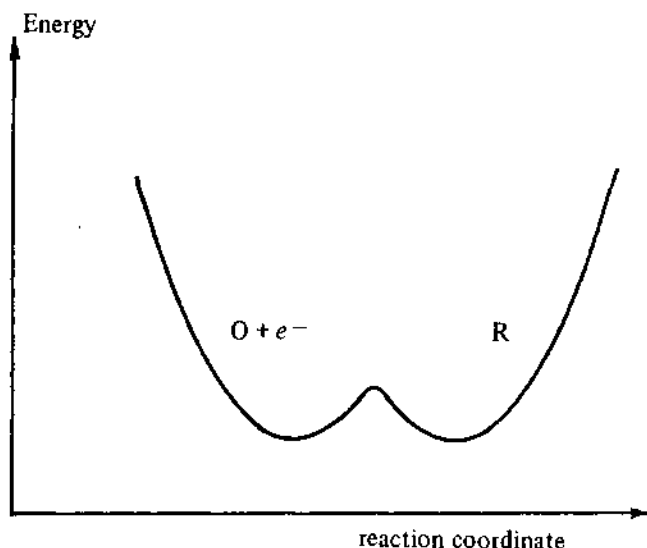
$$\overleftarrow{k} = \kappa Z \exp\left(-\frac{\overleftarrow{\Delta G}^\ddagger}{RT}\right) \quad (3.32a)$$

$$\vec{k} = \kappa Z \exp\left(-\frac{\vec{\Delta G}^\ddagger}{RT}\right) \quad (3.32b)$$

whereas the rate constant at equilibrium was

$$k^\ominus = \kappa Z \exp\left(-\frac{\Theta \Delta G^\ddagger}{RT}\right). \quad (3.32c)$$

(a)



(b)

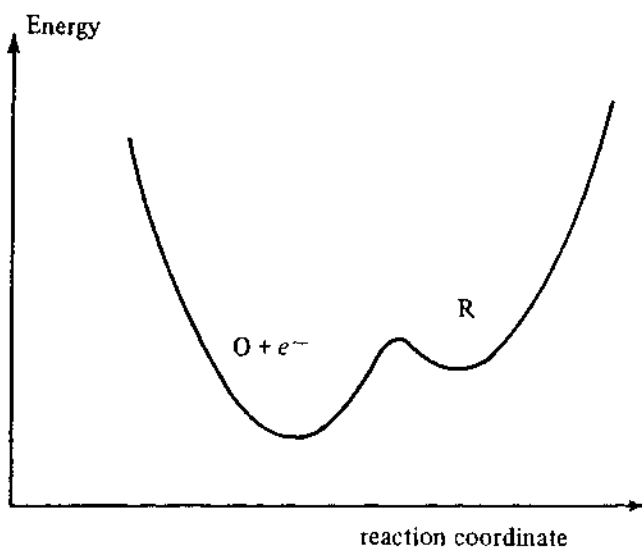


Fig. 3.6 - Energy curves for the reaction $O + ne \Rightarrow R$ for the case where $c_O^\infty = c_R^\infty$. (a) at equilibrium at E_e^\ominus (net current density = 0) and (b) at a potential $E > E_e^\ominus$ (net current density > 0 , i.e. oxidation of R occurs). The relative shift in position of the curves is given by Equation (3.30).

The values of $\vec{\Delta}G^\ddagger$ and $\vec{\Delta}G^\ddagger$ can now be used to obtain the potential dependence of \vec{k} and \vec{k} :

$$\vec{k} = k^\Theta \exp \left[\frac{[-n^2 F^2 (E - E_e^\Theta)^2 / 16^\Theta \Delta G^\ddagger] - \frac{1}{2} nF(E - E_e^\Theta)}{RT} \right] \quad (3.33a)$$

$$\vec{k} = k^\Theta \exp \left[\frac{[-n^2 F^2 (E - E_e^\Theta)^2 / 16^\Theta \Delta G^\ddagger] + \frac{1}{2} nF(E - E_e^\Theta)}{RT} \right]. \quad (3.33b)$$

These equations look more cumbersome than those based on the semi-empirical approach outlined in section 3.1.1 (Equations (3.12a) and (3.12b)), but a comparison of the two sets of equations shows that they are identical if the transfer coefficient α_C is identified as

$$\alpha_C = \frac{1}{2} + \frac{nF(E - E_e^\Theta)}{16^\Theta \Delta G^\ddagger}. \quad (3.34)$$

However, whereas α_C was assumed to be a constant in the empirical theory, this simple treatment based on absolute rate theory suggests that α_C should vary linearly with potential. If the second term in Equation (3.34) is sufficiently small, on the other hand, α_C will approach a potential independent value of 0.5; this will clearly be the case for small changes in potential ($E - E_e^\Theta$) or for large values of $^\Theta \Delta G^\ddagger$ (i.e. for slow reactions).

So far the discussion has been limited to the special case where the bulk concentrations[†] c_O^∞ and c_R^∞ are equal, but the description of the system can be extended to any concentration ratio c_O^∞/c_R^∞ as follows. The equilibrium condition is given by

$$\vec{k} c_O^\infty = \vec{k} c_R^\infty, \quad (3.35)$$

and it is immediately apparent that the energy barrier is no longer symmetrical since Equation (3.35) can be expressed in the form

$$c_O^\infty \exp\left(-\frac{\vec{\Delta}G^\ddagger}{RT}\right) = c_R^\infty \exp\left(-\frac{\vec{\Delta}G^\ddagger}{RT}\right) \quad (3.36)$$

from which it follows that

$$\vec{\Delta}G^\ddagger - \vec{\Delta}G^\ddagger = RT \ln(c_O^\infty/c_R^\infty). \quad (3.37)$$

[†] Note that throughout this chapter, bulk and surface concentrations are considered to be the same. This is because only the kinetics of electron transfer are being discussed and no account need be taken of mass transport processes, i.e. it is assumed that the conditions of mass transport are such that electron transfer is the rate determining step.

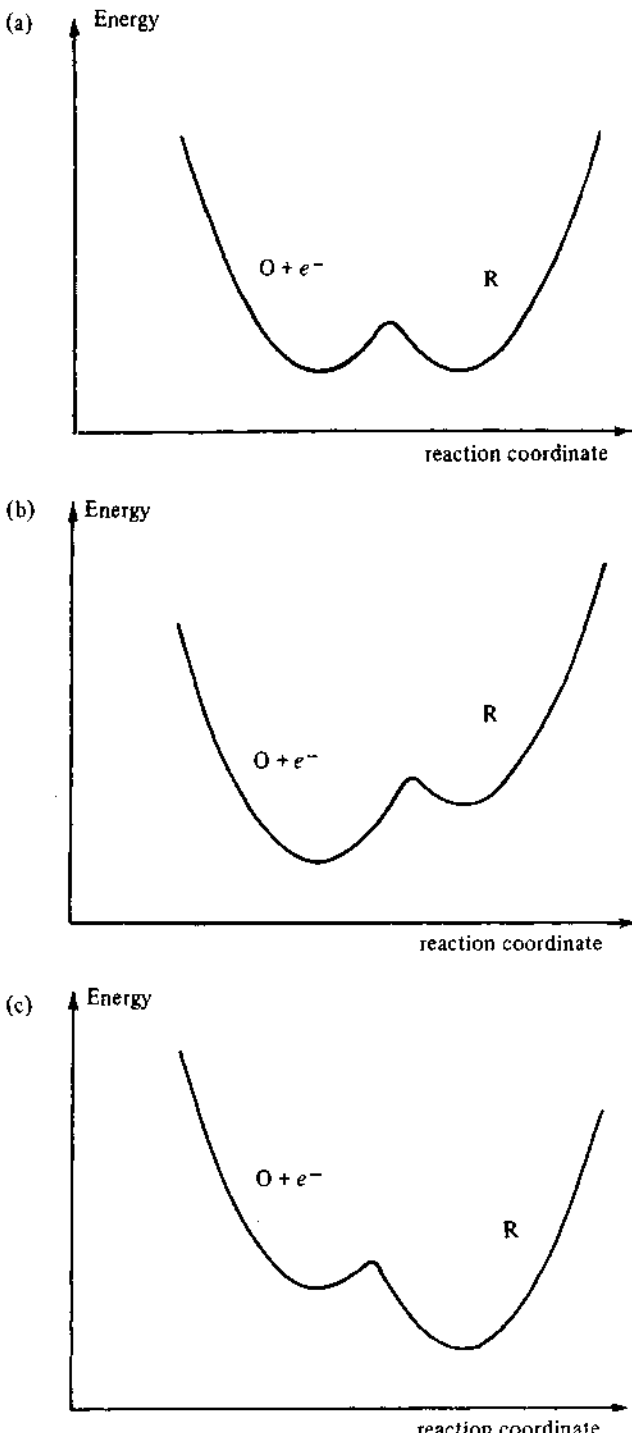


Fig. 3.7 – Changes in shape of the equilibrium energy curves brought about by altering the ratio c_O^∞/c_R^∞ . Note that the equilibrium condition holds in each case (net current density = 0, $E = E_s$). (a) $(c_O^\infty/c_R^\infty) = 1$ (b) $(c_O^\infty/c_R^\infty) = 100$ (c) $(c_O^\infty/c_R^\infty) = 0.01$.

In other words, the effect of changing c_O^∞/c_R^∞ is to move the energy levels apart by an amount $RT \ln(c_O^\infty/c_R^\infty)$. At the same time the equilibrium potential differs from E_e^Θ since

$$E_e = E_e^\Theta + RT \ln(c_O^\infty/c_R^\infty) , \quad (3.15)$$

so that Equation (3.37) can be written in the form

$$\vec{\Delta G}^+ - \vec{\Delta G}^- = nF(E_e - E_e^\Theta) . \quad (3.38)$$

The equilibrium energy diagram is therefore predicted to have the shape shown in Fig. 3.7, and if the derivation of the expressions for the forward and reverse rates is carried out as before, the final expression corresponds to the Butler-Volmer equation, Equation (3.21), except that α_C is now identified as being the potential dependent quantity given by Equation (3.34).

The current-voltage relationship predicted by these simple considerations is similar to the expressions which have been derived by Marcus [12, 13]. Since α_C depends on electrode potential, plots according to the Tafel relations (Equation (3.25)) are no longer expected to be linear; instead they should show a curvature which is related to the value of ${}^\Theta\Delta G^+$, and hence to k^Θ . Fig. 3.8a shows a set of Tafel plots predicted for different values of k^Θ , and the potential dependence of α_C is illustrated in Fig. 3.8b. An interesting feature of the Tafel plots predicted

(a)

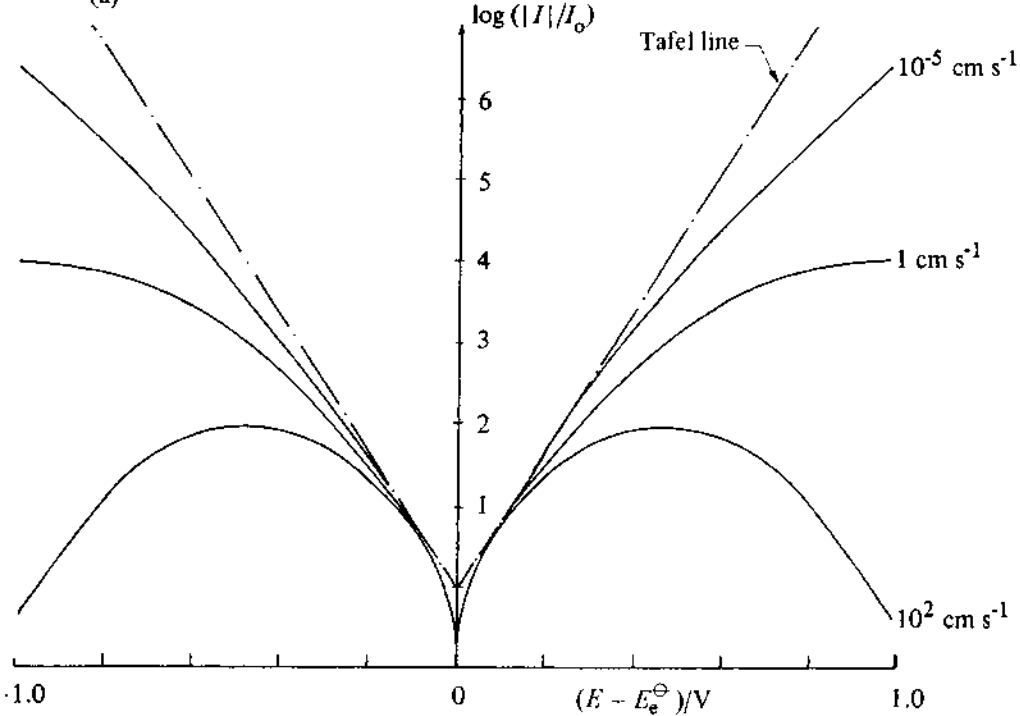


Fig. 3.8 – see legend next page

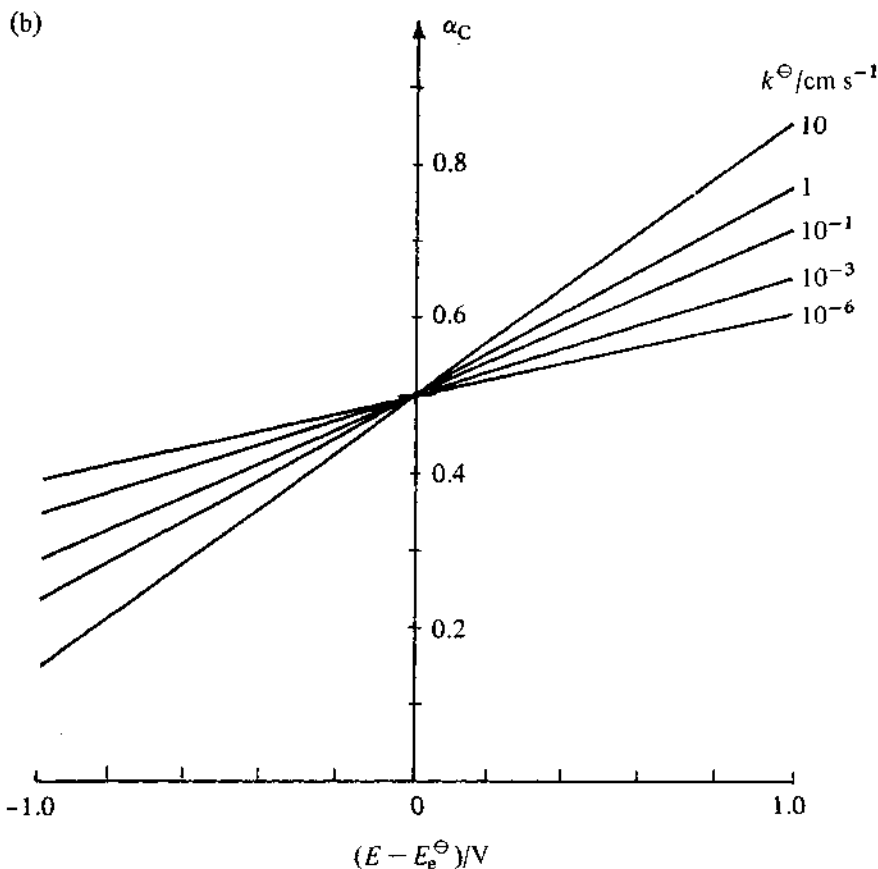


Fig. 3.8 – (a) Normalised Tafel plots, ($\log_{10}(I/I_0)$), for different values of the standard rate constant k^\ominus . The dashed line shows the limiting linear Tafel behaviour, whereas the solid curves predicted by Equation (3.33a) and (3.33b) exhibit curvature. (b) Potential dependence of α predicted by Equation (3.34) for different values of the standard rate constant k^\ominus .

in this way is that at sufficiently high overpotentials the current density passes through a maximum and then begins to fall again. This situation corresponds to the intersection of the parabolic energy curves shown in Fig. 3.9. Although it should be possible to detect the deviation from linear Tafel behaviour predicted by Equation (3.24), in practice the need to allow for other effects such as the influence of the electrical double-layer (see Chapter 5) makes experimental verification difficult. However, several experimental results appear to lend support to the theory outlined here [14, 15]. Even so, the linear Tafel equations account for most experimental data in the laboratory, and will be used throughout the other chapters.

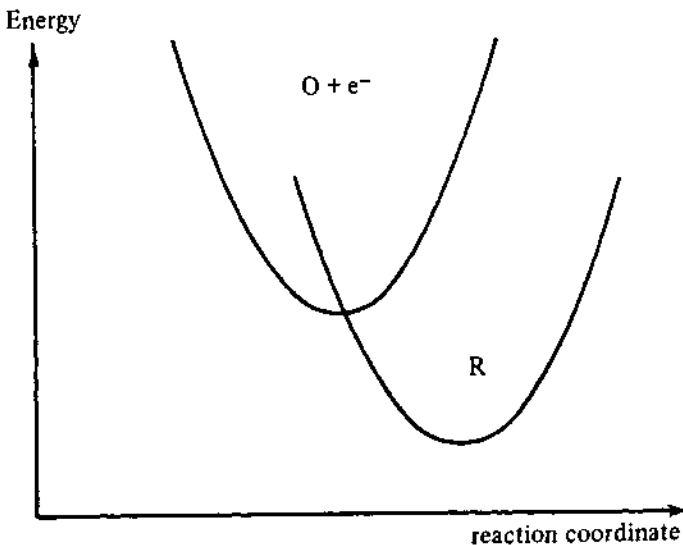


Fig. 3.9 – At high overpotentials the activation energy in one direction is predicted to fall to zero, as shown in the figure. At higher overpotentials the model of intersecting energy curves predicts that the rate will fall again as the point of intersection moves up the left hand side of upper energy curve. This gives rise to a maximum in the Tafel plots (see Fig. 3.8).

3.2.2 An energy diagram for the electron transfer process

The treatment of electron transfer so far has made no distinction between metal and semiconductor electrodes, and the energy diagrams used were borrowed from the theory of chemical kinetics. A more satisfactory energy diagram can be obtained by considering in detail the electronic states in the electrode and electrolyte phases.

The electron energy levels in a solid are grouped together in delocalised energy bands which can be considered to arise from the diffraction of electron waves by the crystal lattice. The population of these energy levels is determined by the Fermi-Dirac distribution function:

$$f_{FD} = \left(1 + \exp \frac{(E - E_F)}{k_B T} \right)^{-1}. \quad (3.39)$$

Near E_F , the Fermi energy, the probability function changes over a narrow range (of the order of $k_B T$) from almost unity to near zero, so that the electrons in a metal can be considered to form a 'Fermi sea' with a maximum energy of E_F . (Note: in this section E can also stand for energy, rather than potential). On the other hand, the electronic energy levels of ions or molecules in the solution phase are localised, and the energy of an electronic state on a particular species involved in electron transfer will change rapidly with time in response to the polarisation fluctuations in the solution. It is therefore necessary to use a normal

distribution function centred on a 'most probable' energy. Since the oxidised and reduced species O and R carry a different electronic charge, they will have different most probable energies as the result of interaction with the solvent dielectric. The distribution of energies about the most probable values for the oxidised and reduced species can then be described by the normal distribution function, and the distribution functions for O and R are therefore represented on the energy diagram as bell-shaped Gaussian curves as shown in Fig. 3.10.

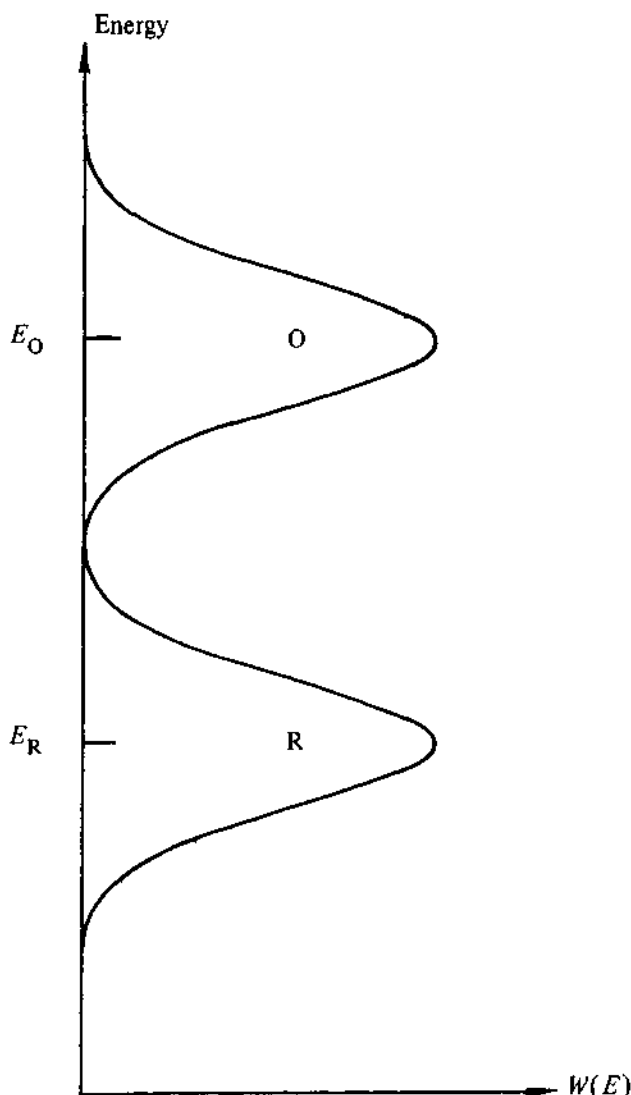


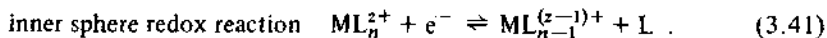
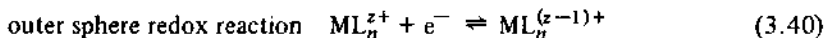
Fig. 3.10 – Temporal probability distribution for electron states of the species O and R. The distribution arises from polarisation fluctuations of the solvent dielectric which cause the electron states to vary with time.

The transfer of electrons across the electrode solution interface can be illustrated on this type of energy diagram as a horizontal movement; electrons are free to move from occupied orbitals on one side of the interface provided that vacant electron states exist at the same energy level on the other side of the interface. At equilibrium, the rates of the forward and reverse electron transfer events must be equal, suggesting that the distribution functions for O and R are situated symmetrically about the Fermi energy in the metal, since in this case the number of occupied states in R that lie above the Fermi level in the metal exactly equals the number of vacant states in O which lie below it.

The diagram shown in Fig. 3.10 is now widely used to describe electron transfer processes at electrodes, and it has the merit that it can be extended readily to the discussion of electron transfer at semiconductor and insulator electrodes [16]. The theoretical basis for the diagram is to be found in the fluctuating energy level model of electron transfer which has been discussed by Marcus [12, 13], Gerischer [17-19], Levich [20], and Dogonadze [21].

3.2.3 The fluctuating energy level model of electron transfer

The first derivation of electron transfer rates by this model was a classical calculation by Marcus [12, 13]. Later Dogonadze et al. [21] and Christov [22] have discussed a quantum mechanical analysis which shows that the ions can be treated satisfactorily by a semi-classical approximation. Gerischer [17-19] has also developed a similar model and applied it to describe electron transfer at semiconductor as well as metal electrodes. The essential element in each of these theories is that the non-equilibrium transition state is assumed to be reached by thermal fluctuations of the solvent dielectric (and ligands) surrounding the reacting species. It should be pointed out that this assumption, although widely accepted, is not without its critics. In particular, Bockris & Khan [23] have drawn attention to a number of fundamental objections to the model, including its failure to take into account the role of the ionic atmosphere in the activation step preceding electron transfer. It is also important to point out that the fluctuating energy level model was developed to describe electron transfer processes in which no chemical bonds are broken or formed. Reactions involving changes in the coordination sphere of metal ions (so-called 'inner sphere' reactions) are excluded, so that the theory is restricted to so-called 'outer sphere' reactions where only changes in the outer solvation sphere occur.



In spite of these limitations, there has been an increasing tendency to apply the qualitative aspects of the theory, such as the energy diagrams, to more complex electrode processes, but it seems unlikely that extensions of the model will lead to a correct understanding, even at the intuitive level, of the activation step in such electrode processes.

The treatments of electron transfer processes by Marcus and by Levich and Dogonadze recognize that the behaviour of the system can be described by using the Born-Oppenheimer approximation to separate the Hamiltonian into two parts:

$$\mathcal{H}\psi_e = U \sum \psi_e \quad (\text{electrons}) \quad (3.42\text{a})$$

$$\mathcal{H}\psi_n = U \sum \psi_n \quad (\text{nuclei}) . \quad (3.42\text{b})$$

The slow subsystem, consisting of the reactant and product and their surroundings (solvent molecules, ligands, other ions, etc.), is adequately represented by the semi-classical approximation, whereas the electrons, of course, must be treated by quantum mechanics. A detailed discussion of these aspects of electron transfer theory has been given by Schmidt [24].

The 'classical' theory of electron transfer developed by Marcus starts with the same kind of 'hard spheres in a dielectric continuum' model that is used to derive the free energy of solvation of an ion. A central role in the theory is played by the *reorganisation energy* λ , which in its simplest definition is given by

$$\lambda = \frac{e^2}{8\pi\epsilon_0 a} \left(\frac{1}{\epsilon_{\text{opt}}} - \frac{1}{\epsilon_{\text{stat}}} \right) \quad (3.43)$$

where ϵ_{opt} and ϵ_{stat} are the values of the optical and static relative permittivities and a is the radius of the ion. A more general expression for λ includes contributions from the ligands in the inner coordination sphere of the ion (see, e.g. [25]).

The central assumption of the theory is that small fluctuations in the dielectric ($\approx k_B T$) can lead to large perturbations in the electronic energy levels. The mean square fluctuation is related to the thermal energy by

$$(E - E_t)^2 = 4\lambda k_B T \quad (3.44)$$

where $(E - E_t)$ represents the deviation from the mean value of the energy (here, of course, the E 's refer to energies, not potentials). For an ion with a radius of 0.3 nm, Equation (3.43) predicts that the reorganization energy, λ , is of the order of 1 eV. The mean square fluctuations of the electronic energy levels are therefore 0.3 eV or more, compared to a value of $k_B T \approx 0.025$ eV at room temperature.

The distribution of energies about the most probable value has already been discussed briefly (see Fig. 3.10). It is described by the normal distribution

$$W(E) = [4\pi\lambda k_B T]^{-1/2} \exp - [(E_{\text{ox}} - E)^2 / 4\lambda k_B T] \quad (3.45)$$

(for the reduced species, E_{ox} is replaced by E_{red}).

The differing polarisation of the dielectric for the oxidised and reduced species leads to a splitting of the energy levels given by

$$E_{\text{ox}} - E_{\text{red}} = 2\lambda . \quad (3.46)$$

The *standard redox Fermi level* is then defined as

$$E_{\text{redox}}^{\ominus} = \frac{1}{2} (E_{\text{ox}} - E_{\text{red}}) . \quad (3.47)$$

The Fermi level is introduced at this point since it is used to describe the population of energy levels by electrons, Equation (3.39). Fig. 3.11 shows the distribution functions for the oxidised and reduced species for a system where $\lambda = 0.25 \text{ eV}$.

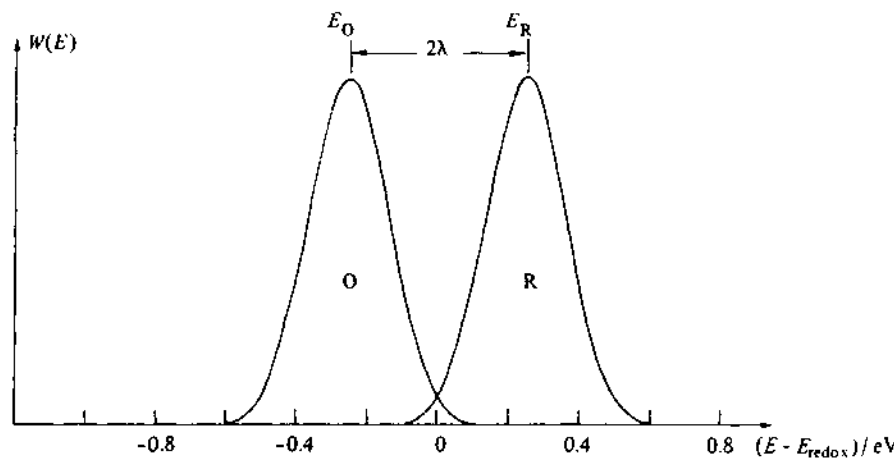


Fig. 3.11 – Energy level distribution calculated from Equation (3.45) for the case where the reorganisation energy $\lambda = 10k_B T$ (0.25 eV at room temperature).

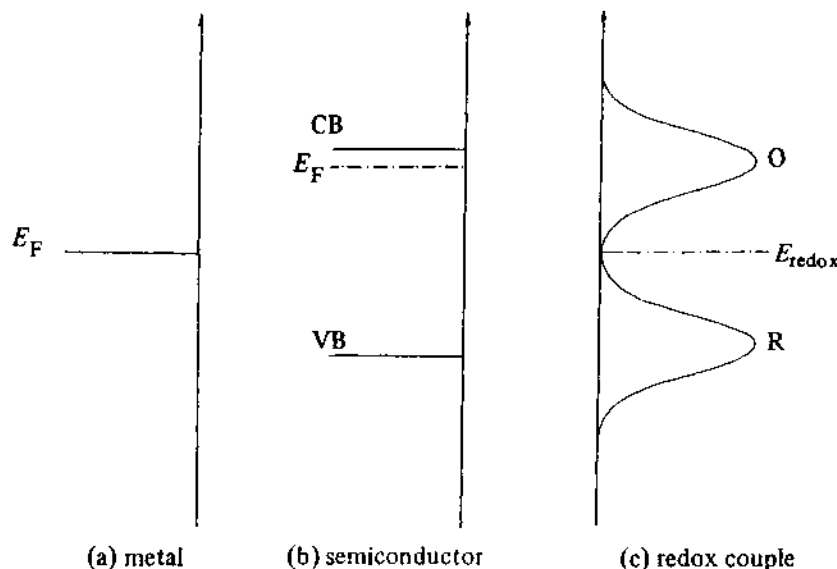


Fig. 3.12 – Energy level diagrams for (a) metals, (b) semiconductors, and (c) redox electrolyte systems.

It is important to remember that these distribution curves represent *temporal* fluctuations of the electronic energy levels; there is a temptation to consider them as energy bands of the type found in solids, but their meaning and origin is quite different. The electron energy levels in metals, semiconductors, and redox systems are contrasted in Fig. 3.12.

The conditions for equilibrium given earlier (see Equations (3.6) and (3.13)) have their equivalent in the present description: The Fermi energy E_F , which determines the probability that an energy level is occupied by an electron, must be the same in the electrode and solution phases at equilibrium, i.e.

$$E_F(\text{electrode}) = E_{\text{redox}} \quad (3.48)$$

This is a thermodynamic definition of equilibrium equivalent to Equation (3.6). The kinetic definition of equilibrium follows from considering the overlap of occupied and vacant states in the solid and in the redox electrolyte. Fig. 3.13 shows a magnified plot of the energy distribution functions near E_F . In the case of a metal electrode, the states involved in electron transfer at equilibrium are in the exponential tails of the distribution functions $W(E)$ for the oxidised and reduced species, and as a consequence electron transfer involves states which are close (within a few $k_B T$) of E_F . In the case of a semiconductor or insulator electrode, on the other hand, the density of electron levels in the solid is zero at

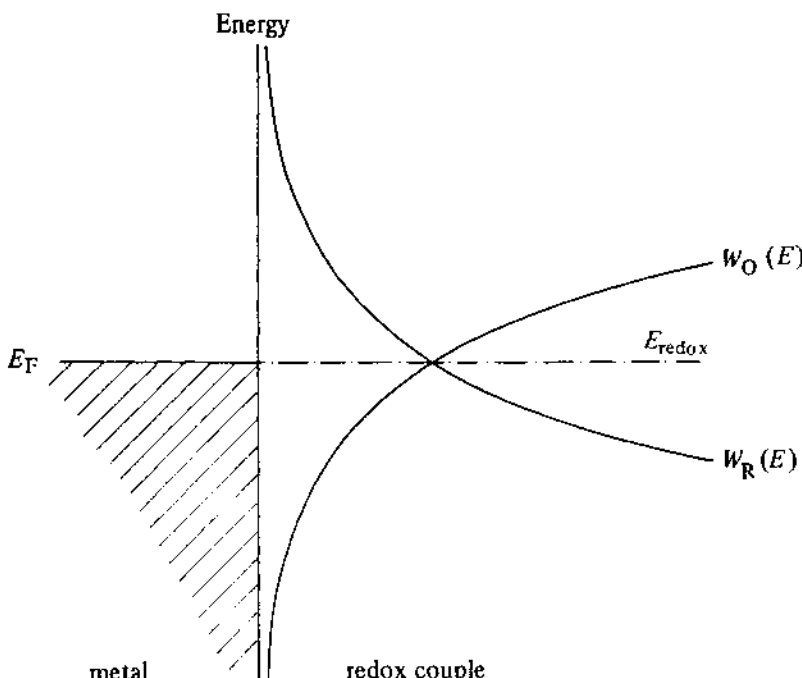


Fig. 3.13 – Magnified plot of the distribution function for the redox electrolyte near E_{redox} showing overlap with electron states in the metal (at equilibrium $E_F = E_{\text{redox}}$).

E_F (unless the material is a degenerate semiconductor). Electron transfer therefore involves states in the O and R distribution envelopes that overlap with the valence or conduction bands. This contrasting situation is illustrated in Fig. 3.14.

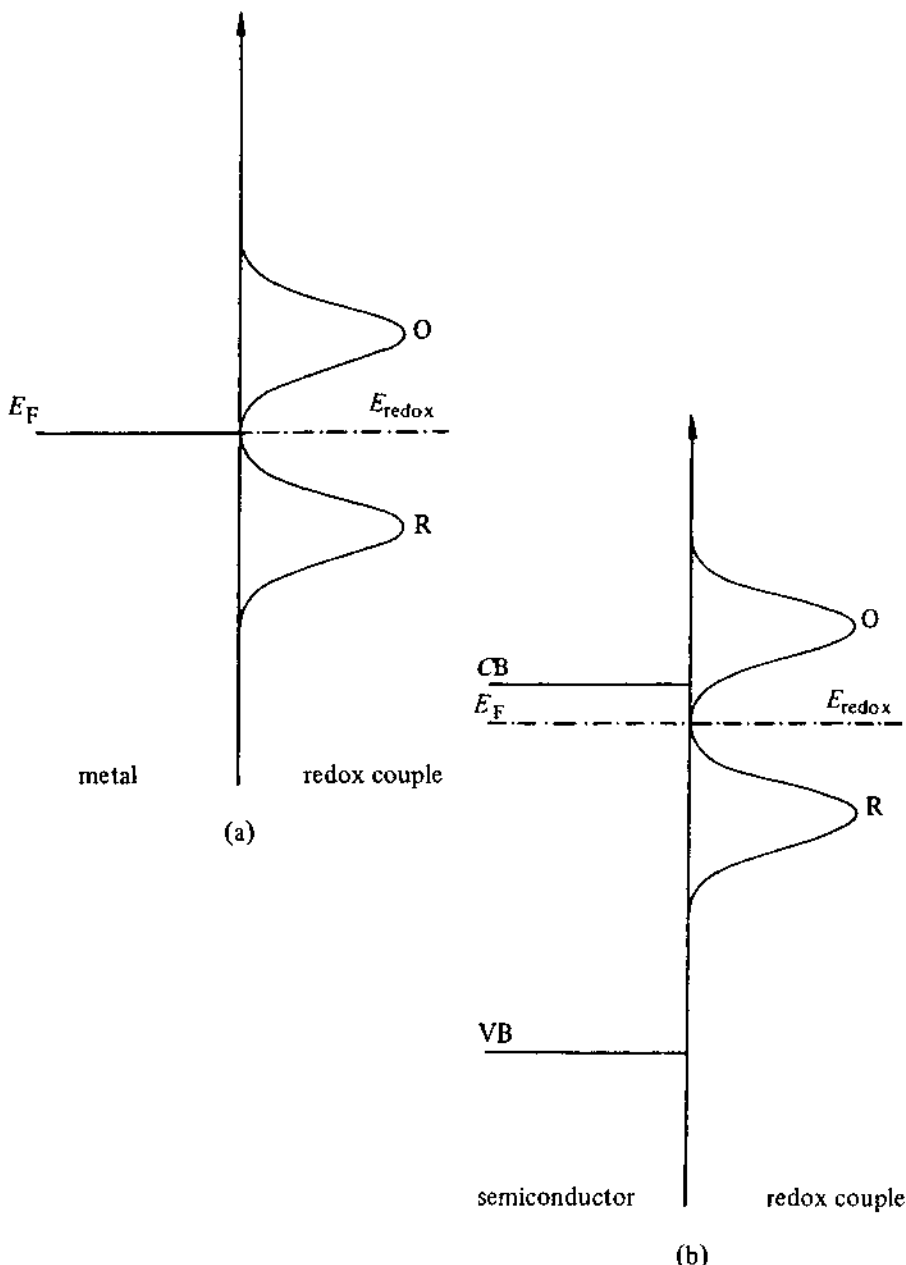


Fig. 3.14 – Comparison of overlap of electron levels at (a) metal and (b) semiconductor electrodes. The figure shows that electron transfer occurs near E_F in the case of the metal, whereas for semiconductors overlap is restricted to the conduction and valence bands since E_F lies in the forbidden gap.

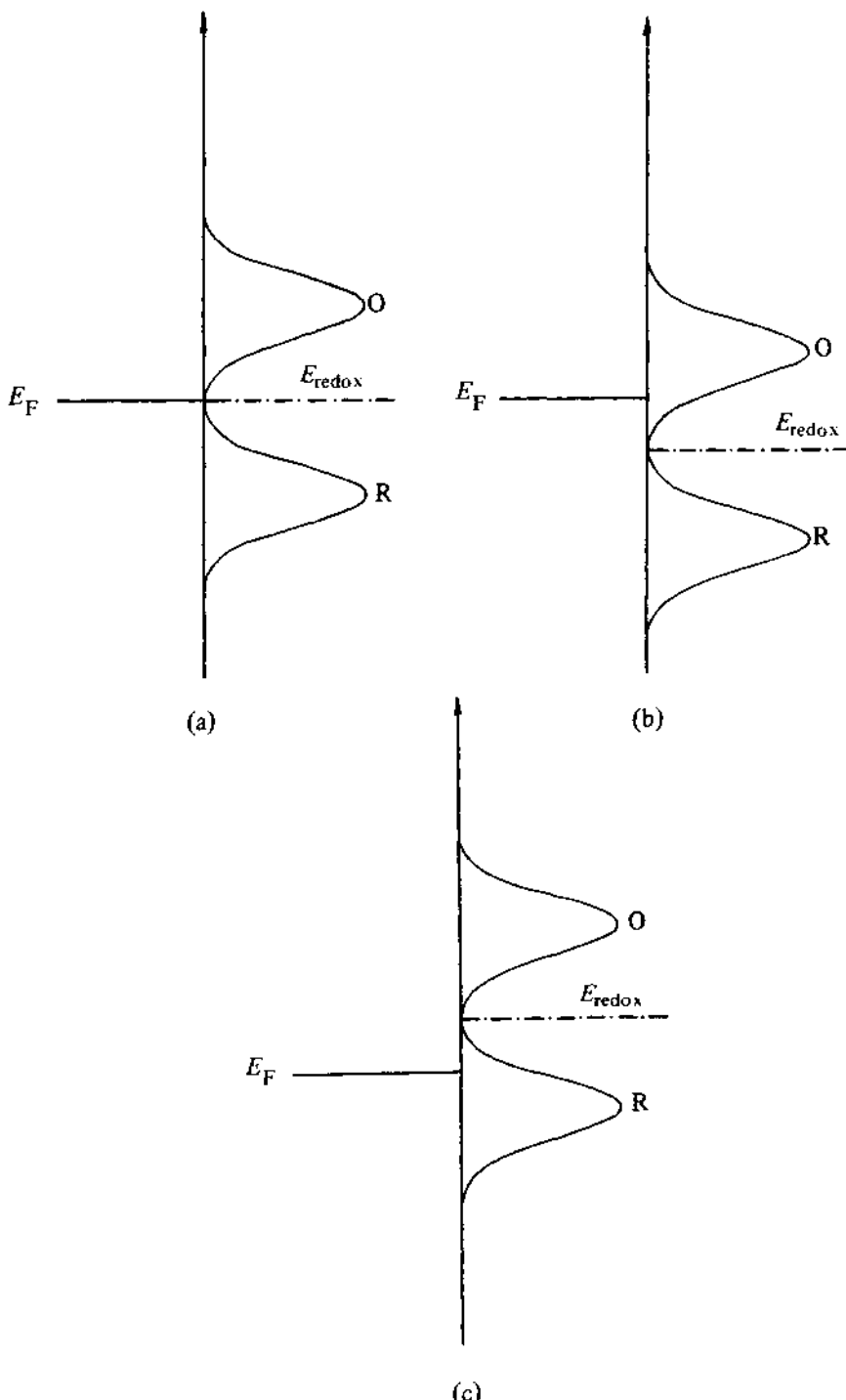


Fig. 3.15 – Shifts of electron energy levels at the metal/electrolyte interface brought about by change in electrode potential. (a) at equilibrium, (b) net cathodic current ($E < E_e$), (c) net anodic current ($E > E_e$).

The influence of electrode potential on electron transfer processes at metal electrodes can be understood with the help of the energy diagrams shown in Fig. 3.15. The relative positions of the electron energy levels in the solution and in the metal are affected by changes in the potential difference across the interface, and the corresponding changes in the overlap of the distribution functions results in either net anodic or cathodic current flow. Exact evaluation of the overlap integrals (assuming that the reorganisation energies for the oxidised and reduced species are the same) leads to the following expression for the current density.

$$I = |e|Z \left[c_R^\infty \exp\left(-\frac{[\lambda + k_B T \ln(c_R^\infty/c_O^\infty) - \eta|e|]^2}{4\lambda k_B T}\right) - c_O^\infty \exp\left(-\frac{[\lambda - k_B T \ln(c_O^\infty/c_R^\infty) + \eta|e|]^2}{4\lambda k_B T}\right) \right] \quad (3.49)$$

(Here $k_B T$ and $|e|$ are used instead of RT and F , since λ is given in electron volts). For $\lambda \gg \eta|e|$ and $\lambda \gg k_B T \ln(c_O^\infty/c_R^\infty)$ Equation (3.49) reduces to

$$I = |e|Z(c_R^\infty)^{1/2}(c_O^\infty)^{1/2} \exp(-\lambda/4k_B T) \left[\exp\left(\frac{|e|\eta}{2k_B T}\right) - \exp\left(-\frac{|e|\eta}{2k_B T}\right) \right] \quad (3.50)$$

or

$$I = I_0 \left[\exp\left(\frac{1}{2}\eta F/RT\right) - \exp\left(-\frac{1}{2}\eta F/RT\right) \right] \quad (3.51)$$

the familiar Butler-Volmer equation where $\alpha_A = \alpha_C = 0.5$. Here I_0 is given by

$$I_0 = |e|Z(c_R^\infty)^{1/2}(c_O^\infty)^{1/2}(\exp -\lambda/4k_B T) \quad (3.52)$$

Comparison of this result with the expressions derived from absolute rate theory establishes the identity

$$\frac{\lambda}{4} = {}^\ominus \Delta G^\ddagger \quad (3.53)$$

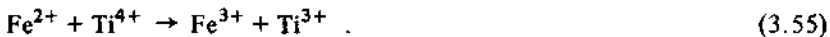
The results of the fluctuation model are therefore formally equivalent to the expressions obtained from absolute rate theory using parabolic energy curves with identical force constants.

3.3 COMPARISON BETWEEN HETEROGENEOUS AND HOMOGENEOUS ELECTRON TRANSFER

The theory outlined here has also been developed to describe homogeneous electron transfer processes. The simplest outer sphere reactions that can be considered involve different oxidation states of the same molecule, e.g.



but the theory also applies to reactions between different ions, e.g.



The application of the fluctuating energy level model to the symmetrical reaction (Equation (3.54)) is of particular interest since it suggests that it should be possible to compare heterogeneous and homogeneous rate constants. The expressions for the rate constant in each case are

$$k^\Theta = Z_{\text{het}} \exp(-\lambda/4RT) \quad (\text{heterogeneous}) \quad (3.56)$$

$$k = Z_{\text{hom}} \exp(-\lambda/2RT) \quad (\text{homogeneous}) \quad (3.57)$$

where Z_{het} is the heterogeneous pre-exponential factor ($\sim 10^4 \text{ cm s}^{-1}$) and Z_{hom} is the homogeneous pre-exponential factor ($\sim 10^{11} \text{ mol}^{-1} \text{ dm}^3 \text{ s}^{-1}$). For simplicity, the transmission factors have been taken to be unity in both cases. Comparison of Equation (3.56) and (3.57) show that the two rate constants are related by the expression

$$k^\Theta/Z_{\text{het}} = (k/Z_{\text{hom}})^{1/2} . \quad (3.58)$$

Table 3.1 shows a comparison between the experimental data for heterogeneous and the corresponding symmetrical homogeneous reactions [9].

Table 3.1 – Comparison of heterogeneous (k^Θ) and homogeneous (k) rate constants for electron transfer reactions (taken from Albery [9])

Oxidised species	$10^{-4} k^\Theta$	$10^{-11} k$
$\text{Fe}(\text{CN})_6^{3-}$	10^{-5}	10^{-3}
MnO_4^-	2×10^{-5}	2×10^{-4}
Fe^{3+}	7×10^{-7}	9×10^{-6}
V^{3+}	4×10^{-7}	4×10^{-7}
Eu^{3+}	3×10^{-8}	6×10^{-8}
$\text{Co}(\text{NH}_3)_6^{3+}$	5×10^{-12}	$< 5 \times 10^{-11}$

The agreement between the two sets of data is reasonably satisfactory. The ability of the Marcus theory to predict values of k and k^Θ has also been tested, and Table 3.2 presents a comparison made by Hale [25] of the experimental and theoretical values of the free energy of activation for electrode processes (the experimental values of ${}^\Theta\Delta G^\ddagger$ have been calculated from k^Θ using Equations (3.53) and (3.56)).

The activation energies were predicted using information about ion size (and ligand stretch frequencies where appropriate), and Table 3.2 shows that reasonable agreement with experimental values is obtained in most cases. One of the main problems in comparisons of this kind is that corrections have to be made for the

electrical work terms associated with bringing the reactant to the reaction site. In the case of heterogeneous electron transfer at a metal, a reactant ion has to move through the diffuse electrical double layer in order to approach sufficiently close to the electrode for electron transfer to occur, and the effective concentration at the reaction site therefore differs from the bulk concentration (it may be greater or smaller depending on the charge on the ion and the potential at the reaction site). For homogeneous reactions, electrical free energy terms must also be considered, even at high concentrations of inert supporting electrolyte. The corrections to experimental heterogeneous rate constants are usually made using the simple equations proposed by Frumkin (these are dealt with in Chapter 5), but these are unlikely to be satisfactory at high concentrations of background electrolyte. At the same time the contribution of the ionic atmosphere to the activation step must become increasingly important at high concentrations, and the possibility of ion pairing must also be taken into account [26].

The most serious obstacle to the experimental verification of the Marcus-Levich-Dogonadze theory is the experimental constraint set by diffusion of reactants. The upper limit for rate constants determined by small-amplitude electrochemical techniques is of the order of $1\text{--}10 \text{ cm s}^{-1}$, and large amplitude methods such as the rotating disc electrode are no longer accurate above about 0.1 cm s^{-1} . The non-linearity in Tafel plots predicted by theory is therefore difficult to verify experimentally since the corrections for diffusion effects lead to a rapid increase in error limits as the overpotential is increased. Novel techniques, for example, using microelectrodes [27] promise to extend the range of rate constants accessible, making possible a more satisfactory comparison of theory and experiment.

Table 3.2 – Comparison of experimental and theoretical values of the standard free energy of activation of electrode processes (taken from Hale [25])

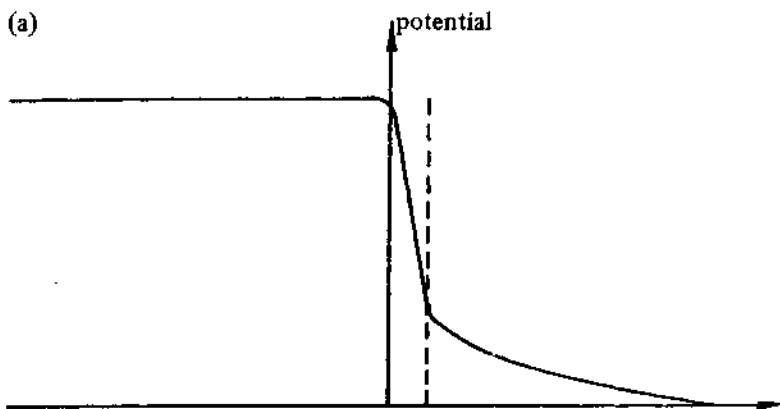
Oxidised species	$k^\ominus/\text{cm s}^{-1}$	${}^\ominus\Delta G^\ddagger_{\text{exp}}/\text{eV}$	${}^\ominus\Delta G^\ddagger_{\text{theory}}/\text{eV}$
$\text{Fe}(\text{CN})_6^{3-}$	9×10^{-2}	0.299	0.310
MnO_4^-	1×10^{-2}	0.355	0.386
WO_4^{2-}	1×10^{-2}	0.355	0.376
$\text{V}(\text{H}_2\text{O})_6^{3+}$	4×10^{-3}	0.379	0.389
$\text{Cr}(\text{H}_2\text{O})_6^{3+}$	1.4×10^{-5}	0.541	0.432
Anthracene	4	0.2	0.223

3.4 COMPARISON OF ELECTRON TRANSFER AT METAL AND SEMICONDUCTOR ELECTRODES

The theories of electron transfer at metal electrodes identify the free energies of activation ΔG^\ddagger and ΔG^\ddagger as being potential dependent quantities. The reason for this is that the potential drop between the solid and solution phases is located largely in a narrow region at the interface (the Helmholtz layer, see

Chapter 5). Changes in electrode potential therefore displace the energies of the reactant and product systems with respect to each other, bringing about corresponding changes in $\Delta\vec{G}^{\ddagger}$ and $\Delta\vec{G}^{\ddagger\ddagger}$. The situation in the case of semiconductor electrodes is different. The total potential difference between the bulk of the semiconductor and the electrolyte phase can be distributed in different ways that depend on the electrode potential and on the conductivity of the solid. If the majority carriers (electrons for an *n*-type semiconductor, holes for a *p*-type semiconductor) are drawn into the surface region by the electrical field, an *accumulation region* is formed, and the semiconductor electrode behaves essentially like a metal. On the other hand, if majority carriers are withdrawn from the surface region, a *depletion region* is formed in the semiconductor. The space-charge associated with ionised donor (or acceptor) states in the depletion region gives rise to a potential drop which is located almost entirely in the semiconductor. Changes in electrode potential then affect only

(a)



charge

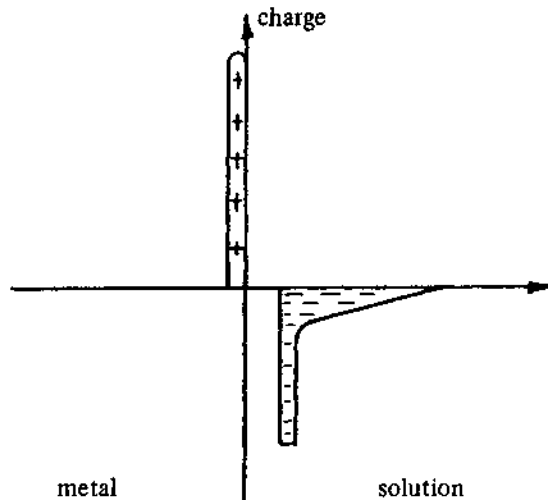


Fig. 3.16 – see legend next page

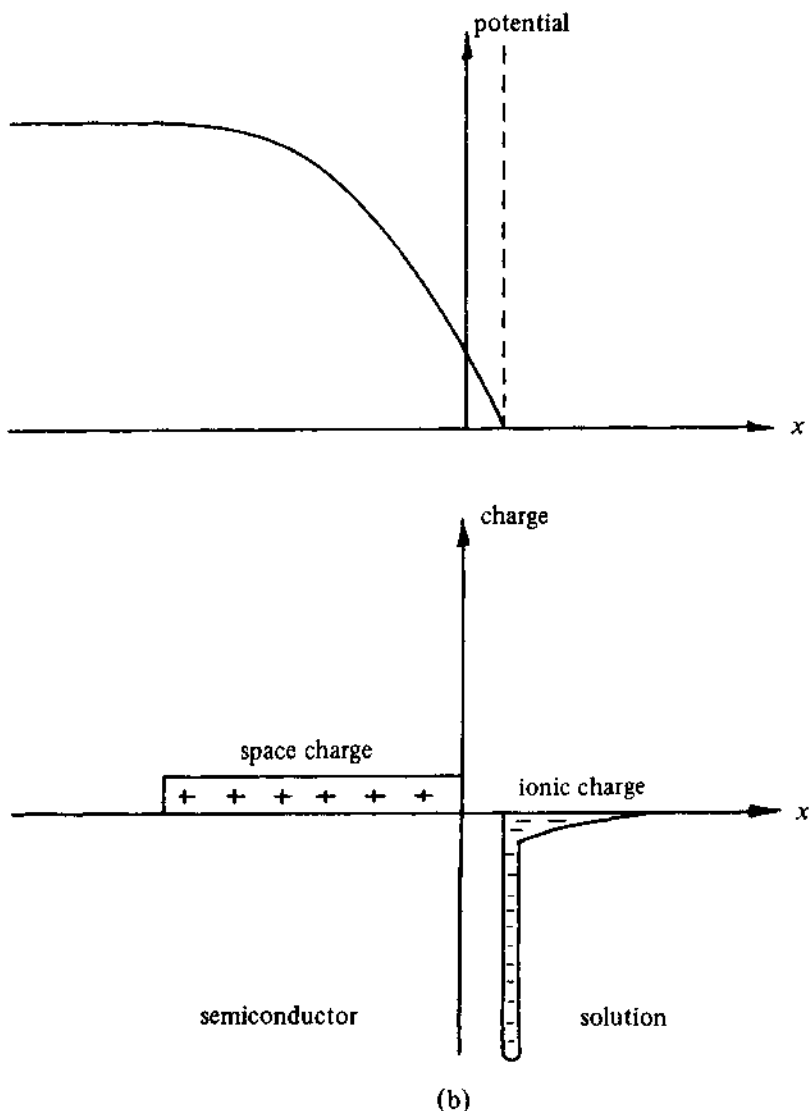


Fig. 3.16 – Comparison of charge and potential distributions at (a) metal and (b) semiconductor electrodes. The profiles shown for the semiconductor apply under depletion conditions, where a space charge region is formed.

the width of the space charge region (typically 10^{-5} cm) and the density of majority carriers at the surface. $\bar{\Delta}G^+$ and $\bar{\Delta}G^+$ are potential independent quantities under these conditions since the potential drop between the surface of the semiconductor and the electrolyte phase is insensitive to changes in electrode potential. The different distributions of charge and potential at metal and semiconductor electrodes are contrasted in Fig. 3.16. The variation of electron

transfer rate with electrode potential is determined in the case of a semiconductor electrode by the density of majority carriers at the surface, which under depletion conditions is described by the Boltzmann relationship.

$$n_s = n_0 \exp(-|e|\Delta\phi_{sc}/k_B T) . \quad (3.59)$$

Here n_s is the surface electron density (or hole density for a p-type semiconductor), n_0 is the bulk electron density, and $\Delta\phi_{sc}$ is the potential drop in the semiconductor. The potential drop in the semiconductor is zero at the *flatband potential* E_{FB} , so that Equation (3.59) can be written in terms of the electrode potential as

$$n_s = n_0 \exp - \left(\frac{|e|(E - E_{FB})}{k_B T} \right) . \quad (3.60)$$

Since the rate of an electrochemical reaction will depend on n_s , Equation (3.60) shows that the apparent cathodic transfer coefficient will approach 1.

Under depletion conditions, the energy levels in the semiconductor are no longer independent of distance from the interface; instead they follow the potential profile as shown in Fig. 3.17.

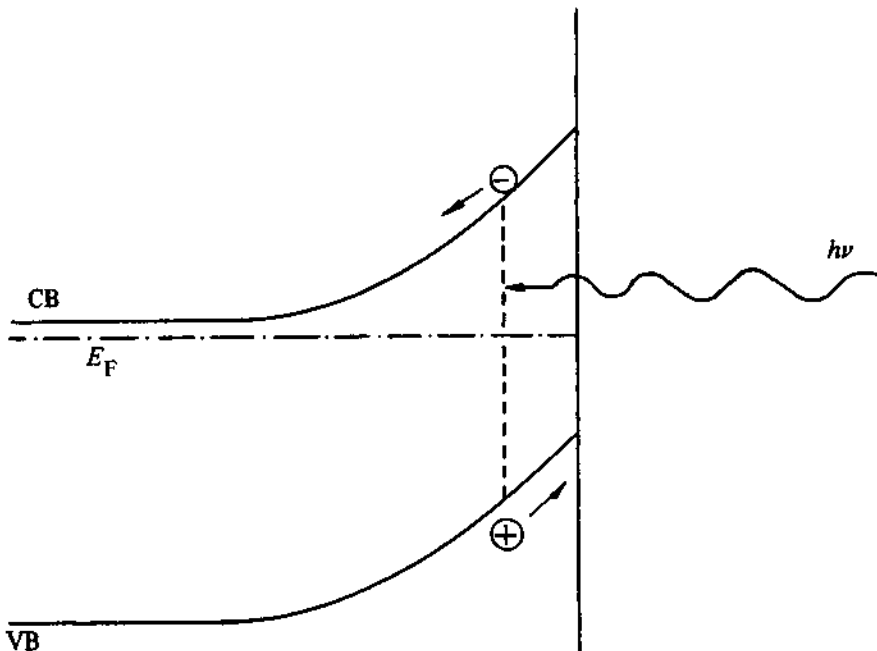


Fig. 3.17 – ‘Band bending’ due to space charge region in semiconductor (n-type). The figure shows that illumination will generate an electron-hole pair that is separated by the electric field, the electron moving into the neutral region and the hole moving towards the interface.

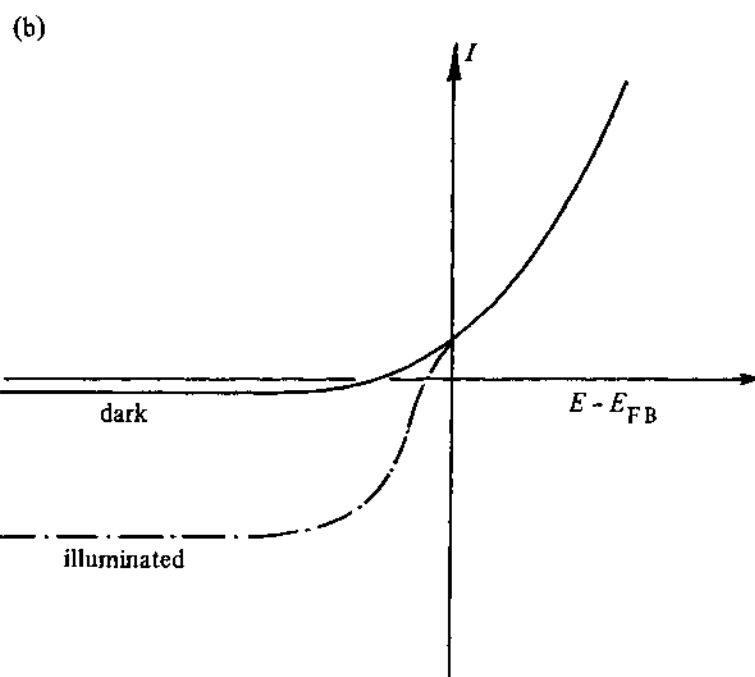
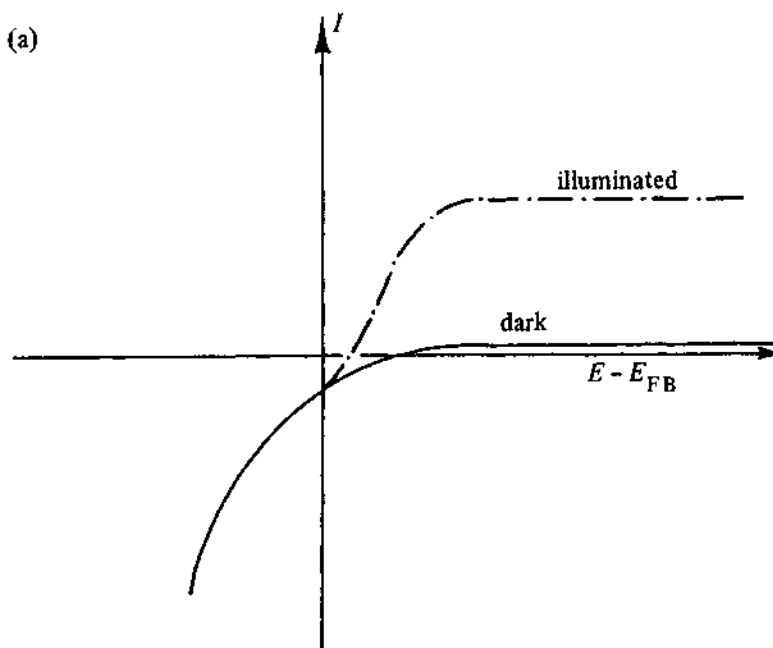
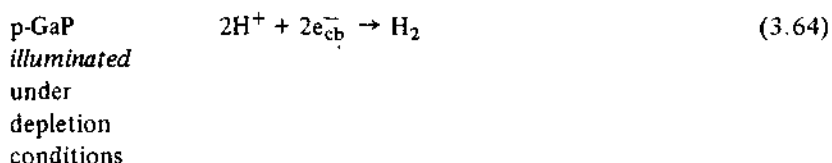
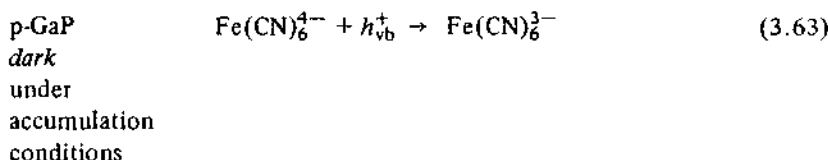
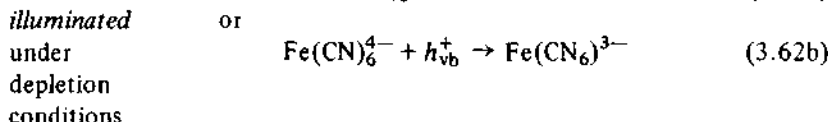
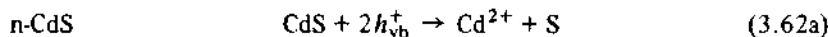
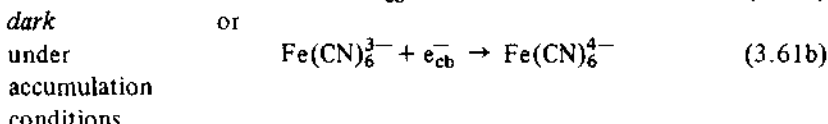
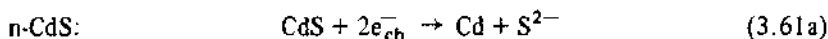


Fig. 3.18 – Current voltage plots for semiconductor/electrolyte junctions in the dark and under illumination (a) n-type, (b) p-type. The photocurrent is linearly proportional to the absorbed photon flux in the saturation region.

A further difference between metal and semiconductor electrodes is that electron transfer at semiconductors can involve minority carriers generated by light, and while in the dark only small currents flow when a depletion layer is formed at the semiconductor solution interface, illumination of the electrode gives rise to much larger photocurrents. The current-voltage curves for semiconductor electrodes are therefore not only dependent on whether the semiconductor is n- or p-type but also on whether the electrode is in the dark or illuminated with light of sufficient energy to promote electrons from the valence band to the conduction band. Instead of the symmetrical Butler-Volmer plots obtained for metal electrodes, essentially diode-like behaviour is expected for extrinsic semiconductor electrodes, as shown in Fig. 3.18.

The electron transfer reactions involved are illustrated by the following examples for n- and p-type semiconductors:



A proper treatment of electron transfer at semiconductor electrodes is beyond the scope of this chapter, but further details can be found, for example, in books by Morrison [16] and Myamlin & Pleskov [28].

It is clear that there are important differences between electron transfer processes at metal and at semiconductor electrodes, and these have been summarised in Table 3.3.

Table 3.3 – Comparison of electron transfer processes at metal and semiconductor electrodes

Metal	Semiconductor
$\Delta\tilde{G}^{\ddagger}$ and $\Delta\tilde{G}^{\ddagger}$ depend on potential	ΔG^{\ddagger} independent of potential under depletion conditions
potential drop located in the Helmholtz layer	potential drop located largely in the semiconductor under depletion conditions
electron transfer occurs near E_F	electron transfer involves the conduction and valance bands (no electron states near E_F)
only small effects of illumination (e.g. photoemission)	illumination can give large photocurrents due to minority carriers

3.5 MULTISTEP ELECTRODE REACTIONS

So far this chapter has been devoted largely to the consideration of simple electron transfer processes in which the chemical environment of the central ion remains essentially unchanged. It is important to make it clear at this point that many electrode processes are more complicated since they involve the formation and rupture of chemical bonds. Electrode reactions are then multistep processes involving a sequence of events, each with characteristic activation energies. Coupled chemical steps may precede or follow electron transfer, or they may occur between two successive electron transfers, e.g. in the ece reaction scheme discussed in Chapters 2 and 6. If the activation energies of chemical steps are unaffected by changes in electrode potential, the formal kinetic treatment of the multistep reaction is straightforward, and well-established diagnostic criteria can be used to deduce mechanistic details from experimental data. Many electrode reactions, however, involve bond formation with the electrode. For example, metal deposition and metal corrosion reactions result in the transfer of atoms as well as electrons between the electrolyte and electrode phases, and the influence of the Galvani potential difference on such a complex process is not clear. In such cases, the cathodic transfer coefficient can deviate considerably from 0.5, reflecting the complex nature of the electrode process. Reactions involving adsorbed intermediates are also common, and the discussion of the hydrogen evolution reaction in Chapter 7 illustrates how the Tafel slopes can be used to deduce the reaction mechanism in such cases.

Many multistep electrode processes involve the transfer of more than one electron, and it seems reasonable to suppose that the most favourable reaction pathway will involve successive rather than simultaneous transfer of electrons. For example, the reaction



involves two discrete electron transfer steps:



In this particular case, the stability of the Cu(I) intermediate depends strongly on the nature of the electrolyte. In the presence of chloride the reaction gives rise to two distinct waves in a current/potential curve, whereas in the absence of complexing ions a single two-electron process appears to occur. Studies with the ring-disc electrode [29] have established, however, that Cu(I) is formed as an intermediate with a measurable lifetime. The existence of lower valent intermediates in other metal ion electrode processes is more controversial, but it seems improbable, for example, that the reduction of Zn²⁺ involves simultaneous transfer of two electrons.

In some electrode reactions it may be appropriate to consider that *partial* charge transfer occurs. In the case of the underpotential deposition of metals, the electrode process leads to the formation of a monolayer or sub-monolayer of metal atoms which interact with the substrate. In the one extreme, the metal-metal bond may have considerable ionic character, so that the reaction approaches ion adsorption, whereas at the other limit an essentially electro-neutral surface atom is formed. These complex electrode processes have been discussed extensively in recent years, and the concept of the electrosorption valency [30] has emerged as a way of describing the nature of the underpotential deposit.

It is clear from this concluding discussion that the theory of simple electrode reactions must be modified considerably to deal with the majority of electrode processes. From the experimental point of view, it is important to measure the anodic and cathodic Tafel slopes as well as the reaction order with respect to all possible reactants (including the supporting electrolyte and the solvent). At the same time, non-electrochemical methods such as infrared and Raman spectroscopy [31, 32] can provide direct molecular information which is essential for the proper understanding of electrode processes.

REFERENCES

- [1] J. Tafel, *Z. physik. Chem.*, **50** (1905) 641.
- [2] J. A. V. Butler, *Trans. Faraday Soc.*, **19** (1924) 734.
- [3] T. Erdey Gruz & M. Volmer, *Z. physik. Chem.*, **150A** (1930) 203.
- [4] K. J. Vetter, *Electrochemical kinetics*, Academic Press, 1967.
- [5] J. O'M Bockris & A. N. Reddy, *Modern electrochemistry*, Plenum Press, 1967.
- [6] J. Koryta, J. Dvorák, & V. Bohácková, *Electrochemistry*, Methuen, 1970.
- [7] B. E. Conway, *Theory and principles of electrode processes*, Ronald Press, (1965).
- [8] P. Delahay, *Double layer and electrode kinetics*, Wiley Interscience, 1965.
- [9] W. J. Albery, *Electrode kinetics*, Clarendon Press, 1975.

- [10] H. Eyring, D. Henderson, & W. Jost (Eds), *Physical chemistry*, Vols. 9A and 9B, Academic Press, 1970.
- [11] J. O'M Bockris & A. N. Reddy, *Modern electrochemistry*, Vol. 1, p. 16, Plenum Press, 1970.
- [12] R. A. Marcus, *J. Phys. Chem.*, **67** (1963) 853.
- [13] R. A. Marcus, *J. Chem. Phys.*, **43** (1965) 679.
- [14] A. N. Frumkin, D. A. Petrii, & N. N. Nickolaeva-Fedorovich, *Electrochim. Acta*, **8** (1963) 177.
- [15] R. Parsons & E. Passeron, *J. Electroanal. Chem.*, **12** (1966) 524.
- [16] S. R. Morrison, *Electrochemistry at semiconductor and oxidised metal electrodes*, Plenum Press, 1980.
- [17] H. Gerischer, *Z. phys. Chem. (Frankfurt)*, **26** (1960) 223.
- [18] H. Gerischer, *Z. phys. Chem. (Frankfurt)*, **27** (1961) 40.
- [19] H. Gerischer, *Z. phys. Chem. (Frankfurt)*, **27** (1961) 48.
- [20] V. G. Levich, *Advances in Electrochem. and Electrochem. Engineering*, **4** (1969) 249.
- [21] R. R. Dogonadze in *Reactions of molecules at electrodes*, (Ed) N. S. Hush, p. 135, Wiley Interscience, 1971.
- [22] S. G. Christov, *Ber. Bunsenges. Phys. Chem.*, **79** (1975) 357.
- [23] J. O'M Bockris & S. U. M. Khan, *Quantum electrochemistry*, Plenum Press, 1979.
- [24] P. P. Schmidt in *Specialist periodical report on electrochemistry*, Vol. 5, Chemical Society, 1975.
- [25] J. M. Hale in *Reaction of molecules at electrodes*, (Ed) N. S. Hush, p. 229, Wiley, Interscience, 1971.
- [26] L. M. Peter, W. Dürr, P. Bindra, & H. Gerischer, *J. Electroanal. Chem.*, **71** (1976) 31.
- [27] M. Wightman, *Anal. Chem.*, **53** (1981) 1125A.
- [28] V. A. Myamlin & Yu. V. Pleskov, *Electrochemistry of semiconductors*, Plenum Press, 1967.
- [29] W. J. Albery & M. L. Hitchman, *Ring-disc electrodes*, p. 78 Clarendon Press, 1971.
- [30] D. M. Kolb, *Adv. Electrochem. Electrochem. Eng.*, **11** (1978) 125.
- [31] A. Bewick, *J. Electroanal. Chem.*, **150** (1983) 481.
- [32] M. Fleischmann, P. Graves, I. R. Hill & J. Robinson, *J. Electroanal. Chem.*, **150** (1983) 33.

4

Convective diffusion systems – the rotating disc and ring-disc electrodes

Convection is defined as the transport of species due to external mechanical forces. In electrochemical systems, it can arise from the movement of the electrode (as with the expanding Hg surface in a dropping mercury electrode or by vibration or rotation of the electrode), agitation of the solution (e.g. with a gas or a stirrer or ultrasonically), or flowing the solution past the electrode surface. In each case, a complete description of the convection requires the solution of a three-dimensional hydrodynamic problem to give in, for example, Cartesian coordinates the components of the velocity of the solution in the directions x , y , and z , i.e. V_x , V_y , and V_z . Convection is, however, only effective in bringing about changes in concentration where there is already a concentration gradient; then the change in concentration of any species due to convection is given by

$$-\frac{\partial c}{\partial t} = V_x \frac{\partial c}{\partial x} + V_y \frac{\partial c}{\partial y} + V_z \frac{\partial c}{\partial z}, \quad (4.1)$$

and this change is superimposed on that due to diffusion. Hence, the total change in concentration with time is given by

$$\frac{\partial c}{\partial t} = D \left[\frac{\partial^2 c}{\partial x^2} + \frac{\partial^2 c}{\partial y^2} + \frac{\partial^2 c}{\partial z^2} \right] - \left[V_x \frac{\partial c}{\partial x} + V_y \frac{\partial c}{\partial y} + V_z \frac{\partial c}{\partial z} \right]. \quad (4.2)$$

In electrochemistry the concentration gradients always occur in the boundary layer close to the electrode surface.

It should be emphasised that when convection is present in a system, it is an important form of mass transport, and current densities 3–100 times greater than the steady state diffusion limited value are common.

In the study of the mechanism and kinetics of electrode reactions, an essential element in the design of an experiment is to provide a mass transport regime where the transport of species to and from the electrode surface may be controlled and varied in a known way. Methods involving convective diffusion offer an excellent way of establishing a defined and reproducible mass transport regime. In order, however, to obtain quantitative information from the experiment it must also be possible to describe exactly the convective diffusion regime in the cell, and the resulting equations must be solvable; then the consequences of changes in the rate of convection may be predicted and used for comparison with experimental data. In fact, few convective diffusion systems are amenable to exact treatment; rotating or vibrating wire electrodes are examples where the mass transport is well defined and reproducible but not calculable. On the other hand, the rotating disc electrode, the rotating ring disc electrode, the dropping mercury electrode, and flow through a channel between parallel or concentric tube electrodes, are cases where exact equations have been obtained.

The rotating disc and rotating ring disc electrodes are now the most popular systems for kinetic and mechanistic studies; particularly the rotating disc electrode, which combines an ease of construction and use with the ability to

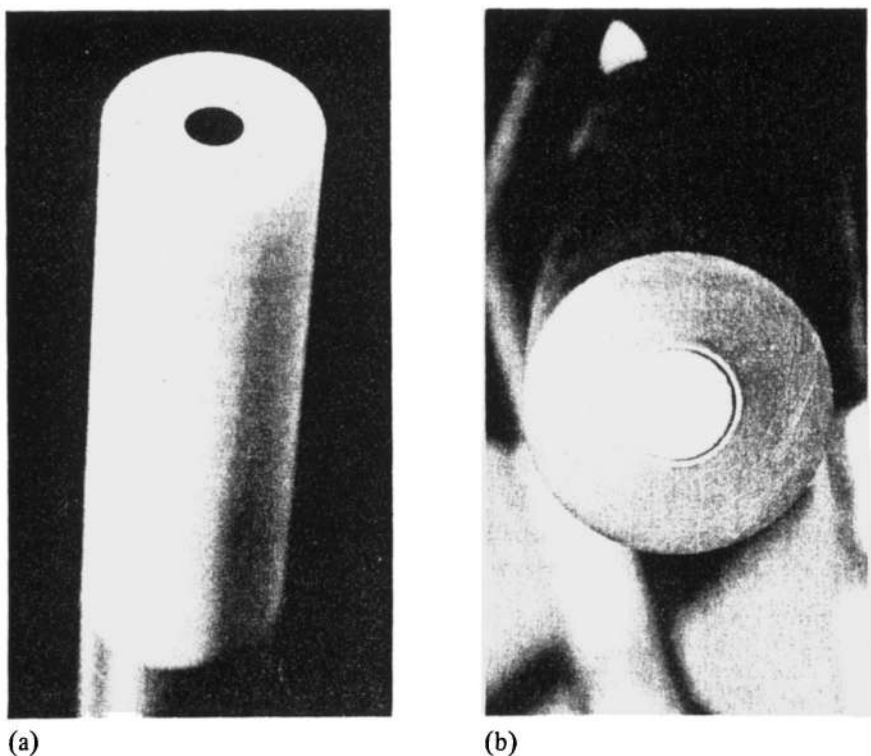


Fig. 4.1 – Photographs of (a) a rotating disc electrode, (b) a rotating ring-disc electrode.

control and vary the rate of mass transport over a very wide range. Hence much of this chapter is dedicated to the discussion of the many elegant experiments possible with such electrodes. Rotating disc and ring disc electrodes are shown in Fig. 4.1. In the former, a disc of the electrode material is surrounded by non-conducting sheath (usually polyethylene, PTFE, or epoxy resin) constructed so that the faces of the electrode and the sheath are flush and only the face of the disc electrode is exposed to the electrolyte solution; the electrode is rotated perpendicular to the face of the disc. In the ring-disc system, a similar disc is separated from a concentric ring electrode by a thin non-conducting gap.

In an industrial environment, quite different convective diffusion regimes are employed, and some common examples are illustrated in Fig. 4.2. Most commonly, the electrolyte solution is flowed through a channel between parallel electrodes or an electrode and a separator (case a), although in some cases there are turbulence promoters in the channel (case b). These introduce eddies into the flow, increasing mixing and the rate of mass transfer (see below). In bed electrodes (cases c and d) the particles perform the dual role of electrode and turbulence promoters. The last example (case e) is the rotating cylinder electrode.

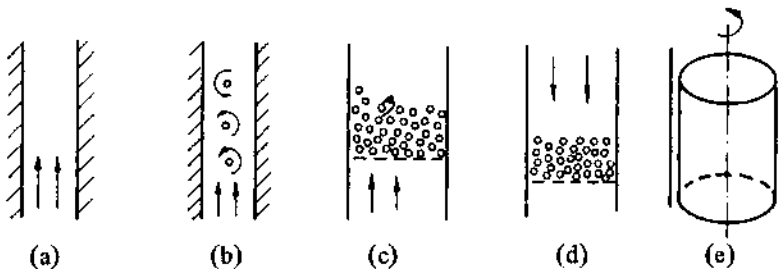


Fig. 4.2 – Convective diffusion regimes commonly found in industrial cells, (a) flow through channel formed by two parallel electrode (or by one electrode and a membrane), (b) flow through such a channel but containing a turbulence promoter (e.g. a set of non-conducting bars or a net), (c) fluidised bed electrode, (d) packed bed electrode, (e) rotating cylinder electrode within a concentric tube.

4.1 HYDRODYNAMICS OF CONVECTIVE DIFFUSION SYSTEMS

4.1.1 Hydrodynamics of the rotating disc system

When a disc electrode surrounded by a non-conducting sheath is rotated in a large volume of solution (i.e. the cell walls do not interfere with the flow pattern), a well defined flow pattern distribution is established. It is illustrated in Fig. 4.3, where it can be seen that the electrode system acts as a pump, pulling the solution vertically upwards towards the disc and then throwing it outwards.

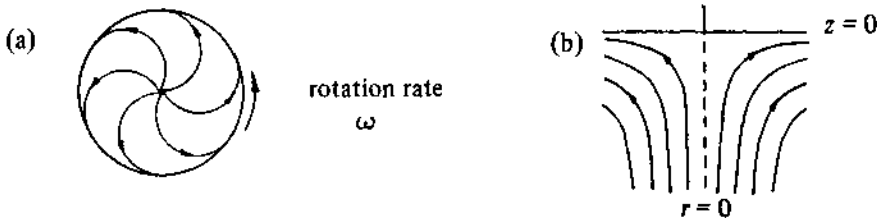


Fig. 4.3 – Flow patterns created by the rotating disc electrode (a) solution flow close to the electrode surface, viewed from below, (b) view from the side showing how the solution is pumped towards the disc, then thrown outwards.

A more quantitative discussion of the flow patterns is most appropriately carried out in cylindrical polar coordinates, see Fig. 4.4, and the solution of the problem is due to Von Karman [1] and Cochran [2] and is described in detail in the book by Levich [3]. It is, however, sufficient for our purposes to be aware of the conclusions of their solution; these are summarised in Fig. 4.5 which shows, in a dimensionless form, the way in which V_z , V_r , and V_θ vary as a function of z , the distance perpendicular to the electrode surface. Of the symbols used in the figure, r_0 is the radius of the disc electrode, ω (s^{-1}) the rotation rate of the disc and ν ($cm^2 s^{-1}$) the kinematic viscosity of the solution (viscosity/density). V_z must be zero at the electrode surface, and it increases with distance from the surface until it reaches a limiting value in the bulk solution; in fact, close to the surface V_z is proportional to z^2 . It can also be seen from the figure, firstly that the rotational movement of the solution is strongest at the surface (indeed the layer immediately adjacent to the surface will rotate at the same rate as the disc itself), but this component of the solution movement drops off quite rapidly with the distance coordinate, z . Secondly, the centrifugal motion V_r , is zero at the surface and also in the bulk, and it goes through a broad maximum a short distance away from the surface.

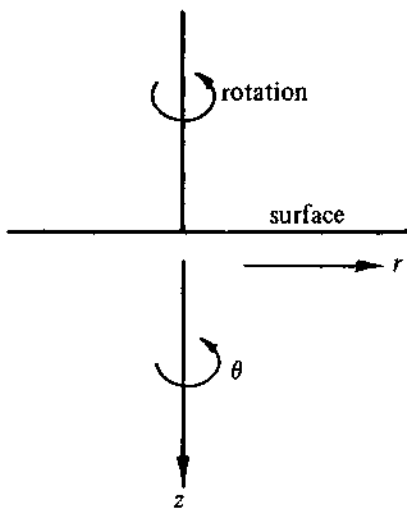


Fig. 4.4 – Cylindrical polar coordinates for the rotating disc

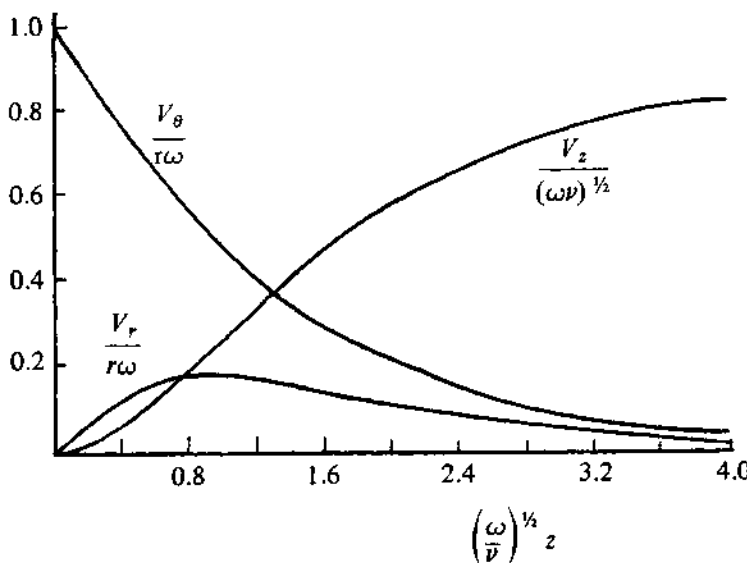


Fig. 4.5 – Dimensionless representation of the variation of the velocity components as a function of distance from the electrode surface.

Equation (4.2) may be written in cylindrical polar coordinates:

$$\frac{\partial c}{\partial t} = D \left[\frac{\partial^2 c}{\partial z^2} + \frac{\partial^2 c}{\partial r^2} + \frac{1}{r} \frac{\partial c}{\partial r} + \frac{1}{r^2} \frac{\partial^2 c}{\partial \theta^2} \right] - \left[V_r \frac{\partial c}{\partial r} + \frac{V_\theta}{r} \frac{\partial c}{\partial \theta} + V_z \frac{\partial c}{\partial z} \right] \quad (4.3)$$

but for the rotating disc electrode, this equation may be simplified considerably because

- (i) the system is totally symmetrical about the centre of the disc. Hence c is not a function of θ , and all terms in $\partial c / \partial \theta$ and $\partial^2 c / \partial \theta^2$ must be zero.
- (ii) provided the radius of the electrode is small compared to that of the sheath, V_z will be independent of r and there will be a uniform supply of material to the disc. Moreover, because of the term $(1/r)(\partial c / \partial r)$ in Equation (4.3), $\partial c / \partial r$ must be zero over the disc (at the centre of the disc, $r = 0$, $\partial c / \partial r$ must be zero, otherwise $(1/r)(\partial c / \partial r)$ will be infinite). Hence $\partial c / \partial r = \partial^2 c / \partial r^2 = 0$.
- (iii) In most experiments only the steady state current is measured and therefore we can take $\partial c / \partial t = 0$.

Making these simplifications and noting the exact solution for V_z close to the surface found by Cochran [2], i.e.

$$V_z = -0.51 \omega^{3/2} \nu^{-1/2} z^2 \quad (4.4)$$

Equation (4.3) becomes

$$\frac{\partial^2 c}{\partial z^2} = \frac{-0.51 \omega^{3/2} \nu^{-1/2}}{D} z^2 \frac{\partial c}{\partial z} . \quad (4.5)$$

Hence the theory of the rotating disc reduces to the solution of Equation (4.5) with the appropriate boundary conditions at $z = 0$ and $z = \infty$.

4.1.2 Hydrodynamics in other cell configurations

In many electrolysis cells it is the solution rather than the electrode which moves, and as an example of such systems, we shall consider briefly the flow of solution over a flat plate. As the solution flows across the plate, two forces act upon it; the first is the cause of the flow and is known as the inertial force (i.e. that generated by the pump or solution head), while the second opposes flow and results from viscous forces between the plate and the solution. Hence as the solution flows over the plate, the layer adjacent to the surface will continuously be slowed down, and the boundary layer, where the rate of flow is less than that in the bulk, will expand into the solution. This is illustrated in Fig. 4.6. The shape of the flow contours and the thickness of the boundary layer will depend on the relative importance of the forces leading to solution flow and those leading to the retardation of flow at the plate/solution interface. Because of the importance of this ratio of inertial/viscous forces, it is given a name, the Reynolds number, Re . This is a dimensionless parameter defined by

$$Re = \frac{\rho l V_0}{\mu} \quad (4.6)$$

where ρ is the electrolyte density, μ its viscosity, V_0 the bulk solution flow rate and l a characteristic length, here the length of the plate.

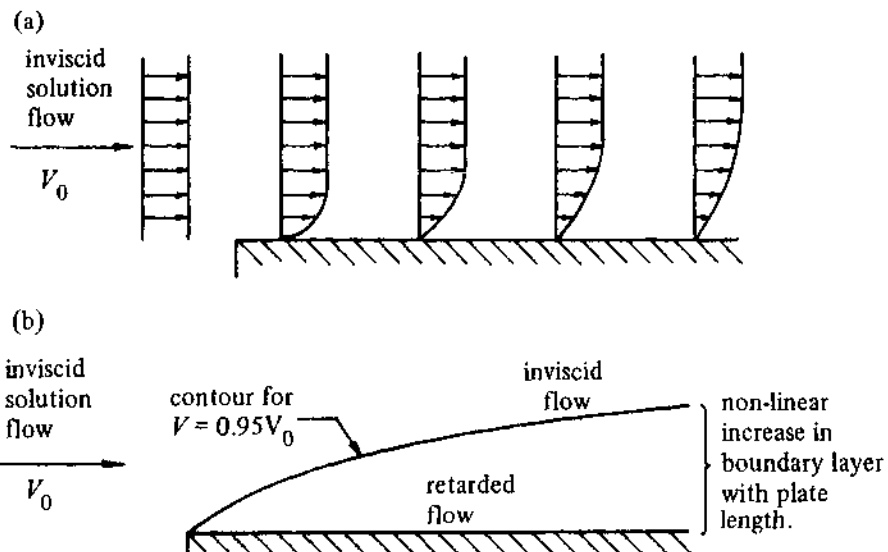


Fig. 4.6 -- Development of a boundary layer during solution flow over a flat plate.

In electrochemistry, it is more usual for the flow to be in a channel formed between two electrodes, between an electrode and a separator, or in a tube. In these cases, see Fig. 4.7, the boundary layers at the two walls must merge at some point, and thereafter a steady state situation will result. Here again, however, the shape of the flow pattern contours will depend strongly on the flow rate and on solution properties, i.e. the Reynolds number.

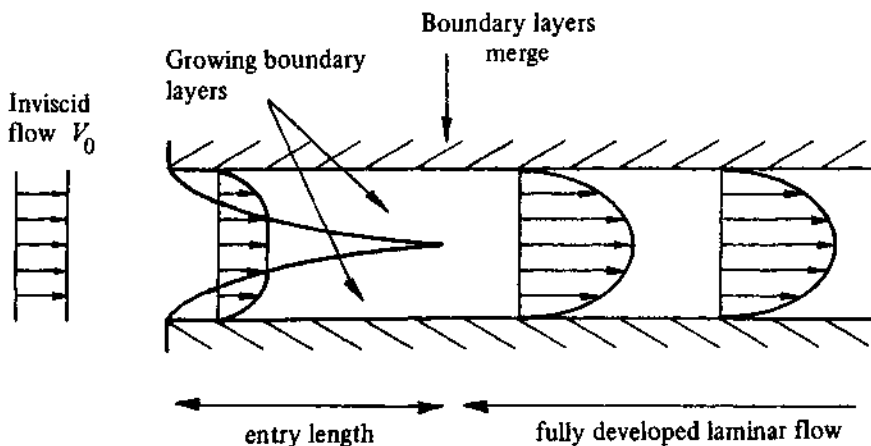


Fig. 4.7 – Development of the boundary layers for solution flowing down a tube or in a channel between two parallel electrodes.

In electrochemistry, a wide variety of complex electrode geometries and flow patterns can be used, and few are amenable to quantitative treatment. Hence the normal approach to the convective diffusion problem is to treat the cell as a 'uniform' or 'averaged' entity, and to seek expressions in terms of space averaged quantities which permit some insight into mass transport conditions in the cell.

Again, in the simple problem of flow over a flat plate it is found that

$$Sh = 0.646 Re^{1/2} Sc^{1/3} \quad (4.7)$$

where the Sherwood, Reynolds and Schmidt numbers, Sh , Re , and Sc , are measures of the average rate of mass transport to the electrode surface, the ratio of inertial/viscous forces in the flow, and the ratio of the rates of transport by convection to that by diffusion respectively. Re is defined in Equation (4.6) above, while the Sherwood number is calculated from the limiting current density (i.e. the current density when the potential of the plate is held at a value where $c^o = 0$):

$$Sh = \frac{II_L}{nFc^\infty D}, \quad (4.8)$$

and the Schmidt number is given by

$$Sc = \frac{\mu}{\rho D} . \quad (4.9)$$

More generally, mass transport in electrolytic cells may be discussed in terms of an expression

$$Sh = k Re^n Sc^m \quad (4.10)$$

where k , n , and m are found from empirical correlations with experimental data.

4.1.3 Laminar vs turbulent flow

All the discussion so far has assumed a laminar flow regime, i.e. that the solution advances in separate, non-mixing layers or elements in a highly organised manner. If, however, the flow or stirring rate is increased sufficiently, the nature of the flow will change. Thereafter, superimposed on the earlier flow pattern, there will be a component of fluid motion which is unsteady and chaotic and leads to mixing between neighbouring solution elements but no net movement of solution. This new type of regime is known as turbulent. It is seldom describable in an exact way, but it leads to high rates of mass transport and good mixing. Hence, it can be very desirable in technological situations, and is therefore often forced at lower flow rates by placing turbulence promoters (bars, rods, particles, etc.) into the solution flow. On the other hand, turbulence will be quite undesirable in a kinetic experiment since the equations, e.g. (4.5), will no longer be applicable.

In the absence of promoters, the transmission from laminar flow to a turbulent regime will again depend on the velocity of movement of the solution and its kinematic viscosity, i.e. on the Reynolds number. In the case of the rotating disc system, the Reynolds number is defined by the equation

$$Re = \frac{\omega r_o^2}{\nu} \quad (4.11)$$

since ωr_o is the velocity of the edge of the disc, and the radius of the disc r_o , is taken as the characteristic distance. The onset of turbulence occurs at a Reynolds number of 10^5 - 10^6 . The higher limit is only applicable for highly polished and perfectly centred discs; any roughness of the surface or eccentricity of the rotation will induce turbulence at a lower rotation rate. Taking typical values for kinematic viscosity (10^{-2} cm 2 s $^{-1}$) and the radius of the disc (0.2 cm), this would suggest an upper limit of $\omega = 2.5 \times 10^4$ s $^{-1}$ (or 2.5×10^5 r.p.m.). In practice such rotation rates can seldom be approached because of vortex formation around the sheath. A more typical upper limit is 1000 s $^{-1}$ (or 10 000 r.p.m.). There is also a minimum rotation rate for the application of the theory. This is because for $Re < 10$ the thickness of the boundary layer becomes comparable to the radius of the disc. Hence the range of rotation rates in the laboratory should be

$$10 < \omega < 1000 \text{ s}^{-1}$$

or

$$100 < \frac{60\omega}{2\pi} < 10000 \text{ r.p.m.}$$

4.1.4 The concepts of a diffusion layer and the mass transfer coefficient

It is frequently helpful to our understanding of experiments with a rotating disc electrode to use a model where the continuously varying flow conditions are replaced by an equivalent system where the zones for diffusion and convection have been completely separated, Fig. 4.8.

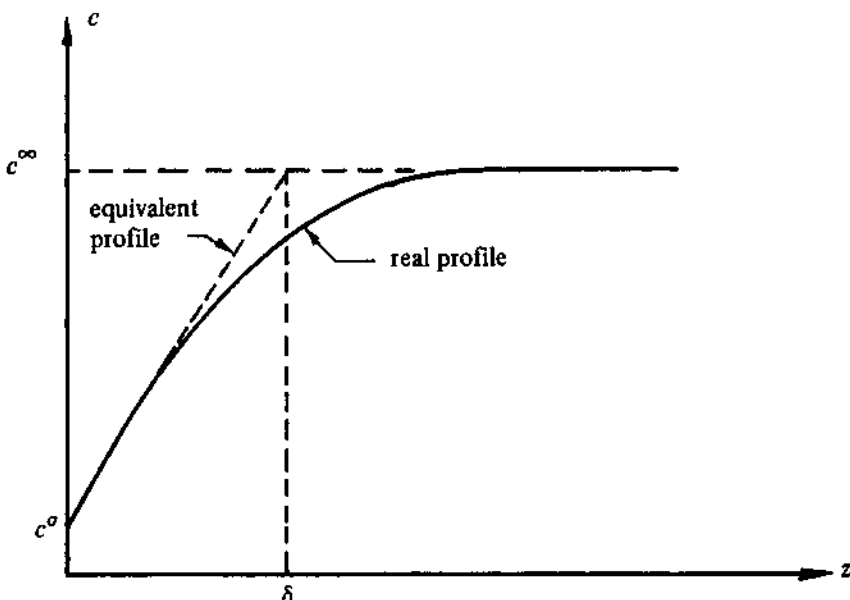


Fig. 4.8 – Concentration profile for the electroactive species using the Nernst diffusion layer model for transport to a rotating disc electrode.

It has already been noted that the flux of material to the rotating disc electrode is uniform over the whole surface, and it is therefore possible to discuss the mass transport processes in a single direction, that perpendicular to the surface (i.e. the z direction). Furthermore, it has been noted that the velocity of movement of the solution towards the surface, V_z , is zero at the surface and, close to the surface, proportional to z^2 . Hence, even in the real situation it is apparent that the importance of convection drops rapidly as the surface is approached. In the Nernst diffusion layer model this trend is exaggerated, and one assumes a boundary layer, thickness δ , wherein the solution is totally stagnant and transport is only by diffusion. On the other hand, outside this layer convection is strong enough for the concentration of all species to be held at their bulk value. This effective concentration profile must, however, lead to the same diffusional flux to the surface (and hence current density) as it found in the real system.

It is also clear from the previous section that the rate of convective diffusion to the disc is strongly dependent on the rotation rate of the disc, but this is readily taken into account in the Nernst diffusion layer model by noting that the stagnant layer thickness will decrease as the rotation rate is increased. In fact, a quantitative relationship has been deduced [3], i.e.

$$\delta = \frac{1.61 \nu^{1/6} D^{1/3}}{\omega^{1/2}} \quad (4.12)$$

when the units of ω are s^{-1} .

The diffusional flux through the Nernst diffusion layer can be conveniently expressed in terms of the mass transfer coefficient, k_m . The flux to the surface is given by the equation

$$J = \frac{D(c^\infty - c^\sigma)}{\delta} \quad (4.13)$$

which may be written as the product of intensive and extensive variables, i.e.

$$J = k_m(c^\infty - c^\sigma) \quad (4.14)$$

The mass transport coefficient may be calculated from the limiting current density (the potential is held at a value where $c^\sigma = 0$).

$$k_m = \frac{I_L}{nF c^\infty} \quad (4.15)$$

The concepts of an equivalent, stagnant boundary layer where transport is only by diffusion and of a mass transfer coefficient are equally applicable and useful to the understanding of all stirred and flowing solution cells.

4.2 THE ROTATING DISC ELECTRODE

In this section, the applications of the rotating disc electrode (RDE) to the study of the mechanism and kinetics of electrode reactions are discussed. It is convenient to subdivide the discussion according to the type of mechanism and subsections will consider total mass transfer control, reversible electron transfer, totally irreversible processes, quasi-reversible electron transfer, and coupled chemical reactions. In general, however, two types of experiment will be of importance. In the first, the shape of the $I-E$ curve at a single rotation rate is analysed; here the RDE is essentially being used to provide a highly controlled mass transfer regime. In the second, the current density, at one or a series of potentials, is investigated as a function of rotation rate. If the RDE is to be used to isolate pure kinetic data from situations where in unstirred solution the steady state current is partially mass transfer controlled, it is a general principle that the current is measured as a function of rotation rate and the data are extrapolated to conditions where the rate of mass transport is infinite, i.e. $\omega = \infty$.

In the final subsection, a further promising but not generally applied experiment is described. The rotation rate of the RDE is modulated and the in-phase current response is used to separate the mass transfer controlled component of the current from kinetically controlled currents.

4.2.1 Experimental factors

The RDE has the considerable practical advantage over techniques such as cyclic voltammetry, potential step, or a.c. methods. The rate of mass transport to the electrode may be varied over a substantial range and in a controlled way without resort to a rapid change in the electrode potential which inevitably leads to the measured current having a contribution from charging the double layer. Since in most experiments with the RDE only (pseudo) steady state currents are measured, the recorded current may be unequivocably equated with the faradic current.

In the early literature [4] there is considerable discussion of the design of cells for RDE experiments. For example, much is made of any eccentricity of the rotation, and it was also held that the non-conducting sheath should be bell shaped. Furthermore, from the theoretical viewpoint, the radius of the sheath should be much larger than that of the active disc, and the cell walls should be well away from the RDE. Fortunately, in practice these factors are seldom important at least over the common range of rotation rates, $10 < \omega < 1000 \text{ s}^{-1}$ or $100 < 60\omega/2\pi < 10000 \text{ r.p.m.}$ Indeed, Fig. 4.9 shows a widely used cell design, and it is also found that the Luggin capillary, apparently in the main flow pattern, is not a problem. Hence, overall it can be said that the design of the RDE and cell is not critical.

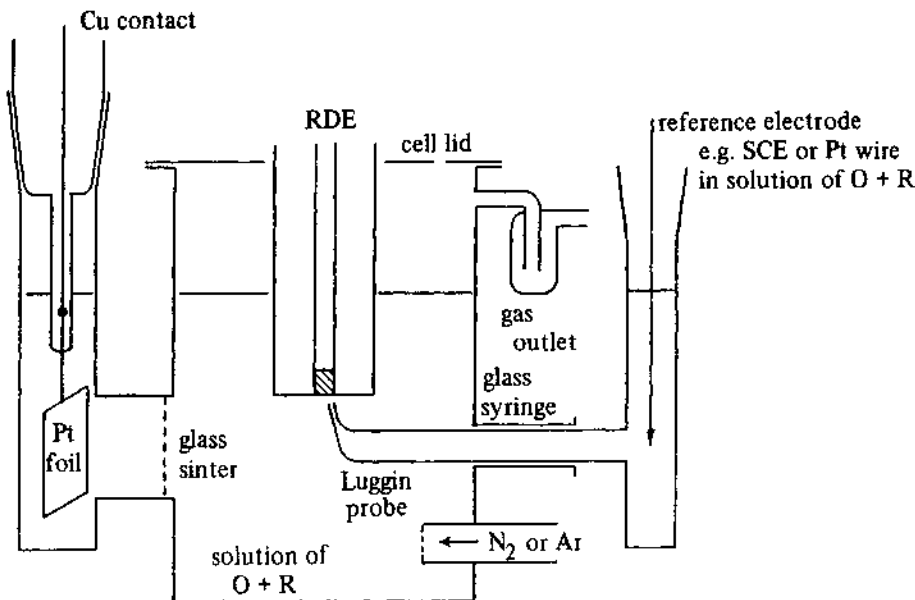


Fig. 4.9 -- Cell used for rotating disc electrode experiments in Southampton.

Problems which do arise in experiments with the RDE are most commonly associated with leakage of solution into any gap between the active disc material and the insulating sheath, and with noise introduced by poor or dirty electrical

contacts. These days the shaft of the RDE is normally linked directly to the motor drive and the electrical contact made either with a high quality carbon brush contact (Ag/C material) or by a wire dipping into a circular trough of mercury around the shaft.

Units are again a problem in rotating disc experiments. In this chapter, the equations are written in terms of angular velocity, $\omega(\text{s}^{-1})$, but other units used experimentally are frequency, f (revolutions s^{-1} or Hz), and revolutions per minute, f' (r.p.m.). These are of course related by $\omega = 2\pi f = (2\pi/60)f'$.

4.2.2 Mass transport control

For potentials where the surface concentration of the electroactive species is zero, the equation relating the limiting current density (for an oxidation) and the rotation rate is found by combining Equations (4.12)-(4.15):

$$I_L = 0.62 nFD^{2/3}\nu^{-1/6}c^\infty \omega^{1/2} \quad (4.16)$$

This expression is known as the Levich equation, and it provides an excellent test that the current is entirely mass transport controlled; a plot of I vs $\omega^{1/2}$ should be linear and pass through the origin, and the slope of such a plot may be used to estimate the diffusion coefficient for the electroactive species, e.g. Fig. 4.10. Except when a chemical reaction limits the current density, the Levich equation will describe the rotation rate dependence of the anodic and cathodic limiting currents at high positive and high negative overpotentials respectively.

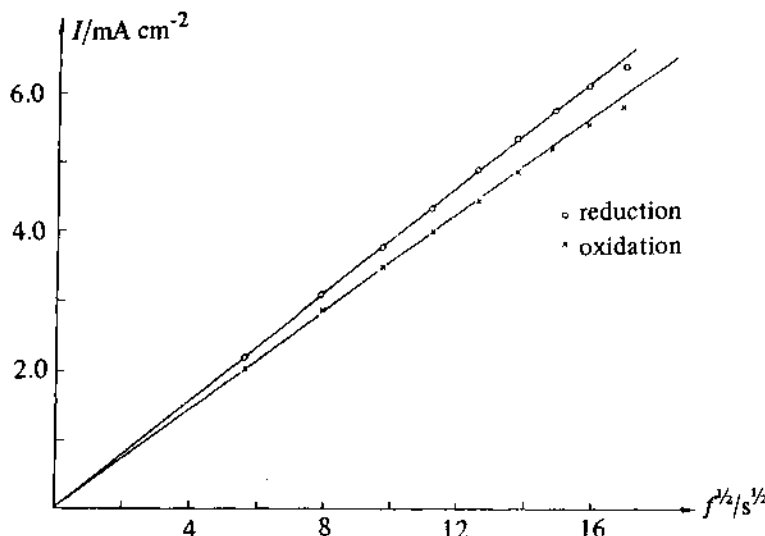


Fig. 4.10 – Plots of I versus $f^{1/2}$ ($\omega = 2\pi f$) at potentials in the plateau regions of the $I-E$ curves in Fig. 4.13(a). Solution contains potassium ferrocyanide (10 mmol dm^{-3}) + potassium ferricyanide (10 mmol dm^{-3}) + potassium chloride (0.5 mol dm^{-3}). Au disc electrode.

4.2.3 Reversible electron transfer

If the standard rate constant for the reaction



is large, the $I-E$ response, at all rotation rates, will appear reversible. At high positive or negative overpotentials, the current density will be given by the Levich equation, but even in the potential range where the current is a strong function of potential (i.e. around the reversible potential), a plot of I vs $\omega^{1/2}$ will be linear. The slope of the plot will, however, be less than that predicted by the Levich equation since the surface concentration of electroactive species will not be zero. The exact form of the $I-\omega^{1/2}$ dependence can be found by combining Equations (4.12) and (4.13) and calculating c^σ from the Nernst equation.

The complete $I-E$ response can also be found by substituting into the Nernst equation:

$$E = E_e^\ominus + \frac{2.3RT}{nF} \log \frac{c_O^\sigma}{c_R^\sigma} \quad (4.18)$$

the ratio of the surface concentrations, c_O^σ/c_R^σ found by manipulation of the following equations resulting from a Nernst diffusion layer model

$$I_L^C = -nFk_m c_R^\infty \quad (4.19)$$

$$I_L^A = nFk_m c_O^\infty \quad (4.20)$$

where I_L^C and I_L^A are the cathodic and anodic limiting current densities respectively (if the solution contains only O or only R, one of these limiting current densities will, of course, be zero) and the equations for the current density at any potential i.e.

$$I = -nFk_m(c_O^\infty - c_O^\sigma) \quad (4.21)$$

$$I = nFk_m(c_R^\infty - c_R^\sigma) . \quad (4.22)$$

The equation which results is

$$E = E_e^\ominus + \frac{2.3RT}{nF} \log \frac{I - I_L^C}{I_L^A - I} \quad (4.23)$$

where for the purpose of analysis of the data, one can take $E_e^\ominus \approx E_{1/2}$. Equation (4.23) should permit the $I-E$ data for all rotation rates and potentials to be collapsed onto a single line.

4.2.4 Irreversible electrode reactions

In the case of an irreversible electrode process



the back reaction may be ignored (i.e. $k = 0$). The I - E curve at an RDE for such a reaction will have the familiar S-shape, and with respect to the dependence of current density on rotation rate, the curve may be broken into three distinct regions:

- (i) in the limiting current plateau region, the current density again depends only on the rate of mass transport and I_L will be proportional to $\omega^{1/2}$;
- (ii) at very low current density, the current density is totally determined by the kinetics of electron transfer, and the rate of mass transport will not affect the current density. Hence I is independent of ω ;
- (iii) in the intermediate zone of mixed control, the current density is partially mass transport controlled, and I must therefore vary with ω . But a plot of I vs $\omega^{1/2}$ is non-linear.

It has been noted above that the approach to obtain \vec{k} in the intermediate zone must be to measure I as a function of ω and then to extrapolate the current density to $\omega = \infty$. Clearly

$$I_{\omega \rightarrow \infty} = -nF\vec{k}c_O^\infty \quad (4.25)$$

The appropriate procedure for the extrapolation of the I - ω data to $\omega = \infty$ may be deduced from the following argument, again based on the Nernst diffusion layer model. The current at any potential in the region of mixed control is given both by the kinetic equation

$$-I = nF\vec{k}c_O^g \quad (4.26)$$

and by the Nernst diffusion layer model

$$-I = nFk_m(c_O^\infty - c_O^g) \quad (4.27)$$

Hence, eliminating I , one obtains

$$c_O^g = \frac{k_m c_O^\infty}{\vec{k} + k_m} \quad (4.28)$$

Now substituting Equation (4.28) into (4.26) and inverting gives

$$-\frac{1}{I} = \frac{1}{nF\vec{k}c_O^\infty} + \frac{1}{nFk_m c_O^\infty} \quad (4.29)$$

but the mass transfer coefficient, $k_m = D/\delta$, and the variation of the diffusion layer thickness with rotation rate is given by Equation (4.12). Using this expression gives the required equation

$$-\frac{1}{I} = \frac{1}{nF\vec{k}c_O^\infty} + \frac{1.61 v^{1/6}}{nFc_O^\infty D^{2/3}} \frac{1}{\omega^{1/2}} \quad (4.30)$$

It can be seen that a plot of $|I|^{-1}$ vs $\omega^{-1/2}$ should be linear, and the intercept can be used to calculate \vec{k} . Moreover, the slopes of these plots, $d|I|^{-1}/d\omega^{-1/2}$, should be independent of potential, while the intercepts (because of \vec{k}) vary strongly with potential. Indeed $\log k$ vs E is a form of Tafel plot and should therefore be linear. Fig. 4.11 shows a set of I^{-1} vs $\omega^{-1/2}$ plots constructed from data for the reduction of oxygen on an aluminium brass [5].

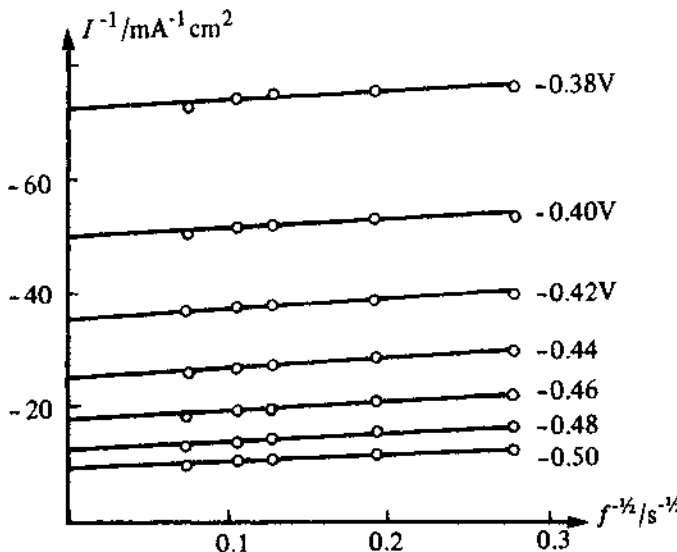


Fig. 4.11 – I^{-1} versus $f^{1/2}$ plots as a function of potential for a rotating aluminium brass electrode in aerated seawater (note $\omega = 2\pi f$). Potentials quoted vs the normal calomel electrode. Reproduced with permission from S. R. Sanchez & D. J. Schiffrian, *Corrosion Science*, 22, (1982), 585.

The Nernst diffusion layer approach can also be used to obtain the equation for the complete I - E response. The result is

$$\log \frac{II_L^C}{I-I_L^C} = \text{const} + \log c_O^\infty - \frac{\alpha_C nF}{2.3RT} E \quad (4.31)$$

for a reduction reaction and

$$\log \frac{II_L^A}{I_L^A - I} = \text{const} + \log c_R^\infty + \frac{\alpha_A nF}{2.3RT} E \quad (4.32)$$

for an oxidation, and these equations may be used to put I - E data from several rotation rates and a series of bulk concentrations onto a single linear plot. Fig. 4.12 shows data from several rotation rates for the reduction of oxygen at gold in 0.1 mol dm^{-3} NaOH; the slope of the graph is $(120 \text{ mV})^{-1}$, confirming that only $1e^-$ is transferred during the rate determining step.

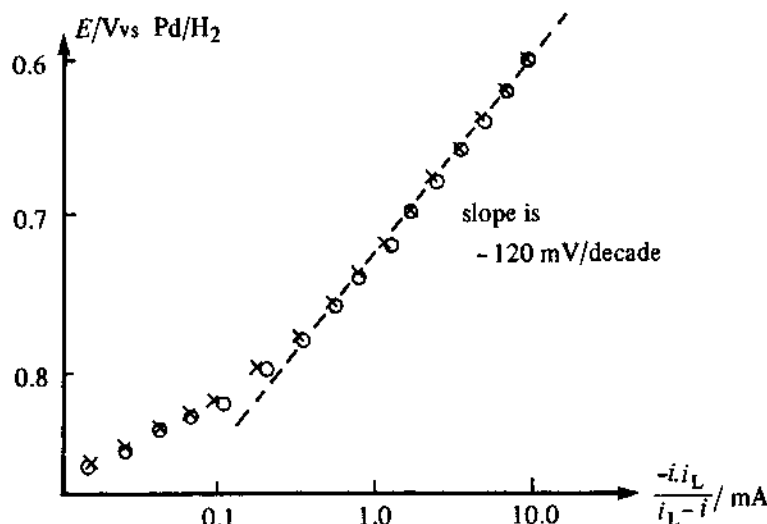


Fig. 4.12 – Test of Equation (4.32) using data for the reduction of oxygen at gold in NaOH (0.1 mol dm^{-3}) from reference [6]. \circ 6400 r.p.m. \times 1600 r.p.m. Electrode area 0.2 cm^2 .

4.2.5 Quasi-reversible electron transfer

In this case, both the forward and back electron transfer processes must be considered. Initially systems



where both halves of the redox couple are solution-free species, will be considered. The $I-E$ curve will clearly have the three zones (i)-(iii) described in section 4.2.4, and to develop a procedure for isolating the kinetic data from the mixed region one again makes use of the Nernst diffusion layer concept. One may write the equations based on equating the fluxes at the disc surface, i.e.

$$k_m(c_O^\infty - c_O^g) = -k_m(c_R^\infty - c_R^g) \quad (4.34)$$

and

$$I = -nFk_m(c_O^\infty - c_O^g) \quad (4.35)$$

and note that the current is also given by

$$I = nF(\vec{k}_R^g - \vec{k}_O^g) . \quad (4.36)$$

Combining these equations leads, after some algebra, to

$$\frac{1}{I} = \frac{1}{nF(\vec{k}_R^\infty - \vec{k}_O^\infty)} + \frac{(\vec{k} + \vec{k})}{nFk_m(\vec{k}_R^\infty - \vec{k}_O^\infty)} \quad (4.37)$$

To find the equation for the dependence of I on ω , we again need to remember that $k_m = D/\delta$ and that δ is given by Equation (4.12). Then

$$\frac{1}{I} = \frac{1}{nF(\vec{k}_R^\infty - \vec{k}_O^\infty)} + \frac{1.61(\vec{k} + \vec{k})v^{1/6}}{nF(\vec{k}_R^\infty - \vec{k}_O^\infty)D^{2/3}} \frac{1}{\omega^{1/2}} \quad (4.38)$$

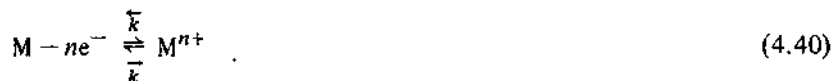
This equation again suggests that the $I-\omega$ data in the potential region of mixed control should be treated by plotting $|I|^{-1}$ vs $\omega^{-1/2}$ and both \vec{k} and \vec{k} can be found using the slope and intercept of the plot. In fact only at potentials close to the reversible potential, say $-2.3RT/2\alpha_C nF < \eta < 2.3RT/2\alpha_C nF$, is it really necessary to consider both the forward and back reaction. Outside this range, the analysis can be greatly simplified, e.g. for cathodic overpotentials $\eta < -2.3RT/2\alpha_C nF$, $\vec{k}_O^\infty \gg \vec{k}_R^\infty$ and $\vec{k} \gg \vec{k}$, and Equation (4.38) simplifies to

$$-\frac{1}{I} = \frac{1}{nF\vec{k}_O^\infty} + \frac{1.61v^{1/6}}{nFc_O^\infty D^{2/3}} \frac{1}{\omega^{1/2}} \quad (4.39)$$

and the kinetic constant can be obtained directly from the intercept.

Fig. 4.13 shows experimental data for the $\text{Fe}(\text{CN})_6^{4-}/\text{Fe}(\text{CN})_6^{3-}$ couple obtained in our laboratories, although the study had been reported in the literature much earlier [7]. Fig. 4.13(a) shows $I-E$ curves at a series of rotation rates of a gold disc electrode, and the three zones (with respect to ω) are clearly seen. At the two extremes of potential, the limiting current plateaux are clearly observed, and it can be seen that $I_L \propto \omega^{1/2}$. Also, at $I=0$ the $I-E$ curves at all ω converge, while in the intervening regions, the current varies with ω but I is not proportional to $\omega^{1/2}$. Furthermore, with increasing ω the plateau is not reached until higher overpotentials, because with the higher rates of mass transport, the range of at least partial kinetic control is extended. Fig. 4.13(b) shows the $|I|^{-1}$ vs $\omega^{-1/2}$ plots for some typical overpotentials, while Fig. 4.13(c) shows the Tafel plots which result from the estimation of \vec{k} and \vec{k} from the mixed region using Equations (4.38) and (4.39).

The case of quasi-reversible electron transfer can also be of interest in the context of the anodic dissolution of metals.



Here, however, the concentration of metal species in the bulk is zero, and the Nernst diffusion layer argument leads to a different equation,

$$\frac{1}{I} = \frac{1}{nF\vec{k}} + \frac{\vec{k}}{\vec{k}} \frac{1.61v^{1/6}}{nFD^{2/3}} \frac{1}{\omega^{1/2}} \quad . \quad (4.41)$$

The plot of I^{-1} vs $\omega^{-1/2}$ is again linear and the slope of the plots will vary with potential because of the term \vec{k}/\vec{k} :

$$\frac{\vec{k}}{k} = \frac{k^\ominus \exp\left(-\frac{\alpha_C nF}{RT} \eta\right)}{k^\ominus \exp\left(\frac{(1-\alpha_C)nF}{RT} \eta\right)} = \exp\left(-\frac{nF}{RT} \eta\right). \quad (4.42)$$

Hence a plot of the slopes of I^{-1} vs $\omega^{-1/2}$ plots against potential is a convenient way of checking n in the corrosion reaction.

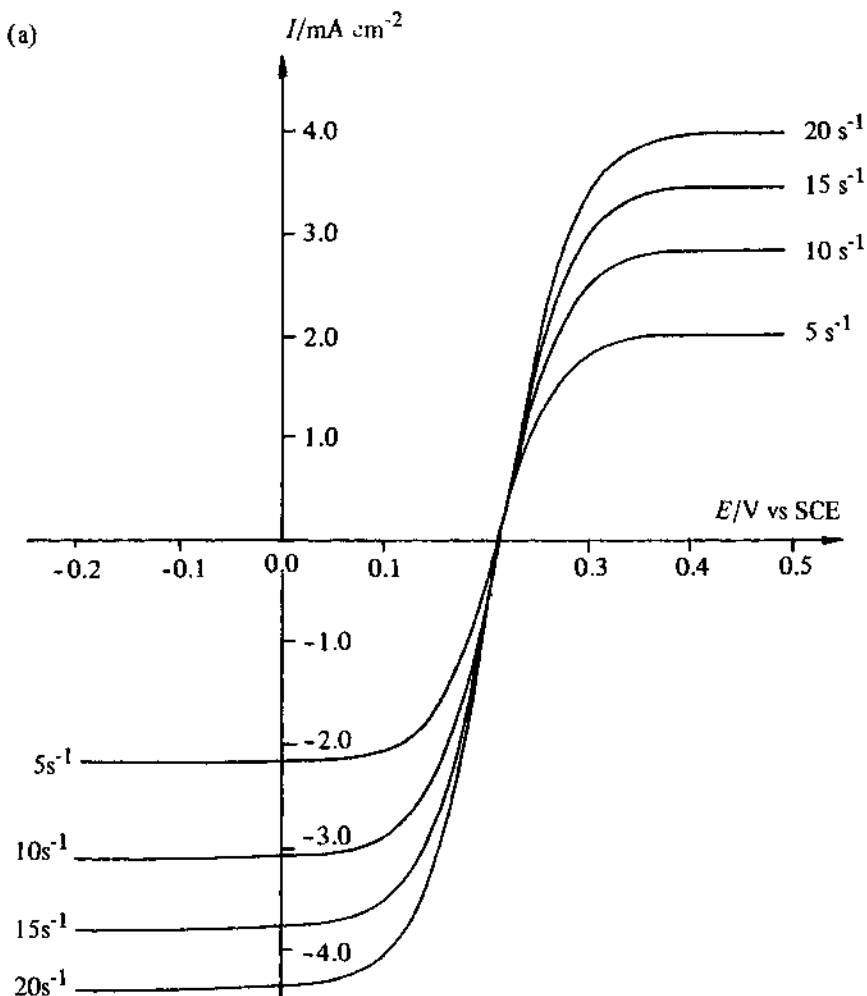


Fig. 4.13 – Experimental data for the study of $\text{Fe}(\text{CN})_6^{4-}/\text{Fe}(\text{CN})_6^{3-}$ couple in KCl (0.5 mol dm^{-3}). $c_O^\infty = c_R^\infty = 10 \text{ mmol dm}^{-3}$. Au electrode (a) $I-E$ curves as a function of rotation rates. (b) I^{-1} vs $f^{-1/2}$ plots ($\omega = 2\pi f$) at a series of potentials. \circ reduction, \times oxidation. (c) Tafel analysis of kinetic currents, i.e. the log of the inverse of the intercepts of (b) vs potential. \bullet uncorrected data. \times data corrected for back reaction.

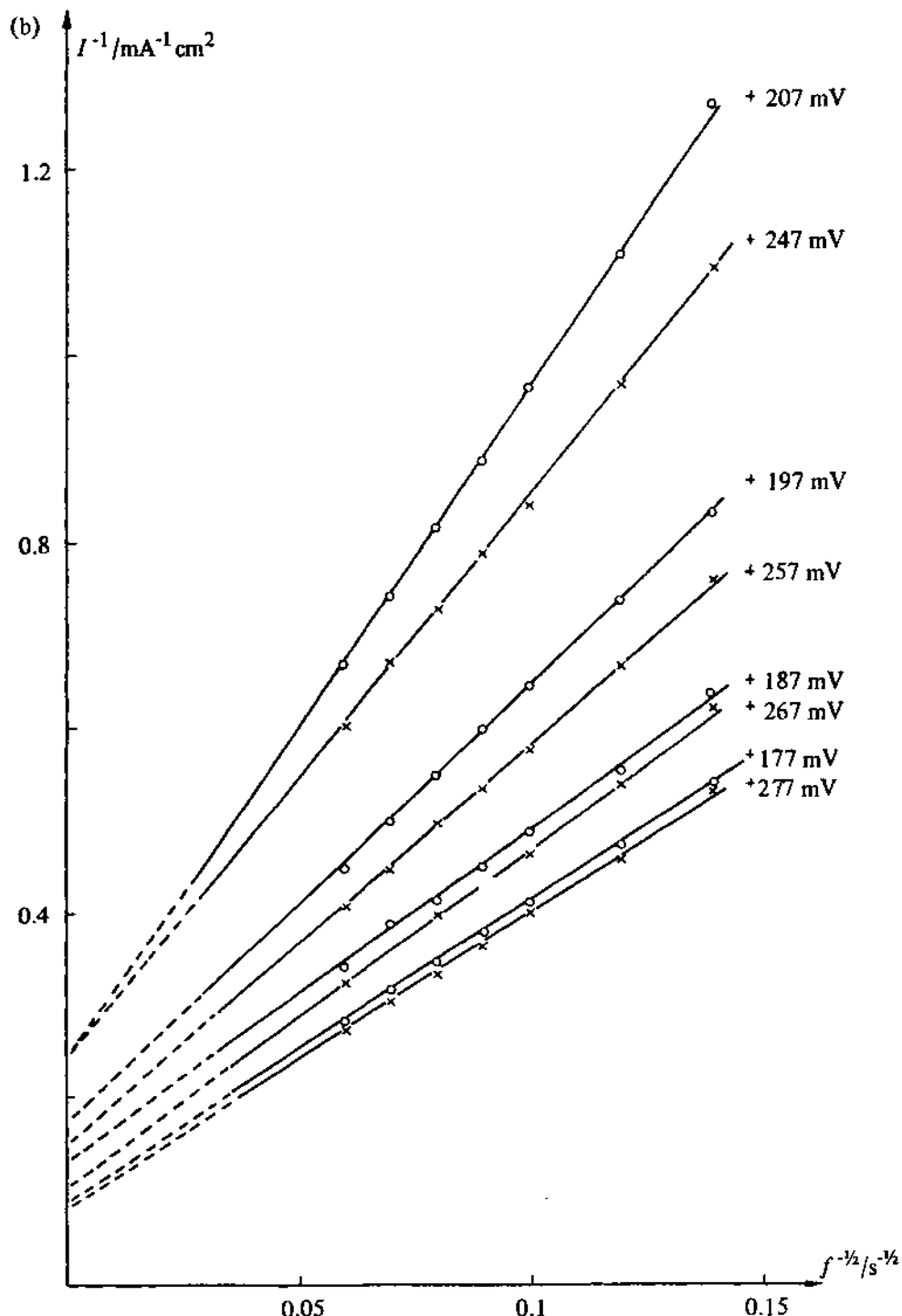


Fig. 4.13 – see legend page 130

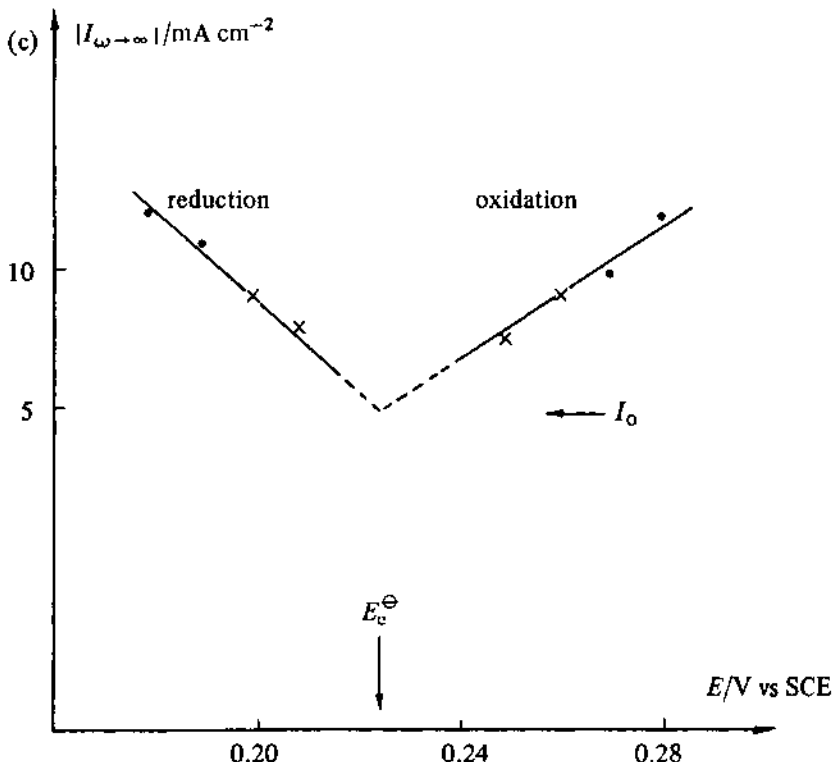
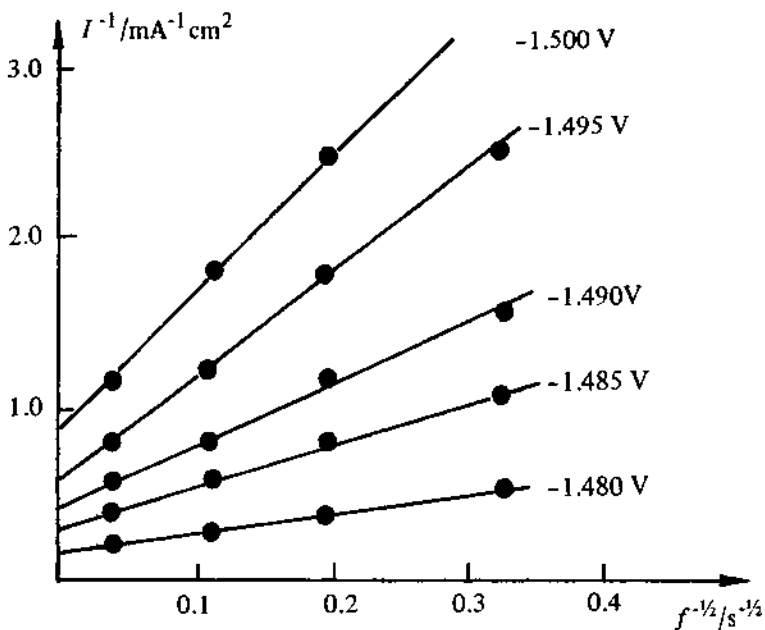


Fig. 4.13 – see legend page 130

Fig. 4.14 - I^{-1} vs $f^{-1/2}$ plots ($\omega = 2\pi f$) for the dissolution of a rotating zinc electrode in NaOH (1 mol dm⁻³). Potentials vs SCE. Reproduced with permission from R. D. Armstrong & G. M. Bulman, *J. Electroanal. Chem.*, 25, (1970), 121.

Whether a rotation rate dependence of the current for metal dissolution is observed depends on the relative values of the rate of dissolution and the rate of mass transport, i.e. the first and second terms in Equation (4.41). For instance, the anodic dissolution of Fe in H_2SO_4 at potentials close to the corrosion potential is slow, and no dependence of the current on rotation rate is observed. In contrast, Fig. 4.14 shows data [8] for a rotating zinc disc electrode in 1 mol dm^{-3} NaOH, and a significant mass transport effect is seen.

4.2.6 Coupled chemical reactions

The study of homogeneous chemical reactions with the RDE is generally carried out by investigating the variation of the limiting current with rotation rate because it leads to greatly simplified boundary conditions when it is certain that the rates of electron transfer at the disc surface are very fast. A corollary is that the $I_L - \omega$ relationship must be dependent on the rate constant of a chemical step; this makes the RDE best suited to the study of ce, ece, or catalytic reactions where either (i) the increase in flux of a reactant puts pressure on a chemical reaction forming the electroactive species e.g. the ce mechanism, or (ii) the rotation rate affects the residence time of an intermediate in the layer at the electrode surface and hence the extent to which it undergoes a chemical reaction within the influence of the electrode, e.g. ece or catalytic mechanisms.

The classical ce reaction is the reduction of acetic acid which occurs by initial dissociation to form a proton, followed by reduction.



This system was first studied by Vielstich & Jahn [9, 10] who deduced the equation

$$-\frac{I_L}{\omega^{1/2}} = 0.62nFD^{2/3}\nu^{-1/6} c_{\text{HOAc}}^\infty + \frac{0.62D^{1/6}\nu^{-1/6}}{K(k_D + k_A)^{1/2}} I_L \quad (4.45)$$

where c_{HOAc}^∞ is the bulk concentration of acetic acid and K is the equilibrium constant (k_D/k_A). If K is known, the two rate constants may be calculated. Fig. 4.15 shows their plot of $I_L/\omega^{1/2}$ vs I_L at a Pt disc in an acetate buffer, and the values $k_D = 4.5 \times 10^5 \text{ s}^{-1}$ and $k_A = 2.6 \times 10^{10} \text{ dm}^3 \text{ mol}^{-1} \text{ s}^{-1}$ were estimated from the data and the known value of k_D/k_A . It should be noted that for a simple electrode reaction $I_L/\omega^{1/2}$ is independent of ω .

The study of ece reactions [11-14] is based on the estimation of n_{app} as a function of ω where

$$n_{\text{app}} \propto \frac{|I_L|}{\omega^{1/2} c^\infty} \quad (4.46)$$

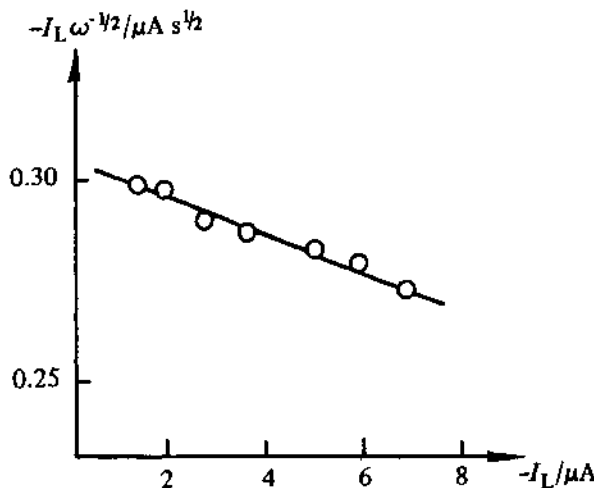
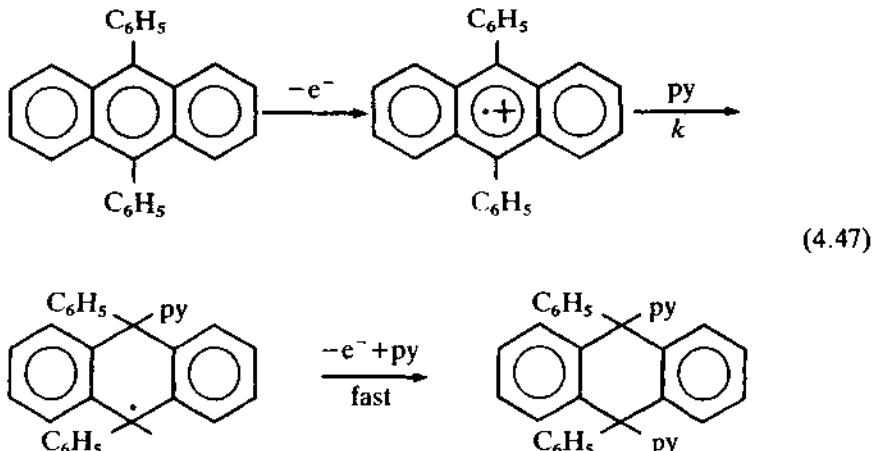


Fig. 4.15 – $I\omega^{-1/2}$ vs I plot for the determination of the rate of dissociation of acetic acid. Pt electrode in acetate buffer, pH 6.7 + KCl (1 mol dm^{-3} KCl). Reproduced with permission from W. Vielstich & D. Jahn, Z. Electrochem., 64, (1960), 43.

A typical ece reaction is the pyridination of diphenyl anthracene (DPA) [14]



and n_{app} will depend on the rate of the chemical step, k , and the rotation rate, ω . If $DPA^{+•}$ reacts close to the surface, the oxidation will involve $2e^-/DPA$ molecule, while if $DPA^{+•}$ is transported away from the surface before reaction with pyridine can occur, only $1e^-/DPA$ will be transferred. Hence if k lies within the appro-

priate range, n_{app} will change from 2 to 1 as ω is increased, see Fig. 4.16. The evaluation of k in practice will depend on the comparison of experimental n_{app} vs ω plots with those obtained from theory [12] or simulation [13, 14].

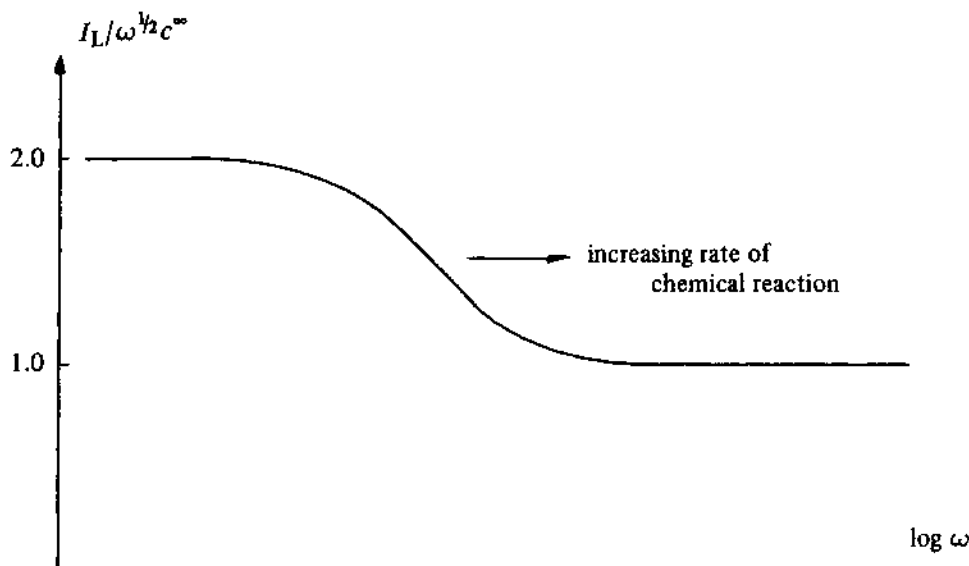


Fig. 4.16 – Normal presentation of rotating disc data for an ece reaction.

4.2.7 The hydrodynamically modulated rotating disc electrode

The idea of this technique [15-17] is to allow the separation of kinetic and mass transport controlled components of a measured current (either in the region of mixed electron transfer/mass transport control or in situations where there are two competing electrode reactions, one mass transport controlled and the other kinetically controlled, (e.g. solvent decomposition) by using a sinusoidal modulation of the rotation rate and employing a phase sensitive detection method to measure the perturbation of the current. Only the mass transport limited component of the current will respond to the modulation.

The modulated angular velocity is

$$\omega^{1/2} = \omega_0^{1/2} + \frac{\Delta\omega^{1/2}}{2} \sin 2\pi ft \quad (4.48)$$

where ω_0 is the rotation rate in the absence of modulation and $\Delta\omega$ and f the amplitude and frequency of the modulation respectively. For practical reasons, the amplitude of the modulation will be small, and the frequency will be determined by the inertia of the motor and electrode system.

The ratio of modulated to mean current is given by

$$\frac{I}{\bar{I}} = \frac{\Delta\omega^{1/2} \sin 2\pi ft}{2\omega_0^{1/2}} \quad (4.49)$$

and the peak to peak value ratio is

$$\frac{\Delta I}{\bar{I}} = \frac{\Delta\omega^{1/2}}{\omega_0^{1/2}} \quad (4.50)$$

for a mass transport limited reaction. ΔI has no contribution due to double layer charging or solvent decomposition reactions, since it depends only on changes brought about by the alteration of the rotation rate and hence of convective mass transport. This is an obvious attraction of the technique for the study of reactions occurring in the presence of spurious phenomena and, indeed, as an analytical tool for the determination of low concentrations of electroactive compounds [19]. The method has been successfully applied to concentrations of metal ions as low as 5×10^{-8} mol/dm⁻³.

Sinusoidal modulation techniques have also been used to study reactions with mixed diffusion and electron transfer control. A simple solution for this case gives for the modulation ratio:

$$\frac{\Delta\omega^{1/2}/\omega_0^{1/2}}{\Delta I/\bar{I}} = 1 + \omega_0^{1/2}/k_E \quad (4.51)$$

where \bar{I} is the average current, and k_E is defined by

$$k_E = \frac{0.62 \nu^{1/6}}{D^{2/3}} (\vec{k} + \vec{k}) \quad (4.52)$$

Hence by measuring the modulation ratio as a function of ω and η , the kinetic parameters can be completely determined [16, 17].

4.3 THE ROTATING RING-DISC ELECTRODE

A photograph of the rotating ring-disc electrode (RRDE) is shown in Fig. 4.1 at the beginning of this chapter, and Fig. 4.17 also illustrates the essential features of the system. It is a view from below and shows the disc electrode surrounded by a concentric ring electrode but with a thin layer of insulating material between.

It was also explained in section 4.1.1 that the rotation of the electrode structure induces a particular flow pattern to the solution. The solution is pulled up at the centre of the rotating structure (i.e. to the disc electrode) and then thrown out radially across the surface of the structure (see also Fig. 4.3 and 4.5). Hence, intermediates formed on the disc are swept out towards

the ring; the ring is therefore effectively downstream to the disc and may be used to give information about solution-free intermediates formed in the electrode reaction at the disc.

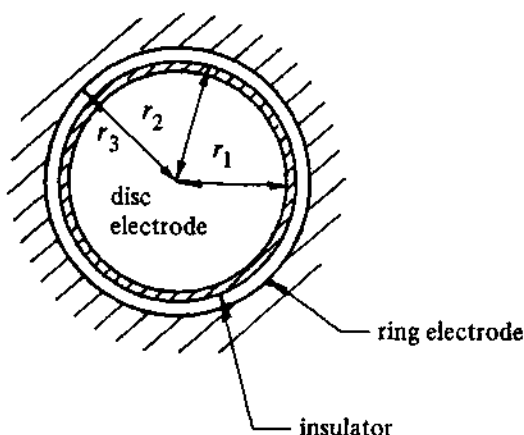


Fig. 4.17 – Critical dimensions of the rotating ring-disc electrode.

The electrical contacts to the ring and disc electrodes are made so that the two electrodes may be controlled independently and, indeed, to obtain the maximum information it is also necessary to have a four electrode potentiostat which will allow the ring and disc electrodes to be potentiostatted independently of each other. The types of experiment that can usefully be performed with a RRDE are illustrated by three examples all using controlled potential operation:

- (i) the disc electrode is held at a constant potential where the reaction of interest takes place, and an $I-E$ curve is recorded at the ring electrode. In principle, this allows identification of solution free intermediates formed in the disc reaction;
- (ii) an $I-E$ curve is recorded at the disc while the ring potential is held constant at a value where a particular intermediate is oxidised or reduced. This allows the definition of the exact potential range where the intermediate is formed;
- (iii) both ring and disc electrodes are held at constant potentials. The disc potential is held at a value where the intermediate is formed and the ring at a value where it may be detected. This is the normal mode of operation for the determination of quantitative kinetics.

In each of the experiments, the rotation rate is an independent variable. Increasing ω will decrease the time it takes for intermediates to be transported from the disc to the ring. The detection of short-lived intermediates requires the use of high rotation rates and the construction of a RRDE with a thin interelectrode gap. Together, these experiments give at least the same flexibility as cyclic

voltammetry for the study of mechanism and kinetics with the additional advantage that solution-free and adsorbed intermediates are directly distinguished (species adsorbed on the disc are not transported to the ring). It should also be noted that the disc and ring electrodes need not be of the same material and, indeed, the material of the ring may be selected for the best response to the species to be detected.

On the other hand, the RDDE electrode is undoubtedly relatively difficult and expensive to construct, and it must be handled and used with caution. The gap between disc and ring needs to be uniform, and the study of short-lived intermediates requires the gap to be thin (for typical values see Table 4.1). Moreover, there must not be any leakage of solution between the electrodes and the sheath (usually PTFE or an epoxy resin).

Much of this section of the chapter will discuss the various types of application of the RRDE.

Table 4.1 – Comparison of calculated and experimentally determined values of collection efficiency (2)

Electrode	A	B	C	D	E
r_1/mm	3.869	4.769	3.480	3.672	3.635
r_2/mm	3.981	4.869	3.860	3.763	3.779
r_3/mm	4.051	5.221	4.375	4.369	4.839
N calculated	0.090	0.214	0.261	0.318	0.402
N determined	0.097	0.215	0.263	0.328	0.404

4.3.1 The collection efficiency

Even if the species formed at the disc electrode is completely stable and free in solution, not all of that formed at the disc will reach the surface of the ring to be detected. Fig. 4.5 shows that the highest radial velocity occurs a short distance away from the surface. Hence it is inevitable that some of the intermediate formed at the disc will be swept past the ring into the bulk solution, Fig. 4.18. It is therefore necessary to define, for each RRDE, the collection efficiency. This is simply the fraction of a completely stable, solution free intermediate formed at the disc which is detected at the ring. Hence for a system



where both O and R are stable and the potentials of the disc and ring are held at appropriate values so that the forward and back reactions respectively are mass transport controlled, the collection efficiency, N, is defined by

$$N = -\frac{i_R}{i_D} \quad (4.54)$$

where i_R and i_D are the ring and disc currents respectively. Couples which have been used for the determination of the collection efficiency include $\text{Fe}(\text{CN})_6^{4-}/\text{Fe}(\text{CN})_6^{3-}$, Br^-/Br_2 and quinone/hydroquinone.

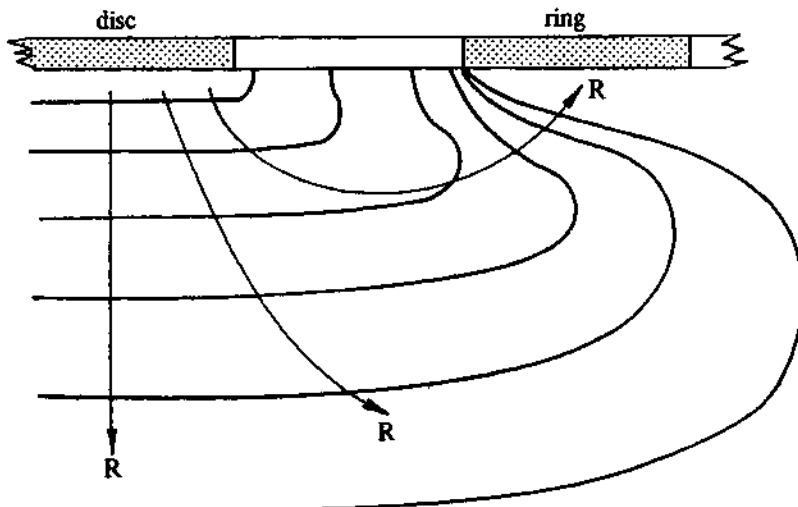


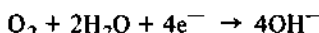
Fig. 4.18 – Concentration contours for an intermediate, R , being formed at the disc and being partially transported to the ring electrode.

The convective-diffusion problem for the RRDE may be solved analytically for the case where the species formed at the disc is completely stable. As a result, the collection efficiency can also be calculated for specified disc and ring dimensions; the analytical solution $N = f(r_1, r_2, r_3)$ is, however, a complex equation, and the interested reader is referred to the book by Albery & Hitchman (see further reading). There is very good agreement between calculated and experimentally determined collection efficiencies, as can be seen from the examples shown in Table 4.1 (also taken from the book by Albery & Hitchman). It should be emphasised that N is not a function of rotation rate since increasing ω will increase the rate of transport to the disc as well as across the gap to the ring.

The next few sections discuss some applications of the rotating ring-disc electrode.

4.3.2 The reduction of oxygen

The reduction of oxygen is a technologically important reaction but in both alkaline media



(4.55)

and acidic media



it is a complex process which can occur via a multitude of mechanisms. In general, however, the mechanisms are of two types, see Fig. 4.19. In the first, complete reduction appears to occur in a single step without formation of solution free intermediates. In the second, reduction of oxygen occurs in two distinct steps with hydrogen peroxide as an identifiable intermediate. Indeed, at some electrodes, e.g. Hg, there may be a range of potentials where hydrogen peroxide is the final product, i.e. oxygen reduction gives *I-E* curves with two waves.

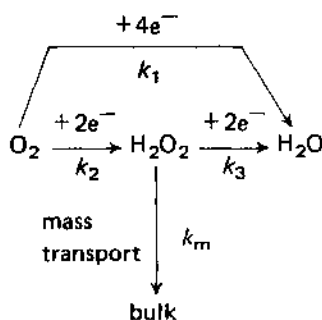


Fig. 4.19 – Routes for the reduction of O_2 in aqueous solution.

The rotating ring disc electrode makes a particularly useful contribution to the study of this system since it both allows differentiation of the two types of mechanism and an estimate of the relative importance of the pathways under conditions where they co-exist. A qualitative example of its application is illustrated in Fig. 4.20 which shows an *i-E* curve at a Pt disc electrode, and the current at a platinum ring when its potential is held at a value where the hydrogen peroxide oxidises. It can be seen that the *i-E* curve at the Pt disc shows only a single reduction wave, implying a complete 4e^- reduction; on the other hand, the response on the ring proves that some hydrogen peroxide is formed during the rising region of the *i-E* curve, and that at Pt the $\text{O}_2/\text{H}_2\text{O}_2$ and $\text{H}_2\text{O}_2/\text{H}_2\text{O}$ processes must occur at very similar potentials.

The equation required to estimate the relative importance of the two types of reaction pathway may be obtained by considering the scheme in Fig. 4.19 and using the concept of mass balance for hydrogen peroxide. Thus it is possible to equate the flux for the formation of hydrogen peroxide with those for its further reduction and diffusion into solution, i.e.

$$k_2 c_{\text{O}_2}^\sigma = k_3 c_{\text{H}_2\text{O}_2}^\sigma + k_m c_{\text{H}_2\text{O}_2}^\sigma \quad (4.57)$$

and hence the surface concentration of hydrogen peroxide is given by

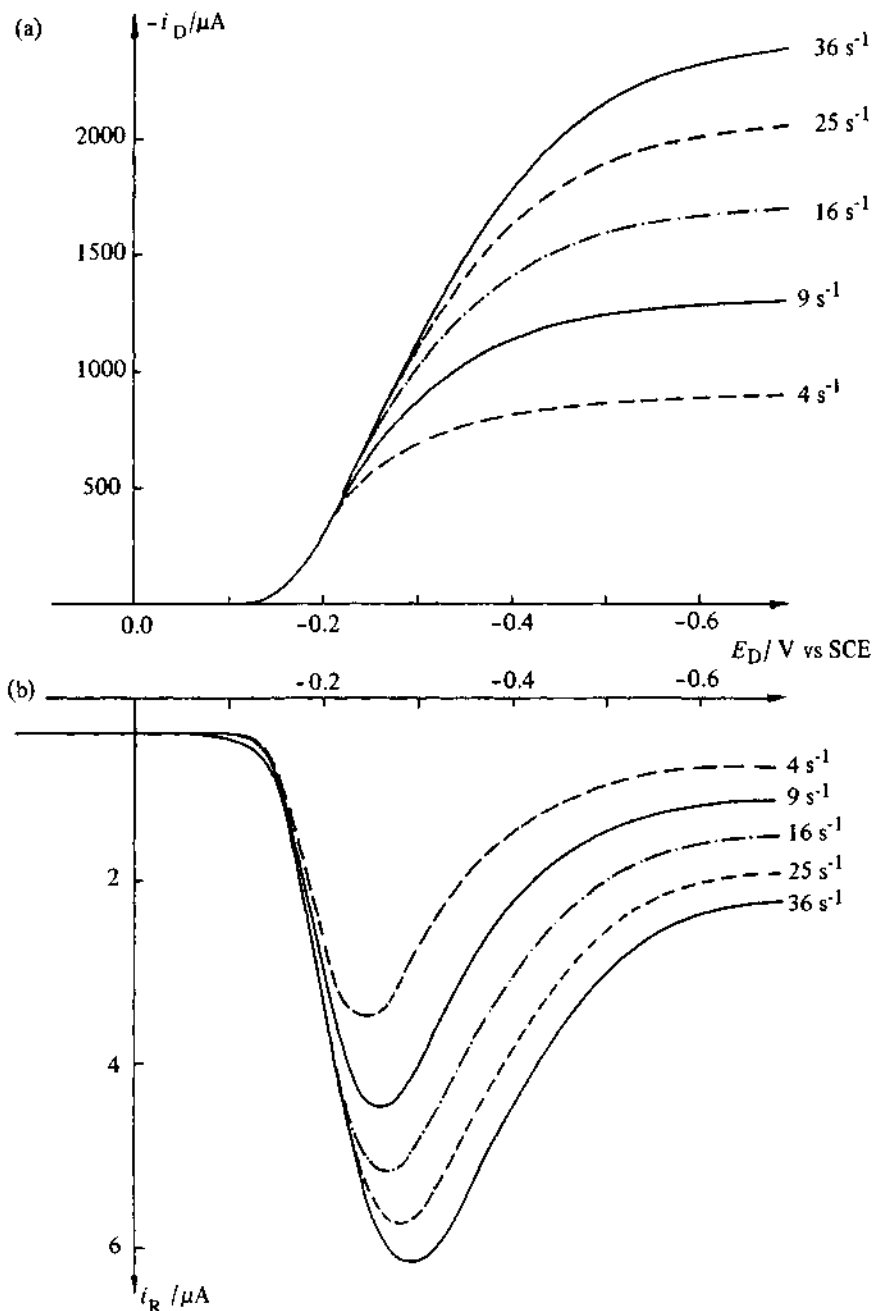


Fig. 4.20 - The electrochemistry of O_2 (saturated) in $\text{NaOH} (0.1 \text{ mol dm}^{-3})$ at a Pt disc/Pt ring electrode. (a) $I-E$ curves at the disc as a function of rotation rate. (b) Response of the ring electrode held at 0.0 V during the potential scan at the disc. At 0.0 V the H_2O_2 is oxidised and hence the amount formed at the disc may be monitored on the ring. It can clearly be seen that the formation of H_2O_2 goes through a maximum at about -0.25 V . At more negative potentials the H_2O_2 is further reduced at the disc.

$$\frac{c_{\text{H}_2\text{O}_2}^{\theta}}{k_m} = \frac{k_2 c_{\text{O}_2}^{\theta}}{k_3 + k_m} . \quad (4.58)$$

The flux of hydrogen peroxide into solution, $k_m c_{\text{H}_2\text{O}_2}^{\theta}$, can be detected at the ring electrode if its potential is held at a value where hydrogen peroxide is oxidised (or reduced). Moreover, the current at the ring depends only on the flux leaving the disc and the collection efficiency. Hence for oxidation at the ring

$$i_R = 2FN k_m c_{\text{H}_2\text{O}_2}^{\theta} . \quad (4.59)$$

The measured disc current is the sum of components for each reduction step

$$-i_D = 4Fk_1 c_{\text{O}_2}^{\theta} + 2Fk_2 c_{\text{O}_2}^{\theta} + 2Fk_3 c_{\text{H}_2\text{O}_2}^{\theta} . \quad (4.60)$$

Combining Equations (4.58), (4.59), and (4.60) and noting that $k_m = D/\delta$ where δ is given by Equation (4.12) for a rotating disc electrode, one obtains

$$\frac{-i_D}{i_R} = \frac{1}{N} \left(\frac{2k_1}{k_2} + 1 \right) + \frac{2k_3 \left(\frac{k_1}{k_2} + 1 \right)}{0.62 \nu^{-1/6} D^{2/3}} \cdot \frac{1}{\omega^{1/2}} . \quad (4.61)$$

This equation shows that much kinetic information may be obtained from a plot of $-i_D/i_R$ versus $\omega^{-1/2}$. For example, if the reduction of oxygen at the material of the disc electrode occurs totally via solution free hydrogen peroxide, $k_1 = 0$ and

$$\frac{-i_D}{i_R} = \frac{1}{N} + \frac{2k_3}{0.62 \nu^{-1/6} D^{2/3}} \frac{1}{\omega^{1/2}} . \quad (4.62)$$

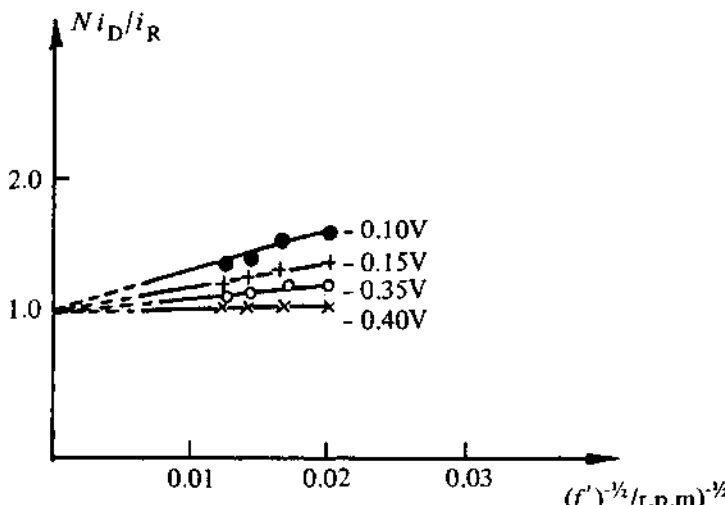


Fig. 4.21 – Application of Equation (4.62) to the study of oxygen reduction at a gold disc electrode using a ring-disc electrode with Pt ring held at 0.4 V. Solution is NaOH (1 mol dm^{-3}). Potentials vs Hg/HgO. Reproduced with permission from R. R. Adzic, N. M. Markovic and A. V. Tripkovic, *Bull. Soc. Chim. Beograd.*, **45**, (1980), 399.

Plots of $-i_D/i_R$ vs $\omega^{-1/2}$ at different potentials will have a common intercept but different slopes from which k_3 may be calculated. Fig. 4.21 shows such a set of data for a gold disc [19]. On the other hand, if both pathways are important both the slopes and intercept will vary with potential [20].

4.3.3 Homogeneous chemical reactions

If the product of the electron transfer reaction at the disc is not completely stable in the solution medium, its concentration will decay as it is convected across the gap from disc to ring, and the ring current will be lower than otherwise expected. It can be seen intuitively that if the rate constant for the decay of the intermediate is large (and the product of the homogeneous chemical reaction is not electroactive at the ring) the ring current will be small. Conversely, if the rate constant is small the ring current will approach the value obtained in the absence of the chemical reaction. Also it is obvious that the ratio of ring/disc currents will depend on the rotation rate of the electrode system since it will determine the time taken for the species to be transported from disc to ring.

In such systems it is normal to define a kinetic collection efficiency, $N_k (= -i_R/i_D)$ which will be a function of the rotation rate, the dimensions of the electrodes and gap, and the rate of the homogeneous chemical reaction. The mathematical solutions required to obtain numerical values for the rate constant are, in general, complex, and many of the dimensionless plots in the literature are obtained by simulation techniques [21].

A simple procedure for studying pseudo first order chemical reactions has been described by Albery & coworkers [22, 23]. A constant current is applied to the disc, and the ring current is monitored. Plots of $-i_R$ vs i_D are found to be linear, but the slopes are a function of ω and the rate constant is found from an analysis of the slopes. Such procedures allow the determination of second order rate constants in the range 3×10^{-2} to $10^7 \text{ dm}^3 \text{ mol}^{-1} \text{ s}^{-1}$.

The range of experiments possible with a rotating ring disc electrode is well illustrated by the studies of the anion radicals of activated olefins in aprotic solvents [24, 25]. In many cases the decay of the anion radicals is by dimerisation. Then the reaction is second order in the intermediate, as may be confirmed by a series of experiments where the disc current is varied and the kinetic collection efficiency is found to decrease with increasing disc current (i.e. flux of anion radical from the disc). The rate constants reported in Table 4.2 were found by comparison of the experimental data with simulated curves. Again, the wide range of rate constants which may be determined by variation of the concentration of olefin and the rotation rate of the electrode should be noted. The behaviour of the anion radical from diethylmaleate (DEM) is, however, quite different, as may be shown with the rotating ring disc electrode. $i-E$ curves for DEM and its trans isomer, diethylfumarate (DEF), at a rotating Pt disc show reduction waves at -1.13 V and -0.70 V vs Ag/Ag^+ respectively. Fig. 4.22 shows i_R vs E plots for a solution of DEM when the disc potential is held at various values. Curve (a) (when the disc potential is held at 0.0 V so no reaction occurs) shows a small wave for the reduction of a low concentration of impurity DEF, and the

beginning of the main wave for the reduction of DEM. For curve (b) the disc potential is held at -0.9 V where the impurity DEF, but not the DEM, is reduced; the ring current is similar to case (a), except that positive to -0.7 V there is a

Table 4.2 – Rate constants for the dimerisation of the anion radical in DMF/ $(C_4H_9)_4NI$ determined with a Pt/Pt ring disc electrode.

Olefin		$k(\text{dm}^3 \text{ mol}^{-1} \text{ s}^{-1})$
R_1	R_2	
$-\text{CO}-\text{OCH}_3$	$-\text{CO}-\text{OCH}_3$	1.1×10^2
C_6H_5	CN	8.8×10^2
CN	CN	7×10^5

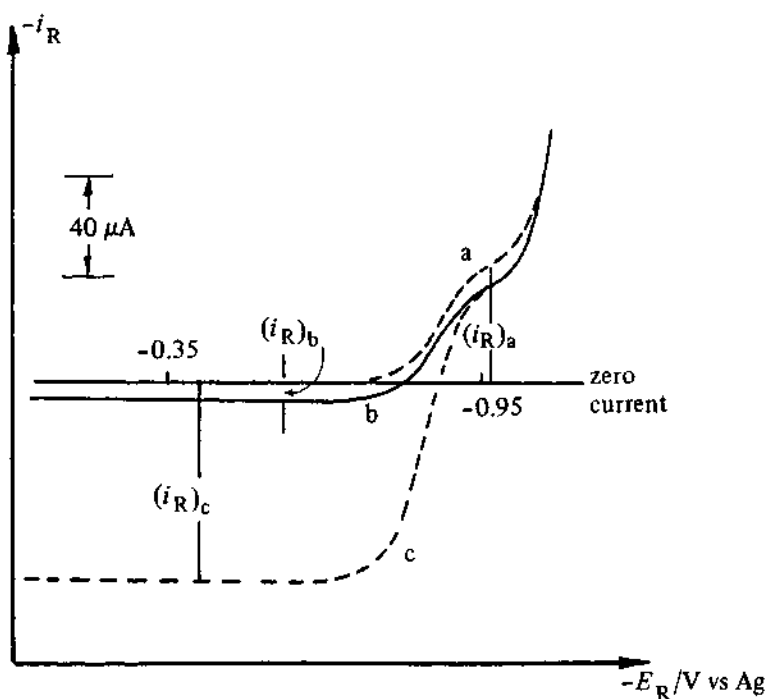


Fig. 4.22 $\sim i_R$ vs E_R plots when the potential of the disc electrode is held at (a) 0.0 V, (b) -0.9 V, and (c) -1.4 V vs Ag reference electrode. The solution is diethyl maleate (3 mmol dm^{-3}) in $\text{DMF}/(C_4H_9)_4\text{NClO}_4$ (0.15 mol dm^{-3}) but the diethyl maleate contains 5–8% diethyl fumarate as an impurity. Rotation rate is 98.6 s^{-1} . Reproduced with permission from A. J. Bard, V. J. Puglisi, J. V. Kenkel, & A. Lomax, *Faraday Disc.*, **56**, (1973), 353.

small anodic current corresponding to oxidation of $\text{DEF}^{\cdot\cdot}$ at the ring. For curve (c) the disc potential is -1.4 V so that both the DEF and DEM are reduced. The i_R-E curve, however, shows no anodic current negative to -0.8 V where oxidation of $\text{DEM}^{\cdot\cdot}$ would be expected, but a large increase in current positive to -0.7 V where $\text{DEF}^{\cdot\cdot}$ is oxidised. Hence it must be concluded that $\text{DEM}^{\cdot\cdot}$ is not sufficiently stable to transport from disc to ring, and it isomerises to $\text{DEF}^{\cdot\cdot}$ which is instead detected at the ring.

4.3.4 The study of corrosion

The rotating ring disc electrode is also a powerful tool for the study of corrosion. The disc is made from the material of interest, while the ring electrode is an inert material. The principal application of the ring disc electrode is to allow, with absolute certainty, distinction between corrosion products which are solids (and remain at the disc surface) and those which are soluble in the solution (and may therefore be detected at the ring electrode). Moreover, the i_R-E characteristic allows the solution free products to be identified. Commonly the disc is left at open circuit so that corrosion is not electrochemically accelerated.

Applications of the rotating disc electrode in corrosion include

- (i) measurement of the instantaneous rate of corrosion to solution free species [26];
- (ii) studies of alloy corrosion [27]. For example, it is possible to demonstrate that in oxygen saturated, chloride media, the corrosion of the alloy, Cu_3OZn , is totally non-selective and there is no tendency for the more electronegative element, Zn, to dissolve more rapidly;
- (iii) the identification of the oxidation states of solution free corrosion products. For example, during the corrosion of molybdenum, Mo(VI) is generally the final oxidation product in solution but both Mo(III) and Mo(V) may be identified as species leaving the corroding surface [28].

4.3.5 Shielding experiments

In a basic shielding experiment the potential of the ring and disc electrodes are held at the same value, where a reaction is mass transport controlled. The ring current under these conditions will be less than expected because some of the electroactive species which would normally be oxidised (or reduced) at the ring will be removed by reaction at the disc. The shielding ring current is given by [29]

$$(i_R)_{\text{SH}} = i_R - Ni_D \quad (4.63)$$

where i_R is the ring current when no electrode reaction occurs at the disc.

Shielding experiments allow precise determination of the quantity of electroactive species consumed at the disc, including material lost in non-faradaic processes such as adsorption or a chemical reaction. Where such non-faradaic processes occur, the experimental shielded ring current will be less than that calculated by Equation (4.63).

Two examples of the many possible applications of the shielding experiment will be given. The first is taken from the paper by Sherwood & Bruckenstein [30] who studied the underpotential deposition of mercury onto gold. Fig. 4.23 shows both the disc current during the deposition of the mercury onto the gold and also $-i_R/N$ as a function of time. There is a clear discrepancy, and therefore there must be a non-faradaic process removing mercurous ions at the disc, i.e. adsorption of mercurous ions must occur in addition to the reduction to mercury metal. The second example concerns the corrosion of zinc in aerated solution [31]; if a zinc disc electrode is allowed to stand at open circuit and an appropriate ring electrode is held at a potential where the reduction of oxygen is mass transport controlled, the ring will be 'shielded' by the chemical reaction of oxygen with zinc. The extent of shielding can be determined by measuring the ring current both when the zinc disc is exposed to solution and when covered by a suitable epoxy resin. Hence, using the shielding Equation (4.63), the rate of corrosion of the metal at open circuit can be measured.

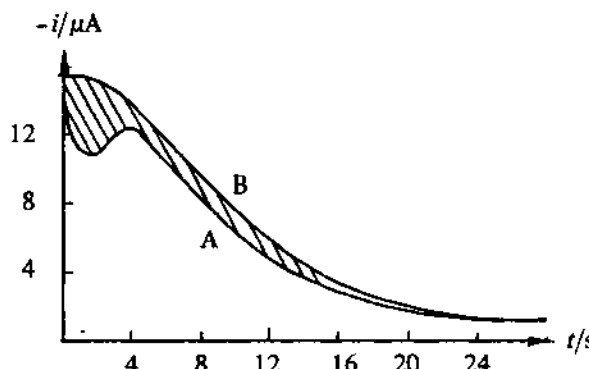


Fig. 4.23 – The application of the shielding effect to the study of the adsorption of Hg_2^{2+} ions during the deposition of an underpotential monolayer of Hg on Au. Solution is Hg_2^{2+} ($2 \times 10^{-5} \text{ mol dm}^{-3}$) in H_2SO_4 (0.2 mol dm^{-3}). Rotation rate 2500 r.p.m.

Curve A is the $-i_D$ vs t transient following the application to the Au disc of a potential step from +0.8 V to +0.4 V, where a monolayer of Hg deposits. Curve B is plot of i_R/N during this experiment when the Hg/Au ring is held at 0.0 V, a value where the reduction of Hg_2^{2+} is mass transport controlled. For a simple reaction the two transients would coincide and the difference corresponds to Hg_2^{2+} removed at the disc by a non-faradic process, i.e. adsorption of Hg_2^{2+} . Reproduced with permission from W. G. Sherwood & S. Bruckenstein, *J. Electrochem. Soc.*, 125, (1978), 1098.

REFERENCES

- [1] T. Von Karman, *Z. Angew. Math. Mech.*, 1 (1921) 233.
- [2] W. G. Cochran, *Proc. Camb. Phil. Soc. Math. Phys. Sci.*, 30 (1934) 345.
- [3] V. G. Levich, *Physicochemical hydrodynamics*, Prentice Hall, 1962.

- [4] A. C. Riddiford, *Advances in Electrochemistry and Electrochemical Engineering*, 4 (1966) 47.
- [5] S. R. de Sanchez & D. J. Schiffrian, *Corrosion Science*, 22 (1962) 585.
- [6] R. W. Zurrilla, R. K. Sen, & E. Yeager, *J. Electrochem. Soc.*, 125 (1978) 1103.
- [7] D. Jahn & W. Vielstich, *J. Electrochem. Soc.*, 109 (1962) 849.
- [8] R. D. Armstrong & G. M. Bulman, *J. Electroanal. Chem.*, 25 (1970) 121.
- [9] W. Vielstich & D. Jahn, *Advances in polarography*, (1960) 281. (Ed) I. Longmuir, Pergamon Press.
- [10] W. Vielstich & D. Jahn, *Z. Electrochem.*, 64 (1960) 43.
- [11] P. A. Malachesky, L. S. Marcoux, & R. N. Adams, *J. Phys. Chem.*, 70 (1966) 4068.
- [12] S. Karp, *J. Phys. Chem.*, 72 (1968) 1082.
- [13] L. S. Marcoux, R. N. Adams, & S. W. Feldberg, *J. Phys. Chem.*, 73 (1969) 2611.
- [14] G. Manning, V. D. Parker, & R. N. Adams, *J. Am. Chem. Soc.*, 91 (1969) 4584.
- [15] B. Miller, M. I. Bellavance, & S. Bruckenstein, *Anal. Chem.*, 44 (1972) 1983.
- [16] B. Miller & S. Bruckenstein, *J. Electrochem. Soc.*, 121 (1974) 1558.
- [17] K. Tokuda & S. Bruckenstein, *J. Electrochem. Soc.*, 126 (1979) 431 & 437.
- [18] B. Miller & S. Bruckenstein, *Anal. Chem.*, 46 (1974) 2026.
- [19] R. R. Adzic, N. M. Markovic, & A. V. Tripkovic, *Bull. Soc. Chim. Beograd.*, 45 (1980) 399.
- [20] H. Wroblowa, Y. D. Pan, & G. Razumney, *J. Electroanal. Chem.*, 60 (1976) 195.
- [21] K. B. Prater & A. J. Bard, *J. Electrochem. Soc.*, 117 (1970) 335.
- [22] W. J. Albery & M. L. Hitchman, *Ring disc electrodes*, Clarendon Press, Oxford, 1971.
- [23] W. J. Albery & S. Bruckenstein, *Trans. Faraday Soc.*, 62 (1966) 1946.
- [24] V. J. Puglisi & A. J. Bard, *J. Electrochem. Soc.*, 119 (1972) 829 and 833, and 120, (1973) 748.
- [25] A. J. Bard, V. J. Puglisi, J. V. Kenkel, & A. Lomax, *Faraday Disc.*, 56 (1973) 353.
- [26] B. Miller, *J. Electrochem. Soc.*, 116 (1969) 1117.
- [27] B. Miller & M. I. Bellavance, *J. Electrochem. Soc.*, 119 (1972) 1510.
- [28] M. N. Hull, *J. Electroanal. Chem.*, 38 (1972) 143.
- [29] W. J. Albery & S. Bruckenstein, *Trans. Faraday Soc.*, 62 (1966) 1932.
- [30] W. G. Sherwood & S. Bruckenstein, *J. Electrochem. Soc.*, 125 (1978) 1098.
- [31] S. Bruckenstein & B. Miller, *Accs. Chem. Research*, 10 (1977) 54.

Further reading

- (1) V. G. Levich, *Physicochemical hydrodynamics*, Prentice Hall, 1962.
- (2) W. J. Albery & M. L. Hitchman, *Ring disc electrodes*, Clarendon Press, 1971.

- (3) Yu V. Pleskov & V. Yu. Filinovskii, *The rotating disc electrode*, Consultants Bureau, 1976.
- (4) A. C. Riddiford, *Advances in Electrochem. and Electrochem. Eng.*, 4 (1966) 47.
- (5) S. Piekarski & R. N. Adams in *Physical methods of chemistry*, Part IIa -- Electrochem. Methods, (Eds) A. Weissberger and B. W. Rossiter, Interscience, 1971.
- (6) F. Opekar & P. Beran, *J. Electroanal. Chem.*, **69** (1976) 1.
- (7) S. Bruckenstein & B. Miller, *Accs. Chem. Research*, **10** (1977) 54.

5

The electrical double layer

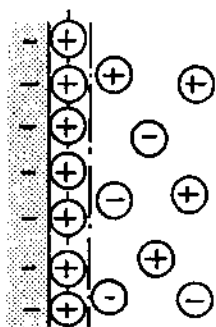
At any interface between two phases and particularly between an electrode and an electrolyte solution, there exists a segregation of positive and negative charge in a direction normal to the phase boundary. These charges may be associated in the form of dipolar molecules or polarised atoms, or they may be free as holes, electrons, or ions. The charge segregation may occur through the preferential adsorption of either positive or negative ions at the interface, through the transfer of charge across the interface, or through the deformation of polarisable molecules by the asymmetrical force field at the interface. The theory of the electrical double layer is concerned with the charge distribution and electrical potentials that arise as a consequence of this charge separation.

The study of the electrical double layer is intimately concerned with the concept of the ideally polarised electrode, which may be defined as an electrode at which no charge transfer can occur, regardless of the potential imposed by an external voltage source. The equilibrium established at such an interface is not chemical as the two phases have no component in common, but is electrostatic like that in a parallel plate capacitor. An important result of this concept is the possibility of a thermodynamic definition of the electrical charge on the metal and solution sides of the double layer. The activation energy for hydrogen evolution at a pure mercury electrode in protonic solvents is so high that this electrode behaves effectively as an ideally polarised electrode over a range of potential of about 2 volts. Mercury is also liquid at room temperature, easily obtained in a high degree of purity, and therefore the majority of studies on the electrical double layer refer to this electrode. Much of what we know has been obtained by macroscopic, thermodynamic experiments, and it is therefore

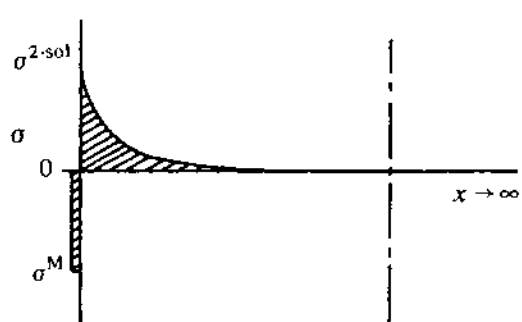
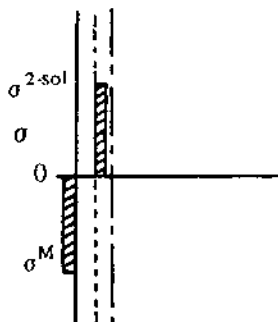
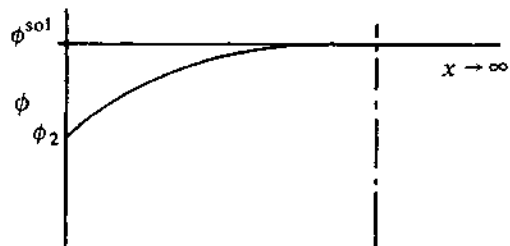
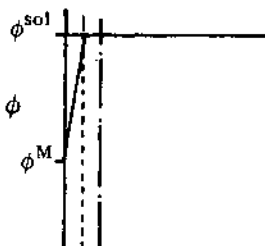
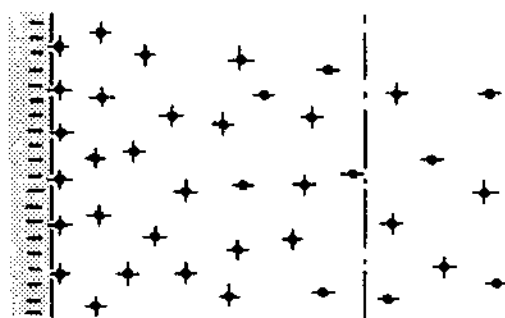
necessary to describe formally the thermodynamic treatment of the electrified interface (section 5.1). The experimental methods used in the study of the double layer are discussed in section 5.5.

A thermodynamic measurement leads to parameters that are macroscopic and relate to the interfacial region as a whole. It is necessary to rationalise these parameters on the basis of structural models for the interfacial region. The simplest model was due to Helmholtz, who envisaged that the excess charge on the metal would be neutralised by a monomolecular layer of ions of opposite charge to that on the metal phase (Fig. 5.1a). This concept of two layers of opposite charge is the origin of the term 'electrical double layer', and although the situation is undoubtedly more complex, the original name still remains.

(a) Helmholtz



(b) Gouy-Chapman



(c) Gouy-Chapman-Stern

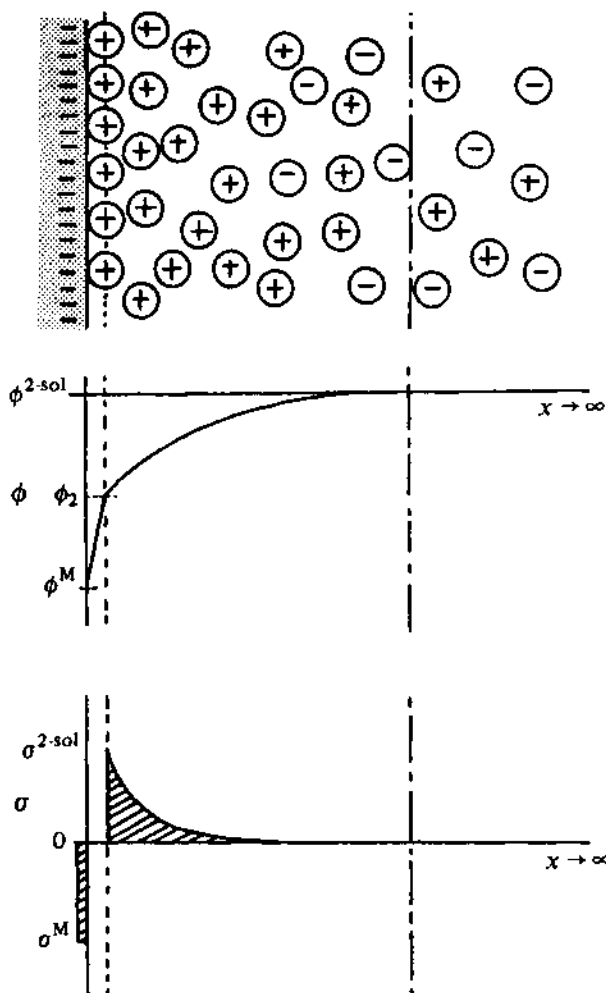


Fig. 5.1 – Schematic models of the ion, potential (ϕ), and charge (σ) distribution in a direction perpendicular to the plane of the electrode as described by (a) Helmholtz, (b) Gouy Chapman, and (c) Stern. Circles represent ions which may or may not be solvated; ---- is the inner Helmholtz plane, and —— · —— is the interphase-solution phase boundary.

Gouy and Chapman realised that in an electrolyte solution, the charges are free to move and are subject to thermal motion. They retained the concepts of the electrostatic theory to describe the coulombic metal-counter ion interaction but, in addition, they allowed for the random motion of the ions. The result is a diffuse layer of charge in which the concentration of counter ions is greatest next to the electrode surface and decreases progressively towards a homogeneous distribution of ions within the bulk electrolyte (Fig. 5.1b).

However, the theory neglects the finite size of the ions, and it was Stern who postulated that ions could not approach the electrode beyond a plane of closest approach, thereby introducing in a crude way the ion size (Fig. 5.1c). Although formulated in a complex manner [1], the basis of Stern's model is a combination of the Helmholtz and Gouy-Chapman approaches. It may be noted that Fig. 5.1 also shows the potential and charge distributions resulting from the models. These will be discussed later.

More recently, Grahame realised that full interpretation of the thermodynamic data required two planes of closest approach; one for specifically adsorbed ions and one for non-specifically adsorbed ions, and a diffuse layer region extending to the bulk electrolyte phase. This structure immediately adjacent to the electrode is shown schematically in Fig. 5.2 and is described in more detail in section 5.2. More recent approaches retain the principles of Grahame's model but attempt to include more quantitatively the role played by the solvent species, and studies of organic adsorption have become important in this respect. Adsorption can be described formally in terms of models based on the two-dimensional analogue of the ideal gas, and this is discussed in section 5.3. Finally, the structure of the interface greatly influences the electrode kinetics as it is precisely in this region where the act of electron transfer occurs. Consequently a knowledge of the potential distribution and the position of the reactant species with respect to the electrode when electron transfer occurs is imperative. These problems are discussed in section 5.4.

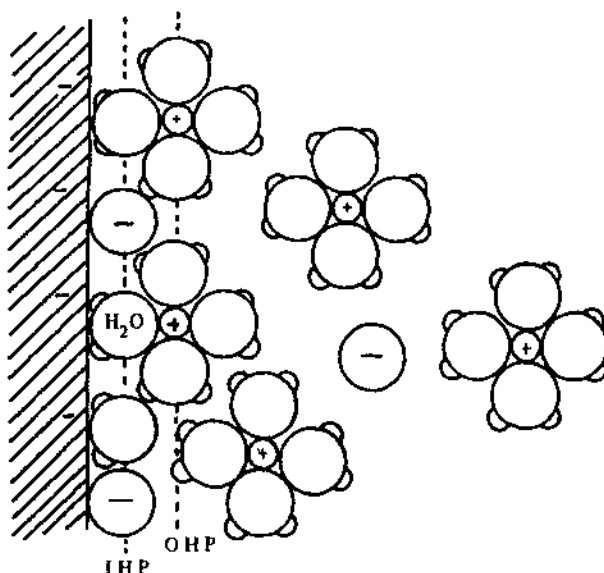


Fig. 5.2 -- Grahame's model of the interfacial region in the immediate vicinity of the electrode; \oplus and \ominus represent cations and anions respectively, and O is a water molecule which may be free or involved in primary solvation. IHP is the inner Helmholtz plane, OHP is the outer Helmholtz plane.

5.1 THE THERMODYNAMICS OF CHARGED INTERFACES

The thermodynamic theory of the ideally polarised electrode has been extensively reviewed in the past few decades [1-5], and the relationship with the ideally non-polarisable interface has been derived in an elegant treatment by Parsons [6]. The starting point in all derivations is the Gibbs-Duhem equation which defines the relationship between the extensive thermodynamic variables. For a bulk phase this has the form:

$$SdT - VdP + \sum_i n_i d\mu_i = 0 \quad (5.1)$$

in which S is the entropy, V is the volume, T is the absolute temperature, P is the pressure exerted on the phase, n_i is the number concentration of component i (molecules, atoms, ions, or electrons), and μ_i is the chemical potential of component i in the phase. For a planar interphase an additional term is necessary to allow for the free energy associated with the formation of the interface; the Gibbs-Duhem equation becomes

$$SdT - VdP + Ad\gamma + \sum_i n_i d\mu_i = 0 \quad (5.2)$$

where γ is the interfacial tension for the electrode/solution interface and A is the surface area. This equation when expressed in terms of unit area of surface, and under conditions of constant temperature and pressure, reduces to the Gibbs adsorption isotherm

$$d\gamma + \sum_i \Gamma_i d\mu_i = 0 \quad (5.3)$$

where Γ_i represents the surface excess concentration of species i in the interphase.

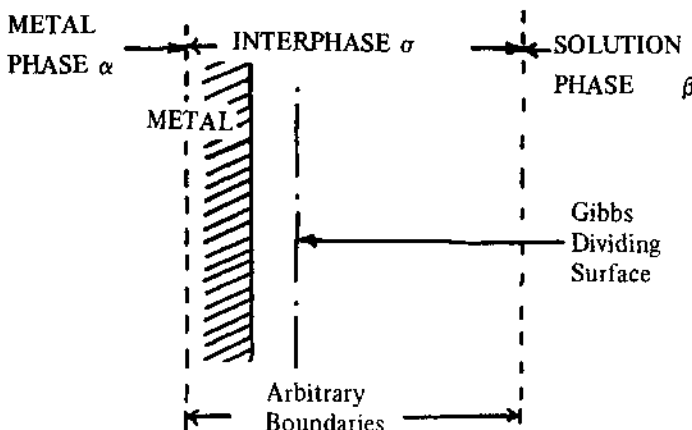
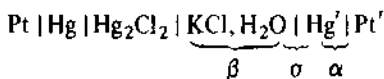


Fig. 5.3 - Model of the electrode-solution interface at equilibrium emphasising the definition of the phases.

In order to use these equations it is necessary to devise a model which enables the surface excess concentration of species i in the interphase to be defined. The interphase itself is defined by enclosing it in two arbitrary planes positioned in such a way that the bulk phases extend homogeneously up to these planes. Any changes in the thermodynamic properties must occur between these planes (Fig. 5.3). If the thickness of the phase is known, then the concentration of species i can be mathematically expressed; this is the Guggenheim model. An alternative approach due to Gibbs introduces a third arbitrary plane called the dividing surface which acts as a reference surface. The concentration of species i can then be expressed in terms of an excess or deficiency of component i at the reference surface with respect to its concentration in the bulk phase.

Let us adopt the Guggenheim description for the interphase, and apply these concepts to a specific experimental cell consisting of a dropping mercury electrode (Hg') in contact with an aqueous electrolyte (KCl) and calomel reference electrode:



σ , α , and β are the interphase, metal phase, and solution phase respectively. The components in the interphase are the ions K^+ , Cl^- and Hg_2^{2+} , the solvent $H_2O(W)$, and the electron, e^- . At constant T and P , Equation (5.3) becomes

$$d\gamma + \Gamma_{K^+} d\tilde{\mu}_{K^+} + \Gamma_{Cl^-} d\tilde{\mu}_{Cl^-} + \Gamma_W d\mu_W + \Gamma_e d\tilde{\mu}_e + \Gamma_{Hg_2^{2+}} d\tilde{\mu}_{Hg_2^{2+}} = 0 \quad (5.4)$$

where $\tilde{\mu}$ is the electrochemical potential of species i . However, this expression may be simplified, since the following equilibria exist in the mercury and the solution phases:

$$\mu_{KCl} = \tilde{\mu}_{K^+} + \tilde{\mu}_{Cl^-} \quad (5.5)$$

$$2\mu_{Hg} = \tilde{\mu}_{Hg_2^{2+}} + 2\tilde{\mu}_e, \quad (5.6)$$

while the interphase as a whole must be electrically neutral and therefore

$$2\Gamma_{Hg_2^{2+}} + \Gamma_{K^+} - \Gamma_{Cl^-} - \Gamma_e = 0 \quad (5.7)$$

Also the chemical potentials in the bulk are subject to the Gibbs-Duhem equation which at constant T and P may be written:

$$\text{Phase } \alpha: n_{Hg} d\mu_{Hg} = 0 \quad (5.8)$$

$$\text{Phase } \beta: n_{KCl} d\mu_{KCl} + n_W d\mu_W = 0 \quad (5.9)$$

Therefore choosing water and Hg as the reference components (eliminating $d\mu_W$ and $d\mu_{Hg}$), imposing the electroneutrality condition, Equation (5.7), and substituting Equations (5.5) and (5.7) into (5.4), leads to:

$$d\gamma + \Gamma_{K^+} d\mu_{KCl}^\beta + (\Gamma_{Cl^-} - \Gamma_{K^+})(d\tilde{\mu}_{Cl^-}^\beta - d\tilde{\mu}_e^{Hg}) = 0 \quad (5.10)$$

where

$$\Gamma_{K^+,W} = \Gamma_{K^+} - \frac{n_{KCl}}{n_W} \Gamma_W \quad (5.11)$$

is the relative surface excess. It should be noted that introducing the Gibbs-Duhem relationship for the bulk phases is equivalent to choosing the Gibbs model to describe the interfacial region, where the dividing surfaces are placed to correspond with zero adsorption of the reference components, Hg and W in phases α and β respectively. The term $(d\tilde{\mu}_{Cl^-}^\beta - d\tilde{\mu}_e^{Hg})$ can be expressed in terms of the actual measured potential difference between the electrodes, E , in the following way. The measured cell potential is given by (where the superscripts always indicate the phase)

$$E = \phi^{Pt'} - \phi^{Pt} \quad (5.12)$$

where ϕ^{Pt} is the Galvani potential of the Pt phase. The electrochemical potential of a species i in phase α is related to the Galvani potential by

$$\tilde{\mu}_i^\alpha = \mu_i^\alpha + zF\phi^\alpha \quad (5.13)$$

where μ_i^α is the chemical potential of component i . Since the chemical potential in any phase of the same material is a constant at constant temperature then:

$$E = -(\tilde{\mu}_e^{Pt'} - \tilde{\mu}_e^{Pt})/F. \quad (5.14)$$

Considering the equilibria at the reference electrode

$$\tilde{\mu}_e^{Pt'} = \tilde{\mu}_e^{Hg'} \quad (5.15)$$

$$\tilde{\mu}_e^{Pt} = \tilde{\mu}_e^{Hg} \quad (5.16)$$

$$\tilde{\mu}_e^{Pt} = \tilde{\mu}_e^{Hg} = \mu_{Hg}^{Hg} - \frac{1}{2}\mu_{Hg_2^{1+}}^{Hg_2Cl_2} \quad (5.17)$$

$$\tilde{\mu}_e^{Pt} = \mu_{Hg}^{Hg} - \frac{1}{2}\mu_{Hg_2^{1+}Cl_2}^{Hg_2Cl_2} + \tilde{\mu}_{Cl^-}^\beta \quad (5.18)$$

Equation (5.14) becomes

$$E = -(\tilde{\mu}_e^{Hg'} - \mu_{Hg}^{Hg} + \frac{1}{2}\mu_{Hg_2^{1+}Cl_2}^{Hg_2Cl_2} - \tilde{\mu}_{Cl^-}^\beta)/F \quad (5.19)$$

and hence by differentiation

$$dE = -(d\tilde{\mu}_e^{Hg'} - d\tilde{\mu}_{Cl^-}^\beta)/F. \quad (5.20)$$

Substituting (5.20) into (5.10), we obtain

$$d\gamma + \Gamma_{K^+,W} d\mu_{KCl} + (\Gamma_{Cl^-} - \Gamma_{K^+})F dE = 0. \quad (5.21)$$

For the cell being considered, the term $(\Gamma_{K^+} - \Gamma_{Cl^-})F$ is the excess charge on the solution side of the interface, σ^{sol} , and because of the electroneutrality

condition and the concept of the ideally polarised electrode this must be equal but of opposite sign to the charge on the metal side of the interface, σ^M . Making this substitution in Equation (5.21) and generalising the equation to allow for neutral species N in the aqueous phase, leads to the equation:

$$-\frac{d\gamma}{dE} = \sigma^M dE_{\mp} + \Gamma_{\pm, w} d\mu_{MX} + \Gamma_{N, w} d\mu_N \quad (5.22)$$

where E_{\mp} is the potential measured with respect to a cation (E_+) or an anion (E_-) reversible electrode, $\Gamma_{\pm, w}$ is the relative surface excess of the cation or anion, and $\Gamma_{N, w}$ is the relative surface excess of the organic species.

5.1.1 The electrocapillary equation

It follows from Equation (5.22) that if the chemical potential of the adsorbing species is maintained constant, the charge density on the electrode is given by the Lippmann equation

$$\left(\frac{d\gamma}{dE} \right)_{T, P, \mu_N, \mu_{MX}} = -\sigma^M = \sigma^{\text{sol}}. \quad (5.23)$$

The interfacial tension is a measurable quantity (see section 5.5), and a typical set of electrocapillary curves for a variety of electrolytes is shown in Fig. 5.4. The curves are approximately parabolic and pass through a maximum value called the *electrocapillary maximum*. Examination of the Lippmann equation shows that the maximum corresponds to the condition when the electrode has no excess charge. At more negative potentials, the electrode surface has a negative excess charge, and at more positive potentials there is a positive surface charge.

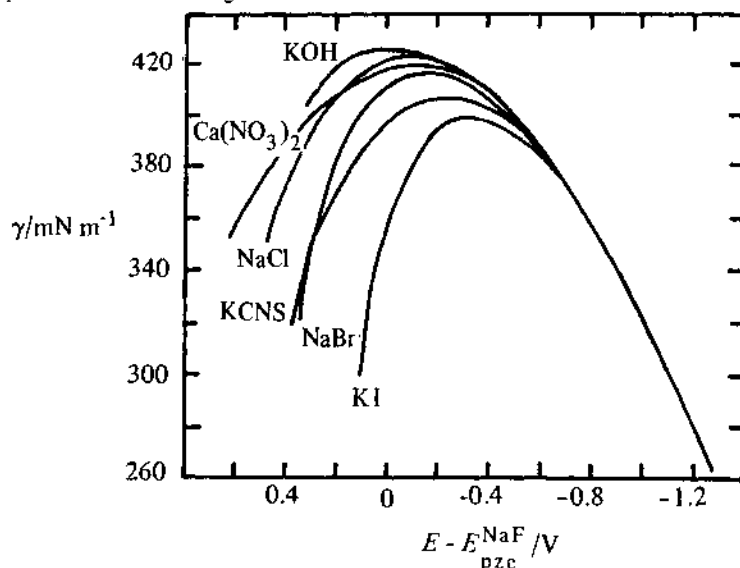


Fig. 5.4 – Electrocapillary curves for a series of 1 mol dm^{-3} aqueous solutions at a mercury electrode. $E_{\text{pzc}}^{\text{NaF}}$ is the potential at the point of zero charge for aqueous NaF. Data taken from D. C. Grahame, *Chem. Rev.*, **41** (1947), 441.

The separation of charge normal to the interface gives it the property of an electrical capacitor. However, the relationship between charge and potential for this capacitor is not generally linear, and consequently it is necessary to define a differential capacity, C .

$$C = \left(\frac{\partial \sigma^M}{\partial E} \right)_{T, P, \mu_N, \mu_{MX}} . \quad (5.24)$$

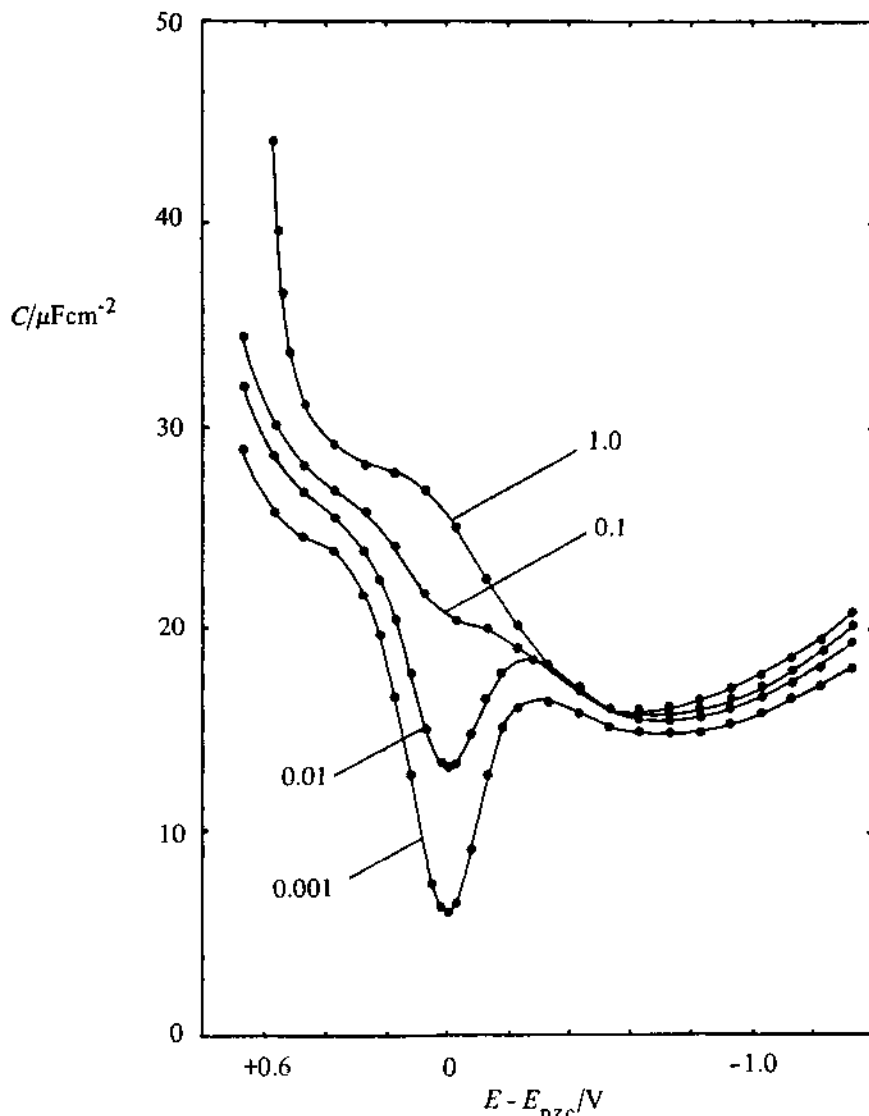


Fig. 5.5 Differential capacity curves for aqueous NaF as a function of concentration (mol dm^{-3}). Data taken from D. C. Grahame, *J. Am. Chem. Soc.*, **76**, (1954), 4819.

It follows from Equations (5.23) and (5.24) that differentiation of the Lippmann equation with respect to potential, yields a relationship between the differential capacity and the interfacial tension

$$\left(\frac{\partial^2 \gamma}{\partial E^2} \right)_{T, P, \mu_N, \mu_{MX}} = - \left(\frac{\partial \sigma^M}{\partial E} \right)_{T, P, \mu_N, \mu_{MX}} = -C . \quad (5.25)$$

The converse of this,

$$\gamma = \gamma_I - \int_{E_I}^E C dE \quad (5.26)$$

provides a useful route for obtaining electrocapillary curves from differential capacity data. The parameters γ_I and E_I are integration constants, so the value of surface tension at one potential needs to be known. The value of the interfacial tension at the electrocapillary maximum and the potential of zero charge (i.e. the potential where the electrode in the electrolyte is neither positively or negatively charged) are usually chosen, but in principle the values at any fixed potential could be used. Typical capacity curves for various concentrations of NaF are shown in Fig. 5.5.

5.1.2 The adsorption of organic molecules

The relative surface excess for neutral molecules can be obtained from surface tension measurements at constant potential and base electrolyte concentration. Under these conditions Equation (5.22) reduces to

$$\left(\frac{\partial \gamma}{\partial \mu_N} \right)_{T, P, E, \mu_{MX}} = -\Gamma_{N,W} . \quad (5.27)$$

To convert this expression into a useful form we note that for ideal solutions, the chemical potential is related to the bulk concentration through the equation:

$$d\mu_N = RT d \ln c_N^\infty . \quad (5.28)$$

It is also convenient to utilise the surface pressure, π , which is defined as

$$\pi = \gamma_0 - \gamma_N \quad (5.29)$$

where γ_0 is the interfacial tension of the solution in absence of the organic compound and γ_N is the value with organic species present. The combination of Equations (5.27), (5.28) and (5.29) gives

$$\Gamma_{N,W} = \frac{1}{RT} \left(\frac{d\pi}{d \ln c_N^\infty} \right)_{T, P, \mu_{MX}, E} . \quad (5.30)$$

Figure 5.6 shows surface excess data for the adsorption of pentaerythritol obtained from surface pressure measurements by the application of Equation

(5.30). In general, maximum adsorption occurs at small charge values ($\approx -2\mu C \text{ cm}^{-2}$ for the monofunctional aliphatic alcohols), and desorption occurs at the extremes of polarisation. This desorption is caused by the preferred adsorption at high fields of the solvent species owing to its large dipole moment. It should be stressed that $\Gamma_{N,W}$ is a relative surface excess defined by

$$\Gamma_{N,W} = \Gamma_N - \frac{n_N \Gamma_W}{n_W} \quad (5.31)$$

where the term $n_N \Gamma_W/n_W$ represents excess water present in the interface. It follows, that for $\Gamma_{N,W}$ to be consistent with the physical interpretation of adsorption, i.e. as being the surface concentration of adsorbate, the identity $n_N \ll n_W$ has to be valid.

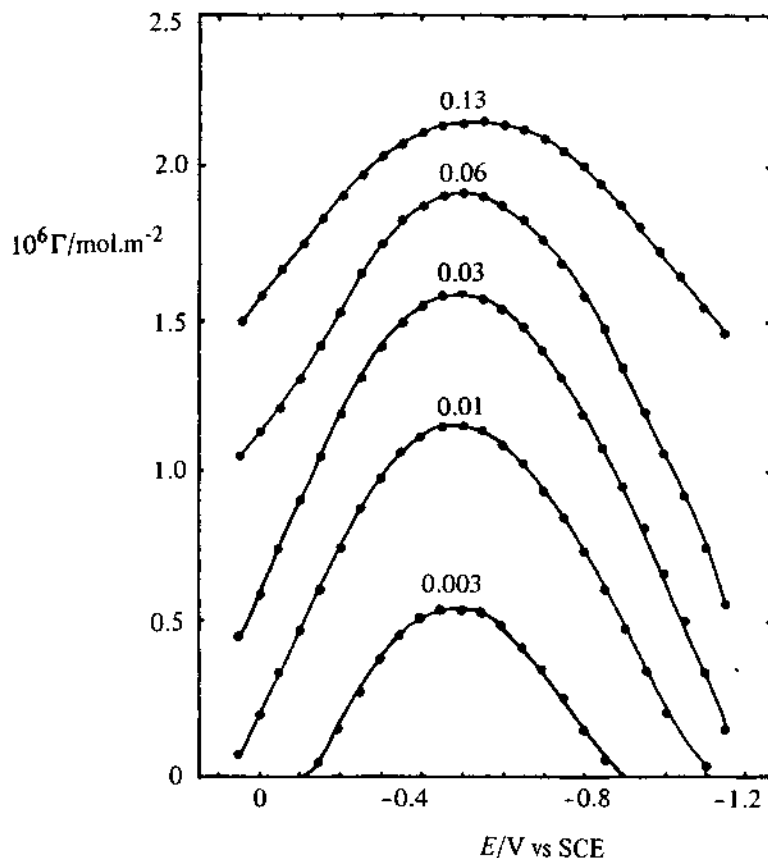


Fig. 5.6 – The relative surface excess as a function of potential for the adsorption of pentaerythritol at a Hg electrode. The concentrations of organic adsorbate are shown in mol dm^{-3} .

5.1.3 The adsorption of ionic species

Adopting a similar strategy to the organic case, the adsorption of an ionic species can be obtained from the relationship:

$$\Gamma_{\pm,w} = \frac{1}{RT} \left(\frac{d\gamma}{d \ln c_{MX}^{\infty}} \right)_{T, P, E_{\pm}, \mu_N} . \quad (5.32)$$

An important consequence of the thermodynamics is that the surface excess obtained depends upon the potential determining ion of the reference electrode. Typical results for a number of electrolytes are shown in Fig. 5.7. Further analysis is possible by working at constant mole fraction or ionic strength, but these

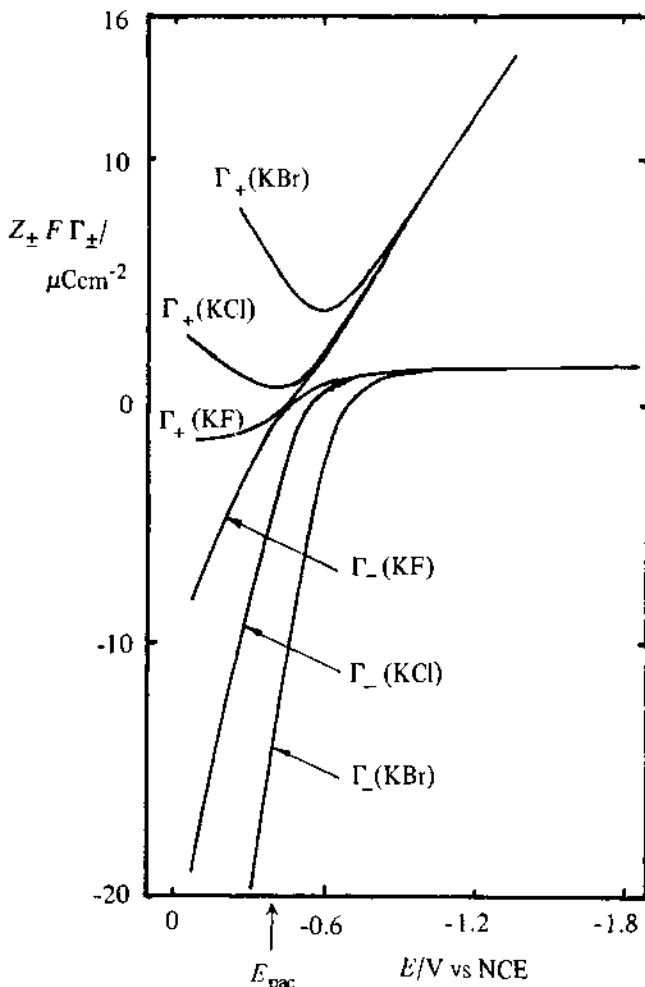


Fig. 5.7 – The charge attributed to cations ($z_+ F \Gamma_+$) and anions ($z_- F \Gamma_-$) in the electrical double layer for 0.1 mol dm^{-3} aqueous solutions at a mercury electrode. Data taken from D. C. Grahame & B. A. Soderberg, *J. Chem. Phys.*, 22 (1954), 449.

methods will not be discussed further. If T and P are experimentally varied, the electrocapillary equation leads to further information about the structure of the double layer.

S.2 THE STRUCTURE OF THE ELECTRICAL DOUBLE LAYER

The thermodynamic treatment of adsorption is macroscopic and only provides information on the interphase as a whole. The currently accepted model for the structure of the interfacial region is due to Grahame [4], and the historical progression leading to its formulation has been discussed previously [1]. The interface is split into three regions: the metal layer, the diffuse layer, and the inner layer. This is shown schematically in Figs. 5.2 and 5.8, along with some of the mathematical notation. The metal layer is homogeneous, and its excess charge resides in a thin two-dimensional layer adjacent to the solution.

The inner layer is only one or two molecular diameters in thickness and contains solvent molecules and sometimes a fractional monolayer of neutral molecules or specifically adsorbed ions. These specifically adsorbed ions are usually anions, but evidence is available that suggests some cations (e.g. caesium) may also specifically adsorb.

The adsorption forces are short range, although the detailed nature of these forces has not yet been completely resolved. The specifically adsorbed ions are generally considered to be unsolvated, especially in the direction of the metal, and the locus of their centres defines the position of the Inner Helmholtz Plane (IHP).

The diffuse layer is the region between the bulk and the Outer Helmholtz Plane (OHP) which is recognised as the plane of closest approach of non-specifically adsorbed species. The properties of this layer can be explained in terms of an equilibrium between thermal motion and the long range coulombic interaction of the ions with the charge on the electrode. It can be regarded as the ionic atmosphere of the metal electrode, and is independent of the chemical nature of the ion.

The mathematical formulation of the diffuse layer region was worked out by Gouy and Chapman and has been treated fully in several reviews [1, 4, 7]. Maxwell-Boltzmann statistics were assumed to relate the concentration of ions at a specified position in the interface to its bulk concentration, c^∞ , and the electrostatic potential;

$$c(x) = c^\infty \exp\left(-\frac{z_i F \phi(x)}{RT}\right). \quad (5.33)$$

However, the potential is also related to the charge density, ρ , through the one-dimensional Poisson equation;

$$\frac{d^2\phi(x)}{dx^2} = -\frac{\rho(x)}{\epsilon\epsilon_0} \quad (5.34)$$

where ϵ is the relative permittivity and ϵ_0 is the permittivity of free space, and combining these two equations followed by integration leads to an expression for the charge on the solution side of the interface, $\sigma^{2\text{-sol}}$, and hence the diffuse layer capacity C^d . The algebra is straightforward but tedious and gives, for a symmetrical 1:1 electrolyte:

$$\sigma^{2\text{-sol}} = -(8RT\epsilon\epsilon_0 c^\infty)^{1/2} \sinh\left(\frac{zF\phi_2}{2RT}\right) \quad (5.35)$$

and

$$C^d = \frac{d\sigma^{2\text{-sol}}}{d\phi_2} = zF\left(\frac{2\epsilon\epsilon_0 c^\infty}{RT}\right)^{1/2} \cosh\left(\frac{zF\phi_2}{2RT}\right). \quad (5.36)$$

These equations are important for electrode kinetics (section 5.4) and for understanding the observed dependence of differential capacity on the concentration of the electrolyte.

A model for the interface and the corresponding potential profile in the absence of specific adsorption is shown schematically in Fig. 5.8(a). This model applies particularly to solutions of the fluorides of the alkali-metals as the fluoride ion, being small, retains its solvation sheath and is unable to penetrate the inner region which therefore consists only of solvent species. The solvent may be present as single molecules or may form two-dimensional solvent clusters. The orientation of the interfacial solvent will be influenced by the charge on the metal and, if it constitutes the hydration shell of an ion situated at the OHP, also by the ionic charge. The excess positive charge on the metal will be balanced in the solution by a diffuse layer of solvated anions. Formally the potential drop across the interface is given by:

$$(\phi^M - \phi^{sol}) = (\phi^M - \phi_2) + (\phi_2 - \phi^{sol}) \quad (5.37)$$

where $(\phi^M - \phi_2)$ and $(\phi_2 - \phi^{sol})$ are the Galvani potential drops across the inner layer and diffuse layer respectively. It follows that:

$$\frac{d(\phi^M - \phi^{sol})}{d\sigma} = \frac{d(\phi^M - \phi_2)}{d\sigma} + \frac{d(\phi_2 - \phi^{sol})}{d\sigma} \quad (5.38)$$

or

$$\frac{1}{C} = \frac{1}{C^i} + \frac{1}{C^d}. \quad (5.39)$$

The observed capacitance, C , is a series combination of the inner layer capacity, C^i , and the diffuse layer capacity. Equation (5.36) predicts an inverted parabolic dependence between C^d and ϕ_2 . Furthermore, the capacity at the minimum decreases with decreasing concentration and is centred symmetrically about the potential of zero charge for a $z:z$ valent electrolyte. Consequently, the diffuse layer contribution only becomes apparent in dilute solutions, as is shown for NaF solutions in Fig. 5.5. As the inner layer contains only solvent molecules, its capacity is independent of NaF concentration so that once C^i is known as a function of potential then the capacity curves at all other concentrations can be calculated. This has been confirmed experimentally. Similar equations have been

derived for unsymmetrical electrolytes, although in this case the diffuse layer capacity is unsymmetrical about the minimum value which is also displaced slightly from the point of zero charge. A recent study has shown that the diffuse layer model works reasonably well for unsymmetrical electrolytes [8]. The Gouy-

(a)

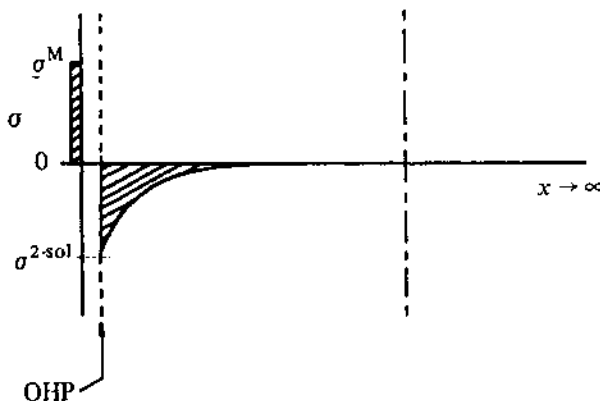
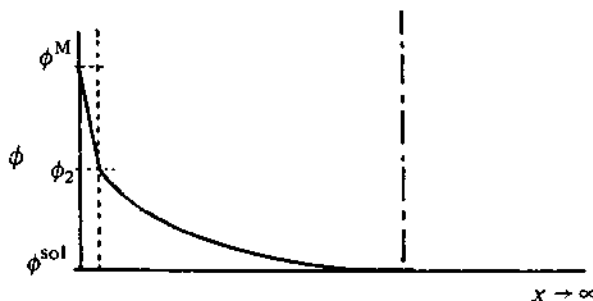
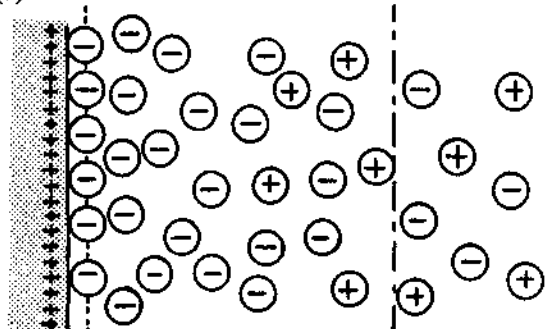


Fig. 5.8 – Schematic models of the ion, potential (ϕ) and charge (σ) distribution across the metal-electrolyte interface for (a) non-specific adsorption, (b) weak specific adsorption and (c) strong specific adsorption. ϕ^M , ϕ_1 , ϕ_2 and ϕ^{sol} are the Galvani potentials at the metal, inner Helmholtz plane (IHP), outer Helmholtz plane (OHP), and bulk solution respectively. σ^M , σ^I , σ^{2sol} represent the excess charge on the metal, inner layer, and diffuse layer respectively. Small circles are unsolvated species; large circles are solvated species.

Chapman model is satisfactory when the adsorption is controlled by the nature of the hydrated cation (i.e. at negative electrode charge). This is indicated by the shape of the electrocapillary curve, which at negative potentials is virtually the same for all the salts shown in Fig. 5.4.

With the possible exception of fluoride ion, specific adsorption occurs as the electrode becomes positively charged and the anion penetrates the inner layer displacing the solvent. If specific adsorption is weak, the positive electrode charge is only partially shielded by the adsorbed inner layer charge, and consequently a diffuse layer of solvated anions is established Fig. 5.8(b). However,

(b)

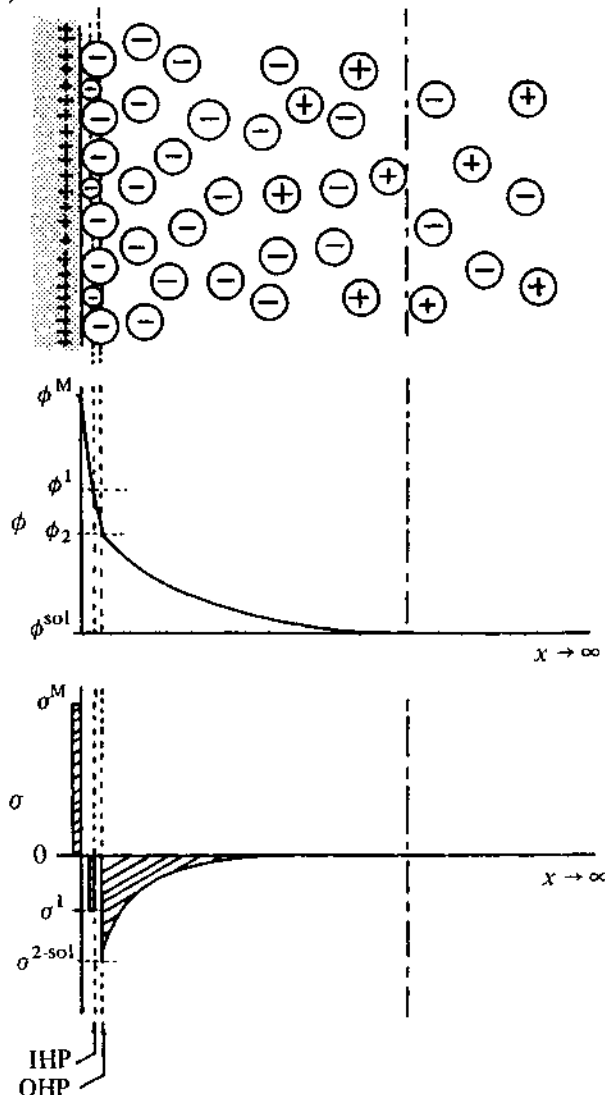


Fig. 5.8 -- See legend page 163

if the metal-ion interaction is strong, then the specifically adsorbed charge may exceed the positive charge on the electrode, effectively causing a charge reversal at the Outer Helmholtz Plane and establishing a diffuse layer region of solvated cations Fig. 5.8(c). The effect is demonstrated by the experimental data in Fig. 5.7. The relative surface excess of K^+ is negative at positive electrode charge values if the electrolyte is KF as expected in the absence of specific

(c)

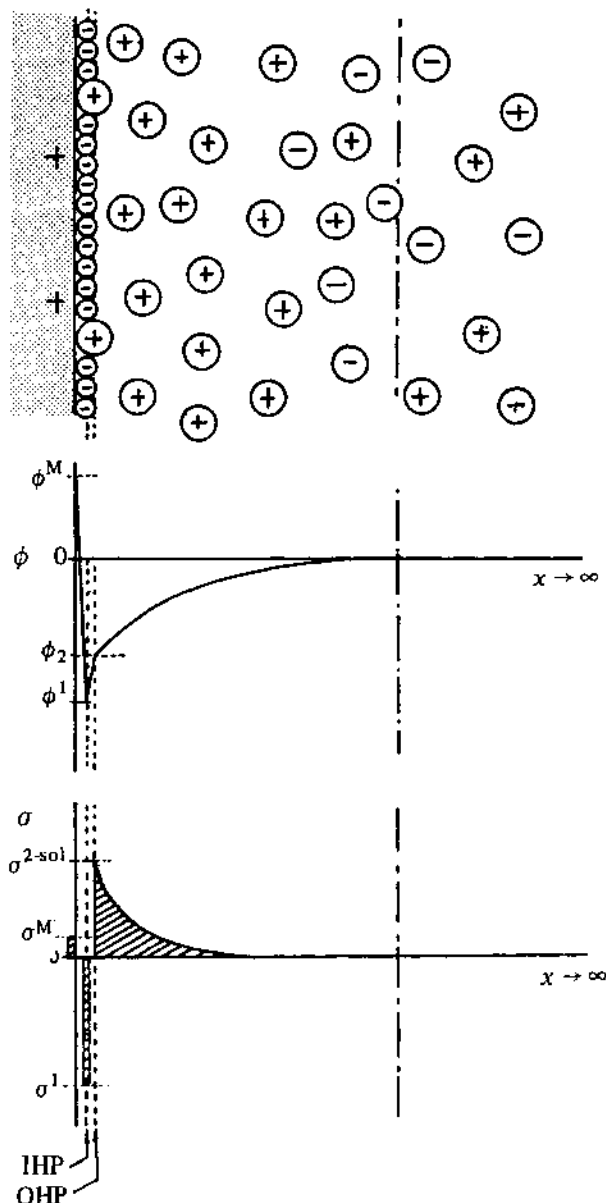


Fig. 5.8 - See legend page 163

adsorption. If the electrolyte is KCl or KBr then specific adsorption of the anion is strong and charge reversal is indicated by the positive surface excess for K^+ at positive charge values. In KBr the mercury-anion interaction is so strong that the adsorption of anions occurs even at negative electrode charge values. A further indication of specific adsorption is a shift in the potential of zero charge with increase in electrolyte concentration (The Esin-Markov effect). Thus specific adsorption of anions is indicated by a negative shift in potential at constant charge density, and vice versa for cations. Non-specific adsorption creates no mechanism for a potential shift to occur, and thus with NaF solutions the point of zero charge is found to be independent of concentration. In aqueous media, the degree of specific adsorption increases in the sequence:



5.3 THE ADSORPTION ISOTHERM

The adsorption isotherm (Γ vs c) describes the relationship at constant temperature, pressure, and electrical variable between the surface concentration, Γ , and bulk concentration of an adsorbed species. Two closely related concepts are the equation of state (π vs Γ) which describes how the surface pressure of the adsorbed layer varies with surface concentration, and the pressure equation (π vs c) describing the relationship between surface pressure and bulk adsorbate concentration. These three relationships are often confused in the literature as they represent equivalent expressions for a particular physical model. The adsorption isotherm and the pressure equation can be obtained from a particular equation of state by substituting the latter into the Gibbs adsorption isotherm and integrating. The results for a number of well known isotherms are given in Table 5.1.

Table 5.1 – Common adsorption isotherms, and their corresponding equations of state

Name	Equation of state	Adsorption isotherm
Henry	$\pi = RT\Gamma$	$\ln \Gamma = \ln \beta c$
Virial	$\pi = RT(\Gamma + B'\Gamma^2)$	$\ln \Gamma + 2B'\Gamma = \ln \beta c$
Langmuir	$\pi = -RT\Gamma_S \ln(1 - \theta)$	$\ln [\Gamma\Gamma_S / (\Gamma_S - \Gamma)] = \ln \beta c$
Frumkin	$\pi = -RT\Gamma_S \{ \ln(1 - \theta) - (g/2)\theta^2 \}$	$\ln [\Gamma\Gamma_S / (\Gamma_S + \Gamma)] + g\Gamma/\Gamma_S = \ln \beta c$
Temkin	$\pi = g\Gamma^2$ $(0.2 < \theta < 0.8)$	$2g\Gamma/RT = \ln \beta c$

B' is the second virial coefficient, g is the interaction parameter, Γ_S is the saturation coverage, and θ is the fractional coverage of the surface.

β is the adsorption coefficient (see Equation (5.42)).

In essence, the isotherm is an attempt to separate the electrode-adsorbate interaction, β , which is manifest in the standard free energy for adsorption, from the lateral adsorbate-adsorbate interactions described formally through fitting parameters such as Γ_S , g , and B' . The physical model inherent in the adsorption isotherm is often most easily seen from the corresponding equation of state by comparison with the analogous three-dimensional PV relationship. For example, expansion of the logarithmic term for small coverage in the Langmuir equation of state reveals that the saturation coverage, Γ_S , represents the finite size of the adsorbing species and therefore, accounts for short range repulsive interaction between neighbouring molecules. Similarly in the Frumkin equation of state, the term $g\theta^2/2$ is a correction to the surface pressure due to long range interactions between adsorbing species analogous to the a/V^2 term postulated by Van der Waals for gases. The Frumkin equation is able to account for both attractive ($a < 0$) and repulsive ($a > 0$) interactions and also a two-dimensional condensation for a critical value of the interaction parameter ($g = 4$).

In contrast to the solid-gas and liquid-gas systems, the metal-solution interface offers the possibility of altering directly the free energy of adsorption by external control of the electrical variable. The choice of potential or charge as the variable has been a matter of controversy for many years, and is still an unresolved problem. Invariably adsorption isotherms for a particular system plotted with the different electrical variables have the same shape. This condition is referred to as congruence, and generally implies that the adsorbate-adsorbate interactions are unaffected by the field which merely influences the metal-adsorbate interaction. In this case, the free energy of adsorption may be formally split into a field dependent component and a chemical term, $\Delta G_{\text{chem}}^\ominus$, which can be attributed in the absence of specific adsorption, to the standard free energy of adsorption at the point of zero charge. The chemical free energy term has values in the range $15\text{--}20 \text{ kJ mol}^{-1}$, which is consistent with physical adsorption forces. The field dependence has generally been found to be linear for ions and for fixed permanent dipoles, consistent with a strong electrostatic interaction with the electrode; a quadratic dependence is found when the adsorption is a property of the polarisability and thickness of the adsorbate and solvent layer as is the case for the adsorption of many neutral organic molecules.

Several problems have arisen with the adsorption isotherm approach. Adsorption at the liquid-solid interface is essentially a solvent replacement reaction, and it is therefore incorrect to adopt the models for adsorption at a gas-solid interface. It is implicit in the Frumkin adsorption isotherm that the adsorbate replaces a single solvent species at the electrode, and in this respect it is surprising that this equation is able to predict successfully the adsorption of a number of large organic molecules (e.g. sucrose [9]). Indeed this success has been used as evidence suggesting that interfacial solvent exists as two-dimensional clusters. Several isotherms have been proposed that allow for more than one solvent species being replaced, but this approach only introduces yet another unknown fitting parameter [10]. Finally the quantitative comparison of literature values for the standard free energy of adsorption is often impossible, owing to an inconsistent definition of the standard state in the surface phase. If the solvent is treated as a continuum, then adsorption from solution may be

represented as an equilibrium between a particle in the bulk, A_b , and on the surface A_s :

$$\mu_{A,s} = \mu_{A,b} \quad (5.40)$$

or

$$\mu_{A,s}^\ominus + RT \ln \frac{\Gamma_{A,s}^*}{\Gamma_{A,s}} = \mu_{A,b}^\ominus + RT \ln \frac{c_{A,b}^*}{c_{A,b}} \quad (5.41)$$

where $\Gamma_{A,s}^*$ and $c_{A,b}^*$ represent the standard states for the species on the surface and in bulk solution respectively.

From the definition of the standard free energy of adsorption, $\Delta G_{ads}^\ominus = \mu_{A,s}^\ominus - \mu_{A,b}^\ominus$, it follows that

$$\Gamma_{A,s} = \beta c_{A,s} \quad (5.42)$$

where β is the adsorption coefficient:

$$\beta = \frac{\Gamma_{A,s}^*}{c_{A,s}^*} \exp - \frac{\Delta G_{ads}^\ominus}{RT} \quad (5.43)$$

The inclusion of the standard state is deliberate to demonstrate that the adsorption coefficient will have units dependent upon the choice of standard states in the bulk and on the surface.

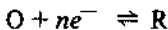
5.4 THE EFFECT OF DOUBLE LAYER STRUCTURE ON ELECTRODE KINETICS

The structure of the interfacial region is not considered in the derivation of the Butler-Volmer equation, and it is implicit in that treatment that the whole potential drop between the metal and the solution is effective in driving the charge transfer reaction. A more exact treatment takes into account the effect of the double layer structure. The simplest model neglects specific adsorption effects and assumes for theoretical convenience that the electroactive species is situated at the Outer Helmholtz Plane when the charge transfer occurs. The corrections are twofold:

- (a) The driving force for the electron transfer reaction is not the metal-solution Galvani potential difference but is the potential difference between the metal and the OHP, ($\phi^M - \phi_2$).
- (b) The concentration of charged electroactive species at the OHP is not the bulk value but is given by the Boltzmann equation as:

$$c_O^{OHP} = c_O^\infty \exp \left(\frac{-z_O F(\phi_2 - \phi^S)}{RT} \right). \quad (5.44)$$

On the basis of this model, the double layer effect for the generalised reaction



may be expressed by the equation

$$I = I_0 \exp\left((\alpha_C n - z_O) \frac{F\Delta\phi_2}{RT}\right) \left[\exp\left(\frac{(1 - \alpha_C)nF\eta}{RT}\right) - \exp\left(\frac{-\alpha_C n F \eta}{RT}\right) \right]. \quad (5.45)$$

and it is useful to define a true exchange current, $I_{0,t}$, by

$$I_0 = I_{0,t} \exp\left((\alpha_C n - z_O) \frac{F\phi_{2,e}}{RT}\right) \quad (5.46)$$

I_0 is the apparent exchange current density,

$I_{0,t}$ is the true exchange current density,

z_O is the charge on the oxidised species

$\Delta\phi_2 = (\phi_2 - \phi_{2,e})$ where ϕ_2 is the potential of the OHP and $\phi_{2,e}$ is the OHP potential at the equilibrium potential for the redox reaction.

The effect of the double layer on the kinetics is contained within the term $\exp[(\alpha_C n - z_O)(F\Delta\phi_2/RT)]$, which is known as the *Frumkin correction*. It is the same for the forward and backward processes in compliance with transition state theory and the importance of the correction depends upon the magnitude and signs of α_C , n , z_O , and $\Delta\phi_2$. If it is assumed that equilibrium prevails within the diffuse layer even when charge transfer occurs and that the diffusion layer is much thicker than the diffuse layer, then Gouy-Chapman theory can be used to calculate the dependence of ϕ_2 on the supporting electrolyte concentration (Equation (5.35)). The combination of these theoretical calculations with experimental σ^M/E data allows the dependence of ϕ_2 on potential to be obtained, as shown in Fig. 5.9. The magnitude of $\Delta\phi_2$ depends upon the position of the

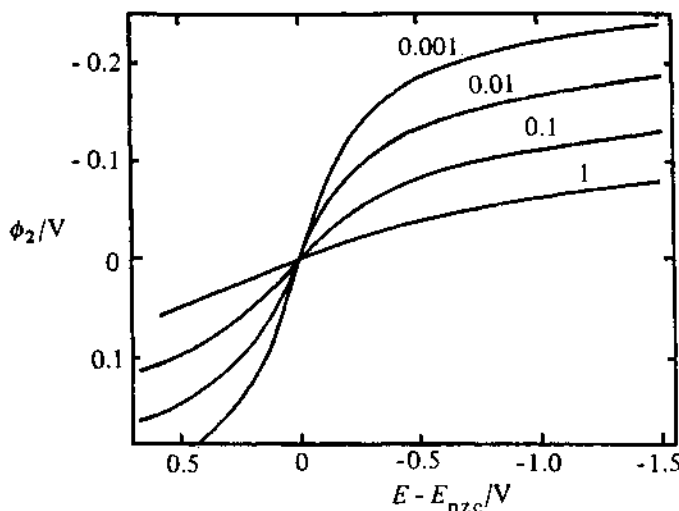


Fig. 5.9 – Potential of the outer Helmholtz plane ϕ_2 as a function of the rational potential for the mercury-aqueous NaF electrode. Concentrations of NaF are indicated on the diagram in mol dm^{-3} . Reproduced with permission from R. Parsons, *Advances in Electrochem. and Electrochem. Eng.*, 1 (1961), 1.

equilibrium potential relative to the point of zero charge. Clearly the effects are most significant in dilute solutions of ions, especially if the equilibrium potential lies close to the potential of zero charge. One of the most important functions of a high concentration of supporting electrolyte is therefore to minimise the effect of the double layer on the kinetics. If the equilibrium potential is situated some distance from E_{pzc} then the effect will be small for small overvoltages but may become significant at larger overvoltages.

A further consequence of these equations is that the Tafel plots may not be linear, or they may be linear with a slope determined by an apparent transfer coefficient α_C^{app} . In the cathodic limit

$$-\alpha_C^{\text{app}} \frac{nF}{RT} = \frac{d \ln -I}{d\eta} = -\alpha_C \frac{nF}{RT} + (\alpha_C n - z_O) \frac{F}{RT} \frac{d\Delta\phi_2}{d\eta} \quad (5.47)$$

and in the anodic limit

$$\alpha_A^{\text{app}} \frac{nF}{RT} = \frac{d \ln I}{d\eta} = (1 - \alpha_C) \frac{nF}{RT} + (\alpha_C n - z_O) \frac{F}{RT} \frac{d\Delta\phi_2}{d\eta}. \quad (5.48)$$

Some model calculations made by Parsons [11] for the reduction of anions and cations on mercury from NaF show how dramatic the deviations can be (Fig. 5.10).

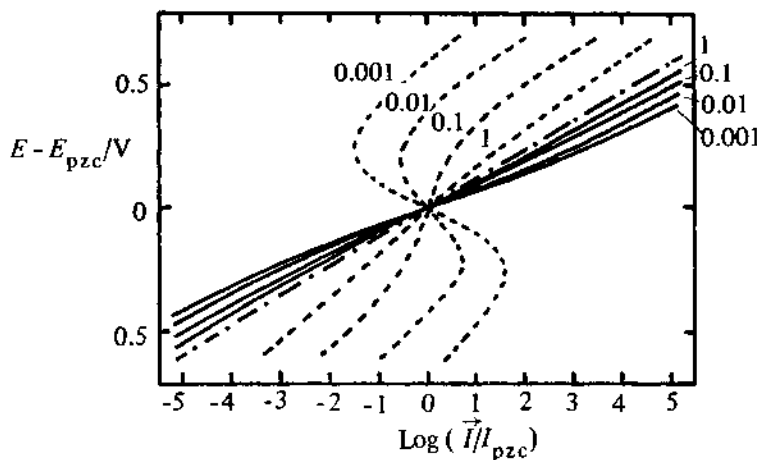


Fig. 5.10 – The effect of the Frumkin correction on the ideal Tafel plot (— · —); for the reduction of monovalent anions (---), and monovalent cations (— · —), for various concentrations of base electrolyte (NaF) indicated in mol dm^{-3} . Reproduced with permission from R. Parsons, *Advanced in Electrochem & Electrochem. Eng.*, 1 (1961), 1.

A more complicated situation arises when one or more of the species present is strongly adsorbed on the metal. If the species is a major component this may lead to total coverage of the surface by an adsorbed layer and complete inhibition

of the electrode reaction. This offers a commercially important way to prevent corrosion, and many organic molecules are corrosion inhibitors. Furthermore, if the adsorbed species is that undergoing reaction, then the kinetics of the electrochemical reaction may be strongly influenced by the degree and rate of adsorption. Finally, it should be observed that if the interface is that between a solution and a semiconductor or between two immiscible liquids, then the considerations of charge separation and potential distribution will apply to both sides of the interface.

5.5 EXPERIMENTAL METHODS

The majority of double layer studies have been made on mercury electrodes by measuring differential capacity or interfacial tension over a potential range where the electrode is ideally polarised. Analysis of the data depends upon the validity of the Gibbs adsorption equation. Direct confirmation of this equation is experimentally difficult, but has been attempted using radiotracer techniques [12] with a moderate degree of success. More recently infrared and Raman spectroscopy, ellipsometry, and other optical methods are providing useful information on the double layer structure. These methods are applicable to solid electrodes and may be less ambiguous than the capacitance method when there is interference from Faradaic processes. Quantitative information may be obtained by investigating the effect that adsorbates have on the kinetics of an electrode reaction.

5.5.1 Differential capacitance measurements

Differential capacitance can be measured with an accuracy of 0.1% using an a.c. impedance bridge [13] in the configuration shown in Fig. 5.11. The equivalent circuit of the cell is given by the double layer capacitance in series with a solution resistance and a capacitance associated with the platinum counter electrode (Fig. 5.11(d)). Providing the counter electrode area is large compared to the area of the mercury drop then, as a consequence of the reciprocal relationship for capacitors in series, the equivalent circuit reduces to the double layer capacitance in series with a solution resistance. The fixed resistors in the bridge network are usually given an equivalent value in order to make the bridge direct reading, and the bridge is balanced when the potentials across the output terminals of the network are equal in magnitude and phase. This corresponds to a minimum amplitude (theoretically zero) in the out of balance signal. The a.c. source is a small amplitude sine wave (typically 8 mV peak to peak) to ensure that any variation in the capacitance produced by the superimposed a.c. signal remains within experimental error. A $0.1\ \mu\text{F}$ blocking capacitor reduces any spurious d.c. output produced by the signal generator, and isolates the polarising circuit from ground.

The detector circuit is isolated from the bridge network by a screened and balanced transformer, and the output signal is amplified, filtered, and displayed on the Y plates of an oscilloscope. However, complications arise when the working electrode is a dropping mercury electrode. The surface area of the

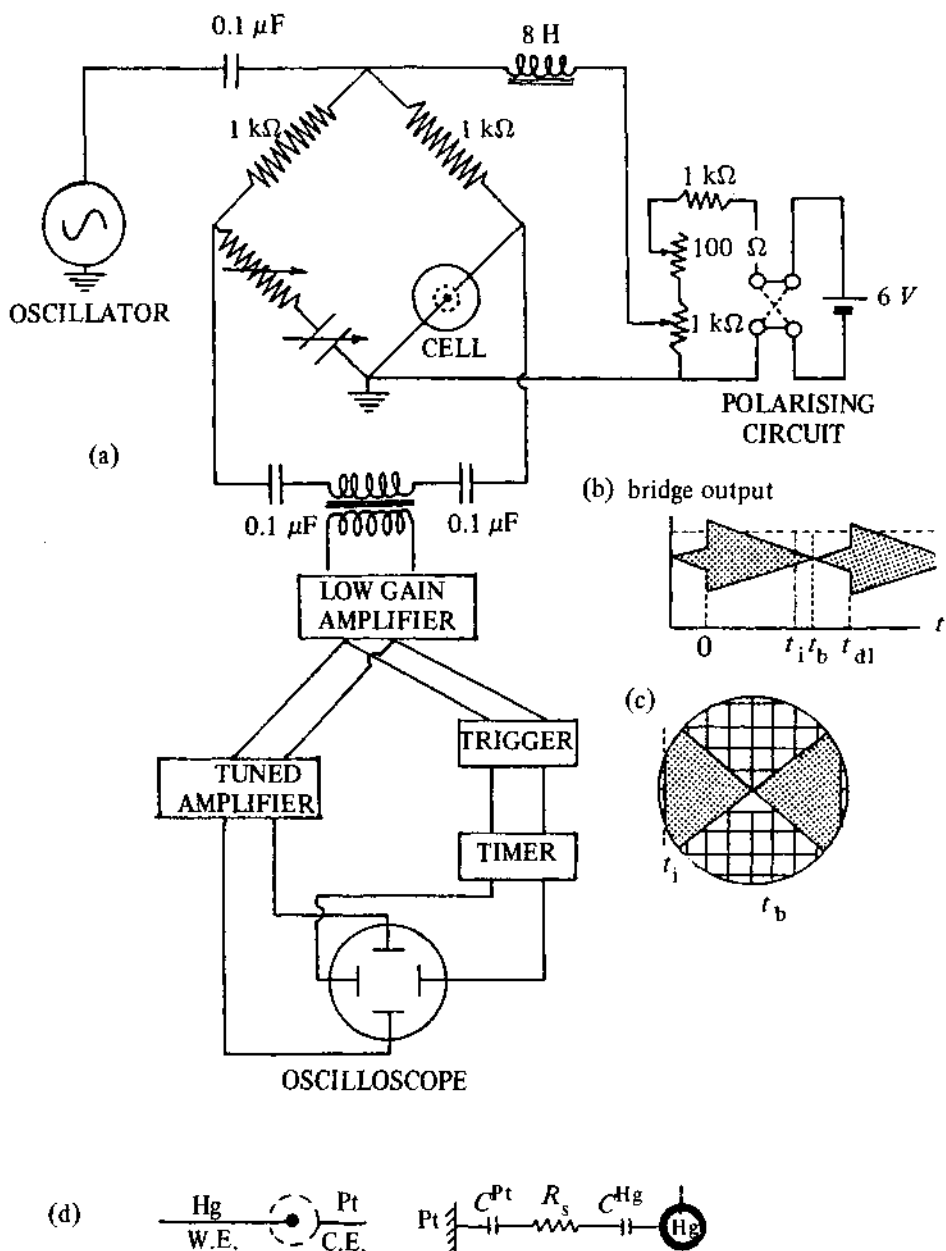


Fig. 5.11 – (a) Schematic diagram of an a.c. impedance bridge for measuring the differential capacitance. (b) Form of the output signal from the bridge during the growth of a mercury drop. (c) Oscilloscope display at balance. (d) Schematic diagram of electrode arrangement and the equivalent circuit for the cell.

mercury interface is continuously increasing, owing to the growth of the drop, and consequently the capacitance and resistance have to be independently adjusted to obtain a unique balance point at a specified instant during the life of the drop. Also as capacitance is an intensive variable, it is necessary to determine simultaneously the area of the drop at the balance time, t_b . The output signal during drop growth is shown in Fig. 5.11(b). The detachment of the drop produces a large change in output signal ($t = 0$) that is used to trigger an interval timer. As the drop grows, the bridge output decreases and passes through a minimum at bridge balance (t_b). The timer is adjusted (t) to trigger the oscilloscope time base in such a manner that the balance point is displayed on the oscilloscope screen (Fig. 5.11(c)). Providing the flow rate of mercury is constant and the back pressure effect negligible, then the area of the drop at the balance time t_b can be calculated from

$$A = 4\pi \left(\frac{3Mt_b}{4\pi\rho_{Hg}} \right)^{2/3} \quad (5.49)$$

where ρ_{Hg} is the density of mercury and M is the flow rate.

A typical cell is shown in Fig. 5.12. A Luggin capillary is unnecessary as the electrode is ideally polarised and only a negligible current should flow (≈ 1 nA). The counter electrode is placed symmetrically about the working electrode, and provision is made for bubbling nitrogen continuously over and/or through the solution in the cell to remove dissolved oxygen. Capillaries are drawn to a fine taper and then cut clean and square at the tip to prevent frequency dispersion in the results. The internal bore is then siliconised using dichlorodimethylsilane to prevent spurious results caused by solution creep. The solution sealed tap is used in the closed position if the experiment requires the formation of a liquid-liquid junction. Finally, the results will be reproducible only if the utmost care is taken to ensure that the solvent and the electrolytes are of the highest possible purity.

The use of a capacitance bridge requires a certain degree of operator skill and patience, as the measurements are tedious and it may take several hours to record a single capacitance curve. An alternative method that is fast, easily adapted to computer control, and may be used for solid-electrolyte systems employs phase sensitive detection techniques to obtain the magnitude and phase relationship between an incoming signal and a reference signal [14]. The reference signal is applied to the cell as a small amplitude sinusoidal voltage superimposed on the polarising d.c. potential. The incoming signal is the response of the experimental cell to the perturbation, i.e. the current. Analysis requires an assumption concerning the equivalent circuit of the system. For the equivalent circuit of a resistor in series with a capacitor the in-phase component of the signal is proportional to the resistance, and the out-of-phase component to the capacitance. The major disadvantage is that the method is less accurate ($\approx 1\%$) than the a.c. bridge techniques (0.1%). Further information may be obtained by measuring phase information as a function of the frequency of the reference signal. This technique is becoming more important owing to the development of

commercial frequency response analysers, and is discussed in more detail in Chapter 8.

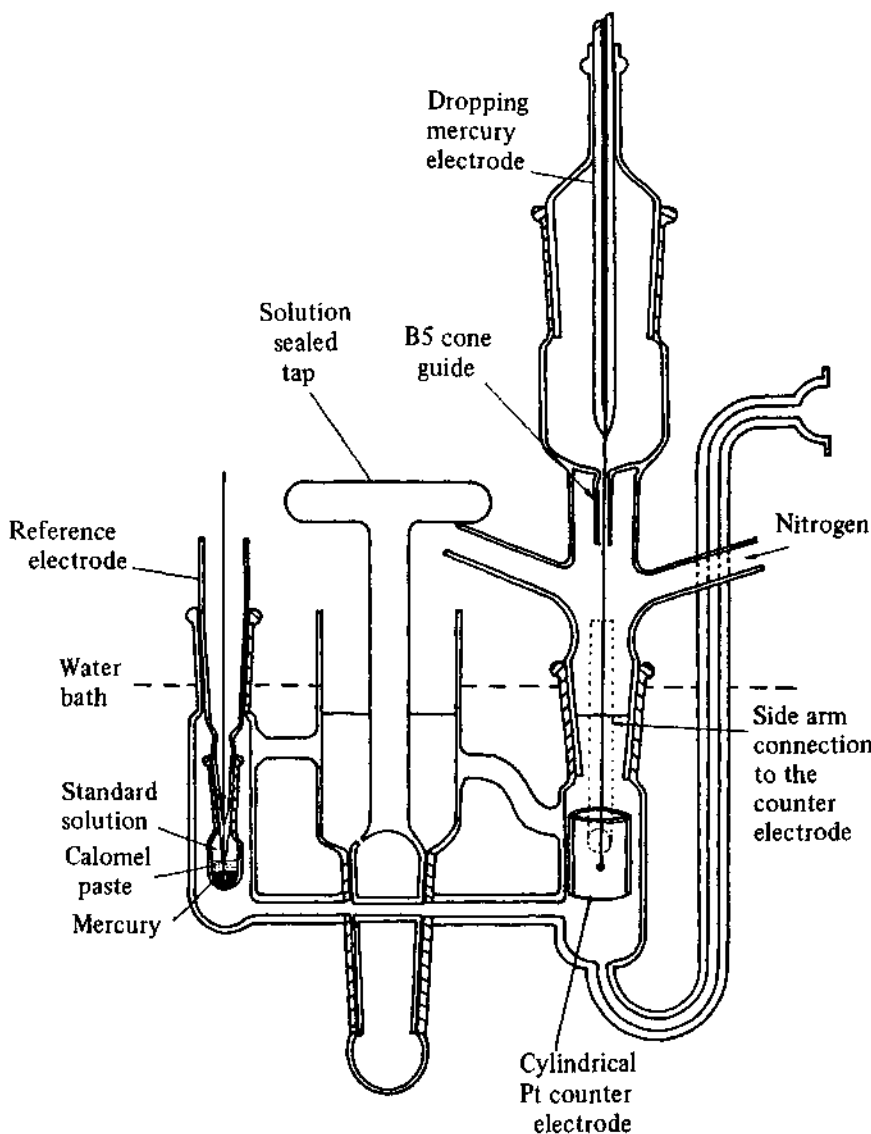


Fig. 5.12 – A cell for the measurement of the differential capacitance at a dropping mercury electrode–solution interface.

5.2.2 Interfacial tension measurements

The two most common methods available to determine the interfacial tension at the mercury-electrolyte interface are the capillary rise method and the maximum

bubble pressure method. These methods rely on the fact that the pressure difference across a curved interface (ΔP) is given by the Young and Laplace equation:

$$\Delta P = \frac{2\gamma}{r} \quad (5.50)$$

where γ is the interfacial tension and r is the radius of curvature. A consequence of this equation is that wetting liquids will rise up a capillary tube until the excess pressure over the curved interface is exactly balanced by the hydrostatic pressure of the liquid in the tube. Therefore, by measuring the height of the liquid rise the interfacial tension can be calculated. This is the principle of the capillary electrometer, but as mercury causes a capillary depression the whole apparatus has to be inverted. All the older measurements were recorded on this type of instrument, but the method is tedious, data acquisition is slow, and eyestrain is a serious problem [15]. More recently, the maximum bubble pressure technique has been developed as this method is easily adapted to computer control [16, 17] with no loss of accuracy (0.04%).

The principle is demonstrated in Fig. 5.13 which shows bubble formation in three stages of growth. Initially the growth of the mercury at the tip of the capillary is such that the curvature of the mercury surface decreases with increasing pressure until the surface is hemispherical, whereupon the curvature starts to increase again as the drop grows. It follows as a consequence of Equation (5.50) that any increase in pressure beyond that for the hemispherical position, P_{\max} , produces an unstable state, and the mercury drop will expand and free itself from the capillary. This maximum pressure is easily determined by superimposing a small a.c. signal on the d.c. polarising potential and detecting the rapid increase in surface area as a sharp increase in the charging current.

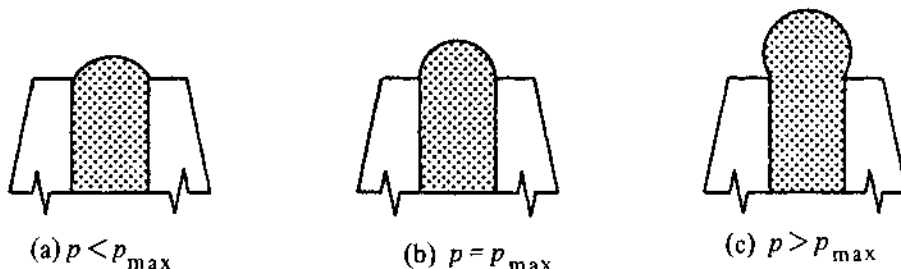


Fig. 5.13 – A schematic diagram illustrating the stages of bubble formation in the extrusion of mercury from a glass capillary, tip facing upwards, on applying an external pressure, P ; (a) is a stable state; (b) hemispherical meniscus; (c) is an unstable state.

A schematic diagram of the apparatus is shown in Fig. 5.14. The pressure system varies in complexity, but the automatic pressure controlling devices available commercially are easily adapted to computer control. Although the capillary rise and maximum bubble pressure electrometers are absolute instruments, they are usually calibrated with a solution of known properties. This avoids the accurate measurement of the radius of the capillary bore.

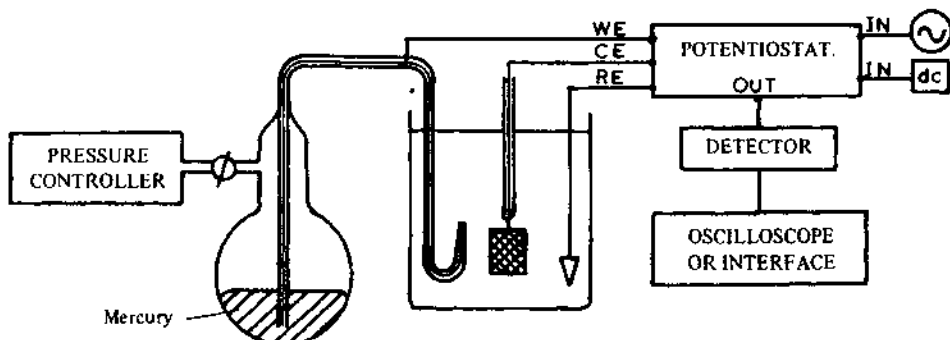


Fig. 5.14 – Schematic diagram of a maximum bubble pressure electrometer.

A further method relies on the fact that the natural drop time of a dropping mercury electrode is proportional to the interfacial tension [18]. Again, drop birth can be detected electrically by the sudden change in impedance, so the method is easily automated. Unlike the other methods there is no adequate theory describing the mechanism of drop detachment, so the proportionality constant is again obtained by calibration with a solution of known properties. The method is extremely sensitive to vibrations and impurities, and consequently it is difficult to obtain results better than 1%. Also as a dropping mercury electrode is used, the system is dynamic and may not be in equilibrium if the rate of adsorption is slow. Similarly, capacitance measurements will be frequency dependent if adsorption is slow compared with the period of a.c. perturbation, and this provides a useful check of whether equilibrium is obtained.

A new method for the measurement of surface and interfacial tension has been developed based on a video digitising technique to measure the drop profile of pendant and sessile drops [19]. The method gives a standard deviation of 0.5%, so the resolution, at present, is less than the maximum bubble pressure technique. It is an extremely useful technique for studying the liquid-liquid interface, and electrocapillary curves of similar shape to those obtained on mercury have been obtained for the water-nitrobenzene interface.

REFERENCES

- [1] R. Parsons, 'Equilibrium Properties of Electrified Interfaces' in *Modern aspects of electrochemistry*, 1 (1954) 103.
- [2] P. Delahay, *Double layer and electrode kinetics*, Interscience, (1965).
- [3] M. Sparnaay, *Electrical double layer*, Pergamon Press, (1972).
- [4] D. C. Grahame, *Chem. Rev.*, 41 (1947) 441.
- [5] D. M. Mohilner in A. Bard (Ed) *Electroanalytical chemistry*, Marcel Dekker, (1966) Vol. 1, p. 241.
- [6] R. Parsons, IUPAC Commission 1:6, *Physical chemistry: Enriching topics from colloid and surface science*, (1975).

- [7] A. J. Bard & L. R. Faulkner, *Electrochemical methods*, John Wiley & Sons, (1980).
- [8] R. Parsons & R. Peat, *Trans. of the SAEST*, **12** (1977) 187.
- [9] R. Parsons & R. Peat, *J. Electroanal. Chem.*, **122** (1981) 299.
- [10] H. P. Dhar, B. E. Conway, & K. M. Joshi, *Electrochim. Acta*, **18** (1973) 789.
- [11] R. Parsons in *Advances in Electrochemistry and Electrochemical Engineering*, Vol. 1, p. 1. (Eds) P. Delahay and C. W. Tobias, Interscience, (1961).
- [12] E. A. Blomgren & J. O'M Bockris, *Nature*, **186** (1960) 305.
- [13] G. J. Hills & R. Payne, *Trans. Faraday Soc.*, **61** (1965) 316.
- [14] D. M. Mohilner, J. C. Kreuser, H. Nakadomari, & P. R. Mohilner, *J. Electrochem. Soc.*, **123** (1976) 359.
- [15] B. E. Conway & L. G. M. Gordon, *J. Phys. Chem.*, **73** (1969) 3609.
- [16] D. J. Schiffrian, *J. Electroanal. Chem.*, **23** (1969) 168.
- [17] J. Lawrence & D. M. Mohilner, *J. Electrochem. Soc.*, **118** (1971) 259, 1596.
- [18] R. G. Barradas & F. M. Kimmerle, *Can. J. Chem.*, **45** (1963) 109.
- [19] H. H. Girault, D. J. Schiffrian, & B. D. V. Smith, *J. Electroanal. Chem.*, **137** (1982) 207.

6

Potential sweep techniques and cyclic voltammetry

Over the past couple of decades potential sweep techniques, such as cyclic voltammetry, have been applied to an ever increasing range of systems, and at the same time the mathematical description of these techniques has been developed sufficiently to enable kinetic parameters to be determined for a wide variety of mechanisms. It is, however, in the area of preliminary mechanistic investigations that sweep techniques, in particular cyclic voltammetry, are probably most useful. An 'electrochemical spectrum' indicating the potentials at which processes occur can be rapidly obtained, while from the sweep rate dependence the involvement of coupled homogeneous reactions is readily identified, and other complications such as adsorption can be recognised. In view of these capabilities, cyclic voltammetry is nearly always the technique of choice when studying a system for the first time, though better techniques probably exist for determining precise kinetic data.

The potential-time waveforms used for sweep measurements are shown in Fig. 6.1. The simplest of these techniques is linear sweep voltammetry (LSV), and this involves sweeping the electrode potential between limits E_1 and E_2 at a known sweep rate, ν , before halting the potential sweep. A generally more useful (and consequently more widely applied) technique is cyclic voltammetry (CV). In this case the waveform is initially the same as in LSV, but on reaching the potential E_2 the sweep is reversed (usually at the same scan rate) rather than terminated. On again reaching the initial potential, E_1 , there are several possibilities. The potential sweep may be halted, again reversed, or alternatively continued further to a value E_3 . In both LSV and CV experiments the cell current is recorded as a function of the applied potential (it should be noted, however, that the potential axis is also a time axis). The sweep rates used in

conventional experiments range from a few mV s^{-1} up to a few hundred V s^{-1} . Rates up to several thousand V s^{-1} have been used, but such high values introduce considerable experimental difficulties (e.g. double layer charging and iR_u drop effects can both be very large) which generally restrict their application. Recently, it has become clear that one good approach to obtaining high quality data at fast scan rates is to use a microelectrode which minimises the charging currents and the effects of uncompensated resistance. The method of recording the voltammogram depends on the sweep rate; up to about 0.5 V s^{-1} an $X-Y$ recorder is most convenient, but above this, the slew rate of the recorder will be insufficient to record the voltammogram without distorting it. In these cases a fast transient recorder, an oscilloscope or microcomputer is required.

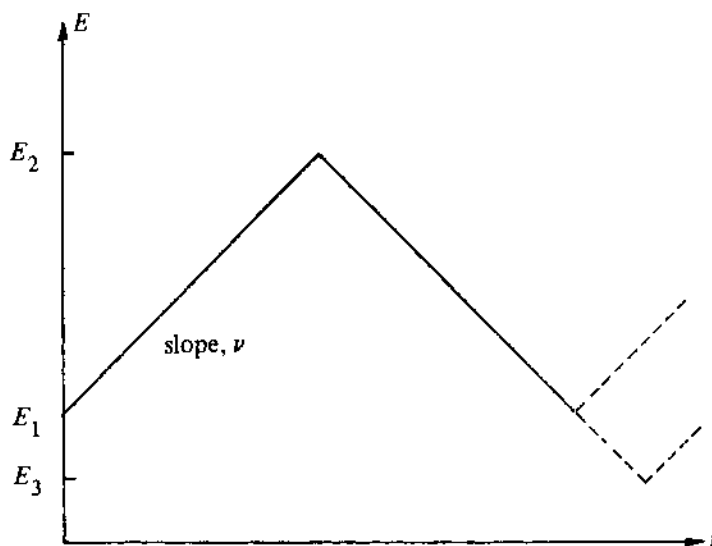


Fig. 6.1 – Potential–time profiles for sweep voltammetry.

When using cyclic voltammetry to study a system for the first time it is usual to start by carrying out qualitative experiments in order to get a feel for the system, before proceeding to semi-quantitative and finally quantitative ones from which kinetic parameters may be calculated. In a typical qualitative study it is usual to record voltammograms over a wide range of sweep rates and for various values of E_1 , E_2 , and E_3 . Commonly, there will be several peaks, and by observing how these appear and disappear as the potential limits and sweep rate are varied, and also by noting the differences between the first and subsequent cycles, it is possible to determine how the processes represented by the peaks are related. At the same time, from the sweep rate dependence of the peak amplitudes the role of adsorption, diffusion, and coupled homogeneous chemical reactions may be identified. The difference between the first and subsequent cyclic voltammograms frequently provides useful mechanistic information. It must, however, be emphasised that kinetic data can only be accurately obtained from an analysis of the first sweep. In cyclic voltammetry v_{anodic} and v_{cathodic}

are generally chosen to be equal, and this is the case that will be considered throughout this chapter; this is not, however, essential, and indeed using different sweep rates can on occasion be useful, e.g. when studying fast homogeneous reactions.

6.1 REVERSIBLE REACTIONS

To see what form voltammograms take let us first consider a simple reversible reaction of the type described by Equation (6.1) and assume that only O is initially present in solution. Throughout this chapter the model electrode reaction will be a reduction process, and all the equations presented therefore relate to a reduction. The extension to an oxidation process is obvious and trivial.



If a very slow linear potential sweep is applied to such a system the voltammogram recorded will appear like a steady state I vs E curve (in fact most steady state measurements are made in this way, rather than point by point). However, as the sweep rate is increased a peak of increasing height develops, as shown in Fig. 6.2. To see why this is so we must consider the shape of the concentration profiles of O as a function of the potential.

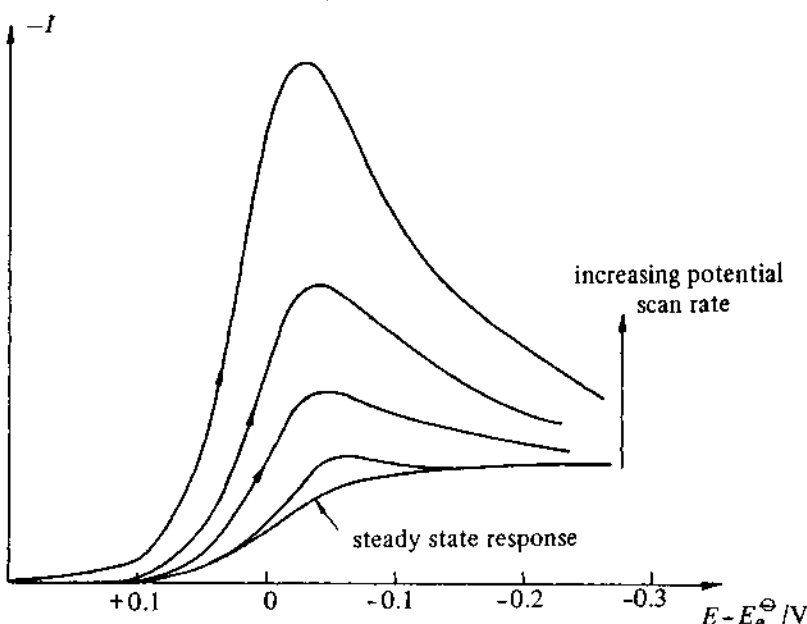


Fig. 6.2 – A series of linear sweep voltammograms for the reaction $\text{O} + e \rightarrow \text{R}$, at several potential scan rates.

As has been seen in earlier chapters, it is assumed that, under steady state conditions, concentrations above a certain distance from the electrode are maintained uniform by natural convection. On the other hand, within the region next to the electrode, known as the *Nernst diffusion layer*, the concentration gradients are essentially linear. The ratio of c_O/c_O^∞ is, for a reversible reaction, given by the Nernst equation, and hence as the potential is made more negative the surface concentration of the reactant must be progressively decreased. The concentration gradient is thereby increased, and hence the current also increases. Eventually the surface concentration of the reactant approaches zero and the steady state concentration profile cannot change further; then the current reaches a plateau value. When the sweep rate is increased, the diffusion layer does not have sufficient time to relax to its equilibrium state; it does not extend as far into solution, and the concentration profiles are not yet linear, as seen in Fig. 6.3. As soon as a potential where O is reduced is reached the surface concentration of O decreases from its bulk value in order to satisfy the Nernst equation and a concentration gradient is set up (Fig. 6.3(a)). As a result a current proportional to the value of this gradient at the electrode surface flows in the external circuit. Once this gradient exists it does not of course remain constant but starts to relax (decrease) owing to diffusion. However, at the same time the electrode potential is still changing, and therefore the surface concentration of O is further decreased (Fig. 6.3(b) and 6.3(c)) until it effectively reaches zero (Fig. 6.3(e)). It can immediately be seen that for any given potential the concentration gradient at the surface is greater than for the steady state case,

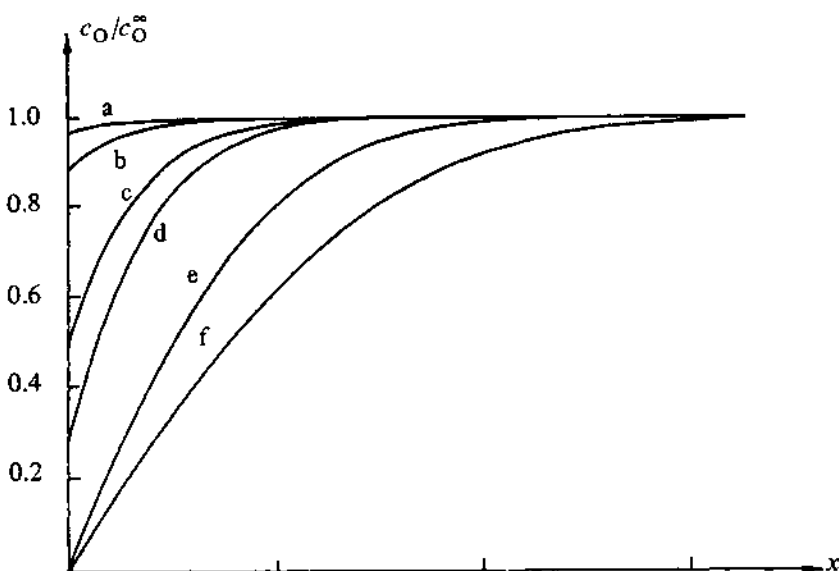


Fig. 6.3 – Concentration-distance profiles for the electroactive species, O, in the reaction $O + e \rightarrow R$ during a linear potential sweep experiment. The curves correspond to the potentials (a) $E_e^\ominus + 90\text{ mV}$, (b) $E_e^\ominus + 50\text{ mV}$, (c) E_e^\ominus , (d) $E_e^\ominus - 28\text{ mV}$, (e) $E_e^\ominus - 128\text{ mV}$, (f) $E_e^\ominus - 280\text{ mV}$.

and therefore the current is larger. Once $(c_O)_{x=0}$ reaches zero the concentration gradient starts to decrease, due to the relaxation effect (Figs. 6.3(e) and (f)) and hence the current flowing must also decrease. Overall, this behaviour gives rise to a peak shaped current-potential response as shown in Fig. 6.2. It can also be seen that the concentration gradients at the surface, and hence currents, will increase with sweep rate as a result of the shorter timescale of the experiment (less relaxation), although the exact dependence is not immediately obvious.

What does the current response look like when the potential sweep is reversed? For slow sweeps, i.e. pseudo steady state experiments, the current should of course directly track the forward one; this is not, however, true for faster sweeps. In these cases when the sweep is reversed there is a significant concentration of R present near the electrode and, indeed, R continues to be formed on the reverse sweep until the potential again approaches E_e^\ominus . However, as the potential approaches E_e^\ominus the R present near the electrode starts to be reoxidised back to O (in order for the surface concentrations to be those required by the Nernst equation) and a reverse current flows. With the changing electrode potential the surface concentration of R eventually reaches zero. Using similar arguments as were used for the forward sweep, it can be shown that the current on the reverse sweep will also exhibit a peaked response, though of course of opposite sign. A typical cyclic voltammogram is shown in Fig. 6.4. It may also be noted that the charge associated with the anodic process is low compared to the forward reduction process. This is because throughout most of the experiment, there is a concentration difference driving R away from the electrode; most of the product, R, therefore diffuses into the bulk solution and cannot be reoxidised on the timescale of a cyclic voltammetric experiment.

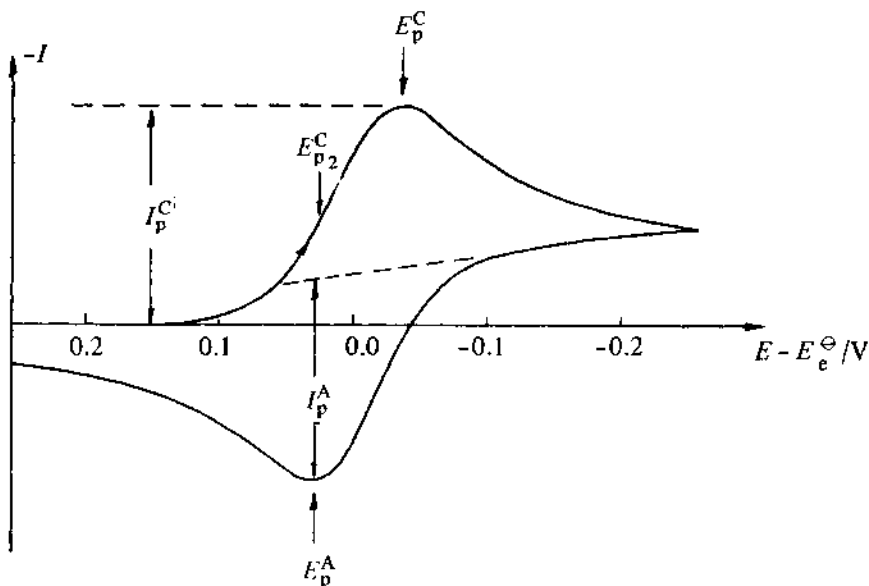


Fig. 6.4 Cyclic voltammogram for a reversible process, $O + z \rightleftharpoons R$. Initially only O present in solution.

In order to determine mathematically the exact form of the cyclic voltammogram it is again necessary to solve Fick's 2nd Law for O and R, Equations (6.2) and (6.3), with the appropriate initial and boundary conditions

$$\frac{\partial c_O}{\partial t} = D_O \frac{\partial^2 c_O}{\partial x^2} \quad (6.2)$$

$$\frac{\partial c_R}{\partial t} = D_R \frac{\partial^2 c_R}{\partial x^2}. \quad (6.3)$$

With just O initially present in solution and assuming $D_O = D_R = D$ the initial and boundary conditions are

$$t = 0, \quad x > 0, \quad c_O = c_O^\infty \quad \text{and} \quad c_R = 0$$

$$t > 0, \quad x = \infty, \quad c_O = c_O^\infty \quad \text{and} \quad c_R = 0$$

$$t > 0, \quad x = 0, \quad D \left(\frac{\partial c_O}{\partial x} \right) + D \left(\frac{\partial c_R}{\partial x} \right) = 0$$

$$\left(\frac{c_O}{c_R} \right)_{x=0} = \exp \left[\frac{nF}{RT} (E - E_e^\ominus) \right]$$

$$-I = nFD \left(\frac{\partial c_O}{\partial x} \right)_{x=0}.$$

For a sweep rate of ν

$$0 < t < \lambda \quad E = E_1 - \nu t$$

$$t > \lambda \quad E = E_1 - 2\nu\lambda + \nu t$$

where E_1 is the initial potential and λ the time at which the sweep is reversed. The solution is quite difficult because of the time dependent potential term, but it can be shown that for planar diffusion [1, 2, 3]

$$I_p = -0.4463 nF \left(\frac{nF}{RT} \right)^{1/2} c_O^\infty D^{1/2} \nu^{1/2} \quad (6.4)$$

This is called the *Randles-Sevcik equation*, and at 25°C this reduces to the form

$$I_p = -(2.69 \times 10^5) n^{3/2} c_O^\infty D^{1/2} \nu^{1/2} \quad (6.5)$$

where I_p , the peak current density (measured as shown in Fig. 6.4) is in A cm⁻², D is in cm² s⁻¹, ν is in V s⁻¹, and c_O^∞ is in mol cm⁻³. Thus we see that the peak current density is proportional to the concentration of electroactive species and to the square roots of the sweep rate and diffusion coefficient. Fig. 6.5 shows a set of typical cyclic voltammograms obtained for a reversible system over a range of sweep rates.

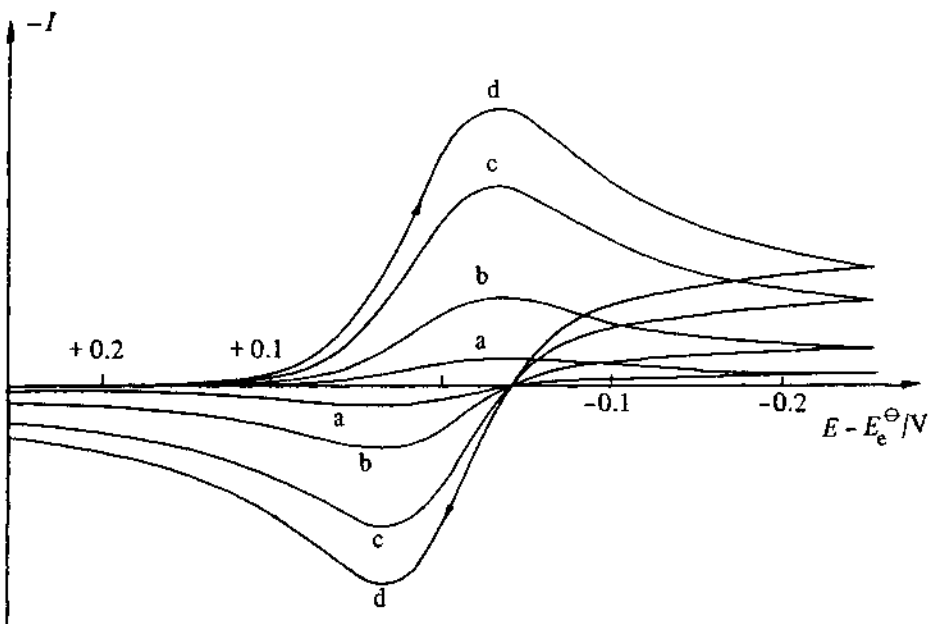


Fig. 6.5 – Cyclic voltammograms for a reversible process, $O + e^- \rightleftharpoons R$ when only O is initially present in solution. The potential sweep rates are (a) ν , (b) 10ν , (c) 50ν , and (d) 100ν .

Having obtained such results, a test of the reversibility of the system is to check whether a plot of I_p as a function of $\nu^{1/2}$ is both linear and passes through the origin (or alternatively whether $I_p/\nu^{1/2}$ is a constant). If this is found to be true then there are further diagnostic tests to be applied, all of which should be satisfied by a reversible system. A complete list of these tests is given in Table 6.1, whilst the symbols used are defined in Fig. 6.4. The direct graphical determination of the reverse peak height, I_p^A , can sometimes be difficult. In these cases one should use the indirect method of Nicholson [4]. When applying these tests of reversibility it is very important that results obtained over a wide range of sweep rates (preferably at least two orders of magnitude) are analysed, or false conclusions may be reached. A failure to satisfy one or more of the conditions in Table 6.1 implies that the electron transfer is not reversible on the timescale of the experiment, and that the process is more complicated than had been assumed.

It must be emphasised that a reversible cyclic voltammogram can only be observed if both O and R are stable and the kinetics of the electron transfer process are fast, so that at all potentials and potential scan rates the electron transfer process on the surface is in equilibrium (remember this is a relative term dependent on a comparison of the rates of the forward and back electron transfer reactions with the prevailing rate of diffusion of material to and from the surface), so that surface concentrations follow (and may be calculated from) the Nernst equation.

Table 6.1 – Diagnostic tests for cyclic voltammograms of reversible processes at 25°C

1. $\Delta E_p = E_p^A - E_p^C = 59/n \text{ mV}$
2. $|E_p - E_{p/2}| = 59/n \text{ mV}$
3. $|I_p^A/I_p^C| = 1$
4. $I_p \propto \nu^{1/2}$
5. E_p is independent of ν
6. at potentials beyond E_p , $I^{-2} \propto t$

6.2 IRREVERSIBLE SYSTEMS

In the case of the reversible system discussed above, the electron transfer rates at all potentials are significantly greater than the rate of mass transport, and therefore Nernstian equilibrium is always maintained at the electrode surface. When the rate of electron transfer is insufficient to maintain this surface equilibrium then the shape of the cyclic voltammogram changes. Fig. 6.6 shows an example of such a system. At low potential sweep rates the rate of electron transfer is greater than that of mass transfer, and a reversible cyclic voltammogram is recorded. As the sweep rate is increased, however, the rate of mass

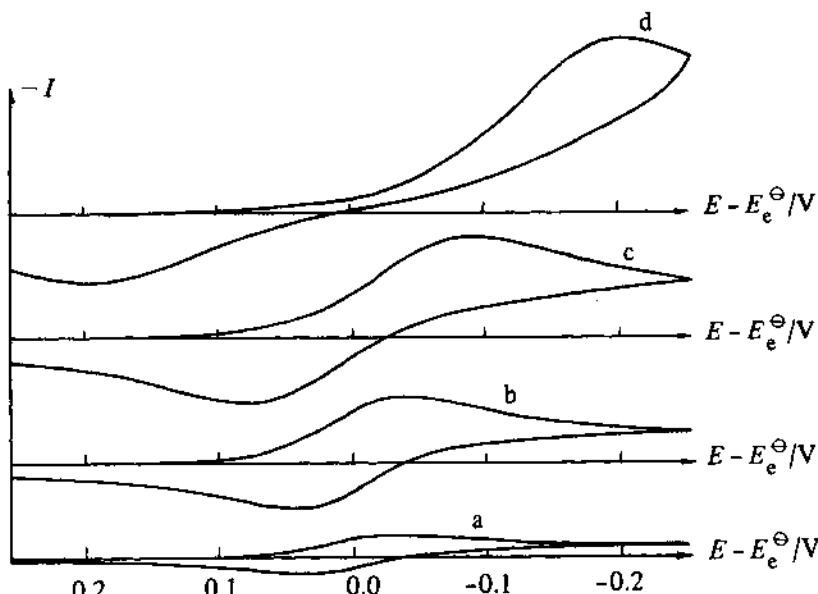


Fig. 6.6 – Simulated cyclic voltammograms for reaction $O + e^- \rightleftharpoons R$ when $D = 10^{-5} \text{ cm s}^{-1}$ and $k^{\ominus} = 10^{-2} \text{ cm s}^{-1}$. Only O initially present in solution. Potential sweep rates (a) 0.13 V s^{-1} , (b) 1.3 V s^{-1} , (c) 4 V s^{-1} , (d) 13 V s^{-1} .

transport increases and becomes comparable to the rate of electron transfer. The most noticeable effect of this is to increase the peak separation. Whilst not normally done, a useful way of studying data such as that of Fig. 6.6 is to normalise the currents for the change in the rate of diffusion, i.e. to replot the data as $I/\nu^{1/2}$ as a function of E . For reversible systems such normalised voltammograms should superimpose at all sweep rates ((provided double layer charging effects can be ignored (see later)). Fig. 6.7 shows normalised cyclic voltammograms for a system such as that used to obtain the data for Fig. 6.6. It can immediately be seen that in addition to the increasing peak separation with increasing sweep rate, the peak height is slightly reduced from that for a reversible system. In the limit for a totally irreversible process the shape of the cyclic voltammogram can again be obtained mathematically by solution of the differential equations described by Equations (6.2) and (6.3), though in this case, whilst the initial and first boundary conditions remain the same as for the reversible case, the boundary condition for $t > 0, x = 0$ becomes.

$$-\frac{I}{nF} = D_O \left(\frac{\partial c_O}{\partial x} \right)_{x=0} = \vec{k}(c_O)_{(x=0)}$$

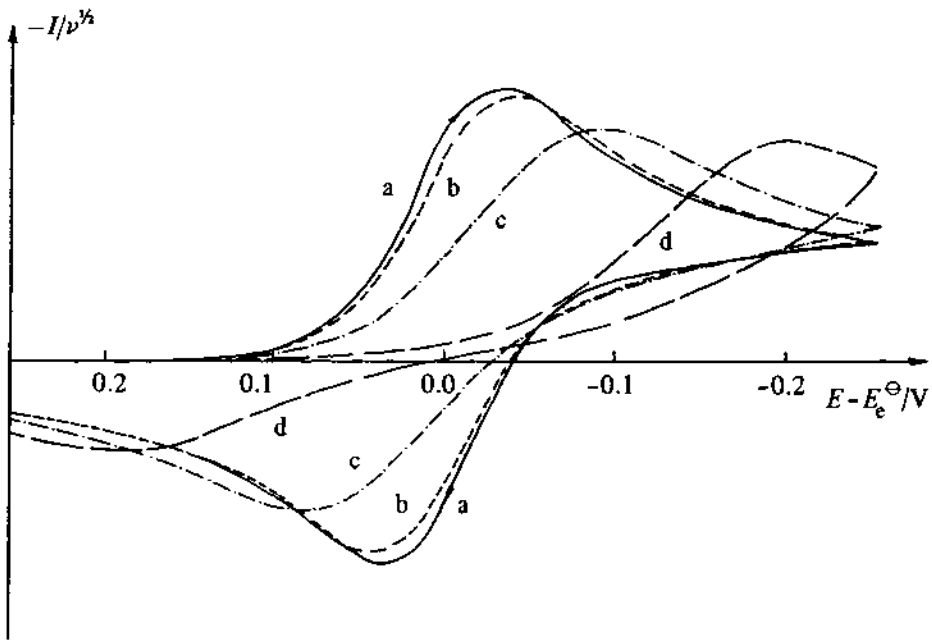


Fig. 6.7 – Normalised cyclic voltammograms. Parameters as Fig. 6.6.

Solution of these differential equations then yields the following equation for the peak current density at 25°C [3]:

$$I_p = -(2.99 \times 10^5) n (\alpha_C n_a)^{1/2} c_O^{\infty} D_O^{1/2} \nu^{1/2} \quad (6.6)$$

where n_α is the number of electrons transferred up to, and including, the rate determining step. Thus, as for the reversible case, the peak current density is proportional to the concentration and to the square root of the sweep rate, but additionally to the square root of the transfer coefficient. For a one electron process and with α_C equal to 0.5 the peak current for the irreversible process is only 78.5% of a reversible one under the same conditions (in addition to depending on α_C this ratio also depends on the number of electrons involved). The reason the peak is smaller is related to the shape of the peak. As the peak for an irreversible process is more drawn out, the surface concentration of O changes more slowly with potential, and at the instant when the surface concentration effectively reaches zero, the concentration profile for O is less steep and the flux to the surface lower.

Probably the most marked feature of a cyclic voltammogram of a totally irreversible system is the total absence of a reverse peak. However, such a feature on its own does not necessarily imply an irreversible electron transfer process, but could be due to a fast following chemical reaction. Other tests must therefore be made. Whereas for the reversible case the value of E_p^C is independent of the sweep rate, for the irreversible case E_p^C is found to vary with the sweep rate as shown below [3].

$$E_p^C = K - \frac{2.3 RT}{2\alpha_C n_\alpha F} \log \nu \quad (6.7)$$

where

$$K = E_e^\ominus - \frac{RT}{\alpha_C n_\alpha F} \left(0.78 - \frac{2.3}{2} \log \left(\frac{\alpha_C n_\alpha F D}{k^\ominus{}^2 R T} \right) \right),$$

i.e. at 25°C it shifts by $30/\alpha_C n_\alpha$ mV for each decade change in ν (it shifts in a negative direction as ν is increased). The shape factor $|E_p - E_{p/2}|$ is also different for the irreversible case, and is given by

$$|E_p - E_{p/2}| = \frac{48}{\alpha_C n_\alpha} \text{ mV at } 25^\circ\text{C}. \quad (6.8)$$

This equation permits the estimation of the factor $\alpha_C n_\alpha$ required for the estimation of D and k^\ominus from Equations (6.6) and (6.7) respectively.

If all the above tests (which are tabulated in Table 6.2) are satisfied, then the process is irreversible, and Equation (6.7) could be used to calculate a value

Table 6.2 – Diagnostic tests for totally irreversible systems at 25°C

-
1. No reverse peak
 2. $I_p^C \propto \nu^{1/2}$
 3. E_p^C shifts $-30/\alpha_C n_\alpha$ mV for each decade increase in ν
 4. $|E_p - E_{p/2}| = 48/\alpha_C n_\alpha$ mV
-

for k^\ominus . Alternatively k^\ominus can be obtained by curve fitting the experimental voltammograms to theoretical curves (usually obtained by digital simulation, see Appendix).

As we saw earlier, it is quite common for a process that is reversible at low sweep rates to become irreversible at higher ones after having passed through a region known as *quasi-reversible* at intermediate values. This transition from reversibility occurs when the relative rate of the electron transfer with respect to that of mass transport is insufficient to maintain Nernstian equilibrium at the electrode surface. In the quasi-reversible region both forward and back reactions make a contribution to the observed current, and the region is generally recognised to have the following boundaries [5]

$$0.3\nu^{1/2} \geq k^\ominus \geq 2 \times 10^{-5}\nu^{1/2} \text{ cm s}^{-1}$$

This change from reversible, to quasi-reversible and finally irreversible behaviour can readily be seen from a plot of I_p as a function of $\nu^{1/2}$ as shown in Fig. 6.8. Diagnostic tests for a system in the quasi-reversible region are given in Table 6.3.

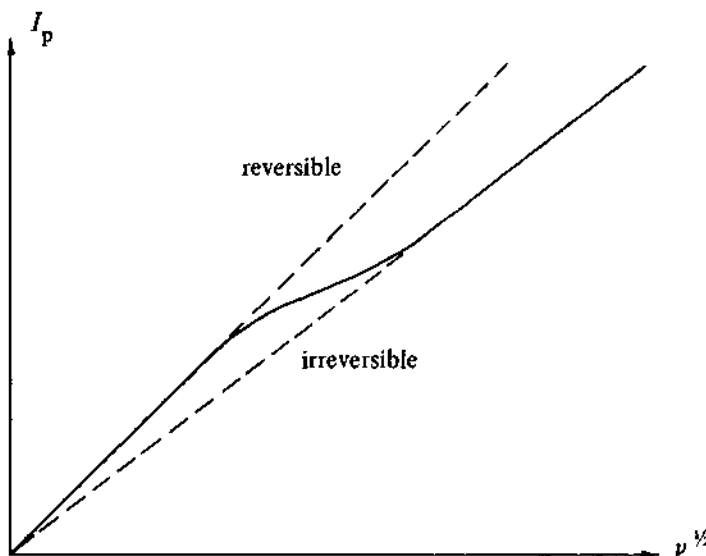


Fig. 6.8 – A plot of the dependence of the peak current density on the square root of the potential sweep rate, showing the transition from reversible to irreversible behaviour with increasing sweep rate $\alpha_c = 0.5$.

Table 6.3 – Diagnostic tests for quasi-reversible systems

1. $|I_p|$ increases with $\nu^{1/2}$ but is not proportional to it
2. $|I_p^A/I_p^C| = 1$ provided $\alpha_C = \alpha_A = 0.5$
3. ΔE_p is greater than $59/n\text{ mV}$ and increases with increasing ν
4. E_p^C shifts negatively with increasing ν

k^\ominus values can be obtained from the analysis of plots such as Fig. 6.8, but it is more usual with cyclic voltammetry to obtain such kinetic data from ΔE_p values. Working curves have been constructed [4] of $n \cdot \Delta E_p$ as a function of the variable ψ defined by

$$\psi = \frac{(RT)^{1/2} k^\ominus}{(nFD\pi\nu)^{1/2}} \quad . \quad (6.9)$$

Such a working curve is shown in Fig. 6.9. By comparing experimental ΔE_p values with the working curve for several ν values, k^\ominus is readily obtained. In favourable cases, using a sweep rate of 1000 V s^{-1} , k^\ominus values as high as 1 cm s^{-1} can be determined. Although it will be discussed more fully later, it is at this point worth mentioning that when determining kinetic parameters from cyclic voltammograms it is very important to ensure that the uncompensated resistance between the end of the Luggin capillary and the working electrode is as small as possible. The effect of iR_u drop is almost identical to that of slow kinetics (i.e. ΔE_p increases with ν), and indeed several reported kinetic studies are, in fact, investigations of uncompensated resistance.

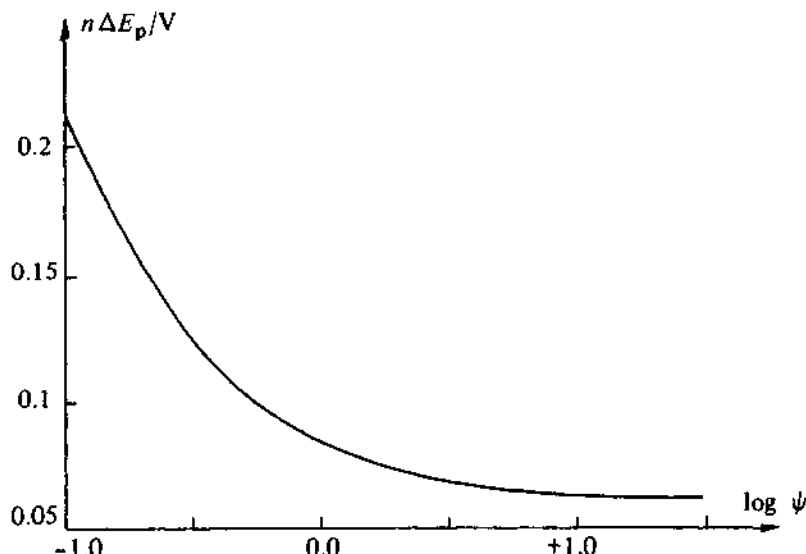


Fig. 6.9 – The working curve of $n\Delta E_p$ vs $\log \psi$ ($\psi = (RT/nFD\pi\nu)^{1/2}k^\ominus$) for the determination of the standard rate constant for electron transfer from the separation of the anodic and cathodic peaks on a cyclic voltammogram.

6.3 COUPLED HOMOGENEOUS REACTIONS

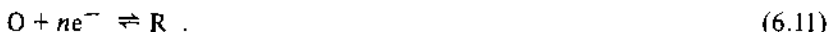
Cyclic voltammetry is probably the most powerful technique available for investigating coupled chemical reactions. Whilst other techniques, e.g. the rotating disc electrode, are suitable for obtaining kinetic data, cyclic voltammetry has the

advantage that it is also ideal for initial mechanistic studies, e.g. the detection and identification of reaction intermediates. In this section the cyclic voltammetry for different types of coupled reaction schemes will be discussed, and the determination of kinetic parameters from such data will be outlined. This is followed by some specific examples of how cyclic voltammetry can be used to investigate such model systems. Modern approaches to more complex mechanisms are discussed later in the chapter.

Before discussing the particular reaction mechanisms it is again worth emphasising that cyclic voltammograms should be recorded over as wide a range of conditions as possible before any attempt is made to interpret the data. In particular the timescale of the experiment should be varied (by using a range of sweep rates) and the potential limits should be changed to investigate whether there are other processes coupled to the one of interest. It is also very helpful to record cyclic voltammograms for both the first and subsequent cycles although only data taken from the first cycle should be analysed to obtain kinetic parameters. Subsequent sweeps may well show peaks not present on the first sweep if electroactive species are formed by following chemical reactions, and then the n th cycle provides an important mechanistic insight. As we have seen earlier, the useful sweep rate range for cyclic voltammetry is from about 10 mVs^{-1} to a few hundred Vs^{-1} . This enables first order rate constants in the range $1\text{-}10^4 \text{ s}^{-1}$ to be determined, whilst for second order processes by choosing the conditions carefully it is possible to study reactions with rates close to the diffusion controlled limit.

6.3.1 The CE mechanism

As we saw in an earlier chapter the ce reaction mechanism can be represented in the following way:



Typical examples of systems that follow such a scheme are the reduction of weak acids and the reduction of formaldehyde in aqueous solution, where it is present in both an electroactive form and an inactive hydrated form. The cases where the electron transfer is reversible and where it is irreversible will both be considered here, but schemes where the chemical reaction is of second or higher order will not be discussed. In these cases kinetic data can only be obtained by either forcing the system into a pseudo first order regime or by comparing experimental data with simulated results.

If first of all we consider the case where the electron transfer is reversible and where the chemical step is very slow, the current will be purely kinetically controlled (i.e. there is no component of diffusion control) and therefore no peaks will be observed on the cyclic voltammogram. Instead a simple steady state type wave will be obtained and the chemical rate constants can be obtained directly from the limiting current using the equation [6]

$$I_L = -nFc_Y^\infty D^{1/2} K(k_1 + k_{-1})^{1/2} \quad (6.12)$$

provided the value of the equilibrium constant, K , is known. At the other extreme, if the chemical reaction is very fast the cyclic voltammogram will be that for a simple diffusion controlled electron transfer. Under intermediate conditions the surface concentration of the reducible species O , and hence the current, will be partially controlled by the kinetics of reaction (6.10) and the shape of the cyclic voltammogram, particularly that of the forward peak, will be slightly different from that for reversible behaviour. The change over from purely kinetic to partial kinetic, to purely mass transport control is a complex function of the relative values of K , k_1 and k_{-1} and ν , but this matter has been considered in detail by Saveant & Vianello [6] and kinetic zone diagrams have been published to which the reader is referred.

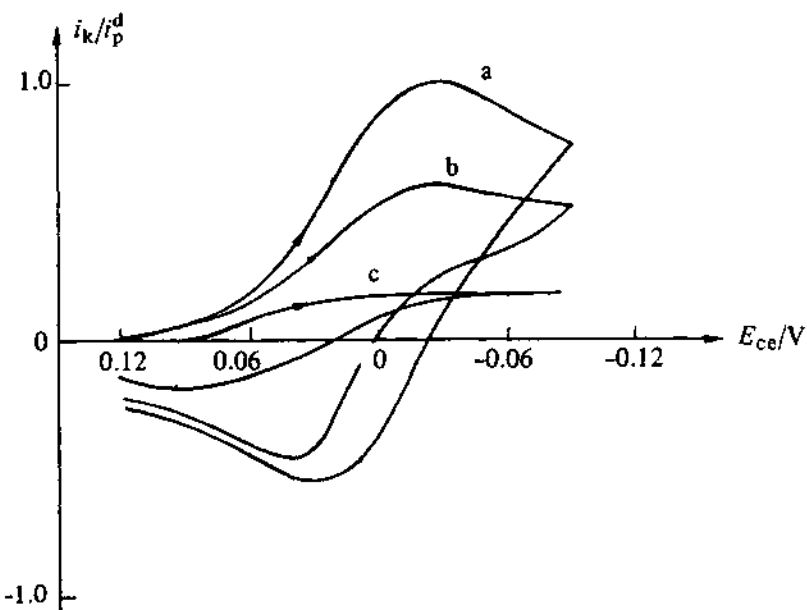


Fig. 6.10 – Theoretical cyclic voltammograms for the ce mechanism. The potential scale is $E_{ce} = E - E_e^\ominus - (RT/F) \ln (k_1/k_1 + k_{-1})$ and the current is normalised by dividing the kinetic current, i_k , by the peak current expected for a reversible reaction, i_p^d . The values of $1/k\lambda^{1/2}$ are (a) 0, (b) 1.0, (c) 10.0.

Table 6.4 – Diagnostic tests for ce mechanism

-
1. $I_p^C/\nu^{1/2}$ decreases as ν increases
 2. $|I_p^A/I_p^C|$ increases with ν and is always greater than, or equal to, unity
-

Fig. 6.10 shows theoretical cyclic voltammograms for the ce system under various conditions. The data are presented as a normalised current plotted as a function of potential for various values of $(K\lambda^{1/2})^{-1}$ where λ is defined by

$$\lambda = \left(\frac{k_1 + k_{-1}}{\nu} \right) \frac{RT}{nF} . \quad (6.13)$$

Thus increasing values of $(K\lambda^{1/2})^{-1}$ correspond to increasing sweep rates for any given system. From this figure a number of diagnostic tests for a ce mechanism can be identified, and these are tabulated in Table 6.4. The theoretical voltammograms were obtained by Nicholson & Shain [3] who also describe how real voltammograms may be analysed to determine rate constants. They show empirically that the ratio of the kinetic peak current, i_p^k , to the value that the current would have been, in the absence of kinetic effects, i_p^d (determined from slow sweep data), is given by

$$i_p^k/i_p^d = \frac{1}{1.02 + 0.471/K\lambda^{1/2}}, \quad (6.14)$$

and Fig. 6.11 shows a working curve obtained from this equation. By determining i_p^k/i_p^d values for a range of sweep rates and fitting these to the working curve, $K\lambda^{1/2}$ values may be obtained from which the kinetic parameters may be determined.

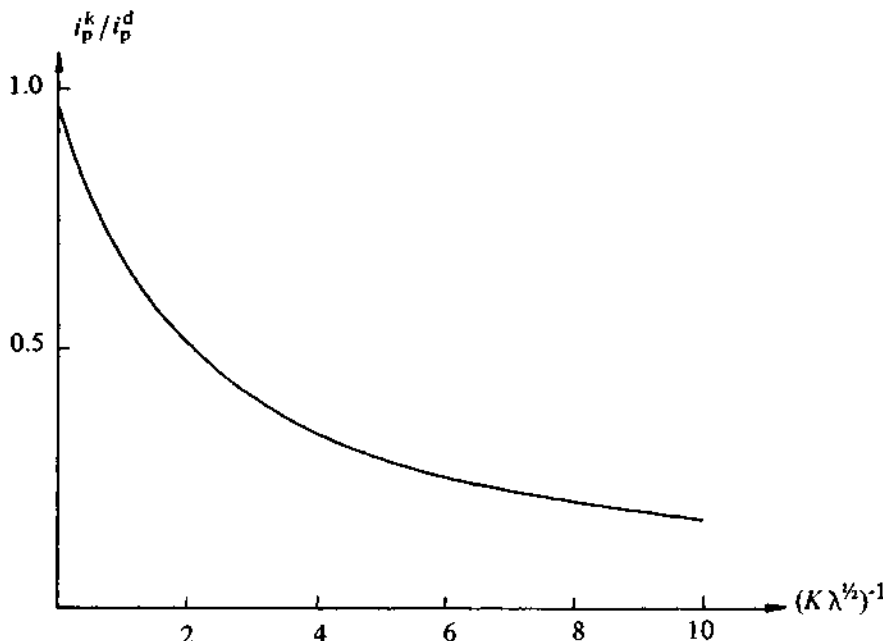


Fig. 6.11 – The working curve for the determination of the rate constant for a chemical reaction preceding the electron transfer process.

Before leaving the ce scheme, we must consider the case where the electron transfer is irreversible. The first thing to be noted is that there is no reverse peak on the voltammogram. The overall behaviour is, however, rather complex since there are several possible limiting cases. Nicholson & Shain [3] have also investigated this system and have determined, again empirically, that the ratio, i_p^k/i_p^d , where i_p^d is the peak current for the simple irreversible electron transfer, should obey the expression

$$\frac{i_p^k}{i_p^d} = \frac{1}{1.02 + 0.531/K\lambda^{1/2}} \quad (6.15)$$

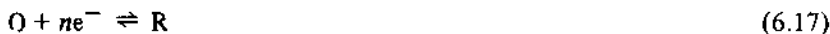
where λ_i is given by

$$\lambda_i = \left(\frac{k_1 + k_{-1}}{\nu} \right) \frac{RT}{\alpha_C n_a F} \quad . \quad (6.16)$$

Equation (6.15) is very similar to Equation (6.14), and kinetic parameters are again obtained by fitting to a working curve.

It is also quite common to meet systems where there is an equilibrium between two electroactive species but the reduction of one occurs at a less negative potential. Then the cyclic voltammogram will show two reduction peaks but the ratio of the peak heights is a function of scan rate; as the scan rate is decreased the first peak will become relatively larger and, indeed, will show the characteristics discussed above for the case where only one of the species is electroactive. The kinetics of the equilibrium is readily obtained by investigating the ratio of the peak currents as a function of scan rates.

6.3.2 The ec reaction



The ec scheme, which is a very common mechanism in organic electrochemistry, is described by Equations (6.17) and (6.18). The cyclic voltammogram observed depends on the relative rates of the two steps. The simplest situation is where the electron transfer is totally irreversible; the presence of the chemical reaction has no effect on the voltammogram obtained and no kinetic data related to the chemical reaction can be derived. This situation leads to the properties in Table 6.2. Similar properties can also arise when the rate of the electron transfer step is relatively fast if the rate constant for the chemical reaction is very large. The full range of other possibilities where the chemical reaction can be reversible or irreversible and the electron transfer either reversible or quasi-reversible has been considered in detail by Nadjo & Saveant [7], and the various kinetic zones have been identified. In this chapter the only case to be discussed in detail is that where the electron transfer is reversible and the chemical reaction is irreversible.

For the similar case where the chemical reaction is reversible the reader is referred to the paper by Nicholson & Shain [3], whilst for all other possibilities the article by Nadjo & Saveant [7] should be consulted.

The effect of a following chemical reaction is of course greatest on the reverse sweep where R is reoxidised. If the chemical reaction is fast, R is rapidly removed from the region near the electrode. At low sweep rates, therefore, no reverse peak is observed, but on decreasing the timescale of the experiment, by increasing the sweep rate, a reverse peak may become increasingly apparent. Fig. 6.12 shows normalised theoretical cyclic voltammograms for the case of reversible electron transfer, irreversible chemical reaction for a range of values of the variable λ given by

$$\lambda = k \left(\frac{RT}{nF} \right) \nu . \quad (6.19)$$

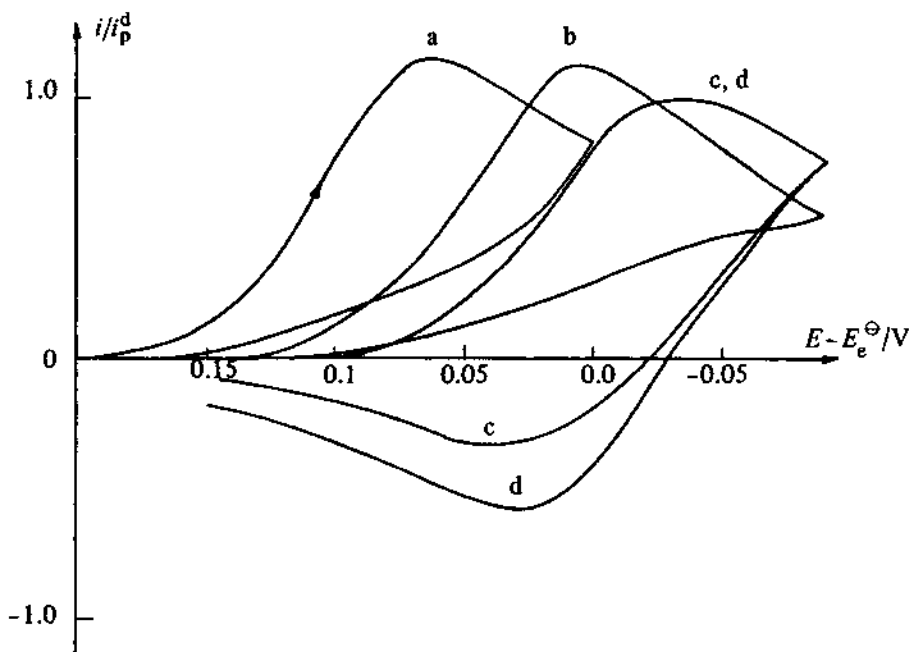


Fig. 6.12 — Theoretical cyclic voltammograms for the ec mechanism for the following values of λ (a) 500, (b) 10, (c) 0.1, (d) 0.01. The current scale is normalised to the peak current in the absence of a chemical reaction.

In the region where no reverse peak is observed, the pure kinetic zone, it can be shown that the chemical reaction has the effect of shifting the cathodic peak potential positive of the E_p^C value for the reversible electron transfer. This is because the coupled chemical reaction reduces the concentration of R at the surface from the value it would have had for a simple electron transfer reaction. The electrode reaction therefore has to work harder to maintain Nernstian equilibrium

at the surface. However, the peak is shifted back $30/n$ mV (at 25°C) in a negative direction for each tenfold increase in ν , provided the chemical reaction is first order in the intermediate produced at the electrode surface (if the chemical reaction is second order in R, $\partial E_p^C / \partial \log \nu = -19.6/n$ mV). Eventually as the sweep rate is increased a reverse peak starts to appear, and the rate of change of E_p with sweep rate decreases. The ratio of the anodic to cathodic peak current continues to increase with the sweep rate until eventually reversible behaviour is observed. It is from the region where a reverse peak is observed, but the ratio $|i_p^A/i_p^C|$ is less than one, that kinetic data can be obtained. This is the region where $5 > \lambda > 0.1$ (a relatively small range). The rate constant is obtained by comparing experimental $|i_p^A/i_p^C|$ ratios with the working curve described by Nicholson & Shain [3] where this ratio is plotted as a function of $\log k\tau$ where τ is the time required to traverse the potential range from the polarographic half wave potential ($E_{1/2}$) to the switching potential (E_2 , the potential at which the sweep is reversed). Such a working curve is shown in Fig. 6.13(a). To ensure reliable values of the rate constant a range of switching potentials and sweep rates should be used. The value of the half wave potential can be obtained from data under reversible conditions where the chemical reaction does not interfere (i.e. at high sweep rates) when E_p^C and $E_{1/2}^C$ are related by Equation (6.20):

$$E_p^C - E_{1/2}^C = -1.109 \frac{RT}{nF} = -\frac{28.5}{n} \text{ mV at } 25^\circ\text{C} . \quad (6.20)$$

An alternative approach based on peak potential measurements arises from the kinetic zone analysis by Nadjo & Saveant [7]. Fig. 6.13(b) shows calculated E_p^C values plotted as a function of $\log \lambda$ for the ec reaction. For values of $\log \lambda \leq -0.95$ the behaviour corresponds to a diffusion controlled system, i.e. the peak potential does not shift with sweep rate, whilst for $\log \lambda \geq 0.28$, E_p^C shifts 30 mV in a negative direction for each tenfold increase in ν . If experimental peak potential data obtained over a sufficiently wide sweep range are plotted as a function of $\log \nu$, then there should be horizontal linear region (diffusion control) an oblique linear region (kinetic control) and a curved region (mixed control) linking them. From the $\log \nu$ values at which the changes occur, the value of k can be found by using the λ values given above.

As with the other schemes discussed here it is useful to have diagnostic tests for the ec mechanism, and these are presented in Table 6.5.

Table 6.5 – Diagnostic tests for ec reactions

-
1. $|I_p^A/I_p^C|$ is less than one but tends to unity as ν is increased
 2. $I_p^C/\nu^{1/2}$ decreases slightly with increasing ν
 3. E_p^C is positive of the value for the reversible case
 4. E_p^C shifts negatively with increasing ν , and in the pure kinetic region shifts by $30/n$ mV per 10 fold increase in ν (this changes to $19/n$ mV for a second order reaction)
-

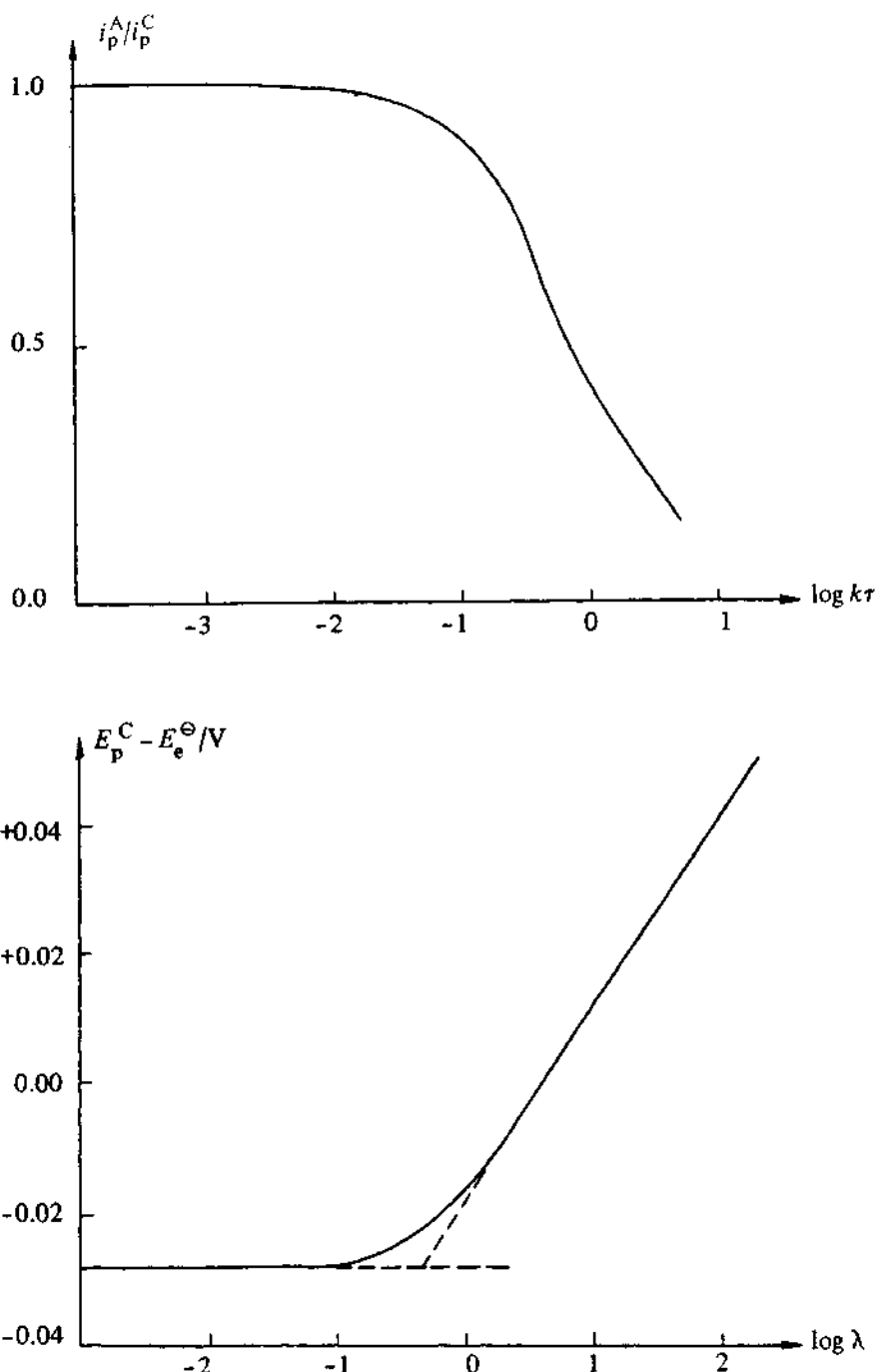


Fig. 6.13 – Working curves for the estimation of the rate constant for a following chemical reaction, an ec system. (a) a plot of the ratio of anodic to cathodic peak currents as a function of $\log k\tau$. τ is the time taken to scan from $E_{1/2}$ to the switching potential. (b) E_p^C as a function of $\log \nu$.

6.3.3 The catalytic mechanism



This is a specific type of following chemical reaction mechanism where the reactant is regenerated chemically. Analysis under second order conditions is difficult, and therefore with such systems it is usual to arrange that $c_X^\infty \gg c_O^\infty$. The concentration of X therefore remains essentially unchanged throughout the experiment, and the chemical reaction can be treated as pseudo first order. We shall discuss here the case where the electron transfer is reversible. Other possibilities are considered in the literature [3, 14].

Under pseudo first order conditions, and where k is small or ν large, the chemical reaction has no effect, and simple reversible behaviour is observed. For larger values of k , or as ν is decreased, however, there is effectively more reactant regenerated, and therefore $|I_p^C|$ values are higher than would be predicted from the Randles-Sevcik equation (Equation (6.4)). The $|I_p^C/\nu^{1/2}|$ values increase with decreasing sweep rate and the peak becomes less pronounced. In the limit the peak disappears altogether and is replaced by a sweep rate independent plateau. This is shown in Fig. 6.14 where normalised theoretical cyclic voltammograms are plotted for several values of λ defined by

$$\lambda = \frac{kc_X^\infty}{\nu} \left(\frac{RT}{nF} \right) \quad (6.23)$$

The current density of the plateau is given by

$$I_L = -nFc_O^\infty(Dkc_X^\infty)^{1/2} , \quad (6.24)$$

and k values can readily be obtained from the experimental value of I_L and Equation (6.24). In certain cases the plateau current is not readily measured; then an alternative method, developed by Nicholson & Shain [3], is used to determine k . This simply relies on comparing the value of the ratio of the peak currents in the presence and absence of X with tabulated data.

The general diagnostic tests for the catalytic mechanism are given in Table 6.6. This mechanism is usually very readily identified as it is the only one in which the $|I_p^C/\nu^{1/2}|$ value increases so markedly on decreasing the sweep rate.

Table 6.6 — Diagnostic tests for catalytic reactions

-
1. $|I_p^C/\nu^{1/2}|$ decreases with increasing ν
 2. I_p^C may reach a limiting value at low sweep rates
 3. $|I_p^C|$ values are greater than predicted by Randles-Sevcik equation
 4. $|I_p^A/I_p^C| \ll 1$
-

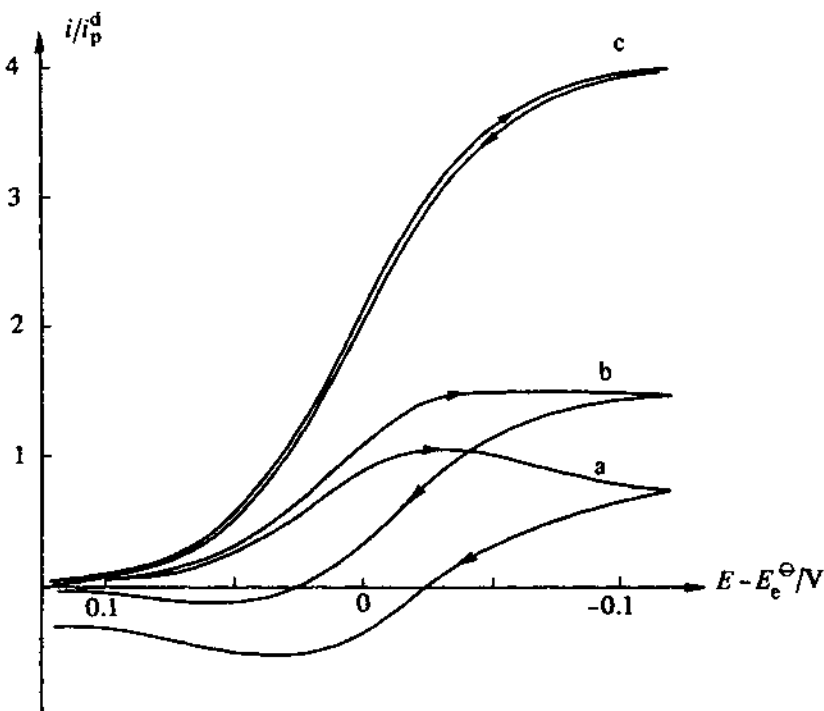


Fig. 6.14 – Theoretical cyclic voltammograms for the catalytic mechanism. The current is normalised with respect to the peak current for a simple reversible process. The curves are for the values of λ (a) 0.04, (b) 0.4, (c) 3.16.

6.3.4 The ece mechanism



This is another specific type of following reaction where the initial reaction product reacts chemically to yield a species O' , which is itself at least as readily reduced as O . This type of reaction sequence is fairly common in multi-electron transfer processes in organic electrochemistry. It was discussed in some detail in an earlier chapter (Chapter 2) on pulse techniques, and the possibility of competing disproportionation reactions was considered. We will only consider here the case where homogeneous electron transfer can be ignored, the electron transfer are reversible, and the chemical reaction is irreversible. Other cases are discussed in the literature [7, 9–11].

If we first just consider the forward peak, then when k is large compared to the rate of mass transport the electrode reaction will appear to be an $(n_1 + n_2)$ electron process, whereas if k is low it will behave like an n_1 electron one. Thus for any given system, as the sweep rate is increased the apparent number of

electrons involved, n_{APP} , will decrease from $(n_1 + n_2)$ towards n_1 . Changes are also observed on the reverse and subsequent sweeps. Fig. 6.15 shows a cyclic voltammogram for an ece system with the rate of mass transport comparable to k . Peaks I and II correspond to the couple O/R, whilst III and IV correspond to the O'/R' couple. Thus for increasing values of k or decreasing sweep rate, peaks III and IV become increasingly apparent.

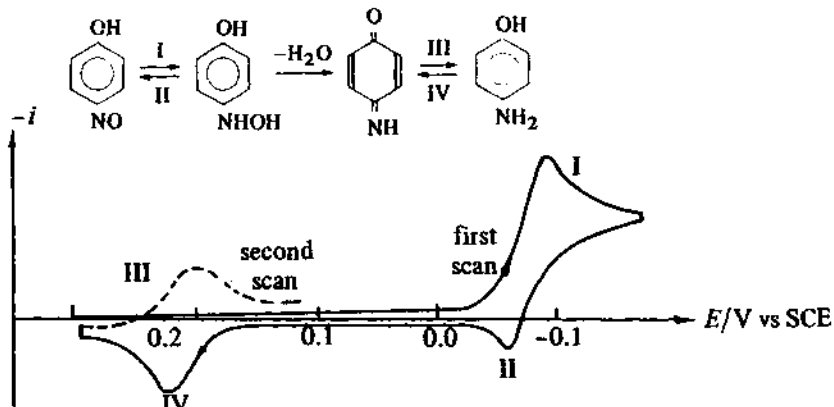


Fig. 6.15 – Cyclic voltammogram for the reduction of p-nitrosophenol in an acetate buffer solution at a mercury drop electrode.

The behaviour of an ece system is most clearly seen by plotting $|I_p^C/\nu^{1/2}|$ for peak I on the first sweep as a function of ν or $\log \nu$ (analogous to the $I t^{1/2}$ vs t plots in chronoamperometry), as is shown in Fig. 6.16 (for $n_1 = n_2 = 1$). At low sweep rates mass transport is slow, and therefore a peak current corresponding to an irreversible two electron process is seen, whereas at high sweep rates only a reversible one electron step is found. Values of k can be found by analysing such $|I_p^C/\nu^{1/2}|$ vs $\log \nu$ plots.

Nicholson & Shain [9] have shown that

$$I_p^C/\nu^{1/2} = -\pi^{1/2} F c_O^{\infty} \left(\frac{D n F}{RT} \right)^{1/2} \{ n_1 \chi c_O^{\infty} + n_2 \phi c_O^{\infty} \} \quad (6.28)$$

where χ and ϕ values are available in tabulated form in the original literature as functions of $(kRT/nF\nu)$. By curve fitting experimental $I_p^C/\nu^{1/2}$ data to Equation (6.28) the value of k can be determined.

Diagnostic tests for ece systems are given in Table 6.7.

Table 6.7 – Diagnostic tests for ece reaction

-
- $I_p^C/\nu^{1/2}$ varies with sweep rate but may reach limiting values at high and low sweep rates
 $|I_p^C/\nu^{1/2}|$ (low ν) $>$ $|I_p^C/\nu^{1/2}|$ (high ν)
 - $|I_p^A/I_p^C|$ increases with sweep rate and tends to one at a high sweep rate
-

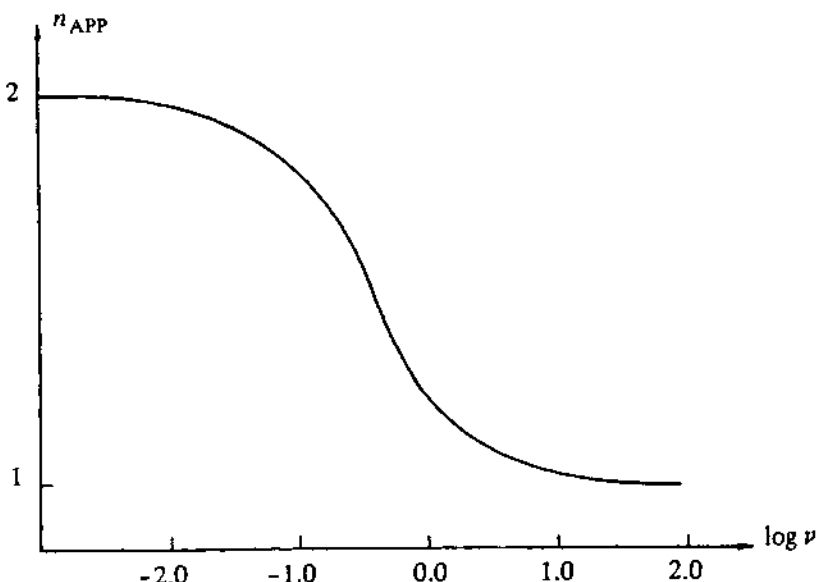


Fig. 6.16 – The theoretical dependence of n_{APP} , as calculated from I_p , on $\log \nu$. Curve calculated for $k = 10 \text{ s}^{-1}$.

6.4 ILLUSTRATIONS OF THE USE OF CYCLIC VOLTAMMETRY FOR THE STUDY OF COUPLED CHEMICAL REACTIONS

All the examples discussed in this section concern reductions in dimethylformamide; the electrode could be a mercury drop or a vitreous carbon disc.

The first example [15] shows how cyclic voltammetry may be used to demonstrate the rapid isomerisation of the anion radical of diethylmaleate (DEM). Fig. 6.17 shows the voltammograms for DEM and diethylfumarate (DEF), the *cis* and *trans* isomers respectively. The reduction of DEF shows a well formed reduction peak, $E_p = -1.41 \text{ V}$ vs SCE, and a coupled anodic peak; above 0.1 Vs^{-1} , the curve has all the properties of a reversible 1e^- process. Below this scan rate, there is evidence for a slow chemical reaction, and more detailed investigations showed this to be dimerisation. The reduction peak for DEM, below 5 Vs^{-1} , is much broader; $E_p = -1.61 \text{ V}$, with no anodic peak corresponding to the reverse process. There is, however, an anodic peak at -1.35 V which is the same potential required for the oxidation of $\text{DEF}^{\cdot-}$. Also on the second and subsequent cycles a new reduction peak is seen to grow at -1.41 V . On increasing the potential scan rate above 50 Vs^{-1} , a small anodic peak is seen where the oxidation of $\text{DEM}^{\cdot-}$ is expected and the anodic peak at -1.35 V becomes relatively smaller (i.e. when corrected for scan rate effects). Finally, the current functions, $I_p^C/c\nu^{1/2}$, for the main reduction peaks for DEF and DEM are almost independent of ν and correspond to reasonable values for a reversible and irreversible 1e^- reduction.

respectively. Hence it may be concluded that the reduction of DEM occurs by the mechanism



Once formed, the $\text{DEF}^{\cdot\cdot\cdot}$ takes part in the electrode reactions



From the variation of I_p^A/I_p^C for the $\text{DEM}/\text{DEM}^{\cdot\cdot}$ couple at the faster scan rates, it is possible to estimate a value, 10 s^{-1} , for the rate constant for isomerisation.

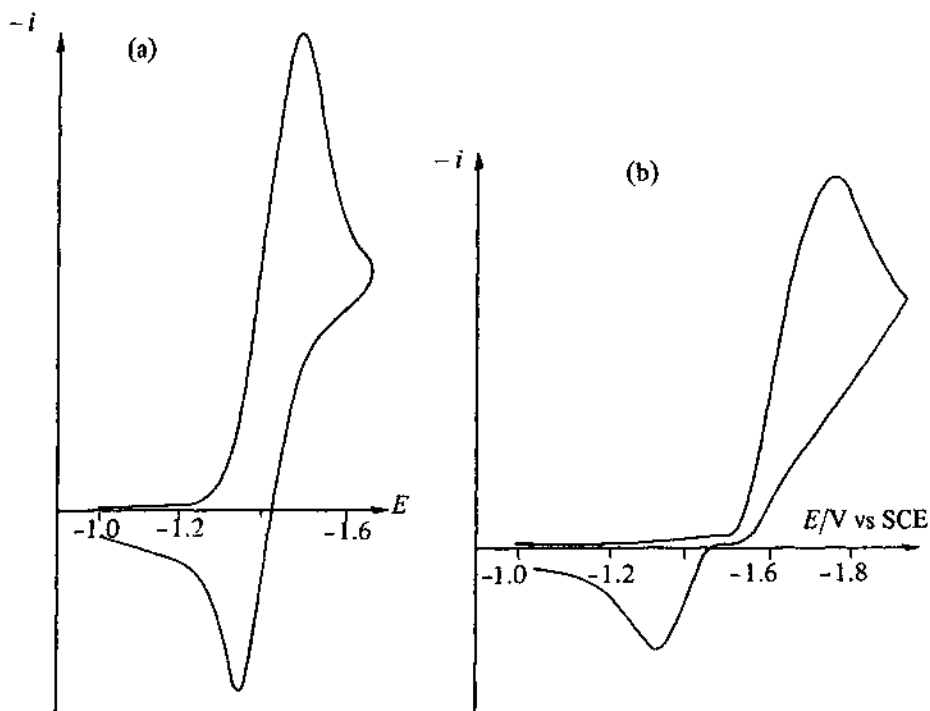


Fig. 6.17 – Cyclic voltammograms of (a) diethylfumarate, 50 mV s^{-1} and (b) diethylmaleate, 5 V s^{-1} , in $\text{DMF}/\text{Bu}_4\text{NBF}_4$ (0.1 mol dm^{-3}). Reproduced with permission from A. J. Bard, V. J. Puglisi, J. V. Kenkel, & A. Lomax, *Trans. Faraday Disc.*, **56** (1973) 353.

Figure 6.18 shows a voltammogram for p-chlorobenzonitrile [16]. The main features are an irreversible peak at -1.96 V and a reversible process at more negative potentials, $E_p^C = -2.32 \text{ V}$. The first peak remains irreversible at all sweep rates investigated even if the scan is reversed at -2.20 V (i.e. before

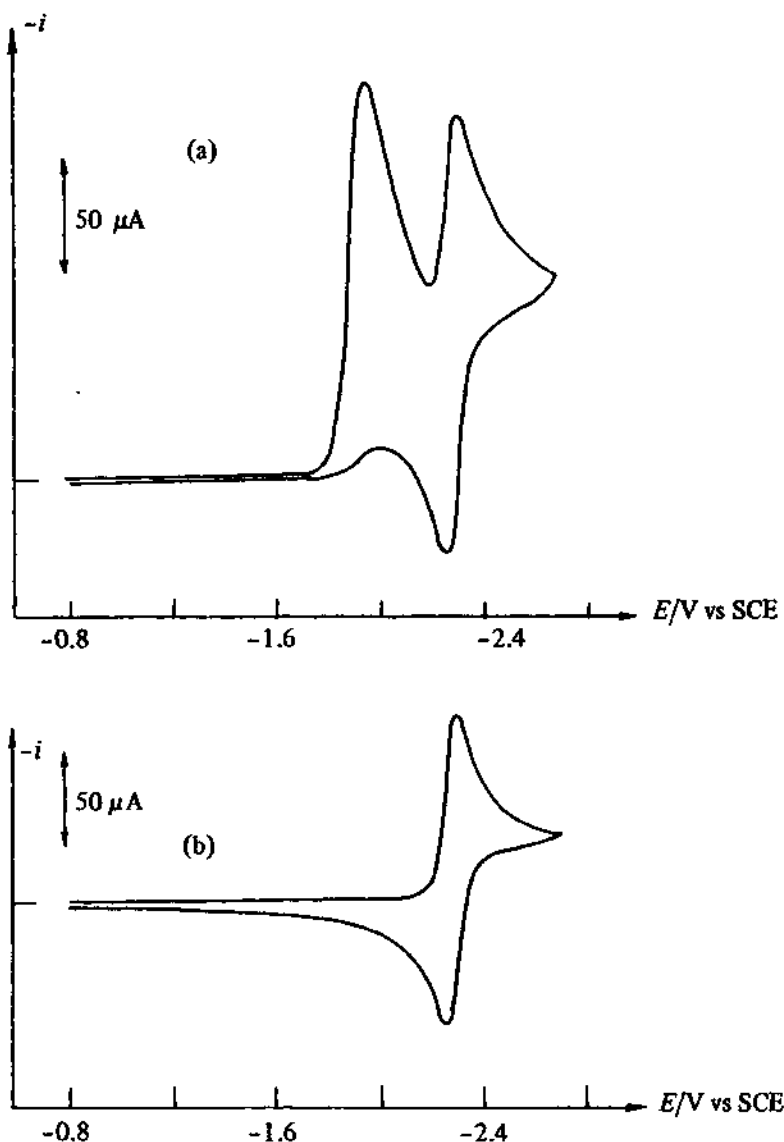
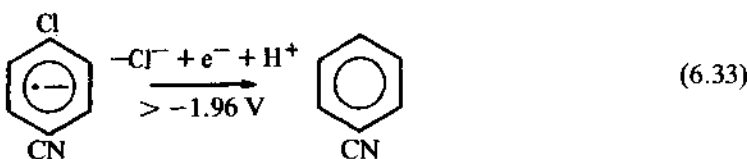
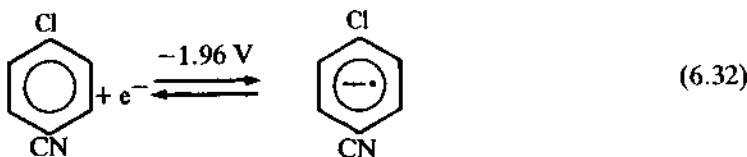


Fig. 6.18 – Cyclic voltammograms of (a) 4-chlorobenzonitrile, (b) benzonitrile at a Pt electrode in $\text{DMF}/\text{Et}_4\text{NClO}_4$ (0.1 mol dm^{-3}). Potential scan rate 0.08 Vs^{-1} . Reproduced with permission from D. E. Bartak, K. J. Houser, B. C. Rudy, & M. D. Hawley, *J. Am. Chem. Soc.*, **94** (1972) 7526.

the second peak), and its current function does not vary significantly with scan rate. The second peak is always about half the size of the first. Hence it may be postulated that the reduction occurs by the mechanism



Two further pieces of evidence confirm this mechanism. Firstly, a cyclic voltammogram for benzonitrile under the same conditions shows a $1e^-$ reversible process at -2.32 V . Secondly, if the electrode is Hg, further peaks (an oxidation peak and a reduction peak on a second cycle) are observed close to zero; they have the characteristics of a process where a surface film is involved, see section 6.5, and are due to the $\text{Hg}/\text{Hg}_2\text{Cl}_2$ couple as may be confirmed by running a cyclic voltammogram for Cl^- in DMF. These peaks are, however, only seen for the solution of chlorobenzonitrile, when the negative limit is chosen beyond the first reduction peak and it can therefore be concluded that chloride is formed in this process. The first peak is clearly a $2e^-$ reduction and is probably an example of an ece reaction; the chemical reaction is, however, fast on the timescale of all experiments reported, and hence the current function corresponding to the $2e^-$ limit is always observed.

Our last example [17] concerns the reduction of the nosylate ester, phenyl 4-nitrobenzenesulphonate. At all potential scan rates, the compound gives three reduction peaks at -0.74 V , -1.23 V and -2.22 V vs SCE, and the first two have coupled anodic peaks. If the potential scan is limited to the range 0 to -1.0 V , the first reduction process can be seen to be a reversible $1e^-$ process at all scan rates, see Fig. 6.19(a). When the scan range is extended to -1.6 V the second reduction step can also be examined. At scan rates above 50 V s^{-1} , $I_p^A/I_p^C = 1$ and the cathodic peak is the same height as that for the peak at -0.74 V . ΔE_p for the second peak is, however, well above 60 mV , typically $150\text{--}200\text{ mV}$. Hence the second electron transfer process is not in equilibrium. Moreover, on slowing down the scan rate, the peak at -1.23 V becomes larger

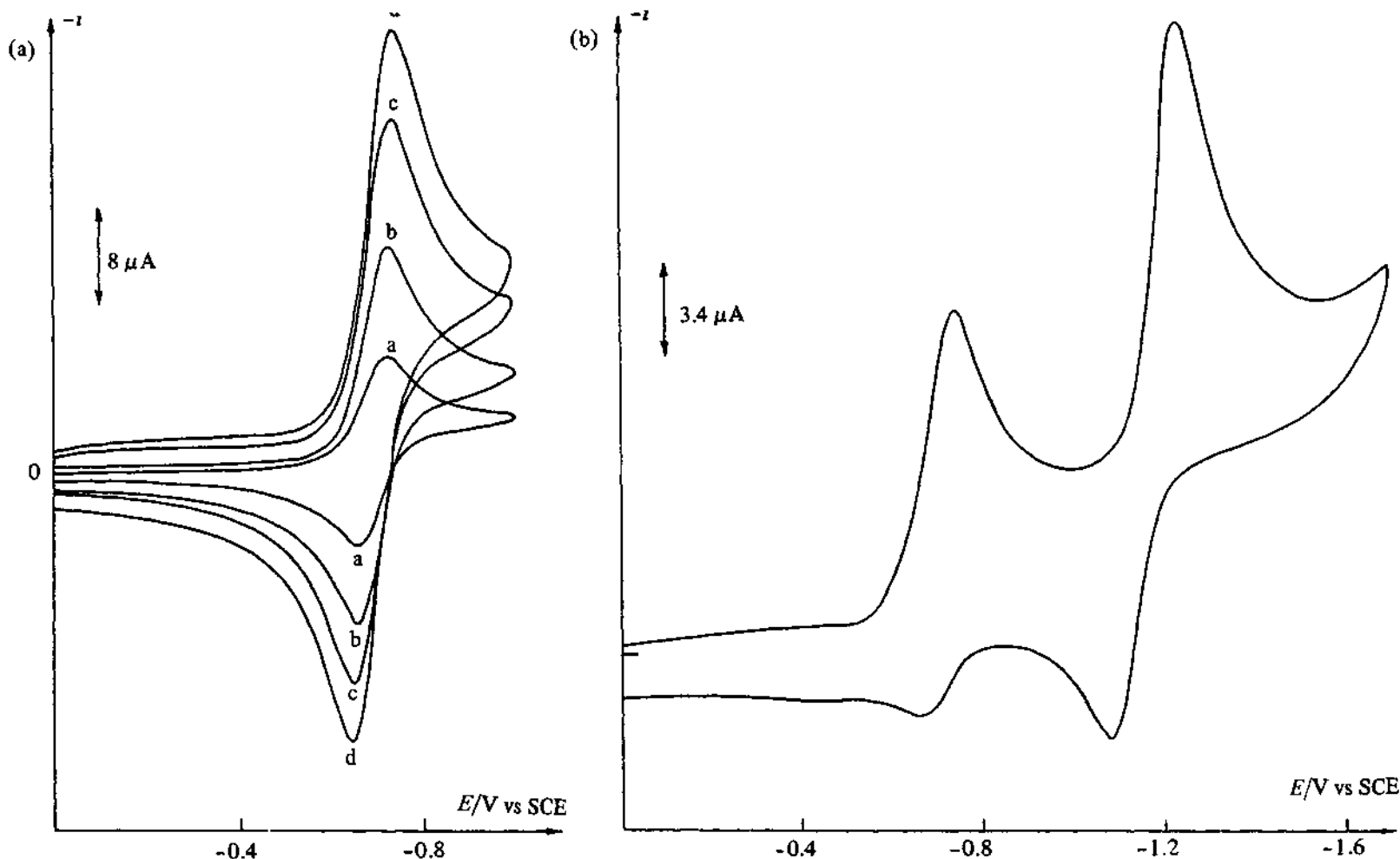
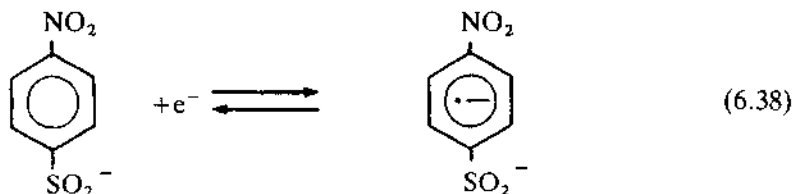
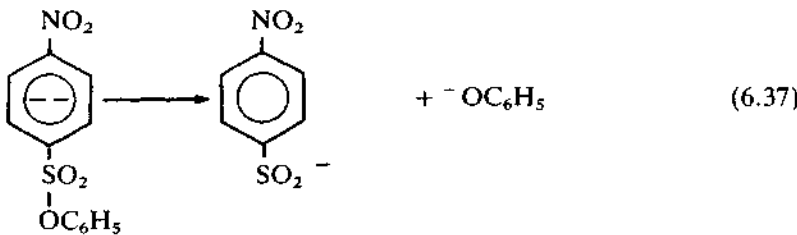
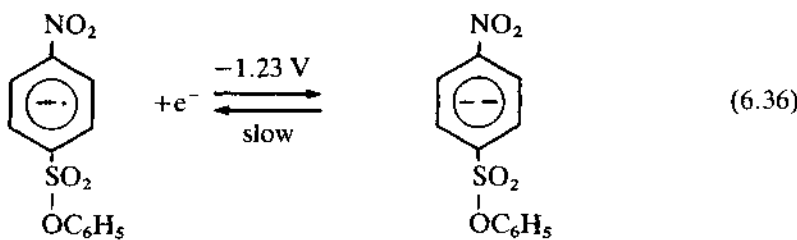
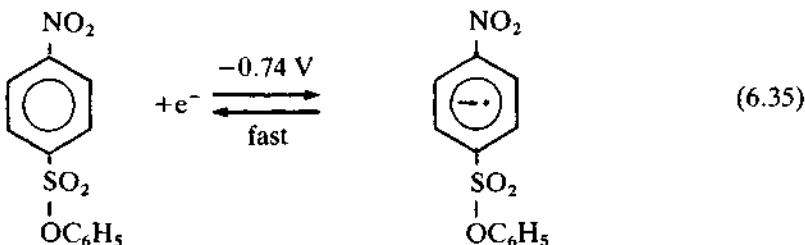


Fig. 6.19 – Cyclic voltammograms for phenyl 4-nitrobenzenesulphonate at vitreous C disc in $\text{DMF}/\text{Bu}_4\text{NBF}_4$ (0.1 mol dm^{-3}). (a) Potential range 0 to -1.0V ; potential scan rates a. 20 mV s^{-1} b. 80 mV s^{-1} c. 200 mV s^{-1} d. 320 mV s^{-1} . (b) Potential range 0 to -1.6V ; potential scan rate 100 mV s^{-1} .

than that at -0.74 V , and $I_p^A/I_p^C < 1.0$. Indeed in the limit, see Fig. 6.19(b), the ratio of the two cathodic peaks becomes 2:1, and the anodic peak for the second reduction process disappears (the anodic peak for the first reduction peak is also distorted and smaller than expected; this always happens when the product of a reaction undergoes a further reduction at more negative potentials, c.f. Fig. 6.19(a) and 6.19(b)). Overall the reduction process at -1.23 V therefore has the characteristics of an ece process, suggesting the mechanism



This mechanism is consistent with the observation that 4-nitrobenzenesulphonate undergoes reduction, $E_p = -1.15\text{ V}$.

These examples are intended to illustrate how variation of the potential scan rate and the potential limits allows cyclic voltammetry to be used to rapidly build up a picture of the electrochemistry of the organic molecules.

Ideally the conclusions should be checked by coulometry and product analysis or spectroelectrochemical methods, and other techniques (e.g. chronoamperometry, RRDE) should be used to confirm the numerical values of rate parameters.

6.5 SURFACE PROCESSES

Thus far this discussion of cyclic voltammetry has assumed that all the reactants and products are freely soluble in the solution, and that surface processes, such as phase formation and removal, and reactant or product adsorption, need not be considered. If the peaks on an experimental cyclic voltammogram exhibit a shape or sweep rate dependence unlike those discussed so far, it is a good indication that surface processes may be involved. Cyclic voltammetry has proved a very useful technique for the quantitative investigation of reactions involving adsorption processes. It is less well suited to the study of surface reactions such as metal deposition and corrosion, other than as a diagnostic tool.

6.5.1 Adsorption

The simplest case to consider of a reaction involving adsorption is that where only the adsorbed forms of O and R are electroactive in the potential range under investigation. This situation can arise for a number of reasons, one of the most common being that the reduction potential of adsorbed O is shifted to a potential well positive of the reduction potential of dissolved O. The analysis of such a system is fairly straightforward as mass transport effects can be ignored. If the electron transfer is reversible then a cyclic voltammogram similar to that shown in Fig. 6.20 will be obtained. The major differences when compared to a voltammogram for a reaction in which both product and reactant are dissolved in solution is that the peaks are sharp and symmetrical, the current rising from essentially zero to a peak value and then falling again to zero, and there is little or no peak separation. Also the charges associated with anodic and cathodic processes are equal. The symmetrical peak arises because of the fixed amount of reactant – only O on the surface at the start of the sweep can be reduced. The actual value of I_p , E_p , and the peak width all depend on the type of adsorption isotherm involved and the relative strengths of adsorption of O and R. For the case where the adsorption can be described by a Langmuir isotherm it can be shown that $E_p^A = E_p^C$, and that the peak current density is given by Equation (6.39).

$$|I_p^C| = \frac{n^2 F^2 \Gamma_O}{4RT} \nu \quad (6.39)$$

where Γ_O is the surface excess of O before the start of the sweep, i.e. the peak current is proportional to the sweep rate, ν , and not its square root. The area under the cathodic peak (remember the potential axis is also a time axis), Q , corresponds to the charge associated with the reduction of the adsorbed layer of O and this enables the surface excess of O to be determined by Equation (6.40)

$$\Gamma_0 = \left| \frac{Q}{nF} \right|. \quad (6.40)$$

For non-Nernstian systems the shape of the cyclic voltammogram changes. For the irreversible case the forward peak ceases to be symmetric, and of course there is no reverse peak. For quasi-reversible reactions there will be a reverse peak but both peaks will be asymmetric and the peak potentials will not be coincident. There is insufficient space here to consider these systems more fully, but further details can be found in the literature [12, 13].

At this point it is probably worth mentioning briefly systems where a reactant has been attached to an electrode by chemical means. Such electrodes, which are known as *chemically modified electrodes*, have received considerable attention recently, largely for possible use in catalysis. They are mentioned here because of their similarity to adsorption systems (the number of reactant sites on the surface is fixed) and because their cyclic voltammetric behaviour can be analysed in a manner identical to that discussed above [14].

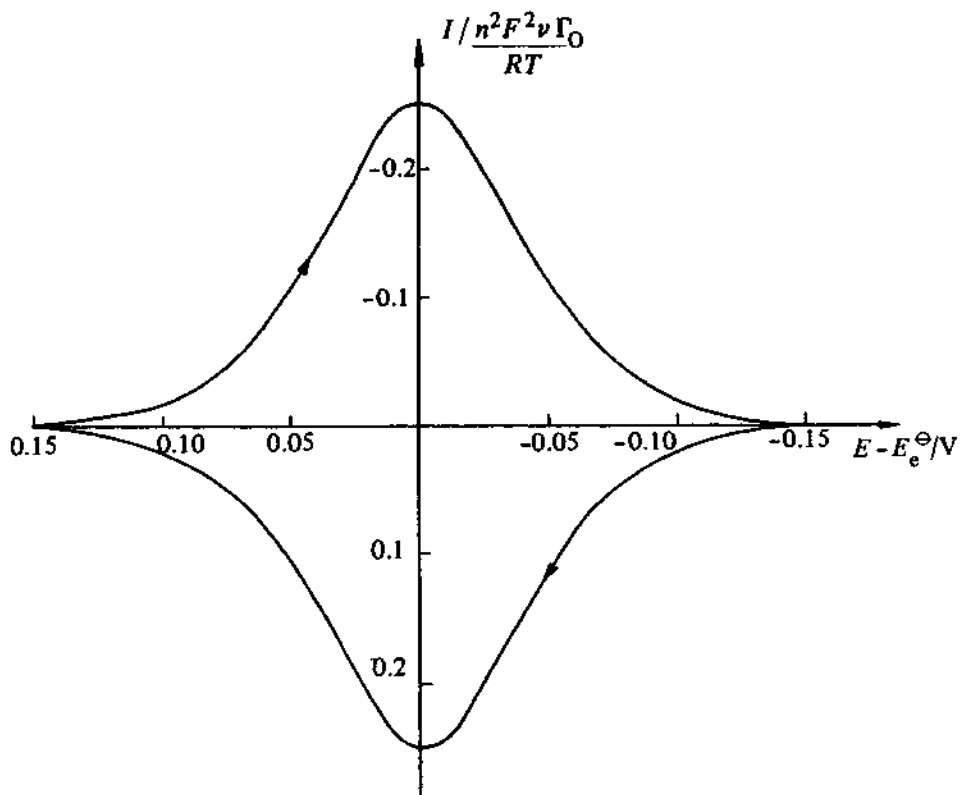


Fig. 6.20 – Theoretical cyclic voltammogram for the reduction of adsorbed O and reoxidation of the product where (a) the free energies of adsorption of O and R are equal and (b) adsorption follows a Langmuir isotherm.

The above discussion has assumed that only the adsorbed species are electroactive; the more general case where both adsorbed and solution species are involved is described by the following equations:

$$\text{O}_{\text{soln}} \rightleftharpoons \text{O}_{\text{ads}} \quad (6.41)$$



$$\text{R}_{\text{soln}} \rightleftharpoons \text{R}_{\text{ads}} \quad (6.43)$$

and has been considered in detail by Wopschall & Shain [18]. Figs. 6.21(a) and (b) show voltammograms corresponding to strong reactant and strong product

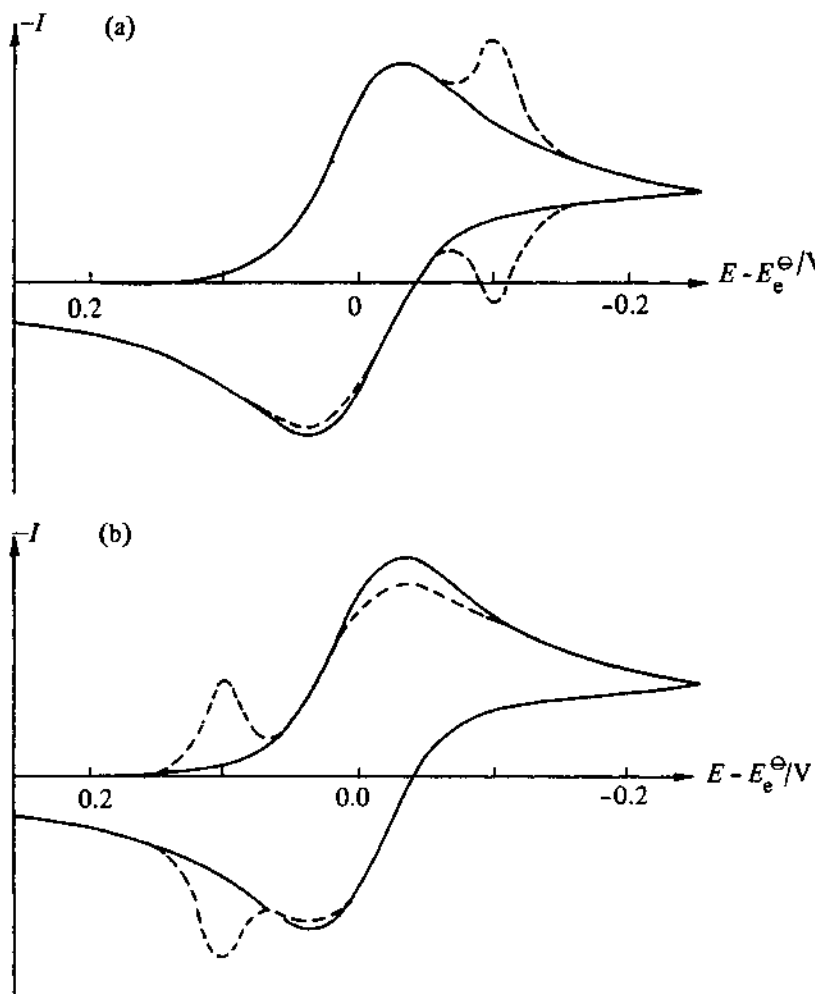


Fig. 6.21 – Theoretical cyclic voltammograms for the reduction of O when (a) O is strongly adsorbed, (b) R is strongly adsorbed. The dashed lines indicate the response with adsorption, and the solid line that for a simple reversible process without adsorption.

adsorption respectively for a process where the electron transfer is reversible. The symmetrically shaped peaks correspond to the reaction of the adsorbed species, whilst the conventionally shaped ones are due to the reaction of solution species. As can be seen, strong reactant adsorption gives rise to a post-peak and strong product adsorption to a pre-peak (an adsorbed reactant is stabilised with respect to electrode reaction and therefore reacts less readily, whereas product adsorption favours reaction). The sweep rate dependence of pre- or post-peaks, and the solution peaks are rather different; whereas the former increase in height proportional to the sweep rate the latter only increase as $\nu^{1/2}$. In addition, the concentration dependence of the two types of peak is also different; the solution peak increases linearly with concentration, whereas an adsorption peak will increase with concentration (not necessarily linearly) until it reaches a limiting value corresponding to complete surface coverage.

A classic example of a system exhibiting strong product adsorption is the reduction of protons at a platinum electrode. As shown in Fig. (6.22), there are two pairs of pre-peaks (other smaller ones are visible in high purity systems) corresponding to adsorption, and desorption, of H at two different types of site. The two types of adsorbed hydrogen are designated H_S and H_W to indicate the relative strengths of adsorption.

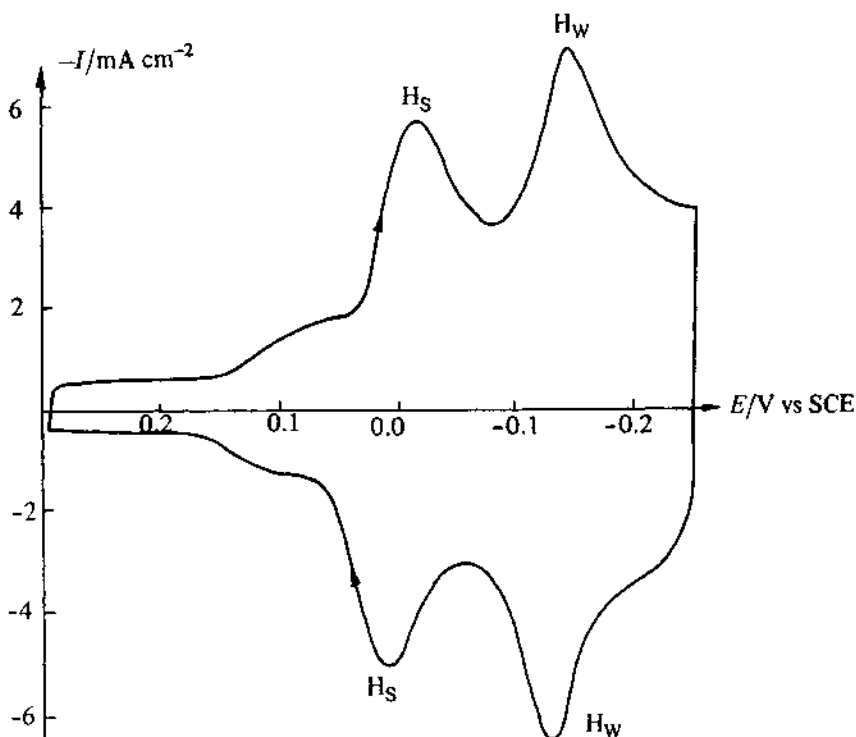


Fig. 6.22 – Cyclic voltammogram for a Pt electrode in $1\text{ mol dm}^{-3}\text{ H}_2\text{SO}_4$ at a potential sweep rate of 42 Vs^{-1} showing the hydrogen adsorption and desorption peaks.

The separation between the adsorption and solution peaks reflects the relative strength of adsorption, and as this strength reduces so too does the peak separation. Thus for weak adsorbates two separate peaks are not discernible; the cyclic voltammogram will however be distorted as shown in Fig. 6.23. In the case of weak reactant adsorption the forward peak will be higher than for a simple reversible system, and the reverse peak will also be enhanced, but less so. For weak product adsorption the situation is reversed; the height of the forward peak hardly changes from the value for a reversible system, though it does shift to positive potentials with increasing scan rate, whereas the reverse peak is significantly enhanced.

The behaviour of systems where the electron transfer is either irreversible or quasi-reversible is fairly similar to the above, and is discussed fully by Wopschall & Shain [18] who also consider the case where there is a coupled following chemical reaction. Other systems with coupled chemical reactions can be analysed in an analogous manner.

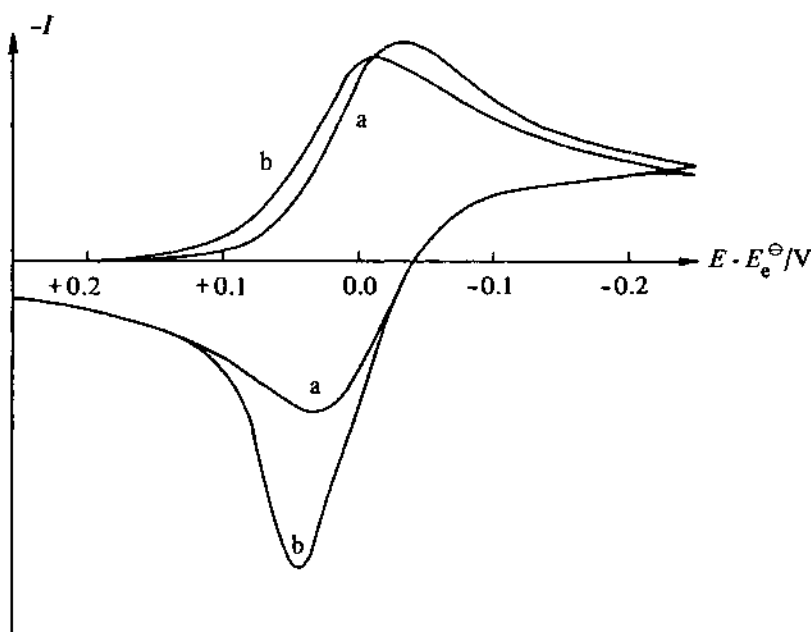


Fig. 6.23 – The effect of weak product adsorption is shown in curve (b). Curve (a) is again the response for a simple reversible system.

6.5.2 Deposition processes

Figure 6.24 shows an example of the type of cyclic voltammogram often encountered in studies of the deposition of metals, or other phases from dilute solution onto a foreign substrate, e.g. Hg on carbon. The forward, i.e. deposition, peak is very similar in shape to that for a process involving only solution soluble species, except that the leading edge is slightly steeper. The major differences are seen

upon sweep reversal. The current trace crosses over the forward sweep, whilst the reverse peak is sharp and symmetrical. This latter feature is simply explained since the reacting material is deposited on the electrode and therefore does not need to diffuse there in order to react. It is thus very like an adsorbed species. The area under this reverse peak, often called a *stripping peak*, corresponds to the amount of material deposited on the electrode during the forward sweep.

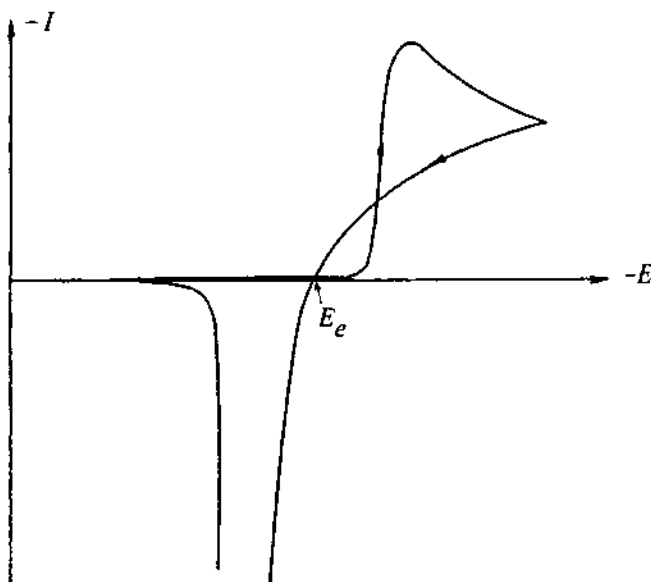


Fig. 6.24 -- Schematic cyclic voltammogram for a metal deposition reaction exhibiting a nucleation overpotential.

The simplest way of explaining the cross-over is to consider a specific example, Pb on carbon. A prerequisite for the growth of lead on the carbon substrate is the formation of thermodynamically stable nuclei on the surface (see Chapter 9). The formation of such nuclei requires a potential more negative than that required to reduce Pb^{2+} cations, and leads to what is known as a *nucleation overpotential*, i.e. the potential has to be more negative to deposit Pb on carbon than on Pb itself. Thus on the forward sweep a potential significantly more negative than the equilibrium potential for the Pb/Pb^{2+} couple in the test solution is required before deposition commences. On the reverse sweep, however, the deposition is occurring on a lead surface and thus continues until the equilibrium potential is reached. The second cross-over on the cyclic voltammogram corresponds to the equilibrium potential (for fast M/M^{n+} couples), and the difference in potential between this point and the potential at which deposition commences on the forward sweep corresponds to the nucleation overpotential. It is worth noting that the nucleation overpotential

on the first sweep will generally be greater than that on the second and subsequent ones, and that different methods of surface preparation also result in different values of the overpotential.

The above discussion was included largely to enable the identification of the cyclic voltammetric behaviour of a deposition process. However, cyclic voltammetry is generally not a good choice of technique for investigations of this type. Electrocrystallisation is discussed in detail in Chapter 9.

6.5.3 Passivation

Passivating layers are particularly important since they are responsible for the stability of many metals and alloys in common use. There is considerable debate in the literature as to how these layers form, and it is not the intention to discuss the various theories here. Essentially an insoluble film of metal salt, or oxide, is formed on the electrode by a reaction such as that in Equation (6.44).



and this layer protects the metal and prevents further dissolution. Fig. 6.25 shows typical voltammograms for passivation processes. The current initially rises as the passivating film grows across the surface, and then falls rapidly as the surface passivates. Depending on the chemical reversibility of the system the passivating layer may or may not be removed when the potential sweep is reversed.

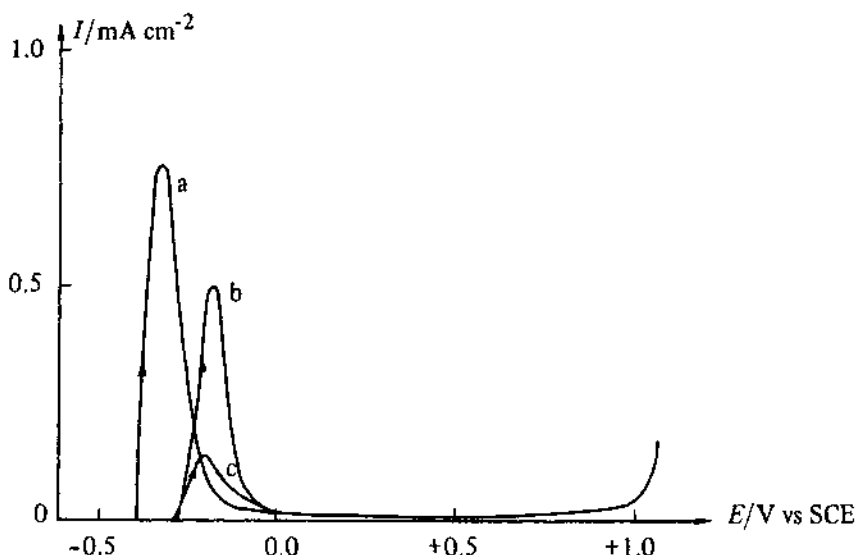


Fig. 6.25 – Linear potential sweeps for various steels in H_2SO_4 (2 mol dm^{-3}) at a sweep rate of 3 mV s^{-1} . The steels are (a) 304, (b) 800, (c) 316 L.

6.6 MORE RECENT DEVELOPMENTS

So far in this chapter, we have considered only traditional cyclic voltammetric experiments where the $I-E$ response is recorded. Moreover, we have taken a rather simplistic view of the mechanisms of homogeneous chemical reactions, assuming that they always follow simple, limiting pathways with a single rate determining step. Studies based on such principles remain important to electrochemistry and are widespread in the literature, but they ignore many mechanistic nuances and lead to imprecise data. This was also the state of the art maybe ten years ago.

It was felt then that

- (a) there was a need to develop techniques able to give information about more complex mechanisms and to discriminate between small differences in mechanism;
- (b) it was necessary to improve the precision with which data (E_p and I_p) could be taken from the experimental voltammograms or to consider analyses which took into account the total shape of the peaks. Alternatively better methods for displaying and analysing the response needed to be developed;
- (c) as always, it was desirable to develop methods of studying mechanism and kinetics when the rate constant for the coupled chemical reaction lay outside the limits of normal cyclic voltammetry, particularly reactions where the half lives of the intermediates were below 1 ms.

The past ten years have seen considerable progress towards the solution of these difficulties, and this section will review briefly both the approaches to the study of complex mechanisms and some of the techniques which have been developed to challenge the above problems. The literature in this field is dominated by the group of Saveant, although significant contributions have come from others such as Parker and Evans. The techniques require a firm grasp of theory, precise experimental work, and either non-commercial equipment or on-line computers. Hence they have not yet been widely applied, although with microcomputers now freely available this should soon change.

6.6.1 Approaches to the study of complex reaction mechanisms

Firstly, we should define the types of complexity which need to be considered when dealing with homogeneous chemical reactions coupled to electron transfer. The most common one is that the conversion of primary intermediates into final product is, in fact, a sequence of several, maybe four or five, elementary steps. In addition to defining the reaction pathway, it is necessary to decide which step is the rate determining one and also to consider the possibility that two steps have approximately the same rate, or that the r.d.s. changes, say with concentration of electroactive species. It is, however, also common in organic electrochemistry to find that the electrode reaction leads to a mixture of products and this is a clear indication of a branch mechanism where two competing reactions have comparable rates; branch mechanisms can even lead to the same product. A further uncertainty arises as to the source of electrons; does the second

electron come from the electrode or from a species in solution (the ece vs disp 1 case has already been discussed in Chapter 2). In addition, in many solutions, disproportionation and conproportionations can complicate the picture which would arise if only electron transfer at the electrode surface were allowed, while the reversibility of chemical reactions can lead to unexpected phenomena. Less commonly, other complexities, e.g. solvation of intermediates or ion pairing, have been introduced into the discussion. The case of such a reaction sequence is illustrated in Table 6.8, using the example of hydrodimerisation of A to DH_2 .

Table 6.8 – Diagnostic criteria for the mechanism of hydrodimerisation of A to DH_2 in the presence of base BH. 298K. From [19-20].

Possible reaction schemes	r.d.s. Medium†	$\frac{\partial E_p}{\partial \log v}$			$\frac{\partial E_p}{\partial \log c_A^\infty}$	$\frac{\partial E_p}{\partial \log c_{BH}^\infty}$
		mV/decade				
(i) radical-radical coupling						
(1) $A + e^- \rightleftharpoons A^{\cdot-}$						
(2) $2A^{\cdot-} \rightleftharpoons D^{\cdot\cdot}$	3	E	19.7	19.7	19.7	19.7
(3) $D^{\cdot\cdot} + BH \rightleftharpoons DH^{\cdot-} + B^-$	2	E	19.7	19.7	0	
(4) $DH^{\cdot-} + BH \rightleftharpoons DH_2 + B^-$						
(1) $A + e^- \rightleftharpoons A^{\cdot-}$	3	B	19.7	19.7	19.7	19.7
(2) $A^{\cdot-} + BH \rightleftharpoons AH^{\cdot-} + B^-$		U	19.7	0	19.7	
(3) $A^{\cdot-} + AH^{\cdot-} \rightleftharpoons DH^{\cdot-}$	2	E	29.6	0	29.6	
(4) $DH^{\cdot-} + BH \rightleftharpoons DH_2 + B^-$						
(ii) radical-substrate coupling						
(1) $A + e^- \rightleftharpoons A^{\cdot-}$						
(2) $A^{\cdot-} + A \rightleftharpoons D^{\cdot\cdot}$	4	E	14.8	29.6	14.8	
(3) $D^{\cdot\cdot} + e^- \rightleftharpoons D^{\cdot\cdot}$	2	E	29.6	29.6	0	
(4) $D^{\cdot\cdot} + BH \rightleftharpoons DH^{\cdot-} + B^-$						
(5) $DH^{\cdot-} + BH \rightleftharpoons DH_2 + B^-$						
(1) $A + e^- \rightleftharpoons A^{\cdot-}$						
(2) $A^{\cdot-} + A \rightleftharpoons D^{\cdot\cdot}$	4	E	19.7	19.7	19.7	19.7
(3) $D^{\cdot\cdot} + A^{\cdot-} \rightleftharpoons D^{\cdot\cdot} + A$	3	E	19.7	39.4	0	
(4) $D^{\cdot\cdot} + BH \rightleftharpoons DH^{\cdot-} + B^-$	2	E	29.6	29.6	0	
(5) $DH^{\cdot-} + BH \rightleftharpoons DH_2 + B^-$						
(1) $A + e^- \rightleftharpoons A^{\cdot-}$						
(2) $A + A^{\cdot-} \rightleftharpoons D^{\cdot\cdot}$	3	E	29.6	29.6	29.6	29.6
(3) $D^{\cdot\cdot} + BH \rightleftharpoons DH^{\cdot-} + B^-$	2	E	29.6	29.6	0	
(4) $DH^{\cdot-} + e^- \rightleftharpoons DH^{\cdot-}$						
(5) $DH^{\cdot-} + BH \rightleftharpoons DH_2 + B^-$						

Table 6.8 – Continued

Possible reaction schemes	r.d.s.	Medium†	$\frac{\partial E_p}{\partial \log \nu}$	$\frac{\partial E_p}{\partial \log c_A^\infty}$	$\frac{\partial E_p}{\partial \log c_B^\infty}$
			mV/decade		
(1) $A + e^- \rightleftharpoons A^-$	4	B	19.7	39.4	19.7
(2) $A + A^- \rightleftharpoons D^-$		U	19.7	19.7	19.7
(3) $D^- + BH \rightleftharpoons DH^- + B^-$	3	E	29.6	29.6	29.6
(4) $DH^- + A^- \rightleftharpoons DH^- + A$	2	E	29.6	29.6	0
(5) $DH^- + BH \rightleftharpoons DH_2 + B^-$					
(1) $A + e^- \rightleftharpoons A^-$	3	B	29.6	29.6	29.6
(2) $A^- + BH \rightleftharpoons AH^- + B^-$		U	29.6	0	29.6
(3) $AH^- + A \rightleftharpoons DH^-$	2	E	29.6	0	29.6
(4) $DH^- + e^- \rightleftharpoons DH^-$	2	E	29.6	29.6	0
(5) $DH^- + BH \rightleftharpoons DH_2 + B^-$					
(1) $A + e^- \rightleftharpoons A^-$	4	B	19.7	39.4	19.7
(2) $A^- + BH \rightleftharpoons AH^- + B^-$		U	19.7	19.7	19.7
(3) $AH^- + A \rightleftharpoons DH^-$	3	B	29.6	29.6	29.6
(4) $DH^- + A^- \rightleftharpoons DH^- + A$		U	29.6	0	29.6
(5) $DH^- + BH \rightleftharpoons DH_2 + B^-$	2	E	29.6	0	29.6
(iii) ion-substrate coupling					
(1) $A + e^- \rightleftharpoons A^-$					
(2) $A^- + e^- \rightleftharpoons A^{--}$	4	E	14.8	14.8	14.8
(3) $A^{--} + A \rightleftharpoons D^{--}$	3	E	14.8	14.8	0
(4) $D^{--} + BH \rightleftharpoons DH^- + B^-$					
(5) $DH^- + BH \rightleftharpoons DH_2 + B^-$					
(1) $A + e^- \rightleftharpoons A^-$	4	B	14.8	14.8	14.8
(2) $A^- + e^- \rightleftharpoons A^{--}$		U	14.8	0	14.8
(3) $A^{--} + BH \rightleftharpoons AH^- + B^-$	3	E	14.8	0	14.8
(4) $AH^- + A \rightarrow DH^-$					
(5) $DH^- + BH \rightarrow DH_2 + B^-$					
(1) $A + e^- \rightleftharpoons A^-$					
(2) $A^- + BH \rightleftharpoons B^- + AH^-$	4	B	14.8	14.8	29.6
(3) $AH^- + e^- \rightleftharpoons AH^-$		U	14.8	-14.8	29.6
(4) $AH^- + A \rightleftharpoons DH^-$	3	E	29.6	0	29.6
(5) $DH^- + BH \rightleftharpoons DH_2 + B^-$					

† Buffered (B); Unbuffered (U); Either (E)

All approaches to the investigation of complex mechanisms must be based on precise data obtained over a wide range of experimental conditions; thus, when possible, cyclic voltammograms should be recorded over several orders of magnitude of sweep rate and of concentration of both electroactive species and other possible participants in the overall chemical change. It is also frequently helpful to vary temperature and to estimate the energy of activation for the rate determining step (r.d.s.).

In situations where a single reaction pathway predominates, considerable progress towards identifying this pathway and the r.d.s. can be made by measuring the variation of peak potential with sweep rate and concentrations and comparing these values with those calculated for all likely mechanisms. This approach has been used by Saveant and coworkers, for example, for the study of hydrodimerisation [19-20],



and Table 6.8 lists their values of $\partial E_p / \partial \log v$, $\partial E_p / \partial \log c_A^\infty$ and $\partial E_p / \partial \log c_{BH}^\infty$ for the likely mechanisms. Thus if these quantities are determined experimentally, most mechanisms can be eliminated; the distinction between the few remaining mechanisms with the same values requires further analysis of the data, e.g. by investigation of the peak shape by convolution, see next section.

Parker and his colleagues have recommended a quite different approach based on reaction orders and activation energies. This method avoids the necessity to treat, in depth, many mechanisms, and has the merit of rapidly transforming the electrochemical results into a language readily understood by all chemists. In early studies [22, 23], the reaction orders were calculated from the shifts in E_p with potential scan rate and concentrations using the expressions

$$\frac{\partial E_p}{\partial \log v} = \frac{1}{b+1} \log \frac{RT}{nF} \quad (6.46)$$

$$\frac{\partial E_p}{\partial \log c_O} = \frac{a+b+x+i-l}{b+1} \log \frac{RT}{nF} \quad (6.47)$$

$$\frac{\partial E_p}{\partial \log c_X} = \frac{x}{b+1} \log \frac{RT}{nF} , \quad (6.48)$$

and hence it is possible to write a rate expression

$$\text{rate} = k_{\text{obs}} c_O^a c_R^b c_X^x c_I^l \quad (6.49)$$

where as usual O and R are the electroactive species and the intermediate formed in the initial electron transfer process respectively, X is any other added reactant (e.g. proton donor), and I is any species formed in the reaction sequence which influences the rate determining step (e.g. OH^-). The rate expression must then

be interpreted in terms of a reaction pathway and r.d.s.. Parker has also emphasised the value of measuring the activation energy and ensuring that it is consistent with the mechanism proposed [23, 24, 25].

Other groups [26, 27] have sought to confirm proposed mechanisms by examining the fit between the experimental I - E response and curves derived by digital simulations of the mechanism (see Appendix). In general, this approach may not provide a critical test of the mechanism, but in some cases where the cyclic voltammograms have unusual features, it can provide convincing evidence for the mechanism.

Saveant and coworkers [28–30] continue to prefer a rigorous mathematical analysis of the likely mechanisms leading to (a) kinetic zone diagrams which express the relationship between the reaction mechanism and both kinetic parameters and reaction conditions, e.g. concentrations. The diagrams also show the conditions where a change of mechanism is likely to occur; (b) dimensionless plots which if fitted over a wide enough range of experimental conditions, provide a convincing test of the mechanism. This approach also shows considerable promise for unravelling mechanisms with competitive pathways.

The recent literature contains many arguments over reaction mechanisms. In assessing these papers, it is important to recognise that electrochemists are now examining mechanisms in very fine detail and addressing questions not normally considered in homogeneous chemistry.

6.6.2 Techniques developed from cyclic voltammetry

In this section, we consider briefly some of the techniques which have been developed to overcome some of the limitations of cyclic voltammetry.

6.6.2.1 Cyclic voltammetry at microelectrodes

In this technique, the experiment is the same as in conventional cyclic voltammetry except that the working electrode is a microelectrode with a diameter 0.5–50 μm . Such low area electrodes have two key advantages for cyclic voltammetry [31]:

- the actual current passing through the cell is very low, maybe a few nA, and hence the problems of iR drop are greatly diminished;
- the double layer charging current decreases much more than the faradaic current, leading to significant improvement in the ratio of faradaic/non-faradaic current.

In consequence, although at conventional electrodes the limit for recording high quality cyclic voltammograms is about 100 V s^{-1} and above this sweep rate the curves become distorted by iR drop and the charging current, at microelectrodes it is possible to obtain good data above 10^4 V s^{-1} . This permits the study of systems with much faster chemical reactions [32, 33]. Moreover, at these high sweep rates, linear diffusion to the microelectrode still predominates (over the spherical component), and the theory needs no modification to that discussed above. (a) above also leads to the possibility of using cyclic voltammetry to study homogeneous chemical reactions in poorly conducting media [34–36], e.g. in benzene or acetonitrile without base electrolyte.

6.6.2.2 Derivative cyclic voltammetry

In derivative cyclic voltammetry [23, 37–39], the experimental I - E response is differentiated electronically, and the result is presented as a plot of dI/dE vs E . dI/dE crosses the E axis at the potential of the peak on the cyclic voltammogram and this potential can be measured with a much higher precision, maybe ± 0.1 mV. In addition the ratio of forward to reverse peaks on the dI/dE vs E curve can be measured accurately, in contrast to conventional cyclic voltammetry where uncertainty over the ‘base line’ always causes difficulty in the measurement of the reverse peak and hence I_p^A/I_p^C . Hence derivative cyclic voltammetry represents simply an improvement in presentation.

6.6.2.3 Ac cyclic voltammetry

In ac cyclic voltammetry, a small amplitude sine wave perturbation is superimposed upon the linear potential scan, and a phase sensitive detector is used to extract and display the in-phase current response as a function of potential. This technique [40–42] is discussed in more detail in Chapter 8, but it is worth noting here that it may have some advantage for the study of fast coupled chemical reactions. At the present stage it is, however, a technique for obtaining numerical parameters when the mechanism is known and there is little in the literature concerning its use as a tool to investigate complex mechanisms.

6.6.6.4 Convolution voltammetry

In all the techniques discussed until now, the interpretation of the mechanism and the estimation of kinetic parameters is based on the analysis of peak currents and peak potentials and their variation with scan rate and concentrations. Such approaches discard much of the information contained within the voltammogram, in particular the shape of the peak.

An alternative approach, which has become possible with the increased availability of cheap mini-and micro-computers capable of rapid data acquisition and treatment, is to transform the whole curve prior to analysis. One such transform that has proved very successful is the convolution [43–46] or semi-integration transform [47].

For any transient electrochemical technique under conditions of semi-infinite linear diffusion, it can be shown that solution of the diffusion equations, when only O is initially present, yields, irrespective of the reaction mechanism, the following expression for the time dependent surface concentration of O.

$$c_O^g(t) = c_O^\infty - \frac{1}{nFAD^{1/2}} \left[\frac{1}{\pi^{1/2}} \int_0^t \frac{i(u)}{(t-u)^{1/2}} du \right]. \quad (6.50)$$

The term inside the square brackets is the convolution transform of the $i(t)$ data which we will denote as $F(t)$ ($I(t)$ is frequently used but tends to be confused with current density), and therefore Equation (6.50) can be rewritten as

$$c_O^g(t) = c_O^\infty - \frac{F(t)}{nFAD^{1/2}} \quad (6.51)$$

where

$$F(t) = \frac{1}{\pi^{1/2}} \int_0^t \frac{i(u)}{(t-u)^{1/2}} du . \quad (6.52)$$

Under purely diffusion controlled conditions, we know that $c_O^g(t)$ is zero, and therefore from Equation (6.51) it can be seen that $F(t)$ reaches a limiting value, F_∞ , given by

$$F_\infty = nFAD^{1/2}c_O^\infty , \quad (6.53)$$

and thus from Equations (6.51) and (6.53)

$$c_O^g(t) = \frac{F_\infty - F(t)}{nFAD^{1/2}} . \quad (6.54)$$

For a simple charge transfer reaction where O is reduced to R without any complications it follows that

$$c_R^g(t) = \frac{F(t)}{nFAD^{1/2}} , \quad (6.55)$$

and therefore for a Nernstian system

$$E = E_{1/2} + \frac{RT}{nF} \ln \frac{F_\infty - F(t)}{F(t)} . \quad (6.56)$$

Equation (6.56) is identical in form to those describing steady state voltammograms at stationary or rotating electrodes, and thus a convolution voltammogram where $F(t)$ is plotted as a function of E has the same appearance as these steady state plots.

The convolution transformation described by Equation (6.50) is readily performed on a small computer using numerical techniques, and Fig. 6.26 shows a typical cyclic voltammogram for a reversible system and the corresponding convolution voltammogram. It can be seen immediately that the convolution voltammogram retraces itself on the back sweep, and this is one test of a reversible process, the other being that a plot of the left-hand side of Equation (6.56) varies linearly with E .

For non-reversible processes and those involving coupled chemical reactions Equation (6.56) will no longer hold; however, Saveant and coworkers [43-46] have derived similar linear plots of logarithmic functions of $F(t)$ as a function of E to enable kinetic parameters to be determined. Some examples of these functions are given in Table 6.9; others can be found in the literature. One important feature of all these functions is that they are independent of sweep rate, and therefore plots at various values of v ought to superimpose. This is a very useful test of whether the correct mechanism has been chosen.

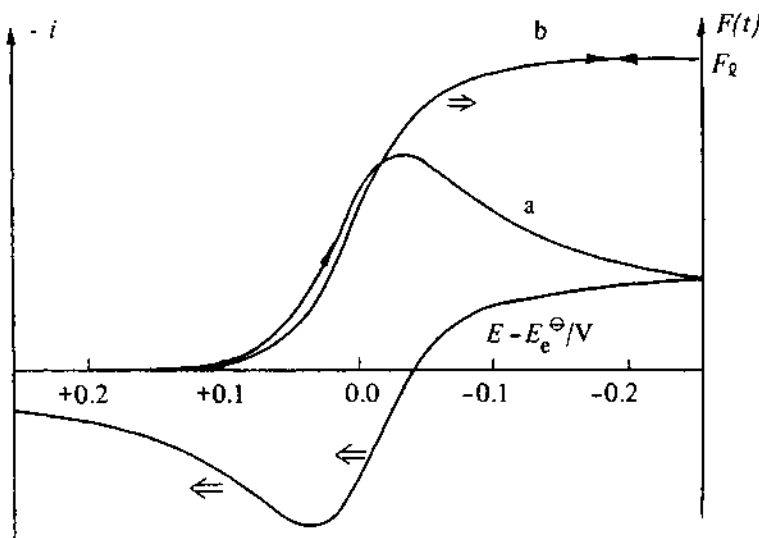


Fig. 6.26 – (a) Cyclic voltammogram and (b) convolution voltammogram for a reversible one electron transfer process.

Table 6.9 – Logarithmic functions for convolution voltammetry

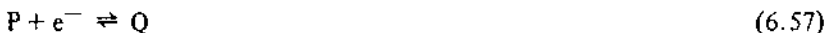
Mechanism	Function
Reversible	$E = E_e^\ominus + \frac{RT}{nF} \ln \frac{F_\text{Q} - F(t)}{F(t)}$
Irreversible	$E = \frac{RT}{\alpha_C nF} \ln \frac{k^\ominus}{D^{1/2}} + \frac{RT}{\alpha_C nF} \ln \frac{F_\text{Q} - F(t)}{F(t)}$
Quasi-reversible	$E = \frac{RT}{\alpha_C nF} \ln \frac{k^\ominus}{D^{1/2}} + \frac{RT}{\alpha_C nF} \ln \frac{F_\text{Q} - F(t) - F(t) \exp(nF/RT)(E - E_{1/2})}{i(t)}$
CE	$E = E_e^\ominus - \frac{RT}{2nF} \ln k_{-1} + \frac{RT}{nF} \ln \frac{F_\text{Q} - F(t)}{F_\text{Q}}$
EC	$E = E_e^\ominus + \frac{RT}{2nF} \ln k + \frac{RT}{nF} \ln \frac{F_\text{Q} - F(t)}{F_\text{Q}}$
ECE	$E = E_e^\ominus + \frac{RT}{2nF} \ln \frac{(k_1 + k_{-1})}{(1 + K)^2} + \frac{RT}{nF} \ln \frac{F_\text{Q} - F(t)}{i(t)}$
DISP 1	$E = E_e^\ominus + \frac{RT}{2nF} \ln \frac{(k_1 + k_{-1})}{2(1 + K)} + \frac{RT}{nF} \ln \frac{F_\text{Q} - F(t)}{i(t)}$

A further advantage of the convolution method is that iR_u drop is very easily accounted for. In the case of conventional cyclic voltammetry, the non-linearity of the sweep makes data analysis difficult; however, in convolution voltammetry all that is necessary is to replace E by $E + iR_u$ when plotting the voltammogram [43].

6.6.2.5 Homogeneous redox catalysis

During the period 1978–80, Saveant's group published a series of papers [48–51] in which they describe a new type of experiment which allows both the study of reaction mechanisms and the determination of kinetic parameters for reactions involving intermediates with a half life down to 1 ns (cf 0.1 ms for conventional cyclic voltammetry); it is also possible to measure standard potentials for processes which by other electrochemical techniques appear totally irreversible. The papers develop the theory, present the essential working curves, and illustrate the application of the method; more recently, many other groups are using the method. Surprisingly, the method, known as *redox catalysis*, requires only slow scan cyclic voltammetry (or polarography or RDE studies), and hence experimentally is very straightforward.

The experiment involves recording the cyclic voltammograms for the redox catalyst couple P/Q in the absence and presence of the substrate, A, whose reduction leads to the reactive intermediate of interest, B, by a single electron transfer, i.e.



The method is usually applied to systems where the cyclic voltammetry of A shows a totally irreversible peak either because the electron transfer is slow



or because B is totally unstable



two situations which lead to different peak widths and $\partial E_p / \partial \log v$, see earlier.

Now in redox catalysis, the information about Reactions (6.58) and/or (6.59) is obtained by measuring the ratio of peak currents i_p/i_p^d (or, in principle, the shift of E_p for the P/Q couple) as a function of (i) the concentration of P,

c_P^∞ , (ii) the excess factor, $\gamma = c_A^\infty/c_P^\infty$, and (iii) the potential scan rate. i_P^d is the peak current for a solution of P alone, and i_P that for the reduction of P in the presence of A at the same scan rate.

The redox catalyst (commonly an aromatic hydrocarbon) is chosen so that (i) P and Q are stable in the medium in the absence of A, (ii) Reaction (6.57) is always in equilibrium (the standard rate constant for the P/Q couple should be large), (iii) $E_{P/Q}^\Theta - E_{A/B}^\Theta$ has an appropriate value.

The measured catalytic current for the reduction of P in the presence of A can be determined by three different situations depending on the relative kinetics of Reactions (6.58) and (6.59).

(a) *Case 1:* When Reaction (6.59) is much faster than the reverse of (6.58). Then all of B will disappear by Reaction (6.59) and the catalytic current will depend solely on the rate of Reaction (6.58). This situation is analogous to the direct electrode Reaction (6.60). Here k_1 may be determined from i_P/i_P^d .

(b) *Case 2:* When Reaction (6.59) is slow compared to the reverse of Reaction (6.58).

Now Reaction (6.58) may be treated as an equilibrium and the catalytic current is determined both by the position of equilibrium, i.e. $E_{P/Q}^\Theta - E_{A/B}^\Theta$, and the rate of Reaction (6.59). Then i_P/i_P^d is a function of kk_1/k_2 . This case is analogous to the direct electrode Reaction (6.61) + (6.62).

(c) *Case 3:* When Reaction (6.59) and the reverse of Reaction (6.58) have approximately the same rate.

This situation is the most complex and progress can only be made if k or k_1/k_2 are independently known.

Note that the rds in the sequence (6.57)-(6.59) depends on the relative rates of two steps. This is also the case in the direct electrode reaction. Thus, for example, the electron transfer step will appear irreversible either if it is slow or if the following chemical reaction is very fast.

Table 6.10 – Tests to confirm that the kinetics of the system are appropriate to Case 1

-
1. $i_P/\gamma i_P^d$ increases with increasing c_P^∞ and c_A^∞
 2. k_1 as estimated from dimensionless plots is independent of γ, v and c_P^∞
-

Table 6.11 – Tests to confirm that the kinetics of the system are appropriate to Case 2

-
1. $i_P/\gamma i_P^d$ increases with c_A^∞ but is independent of c_P^∞
 2. kk_1/k_2 as estimated from dimensionless plots is independent of γ, v and c_P^∞
-

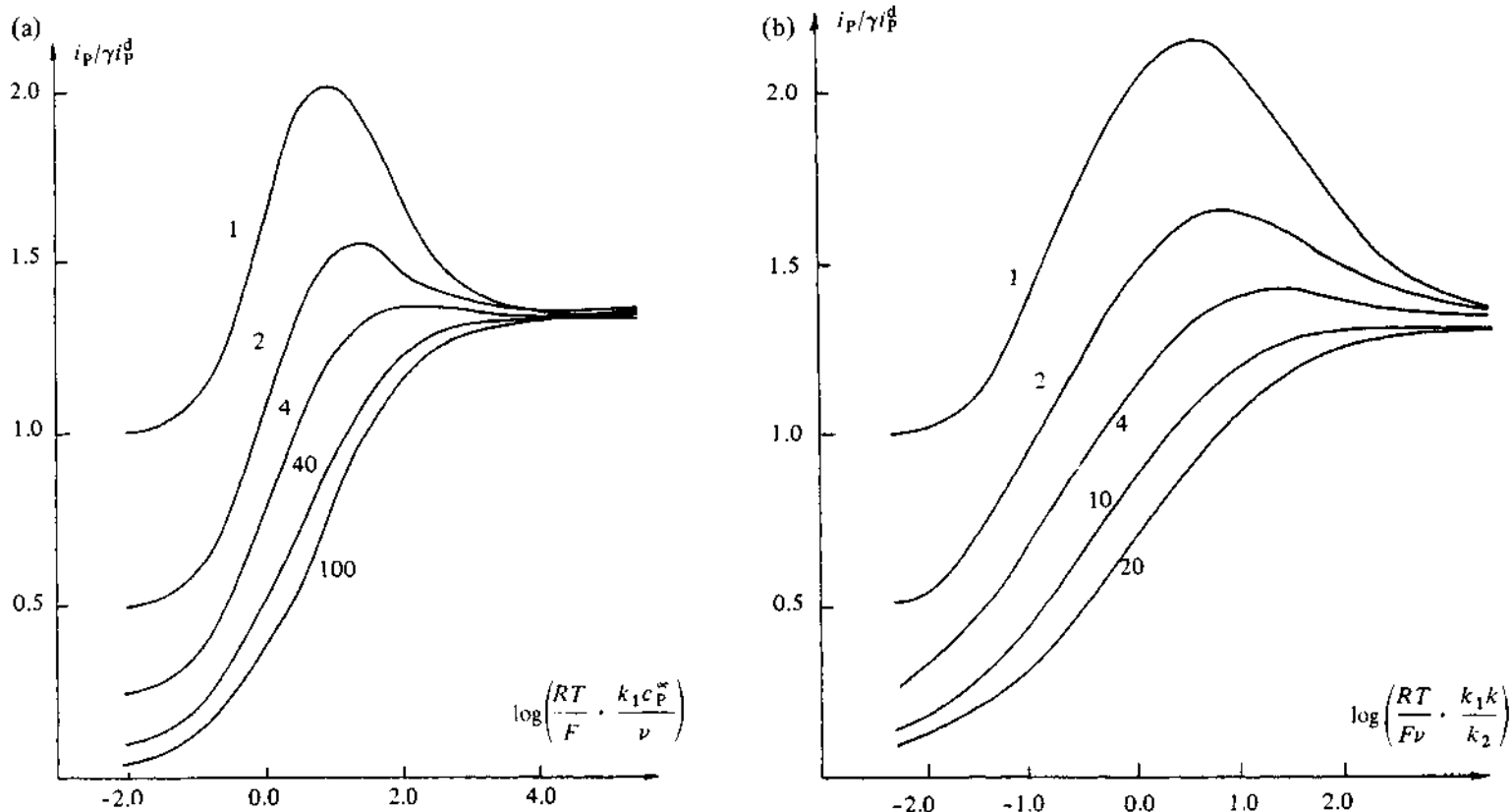


Fig. 6.27 – Dimensionless plots for determining rate constants from redox catalysis experiments (a) Case 1 systems where k_1 may be determined, (b) Case 2 systems where k may be estimated. The numbers on the curves indicated the excess factor $\gamma = c_A^x/c_P^o$. The figure is drawn from tables supplied by J. M. Saveant.

Distinction between the limiting Cases 1 and 2 may be made on the basis of the tests in Table 6.10 and 6.11. In each case, test 1 is a straightforward analysis of the experimental data, but test 2 requires the use of dimensionless plots such as those shown in Fig. (6.27).

If a system shows Case 1 behaviour, then it is only possible to calculate a rate constant for the solution electron transfer. If, however, data are recorded for several catalyst couples, a plot of $\log k_1$ vs $E_{P/Q}^\ominus$ can lead to the standard potential for the A/B couple. Indeed this method was used to determine standard potentials for the $1e^-$ reduction of a series of aryl halides [50].

Case 2 is the one of interest for the determination of the half life of an unstable intermediate. The redox catalysis experiments illustrated by the data of Fig. 6.28, lead only to a value of kk_1/k_2 . Fortunately k can be extracted by several procedures, the simplest by combining the redox catalysis data with data from cyclic voltammograms for the direct reduction of A.

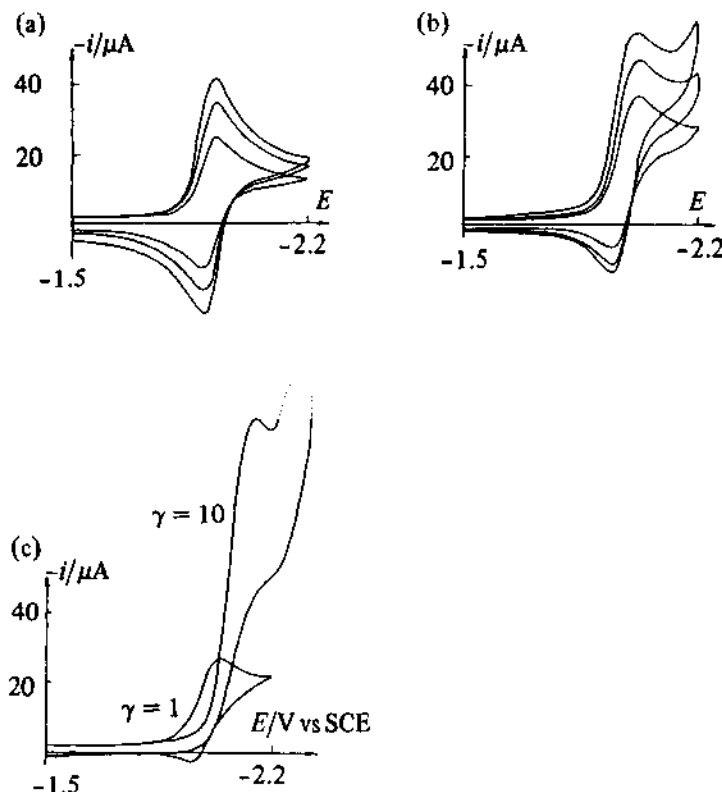


Fig. 6.28 — Cyclic voltammograms in $\text{DMF}/\text{Bu}_4\text{NBF}_4$ (0.1 mol dm^{-3}) (a) anthracene (2 mmol dm^{-3}) at sweep rates of $0.1, 0.2$ and 0.3 Vs^{-1} , (b) as (a) but solution also contains $p\text{-CH}_3\text{C}_6\text{H}_4\text{SO}_2\text{OCH}_3$ (2 mmol dm^{-3}), (c) anthracene (2 mmol dm^{-3}) in the presence of $p\text{-CH}_3\text{C}_6\text{H}_4\text{SO}_2\text{OCH}_3$ for the two values of γ shown; potential scan rate 0.05 Vs^{-1} .

So far we have only discussed systems where the reduction of A is a 1e reduction. This is, of course, unusual, and it is common for the product from the decomposition of B to be further reducible. It has been shown that such mechanisms may be handled by the expedient of calculating $i_p/2\gamma i_p^D$ (instead of $i_p/\gamma i_p^D$) and using the working curve for 2γ .

6.7 EXPERIMENTAL PROBLEMS ASSOCIATED WITH LINEAR SWEEP AND CYCLIC VOLTAMMETRY

6.7.1 Double layer charging effects

As with all transient techniques there is, in addition to the faradaic current which has already been discussed, also a double layer charging current contribution as given by Equation (6.63):

$$I_{dl} = C_{dl}v \quad (6.63)$$

where

$$I_{total} = I_{faradaic} + I_{dl} . \quad (6.64)$$

It can be seen immediately that whilst $I_{faradaic}$ is proportional to $v^{1/2}$, the charging current is proportional to v . Typical values for C_{dl} lie between 20 and $40\mu\text{F cm}^{-2}$, therefore, at 100mVs^{-1} , I_{dl} will be between 2 and $4\mu\text{A cm}^{-2}$ and will usually be small compared to the faradaic current. At 100Vs^{-1} , however, the values becomes 2 to 4 mA cm^{-2} and is no longer negligible. Thus the double layer charging current distorts cyclic voltammograms recorded at high sweep rates, and the effect is worse if C_{dl} varies (as it frequently will) over the potential range of interest. It is this effect which imposes one of the major limitations on the maximum value of sweep rate that may be used successfully.

To some extent the influence of double layer charging currents may be reduced by subtracting from the $I-E$ curve for the test solution, the $I-E$ curve for the electrolyte solution in the absence of the electroactive species. This technique assumes that the double layer capacitance/potential curve is unchanged by the presence of electroactive species. A better approach may be to use a microelectrode. With solid electrodes, changes in oxidation state of the surface lead to similar distortions of the $I-E$ response and then the problem is even more difficult as the surface film may effect the rate of other electron transfer processes.

6.7.2 iR_u drop

The problem of iR_u drop is discussed in detail in Chapter 11, and has also been discussed in a recent review [22]. However, it is worth briefly mentioning how it manifests itself in a cyclic or linear sweep voltammetry experiment. As a result of iR_u drop the applied voltage is changed from the desired value, E , to $E - iR_u$, and since i varies during a scan the sweep is no longer linear. This has the effect of decreasing peak heights and increasing peak separations. Since the behaviour is so similar to that expected for a slow electron transfer step, an iR_u drop

problem is often mistaken for this. Great care must therefore be taken to ensure iR_u drop is not affecting the system under study before proceeding to analyse the results. This is, of course, particularly the case when interpretation of the data depends on measurement of shifts in peak potentials and/or the experiments involve large currents, i.e. high concentrations and/or high sweep rates.

The best way to check that the experimental response is free from the influences of iR_u drop is to run a voltammogram for a couple known to behave reversibly, e.g. $\text{Cp}_2\text{Fe}/\text{Cp}_2\text{Fe}^+$, and check that under the experimental conditions (including cell, solvent, electrolyte, concentration of electroactive species, potential scan rate) it has the expected response.

REFERENCES

- [1] J. E. B. Randles, *Trans. Faraday Soc.*, **44** (1948) 327.
- [2] A. Sevcík, *Coll. Czech. Chem. Comm.*, **13** (1958) 349.
- [3] R. S. Nicholson & I. Shain, *Anal. Chem.*, **36** (1964) 706.
- [4] R. S. Nicholson, *Anal. Chem.*, **37** (1965) 1351.
- [5] H. Matsuda & Y. Ayabe, *Z. Electrochem.*, **59** (1955) 494.
- [6] J. M. Saveant & E. Vianello, *Electrochim. Acta*, **8** (1963) 905, **12** (1967) 629 and **12** (1967) 1545.
- [7] L. Nadjo & J. M. Saveant, *J. Electroanal. Chem.*, **48** (1973) 113.
- [8] J. M. Saveant & E. Vianello, *Electrochim. Acta*, **10** (1973) 905.
- [9] R. S. Nicholson & I. Shain, *Anal. Chem.*, **37** (1965) 178 and 190.
- [10] J. M. Saveant, *Electrochim. Acta*, **12** (1967) 753.
- [11] M. Mastragostino, L. Nadjo, & J. M. Saveant, *Electrochim. Acta*, **13** (1968) 721.
- [12] E. Laviron, *J. Electroanal. Chem.*, **52** (1974) 355, 395.
- [13] S. Srinivasan & E. Gileadi, *Electrochim. Acta*, **11** (1966) 321.
- [14] A. P. Brown & F. C. Anson, *Anal. Chem.*, **49** (1977) 1589.
- [15] D. E. Bartak, K. J. Houser, B. C. Ruby, & M. D. Hawley, *J. Am. Chem. Soc.*, **94** (1972) 7526.
- [16] A. J. Bard, U. J. Puglisi, J. V. Kenkel & A. Lomax, *Disc. Faraday Soc.*, **56** (1973) 353.
- [17] D. Pletcher & N. Stradiotto, *J. Electroanal. Chem.*, **186** (1985) 211.
- [18] R. H. Wopschall & I. Shain, *Anal. Chem.*, **39** (1967) 1514, 1527, 1535.
- [19] E. Lamy, L. Nadjo, & J. M. Saveant, *J. Electroanal. Chem.*, **42** (1973) 189.
- [20] E. Lamy, L. Nadjo, & J. M. Saveant, *J. Electroanal. Chem.*, **50** (1974) 141.
- [21] L. Nadjo & J. M. Saveant, *J. Electroanal. Chem.*, **44** (1973) 169.
- [22] O. Hammerich, B. Svensmark, & V. D. Parker in *Organic electrochemistry*, (Eds) M. M. Baizer & H. Lund, Marcel Dekker, 1983.
- [23] V. D. Parker, *Electroanal. Chem.*, **14** (1986), 1.
- [24] V. D. Parker, *Acta Chem. Scand. B*, **35** (1981) 51.
- [25] B. Aalstad, A. Ronlan, & V. D. Parker, *Acta Chem. Scand. B*, **36** (1982) 199.
- [26] S. W. Feldberg & L. Jeftic, *J. Phys. Chem.*, **76** (1972) 2439.
- [27] T. Matsue & D. H. Evans, *J. Electroanal. Chem.*, **168** (1984) 287.

- [28] C. Amatore, F. M'Halla, & J. M. Saveant, *J. Electroanal. Chem.*, **123** (1981) 219.
- [29] C. Amatore & J. M. Saveant, *J. Electroanal. Chem.*, **144** (1983) 59.
- [30] C. Amatore, M. Gareil, & J. M. Saveant, *J. Electroanal. Chem.*, **147** (1983) 1.
- [31] M. Wightman, *Anal. Chem.*, **53** (1981) 1125A.
- [32] J. O. Howell & R. M. Wightman, *Anal. Chem.*, **56** (1984) 524.
- [33] J. O. Howell, J. M. Goncalves, C. Amatore, L. Klasinc, R. M. Wightman, & J. K. Kochi, *J. Am. Chem. Soc.*, **106** (1984) 3968.
- [34] A. M. Bond, M. Fleischmann, & J. Robinson, *J. Electroanal. Chem.*, **168** (1984) 299.
- [35] A. M. Bond, M. Fleischmann, & J. Robinson, *J. Electroanal. Chem.*, **172** (1984) 11.
- [36] R. A. Lines & V. D. Parker, *Acta Chem. Scand. B* **31** (1977) 369.
- [37] E. Ahlberg & V. D. Parker, *J. Electroanal. Chem.*, **121** (1981) 57.
- [38] E. Ahlberg & V. D. Parker, *J. Electroanal. Chem.*, **121** (1981) 73.
- [39] V. D. Parker, *Acta Chem. Scand. B* **35**, (1981) 373.
- [40] A. M. Bond, R. J. Halloran, I. Ruzic, & D. E. Smith, *Anal. Chem.*, **48** (1976) 872.
- [41] A. M. Bond, R. J. Halloran, I. Ruzic, & D. E. Smith, *Anal. Chem.*, **50** (1978) 216.
- [42] A. J. Bard & L. R. Faulkner, *Electrochemical methods*, Wiley 1980.
- [43] J. C. Imbeaux & J. M. Saveant, *J. Electroanal. Chem.*, **44** (1973) 169.
- [44] F. Ammar & J. M. Saveant, *J. Electroanal. Chem.*, **47** (1973) 215.
- [45] L. Nadjo, J. M. Saveant, & D. Tessier, *J. Electroanal. Chem.*, **52** (1974) 403.
- [46] J. M. Saveant & D. Tessier, *J. Electroanal. Chem.*, **61** (1975) 251 and **65** (1975) 57.
- [47] K. B. Oldham, *Anal. Chem.*, **44** (1972) 196.
- [48] C. P. Andrieux, J. M. Dumas-Bouchiat, & J. M. Saveant, *J. Electroanal. Chem.*, **87** (1978) 39; **87** (1978) 55; **88** (1978) 43 and **113** (1980) 1.
- [49] C. P. Andrieux, J. M. Dumas-Bouchiat, F. M'Halla, & J. M. Saveant, *J. Electroanal. Chem.*, **113** (1980) 19.
- [50] C. P. Andrieux, C. Blocman, J. M. Dumas-Bouchiat, & J. M. Saveant, *J. Am. Chem. Soc.*, **101** (1979) 3431.
- [51] C. P. Andrieux, C. Blocman, J. M. Dumas-Bouchiat, F. M'Halla & J. M. Saveant, *J. Am. Chem. Soc.*, **102** (1980) 3806.
- [52] J. M. Saveant & K. B. Su, *J. Electroanal. Chem.*, **171** (1984) 341.

Further reading

- (1) R. N. Adams, *Electrochemistry at solid electrodes*, Marcel Dekker, 1969.
- (2) Chapters VI and VII in *Physical methods of chemistry - Part IIa electrochemical methods*, (Eds) A. Weissberger & B. W. Rossiter, Interscience, 1971.
- (3) A. J. Bard & L. R. Faulkner, *Electrochemical methods*, John Wiley and Sons, 1980.
- (4) D. D. MacDonald, *Transient techniques in electrochemistry*, Plenum Press, 1977.

- (5) O. Hammerich, B. Svensmark, & V. D. Parker in *Organic electrochemistry*, (Eds) M. M. Baizer and H. Lund, Marcel Dekker, 1983.
- (6) *Laboratory techniques in electroanalytical chemistry*, Eds. P. T. Kissinger & W. R. Heineman, Marcel Dekker, 1984.

7

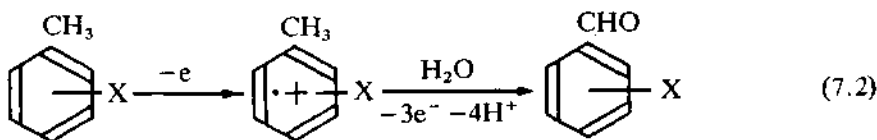
Electrocatalysis

Many chemical reactions, although thermodynamically very favourable, do not by themselves occur at a significant rate. For such reactions to be useful, it is necessary to find a homogeneous or heterogeneous catalyst which will increase the rate of reaction, maybe by several orders of magnitude. Likewise, in the absence of a catalyst, many electrode reactions occur, if at all, only at very high overpotentials because of poor kinetics, i.e. such electrode reactions have a low exchange current density. The objective of electrocatalysis is therefore to seek to provide alternative, lower energy of activation pathways and hence to permit such electrode reactions to occur at high current density close to the equilibrium potential. Electrocatalysis is important to many applications of electrochemistry since the energy efficiency of any cell is determined, in part, by the overpotentials necessary at the anode and cathode. In fact, the overpotential at each electrode will, for each current density, be given by the Tafel equation (written for an oxidation)

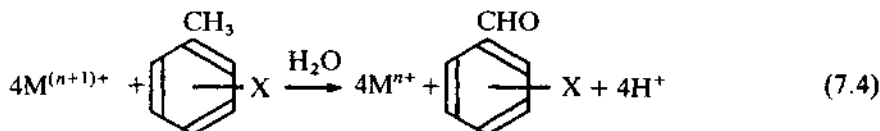
$$\eta = \frac{2.3RT}{\alpha_A nF} [\log I - \log I_0] , \quad (7.1)$$

and it should be noted that the overpotential required depends on both the exchange current density and the Tafel slope.

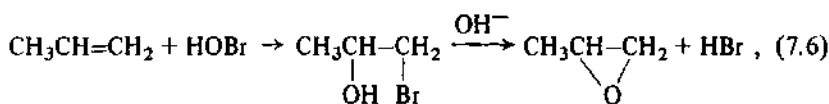
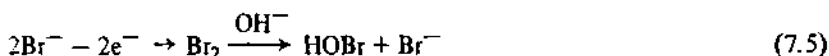
The catalysis of electrode reactions is possible both by species attached to the electrode surface and by species dissolved in the electrolyte. Examples of the latter include the oxidation of toluenes to benzaldehydes and of propylene to propylene oxide. In aqueous solution, the removal of an electron from toluenes



is found to occur only at low rates at high overpotentials; the addition of some metal ions, M^{n+} (e.g. Ag^+ , Ce^{3+} , Mn^{2+} , Co^{2+}) to the solution allows the reaction scheme



and hence the reaction occurs at the potential of the $M^{n+}/M^{(n+1)+}$ couple. The oxidation of propylene to propylene oxide is probably unknown as a direct electrode reaction, but in the presence of bromide ion in slightly alkaline solution, say pH 9, the conversion is possible in high yield by the route



and the process occurs at the potential of the Br^-/Br_2 couple.

The term *electrocatalysis* is, however, more commonly applied to systems where the oxidation or reduction requires bond formation, or at least a strong interaction of the reactant, intermediates, or the product with the electrode surface. The catalyst is the electrode material itself or a species adsorbed from solution. This chapter will discuss this more limited definition of electrocatalysis (note also that simple electron transfer reactions which are pictured as occurring by an outer sphere mechanism and may have very high exchange current densities, are not normally considered within electrocatalysis – in this book they are dealt with in Chapter 3).

7.1 ELECTRODE REACTIONS INVOLVING ADSORBED INTERMEDIATES

A number of reactions of this type, for example hydrogen evolution, oxygen reduction and evolution, chlorine formation, and methanol oxidation, are of great importance in applied electrochemistry. Indeed, a major achievement of electrocatalysis was the development of DSA electrodes (dimensionally stable anodes) for chlorine manufacture. The catalyst is a ruthenium dioxide coating on a titanium substrate (the coating sometimes also contains other species e.g. TiO_2 , Pt metals), and these anodes can maintain very high current densities, $0.1\text{--}1.0 \text{ A cm}^{-2}$, at an overpotential of only $30\text{--}70 \text{ mV}$. This is in contrast with the 500 mV overpotential essential with the previously used graphite anodes. On the other hand, the failure to develop electrocatalysts for the oxidation of primary fuels (e.g. hydrocarbons, alcohols, and carbon monoxide) and for the reduction of oxygen has slowed down the development of fuel cells.

How may electrode reactions which involve surface chemistry be recognised in the laboratory? Most obviously, the I - E characteristics will depend very strongly on the choice of electrode material, and with some electrodes, at least, the reaction will occur up to several volts away from the reversible potential. More detailed analysis of the I - E data will reveal that:

- (i) the exchange current densities will vary with electrode material. For example the I_0 values for H_2 evolution in 1 mol dm^{-3} acid range from 10^{-12} to $10^{-3} \text{ A cm}^{-2}$, see Table 7.1;
- (ii) the Tafel slope is commonly not $\beta = \alpha nF/2.3RT$ or $(120 \text{ mV})^{-1}$ for a reaction where $\alpha = 0.5$, $n = 1$. Values of $\beta/2$, $\beta/3$, and $\beta/4$ are common, and the Tafel slope may also depend on electrode material, indicating a change in reaction mechanism. The Tafel slopes which are β/m may be interpreted in terms of mechanism, as will be discussed below.
- (iii) the temperature dependence of the Tafel slope may not be straightforward. This was first noted by Conway *et al.* [1, 2] for the hydrogen evolution reaction in methanol, and has also been found by Yeager [3] for oxygen reduction in phosphoric acid.

In electrocatalytic processes where the rate determining step is a surface reaction, the measured current density (in terms of the geometric area of the electrode) depends on both the genuine catalytic activity of the surface and also the real surface area, i.e. the roughness of the surface. This is in contrast to a mass transport controlled reaction where the current is independent of the surface roughness provided that the rugosity is small compared to the diffusion layer thickness, ca. 10^{-2} cm . Hence clearly in catalytic electrode design the surface should be as rough as possible to give the highest apparent current density. On the other hand, in the laboratory, a knowledge of the roughness and, hence, real surface area is essential to the interpretation of data at catalytic surfaces. Another recent observation is that Tafel slopes can vary with surface roughness and, for example, the success of NiMo coatings on steel as catalysts for hydrogen evolution in concentrated caustic soda has been attributed, at least in part, to the resulting steepness of the log I - E plots [4].

The selection of electrocatalysts for a particular reaction remains largely an empirical process, and catalyst design is still very much a goal for the future. Electrocatalysts are almost always transition metal species, and analogies with homogeneous as well as gas phase heterogeneous catalysis are to be expected. Certainly our knowledge of the factors which determine the activity of electrocatalysts lags behind that available in homogenous catalysis where, for example, Meyer [5] has been able to discuss the choice of ligands and oxidation state to permit $\text{Ru}(\text{bipy})_n$ complexes to carry out $1e^-$ oxidation, $2e^-$ oxidation, hydride or oxygen atom transfer. So far in electrocatalysis, it has only been possible to consider qualitatively the importance of the oxidation state of the metals, the spacing of catalyst centres, and electronic factors due to the surrounding metal atoms, lattice (e.g. oxide or sulphide), or ligands.

It is, however, possible to identify several types of electrocatalysts, for example

- (i) single metals, e.g. Pt, Ni, Pd;
- (ii) two component catalysts, e.g. PtSn for CO or CH_3OH oxidation [6], where the two metals are present to perform different roles, the Pt to catalyse the adsorption of the CO or fragments of CH_3OH and the Sn to allow ready formation of oxide to complete the oxidation of the organic fragments;
- (iii) transition metal compounds or complexes and some alloys where it may be envisaged that the role of other components is only to modify the environment of the main catalytic atoms.

But a detailed examination of each reveals many unanswered questions. In the simplest class, the single metals, it is commonly desirable to deposit them on a cheaper substrate, and then one would like to know the effect on the activity of the choice of substrate and the form of the deposit (the shape and size or the catalyst centres or the thickness of the deposit). Certainly such effects are to be observed as illustrated by studies of Pt deposited on Au and C [7] and of Ru on Hg and C [8, 9]. In addition, the reasons why a particular metal is the best catalyst for a reaction are not fully resolved, while the role of special lattice sites and the possibilities for selective poisoning [10, 11, 12] are other interesting questions. Further studies are clearly required, and many insights will come from investigations using single crystals. It is already clear that the catalytic activity of the single crystal faces of Pt for H_2 adsorption [13, 14, 15] and formic acid oxidation [16] are quite different, and inevitably the activity of polycrystalline Pt is a weighted average of these. It should also be noted that the organisation of electrocatalytic reactions on a molecular level also needs to be understood. The oxidation of a monolayer of carbon monoxide on Pt [17] and of formic acid on Pt/Pb surfaces [18] are two systems which have been examined with this question in mind.

It is clear that electrocatalytic reactions are complex, and their study will require the use of the widest possible range of techniques. The best electrochemical approach, however, is often the measurement of steady state currents as a function of potential (note the current is generally well below that where mass transport limitations are important) and comparison of the experimental

Tafel slopes with those calculated for all feasible mechanisms. Additional information comes from cyclic voltammetry, potential step techniques, and capacitance measurements, while several *in situ* and *ex situ* spectroscopic techniques are beginning to give a detailed insight into the electrode-solution interface during electrocatalytic reactions [19] (see also Chapter 10).

In this chapter we shall illustrate the above discussion by dealing with the H₂ evolution reaction in some detail, and then consider some general principles of catalyst design and other reactions more briefly.

7.2 THE HYDROGEN EVOLUTION REACTION

The hydrogen evolution reaction is historically very important. It has been widely studied using both a broad range of solution conditions and electrode materials, and these investigations have contributed much towards our understanding of electrode reactions. It is also of importance in technology since it is the cathode reaction in water electrolysis and some chlor-alkali cells, a competing reaction in many metal deposition reactions and organic reductions, and it is also one of the reactions in corrosion. Moreover, the reaction is interesting in that it occurs at widely differing rates on different metals, see Table 7.1.

Table 7.1

Metal	$-\log (I_o/\text{A cm}^{-2})$	Metal	$-\log (I_o/\text{A cm}^{-2})$
Ag	5.4	Ni	5.2
Au	5.5	Pb	12.2
Cd	11.0	Pd	2.3
Co	5.2	Pt	3.6
Cr	7.4	Rh	2.8
Cu	6.7	Ru	2.1
Fe	6.0	W	7.0
Hg	12.5	Zn	10.5

Exchange current densities for the hydrogen evolution reaction in 1 mol dm⁻³ H₂SO₄.

In acid solution, the overall reaction is



and in neutral and basic media



This discussion will assume an acidic medium, although the modifications to include higher pH are obvious. The adsorbed hydrogen atom, formed by the reaction

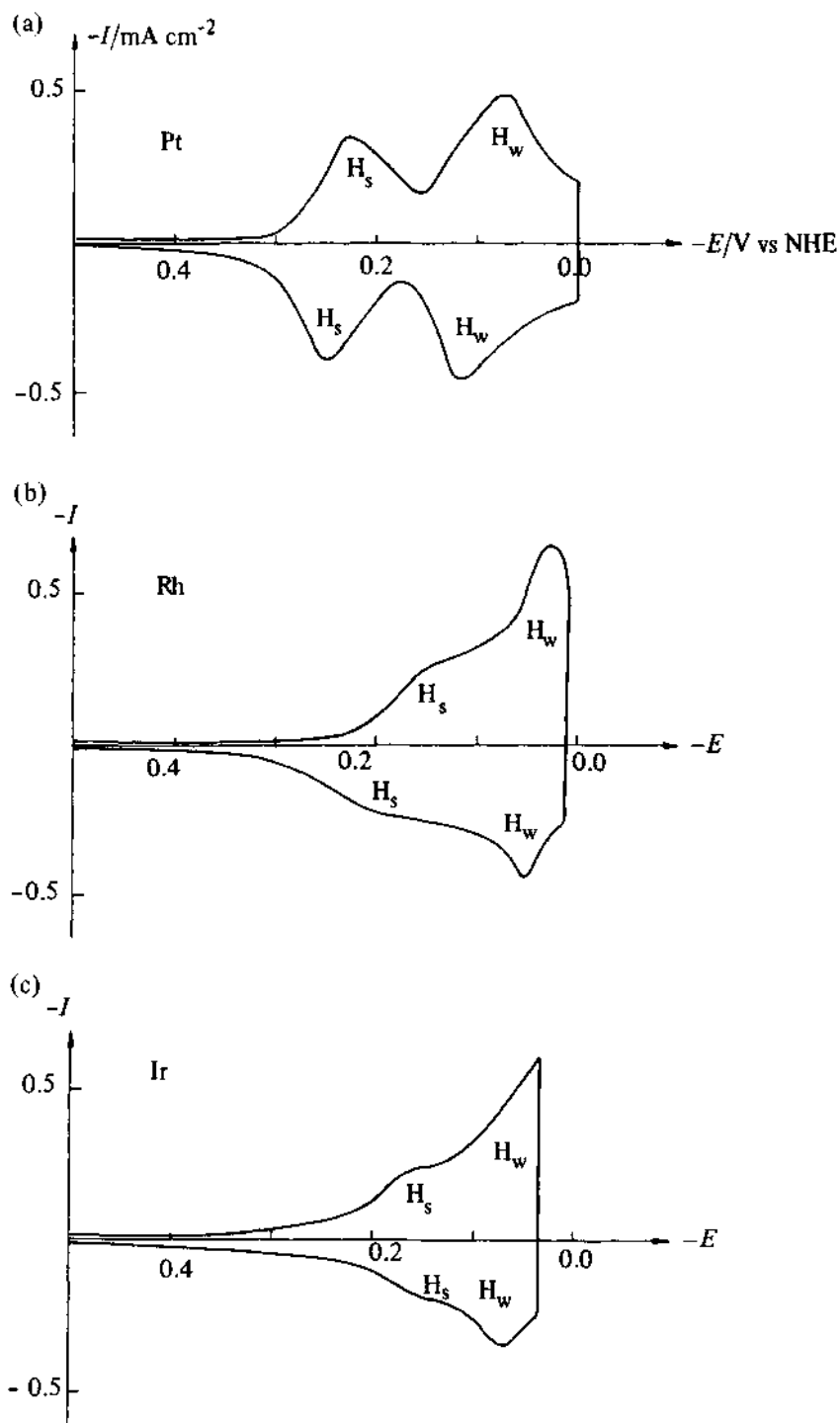


Fig. 7.1 – Cyclic voltammograms of (a) Pt, (b) Rh, and (c) Ir run at 0.1 V s^{-1} in H_2SO_4 (1 mol dm^{-3}) to show the hydrogen adsorption and desorption regions.



plays a key role in the mechanism and kinetics of the hydrogen evolution reaction, changing both its thermodynamics and kinetics. Firstly, the formation of an adsorbed species changes the free energy of the electron transfer step by an amount equal to the free energy of formation of the bond between the hydrogen atom and the surface. As a result, Reaction (7.9) can occur at a potential that is $-\Delta G_{\text{ADS}}^\ominus/F$, positive of the equilibrium potential for Reaction (7.7); hence the stronger the M-H bond, the larger is this shift in the reversible potential. Indeed, the adsorption of hydrogen on many metals can be clearly detected using cyclic voltammetry. Fig. 7.1 shows cyclic voltammograms for several metals in acid solution, and 'adsorption peaks' (see Chapter 6) are to be seen at potentials just positive to those where hydrogen gas is evolved. The 'desorption peaks' are present on the reverse scan. Adsorption and desorption peaks are characterised, particularly at high scan rates by their sharp, more symmetrical shape, their peak currents are proportional to potential scan rate, and the charges for the adsorption and desorption processes should be equal and independent of potential scan rate. The voltammogram for Pt shows that there are at least two types of hydrogen on the surface since there are two distinct adsorption peaks and two desorption peaks on the reverse sweep. The two types are called 'strongly' and 'weakly' adsorbed hydrogen, the former giving rise to the more positive peak since a higher free energy of adsorption is necessary for the larger shift in potential.

Secondly, the existence of adsorbed hydrogen atoms on the surface makes possible alternative reaction routes, and two mechanisms are generally considered important, namely



where the adsorbed hydrogen atoms are written in a way to emphasise the importance of the electrode material in determining the properties of the bond.

It may be noted immediately that both mechanisms require the formation and then the cleavage of a M-H bond. Hence while a variation of the cathode, so as to increase the free energy of adsorption, will increase the formation of the adsorbed species, it will slow down the second step in the overall process. As a result, it is to be expected that the maximum rate of hydrogen evolution will occur at intermediate values of $\Delta G_{\text{ADS}}^\ominus$ which lead to a significant but not monolayer coverage by adsorbed hydrogen atoms. This is indeed observed, and Fig. 7.2 shows a 'volcano plot' of exchange current density vs $\Delta G_{\text{ADS}}^\ominus$ for a series of metal cathodes. Similar dependences of rate parameters on the free energy of adsorption of an intermediate are common in gas phase catalysis.

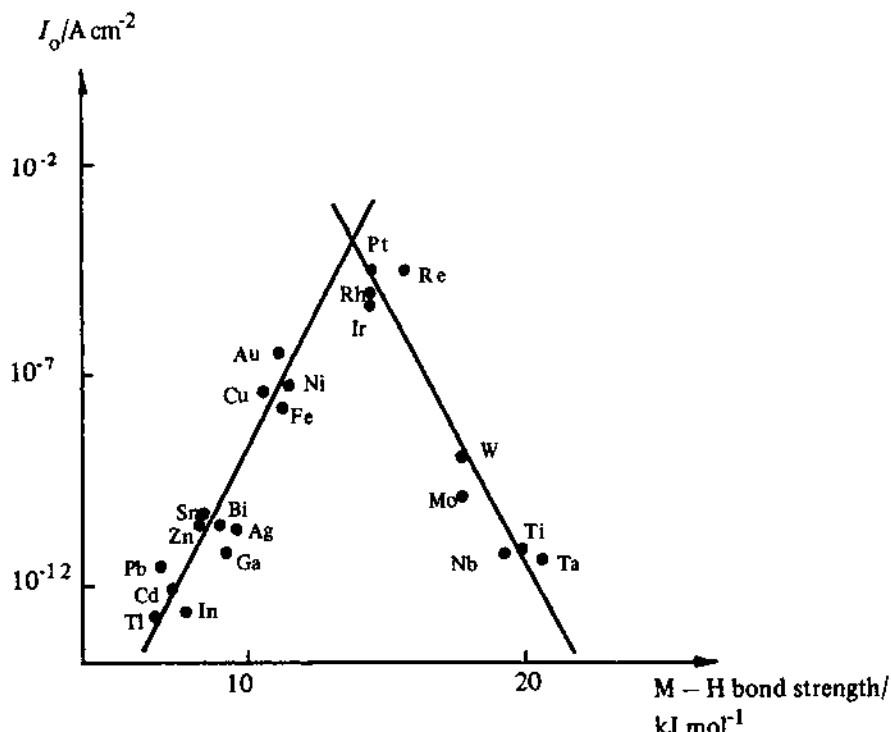


Fig. 7.2 – Dependence of the exchange current density for the hydrogen evolution reaction in 1 mol dm^{-3} acid on the strength of the metal–hydrogen bond formed with the metal of the electrode. Data taken from S. Trasatti, *J. Electroanal. Chem.*, **39**, (1972), 163.

Experimental investigations of hydrogen evolution at many cathodes have shown a wide variation in the Tafel slope, exchange current density, and dependence of current on pH. This is typical of reactions which involve a specifically adsorbed intermediate. We should now illustrate the procedure for deriving the Tafel slopes for such reaction mechanisms. It will be assumed that the fractional coverage of the surface by adsorbed hydrogen atoms can be estimated from the Langmuir isotherm. Similar derivations are possible for the Frumkin or other isotherms, but the algebra and the results are more complex.

7.2.1 Step A as the slow step

The formation of the adsorbed hydrogen atom as the first step is common to both mechanisms. Hence where this is the rate determining step we cannot be certain of the overall mechanism. The rate of step A (and hence the rate of the overall sequence when it is the rate determining step) may be written

$$\vec{v}_A = \vec{k}_A c_{H^+} (1 - \theta) \quad (7.10)$$

where \vec{k}_A is the rate constant for step A in the forward direction, potential dependent since the reduction of proton involves the transfer of an electron. The rate of reaction, \vec{v}_A , also depends on the concentration of the electro-active species and the fraction of surface free of adsorbed hydrogen atoms and therefore available for the reaction. If step B or C is always fast compared to step A, θ must be small and $(1 - \theta) \rightarrow 1$. Hence the current density for this mechanism may be written

$$\begin{aligned} I &= F\vec{k}_A c_{H^+} \\ &= Fk_A c_{H^+} \exp\left(\frac{-\vec{\alpha}_A F}{RT} E\right) \end{aligned} \quad (7.11)$$

where here $\vec{\alpha}_A$ is the transfer coefficient for step A. Hence

$$\log I = \log Fk_A + \log c_{H^+} - \frac{\vec{\alpha}_A F}{2.3RT} E. \quad (7.12)$$

It can be seen that the current is first order in proton concentration, and assuming that the transfer coefficient, $\vec{\alpha}_A \approx 0.5$, the Tafel slope, $\partial \log I / \partial E$, is $(120 \text{ mV})^{-1}$.

7.2.2 Mechanism I, rate determining step – reaction B

In this case the current is given by

$$I = 2Fk_B\theta^2 \quad (7.13)$$

where k_B is a chemical rate constant. The coverage by hydrogen atoms, θ , can in the steady state be found using the quasi-equilibrium assumption, $d\theta/dt = 0$ or

$$\vec{v}_A = \vec{v}_A' + \vec{v}_B. \quad (7.14)$$

In fact, $\vec{v}_B \ll \vec{v}_A$ under all conditions and close to the equilibrium potential $\vec{v}_B \approx \vec{v}_A'$, and hence we may treat step A as an equilibrium and write $\vec{v}_A = \vec{v}_A'$ or

$$\vec{k}_A c_{H^+} (1 - \theta) = \vec{k}_A' \theta$$

and hence

$$k_A c_{H^+} (1 - \theta) \exp\left(-\frac{\vec{\alpha}_A F}{RT} E\right) = k'_A \theta \exp\left(\frac{(1 - \vec{\alpha}_A) F}{RT} E\right) \quad (7.15)$$

which reduces to

$$\frac{\theta}{1 - \theta} = K c_{H^+} \exp\left(-\frac{F}{RT} E\right) \quad (7.16)$$

where $K = k'_A/k_A$. Rearranging this expression gives

$$\theta = \frac{Kc_{H^+} \exp\left(-\frac{F}{RT}E\right)}{1 + Kc_{H^+} \exp\left(-\frac{F}{RT}E\right)} . \quad (7.17)$$

Close to the equilibrium potential $Kc_{H^+} \exp[-(F/RT)E] < 1$, and hence

$$\theta \approx Kc_{H^+} \exp\left(-\frac{F}{RT}E\right) , \quad (7.18)$$

and substitution into equation (7.13) gives

$$I = 2Fk_BK^2c_{H^+}^2 \exp\left(-\frac{2F}{RT}E\right) \quad (7.19)$$

or

$$\log I = \log 2Fk_BK^2 + 2\log c_{H^+} - \frac{2F}{2.3RT}E . \quad (7.20)$$

For this mechanism the Tafel slope is therefore $(30\text{mV})^{-1}$, and the current varies as the square of the proton concentration.

7.2.3 Mechanism II, rate determining step – reaction C

The rate of reaction C is given by

$$\vec{v}_C = \vec{k}_C c_{H^+} \theta \quad (7.21)$$

since it depends on the concentration of protons and the fraction of the surface covered by M–H; \vec{k}_C is again potential dependent, since reaction C involves the transfer of an electron. Two simple forms of rate expression may be obtained for low and high overpotentials.

At low overpotentials $\vec{v}_A \gg \vec{v}_C$ and $\vec{v}_A \gg \vec{v}_B$, and the coverage, θ , may again be found by applying the same argument as in (7.2.2) above. The coverage is again given by Equation (7.18), and the current for this mechanism is given by

$$\begin{aligned} I &= 2Fk_C K c_{H^+}^2 \exp\left(-\frac{F}{RT}E\right) \exp\left(-\frac{\vec{\alpha}_C F}{RT}E\right) \\ &= 2Fk_C K c_{H^+}^2 \exp\left(-\frac{(1 + \vec{\alpha}_C)F}{RT}E\right) . \end{aligned} \quad (7.22)$$

Hence

$$\log I = \log 2Fk_C K + 2\log c_{H^+} - \frac{(1 + \vec{\alpha}_C)F}{2.3RT}E \quad (7.23)$$

and the Tafel slope, assuming $\vec{\alpha}_C = 0.5$, will be $(40\text{mV})^{-1}$, while the current will depend on the square of the proton concentration.

At high overpotentials, $\vec{v}_C \gg \vec{v}_A$ and then θ may be obtained by noting that $\vec{v}_A \approx \vec{v}_C$ or

$$k_A c_{H^+} (1 - \theta) \exp\left(-\frac{\vec{\alpha}_A F}{RT} E\right) = k_C c_{H^+} \theta \exp\left(-\frac{\vec{\alpha}_C F}{RT} E\right). \quad (7.24)$$

Then assuming $\vec{\alpha}_A = \vec{\alpha}_C$, θ is clearly independent of potential, and the rate expression for this mechanism is

$$I = 2Fk_C c_{H^+} K \exp\left(-\frac{\vec{\alpha}_C F}{RT} E\right) \quad (7.25)$$

or

$$\log I = \log 2Fk_C K + \log c_{H^+} - \frac{\vec{\alpha}_C F}{2.3RT} E, \quad (7.26)$$

and the reaction becomes first order in proton with a Tafel slope of $(120 \text{ mV})^{-1}$.

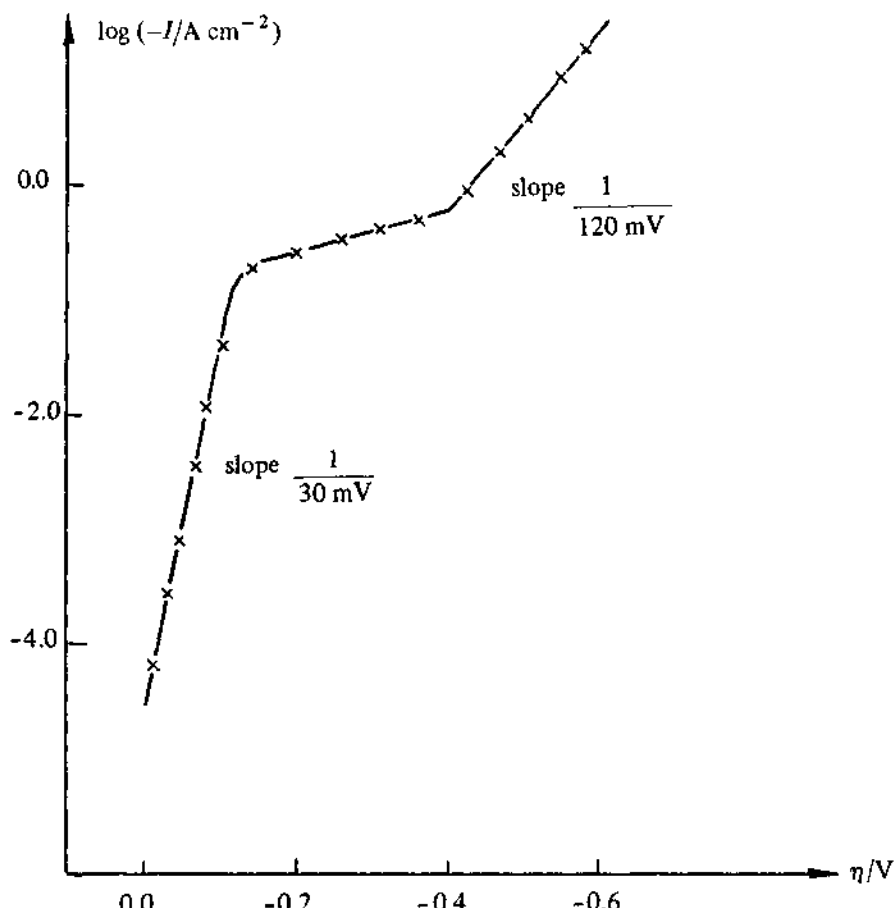


Fig. 7.3 – Steady state $I-\eta$ characteristic for a Pt cathode in $5 \text{ mol dm}^{-3} \text{ H}_2\text{SO}_4$. The data are corrected for IR drop using a current interruption technique.

Table 7.2 summarises the conclusions for the mechanisms which have been considered. While the mechanisms and different rate determining steps lead to several values for the reaction order and Tafel slope, the experimental observations will not be totally diagnostic because different mechanisms can lead to the same values. Moreover, there are many more mechanistic possibilities than have been discussed here. On the other hand, the behaviour described by the data in Table 7.2 is often observed. Platinum is an example of a cathode material where two Tafel regions are observed, see Fig. 7.3. Close to the equilibrium potential, a Tafel line, slope $(30 \text{ mV})^{-1}$ is observed, while at high overpotentials a further linear region, slope $(120 \text{ mV})^{-1}$, can be seen.

Table 7.2 Tafel slopes and reaction orders for four mechanisms of the hydrogen evolution reaction.

Mechanism	Rate determining step	Over-potential range	Tafel slope	Reaction order $\left(\frac{\partial \log I}{\partial \log C_{H^+}} \right)_E$
I or II	A	all	$(120 \text{ mV})^{-1}$	1
I	B	low	$(30 \text{ mV})^{-1}$	2
II	C	low	$(40 \text{ mV})^{-1}$	2
		high	$(120 \text{ mV})^{-1}$	1

More detailed information about the structure of the hydrogen species adsorbed onto platinum metals is now becoming available as a result of studies by pulse modulated reflectance spectroscopy using both UV/visible [21] and IR [22] irradiation. In these experiments the spectrum for the surface is separated from the absorption by the electrolyte by modulating the potential between the double layer region and a value where the H-adsorption occurs. Hence the response is a difference in reflectivity for the surface at two potentials. In the UV-visible range, well defined spectra are obtained for both weakly and strongly adsorbed hydrogen at platinum, see Fig. 7.4. The difference in reflectivity, ΔR , during the potential modulation, however, is of different sign for the two species. The sign of the change for strongly adsorbed hydrogen corresponds to an increase in electron concentration in the metal during adsorption, and this is compatible with the adsorbed species being a screened hydrogen atom at interstitial sites, donating electrons into the metal conduction band. On the other hand, the spectrum for the weakly adsorbed hydrogen is consistent with a hydrogen covalently bonded to a platinum atom. Strongly adsorbed hydrogen does not give a defined IR spectrum, but the weakly bound entity does. Its spectrum is too complex to be interpreted in terms of a simple Pt-H species (moreover, the spectrum is quite different from that for H adsorbed from the gas phase).

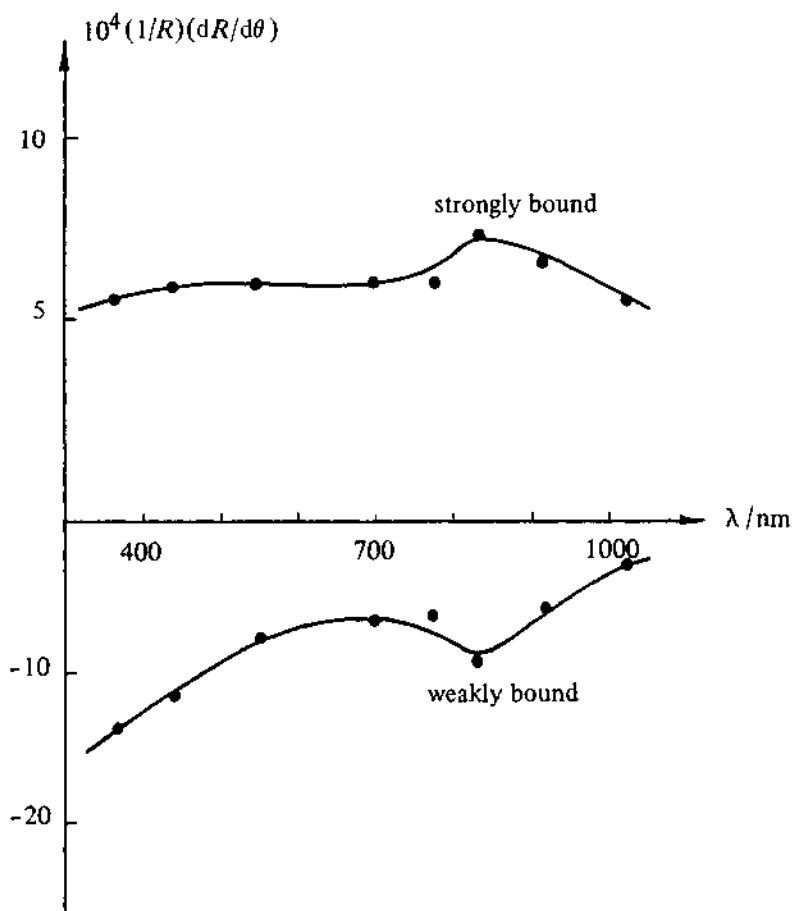


Fig. 7.4 – Wavelength dependence of $(1/R)(dR/d\theta)$ for strongly and weakly adsorbed hydrogen; p-polarised light with 45° angle of incidence.

Rather it is taken as an indication that the adsorbed H atoms are extensively hydrogen bonded to water molecules; the simplest structure consistent with all the data obtained from experiments with H_2O , D_2O , and $\text{H}_2\text{O}/\text{D}_2\text{O}$ mixtures is a structure where three hydrogen atoms are bridged by two water molecules. More extensive structures are also probable. Hence Fig. 7.5 summarises the present conclusions concerning the structure of weakly adsorbed hydrogen at platinum.

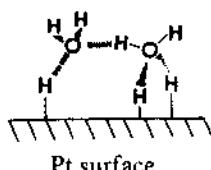


Fig. 7.5 – Sketch of Pt surface covered by weakly adsorbed hydrogen showing interaction of water molecules with the Pt-H species.

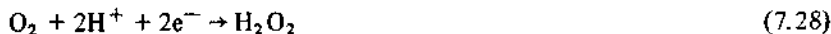
7.3 THE OXYGEN EVOLUTION AND REDUCTION REACTIONS

Oxygen evolution is the counter electrode reaction in several electrolytic processes (e.g. metal extraction, chromium plating, several organic electrosyntheses) while oxygen reduction is the desired cathode reactions in fuel cells and metal-air batteries, a potential cathode reaction in improved chlor-alkali cells and a component reaction in corrosion.

It has proved particularly difficult to identify catalysts for the reduction process. The reduction of oxygen can lead to different products; in aprotic solvents the $1e^-$ -reduction to superoxide



standard potential approx. -0.7 V , is observed. In aqueous acid, the reactions



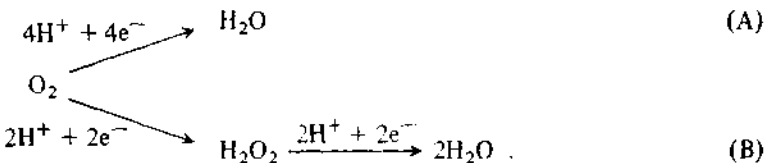
standard potentials $+0.68\text{ V}$ and $+1.23\text{ V}$ respectively, are both possible under some conditions, e.g. with appropriate choice of electrode material. With increasing pH, the potentials shift negative by 60 mV/pH unit, and in neutral or basic solutions the reactions should be written



From the viewpoint of energy efficiency, it is always desirable to have the complete $4e^-$ reduction, Reactions (7.29) or (7.31), since this reduction allows the cathode to take up a more positive potential.

The selection of cathodes for oxygen reduction poses a materials problem. Particularly in acid solution, few materials are stable to anodic dissolution at potentials close to the equilibrium potential for oxygen reduction where a good catalyst would operate. Moreover, even with the more noble metals which do not dissolve, the study of oxygen reduction is hampered by oxidation and/or reduction of their surface within the potential range of interest; this makes the experimental data for oxygen reduction less precise, and perhaps also leads to a change in mechanism when the electrode surface changes from metal oxide to metal or vice versa. In this respect the oxygen evolution reaction is easier to study since it generally occurs on a fully oxidised anode surface, and for such surfaces its study gives information relevant to its reverse reaction, providing the principle of microscopic reversibility may be applied.

In any case, the oxygen electrode is a complex system, and the overall reaction in either direction requires the transfer of four electrons and four protons. As a result, it is possible to write a very large number of reaction mechanisms, but they are essentially of two types

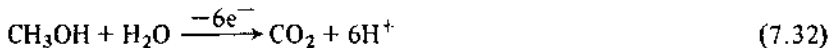


The first leads to water as the only identifiable product, while in the other the reduction to water clearly occurs in two steps with hydrogen peroxide as an intermediate. Indeed, in some conditions the reaction stops at the hydrogen peroxide stage, e.g. at mercury, oxygen is reduced in two well defined steps, separated by up to 1 V. In this mechanism catalysts may well have the role of ensuring the rapid and total disproportionation of the hydrogen peroxide to oxygen and water. Route A implies the cleavage of the O–O bond by dissociative adsorption at an early stage in the reduction, whereas in route B the first step is the reduction of oxygen to superoxide (or HO_2^+ to HO_2^-). The two types of mechanism are most readily distinguished by an experiment with a rotating ring-disc electrode (see Chapter 4). Oxygen is reduced at a rotating disc of the active material, and any hydrogen peroxide formed is monitored on a ring electrode surrounding the disc and separated from it by a thin layer of insulator; in general the disc and ring electrode may be controlled independently. At least fourteen reaction pathways for oxygen reduction have been considered [23], and taking into account the various possible rate determining steps, the anodic and cathodic Tafel slopes for 53 mechanisms for the oxygen electrode system have been established. In these circumstances, the mechanism can seldom be established with certainty, and reliable kinetic parameters cannot be obtained. Certainly, comparison between electrode materials, where the products and mechanisms may be different, is not possible. Even so, the reduction of oxygen is clearly always a slow reaction, and the best of the metals, platinum, requires an overpotential of over 0.5 V for a current density above 10 mA cm^{-2} . At other metals, e.g. Hg and some carbons, the overpotential may need to be of the order of 1.5 V.

Route A offers the best chance of effective electrocatalysis and is also necessary to ensure the full free energy output from the 4e^- -reduction and an approach to the equilibrium potential of 1.23 V. The O–O bond in oxygen is, however, strong, and it is therefore not surprising that good catalysts have not proved easy to find. Recent research studies have concentrated on various mixed oxides (e.g. spinels, bronzes, and perovskites) and transition metal complexes (e.g. metal porphyrins). To the present time, however, dispersed Pt electrodes remain the best catalytic cathodes for oxygen reduction, allowing practical current densities at an overpotential of 350–600 mV. For oxygen evolution in alkaline media, some semiconducting oxides, e.g. NiCo_2O_4 , give quite good performance [24], but the best anodes seem to be those based on Ir/RuO₂ coatings of Ti which give practical current densities at an overpotential of 200 mV [25].

7.4 FUEL CELL ANODE REACTIONS

If the complete oxidation of small organic molecules (e.g. CH₃OH, C₂H₅OH, HCHO, HCOOH, CO) to carbon dioxide could be achieved close to the reversible potentials and this electrode were coupled with a good oxygen cathode, an energy efficient fuel cell would be possible. The electrode reactions would be, using methanol as the example,



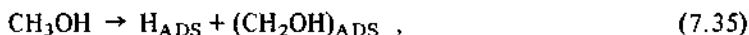
and the overall cell reaction



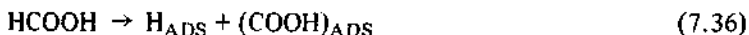
To the present time, it has not been possible to obtain a reasonable performance from anodes with a primary fuel feed, and the candidate systems are based on H₂ (as in phosphoric acid cells at 573K) or H₂ + CO (molten carbonate cells at 973K).

Two major problems arise with the anodic oxidation of small organic molecules to carbon dioxide.

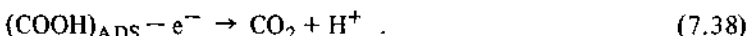
- (i) The direct removal of an electron from organic fuels in solution occurs only at very positive potentials. Hence an oxidation close to the reversible potential is dependent on predissociation of the molecule to give more readily oxidised fragments. In the case of methanol the first step is



although this will be followed by other, probably faster, reactions to give CHOH, CHO, and CO adsorbed on the surface. At all anode materials studied, such reactions are slow and limit severely the current density. The exception is formic acid where the cleavage of the C–H bond in the reaction

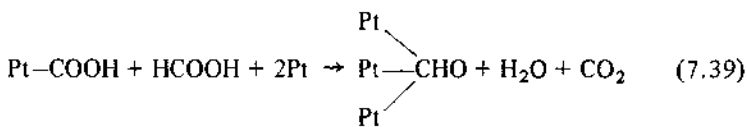


is quite fast at several precious metals [18], and is followed by two rapid electron transfer reactions [26]



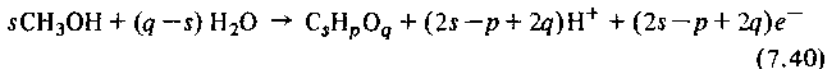
- (ii) Some of the species formed in the surface reactions are very strongly adsorbed, and hence only oxidised at very high potentials. Such species act as poisons by reducing the number of catalytic sites for the desired reaction and therefore the current density. Such a reaction rapidly decreases the activity of a Pt surface for the oxidation of formic acid.

It has been suggested [26] that the poison is formed by a reaction such as

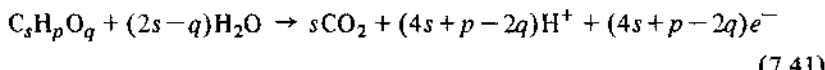


in parallel with the desired oxidation, Reaction (7.38). Evidence for the nature of the reaction comes from the strong inhibition of poison formation by sub-monolayer amounts of metals, e.g. Pb, deposited onto the Pt. It has been suggested that the oxidation of formic acid requires only two adjacent Pt sites, see Reactions (7.36)–(7.38), while the formation of the poison requires three sites; the effect of the adatoms is to break up the Pt surface so there are many places where there are two adjacent Pt sites but few where there are more than two such sites [10, 11, 12, 18, 27]. Pt surfaces partially covered by metal adatoms are effective catalysts for formic acid oxidation, and, indeed, the process can be mass transport controlled. This technique does not work for more interesting fuels, e.g. CH₃OH, because of the inherent slow rate of Reaction (7.35), and then the inhibition of the formation of poisons is not sufficient to increase the current density.

In most of these oxidation reactions, the surface is covered by several adsorbed fragments, and the ratio (and hence the electrochemical response) will vary with time and total coverage. Generally the coverage by the organic fragments cannot be described by isotherms, since their formation is quite irreversible and it is even difficult to define the structure of the adsorbates with certainty. The traditional electrochemical approach to defining the surface species and their coverage is based on the measurement of charges for the adsorption and complete oxidation of the organic compound. For example, with methanol [28], for the two steps



at a potential where C_sH_pO_q is stable and



at very positive potentials where all the adsorbed fragment may be oxidised to carbon dioxide. Both charges may be ‘normalised’ to the number of Pt sites covered by such fragments by measuring the charge for the adsorption of hydrogen in the presence of the organic compound and at the clean Pt surface (the ratio allows the determination of the fraction of the surface free from adsorbate). But such studies allow only the definition of the stoichiometry of the ‘average fragment’ on the surface if there are several present. The accurate estimation of s, p, q also requires subtraction of double layer and oxide formation charges, and unfortunately there is not a totally certain way to make such corrections.

A recent approach to the study of fuel cell oxidations has used mass spectroscopy directly coupled to the cell [29], since the mass spectrum allows a clear definition of whether an observed current is due to the formation of CO_2 or merely the oxidation of hydrogen. *In situ* IR spectroscopy is another promising method; these experiments clearly show that adsorbed carbon monoxide is formed during the pulsed oxidation of all small molecules containing carbon. Unfortunately, the time taken to record a spectrum, typically 10 minutes, and the pulse modulation essential to obtain the sensitivity, make uncertain the interpretation of these observations in the context of data obtained on 'clean' surfaces after only a few milliseconds.

Overall, however, there is no doubt that the major need is the development of much more active catalysts where the initial predissociation step occurs more rapidly.

7.5 THE DESIGN OF ELECTROCATALYSTS

It is not sufficient for an electrode material to exhibit good catalytic properties under laboratory conditions. In practice, it is often essential for the electrode to catalyse specifically only one reaction; for example, it is a prerequisite for an anode for a chlorine cell to oxidise chloride ion at low overpotential, but also it must not promote oxygen evolution, the thermodynamically preferred reaction. Furthermore, it must be possible to design and construct an electrode from the catalyst material. Since the measured current density is proportional to the real surface area, practical catalytic electrodes are manufactured with a microscopically rough surface. Also the catalyst may be expensive, and best use of material may require the dispersing of the active component in a cheaper matrix and/or applying it as a coating (e.g. by spray or plating methods) on a cheaper metal.

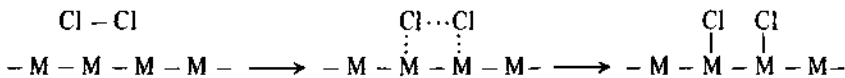
When the catalyst is a metal it will commonly be deposited in a high surface area form or dispersed onto a conducting support. If it is not a metal, it may be necessary to mix it with an inert conductor and a binder and press onto a supporting grid, or to develop a technique for coating onto an inert metal. For industrial application, the electrocatalyst must be mechanically stable, be resistant to corrosion in the electrolysis medium (both on load and on open circuit), and also maintain its catalytic activity for a long period. Indeed it is these properties which earned the name 'dimensionally stable anodes' for the chlorine electrodes. Finally, from an applied point of view, we should recognise that many electrode reactions of importance involve the evolution of a gas; since collection of gas bubbles in the interelectrode gap must have an adverse effect on the cell voltage, the catalytic electrodes will also be designed to release the gas rapidly and to pass the gas out of the interelectrode space. This is achieved by macro-shaping of the electrode, e.g. designing the electrode with louvres. Other electrode reactions require a gas as the reactant, and then the electrodes are designed as porous structures with the gas entering from the side away from the electrolyte. The electrode is manufactured by compressing the catalyst, a conducting powder (e.g. a carbon), and perhaps a hydrophobic material (e.g. PTFE) onto a conducting grid, and the gaseous reactant is passed over the back

of the electrode so that a three phase interface between gas, electrolyte, and catalyst can form within the pores for the reaction to occur. Recent gas electrodes are duplex structures with a more porous layer on the gas side and a less porous layer containing the catalyst; such structures permit the three-phase interface to be more readily controlled.

What factors determine the activity of electrocatalysts and are likely to introduce specificity into an electrode reaction? At the present time, a complete answer to this question is not possible, and we have certainly not reached the stage where it is possible to design electrocatalysts from theoretical considerations. On the other hand, a number of general principles can be set out. Thus while metals, alloys, semiconductors (particularly oxides), and complexes have been shown to exhibit catalytic properties, invariably catalysts are based on transition metals, and it seems that the design of a catalyst requires the placing of transition metal ions or atoms in a matrix which serves to optimise their electronic configuration and position with respect to each other.

The dependence of electrocatalysis on adsorption has already been emphasised, and therein lies the explanation of the success of transition metals as catalysts; they have unpaired d-electrons and unfilled d-orbitals which are available to form bonds with the adsorbate. The free energy of adsorption will, however, depend strongly on the number of unpaired electrons/atom and also on their energy levels, and hence it is not surprising that activity varies with the transition metal and may be modified by alloying or placing in a non-metallic lattice. In the limit the lattice and adsorbate may be considered as ligands in a metal complex. The observation that the rate of hydrogen evolution passes through a maximum when plotted versus free energy of adsorption is equally true of other electrocatalytic processes, and hence the objective should be to tailor the electronic environment of the metal to obtain the free energy of adsorption which leads to the maximum current density.

In addition to electronic factors, the geometric arrangement of catalyst centres will also be important. All electrocatalytic reactions involve the formation or cleavage of bonds, and it is likely that such processes will be substantially increased in rate if they can occur as concerted reactions, i.e. for example, in the reduction of chlorine, the bond between the surface and the chlorine atoms forms at the same time as the Cl—Cl bond is broken.



Such mechanisms require the correct spacing of the adsorption sites. Here the sites are written as the metal atoms themselves, but it is also possible that adsorption occurs at interstitial positions, although the argument would remain the same. The adsorption of larger molecules may involve adsorption at more than one site, and this will also require the appropriate site spacings.

To summarise the conclusions concerning catalyst design, we shall again look at oxygen reduction; how can we set out to find the most suitable catalyst? Certainly it is desirable to promote the dissociative adsorption of oxygen to give M—O bonds of intermediate strength so that the oxygen atom can readily be

reduced to water (oxide). These processes will require the correct spacing of catalyst sites and the optimum electronic energy levels to ensure the appropriate free energy of adsorption. In addition, it may be advantageous for the oxygen molecule to be able initially to form a π -complex at the surface, and the final step may be assisted by polarisation of the M–O bond. The various stages in the overall process may require different properties from the transition metal, and one way of facilitating this is to use transition metals where the oxidation state may readily be altered. It must be said, however, that few catalysts lead to a lower overpotential than platinum metal, and this will also be the case for the hydrogen electrode, the oxidation of ethylene, methanol, and carbon monoxide and chlorine evolution. Hence our search is largely limited to catalysts with a similar performance but which are cheaper. Present studies largely relate to non-stoichiometric oxides and metal complexes where inorganic chemistry would indicate that the oxide lattice or ligands may be tailored closely. Hence recent studies of the electrocatalytic reduction of oxygen have concentrated on various oxides including cobaltites [31], delafossites [32], and perovskites [33] and Fe or Co phthalocyanines and porphyrins either in solution or adsorbed on a carbon surface (for references see further reading, refs (8, 9, 13)). The synthesis of dimeric cofacial porphyrins [34, 35], which permit both control of the electronic environment of the two metal centres via the ligand structure and control of the metal–metal distance and hence the ability of oxygen to interact with both metal centres, has caused particular excitement, and, indeed, such molecules can be very good catalysts. Stability is, however, a problem. On the other hand, our confidence in the interpretation of electrocatalysis in terms of structure has been shaken by the observation of several groups [3, 36, 37] that heat treatment up to 900°C of metal complexes on carbon leads to more active and more stable catalysts. Since it is most unlikely that the ligands survive such treatment and the structure of the product is uncertain, such catalysts clearly require further characterisation. Moreover, Pt always fights back, and not only does it remain the best catalyst but the loading continues to decrease. Using special procedures for making small crystallites, electrodes with loadings as low as a few mg cm^{-2} on graphite are excellent catalysts [3].

REFERENCES

- [1] B. E. Conway & D. J. MacKinnon, *J. Electrochem. Soc.*, **116** (1969) 1665.
- [2] B. E. Conway, D. J. MacKinnon, & B. V. Tilak, *Trans. Faraday Soc.*, **66** (1970) 1203.
- [3] E. Yeager, *The Physics and Chemistry of Electrocatalysis, Electrochemical Society Meeting, San Francisco, 1983*.
- [4] B. V. Tilak, *Electrochemical Society Meeting, San Francisco, 1983*.
- [5] T. Meyer, *Proc. The Physics and Chemistry of Electrocatalysis, Electrochemical Society Meeting, San Francisco, 1983*.
- [6] S. Motoo & M. Watanabe, *J. Electroanal. Chem.*, **110** (1980) 103 and 111 (1980) 261.

- [7] Jiang Lin-Cai & D. Pletcher, *J. Electroanal. Chem.*, **149** (1983) 237.
- [8] M. Fleischmann, J. Koryta & H. R. Thirsk, *Trans. Faraday Soc.*, **63** (1967) 1261.
- [9] M. Fleischmann & M. Grenness, *J. Chem. Soc., Faraday Trans. I*, **66** (1972) 2305.
- [10] H. Angerstein-Kozlowska, B. MacDougall & B. E. Conway, *J. Electrochem. Soc.*, **120** (1973) 756.
- [11] R. R. Adzic, D. N. Simic, D. M. Drazic, & A. R. Despic, *J. Electroanal. Chem.*, **80** (1977) 81.
- [12] S. Bruckenstein, *Proc. The Physics and Chemistry of Electrocatalysts, Electrochemical Society Meeting, San Francisco, 1983*.
- [13] P. N. Ross, *J. Electroanal. Chem.*, **76** (1977) 139.
- [14] E. Yeager, W. O'Grady, M. Woo, & P. Hagans, *J. Electrochem. Soc.*, **125** (1978) 348.
- [15] J. Clavilier, R. Parsons, R. Durand, C. Lamy, & J. W. Leger, *J. Electroanal. Chem.*, **124** (1981) 321.
- [16] C. Lamy, J. M. Leger, & J. Clavilier, *J. Electroanal. Chem.*, **135** (1982) 321.
- [17] C. McCullum & D. Pletcher, *J. Electroanal. Chem.*, **70** (1976) 277.
- [18] D. Pletcher & V. Solis, *J. Electroanal. Chem.*, **131** (1981) 309.
- [19] J. Robinson in *Specialist periodical reports on electrochemistry*, Volume 9, Royal Society of Chemistry, 1984, p. 101.
- [20] S. Trasatti, *J. Electroanal. Chem.*, **39** (1972) 163.
- [21] A. Bewick, K. Kunimatsu, J. Robinson, & J. R. Russell, *J. Electroanal. Chem.*, **119** (1981) 175.
- [22] A. Bewick & J. W. Russell, *J. Electroanal. Chem.*, **132** (1982) 329.
- [23] J. O'M Bockris & S. Srinivasan, 'Fuel cells: their electrochemistry', McGraw-Hill 1969 p. 437.
- [24] A.C.C. Tseung & S. Jasem, *Electrochim. Acta*, **22** (1977) 31.
- [25] A. J. Scarpellino & G. L. Fisher, *J. Electrochem. Soc.*, **129** (1982) 515 and 522.
- [26] A. Capon & R. Parsons, *J. Electroanal. Chem.*, **44** (1973) 1 and **45** (1973) 205.
- [27] R. R. Adzic, D. N. Simic, D. M. Drazic, & A. R. Despic, *J. Electroanal. Chem.*, **61** (1975) 117 and **65** (1975) 587.
- [28] M. W. Breiter, *Discussions of the Faraday Soc.*, **45** (1968) 79.
- [29] O. Wolter & J. Heitbaum, *Ber. Bunsen. Phys. Chem.*, **68** (1964) 2 and 6 and *J. Electroanal. Chem.*, **185** (1985) 163.
- [30] B. Beden, C. Lamy, A. Bewick, & K. Kunimatsu, *J. Electroanal. Chem.*, **121**, (1981) 343.
- [31] V. S. Vilinskaya, N. G. Bulavaina, V. Ya. Shepelev, & R. Kh. Burshtein, *Sov. Electrochem.*, **15** (1979) 805.
- [32] P. F. Garcia, R. D. Shannon, P. E. Bierstedt, & R. B. Flippin, *J. Electrochem. Soc.*, **127** (1980) 1974.
- [33] Y. Matsamura & E. Sato, *Electrochim. Acta*, **25** (1980) 585.
- [34] J. P. Collman, M. Marrocco, P. Denisevich, C. Koval, & F. C. Anson, *J. Electroanal. Chem.*, **101** (1979) 117.
- [35] J. P. Collman, P. Denisevitch, Y. Konai, M. Marrocco, C. Koval, & F. C.

- Anson, *J. Am. Chem. Soc.*, **102** (1980) 6027 and **105** (1983), 2694 and 2699.
- [36] J. A. R. Van Veen, J. F. Van Baar, C. J. Kroese, J. G. F. Coolegem, N. de Wit, & H. A. Colijn, *Ber. Bunsen. Phys. Chem.*, **85** (1981), 693.
- [37] J. A. R. Van Veen, J. F. Van Baar, & C. J. Kroese, *Ber. Bunsen. Phys. Chem.*, **85** (1981) 700.

Further reading

- (1) J. O'M Bockris & A. K. N. Reddy, *Modern electrochemistry*, Plenum Press, 1970.
- (2) J. O'M Bockris & S. Srinivasan, *Fuel cells: their electrochemistry*, McGraw-Hill, 1969.
- (3) M. W. Breiter, *Electrochemical processes in fuel cells*, Springer Verlag, 1968.
- (4) J. P. Hoare, *The electrochemistry of oxygen*, Interscience, 1968.
- (5) H. Kita & T. Kurisu, *J. Res. Inst. Catalysis, Hokkaido Univ.*, **21** (1973) 200.
- (6) E. Yeager, *Surface Science*, **101** (1980) 1.
- (7) K. Kimushita & P. Stonehart, *Modern Aspects of Electrochemistry*, **12** (1977) 183.
- (8) *Proc. The Physics and Chemistry of Electrocatalysis, Electrochemical Society Meeting, San Francisco*, 1983.
- (9) E. Yeager, *J. Electrochem. Soc.*, **128** (1981) 160C.
- (10) D. Pletcher, *J. Applied Electrochem.*, **14** (1984) 403.

Hydrogen evolution

- (10) A. N. Frumkin, *Advances in Electrochemistry and Electrochemical Engineering*, **1** (1961), 65 and **3** (1963) 287.
- (11) S. Trasatti, *J. Electroanal. Chem.*, **39** (1972) 163.
- (12) E. W. Broaman & A. T. Kuhn, *J. Electroanal. Chem.*, **49** (1974) 325.

Oxygen reduction and evolution

- (13) D. J. Schiffrin, *Specialist periodical reports on electrochemistry*, Volume 8, The Royal Society of Chemistry, 1983.
- (14) E. Yeager, *National Bureau of Standards Special Publication*, **455** (1975) 203.
- (15) A. J. Appleby, *Modern Aspects of Electrochemistry*, **9** (1974) 369.

Chlorine evolution

- (16) S. Trasatti & W. E. O'Grady, *Advances in Electrochemistry and Electrochemical Engineering*, **12** (1981) 177.

8

A.C. techniques

Methods employing excitation of an electrochemical cell by a sinusoidal signal and analysis of the currents produced were first employed as a way of measuring the rate constants of fast electron transfer reactions. In any measurement of fast reactions by whatever technique, information has to be obtained at short times, otherwise diffusion rather than kinetics becomes the rate determining process. The a.c. bridge was for a time the only instrumental technique available to allow measurements on the millisecond timescale and below, and the basics of present-day a.c. techniques and methods of analysis were worked out using an electrochemical cell at equilibrium as the unknown arm of a Wheatstone bridge. Modern instrumentation allows a.c. measurements to be made far more expeditiously than with a manually balanced bridge, so permitting continuous recording of a.c. parameters under dynamic rather than equilibrium conditions, e.g. in cyclic voltammetry or polarographic experiments. At the other end of the timescale, a.c. techniques are now important in corrosion studies, where rapid response is of lesser importance than complete analysis of what are often complicated processes involving surface and solution reactions. Here, modern computational methods have been essential in the application of a.c. methods.

8.1 A.C. THEORY

In order to work with electrochemical cells in a.c. circuits, some basic understanding of a.c. theory is necessary. The following outline uses the so-called *phasor* concept of the sinusoidal alternating current, in which voltages and currents are thought of as rotating vectors and are represented in the *complex plane* (Argand diagram).

Representing a sinusoidal voltage as

$$E = \Delta E \sin \omega t , \quad (8.1)$$

where ω is the angular frequency ($= 2\pi f$ where f is in hertz), E is the instantaneous value, and ΔE is the maximum amplitude. The value is seen to be a projection on the zero axis in the polar diagram, Fig. 8.1, where the phasor \mathbf{E} is the rotating vector representing the sinusoidal voltage. Usually we wish to describe the relationship between the voltage and the current in a circuit. In most cases the current will also be sinusoidal and of the same frequency ω , but different in amplitude and phase from the voltage (lagging or leading in phase), and can be represented as

$$i = \Delta i \sin(\omega t + \phi) . \quad (8.2)$$

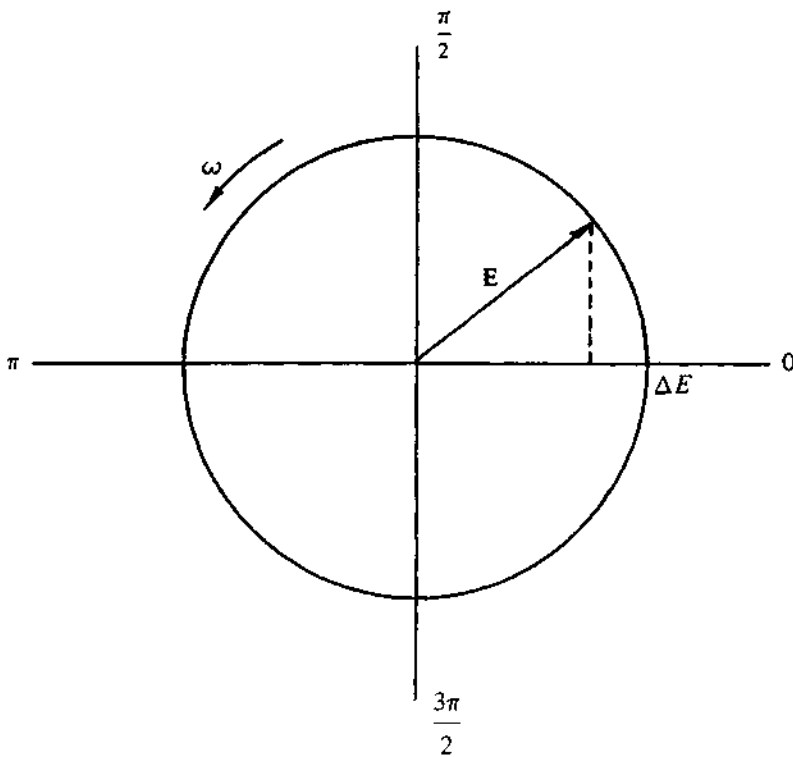


Fig. 8.1 ~ Phasor diagram for an alternating voltage $E = \Delta E \sin \omega t$ where ΔE is the maximum amplitude. The phasor is the rotating vector \mathbf{E} .

In phasor terms, the rotating vectors are now separated on the polar diagram by the angle ϕ , Fig. 8.2. The response of simple circuit elements to the voltage \mathbf{E} can be seen by applying Ohm's law, which for a pure resistance of value R is:

$$i = \frac{E}{R} . \quad (8.3)$$

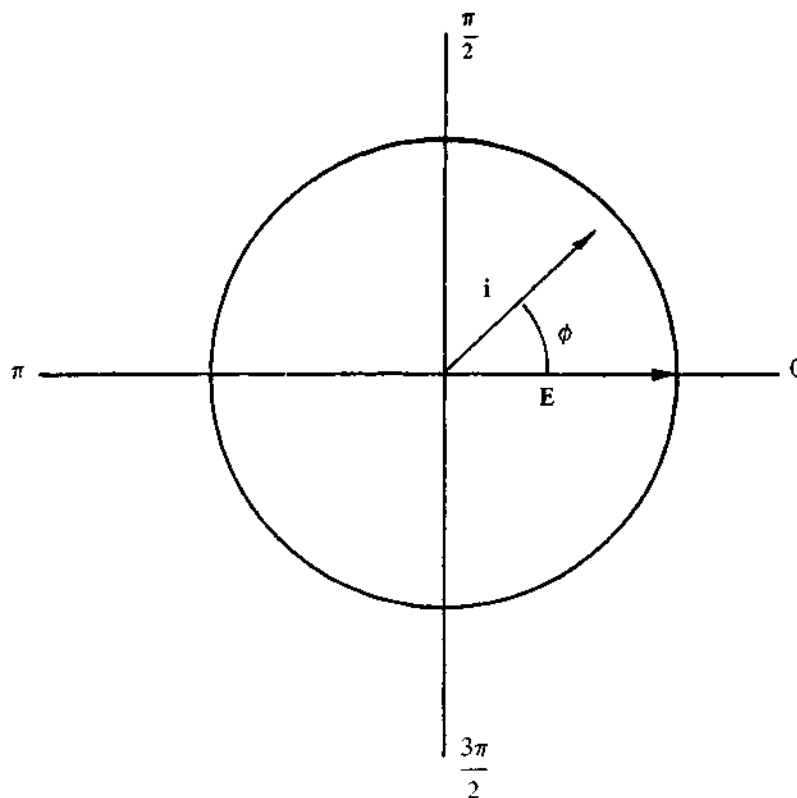


Fig. 8.2 - Phasor diagram showing current and voltage phasors separated by the phase angle ϕ .

This means that the phase angle ϕ is zero. For a capacitor, we need to apply the definition of capacitance, C , from the relation between the potential, E , across the plates to the charge q residing on the plates:

$$q = CE . \quad (8.4)$$

On differentiating to get the current, i ,

$$i = \frac{dq}{dt} = C \frac{dE}{dt} \quad (8.5)$$

which from (8.1) is

$$i = \omega C \Delta E \cos \omega t . \quad (8.6)$$

Replacing $1/\omega C$ by the symbol X_c (called the capacitive reactance) we have

$$i = \frac{\Delta E}{X_c} \sin(\omega t + \pi/2) . \quad (8.7)$$

which is similar in form to the Ohm's law expression for a resistor (8.3), but with R replaced by X_c and a phase angle not of zero but of $\pi/2$. The phase angle is positive, so the current is said to lead the voltage.

At this point it is helpful to introduce complex notation, in which magnitudes on the ordinate axis are multiplied by $j = \sqrt{-1}$. Current and voltage are regarded as phasors, i.e. rotating vectors, the notation for which is simplified by defining the phasor \mathbf{E} as

$$\mathbf{E} = E \sin \omega t . \quad (8.8)$$

In mathematical terms the components of the phasors \mathbf{E} and i can be represented in an Argand diagram with the real component on the abscissa and the imaginary component on the ordinate. Fig. 8.3 and 8.4 show equivalent representations in both phasor and i - t or E - t form. In Fig. 8.4 the voltage is measured with respect to the current, so the \mathbf{E} phasor has a phase angle of $-\pi/2$. Then we can write

$$\mathbf{E} = -jX_c i \quad (8.9)$$

which is of similar form to Ohm's law, but with a complex number $-jX_c$ replacing resistance. X_c , of course, depends on the reciprocal of the frequency and the reciprocal of the capacitance, but has the units of ohms.

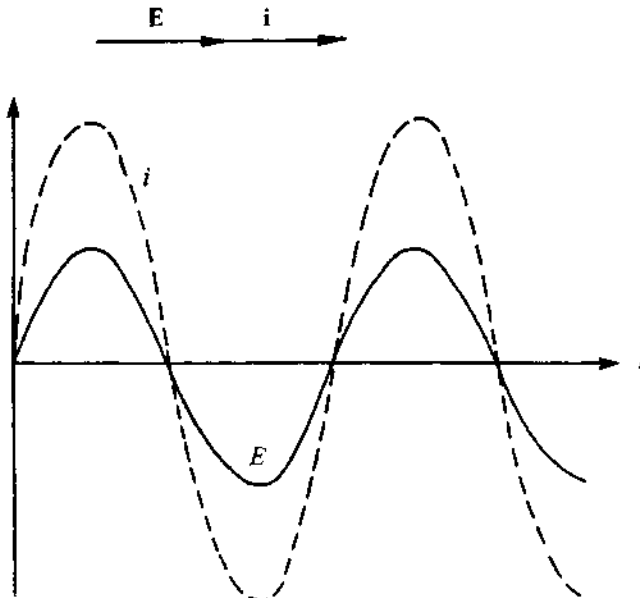


Fig. 8.3 – Equivalent representations in phasor and time axis form of current and voltage relationships in a purely resistive circuit where the phase angle is zero.

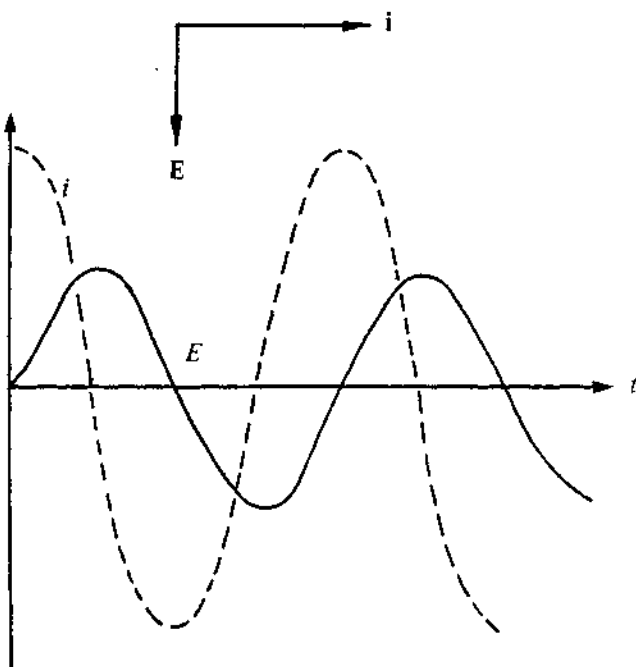


Fig. 8.4 – Equivalent representations in phasor and time-axis form of current and voltage relationships in a circuit with capacitive reactance showing a 90° phase angle.

For a resistor and a capacitor connected in series, the sum of the voltage drops across each element must sum to the total of \mathbf{E} , so in phasor notation

$$\begin{aligned}\mathbf{E} &= \mathbf{E}_R + \mathbf{E}_C \\ &= \mathbf{i}(R - jX_C)\end{aligned}\quad \text{or } \mathbf{E} = \mathbf{i}Z \quad (8.10)$$

where $Z = (R - jX_C)$ is called the *impedance*.

The current will no longer be in phase or 90° out of phase with the voltage, but can be obtained simply from the Argand diagram, Fig. 8.5. If the phase angle is denoted by ϕ :

$$\tan \phi = \frac{X_C}{R} = \frac{1}{\omega RC} \quad . \quad (8.11)$$

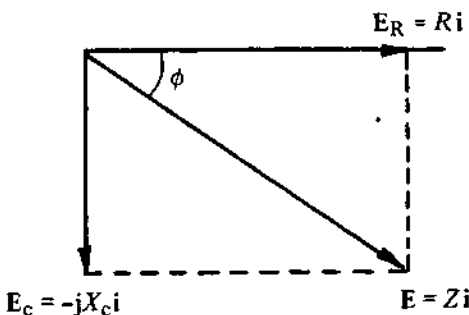


Fig. 8.5 – Phasor diagram for a series resistor and capacitor, showing E the voltage across the combination of R and C , and the resistive and capacitive components Ri and $jX_c i$.

Because of the simple relation between complex impedance and E and i , an alternative diagram giving the same information in terms of impedances only can be plotted, Fig. 8.6. For series circuits, the overall impedance is the vector sum of the reactances of the separate elements. Again by analogy with the rule for resistive circuits, the overall impedance for parallel combinations is the reciprocal of the sum of the reciprocal impedances of each circuit component. The quantity defined by the reciprocal impedance $1/Z$, called the *admittance* Y , is often useful in describing the behaviour of combinations of impedances. The generalised Ohm's law is then

$$i = EY \quad (8.12)$$

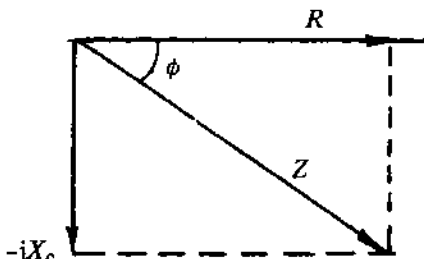


Fig. 8.6 – Argand diagram showing the same relationships as in Fig. 8.5 but in terms of impedances only.

In using vector notation for phasors, further economy of notation can be achieved by introducing the polar forms:

$$\mathbf{E} = E \exp j\phi \quad (8.13)$$

$$\mathbf{i} = i \exp j\phi \quad (8.14)$$

$$\mathbf{Z} = Z \exp j\phi \quad (8.15)$$

$$\mathbf{Y} = \frac{1}{Z} \exp -j\phi , \quad (8.16)$$

that is, \mathbf{Y} has the magnitude of $1/Z$ and an equal (but opposite) phase angle.

8.2 MEASURING THE IMPEDANCE OF AN ELECTROCHEMICAL CELL

There are some general considerations to be borne in mind in any a.c. method.

(a) Frequency of the exciting signal

The range of frequencies should be as wide as possible if a.c. methods are to be used in a diagnostic way. Ideally this means a range of 6 to 7 decades of frequency, e.g. 10^{-2} to 10^5 Hz, if all the theoretical tools available, including Kramers-Krönig analysis, (*vide infra*), are to be used to their full potential.

(b) Linearity

In the sense that the rates of elementary reaction steps are exponentially dependent upon the potential, electrochemical processes are inherently non-linear. The a.c. theories that are most fully developed, however, are all *linear* theories, which means that in order to use them the amplitude of the exciting signal must be kept small enough that the system becomes linear to a close approximation (i.e. the linear approximation to the Butler-Volmer equation may be used see Equation (1.34)). The permissible amplitude varies with the system under test and with frequency, but as a general rule a peak-to-peak amplitude of 10 mV should not be exceeded without some particular indication that it is safe to do so, and with the knowledge that even this low level of perturbation may cause problems. Non-linearities manifest themselves by the production of harmonics of the exciting signal in the cell response, and so a detection system such as a spectrum analyser can be used to detect their presence and measure their amplitudes. An oscilloscope should be used routinely to monitor the a.c. component of cell current as a way of showing up any gross non-linearities as a visible distortion of the sine wave response. A further simple check is to carry out analyses with a different amplitude of excitation, any differences of response pointing to non-linearities as a problem.

(c) Spurious responses

A.c. techniques are notoriously prone to falsification by spurious effects in the measurement circuitry. It is difficult to design potentiostats which do not display phase shifts at high frequencies while still having a high enough gain. Stray capacitance between connecting leads to earth and between the leads themselves, and self inductance of leads and structures within the cell, will always be a problem at very high frequencies.

Good cell design can help to alleviate some of these problems, and attention should be paid to the following points. The working electrode and the counter electrode should be symmetrically disposed so as to provide a very uniform

distribution of current. The Luggin capillary should be placed close, but not too close, to the working electrode, thus minimising uncompensated ohmic resistance but avoiding shielding effects that cause uneven current distribution. The capillary should preferably be straight and short, and should not be of too fine a calibre, or its resistance will be high. The reference electrode itself should be of as low a resistance as possible and should be buffered by a high input impedance unity-gain amplifier connected to it by a short lead to minimise the RC time constant of the reference circuit (see also Chapter 11).

Random electrical noise or pickup at mains frequency is also likely to be a problem because of the need to keep the exciting signal small. Careful shielding of the cell and detection circuits will usually be needed to reduce this kind of interference to an acceptable level.

Several distinct types of instrumentation are available for measuring electrochemical impedances using sine wave excitation, the most often used being described in detail below.

8.2.1 Wheatstone bridge

Historically, the a.c. Wheatstone bridge in its various elaborated forms has been most important in laying the foundations of a.c. electrochemical experiments. One example of a bridge circuit is shown in Fig. 8.7.

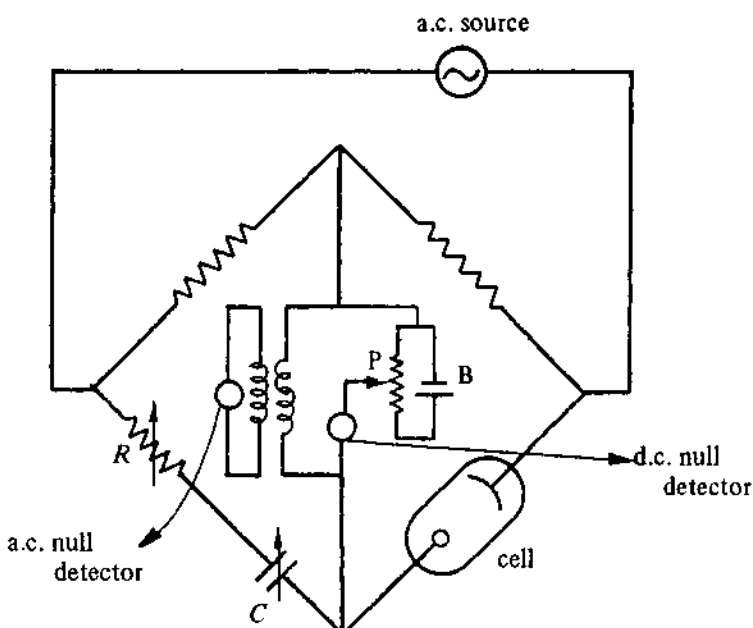


Fig. 8.7 – Simple Wheatstone bridge adapted to measurement of the impedance of an electrochemical cell at the open-circuit potential by the incorporation of a d.c. polarising source consisting of the battery (B) and potentiometer (P). The d.c. null detector is a sensitive galvanometer; the a.c. detector is an oscilloscope or a.c. microvoltmeter.

The typical electrochemical cell is not a passive element, i.e. it generates a potential difference or it needs to have a potential difference impressed upon it to bring it to the condition required by the experiment. Therefore the bridge has both an a.c. and a d.c. detector, the latter also serving as a source of whatever steady current is taken by the cell. In this case it consists of a battery and potentiometer. Balance of the bridge is indicated by an a.c. detector, which may take the form of a tuned amplifier/meter combination, an oscilloscope, or some other form of sensitive a.c. voltmeter.

Both R and C have to be balanced simultaneously, which in the simplest forms of bridge means adjusting them successively in an iterative approach to the a.c. signal minimum. This is a slow process which means that the method is suitable only for static or very slowly changing systems. This arrangement yields the series equivalent of the total cell impedance, which includes several impedances such as that of the working electrode, the counter electrode, and the resistance of the electrolyte separating them; the latter is usually purely resistive. It is desirable to eliminate the counter electrode impedance, and this can usually be done by making its impedance negligibly small in comparison with that of the working electrode, e.g. by increasing its surface area and using a highly reversible system such as a metal-insoluble metal salt counter electrode. Although the solution resistance cannot be reduced to zero, it can sometimes be reduced to a negligible value, but usually it will be present as an important contribution to the overall impedance. As it is generally constant, however, it may be possible to determine its value or allow for it quantitatively.

The main disadvantage of bridge circuits is that they do not lend themselves to dynamic measurements. They also have a restricted frequency range, and cannot be used below about 10 Hz.

8.2.2 Analogue a.c. analysers

Modern electronics provides a wide variety of methods for automatically measuring impedance or admittance, most of them based on potentiostatic control of the working electrode potential. Instead of compensating for the real and complex part of the admittance with a known R and C (the bridge method), the a.c. part of the cell current is measured. From the Argand diagram it is apparent that two quantities are necessary to define the complex impedance. There is a choice of measurables, however. Either the total a.c. amplitude and the phase angle, or alternatively the real and complex parts of the impedance, can be measured – the two methods requiring different instrumentation.

A general apparatus for these measurements is shown in Fig. 8.8.

The a.c. analyser would in the first method comprise two dissimilar instruments: an a.c. voltmeter giving an output proportional to the total amplitude of the alternating current, and a phase angle meter. The latter has two inputs, the a.c. itself and a reference which is taken from the sine wave source at the input of the potentiostat. By the use of switching techniques, an output is produced proportional to the phase difference between these signals but independent of their magnitude, Fig. 8.9.

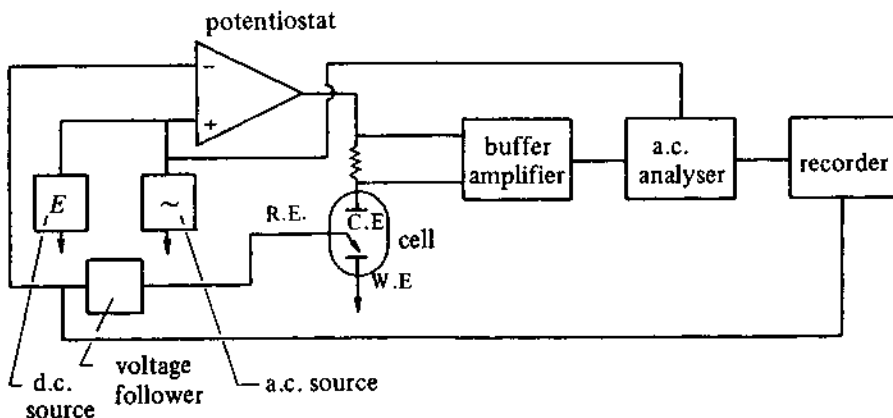


Fig. 8.8 – General apparatus for a.c. analysis of a reaction as a function of electrode potential.

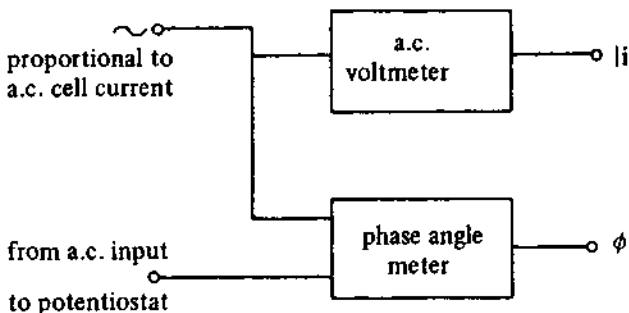


Fig. 8.9 – A.c. analyser giving output signals proportional to the total alternating current and the phase angle.

The second method uses a pair of phase sensitive detectors (p.s.d.s.) which differ only in the source of their reference inputs. Each takes the alternating cell current as one input and has as reference, either the potentiostat input a.c. or the latter signal shifted by 90° . The separate outputs of these p.s.d.s. are proportional to the in-phase component or the 90° (i.e. quadrature) component.

Instruments for both these methods are commercially available, or can be made using standard operational amplifier techniques [1]. An instrument incorporating two p.s.d.s. with synchronisation for the dropping mercury electrode has been described by de Levie & Husovsky [2]. Both of these techniques are convenient in that they give analogue displays of the measured quantities. By using a swept-frequency oscillator, both quantities can be recorded as a function of frequency on an $X-Y$ recorder.

The results from phase angle meters are inherently rather susceptible to pick-up at mains frequencies. Phase sensitive detectors, however, have good rejection of adventitious frequencies and are insensitive to harmonics of the exciting frequency. Problems can arise, however, if the signal-to-noise ratio is small, as a high amplitude noise signal can drive the input circuitry into saturation. The p.s.d. is then said to 'limit on noise', and its output becomes a highly non-linear function of the true signal. This effect can be overcome by pre-filtering the signal, but great care has to be taken not to introduce spurious phase shifts in this way. If a wide frequency range is being covered then a series of filters with different cut-off frequencies will be needed. The low frequency limit of the p.s.d. technique is in the range 0.1 to 1 Hz.

8.2.3 Sine wave correlation

The process of sine wave correlation can be described as the multiplication of the measured signal with a sine wave reference derived from the exciting signal. The resulting signal is then integrated over a whole number of cycles of the reference wave, to give a response that is unaffected by harmonics of the reference frequency. Moreover, the random noise components are reduced in proportion to the length of the integration period. In practice, two reference signals are used which are in-phase and in quadrature with the exciting signal. The correlator outputs are then proportional to the real part and the imaginary part of the admittance (Fig. 8.10). Instruments are commercially available [3], which can carry out this correlation analysis, providing also the exciting signal which is programmable in amplitude and frequency in the range 10^{-3} Hz to 10^4 Hz. All of the functions can be controlled by an external computer, and the outputs are available in both analogue and digital form.

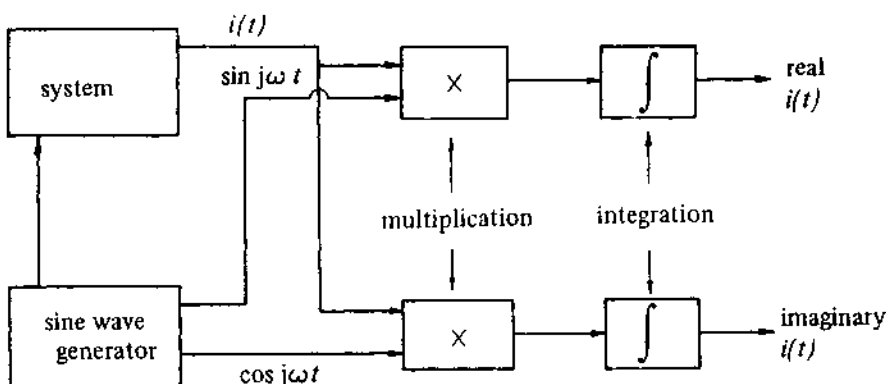


Fig. 8.10 -- Schematic of a sine wave correlator showing the process of multiplication of the system output $i(t)$ with reference signals in-phase and in quadrature with the excitation signal. The resultant signals are integrated over a whole number of cycles to give the real and imaginary parts of the function $i(t)$.

8.2.4 Fourier transform methods

The methods so far described are frequency scanning methods, i.e. a separate measurement is made at each frequency required. A radically different approach employs multiple-frequency excitation and Fourier transformation of the resulting signal into the real and complex spectra. Smith and co-workers [4] have shown that the best kind of excitation signal is phase-varying, odd harmonic pseudo-random white noise. This can be generated by computer so that the amplitude of all the component frequencies (10-20, over a 2 or 3 decade frequency range) is equal. This signal is superimposed on a d.c. bias and fed to the input of the potentiostat and to the Fourier analyser. The analyser, which is a special purpose computer, also receives the output response current from the

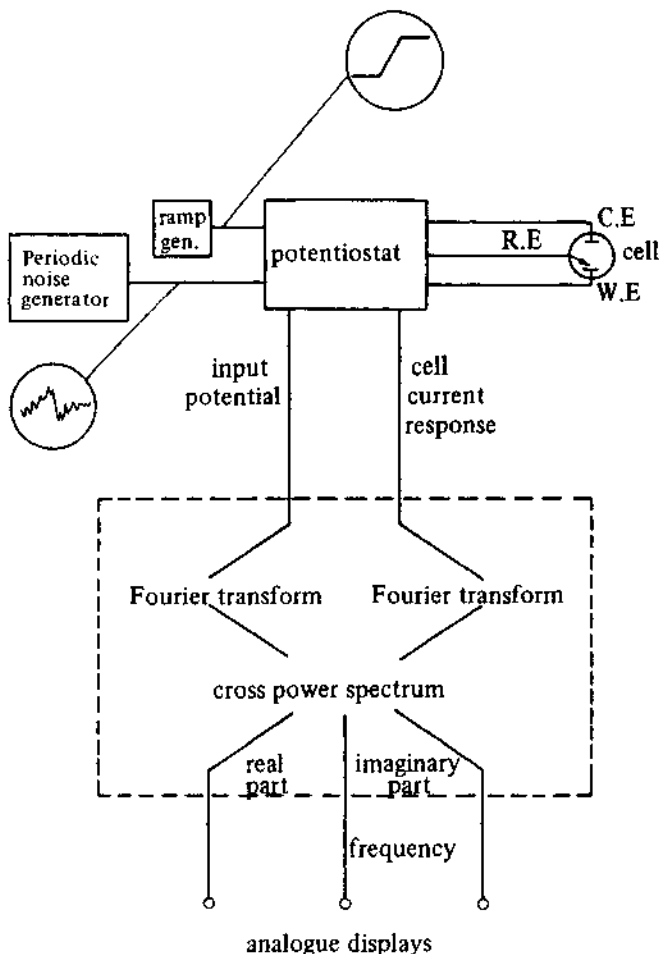


Fig. 8.11 – Schematic of the main processes in Fourier transform analysis. In this case the excitation is by pseudo-random noise, but other forms such as multi-frequency sine wave excitation can be used. The signal processor is a special purpose computer that carries out timed sampling of a fixed number of points which are transformed to give the real and imaginary components of the cell current as a function of frequency.

potentiostat, and carries out a Fourier transform analysis on a sampled section of the response, which may be as short as 0.1 s (Fig. 8.11). This is followed by computation of the cross power spectrum and resolution into the real and imaginary components. From this, further processing can yield a phase angle versus frequency analysis, or the response at some higher harmonic of the excitation frequency. In a favourable situation this method can be very fast; it is feasible to obtain a response spectrum on the timescale of the life-time of a single mercury drop in a polarographic experiment [5]. The method therefore would appear to have advantages compared to the sine wave correlation method, which necessarily has to measure one frequency at a time. It should be realised, however, that the Fourier Transform (FT) process is inherently more subject to disturbance by noise and by other coherent frequencies such as harmonics and pick-up from external sources. The only way to discriminate against noise is to average the signal, which again multiples the time needed for a measurement.

The question of resolution on the frequency axis in the FT method is also worthy of careful consideration. An FT analysis presents a fixed number of points which are equally spaced on the frequency axis. This represents an inefficient distribution of data, which are needlessly closely spaced at high frequencies but sparse at low frequencies — a logarithmic distribution with a fixed number of points per *decade* is better. To cover low frequencies adequately, it may therefore be necessary to carry out analyses over different ranges, which again multiples the time for a complete measurement.

These factors have been considered in more detail by Gabrielli *et al.* [6], who compare sine wave correlation methods with those employing random (white noise) excitation signals.

8.3 APPLICATIONS OF IMPEDANCE ANALYSIS

8.3.1 Impedance of a simple electron transfer reaction

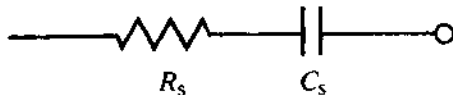
One of the simplest electrochemical systems to analyse is that of a rapid reaction at its equilibrium, open circuit potential E_e , i.e. with no net current flowing. Under a.c. excitation (and in this and subsequent examples it is assumed that the excitation of potential of the working electrode is small, which means ideally less than 5 mV peak-to-peak) the net current is, of course, still zero, but the current-potential relationship is approximately linear rather than exponential.

Consider the reaction



where both reactant and product are soluble. In order to evaluate the a.c. response of the system, two kinds of information are needed. Firstly, the forward and reverse rate constants, or the exchange current density, I_0 . This quantity is usually the desired parameter to be measured in this kind of experiment. Secondly, the rates of diffusion of the species O and R at the working electrode as a function of time during the a.c. cycle are needed.

When the a.c. signal is first impressed, a time-dependent diffusion layer is created. As no net current flows, a steady state is set up after a few cycles. This coupled diffusion and electrochemical problem has been solved with the following result [8]. Assuming that the impedance can be expressed as a series combination of a resistor and a capacitor:



it is found that:

$$R_s = R_{ct} + \sigma/\omega^{1/2} \quad (8.18)$$

$$C_s = 1/\sigma\omega^{1/2} \quad (8.19)$$

R_{ct} is called the charge transfer resistance and C_s is the pseudo-capacitance. It is then assumed that close to the reversible potential the relationship between current and potential is linear rather than logarithmic, which is true for an excursion less than five millivolts either side of the reversible potential. Then it is found that, for a planar diffusion field,

$$R_{ct} = \frac{RT}{nF i_0} \quad (8.20)$$

and

$$\sigma = \frac{RT}{2^{1/2} n^2 F^2 A D^{1/2}} \left[\frac{1}{c_O^\infty} + \frac{1}{c_R^\infty} \right] \quad (8.21)$$

where A is the electrode area, D is the diffusion coefficient for species in solution, and c_O^∞ and c_R^∞ are bulk concentrations. Thus R_{ct} is characteristic of the exchange current, i_0 , and therefore of k^\ominus the rate constant at equilibrium, whereas σ has to do with the diffusion parameters of the system. Rewriting (8.19) as

$$1/\omega C_s = \sigma/\omega^{1/2}, \quad (8.22)$$

then from (8.18)

$$R_s - 1/\omega C_s = R_{ct} = RT/nF i_0 \quad (8.23)$$

so that a plot of R_s against $1/\omega^{1/2}$ should yield a straight line of slope σ and intercept on the ordinate equal to R_{ct} , from which i_0 can be found. Furthermore, the term $1/\omega C_s$ when plotted against $1/\omega^{1/2}$ should have the same slope σ . The quantities R_s and C_s are those given directly from the bridge configuration of Fig. (8.7), but equivalent values of R_s and C_s can be obtained at a given frequency whatever method of a.c. analysis is used. Both these plots should be done when looking at a new system, as the linearity of each, with equal slopes, is valuable confirmation that the process is indeed a single charge transfer process without other complications [7].

Looking again at the overall impedance we have

$$Z = R_s + 1/j\omega C_s \quad (8.24)$$

$$= R_{ct} + \sigma/\omega^{1/2} + j\sigma/\omega^{1/2}. \quad (8.25)$$

This is the sum of two terms, a simple resistive component which is small when i_0 is large, and a reactance which can be regarded as a frequency-dependent resistance. This special reactance is called the Warburg impedance Z_W , sometimes drawn ---W--- . If R_{ct} approaches zero, then the total impedance is Z_W , whose magnitude is

$$\begin{aligned} |Z_W| &= [(\sigma/\omega^{1/2})^2 + (\sigma/\omega^{1/2})^2]^{1/2} \\ &= (2/\omega)^{1/2}\sigma. \end{aligned} \quad (8.26)$$

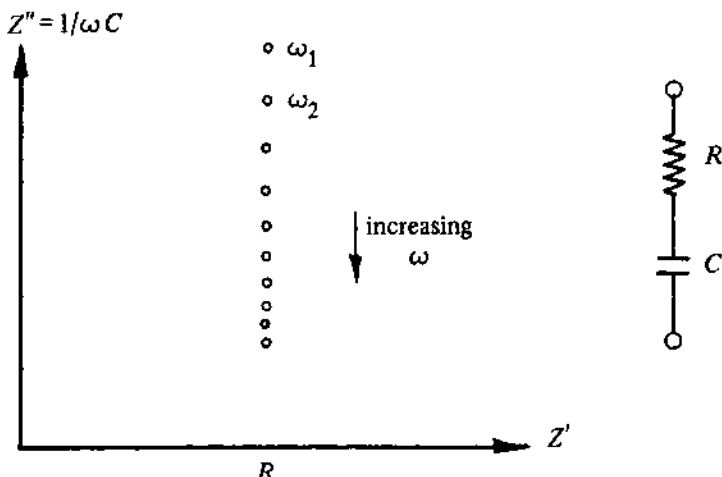
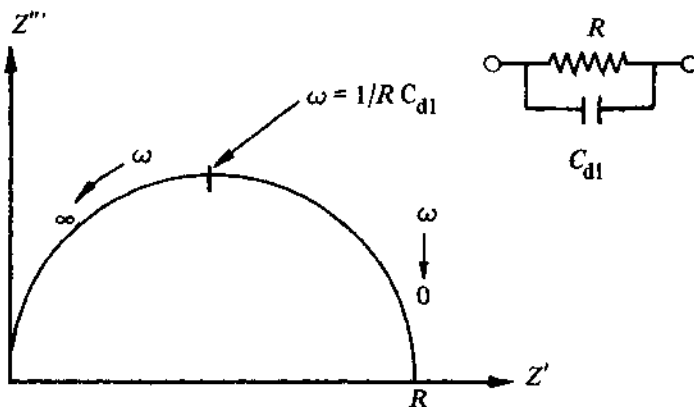
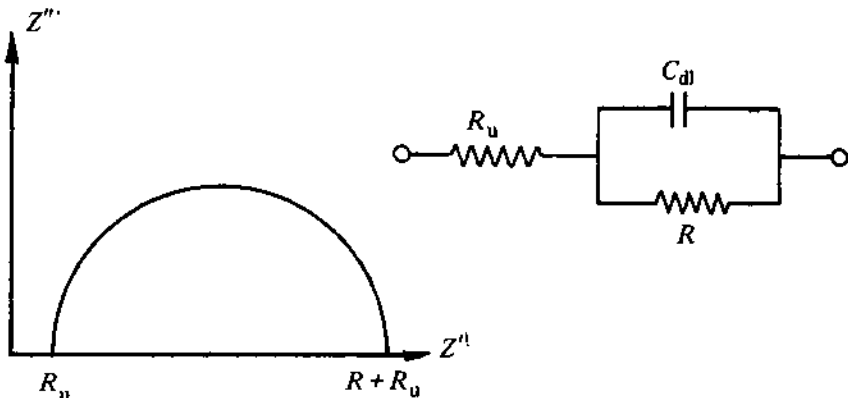
Since both real and complex parts of Z_W are equal, it is characterised by a constant phase angle of $\pi/4$ (45°), independent of frequency.

The relative size of R_{ct} and Z_W at any given frequency is a measure of the balance between kinetic and diffusion control. If i_0 is very large, $R_{ct} \rightarrow 0$ and will be too small to measure so that only the Warburg impedance will be observed. On the other hand, a very sluggish electrochemical reaction will have a high (and possibly difficult to measure) value of R_{ct} which will be the dominant term.

The foregoing analysis has neglected the fact that all electrodes exhibit a capacitance, C_{dl} , the so-called double layer capacitance, quite independent of any Faradaic reaction, which as we have seen, contributes a pseudo-capacitance C_s to the overall impedance. If there is any solution resistance R_u between the point at which the potential is measured (usually the tip of the Luggin capillary) and the working electrode, this too will appear as part of the measured total impedance.

The effect of C_{dl} and R_u can be accounted for if their values are known. They can sometimes be determined by making measurements in the absence of the electroactive couple O/R. However, determining these components separately adds greatly to the complication of the experiment and the analysis. A method of analysis which can often circumvent the need to make separate measurements derives from a procedure long used in electrical engineering and adapted to electrochemical applications originally by Sluyters and co-workers [8]. This is the so-called *complex plane impedance analysis*.

Considering a simple circuit such as a series resistance and capacitance, with an impedance $Z = R + 1/j\omega C$, it can be seen that the real part of Z is simply R , and the imaginary part is $1/\omega C$. Plotted on an Argand diagram of $Z = Z' + Z''$ we shall therefore have the response shown in Fig. 8.12. The graph is a series of points at different ω values, the value of Z'' approaching zero at infinite frequency where the capacitance is effectively a short circuit. The graph representing a parallel combination is a semi-circle (Fig. 8.13). At low frequencies the impedance is purely resistive, because the reactance of C is very large. The next step in complication is to add a series resistance, which might represent an

Fig. 8.12 – Complex plane (Argand) diagram for a series RC circuit.Fig. 8.13 – Complex plane impedance diagram for a parallel RC circuit. This is the simplest possible analogue of a Faradaic reaction at an electrode with an interfacial capacitance C_{dl} .Fig. 8.14 – Complex plane diagram as in Fig. 8.13 with the addition of R_u , an uncompensated solution resistance.

uncompensated solution resistance. This has the effect of translating the semi-circle along the Z' axis, Fig. 8.14. One can now build a realistic model of a simple electrochemical cell by identifying C as the double layer capacitance, which will always be in parallel with the reaction impedance. Therefore R can now be resolved into the charge transfer resistance in series with the Warburg impedance as before, see Fig. 8.15. A full analysis of this series-parallel configuration, usually called the *Randles equivalent circuit* [7], has two limiting cases. At low frequencies as $\omega \rightarrow 0$ the real and imaginary parts of Z are found to be:

$$Z' = R_u + R_{ct} + \sigma\omega^{-1/2} \quad (8.27)$$

$$Z'' = \sigma\omega^{-1/2} + 2\sigma^2 C_{dl} \quad (8.28)$$

from which

$$Z'' = Z' - R_u - R_{ct} + 2\sigma^2 C_{dl}. \quad (8.29)$$

This is the equation of a straight line of unit slope and with an intercept on the real Z' axis of $R_u + R_{ct} - 2\sigma^2 C_{dl}$.

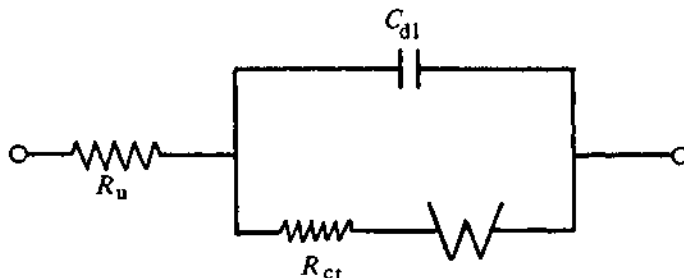


Fig. 8.15 — Equivalent circuit for an electrode reaction with double layer capacitance C_{dl} and uncompensated solution resistance R_u . The reaction resistance has been resolved into the charge transfer resistance R_{ct} and a Warburg impedance.

At high frequencies where the Warburg impedance is negligible in relation to R_{ct} the two components are:

$$Z' = R_u + \frac{R_{ct}}{1 + \omega^2 C_{dl}^2 R_{ct}^2} \quad (8.30)$$

$$Z'' = \frac{C_{dl} R_{ct}^2 \omega}{1 + \omega^2 R_{ct}^2 C_{dl}^2}. \quad (8.31)$$

Eliminating ω gives

$$(Z' - R_u - R_{ct}/2)^2 + (Z'')^2 = (R_{ct}/2)^2 \quad (8.32)$$

which is the equation of a circle centred on $Z' = R_u + R_{ct}/2$ with a radius of $R_{ct}/2$. A plot of the whole expression for Z'' vs Z' has the form shown in Fig 8.16. In this plot both the kinetically controlled (semicircular) and diffusion controlled (linear, unity slope) regions are displayed. However, a real system studied over a realistic frequency range (say 0.01 Hz to 10^4 Hz) might show only one of these regions [9]. For the $\text{Zn}^{2+} \rightarrow \text{Zn(Hg)}$ reaction in HClO_4 , for example, the onset of Warburg impedance behaviour is only just discernible at 20 Hz. In this case R_{ct} can be found by extrapolating experimental points on a semicircle to intercept the Z' axis. On the other hand the $\text{Hg}_2^{++} \rightarrow \text{Hg}$ reaction in HClO_4 shows a straight line relationship from 20 Hz to 20 kHz without any break to a semicircle. It is therefore a highly reversible reaction whose I_o cannot be measured by this means.

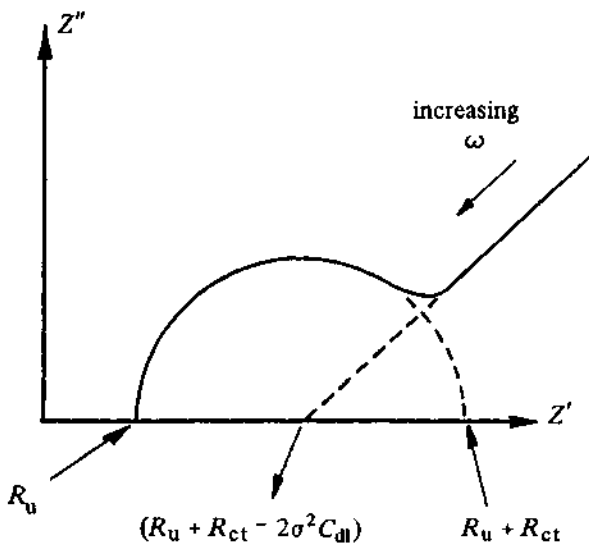
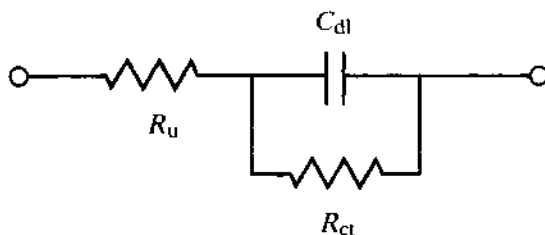


Fig. 8.16 – Complex plane impedance plot for the circuit of Fig. 8.15.

8.3.2 Measurement of interfacial capacitance

It was shown in the section on complex plane analysis that the double layer capacitance C_{dl} is obtainable from the maximum value of Z'' in the semicircular region, where $1/\omega C = R_{ct}$. There are situations, however, where C_{dl} is the prime quantity of interest, and in these cases the faradaic current is either zero or very small ($R_{ct} \rightarrow \infty$). Small-signal sinusoidal excitation is then a good way of measuring C_{dl} , and the analysis is a good deal simpler than the full complex plane analysis which is required when R_{ct} is small.

The equivalent circuit is



When R_u is zero and $R_{ct} \rightarrow \infty$, the admittance of the working electrode is simply that of C_{dl} , and so C_{dl} can be found from the amplitude of the excitation signal and the amplitude of the alternating current flowing, which will be entirely in quadrature with the excitation.

A real system which approaches this ideal closely is that of a mercury electrode at a potential where it is perfectly polarised. In aqueous KCl solution, for example, there is a region extending to about -1.8 V vs the $\text{Hg}/\text{Hg}_2\text{Cl}_2$ potential where the ideal condition of purely capacitance impedance holds good.

When a pair of in-phase and quadrature p.s.d.s. are used to analyse the current flowing in such a system, the in-phase current is zero and the quadrature current is directly proportional to the value of C_{dl} . The in-phase current therefore provides a convenient indicator of non-ideality (which can be produced by an appreciable uncompensated solution resistance, R_u , or a significant faradaic reaction) and can be used, as shown by de Levie [2], as a continuous monitor of correct cell conditions.

When the system is known to approach the ideal, it is not even necessary to measure the current phase-selectively, a measurement of the total a.c. being sufficient to characterise C_{dl} . This technique has been termed *tensammetry*, the applications of which have been described in detail by Breyer & Bauer [10]. In view of the fact that R_{ct} is large for irreversible processes, tensammetry may be a useful technique, even if a faradaic current, easily detectable by ordinary d.c. polarography, is flowing. A good example of this is oxygen reduction at mercury in aqueous solution, which gives two irreversible reduction waves. The double layer capacitance of mercury can be measured by tensammetry, therefore, without the necessity to deoxygenate the solution.

A comprehensive treatment of the information about double layer structure and adsorption of organic surfactants that can be obtained for both solid and liquid metals by measurements of double layer capacitance has been published by Damaskin, Petrii, & Batrakov [11] (see also Chapter 5).

8.3.3 A.C. voltammetry

This term is used to cover a range of techniques in which the mean potential is controlled potentiostatically and swept over a range while a small amplitude, relatively high frequency alternating potential superimposed on the slowly-varying sweep is used to excite a sinusoidal response in the current, which is

then the recorded variable. Two distinct regimes are operative *vis-à-vis* diffusion in these experiments. The average potential serves to define the average surface concentrations of O and R. These are modulated, on a much shorter timescale, by the alternating potential, so that the 'a.c.' diffusion layer is much thinner than the pseudo-steady state diffusion layer produced by the fact that the average potential is no longer equal to E_e , the equilibrium value.

Among the experimental possibilities are: the mean potential may be swept in one direction or cyclically, the fundamental a.c. response or a higher harmonic may be recorded, and the method may be applied to dropping mercury, sessile drop, or solid electrodes. In all these cases, there is usually some advantage to be gained over the corresponding d.c. technique, be it conventional cyclic voltammetry or direct-current polarography, although this is obtained, of course, at the expense of some instrumental elaboration. Typical advantages include greater precision and sensitivity to faradaic currents, greater ease of measuring data because of the peaked shape of the a.c. curves, a high degree of immunity to double-layer charging effects, and in some cases good selectivity in terms of the mechanism of follow-up chemical reactions.

8.3.3.1 A.C. Polarography

Polarography is here taken to mean the use of a dropping mercury electrode (D.M.E.) with a potential scan that is slow enough that each drop sees a virtually constant potential. Considering a reversible system, we have seen that the current leads the potential phasor by 45° . The amplitude I of the current density is measured for a fixed amplitude ΔE of the alternating potential, and is given by

$$I = \frac{n^2 F^2 \omega^{1/2} D^{1/2} c_O^\infty \Delta E}{4RT \cosh^2 a/2} \quad (8.33)$$

where $a = (E_{dc} - E_{1/2})nF/RT$.

This is the equation of a symmetrical bell-shaped curve (Fig. 8.17(a)) centred on $E_{1/2}$, peak height I_p . Rewriting the equation in terms of peak height gives:

$$E_{dc} = E_{1/2} + \frac{2RT}{nF} \ln \left[\left(\frac{I_p}{I} \right)^{1/2} - \left(\frac{I_p - I}{I} \right)^{1/2} \right]. \quad (8.34)$$

When considering these expressions, it should be remembered that a dropping electrode will give an oscillating current as the drop grows and falls, see Fig. 8.17(b), the exact shape of the recorded polarogram depending upon the damping time constant of the recorder.

The main features of the curve, however, are best seen with the averaged, smooth curve, and they can be summarised as showing a direct proportionality between I_p and n^2 , $\omega^{1/2}$ and c_O^∞ . The width at half-peak is $90/n$ mV at 298 K. The shape of the curve depends on the same approximations holding true as before, i.e. the diffusion field is effectively planar, and ΔE is small enough (about $10/n$ mV or less) for the current-potential relationship to be linear.

The foregoing analysis applies to reversible systems, i.e. those exhibiting a

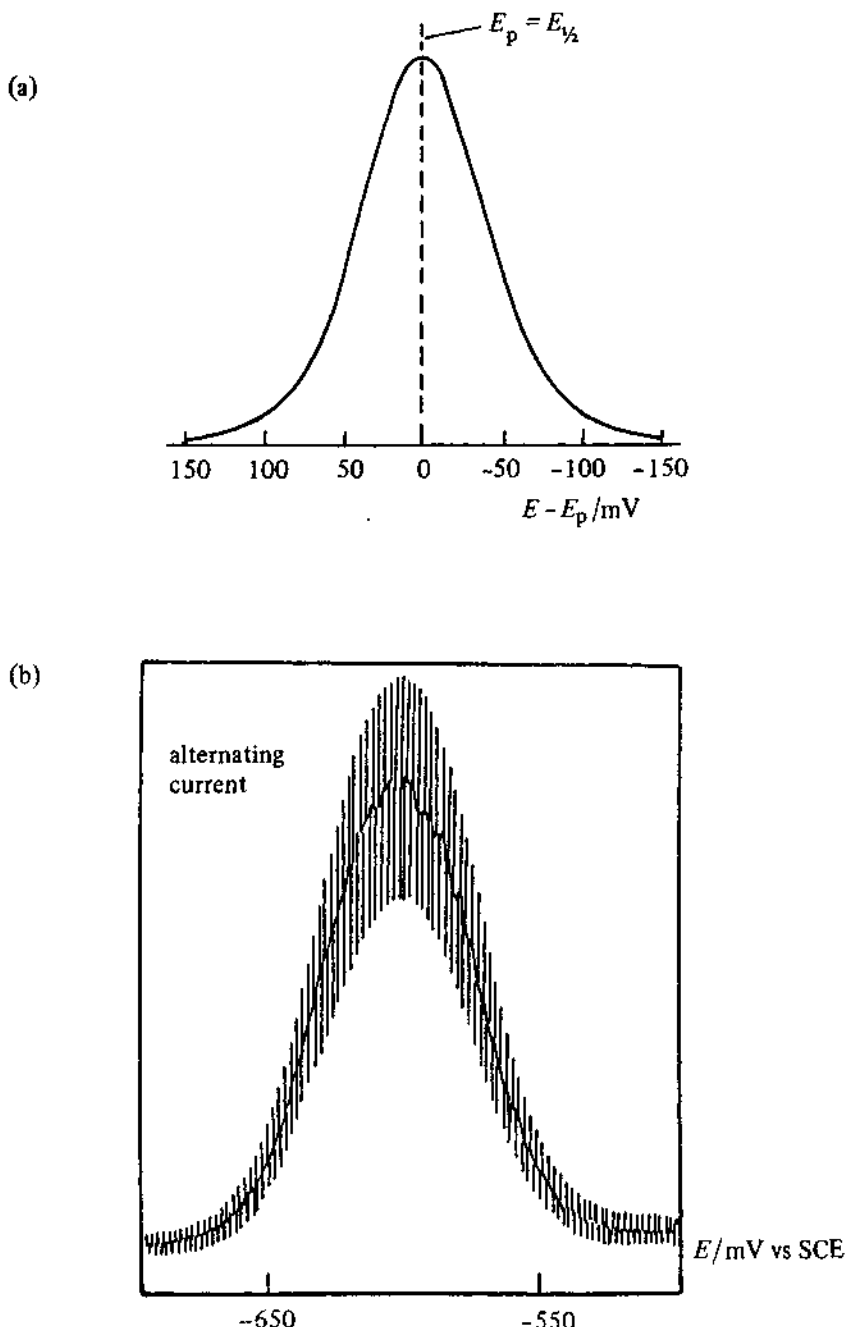


Fig. 8.17 – (a) Shape of a reversible a.c. voltammetric peak following Equation (8.34) with $n = 1$. (b) An a.c. polarogram for Cd^{2+} (3 mmol dm^{-3}) in Na_2SO_4 (1 mol dm^{-3}) with $\Delta E = 5 \text{ mV}$, $\omega/2\pi = 320 \text{ Hz}$. Reproduced with permission from D. E. Smith, *Anal. Chem.*, **35** (1963), 1811.

Warburg impedance. As we have seen, some systems can move to partial or total kinetic control as ω is increased. In these regions, called *quasi-reversible* and *irreversible* respectively, the symmetrical bell-shaped a.c. polarogram is no longer observed, the response becoming skewed and the peak height falling dramatically, see Fig. 8.18. Limiting behaviour is reached when the frequency is so high that $R_{ct} \gg \sigma/\omega^{1/2}$ so that the current is entirely limited by kinetics. I_p will then be independent of ω .

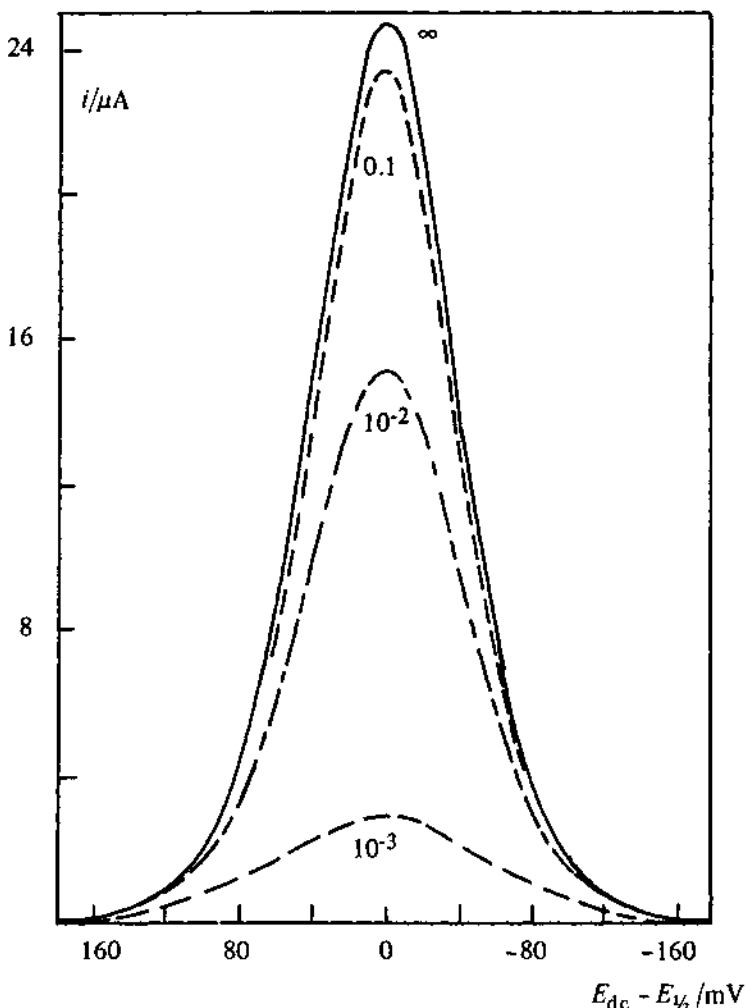


Fig. 8.18 – Calculated a.c. polarograms for quasi-reversible systems, showing decreasing peak height with decreasing exchange current at fixed frequency (2000 s^{-1}); $\Delta E_p = 5\text{ mV}$. Exchange current densities shown in A cm^{-2} . Reproduced with permission from D. E. Smith, *Electroanal. Chem.*, 1 (1966), 1.

Other systems may be so irreversible that the Warburg response is not seen at any frequency, however low. In these cases the peak height will always be very small in comparison with that for a reversible couple. This would naturally be seen as a disadvantage from the point of view of analytical chemistry, but the discrimination of the a.c. method against irreversible systems can be a positive advantage. For example, the reduction of oxygen is irreversible, and so in a.c. polarography the necessity for deoxygenation of the electrolyte can be avoided when reversible systems are being studied.

The peak potential is displaced slightly away from $E_{1/2}$ with increasing irreversibility, but in the absence of ohmic drop errors the peak height is always proportional to bulk concentration.

8.3.3.2 Linear and cyclic a.c. sweep voltammetry

With stationary electrodes the diffusion layer cannot be renewed periodically as happens with the DME, so the question arises as to what shape should be expected for the alternating current during a slow potential sweep when the diffusion layer is growing continuously during the potential scan.

For reversible processes the answer turns out to be satisfactorily simple. The shape of the bell-shaped curve is just the same as for the D.M.E. average current. The shape does not change with scan rate, and the a.c. curve during a

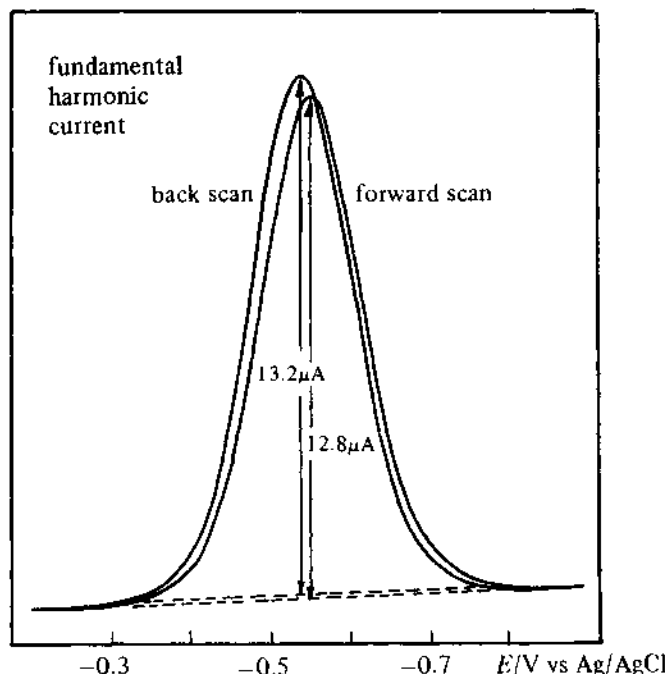


Fig. 8.19 – Cyclic a.c. voltammogram for 1 mmol dm^{-3} tris(acetylacetone) Fe(III) in acetone containing 1 mol dm^{-3} tetraethylammonium perchlorate at a Pt electrode, $\Delta E = 5 \text{ mV}$, $v = 100 \text{ mV s}^{-1}$ at a frequency of 400 Hz. Reproduced with permission from A. M. Bond, R. J. Halloran, I. Ruzic, & D. E. Smith, *Anal. Chem.*, 48 (1976), 872.

reverse scan *retraces* the forward scan. This superimposition is a good indication of reversibility. The peaked curve has a baseline of zero, which means that it may be easier to use in analytical applications than the cyclic voltammogram.

When there is a degree of irreversibility this is manifest in the cyclic voltammogram as a larger peak separation and a lowering of the forward and reverse peaks. As might be expected, irreversibility shows up in the a.c. response in a similar way (Fig. 8.19). The peaks on the forward and reverse scans are separated and are of unequal height. Fuller reviews of a.c. methods in analytical chemistry are available [12, 13].

The theory of cyclic voltammetry for reactions complicated by follow-up chemical steps or catalytic effects is in a quite highly developed state (see Chapter 6). Methods using a superimposed sine wave have been used in these circumstances [14], but the theory is as yet not so complete. Again, the incentive to use the a.c. technique stems mainly from the more convenient shape of the responses and the higher precision obtainable.

8.3.4 Impedance analysis of more complicated systems

8.3.4.1 Mass transfer – forced convection

The solution given previously for the a.c. impedance of a diffusion-limited current was for the case of linear diffusion, i.e. convection processes, whether natural or forced, being negligible. The impedance for situations of forced convection, e.g. the rotating disc electrode and the streaming mercury electrode, have also been worked out by applying the Nernst diffusion layer concept. This assumes that the diffusion layer has a certain fixed thickness δ dependent on the stirring conditions (e.g. the rotational speed of a rotating disc), and that the concentration profiles of reactants and products are linear across the diffusion layer. The expression for the mass transfer impedance has the following form [8] :

$$Z' = \sigma\omega^{-1/2} \frac{\sinh(2u) + \sin(2u)}{\cosh(2u) + \cos(2u)} \quad (8.35)$$

$$Z'' = \sigma\omega^{-1/2} \frac{\sinh(2u) - \sin(2u)}{\cosh(2u) + \cos(2u)} \quad (8.36)$$

where $u = \delta(\omega/2D)^{1/2}$ and σ is defined in Equation (8.21). If $\delta \rightarrow \infty$, as with an unstirred solution, this expression gives Z equal to a Warburg impedance. Moreover, the Warburg impedance should always be obtained when the frequency is high enough such that the diffusion layer thickness is much smaller than the hydrodynamic layer thickness.

8.3.4.2 Porous electrodes

Calculating the impedance of a porous electrode is a difficult task which has usually been approached by proposing a shape for a single pore and modelling the electrode as an assembly of such pores of randomly distributed size. In calculating pore impedances the analogy with distributed electrical impedances

can be invoked. Although generalisations are hard to find, it has been claimed [15] that if the local impedance at a pore wall is Z , then the total impedance measured from outside the pore should be $Z^{1/2}$, and this has been experimentally verified in certain cases.

8.3.4.3 Reaction with adsorbed intermediates

The impedance of a heterogeneous reaction of the type



has been studied by a number of workers. The approach of Schumann [16] and Epelboim and co-workers [19] was to adopt the assumptions that the intermediate X is adsorbed according to the Langmuir isotherm, and that the electron transfer reactions follow the Tafel law. The impedance was calculated for finite and infinite diffusion fields for the reactant A .

For the case where the rate is entirely kinetically controlled, the following expression for the impedance was derived:

$$Z = \frac{1}{FA} \frac{k_1 c_A + k_2}{k_1 k_2 c_A \left[b_1 + b_2 + \frac{(b_1 - b_2)(-k_1 c_A + k_2)}{j\omega\beta + k_1 c_B + k_2} \right]} \quad (8.39)$$

where β is the maximum fractional surface occupancy of X , and b_1 and b_2 are Tafel law transfer coefficients.

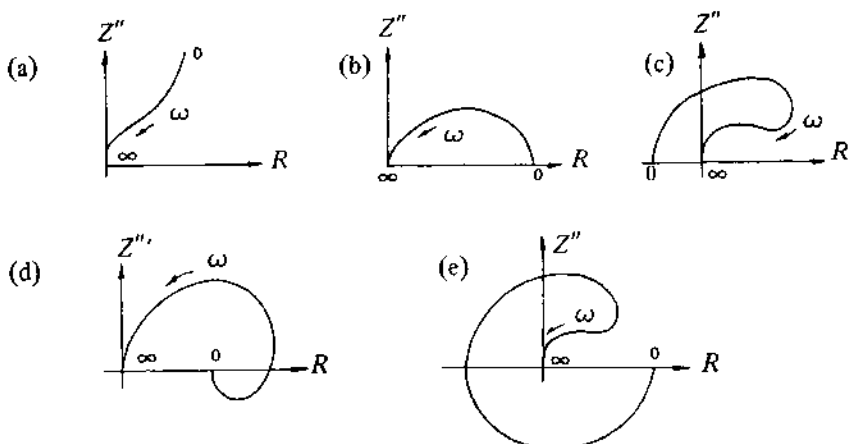


Fig. 8.20 – Possible shape of complex impedance plots characteristic of (a) a single passivating reaction, (b)-(e) passivation coupled with other reactions. Reproduced with permission from D. Schumann, *J. Electroanal. Chem.* 17 (1968), 45.

This equation is notable for the different aspects of the complex plane plots of Z that are predicted as the relative magnitudes of k_1 and k_2 are changed (i.e. for different points on the polarisation curve). Both capacitive (semicircles above the axis) and inductive behaviour (semicircles below the Z' axis) can be generated (see Fig. 8.20). An alternative approach with fewer assumptions has been taken by Armstrong *et al.* [17], who have extended the calculations to cover systems with a coupled homogeneous reaction and with a soluble intermediate species. These results have been reviewed by Armstrong, Bell & Metcalfe [14].

8.3.4.4 Anodic behaviour of metals

The anodic behaviour of metals encompasses several well-defined phenomena, such as active dissolution, passivity, and the active-passive transition, inhibition of dissolution, formation of bulk oxides, as well as other less well classifiable behaviour. The anodic behaviour of iron in sulphuric and nitric acids has generated a great number of papers and the following example can be taken as an indication of the complexity of the processes involved.

In the study of the anodic behaviour of iron [18], a rotating ring electrode was employed to measure the 'steady state' curve for iron dissolution in 1 mol dm^{-3} sulphuric acid. The observed current-voltage result is the 'bell-shaped' curve (Fig. 8.21) which has a region of negative resistance on the passive branch. The

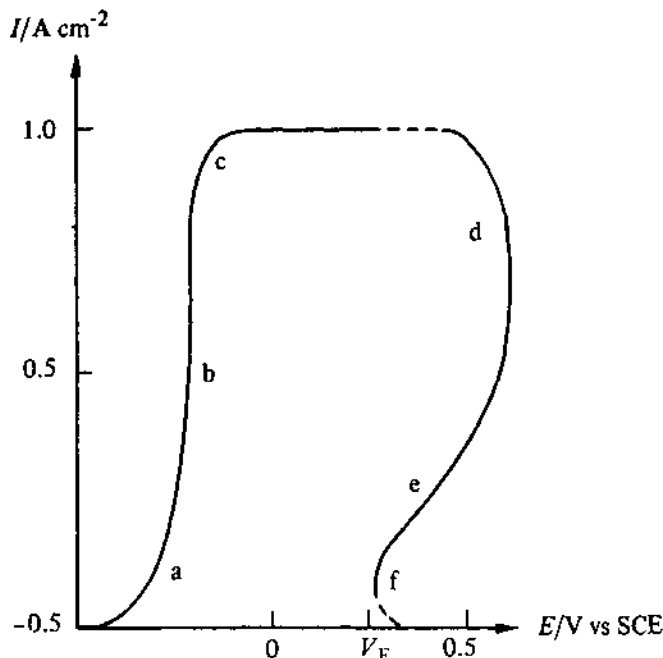
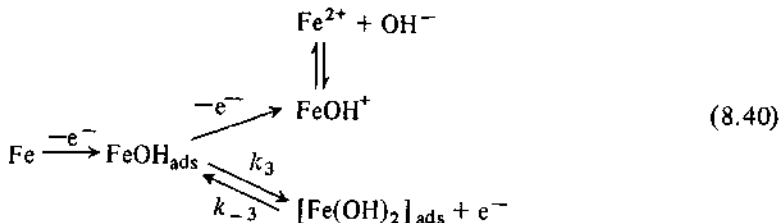


Fig. 8.21 – Dissolution of an iron rotating electrode in 1 mol dm^{-3} H_2SO_4 solution. Sections a, b and c show active dissolution, sections d, e and f show passivity. Reproduced with permission from I. Epelboin, C. Gabrielli, M. Keddam, & H. Takenouti, *Electrochim Acta*, 16 (1966), 913.

mechanism adopted proposes that iron dissolves through two consecutive single electron steps coupled by an intermediate adsorbed species FeOH_{ads} .



FeOH^+ decomposes in the solution by a fast chemical step, while passivation is brought about by the adsorption of $\text{Fe}(\text{OH})_2$. Fe_2O_3 is also thought to be involved in the passivation process. Other equilibria are necessary to account for the large currents observed in spite of the very low OH^- concentrations present in this strong acid solution. The assumptions necessary to calculate the current for this mechanism include those of Langmuir adsorption, Tafel rate law and, and certain others on the rates of diffusion. A polarisation curve was calculated, and by differentiation at various points the complex impedance as a function of frequency was obtained. Good agreement between theory and experiment was claimed. The steady state and impedance diagrams are shown in Fig. 8.22. The curves show features such as negative resistance and inductance noted previously for complex reaction schemes involving adsorbed intermediates.

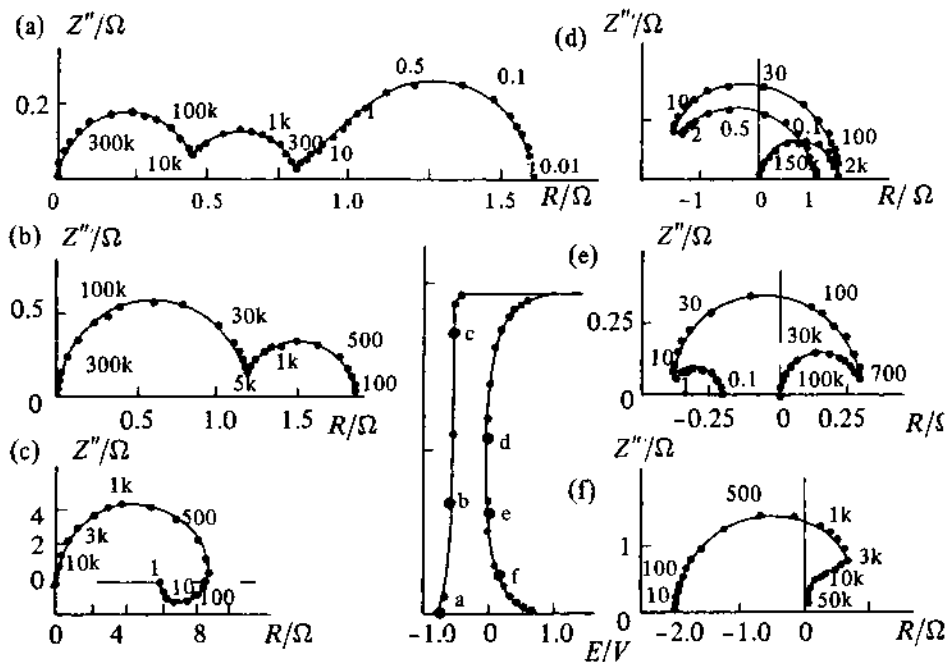


Fig. 8.22 – Calculated impedance diagrams for iron dissolution (a-f). These are derived from the points indicated on the simulated polarization curve (A). Reproduced with permission from I. Epelboin, C. Gabrielli, M. Keddam, & H. Takenouti, *Electrochim. Acta*, 16, (1966), 913.

The subject of the study of passivation processes by impedance analysis has been extensively reviewed by Epelboin *et al.* [19]. Other areas where the impedance method has been developed include solid electrolytes and superionic conductors [20], electrocrystallisation [21] and state-of-charge testing of primary batteries [22]. Numerous other examples of the use of a.c. techniques have been collected together by Gabrielli [23].

8.4 GRAPHICAL REPRESENTATION OF RESULTS

8.4.1 Bode plots vs complex plane diagrams

The papers referred to in the section on a.c. analysis of complex systems have all presented results as plots in the complex impedance (or admittance) plane, and this is very often a good way to gain a synoptic view of a system. However, it is not always true that it is the best way, as has been pointed out by Cahan [24], who advocates the Bode plot as a clearer way of presenting impedance data. This consists of two curves, that of the logarithm of the modulus of the impedance, ($\log |Z|$), and of the phase angle, ϕ , plotted with a common abscissa of log frequency. On such a plot, a pure resistance is represented by a horizontal line and a constant ϕ of 0° , while a pure capacitance is a straight line of slope -1 and a constant ϕ of -90° . A Warburg impedance is a straight line of slope $-\frac{1}{2}$ and a ϕ of -45° .

The Bode plots for some simple equivalent circuits are shown in Figs. 8.23 and 8.24. The rounded transition between horizontal and sloping section is usually called a corner, and the frequency of the intersection of lines extrapolating the

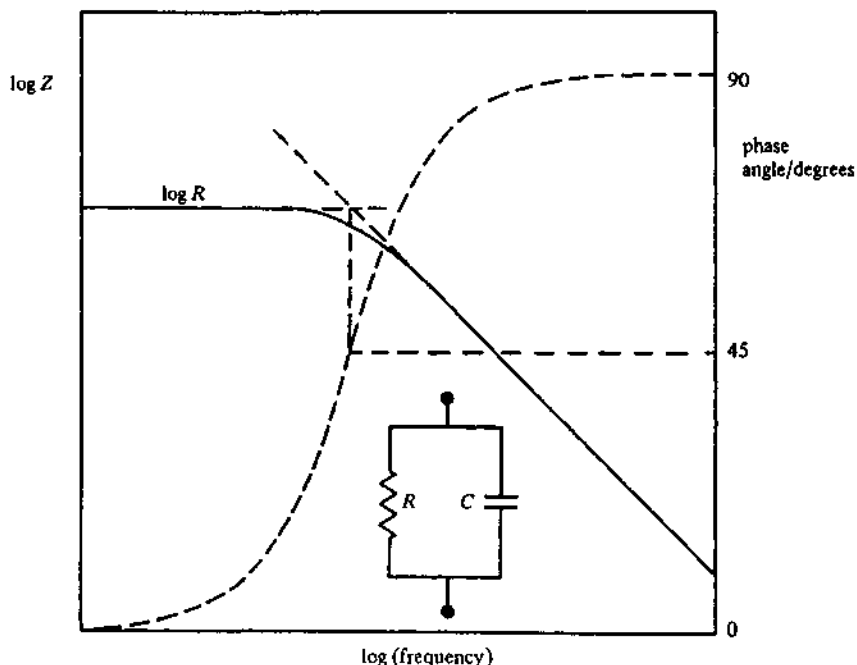


Fig. 8.23 -- Bode plot for a parallel RC circuit.

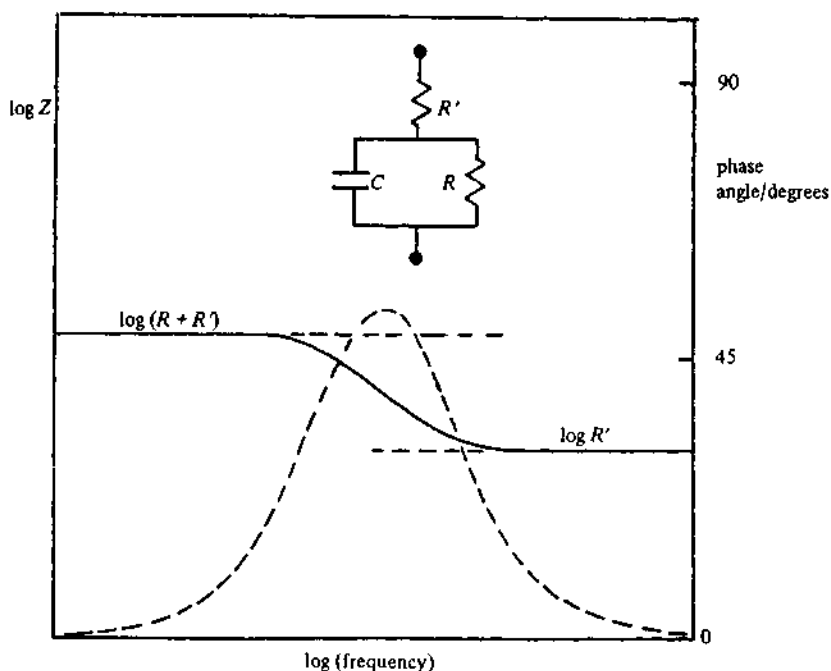


Fig. 8.24 – Bode plot for a series-parallel three-element circuit.

straight sections is the corner frequency. In theoretical Bode diagrams, the $\log |Z|$ plots are often approximated by straight lines, omitting the rounded transitions. It is noticeable that the phase plots are more 'sensitive' in that they show a marked departure from their asymptotic values about one frequency decade earlier and later than do the $\log |Z|$ lines.

The transitions between asymptotic values do, of course, mark those frequency regions where the ohmic and capacitive reactions have comparable values, with neither one completely dominant, so their counterpart in the complex plane plots are semicircular sections.

Frequencies are not indicated explicitly on the complex plane plot, and individual points have to be labelled with the measured value of f . This can be difficult to do because of overcrowding on the plot. Moreover, a change in value, for example of a capacitance, still retains the overall aspect of a semi-circle, the change being apparent only in the different position of a given frequency on the curve. In the Bode plot, a separate curve can be plotted which is displaced on the frequency axis. It should be apparent that, although the type of curve that is plotted will to some extent be a matter of taste, the Bode representation is more suited to systems that have several time constants and where one or more of these is changing e.g. with time or with electrode potential. Because the complex impedance plane has linear axes, more than one diagram will usually be necessary if the time constants are widely separated, as otherwise parts of the plot will be too cramped.

8.4.2 Kramers-Kronig analysis

The Kramers-Kronig relationships between the real and complex parts of quantities representing physical quantities such as absorbance and impedance have long been known to scientists in such fields as optics and radio engineering, but it has only fairly recently been pointed out [25] that they are a useful adjunct to electrochemical impedance analysis.

The relationships are integral equations which can be written in various forms [26]. Choosing a logarithmic form for phase shift ϕ and impedance modulus $|Z|$:

$$\phi_c = \frac{1}{\pi} \int_{-\infty}^{\infty} \frac{d \ln |Z|}{du} \ln \left| \frac{\omega + \omega_c}{\omega - \omega_c} \right| du \quad (8.41)$$

where $u = \ln(\omega/\omega_c)$

$$\ln \frac{Z_c}{Z_\infty} = -\frac{1}{\pi \omega_c} \int_{-\infty}^{\infty} \frac{d(\omega \phi)}{du} \ln \left(\operatorname{coth} \frac{|u|}{2} \right) du \quad (8.42)$$

$$\ln \frac{Z_c}{Z_0} = -\frac{\omega_c}{\pi} \int_{-\infty}^{\infty} \frac{d\phi}{du} \ln \left(\operatorname{coth} \frac{|u|}{2} \right) du . \quad (8.43)$$

Equation (8.41) gives the phase shift ϕ_c at one particular frequency ω_c as an integral of the impedance modulus over *all* frequencies. Equations (8.42) and (8.43) similarly give the impedance modulus compared with the impedance at infinitely high frequency or zero frequency as an integral of the phase shift over all frequencies.

The K-K relationships are purely mathematical ones which can be obtained from the properties of continuous functions of a complex variable. To be applicable to a physical system, that system must have the following properties:

- (i) The system should be causal, i.e. the applied voltage causes the measured current to flow.
- (ii) The relationship between current and potential should be linear.
- (iii) The system should be stable, i.e. if the applied potential is removed the current will fall to zero.
- (iv) The impedance should be finite at all frequencies, including $\omega = 0$ and $\omega = \infty$.

There are certain difficulties in applying the K-K criteria to electrochemical systems, the most obvious of which is that an integration over an *infinite* range of frequencies is required. In practice, infinite means over a very wide range of frequencies, and as a rule of thumb the range can be taken as extending two decades below the minimum, through to two decades above the maximum frequency at which any variation in phase is apparent. For the simplest system therefore a four-decade frequency range is required, and many systems will require a six- or seven-decade range.

The four conditions may not be as easy to satisfy as may be thought at first glance, and the finiteness condition (iv) poses theoretical difficulties when the system contains a Warburg impedance. The Warburg impedance is infinite at zero frequency, although in practice this would imply a diffusion layer of infinite thickness. It has been shown [25], however, that because the contribution of the Warburg impedance to the integrals is low at very low frequencies, the complementary integrals are well-behaved.

It is important to realise that the complementarity between phase and impedance modulus implied in Equations (8.41)-(8.43) is a property of any passive network composed of resistors, capacitors and inductors. Such a network is said to be K-K transformable. Therefore if an electrochemical system is to be represented by an equivalent passive network, which is one of the objectives in impedance analysis, the measured impedance must be K-K transformable. Note that this is a necessary but not a sufficient condition, i.e. the fact that a measured response satisfies the K-K integral equations is not a guarantee that it is a true response from the electrochemical system under investigation!

Cahan & Chen [27] have retrospectively analysed some published impedance data on corroding systems and found that although apparently well-behaved semicircular plots were obtained in the complex plane, the data were not K-K transformable and could not be represented as an equivalent passive network as has been claimed. Corroding systems and those involving electrodeposition are bound to be suspect as far as criteria (iii) and (iv) (stability and finiteness) are concerned, because any area change brought about by the exciting signal at low frequencies may not be exactly reversed during the negative part of the cycle. A K-K analysis should therefore form part of any thorough-going study of impedance.

REFERENCES

- [1] R. Greef, *J. Phys. E*, **11** (1978) 1.
- [2] R. de Levie & A. A. Husovsky, *J. Electroanal. Chem.*, **20** (1969) 181.
- [3] *The 1170 and 1250 families of frequency response analyser*, Schlumberger-Solartron Electronic Group Ltd.
- [4] D. E. Smith, *Anal. Chem.*, **48** (1976) 221A and 517A.
- [5] S. C. Creason, J. W. Hayes, & D. E. Smith, *J. Electroanal. Chem.*, **47** (1973) 9.
- [6] C. Gabrielli, F. Huet, M. Keddam, & J. F. Lizée, *J. Electroanal. Chem.*, **138** (1982) 201.
- [7] J. E. B. Randles, *Disc. Faraday Soc.*, **1** (1947) 11.
- [8] M. Sluyters-Rehbach & J. H. Sluyters, *Electroanalytical chemistry* (A. J. Bard (Ed)), Vol. 4, Ch. 1, Marcel Dekker, (1970).
- [9] J. H. Sluyters & J. J. C. Oomen, *Rec. Trav. Chim.*, **79** (1960) 1101.
- [10] B. Breyer & H. H. Bauer, *Alternating current polarography and tensammetry*, Vol. 13 in *Chemical analysis*, P. J. Elving & I. M. Kolthoff (Eds), Wiley Interscience (1971).
- [11] B. B. Damaskin, O. A. Petrii, & V. V. Batrakov *Adsorption of organic compounds on electrodes*, Plenum Press, (1971).

- [12] A. J. Bard & L. R. Faulkner, *Electrochemical methods – fundamentals and applications*, Wiley, N.Y. (1980).
- [13] D. D. Macdonald, *Transient techniques in electrochemistry*, Plenum Press, N.Y. (1977).
- [14] R. D. Armstrong, M. F. Bell, & A. A. Metcalfe, *Electrochemistry* (Specialist Periodical Report) Vol. 6, Royal Society of Chemistry, London (1978) p. 98-127.
- [15] R. de Levie, *Advances in electrochemistry and electrochemical engineering*, Vol. 6, Wiley Interscience, N.Y. pp. 329-397 (1967).
- [16] D. Schumann, *J. Electroanal. Chem.*, 17 (1968) 45.
- [17] R. D. Armstrong, W. P. Race, & H. R. Thirsk, *J. Electroanal. Chem.*, 16 (1968) 517.
- [18] I. Epelboin, C. Gabrielli, M. Keddam, & H. Takenouti, *Electrochim. Acta*, 20 (1975) 913.
- [19] I. Epelboin, C. Gabrielli, M. Keddam, & H. Takenouti, *Comprehensive treatise on electrochemistry*, J. O'M Bockris, B. E. Conway & E. Yeager (Eds), Vol. 4, Plenum Press (1981).
- [20] R. D. Armstrong & K. Taylor, *J. Electroanal. Chem.*, 63 (1975) 9.
- [21] R. D. Armstrong & A. A. Metcalfe, *J. Electroanal. Chem.*, 71 (1976) 5.
- [22] S. A. G. R. Karunathilaka, N. A. Hampson, R. Leek, & T. J. Sinclair, *J. Appl. Electrochem.*, 10 (1980) 603.
- [23] C. Gabrielli *Identification of electrochemical processes by frequency response analysis*, Publication No. 004/83, Schlumberger Solartron Electronic Group Ltd.
- [24] B. D. Cahan & C. T. Chen, *J. Electrochem. Soc.*, 129 (1982) 700.
- [25] R. L. van Meirhaege, E. C. Dutoit, F. Cardon, & W. P. Gomes, *Electrochim. Acta*, 21 (1976) 39.
- [26] H. W. Bode, *Network analysis and feedback amplifier design*, D. van Nostrand, N.Y., (1945).
- [27] B. D. Cahan & C. T. Chen, *J. Electrochem. Soc.*, 129 (1982) 474.

9

ElectrocrySTALLISATION

Many important electrode reactions involve the formation of a solid phase, either as the result of the reduction of ions in solution, as in the case of metal deposition, or by oxidation of the electrode and subsequent reaction with anions to form an anodic film. The term *electrocrySTALLISATION* is used to describe electrode processes of this kind.

ElectrocrySTALLISATION involves a number of distinct steps which form the subject of this chapter:

- (1) diffusion of ions in solution to the electrode surface,
- (2) electron transfer,
- (3) partial or complete loss of the solvation sheath, resulting in the formation of ad-atoms,
- (4) surface diffusion of ad-atoms,
- (5) clustering of ad-atoms to form *critical nuclei* on a perfectly smooth surface or on a foreign substrate,
- (6) incorporation of ad-atoms at lattice sites,
- (7) development of crystallographic and morphological characteristics of the deposit.

These steps are illustrated schematically in Fig. 9.1.

Although, in practical terms, the last of these steps is of most interest, it is necessary to look more closely at the earlier stages of the electrocrySTALLISATION process in order to gain a fundamental understanding of the thermodynamics and kinetics of electrocrySTALLISATION. Unfortunately, the complexity of commercially important electrodeposition processes has restricted attempts at satisfactory

theoretical description, although the use of computer simulation methods offers the hope that a complete kinetic and mechanistic description may eventually be possible.

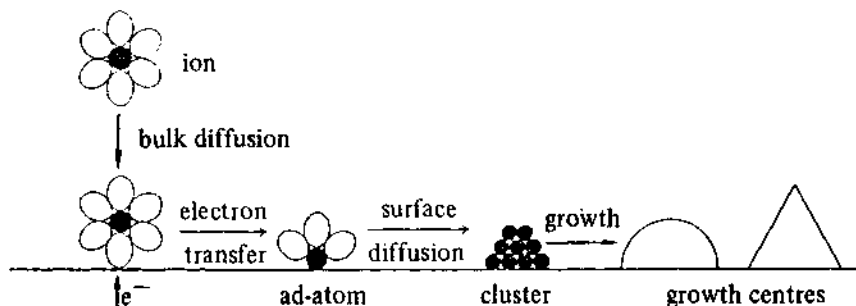


Fig. 9.1 ~ Some of the steps involved in the electrocrystallisation of a metal on a substrate of a different material such as carbon.

9.1 PHASE FORMATION FROM THE VAPOUR PHASE

9.1.1 Thermodynamic aspects

A proper thermodynamic description of electrochemical phase formation is necessarily complicated by the need to consider the changes in energy and entropy associated with the process as a whole. Fortunately, electrocrystallisation has many features in common with the growth of a solid phase from its supersaturated vapour, and it is useful to examine this simpler process first. In the case where two phases but only one component are present, phase formation involves the incorporation of atoms or molecules into a pre-existing surface of the solid, and the enthalpy change is therefore related to the transition



where ΔH_s is the enthalpy of sublimation. The solid is at equilibrium with its own vapour when the partial molar Gibbs free energy, or chemical potential, of the gas is exactly equal to that of the solid:

$$\mu_{M(g)} = \mu_{M(s)} \quad (9.2)$$

The chemical potential of the gas is related to its pressure (assuming ideal gas behaviour) by the expression

$$\mu_{M(g)} = \mu_{M(g)}^\ominus + RT \ln(p^*/p^\ominus) \quad (9.3)$$

so that Equation (9.2) effectively defines the equilibrium vapour pressure, p^* ; at a particular temperature. It follows from Equations (9.1) and (9.2) that spontaneous growth of the solid phase can only occur if the vapour pressure

exceeds p^* , in which case the vapour is said to be *supersaturated*. In practice, supersaturation of the vapour can be achieved by starting with the system at equilibrium and then lowering the temperature or increasing the pressure of the vapour. The free energy change associated with growth of the solid phase in the latter case is then given by

$$\Delta G = -RT \ln(p/p^*) \quad (\text{at constant } T) \quad (9.4)$$

where (p/p^*) is referred to as the *supersaturation ratio*.

The preceding treatment implies that the equilibrium vapour pressure depends only on the temperature of the system concerned. This will be true when the solid phase is present as a macroscopic solid with large surface area, but if the solid phase (or liquid phase) is present as small crystallites or droplets, the contribution of surface free energy must be taken into account.

9.1.2 Homogeneous nucleation from the vapour phase

Consider a spherical droplet of pure solid or liquid in contact with its vapour. The equilibrium is given by Equation (9.2), but it is now necessary to take account of the surface contribution to the total free energy. The equilibrium vapour pressure, p_r^* , under these circumstances depends on the radius of curvature, r , of the surface according to the *Kelvin equation*:

$$\ln(p_r^*/p_\infty^*) = \left(\frac{2\gamma\bar{V}}{RT} \right) \frac{1}{r} \quad (9.5)$$

where γ is the molar surface free energy (surface tension), \bar{V} is the molar volume of the condensed phase, and p_∞^* is the equilibrium vapour pressure in the limit that the radius of curvature tends to infinity ($1/r \rightarrow 0$). Equation (9.5) is important, since in principle the formation of a new phase must involve growth centres with radii of atomic dimensions. Although in fact these *nuclei* are so small that the use of bulk values of γ and \bar{V} may be suspect, it is clear that small centres should be inherently unstable unless the vapour pressure considerably exceeds the equilibrium value p^* .

If the free energy changes associated with the formation of the bulk and of the surface are considered separately, the overall free energy change has the following components (for a spherical centre)

$$\Delta G_{\text{surface}} = 4\pi r^2 \gamma \quad (9.6a)$$

and

$$\Delta G_{\text{bulk}} = \frac{4}{3}\pi r^3 \Delta G_v \quad (9.6b)$$

where ΔG_v is the free energy change *per unit volume* associated with the formation of the bulk phase. From Equation (9.4) it follows that

$$\Delta G_v = -\frac{RT}{\bar{V}} \ln(p/p^*) . \quad (9.7)$$

For $p > p^*$, ΔG_v is always a negative quantity, whereas γ the surface free energy, is positive. For a given value of p^* the surface and volume contributions therefore combine to produce a maximum in ΔG as a function of the radius of the nucleus as shown in Fig. 9.2. The following critical parameters can be defined:

r_c — the critical radius at which $(\partial \Delta G / \partial r) = 0$

and

ΔG_c — the critical free energy.

For a nucleus to evolve into a stable entity, its radius must exceed r_c . Fig. 9.2 makes it clear that this can only occur if thermal fluctuations in the system allow it to overcome the energy barrier ΔG_c , so that ΔG_c can be thought of as the free energy of activation for homogeneous nucleation from the vapour phase.

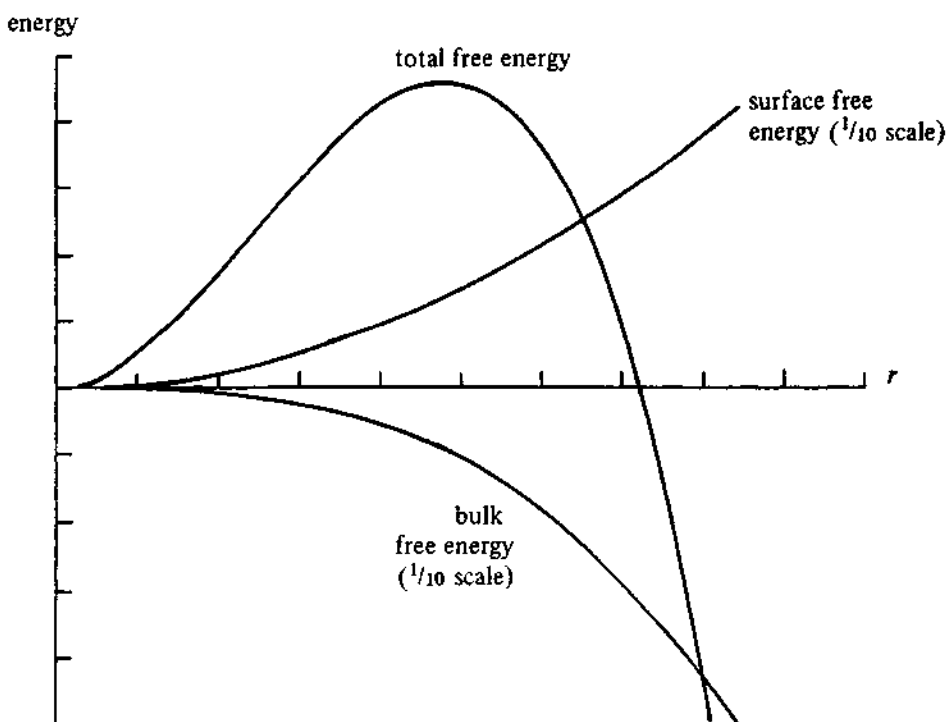


Fig. 9.2 — Schematic free energy curves for the homogeneous nucleation and growth of a spherical mercury droplet from the vapour phase. The contributions to the total free energy made by the surface and the volume are shown on a reduced scale.

9.2 ELECTROCHEMICAL PHASE FORMATION

9.2.1 The thermodynamics

In the case of electrochemical phase formation, equilibrium is established by electron transfer. Since the growth of the new phase occurs at the boundary between the electrode material and the solution, the nucleation process must be heterogeneous. Although it is necessary to take the properties of the substrate into account, it is also instructive to pursue the analogy with homogeneous nucleation from the vapour by assuming that the contact area between nuclei and the electrode is vanishingly small, i.e. that small spherical droplets are formed on a foreign electrode material. If the electrode process is of the general type,



the equilibrium electrode potential, E_e , is given by the Nernst equation, Equation (3.11). Under these equilibrium conditions the surface activity of ad-atoms has its equilibrium value $a_{M_{ads}}^*$. If the electrode potential is now changed to some new value ($E_e + \eta$), where η is the overpotential, the surface activity of ad-atoms will be determined by the relationship

$$\frac{a_{M_{ads}}}{a_{M_{ads}}^*} = \exp(-nF\eta/RT) . \quad (9.9)$$

The free energy of formation of the condensed phase is therefore, by analogy with Equation (9.7),

$$\Delta G_v = nF\eta/\bar{V} . \quad (9.10a)$$

or if \bar{V} is replaced by M/ρ , where M is the molecular weight and ρ the density of the deposit;

$$\Delta G_v = nF\rho\eta/M . \quad (9.10b)$$

The total free energy, ΔG_{net} , for a spherical nucleus resting on an electrode surface is therefore given by

$$\Delta G_{net} = \Delta G_{bulk} + \Delta G_{surf} \quad (9.11a)$$

or

$$\Delta G_{net} = \frac{4\pi r^3 \rho n F \eta}{3M} + 4\pi r^2 \gamma . \quad (9.11b)$$

A set of curves calculated from Equation (9.11b) is shown in Fig. 9.3. It is clear that the critical radius and the critical free energy depend on overpotential, and differentiation of Equation (9.11b) with respect to r gives the expressions for the maximum in the free energy curve:

$$\Delta G_c = \frac{16\pi M^2 \gamma^3}{3\rho^2 n^2 F^2 \eta^2} \quad (9.12a)$$

$$r_c = \frac{-2M\gamma}{nF\eta\rho} . \quad (9.12b)$$

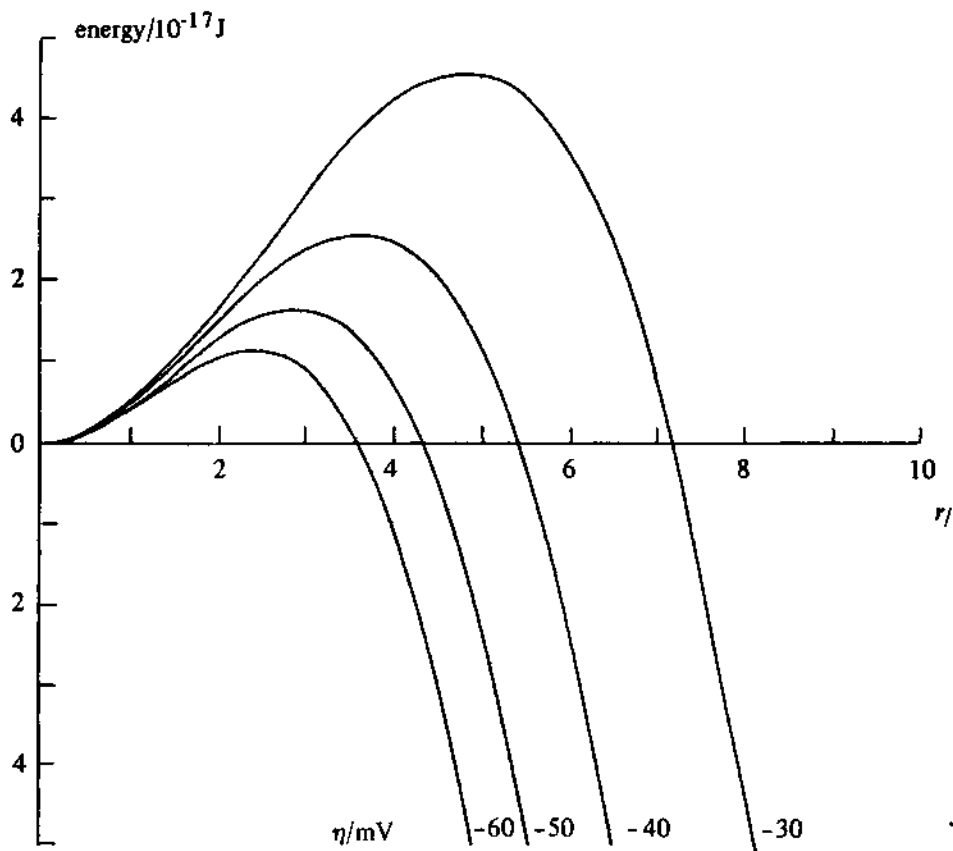


Fig. 9.3 – Free energy curves for the electrochemical nucleation of a spherical mercury centre at different overpotentials. Note that an increase in overpotential is equivalent to an increase in the supersaturation ratio in the case of nucleation and growth from the vapour phase.

An important prediction of the classical theory of electrochemical nucleation is therefore that the free energy of activation should depend on $1/\eta^2$ as shown in Fig. 9.4.

The preceding treatment corresponds to the case where nucleation is essentially homogeneous in the sense that it does not involve the substrate except in the electron transfer step. In practice, however, phase growth often involves a pre-existing surface of the same material. The free energy changes associated with the formation of a circular patch of radius r and height h (Fig. 9.5) under these conditions are given by

$$\Delta G_{\text{net}} = \Delta G_{\text{bulk}} + \Delta G_{\text{surf}} , \quad (9.13a)$$

that is,

$$\Delta G_{\text{net}} = \frac{\pi r^2 h n F \eta}{V} + 2\pi r h \gamma . \quad (9.13\text{b})$$

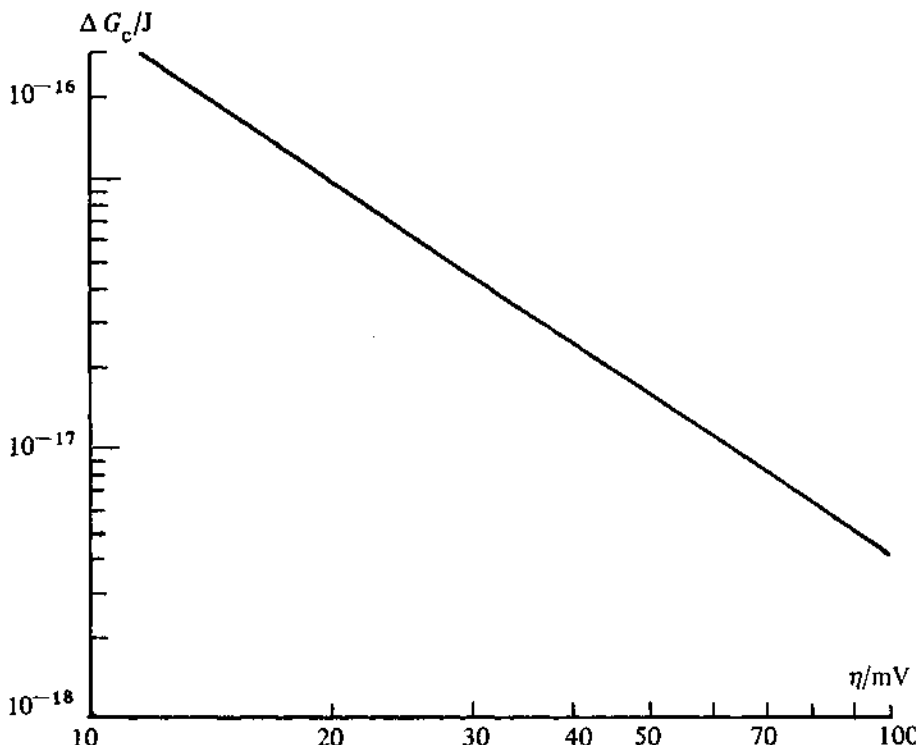


Fig. 9.4 – A double logarithmic plot of the critical free energy, ΔG_c , as a function of overpotential. The plot illustrates the inverse dependence of ΔG_c on η^2 (Equation (9.12a)) predicted by the classical theory of nucleation.



Fig. 9.5 – A disc-shaped growth centre which is considered in the treatment of the growth of monolayer deposits. The centre expands by incorporation of new material at its edges, but its height remains constant.

The important point to note here is that the new surface area created by the formation of such a patch of material is restricted to the edge of the disc. The corresponding free energy changes as a function of radius are shown in Fig. 9.6. The critical radius and critical free energy are now given by

$$r_c = -\gamma \bar{V}/nF\eta \quad (9.14a)$$

$$\Delta G_c = -\pi h\gamma^2 \bar{V}/nF\eta , \quad (9.14b)$$

or if \bar{V} is replaced by M/ρ ,

$$r_c = -\gamma M/nF\rho\eta \quad (9.15a)$$

and

$$\Delta G_c = -\pi h\gamma^2 M/nF\rho\eta . \quad (9.15b)$$

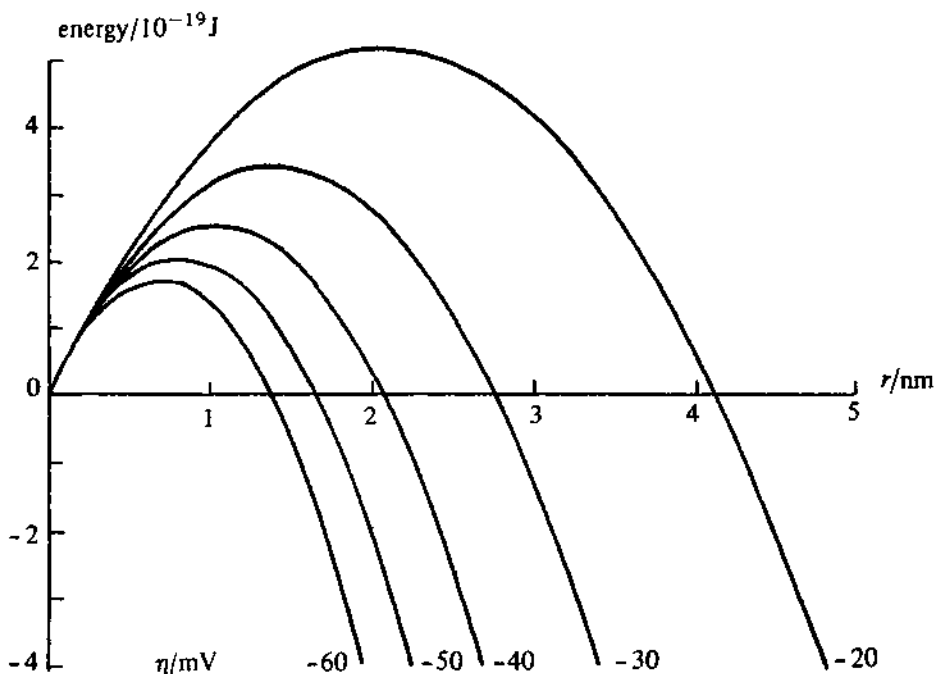


Fig. 9.6 -- Typical free energy curves calculated for the formation of a monolayer deposit of a metal on a pre-existing surface of the same material. Note that in this case the new area created by the expansion of the growth centre is associated only with its edge.

The 'classical' approach to nucleation outlined above is subject to criticism on several grounds. In the first place, the thermodynamic properties of small clusters are assumed to be identical to those of the bulk phase at equilibrium. At the same time, the subdivision of free energy terms into bulk and surface

contributions implies an abrupt discontinuity in the molecular environment at the interface, whereas the surface thickness of the liquid–vapour transition has been calculated to correspond to several molecular diameters. The properties of small clusters of atoms (less than a few hundred) will therefore differ appreciably from those of the bulk material. The small values of critical radius calculated from the classical theory (see Fig. 9.3) therefore reveal an internal inconsistency which probably restricts the use of the theory to a formal qualitative description of the nucleation process.

9.2.2 Microscopic aspects of phase formation

At the microscopic level, the process of phase growth involves incorporation of atoms at lattice sites in the surface of the solid. A real crystal surface presents a richly differentiated array of sites at which an atom can be incorporated; only in rare cases will the surface be perfectly uniform at the atomic level, and even single-crystal surfaces have distinguishable surface sites. The electrochemical growth of solid phases under most conditions involves structural defects such as screw dislocations, and the thermodynamic treatment outlined in the preceding sections is no longer appropriate. The fact that growth on a perfect single crystal surface involves a number of different sites was first discussed by Kossel and Stranski [1, 2] in the context of crystal growth from the vapour phase. The difference in energy associated with the incorporation (or removal) of atoms from different sites can be related to the effective coordination number of the sites. Fig. 9.7 shows that the following sites can be characterised by their cubic coordination number, m .

- | | |
|-----------------------|-----------|
| (i) surface sites | $(m = 1)$ |
| (ii) edge sites | $(m = 2)$ |
| (iii) kink sites | $(m = 3)$ |
| (iv) edge vacancies | $(m = 4)$ |
| (v) surface vacancies | $(m = 5)$ |

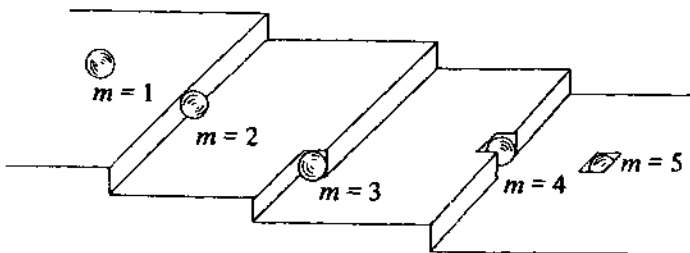


Fig. 9.7 – The cubic coordination sites considered in the Kossel–Stranski theory of phase growth. The different sites are conveniently distinguished by their cubic coordination number, m , as shown in the figure.

In the case of crystal growth from the vapour phase, the energy change involved in lattice incorporation can be related approximately to the enthalpy of subli-

mation, and it is clear that the most favourable sites for deposition are those with high values of m . In the case of electrochemical nucleation the situation is more complicated, since it is possible that the charge-transfer reaction does not produce a neutral atom, but rather a species which has some residual or partial charge and which retains part of its hydration sphere as shown in Fig. 9.8. Conway & Bockris [3] have attempted to calculate the energy changes involved in the formation of these *ad-ions*, and they have concluded that charge transfer reactions are favoured on the plane surfaces, rather than at steps or kinks. Lattice growth at step or kink sites must therefore involve surface diffusion of surface ad-ions. Lattice incorporation at different sites results in further loss of the hydration sheath until eventually the atom is incorporated into the surface and becomes indistinguishable from its neighbours.

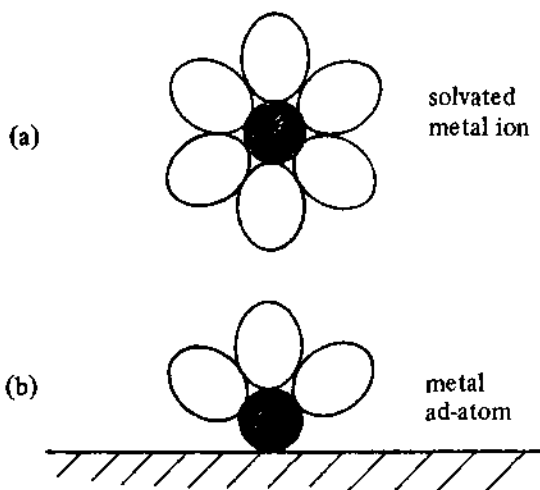


Fig. 9.8 – The formation of an ad-atom by the reduction of a solvated metal ion in solution. The ad-atom may still retain a partial solvation sphere since there can be a dipole associated with the ad-atom/substrate interaction.

The problem with this simple picture is that real macroscopic solids are not perfect. The growth of crystals nearly always involves structural defects in the solid, the best known example being the spiral growth which takes place at emergent screw dislocations as shown in Fig. 9.9. The theory of crystal growth at spiral dislocations has been developed by Burton, Cabrera, & Frank [4], and extensions to the electrochemical case are relatively straightforward [5, 6]. The interaction of closely spaced screw dislocations can lead to macroscopic steps which reveal the shape of the dislocation; an example is shown in Fig. 9.10. The most important property of the screw dislocation is that it propagates as atoms are incorporated, maintaining an energetically favourable condition for further growth (or removal). By contrast, a crystal plane without dislocations will eventually require the incorporation of atoms onto the plane, the least energetically favourable situation, and growth therefore slows considerably

when this stage is reached. It has proved possible to grow dislocation free metal crystals by electrochemical methods, and a series of elegant studies by Budevski and co-workers [7] has demonstrated the periodic nature of crystal growth which follows from the Kossel-Stranski model.

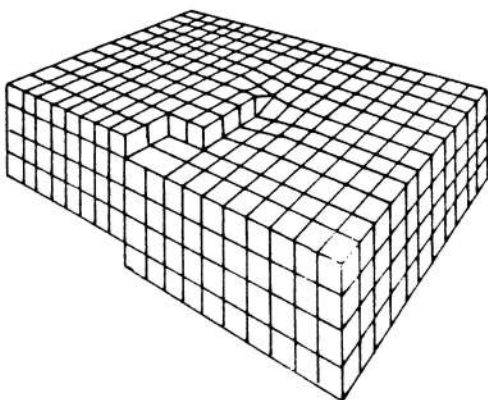


Fig. 9.9 – The formation of a screw dislocation by the displacement of atoms shown in the figure creates an edge at which lattice incorporation can occur. The edge then propagates, allowing further growth without the need for the formation of new growth centres by nucleation.



Fig. 9.10 – Screw dislocation on a copper surface grown in $\text{CuSO}_4 (1 \text{ mol dm}^{-3}) + \text{H}_2\text{SO}_4 (1 \text{ mol dm}^{-3})$ at 298K and under pulsed current conditions. Reproduced with permission from H. Seiter, H. Fischer, & L. Albert, *Electrochim. Acta*, 2, (1960), 97.

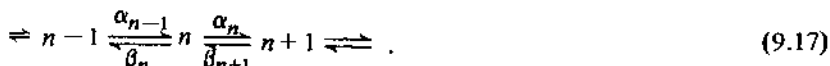
9.2.3 Kinetics of nucleation

The treatment of electrochemical kinetics is greatly simplified by the use of the concept of the *rate determining step*. In the case of electrocrysallisation, any one of the first six steps listed at the beginning of this chapter can be the slowest – and hence rate-determining step, but it is convenient to consider for the moment that electron transfer and subsequent changes in solvation are rapid. On the other hand, if the formation of a critical nucleus is necessary for phase growth to occur, the rate of electrocrysallisation may be largely determined by the frequency with which new growth centres appear. The thermodynamic treatment of phase formation outlined in section 9.2.1 demonstrates that the free energy of a centre passes through a maximum at the critical radius r_c . Centres with radii less than r_c are therefore unstable, whereas those with radii exceeding r_c will tend to grow. The formation of critical nuclei must therefore occur by thermal fluctuations of the system, and the rate constant for nucleation is related to the energy barrier ΔG_c by an expression of the form

$$A = F \exp(-\Delta G_c/k_B T) \quad (9.16)$$

where F is a pre-exponential factor.

A more satisfactory understanding of the kinetics of nucleation is obtained by considering the formation of clusters of atoms by the subsequent addition of monomers or ad-atoms [8]. In the steady state, the rates of addition and loss of monomers must be equal, and the distribution of clusters is determined by equilibria of the form



As the cluster size increases towards a critical value, the point is approached where further addition of monomer results in the formation of a stable growth centre, and the centre is no longer involved in the steady state distribution. This can be accounted for by considering that supercritical clusters are removed and reintroduced as the equivalent amount of monomer, and solution of the set of steady state equations based on Equation (9.17) then leads to the steady state nucleation rate, J_s , as

$$J_s = Z \alpha_{n^*} \bar{c}_{n^*} \quad (9.18)$$

where α_{n^*} is the rate at which monomers are added to the critical cluster of n^* atoms, \bar{c}_{n^*} is the equilibrium concentration of critical clusters, and Z is a dimensionless ‘non-equilibrium’ factor, usually called the *Zeldovich factor*, which accounts for the fact that clusters are removed from the steady state distribution as they approach the critical size. The equilibrium concentration of critical clusters is related to the concentration of monomers by the Boltzmann expression

$$\bar{c}_{n^*} = \bar{c}_1 \exp\left(-\frac{\Delta G_{n^*}}{k_B T}\right) \quad (9.19)$$

so that the nucleation rate depends on ΔG_{n*} , which is identical with ΔG_c in the thermodynamic treatment.

The kinetics of heterogeneous nucleation differs from the treatment given above, since nuclei may form at preferred or active sites on a surface. The value of ΔG_n^* therefore depends on the nature of the substrate, and, in the case of electrocrystallisation, on the electrode potential. If we define the number of active sites under particular experimental conditions as N_0 , the rate of appearance of stable growth centres is expected to follow first order kinetics, with the number density of centres given by

$$N(t) = N_0 [1 - \exp(-At)] . \quad (9.20)$$

In the limit that $At \gg 1$, Equation (9.20) becomes

$$N(t) = N_0 , \quad (9.21)$$

whereas for small values of At the nuclear number density is given by

$$N(t) = N_0 At \quad (9.22a)$$

$$\text{or } N(t) = A't . \quad (9.22b)$$

In these expressions A is the first order nucleation rate constant, and the limiting cases described by Equations (9.21) and (9.22) are referred to as *instantaneous* and *progressive* nucleation respectively. They have been used extensively as part of the description of nucleation and growth on foreign substrates (discussed in sections 9.3 and 9.4).

9.2.4 Surface diffusion

In the case where electrocrystallisation occurs at a preexisting surface of the bulk phase, the slowest step may involve the diffusion of ad-atoms or ad-ions to the sites at which they are incorporated into the crystal lattice. A growing surface will generally have a high density of growth sites at which lattice incorporation occurs. The sites will often be at spiral dislocations, or if the crystal surface is free of defects, they will be of the type described by the Kossel-Stranski theory. In the case of a growing spiral dislocation, the surface is characterised by a number of steps and the incorporation of atoms at these steps gives rise to a surface diffusion flux. If we assume that the concentration of ad-atoms, c_{ad} , at the steps approaches the equilibrium value \bar{c}_{ad} , the solution of the diffusion problem is straightforward since the boundary conditions are

$$c_{ad}(0) = \bar{c}_{ad} \quad (9.23)$$

$$c_{ad}(2x_0) = \bar{c}_{ad} \quad (9.24)$$

where $2x_0$ is the separation between two adjacent steps.

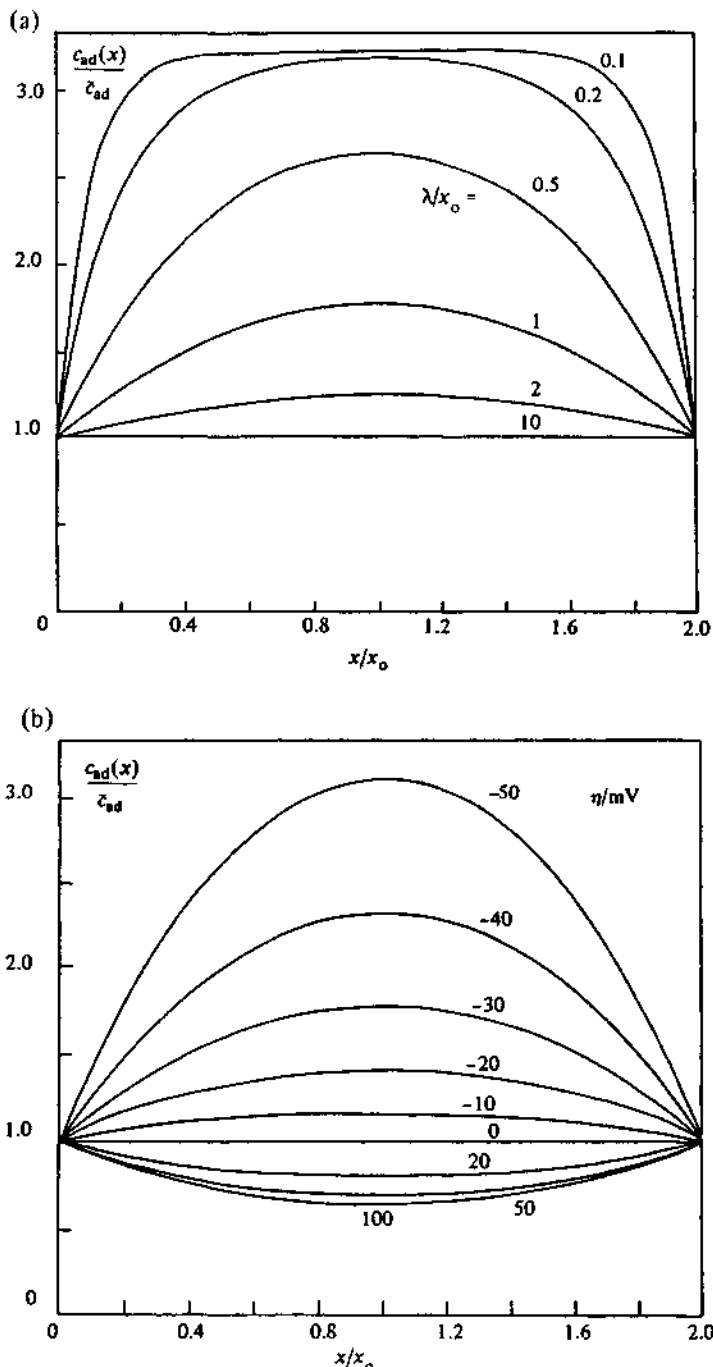


Fig. 9.11 – (a) Distribution of ad-atom concentration between two parallel steps at a distance $2x_0$ from each other as a function of the penetration, λ/x_0 , of surface diffusion. Overpotential -30 mV . (b) Distribution of ad-atom concentration between two parallel steps at a distance $2x_0$ from each other for different values of the overpotential. $\lambda/x_0 = 1$.

The solution of this problem was first given by Cabrera & Burton [9] for the case of vapour phase deposition, the Lorenz [10] has adapted it to the electrochemical case. The solution has the form

$$\frac{c_{ad}(x)}{\bar{c}_{ad}} = \left(\exp \frac{-zF\eta}{RT} \right) + \left[1 - \exp \left(\frac{-zF\eta}{RT} \right) \right] \cdot \exp \left(\frac{-x}{\lambda_0} \right) \frac{1 + \exp \left(-\frac{2(x_0 - x)}{\lambda_0} \right)}{1 + \exp \left(-\frac{2x_0}{\lambda_0} \right)} \quad (9.25)$$

where λ_0 , is given by

$$\lambda_0 = \left(\frac{zFD\bar{c}}{I_0} \right)^{1/2} \exp \left(-\frac{(1 - \alpha_C)nF\eta}{2RT} \right) \quad (9.26)$$

and is referred to as the surface diffusion penetration depth. Here I_0 is the exchange current density, α_C is the cathodic transfer coefficient, and η is the overpotential. If I_0 is small, $\lambda/x_0 \gg 1$ and Equation (9.25) approaches the expression obtained for the case of pure electron transfer control. If, on the other hand, I_0 is large, the situation corresponds essentially to pure diffusion control. Fig. 9.11 illustrates the profiles of surface concentration which are predicted by Equation (9.25) for different values of λ/x_0 and for different overpotentials. The local current density has been derived from Equation (9.25) by Damjanovic & Bockris [11];

$$I = I_0 \left[\exp \left(\frac{(1 - \alpha_C)nF}{RT} \eta \right) - \exp \left(\frac{-\alpha_C nF}{RT} \eta \right) \right] \cdot \frac{\exp \left(\frac{x_0 - x}{\lambda_0} \right) + \exp \left(-\frac{x_0 - x}{\lambda_0} \right)}{\exp \left(\frac{x_0}{\lambda_0} \right) + \exp \left(-\frac{x_0}{\lambda_0} \right)} \quad (9.27)$$

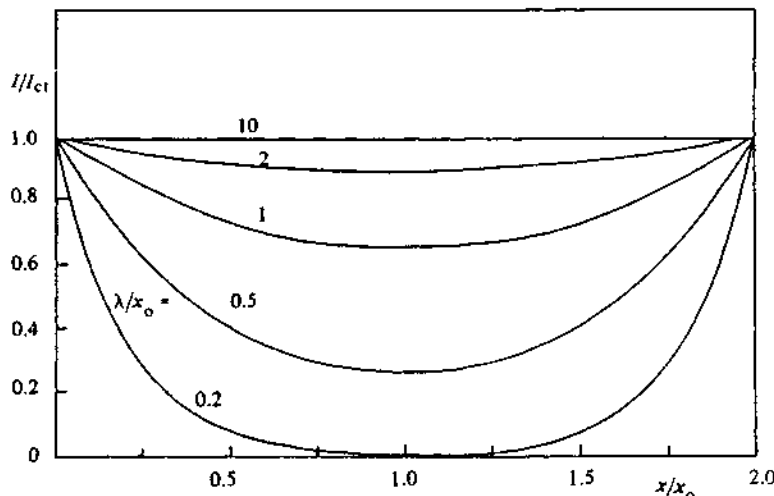


Fig. 9.12 – Distribution of local current density between two parallel steps at a distance $2x_0$ from each other for different values of diffusion penetration λ/x_0 .

The distribution of local current density is shown as a function of the ratio x_0/λ_0 in Fig. 9.12.

The circularly symmetrical diffusion of ad-atoms to kink sites has also been considered [12] as well as diffusion processes at screw dislocations [13], and further details may be found, for example, in Vetter's book [14].

9.3 NUCLEATION AND GROWTH OF MONOLAYERS

The growth of metals on inert substrates like carbon, as well as the formation of anodic films, for example during corrosion, involve as a first step the formation of a nucleus of the new phase. The theoretical treatment of these systems has been dominated by geometrical considerations concerned with the shape and size of the growing centres. The growth of very thin anodic films on mercury and amalgam electrodes has received particular attention, the electrocristallisation of calomel [15] being the classical example, and more recently the growth of silver on the dislocation free surfaces of single crystals has been studied in detail [7]. An example of the current transients observed in potential step experiments is shown in Fig. 9.13. In both cases the growth of the deposit involves nucleation of centres which can be thought of as discs one atom or one molecule thick. These growth centres expand and coalesce to form the monolayer deposit, and further growth then requires the nucleation of new growth centres on the freshly generated surface; The growth of monolayer deposits in this way is referred to as *two-dimensional electrocristallisation*. If the rate determining step in the electrocristallisation process is the incorporation of atoms or molecules at the expanding periphery of the centres (Fig. 9.14), the current flowing into a single growth centre will be

$$i = nFk2\pi rh \quad (9.28)$$

where k is the rate of incorporation expressed in $\text{mol cm}^{-2} \text{s}^{-1}$. The amount of charge required to form the cylinder of new material is

$$Q(r) = \frac{\pi r^2 h n F p}{M} \quad (9.29)$$

The derivative of Equation (9.29) gives the instantaneous current into the centre as

$$i(r,t) = \frac{2\pi h n F p r(t)}{M} \cdot \frac{dr(t)}{dt} \quad (9.30)$$

It follows that the rate of radial expansion is given by

$$\frac{dr(t)}{dt} = \frac{Mk}{p} \quad (9.31)$$

The radius at any time is obtained by integration of Equation (9.31) as

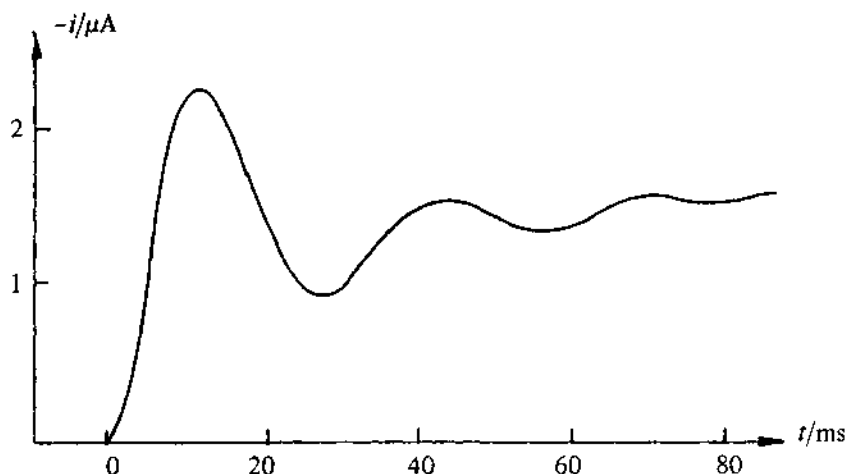


Fig. 9.13 – Current transient observed for the deposition of silver on a dislocation free surface of a silver single crystal. Data taken from E. B. Budevski, *Progress in Surface and Membrane Science*, 11, (1976), 71.

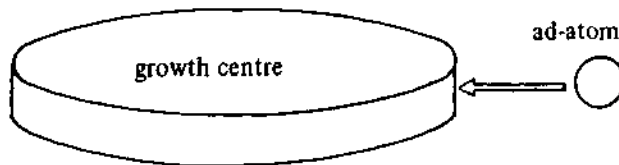


Fig. 9.14 – The slowest step is assumed to involve the incorporation of atoms or molecules at the periphery of the expanding growth centre.

$$r(t) = \frac{Mk}{\rho} t \quad (9.32)$$

which, when substituted into Equation (9.28), yields

$$i = \frac{2\pi n F k^2 h M}{\rho} \cdot t . \quad (9.33)$$

The current associated with the growth of an isolated disc shaped nucleus is therefore expected to increase linearly with time. In practice, of course, it is extremely difficult to observe the growth of a single nucleus, so that it is necessary to take into account the way in which the growth centres are formed. The limiting cases of Equation (9.21) and (9.22) are useful here. If the nucleation of growth centres is essentially instantaneous, the net current density corresponding to a number density of N_0 of isolated centres is

$$I = \frac{2N_0\pi n F k^2 h M}{\rho} \cdot t . \quad (9.34)$$

If, on the other hand, the nucleation of growth centres is progressive, Equation (9.22), the net current density becomes

$$I = \frac{2AN_0\pi n F k^2 h M}{\rho} \cdot t^2 . \quad (9.35)$$

It is therefore clear that the time dependence of the growth current depends on the nucleation law. However, the derivation of Equation (9.34) and (9.35) was made by assuming that the centres grow independently of each other. This may be true in the early stages of growth when the centres are widely spaced, but as radial growth proceeds, adjacent centres will come into contact, reducing the edge area available for the incorporation of materials into the lattice. This situation also occurs in homogeneous phase formation, and it is referred to as the *overlap problem*. It has been treated theoretically by introducing the notion of the *extended area*. This is the notional area which would be covered by the centres if the 'overlap' were not taken into consideration. This idea is illustrated in Fig. (9.15). It can be shown [16] that the normalised area covered, S , is related to the normalised extended area S_{ex} by the expression

$$S = 1 - \exp(-S_{ex}) . \quad (9.36)$$

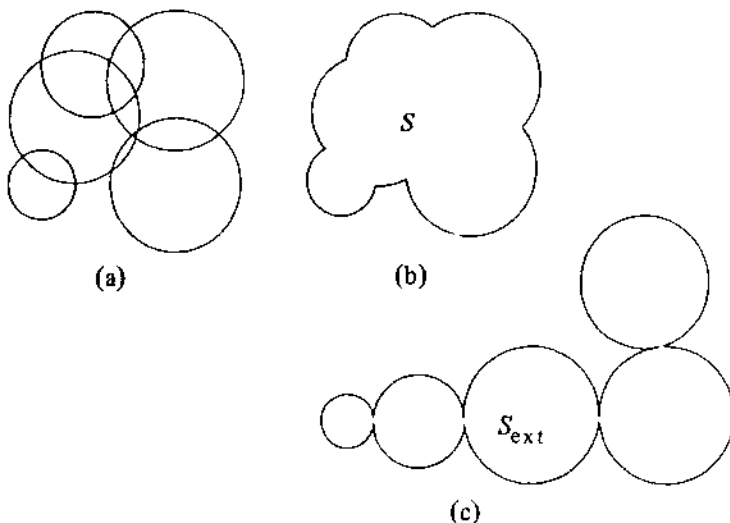


Fig. 9.15 – The overlap problem. The Avrami theorem (Equation (9.36)) relates the true surface area, S , to the nominal 'extended area' S_{ex} . The figure illustrates how the overlap of growth centres shown in (a) gives rise to the real area corresponding to (b) and the 'extended area' shown in (c).

As S_{ex} becomes very large, S tends towards 1, i.e. the surface is completely covered. Equation (9.36) is known as the *Avrami theorem*. The charge density associated with this notional extended area is given by

$$Q_{\text{ex}} = \int_0^t I_{\text{ex}} dt \quad (9.37)$$

where I_{ex} is given by either Equations (9.34) or (9.35), depending on the type of nucleation involved. Q_{ex} can also be related to the total charge density, Q_{mon} , required to form a monolayer of the deposit, since

$$Q_{\text{ex}} = S_{\text{ex}} \cdot Q_{\text{mon}} . \quad (9.38)$$

It follows that the 'extended' current density, I_{ex} is

$$I_{\text{ex}} = Q_{\text{mon}} \cdot \frac{dS_{\text{ex}}}{dt} , \quad (9.39)$$

and also

$$I = Q_{\text{mon}} \cdot \frac{dS}{dt} . \quad (9.40)$$

Since S and S_{ex} are related by the Avrami theorem, it follows that

$$I = I_{\text{ex}} \exp(-S_{\text{ex}}) . \quad (9.41)$$

It is now a simple matter to obtain the currents for each limiting case of the nucleation law. For instantaneous nucleation, Q_{ex} is obtained by integration of Equation (9.39):

$$Q_{\text{ex}}(\text{instantaneous}) = \frac{\pi n F M h N_o k^2 t^2}{\rho} , \quad (9.42)$$

and since $Q_{\text{mon}} = hpnF/M$, it follows that the extended area is this case is

$$S_{\text{ex}}(\text{instantaneous}) = \frac{\pi N_o k^2 t^2 M^2}{\rho^2} , \quad (9.43)$$

so that the current can be derived by substitution of Equation (9.39) and (9.43) into (9.41)

$$I(\text{instantaneous}) = \frac{2\pi n F M h N_o k^2 t}{\rho} \exp\left(-\frac{\pi N_o M^2 k^2 t^2}{\rho^2}\right) . \quad (9.44)$$

An identical treatment for progressive nucleation leads to the expression

$$I(\text{progressive}) = \frac{\pi n F M h A N_o k^2 t^2}{\rho} \exp\left(-\frac{\pi M^2 A N_o k^2 t^3}{3\rho^2}\right) . \quad (9.45)$$

The effect of the exponential term introduced by the Avrami theorem is to introduce a maximum into the current transient, and at long times the current approaches zero.

These two equations can be reduced to a more convenient form by using the coordinates of their respective maxima (I_m, t_m) to obtain expressions in terms of the reduced variables

$$\frac{I}{I_m} = \frac{t}{t_m} \exp\left(-\frac{(t^2 - t_m^2)}{2t_m^2}\right) \quad (9.46)$$

in the case of instantaneous nucleation, and

$$\frac{I}{I_m} = \frac{t^2}{t_m^2} \exp\left(-\frac{2(t^3 - t_m^3)}{3t_m^3}\right) \quad (9.47)$$

in the case of progressive nucleation. The shapes of the reduced current transients predicted for instantaneous and for progressive nucleation are contrasted in Fig. 9.16.

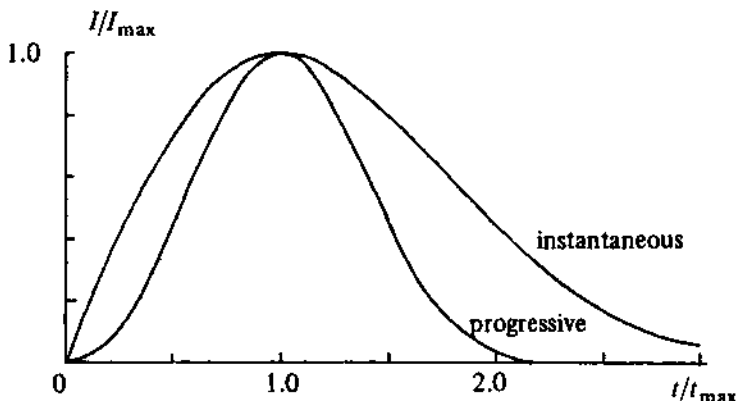


Fig. 9.16 – Dimensionless plots according to Equations (9.46) and (9.47) for the growth of monolayer deposits by the instantaneous and progressive nucleation mechanisms respectively.

The nucleation and growth of many anodic films on mercury or on amalgam substrates gives rise to potentiostatic transients which follow the shapes predicted by Equation (9.46) or (9.47) [17], and Fig. 9.17 compares an experimental transient for the growth of monolayers of HgS with the reduced variable curve for progressive nucleation. In many systems electrocrysallisation of subsequent monolayers takes place, and theoretical treatments for this case, involving extensions of the theory outlined here, have appeared in the literature [18].

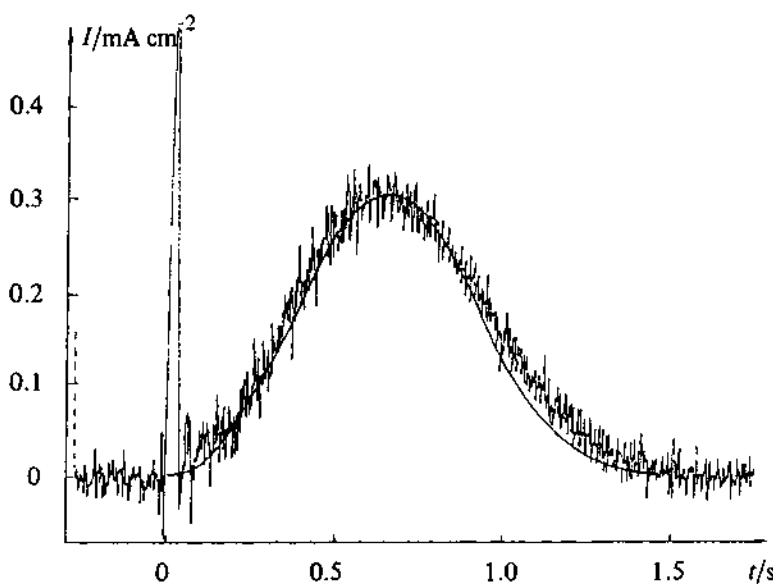


Fig. 9.17 -- Experimental transient for the deposition of a monolayer of HgS on a mercury electrode in $0.1 \text{ mol dm}^{-3} \text{ Na}_2\text{S} + 1.0 \text{ mol dm}^{-3} \text{ NaHCO}_3$, illustrating the fit predicted by Equation (9.47) for the progressive nucleation of a monolayer. The charge under the transient corresponds to the formation of a monolayer of HgS in the (001) plane.

9.4 NUCLEATION AND GROWTH OF THREE-DIMENSIONAL CENTRES

9.4.1 Rate determining step—lattice incorporation

The electrocrystallisation of a new phase on a foreign substrate may involve in its early stages the formation of three-dimensional growth centres which subsequently overlap to give a continuous deposit. The geometry of the growth centre is sensitive to the interaction between the deposit and substrate materials, and this is particularly evident in the case of a liquid metal deposit like mercury where the contact angle with the substrate determines whether a hemispherical or cap-shaped nucleus is formed. If the substrate is completely wetted by the mercury, we might expect a monolayer film to form. The shape of solid growth centres is more complex, but it is instructive to consider simple geometries which lead to analytical expression for the current transient under potentiostatic conditions. Suppose, for example, that the growth centre can be represented as a right circular cone growing on a foreign substrate as shown in Fig. 9.18. Growth parallel to the surface takes place with a rate constant k_3 , and that perpendicular to the surface with a rate constant k'_3 (the units of these rate constants are $\text{mol cm}^{-2} \text{s}^{-1}$). The total current into the growing cone can be obtained by integration of the contributions of a stack of discs. The solution of the problem involving growth of a number of discrete centres must take account of their overlap, and the expressions for instantaneous ($N = N_0$) and progressive ($N = A_3 t$) nucleation have the form [19]:

instantaneous nucleation

$$I = nFk'_3 \left(1 - \exp\left(-\frac{\pi M^2 k_3^2 N_o t^2}{\rho^2}\right) \right) \quad (9.48a)$$

progressive nucleation

$$I = nFk'_3 \left(1 - \exp\left(-\frac{\pi M^2 k_3^2 A_3 t^3}{3\rho^2}\right) \right). \quad (9.48b)$$

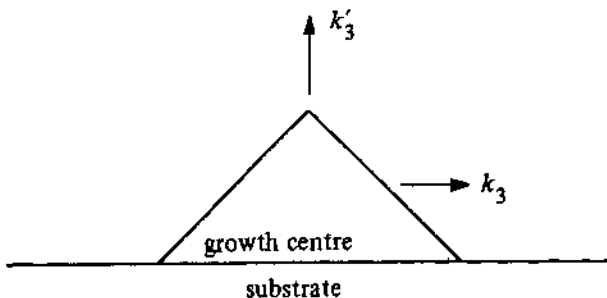


Fig. 9.18 – Growth of three-dimensional centres; the right circular cone. Growth in directions perpendicular and parallel to the substrate is defined by the rate constants k'_3 and k_3 respectively.

The general behaviour of these expressions for the current density can be seen by examining their limiting forms. At short times the arguments of the exponential terms are sufficiently small that expansion gives

instantaneous nucleation

$$I \approx \frac{nFk'_3 \pi M^2 k_3^2 N_o}{\rho^2} t^2 \quad (9.49a)$$

progressive nucleation

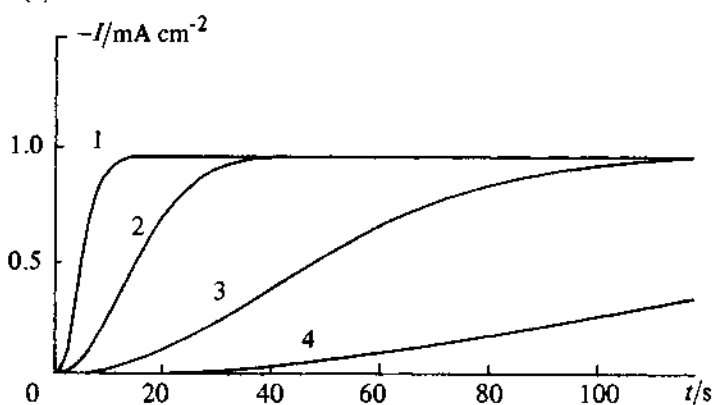
$$I \approx \frac{nFk'_3 \pi M^2 k_3^2 A_3}{3\rho^2} t^3. \quad (9.49b)$$

In both cases the current density approaches nFk'_3 at long times, since the remaining growth is restricted to the perpendicular direction. Fig. 9.19 illustrates the current transients corresponding to Equations (9.48a) and (9.48b).

Other geometries have been considered using a similar approach, and a recent detailed examination of different three-dimensional models has been given by Bosco & Rangarajan [20]. The solutions in the case of hemispherical growth centres are particularly interesting since they show maxima and minima in the approach to the final current density. The transients computed for instan-

taneous and progressive nucleation are illustrated in Fig. 9.20, and the reader is referred to the papers of Bosco & Rangarajan for further details. Abyaneh [25] has given a more exact treatment of this problem which shows that only one maximum is observed. Fig. 9.21 shows that the growth of PbO_2 on Pt is characterised by transients which resemble those derived for hemispherical centres [20], although an alternative explanation in terms of birth and death of cone shaped centres was considered by Abyaneh & Fleischmann [21] for the case of Ni on C.

(a)



(b)

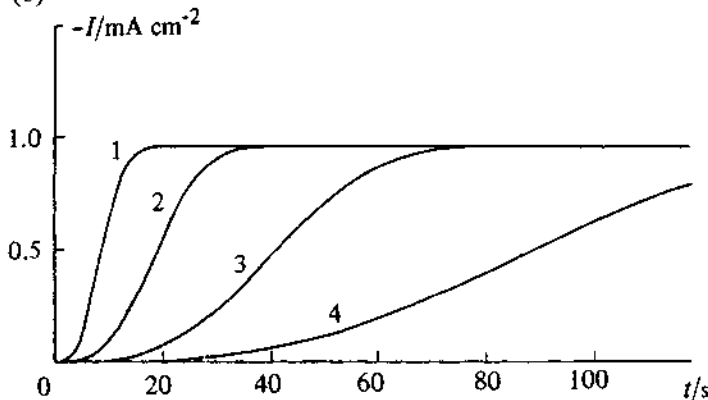


Fig. 9.19 – (a) Current transients calculated from Equation (9.48a) for the growth of right circular cones formed by instantaneous nucleation. $k_3 = 10^{-8} \text{ mol cm}^{-2} \text{ s}^{-1}$, $n = 1$, $M = 100 \text{ g mol}^{-1}$, $\rho = 10 \text{ g cm}^{-3}$. N_0 values (cm^{-2}) are (1) 10^{12} , (2) 10^{11} , (3) 10^{10} , (4) 10^9 . (b) Current transients calculated from Equation (9.49b) for the growth of right circular cones formed by progressive nucleation. A' values ($\text{cm}^{-2} \text{ s}^{-1}$) are (1) 10^{12} , (2) 10^{11} , (3) 10^{10} , and (4) 10^9 . Other values are the same as those used for (a).

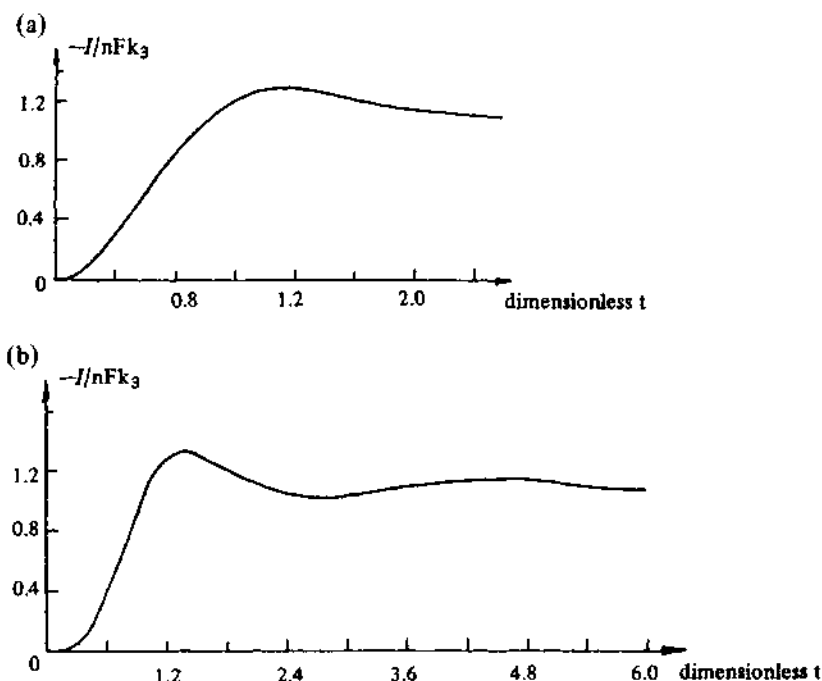


Fig. 9.20 – (a) Current transients calculated for the growth of hemispherical centres formed by instantaneous nucleation (b) Current transients calculated for the growth of hemispherical centres formed by progressive nucleation. Reproduced with permission from E. Bosco & S. K. Rangarajan, *J. Electroanal. Chem.*, 134, (1982), 213.

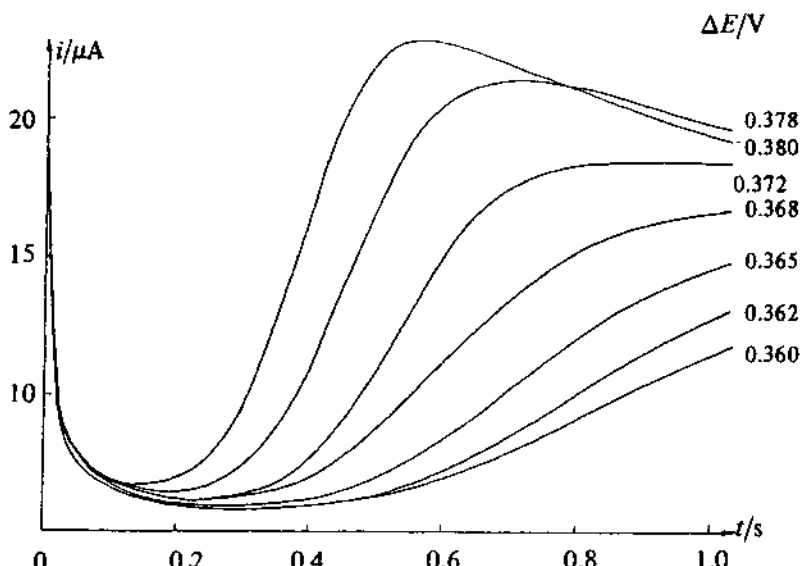


Fig. 9.21 Current transients for the deposition of lead dioxide on platinum. The figures on the transients refer to the height of the potential step used. Electrolyte 1 mol dm^{-3} sodium acetate, 1 mol dm^{-3} acetic acid, 1 mol dm^{-3} lead acetate.

9.4.2 Rate determining step – diffusion

The preceding discussion presupposed that the slowest step in the growth of a three-dimensional deposit involved incorporation of material into the lattice. In practice, of course, this may not be the slowest step, so brief consideration will be given to the particular case of diffusion controlled growth of three-dimensional centres.

At high overpotentials the current density at a spherical electrode of constant radius r_0 is given by the sum of two terms:

$$I(t) = nFc^\infty \left(\frac{D}{\pi t} \right)^{1/2} + \frac{nFDc^\infty}{r_0}. \quad (9.50)$$

If r_0 is sufficiently small, the first term in Equation (9.50) can be neglected, and the current density at a microscopic spherical growth centre can therefore be written as

$$I(t) \approx \frac{nFDc^\infty}{r(t)}. \quad (9.51)$$

Hills, Schiffrin, & Thompson [22] have derived expressions for the current transients in the two limiting cases of instantaneous and progressive nucleation by the following argument. The instantaneous current is related to the rate of change of volume of the centre, since

$$i(t) = \frac{nF\rho}{M} \frac{dV(t)}{dt}, \quad (9.52)$$

and it therefore follows that the current at an isolated hemispherical centre is given by

$$i(t) = \frac{nF\pi(2Dc^\infty)^{3/2}M^{1/2}}{\rho^{1/2}} t^{1/2}. \quad (9.53)$$

At lower overpotentials, the surface concentration of reactant is significantly greater than zero, and Equation (9.51) becomes

$$I(t) = \frac{nFD(c^\infty - c^\sigma)}{r_0}, \quad (9.54)$$

and since the ratio (c^σ/c^∞) is assumed to be determined by the Nernst equation, it follows that current into a growing hemisphere is

$$i(t) = \frac{nF\pi(2Dc^\infty)^{3/2}M^{1/2}}{\rho^{1/2}} \left[1 - \exp\left(-\frac{nF}{RT}\eta\right) \right]^{3/2} t^{1/2}. \quad (9.55)$$

Plots of Equation (9.55) for different values of overpotential are shown in Fig. 9.22, which also illustrates an experimental transient obtained for the deposition of a single mercury centre on a carbon micro-electrode [23].

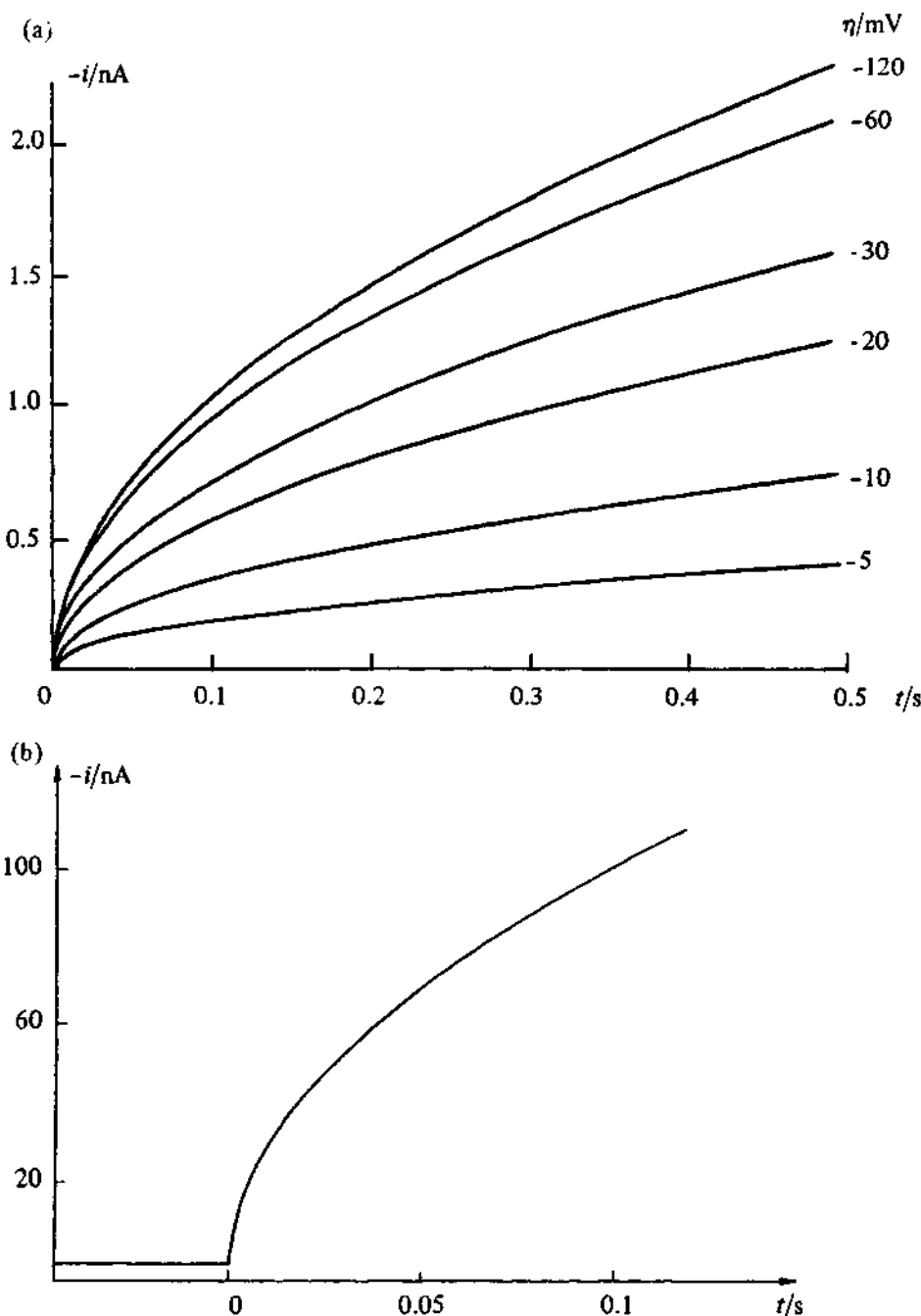


Fig. 9.22 – (a) Current transients calculated from Equation (9.55) for different overpotentials. The transients show the typical $t^{1/2}$ behaviour expected for the growth of a single centre under diffusion control. (b) Experimental transient for the growth of a single mercury centre on a carbon fibre microelectrode from $Hg_2(NO_3)_2$ solution (taken from B. Scharifker, PhD thesis, University of Southampton, 1979).

In general, of course, a large number of growth centres are formed on the substrate, and the interaction of their diffusion fields leads to an intractable problem for which only approximate treatments have been attempted. At very short times the interaction of the diffusion fields can be assumed to be negligible, and the two limiting cases of instantaneous and progressive nucleation of growth centres follow directly from Equation (9.55) by multiplication by the nuclear number density (N_0 in the instantaneous case or $A't$ in the progressive case). The diagnostic criterion is therefore the time dependence of the current density at short times. The current is proportional to $t^{1/2}$ if nucleation is instantaneous, and proportional to $t^{3/2}$ if nucleation is progressive. In practice, however, experimental transients are often distorted at short times by currents due to double layer charging and ad-atom formation, and a clear analysis of nucleation mechanism is not always possible.

The effect of the overlap between the diffusion fields of a random array of growing centres has been considered by Scharifker [24] and by Bosco & Rangarajan [20]. Both treatments are approximate. The expressions derived by Scharifker are

$$I(t) = \frac{nFD^{1/2}c^\infty}{\pi^{1/2}t^{1/2}} [1 - \exp(-N_0\pi kDt)] \quad (9.56a)$$

for instantaneous nucleation, where $k = (8\pi c^\infty M/\rho)^{1/2}$, and

$$I(t) = \frac{nFD^{1/2}c^\infty}{\pi^{1/2}t^{1/2}} \left[1 - \exp\left(-\frac{A'\pi kDt^2}{2}\right) \right] \quad (9.56b)$$

for progressive nucleation, where

$$k = \frac{4}{3} \left(\frac{8\pi c^\infty M}{\rho} \right)^{1/2} .$$

The transients predicted by Equation (9.56a) and (9.56b) are illustrated in Fig. 9.23. At short times, the transients approach those predicted for the growth of non-interacting centres, whereas at long times they approach the limiting form

$$I(t) = \frac{nFD^{1/2}c^\infty}{\pi^{1/2}t^{1/2}} \quad (9.57)$$

corresponding to semi-infinite diffusion to a planar surface. The time and current corresponding to the maximum in each transient are given by

$$t_m = 1.26/N\pi kD \quad (\text{instantaneous}) \quad (9.58a)$$

$$t_m = (4.67/AN_0\pi kD)^{1/2} \quad (\text{progressive}) \quad (9.58b)$$

and

$$I_m = 0.638nFDc^\infty k^{1/2} N_0^{1/2} \quad (\text{instantaneous}) \quad (9.59a)$$

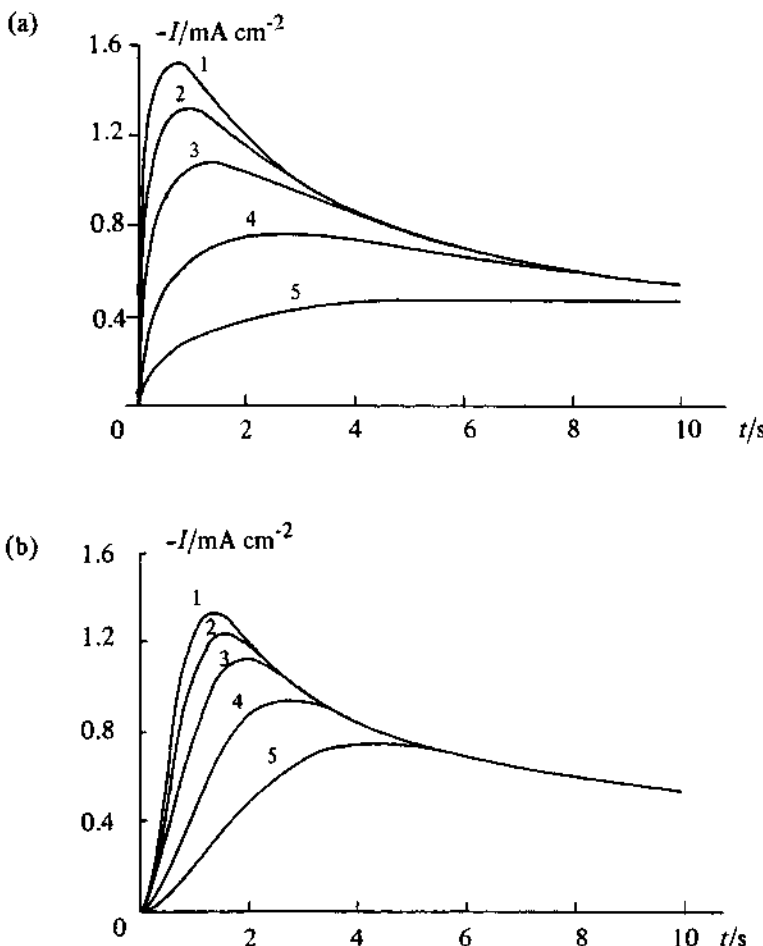


Fig. 9.23 – (a) Current transients calculated from Equation (9.56a) for the growth under diffusion control of a number of centres formed by instantaneous nucleation. N_0 values (cm^{-2}), (1) 10^6 , (2) 7.5×10^5 , (3) 5×10^5 , (4) 2.5×10^5 , (5) 10^5 . Other values $c^\infty = 10^{-5} \text{ mol dm}^{-3}$, $D = 10^{-5} \text{ cm}^2 \text{s}^{-1}$, $M = 200 \text{ g mol}^{-1}$, $\rho = 13.6 \text{ g cm}^{-3}$. (b) Current transients calculated from Equation (9.56b) for the growth under diffusion control of centres formed by progressive nucleation. AN_0 values ($\text{cm}^{-2} \text{s}^{-1}$); (1) 10^6 , (2) 7.5×10^5 , (3) 5×10^5 , (4) 2.5×10^5 , (5) 10^5 . Other values as in (a).

$$I_m = 0.462nFD^{3/4}c^\infty k^{1/4}(AN_0)^{1/4} \quad (\text{progressive}) \quad (9.59b)$$

The product $I_m^2 t_m$ does not contain the quantities k , A , or N , and Scharifker suggests that it is therefore a useful diagnostic criterion for the type of nucleation behaviour. For instantaneous nucleation,

$$I_m^2 t_m = 0.163(nFc^\infty)^2 D , \quad (9.60a)$$

whereas for progressive nucleation

$$I_m^2 t_m = 0.260(nFc^\infty)^2 D . \quad (9.60b)$$

One of the most widely studied examples of the electrocrystallisation of three-dimensional centres under diffusion control is the deposition of mercury on glassy carbon [26]. A typical family of experimental transients is shown in Fig. 9.24, and it can be seen that they approach closely the shape predicted theoretically by Scharifker.

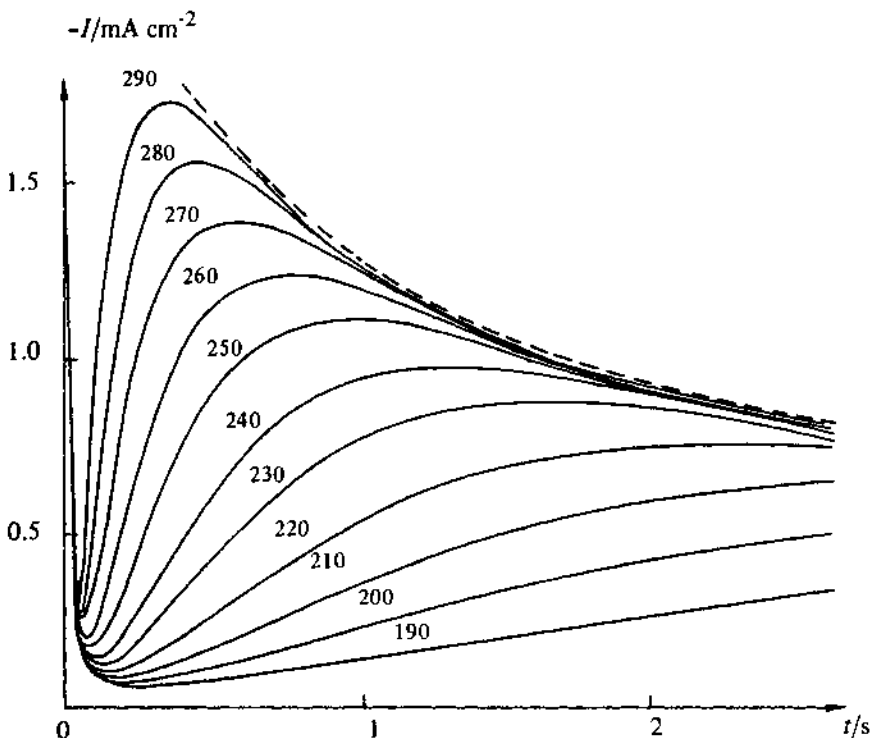


Fig. 9.24 – Experimental current transient for the deposition of mercury on vitreous carbon from $\text{Hg}_2(\text{NO}_3)_2$ solution. The figures refer to the overpotentials. Data taken from B. Scharifker, PhD thesis, University of Southampton, 1979.

9.5 CRYSTAL ORIENTATION AND MORPHOLOGY OF POLYCRYSTALLINE DEPOSITS

The initial stages in the formation of an electrodeposited layer have been discussed in considerable detail in this chapter. From a practical of view, it is also important to consider the thickening of deposits to form layers of macroscopic thickness. The morphology and mechanical properties of metal deposits are of primary interest in plating technology, and the composition of most plating baths is

complicated since brightening and levelling agents are present in order to control these properties. A large reservoir of empirical information about plating conditions has been built up, but it is probably true to say that in the majority of cases the exact function of each component of a particular bath is not known in any detail. The structures of metal deposits apparently depend on many parameters, some of which are ill-defined. Some idea of the extent of the variety of morphologies can be gained by reference to the book by Fischer [27].

The growth of metal deposits appears in many cases to proceed by a layer by layer mechanism. The expansion of three-dimensional growth centres can be inhibited, for example by the adsorption of organic additives, and growth parallel to the initial surface effectively ceases until a new set of centres is formed. These 'birth and death' processes have been discussed by Abyaneh & Fleischmann [21]. A characteristic of this type of growth is the appearance of macroscopic steps which move across the surface during the deposition. The linear expansion rate, v , of a step in the tangential direction is related to the step height, h , by the expression

$$v = \frac{I \cdot M}{nFpl} \quad (9.61)$$

where l is the length of the expanding step. Hence if v and l are known, the step height can be calculated.

Fischer [27] has classified polycrystalline metal deposits into the following groups:

- (a) Type F1 (Field oriented isolation type). In these deposits crystals grow along the direction of the current lines, and metal sponges without orientation are also formed.
- (b) Type B1 (Base oriented reproduction type). These crystal deposits reproduce the crystal orientation of the substrate. There are coarse and compact limiting forms of this type of growth.
- (c) Type FT (Field oriented texture type). These deposits consist of finely bunched crystallites growing in the direction of the current lines.
- (d) Type UD (Unoriented dispersion type). This deposit consists of irregular closely packed crystallites which show no preferred orientation.

The different growth forms depend on bath composition, temperature, convection, and the presence of additives, but the interaction of these factors is clearly complex, and it is therefore not surprising that detailed mechanisms have not been established except in the simplest cases. Details on plating can be found in books by Gabe [28] and Pletcher [29]. In practice, a uniform hard deposit is desired, and steps must be taken to prevent the formation of loose deposits consisting of dendrites or powder. Loose deposits of this kind are generally formed under mass transfer control, and one function of additives is to inhibit the rates of charge transfer and lattice incorporation so that they become slower than the rate of mass transfer. Barton & Bockris [30] as well as Hamilton [31] have developed theoretical descriptions of dendrite formation which consider the spherical diffusion geometry at the tip of the growing crystallites.

Understanding of bulk electrocrysTALLISATION processes and the role of organic additives may be advanced by the use of the range of *in situ* spectroscopic techniques which have been developed recently. For example, Fleischmann *et al.* [32] have studied the adsorption of heterocyclic additives on copper using *in situ* Raman spectroscopy, and it has also been shown that *in situ* X-ray techniques can give structural information about the early stages on metal deposition [33].

9.6 ELECTROCRYSTALLISATION OF ANODIC FILMS

The deposition of two-dimensional anodic films has already been considered briefly. The anodisation of metals such as aluminium is of technological importance, and the mechanism of film growth in this case clearly differs from that of metal deposition. In the early stages of nucleation and growth of an anodic film a thin continuous layer of essentially insulating material may be formed. In this case the electrode is said to be *passive*. Further growth of this insulating layer requires the migration of ionic species, and this only occurs at a measurable rate in the presence of large impressed electric fields of the order of 10^6 V cm^{-1} . This type of electrode process is referred to as *field-assisted migration*. The barriers to migration of ions through a continuous insulating deposit can be represented in the way shown in Fig. 9.25. In the absence of space-charge, the electric field in the film is uniform, so that the barrier heights for the forward and reverse directions of ion transfer are changed as shown in the figure. The net current density is obtained as the sum of the ionic currents in the forward and reverse directions. The resulting expression was first derived by Cabera & Mott and by Verwey [34].

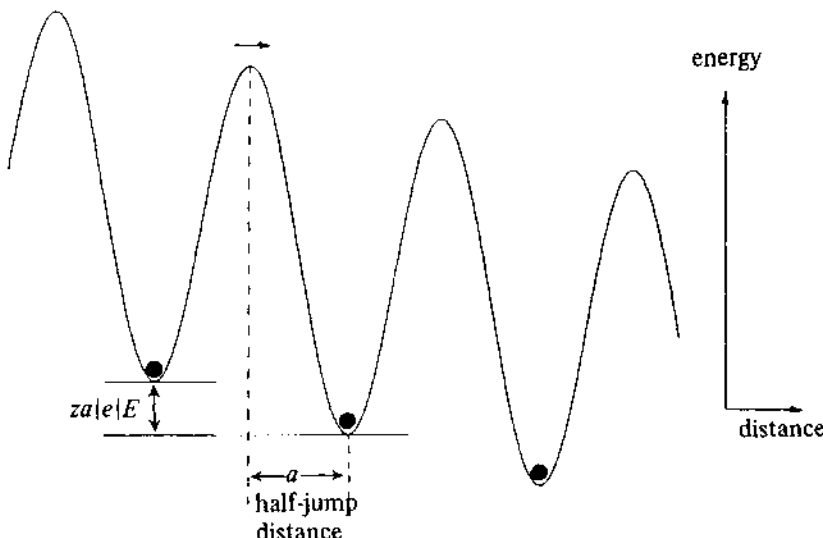


Fig. 9.25—Modification of the energy barrier for ions brought about by the electric field in an oxide film. The barrier for the forward direction is lowered by an amount $za|e|E$, where a is the 'half jump distance' (shown in the figure), E is the electric field (assumed to be uniform), and $z|e|$ is the charge on the migrating ion.

$$I = NvzF \exp(-\Delta G^\ddagger/RT) \sinh(zAF/RT) \quad (9.62)$$

where N is the concentration of mobile ions (mol cm^{-2})

v is a frequency factor

ΔG^\ddagger is the free energy of activation for ion diffusion

a is the half jump distance (see Fig. 9.25) and zF is the charge per mol on the migrating ions.

Since the current density is determined by the field, the electrode potential rises linearly with time if the oxide is grown at constant current. Fig. 9.26 shows a set of potential transients obtained for the growth of the TiO_2 film on titanium [35]. Transients of this kind can be analysed in order to obtain information about the exchange current density, I_0 , and the half jump distance, a .

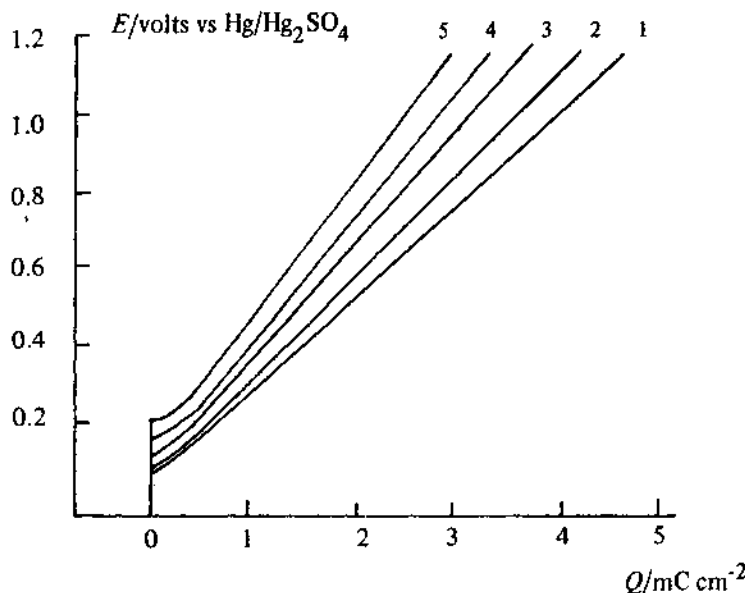


Fig. 9.26 -- Galvanostatic (constant current) transients for the growth of the anodic oxide film on a titanium electrode in $1.0 \text{ mol dm}^{-3} \text{ H}_2\text{SO}_4$. The current densities in mA cm^{-2} are: (1) 0.06, (2) 0.12, (3) 0.60, (4) 1.2, and (5) 6.0. Note that the potential is displayed against charge (i.e. $I \propto t$) rather than against time. The increase in slope of the transients with current density therefore corresponds to an increase of the electric field. (Data taken from J. F. McAleer PhD Thesis, University of Southampton, 1980).

9.7 ELECTROCRYSTALLISATION PROCESSES IN OTHER ELECTROCHEMICAL SYSTEMS

This chapter has been devoted so far to a discussion of the fundamental aspects of electrocristallisation. The applications of electrochemical phase formation in metal plating and anodisation have already been mentioned, but it is important

to point out that the formation (or dissolution) of solid phases is also important in corrosion and in the mechanisms of battery electrochemistry. The corrosion of a metal such as iron can result in the formation of oxide films by a dissolution/precipitation mechanism, and the morphology and permeability of the resulting oxide layer partly determines the rate of attack of the metal. Further examples of electrocrystallisation are readily found in battery electrochemistry. For example, in the lead-acid system, the charge/discharge processes involve the electrocrystallisation of Pb, PbO₂, and PbSO₄. Control of crystal morphology in the battery plates is essential to ensure stability and cycle life, and for this reason additives known as expanders (e.g. lignosulfates) are added to the battery paste.

REFERENCES

- [1] I. N. Stranski, *Z. Physik. Chem.*, **136** (1928) 259.
- [2] see also K. J. Vetter, *Electrochemical kinetics*, p. 283, Academic Press, N.Y. 1967.
- [3] B. E. Conway & J. O'M Bockris, *Electrochimica Acta*, **3** (1961) 340.
- [4] W. K. Burton, N. Cabrera, & F. C. Frank, *Trans. Roy. Soc.*, **A243** (1951) 299.
- [5] D. A. Vermilyea, *J. Chem. Phys.*, **25** (1956) 1254.
- [6] M. Fleischmann & H. R. Thirsk, *Electrochim. Acta*, **2** (1960) 22.
- [7] E. B. Budevski, *Progress in surface and membrane science*, (Eds) D. A. Cadenhead and J. F. Daniell, **II** (1976) 71 Academic Press.
- [8] J. B. Zeldovich, *Acta. Phys. URSS*, **18** (1943) 1.
- [9] N. Cabrera & W. K. Burton, *Disc. Faraday Soc.*, **5** (1949) 50. See also [4].
- [10] W. Lorenz, *Naturf.*, **9a** (1954) 716.
- [11] A. Damjanovic & J. O'M Bockris, *J. Electrochem. Soc.*, **110** (1963) 1035.
- [12] W. Lorenz, *Z. Elektrochem.*, **57** (1953) 382.
- [13] D. A. Vermilyea, *J. Chem. Phys.*, **25** (1956) 1254 See also M. Fleischmann & H. R. Thirsk, *Electrochim. Acta*, **2** (1960) 22.
- [14] K. J. Vetter, *Electrochemical kinetics*, Academic Press, N.Y., 1967.
- [15] A. Bewick, M. Fleischmann, & H. R. Thirsk, *Trans. Faraday Soc.*, **58** (1962) 2200.
- [16] M. Avrami, *J. Chem. Phys.*, **7** (1939) 1130; **8** (1940) 212; **9** (1941) 177. See also U. R. Evans, *Trans. Faraday Soc.*, **41** (1945) 365.
- [17] J. A. Harrison & H. R. Thirsk, *A Guide to the study of electrode kinetics*, Academic Press 1972.
- [18] S. K. Rangarajan, *J. Electroanal. Chem.*, **46** (1973) 125.
- [19] R. D. Armstrong, M. Fleischmann, & H. R. Thirsk, *J. Electroanal. Chem.*, **11** (1966) 205.
- [20] E. Bosco & S. K. Rangarajan, *J. Electroanal. Chem.*, **134** (1982) 213.
- [21] M. Y. Abyaneh & M. Fleischmann, *J. Electroanal. Chem.*, **119** (1981) 187.
- [22] G. J. Hills, D. J. Schiffrian, & J. Thompson, *Electrochim. Acta*, **19** (1974) 657.
- [23] B. R. Scharifker, PhD Thesis, University of Southampton, 1979.
- [24] B. R. Scharifker & G. J. Hills, *Electrochim. Acta*, **28** (1983) 879.

- [25] M. Y. Abyaneh, *Electrochim. Acta*, **27** (1982) 1329.
- [26] G. A. Gunawardena, G. J. Hills, & I. Montenegro, *Electrochim. Acta*, **23** (1977) 693.
- [27] H. Fischer, *Electrolytische abscheidung und elektrokristallisation von metallen*, Springer Verlag, 1954.
- [28] D. Gabe, *Principles of metal surface treatment and protection*, Pergamon Press, 1978.
- [29] D. Pletcher *Industrial electrochemistry*, Chapman & Hall Ltd, 1982.
- [30] J. L. Barton & J. O'M Bockris, *Proc. Roy. Soc. London*, **A268** (1962) 485.
- [31] J. F. Hamilton, *Electrochim. Acta*, **8** (1963) 731.
- [32] M. Fleischmann, I. R. Hill & G. Sundholm, *J. Electroanal. Chem.*, **158** (1983) 153.
- [33] M. Fleischmann, P. Graves, I. Hill, A. Oliver, & J. Robinson, *J. Electroanal. Chem.*, **150** (1983) 33.
- [34] For a review see L. Young, *Anodic oxide films*, Academic Press, 1961.
- [35] J. F. McAleer, PhD Thesis, University of Southampton, 1980.

10

Spectroelectrochemistry

The various techniques for the elucidation of reaction mechanisms and the determination of kinetic parameters that have been described in earlier chapters rely on making current or potential measurements, often as a function of parameters such as sweep rate, time, or electrode rotation rate. One of the useful features of these electrochemical techniques is that the current is a direct measure of the reaction rate, and therefore the rate parameters relating to a simple process are fairly readily determined. The principle disadvantage of this approach is that such purely electrical measurements lack molecular specificity, i.e. the current only represents the aggregate rate of all processes occurring, and no direct information about the identity of reaction products or intermediates is available. In a similar way, most studies of electrode/electrolyte solution interfacial structure rely on capacitance measurements and comparing results with theoretical values obtained from calculations based on bulk properties (see Chapter 5), i.e. again no information at the molecular level is obtainable. It is therefore very clear that there is a need for techniques capable of probing the electrode/electrolyte interfacial region to provide this type of data. In particular it would be useful to be able (i) to identify reaction intermediates, (ii) to monitor the time dependent concentration of these, and other species, as well as (iii) to be able to study surface properties such as adsorbate orientation, ordering, and coverage.

In conventional solution chemistry this type of data is obtained through the application of one or more of the many spectroscopic techniques, such as IR and N.M.R. spectroscopies, now routinely available. Since the early 1960s a considerable effort has been expended in adapting some of these spectroscopies so that they can be applied *in situ* in an electrochemical cell. In addition,

totally new techniques for the study of the electrode/solution interface have been developed. This field, known as *spectroelectrochemistry*, is currently one of the most active areas of electrochemical research, and many of the techniques that have been developed are now being routinely applied.

In the space available here it would be impossible to describe in any detail all the spectroelectrochemical techniques that have been used, and in any case this area has been recently reviewed [1]. Instead the aim is to concentrate on a few of the most widely applied, and most useful, ones, to discuss the experimental requirements, and to give examples of the type of information that can be obtained. The bulk of the discussion will be concerned with those techniques which utilise UV-visible light, as it is in this area that greatest progress has been made. Recent developments using IR radiation as well as non-optical techniques will also be briefly discussed. Readers interested in assessing the current state of the art should consult the proceedings of recent conferences in this area [2].

10.1 UV-VISIBLE OPTICAL TECHNIQUES

10.1.1 The optically transparent electrode

The first widely applied spectroelectrochemical technique was UV-visible spectroscopy using optically transparent electrodes (OTE), and it is also one of the simplest to implement. A beam of monochromatic UV-visible light is directed perpendicularly through an OTE, then through the diffusion layer next to the electrode and the bulk solution, before passing out of the electrochemical cell through an exit window and being detected. Such a beam is of course attenuated by any absorbing species in its path, and thus both spectral and temporal information about the concentrations of such species in the diffusion layer at the electrode can be obtained. Fig. 10.1 shows a schematic diagram of the experimental configuration.

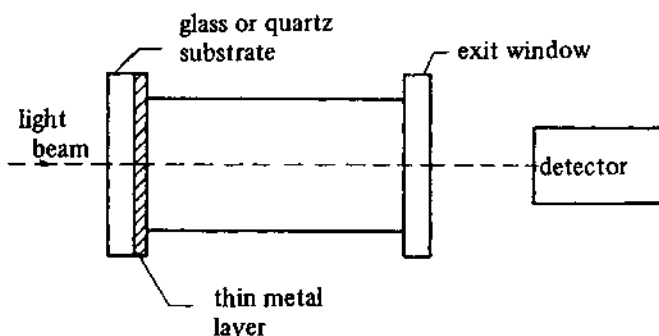


Fig. 10.1 – A schematic diagram of the optical configuration for an experiment with an optically transparent electrode.

It will be immediately apparent that the principal requirement for this technique is a suitable electrode material that is also transparent to UV-visible light. The first such electrodes consisted of a thin layer of doped SnO_2 on a

glass substrate, but these suffered from a number of problems, in particular their low conductivity and their instability in certain solvents. The electrodes now most frequently used are made by evaporating, or sputtering, 10–100 nm thick layers of Pt or Au onto glass substrates, often with a thin metal oxide undercoat to improve adhesion. These electrodes have resistivities between 20Ω and 5Ω per square, transmission in the visible part of the spectrum varying between 85% and 20%, and they are very stable. Alternative substrates to glass include quartz and polyester sheets, whilst other film materials include silver, copper, mercury, and carbon. The techniques required for the preparation of these OTEs are discussed by Von Benken & Kuwana [3], and Fig. 10.2 shows how they are incorporated into a typical cell.

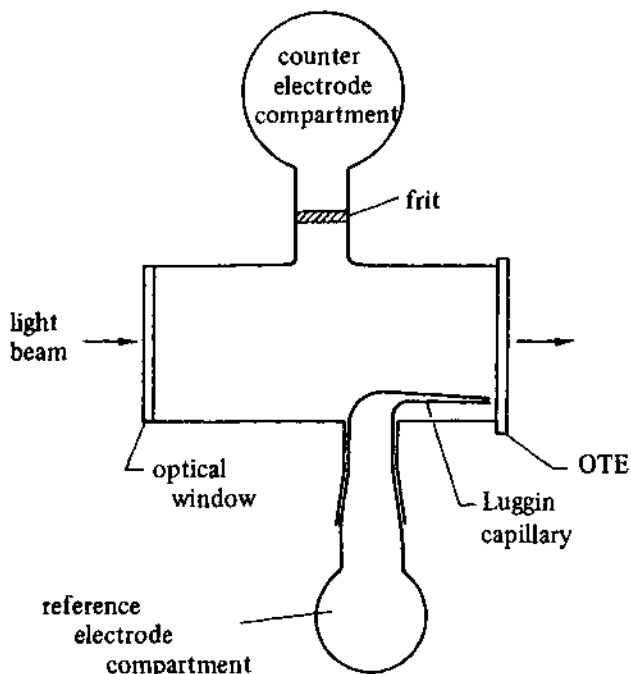
In the simplest type of experiment a cell, like that shown in Fig. 10.2, can be placed directly in the sample compartment of a commercial UV-visible spectrometer, and long lived highly coloured species can be monitored. In general, however, electrochemical intermediates will not have large enough extinction coefficients or may be too short lived for this approach to be satisfactory. Then the spectrometer must either be modified to permit optical transient recording, signal averaging and phase sensitive detection, or alternatively a purpose built optical system can be used. All that is required is a stable light source (Xe and Hg/Xe arc lamps have the advantage of high intensity, though tungsten filament lamps have also been successfully used), a high throughput monochromator, and a photodetector (photomultiplier or photodiode), in addition to simple components such as lenses and optical benches.

Let us first consider how we might investigate a simple reaction of the type described by Equation (10.1)

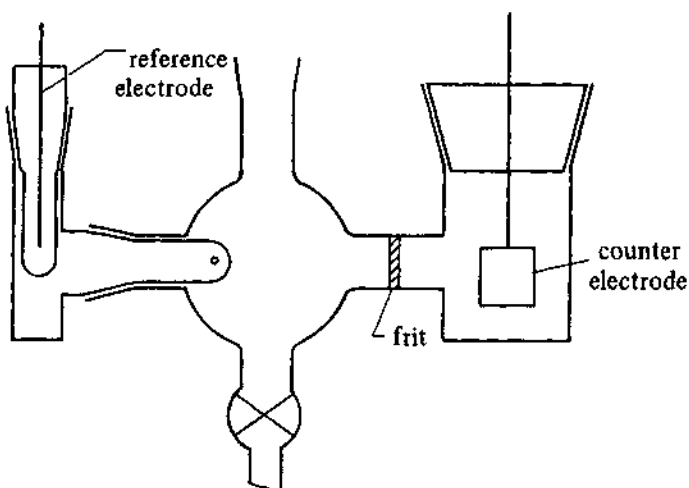


where only O is initially present and only R is coloured. The first requirement is to obtain a spectrum of R. If R is highly coloured and/or the solution is highly concentrated, it is only necessary to set the electrode potential to a value at which O is reduced to R at a diffusion controlled rate, allow the system to reach a steady state, and then record the absorbance as a function of wavelength. Generally this will not be possible, and it will be necessary to enhance the signal-to-noise ratio in some way. The simplest approach is to chop the light beam at a defined rate and to use a lock-in amplifier to 'tune in' to the chopping frequency. An even more effective technique is to modulate the electrode potential and again use phase sensitive detection. The electrode potential is modulated between a value where O is reduced to R at a diffusion controlled rate, and a value where the reverse process occurs, using a square wave; a typical modulation frequency is 30 s^{-1} . A lock-in amplifier tuned to the modulation frequency is then used to detect that part of the optical signal (photomultiplier or photodiode output) that is modulated in phase with the potential modulation. The output of the lock-in amplifier is then recorded as a function of wavelength. In both the above cases the optical signal has to be normalised with respect to the lamp intensity as this will vary with wavelength.

A more elegant, but more expensive, way of obtaining spectra is to use a rapid scanning spectrometer (RSS) [4, 5]. This enables a 1000 point, 450 nm



Top view



Front view

Fig. 10.2 -- A cell for experiments with an optically transparent electrode under conditions of semi-infinite linear diffusion.

wide spectrum in the range 240–800 nm to be swept and acquired every 5 ms, and by signal averaging these spectra a sensitivity of about 10^{-4} absorbance units is possible. A recently developed alternative to the RSS is to use a photodiode array detector which has similar speed and resolution but potentially higher sensitivity and should be more reliable as it has no moving parts. An instrument of this type is described by Rhodes & Kadish [6].

Having obtained a spectrum for R it is usual to investigate the kinetics of its formation. This is easily done by making optical transient measurements. The wavelength is fixed at a value close to an absorbance maximum, and the absorbance change in response to a potential modulation is monitored. The most frequently applied potential modulation is a potential step and signal averaging is usually required to obtain an acceptable signal to noise ratio.

The total absorbance [$A(t, \lambda)$] is given by the integration of the concentration profile [$c(x, t)$] of the coloured species because the beam passes through the diffusion layer perpendicular to the surface, i.e.

$$A(t, \lambda) = \epsilon(\lambda) \int_0^\infty c(x, t) dx \quad (10.2)$$

where $\epsilon(\lambda)$ is the molar absorptivity at the wavelength λ . Thus for a potential step experiment where the reaction is diffusion controlled and R is the only absorbing species, $A(t, \lambda)$ is given by the integration of the Cottrell equation, Equation (2.16) and is found to increase with $t^{1/2}$ as described by Equation (10.3):

$$A(\lambda, t) = \frac{2c_0^\infty \epsilon(\lambda) D^{1/2} t^{1/2}}{\pi^{1/2}} \quad (10.3)$$

where the various symbols have their usual meanings. Fig. 10.3 shows a typical A vs t curve for a diffusion controlled reaction. Any deviation from this type of behaviour is a clear indication either that the process is not reversible or alternatively that the mechanism is not as simple as was thought. In either case, it is possible to obtain mechanistic and kinetic data from the recorded A - t transients. In general it is possible to obtain A - t transients with a resolution of 5–10 μ s which makes possible the determination of bimolecular rate constants for coupled reactions as high as $10^9 \text{ dm}^3 \text{ mol}^{-1} \text{ s}^{-1}$.

Kinetic parameters are obtained from A - t transients by fitting experimental data to model calculations. Where possible these are made analytically but generally they are the result of computer simulations, usually carried out using the finite difference method (see Appendix). Details of the techniques used are given by Kuwana & Winograd [7], whilst Hanafey *et al.* [8] discuss the use of double potential step optical measurements which are very effective at differentiating between reaction mechanisms.

Before proceeding to discuss a specific example of the type of study described above it should be noted that the kinetic parameters are obtained from optical data recorded at a single wavelength. This is satisfactory for simple reactions with only one absorbing species present but can lead to problems if there are

several coloured components. In these cases the transient behaviour over a wide spectral range should be studied. This is most effectively done by using either an RSS system or one based on photodiode array detection.

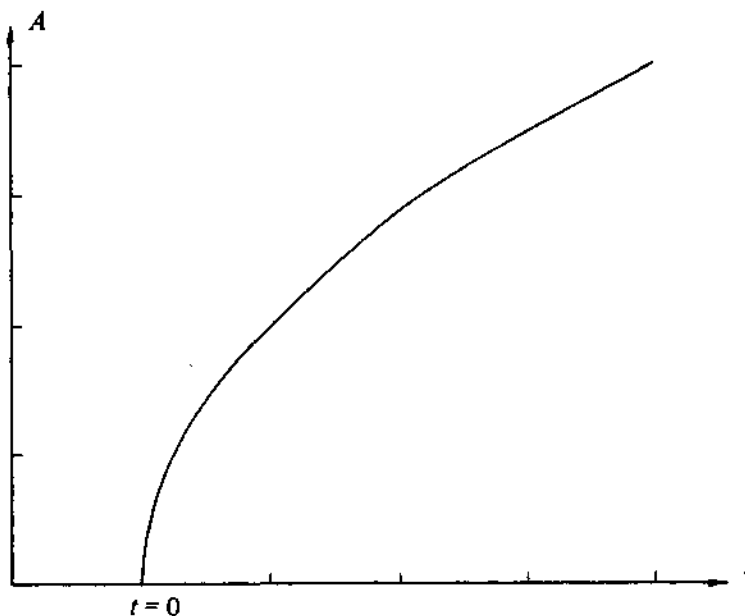
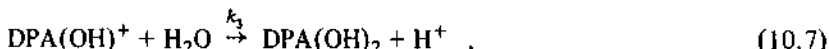
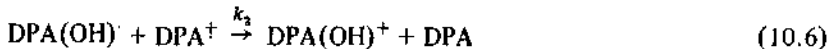


Fig. 10.3 – Absorbance-time curve for the formation of a coloured species under conditions of diffusion control.

Whilst OTEs have been successfully used to investigate a wide range of reaction types, the major application has been in the study of systems which involve coupled chemical reactions. An example of this type of study is that of the oxidation of diphenylanthracene (DPA) in the presence of water by Blount & Kuwana [9]. By monitoring the absorbance due to the radical cation of DPA, the first oxidation product, the reaction was shown to follow the scheme



rather than the ece and disp mechanisms that had previously been suggested on the basis of conventional electrochemical experiments. Fig. 10.4 shows an absorbance-time transient at a wavelength corresponding to an absorbance

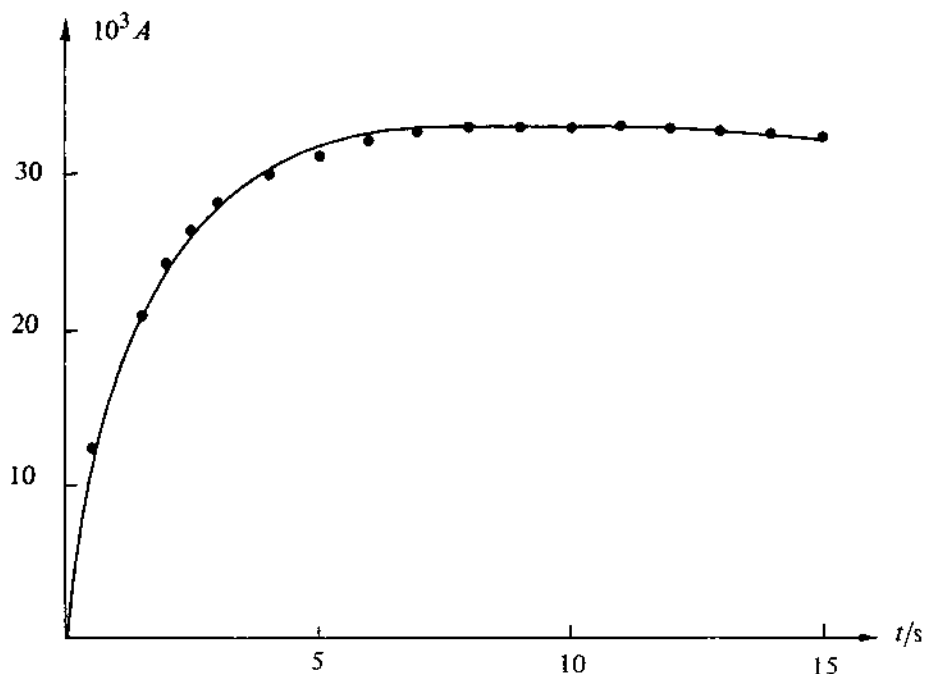


Fig. 10.4 – Experimental absorbance–time curve for the radical cation of DPA formed by oxidation of diphenylanthracene (DPA), in acetonitrile/water (10 mol dm^{-3}). Data taken from H. N. Blount & T. Kuwana, *J. Electroanal. Chem.*, 27, (1970), 464.

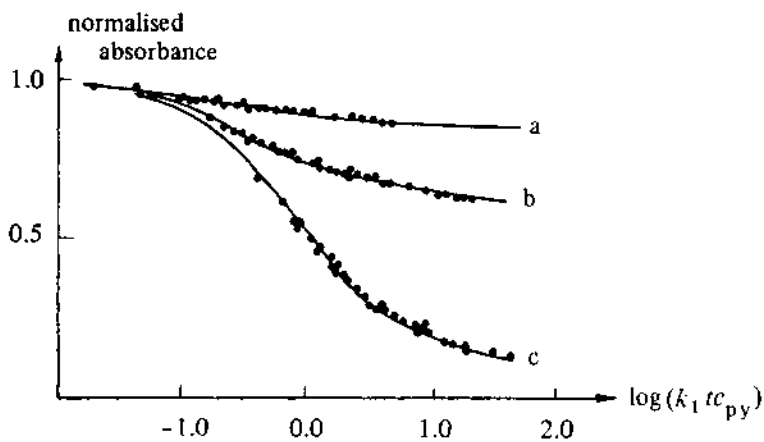


Fig. 10.5 – A comparison of experimental (points) and simulated (solid lines) spectroelectrochemical responses for the oxidation of DPA in CH_3CN containing pyridine (py). The curves are calculated for

(a) $c_{\text{py}}/c_{\text{DPA}} = 0.054$ and $k_1 = 1.7 \pm 0.4 \times 10^4 \text{ dm}^3 \text{ mol}^{-1} \text{ s}^{-1}$

(b) $c_{\text{py}}/c_{\text{DPA}} = 0.207$ and $k_1 = 1.8 \pm 0.3 \times 10^4 \text{ dm}^3 \text{ mol}^{-1} \text{ s}^{-1}$

(c) $c_{\text{py}}/c_{\text{DPA}} = 1.022$ and $k_1 = 1.8 \pm 0.3 \times 10^4 \text{ dm}^3 \text{ mol}^{-1} \text{ s}^{-1}$

Data taken from H. N. Blount, *J. Electroanal. Chem.*, 42, (1973), 271.

maximum of DPA^+ , and it can clearly be seen that at long times the absorbance starts to fall due to the presence of the following chemical reactions, whereas for the diffusion controlled reaction, Fig. 10.3, the absorbance continues to rise. By fitting data such as that in Fig. 10.4 to simulated results the mechanistic assignment was made and the value of k_1 was obtained. It was subsequently shown by Blount [10] that the oxidation of DPA in the presence of pyridine follows the same type of mechanism, and Fig. 10.5 shows dimensionless plots of the experimental optical transient data fitted to simulated results.

A further important application of experiments of this type is in the differentiation between ece and disp 1 reactions (see discussion in Chapter 2 and Equations (2.43) to (2.46)), which is difficult by conventional electrochemical methods. The technique used is to monitor the optical signal at an absorbance maximum of the product of the first redox reaction, as the potential is first pulsed into the diffusion controlled region and then as the cell is subsequently open circuited. Fig. 10.6 shows simulated A vs t curves [11] for the two reaction schemes. Since the behaviour is so different, the differentiation is a simple matter.

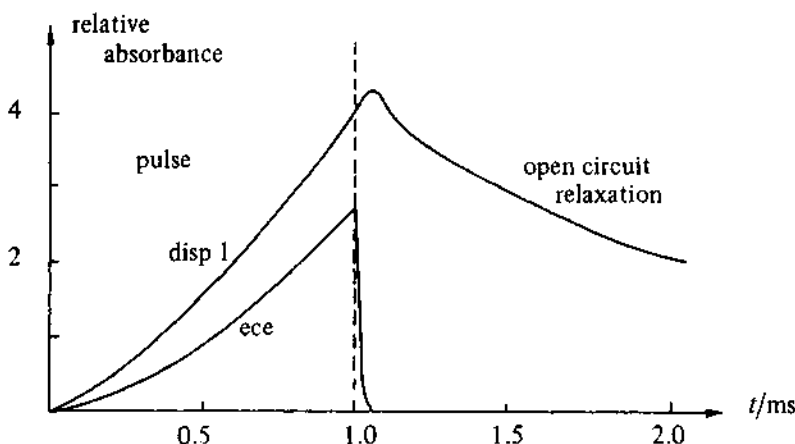


Fig. 10.6 – A comparison of absorbance-time curves for a potential step followed by open circuit relaxation for the ece and disp 1 mechanisms. Reproduced with permission from A. Bewick, J. M. Mellor, & B. S. Pons, *Electrochim. Acta*, 23, (1978), 77.

10.1.2 The optically transparent thin layer electrode

At about the same time as OTEs were first used in spectroelectrochemistry an alternative design, known as the optically transparent thin layer electrode (OTTLE), appeared. In its original form [12] this consisted of a piece of gold minigrid (a thin gold sheet with typically 100–2000 perforations per inch) sandwiched between two glass microscope slides held together by a 100 μm thick adhesive spacer, as shown in Fig. 10.7. The holes in the minigrid were of such a size that the OTTLE transmitted between 20% and 80% of visible

light, whilst the electrode still behaved essentially as though it were planar. As also shown in Fig. 10.7, the OTTLE is then placed in a cup of solution containing both a secondary and reference electrode and is filled either by capillary action or by applying a vacuum to the top of the electrode assembly. The thin layer cell is positioned in the solution cup such that only the bottom few millimetres are immersed, and thus a light beam can pass unobstructed through the thin layer. In addition to gold minigrids a range of other electrode materials has been used including evaporated metal films, nickel and copper minigrids, mercury electrodeposited on a minigrid, and reticulated vitreous carbon; a variety of other cell designs have also appeared. These alternatives have been recently reviewed [1]. The major advantages of OTTLEs are that they can be constructed both quickly and cheaply, and can be mounted directly in a conventional spectrometer.

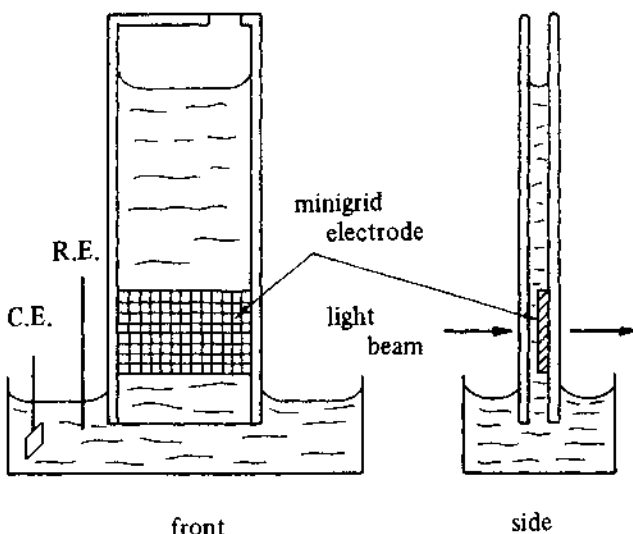


Fig. 10.7 ... A schematic diagram of a cell incorporating an OTTLE.

There are two major differences between OTE and OTTLE systems. Firstly there is considerable iR drop in the OTTLE, and therefore it is unsuitable for fast kinetic studies. Secondly it is possible to convert all of the electroactive species in the light path to product in a very short time (typically less than a minute). In view of these differences OTEs, and OTTLEs have rather different applications.

The simplest type of experiment with an OTTLE is aimed simply at identifying reaction products. The electroactive species in solution is electrolysed at constant potential until the current decreases to zero (typically 30–60 s), and then the spectrum of the product is recorded. Provided this product contains a strong chromophore, a conventional spectrometer is usually adequate; alternatively an RSS or photodiode array system is used. In view of the timescale

of this experiment the spectrum recorded is that of the final product of the reaction, and not necessarily that of the initial product of the electron transfer. This contrasts with OTE studies where it is this initial product that is usually studied.

Over recent years the major use of OTTLEs has been in determining standard potentials and n values for redox couples. The simplest way of describing how this is done is to consider a specific example; the redox couple formed by the bis(salicylaldehyde)ethylenediimine complexes of Co(I) and Co(II) [13]. Initially a solution of the Co(II) complex is prepared. Progressively more negative potentials are applied, and at each potential the current is allowed to fall to zero before a spectrum is recorded. Fig. 10.8 shows a series of such spectra for the above couple. From these spectra it is possible to determine the concentrations of the two halves of the redox couple, and hence from the Nernst equation

$$E_e = E_e^\ominus + \frac{2.3RT}{nF} \log \frac{c_O}{c_R} \quad (10.8)$$

it can be seen that by plotting $\log (c_O/c_R)$ as a function of the applied potential it is a simple matter to find the value of E_e^\ominus (from the intercept) and n (from the gradient). An extension of this type of study is the investigation of redox couples based on large, frequently biologically important molecules, e.g. cytochrome C, where the rate of heterogeneous electron transfer is low and where direct measurement of standard potentials is consequently difficult. In this case a mediator is used to couple the redox system to the electrode potential.

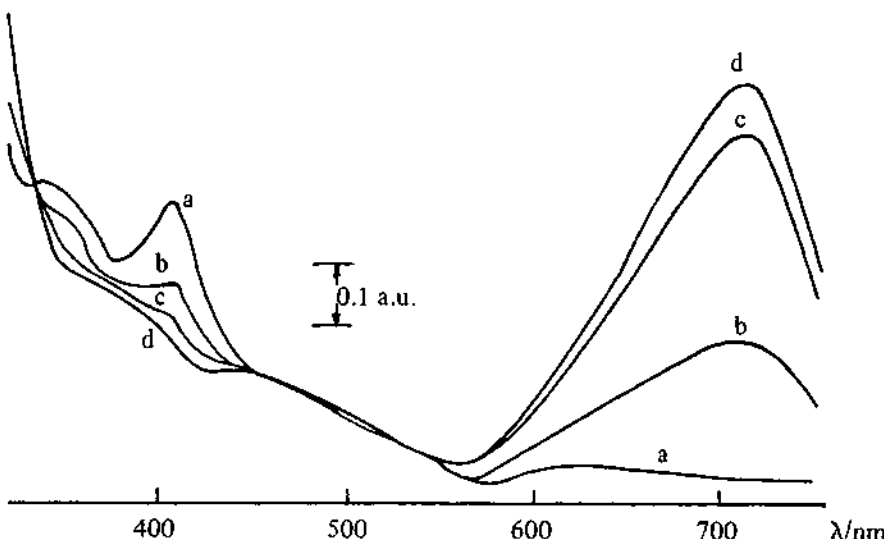
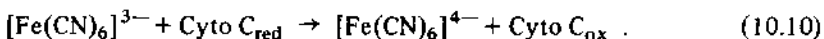


Fig. 10.8 – Spectra of the cobalt complexes of bis(salicylaldehyde) ethylenediiamine obtained at an OTTLE at (a) -0.90 V, (b) -1.18 V, (c) -1.25 V, (d) -1.45 vs SCE. Data taken from D. F. Rohrbach, E. Deutsch, & W. R. Heineman in G. Mamantov (Ed), *Characterisation of non-aqueous solvents*, Plenum Press, 1978.

A commonly used mediator is the ferricyanide/ferrocyanide couple, and Equations (10.9) and (10.10) show the reaction sequence involved:



The mediator is oxidised or reduced at the electrode, and in turn oxidises or reduces the biocomponent with regeneration of the mediator. The OTTLE experiment is essentially the same as that described above; spectra recorded at fixed potentials being used to determine the concentration of the reduced and oxidized forms of redox couple from which the E_e^\ominus and n value may be deduced.

10.1.3 Reflection techniques

The transmission techniques described above, particularly the OTE, have proved very successful for investigating simple electron transfer reactions and in investigating coupled homogeneous chemical reactions. They are not, however, so well suited to the investigation of surface properties and surface reactions, e.g. in electrocatalysis and corrosion. This is because the transparent electrodes used frequently behave, both optically and electrochemically, in a different way to those prepared from bulk materials, and it is anyway essentially impossible to prepare OTEs of many metals of interest, or of single crystals which are now widely used in surface studies. For such investigations reflection methods are much more suitable as these generally use conventional bulk electrodes. It should however be emphasised that great care must be taken in preparing electrode surfaces with reproducible electrochemical and optical properties. This usually involves initial mechanical polishing to a mirror finish followed by chemical or electrochemical polishing to remove the strained surface layer. Without careful preparation, it is impossible to obtain reproducible optical data for surface processes.

10.1.3.1 Ellipsometry

Ellipsometry was in fact the earliest optical technique to be applied to the study of electrode processes. It involves the determination of the change in polarisation state of an obliquely incident light beam upon specular reflection at a surface. In order to fully define a monochromatic light beam it is necessary, in addition to knowing the frequency, amplitude, and direction of propagation, to include information about the electric and magnetic vectors which describe the polarisation state. Since these vectors are orthogonal and related in amplitude it is, in fact, only necessary to consider one of them, and it is the electric vector that is usually chosen. If this vector lies in a plane then the beam is said to be *plane polarized*, and further if this plane lies parallel to the plane of incidence at a surface the beam is said to be *p-polarised*, whereas a beam polarised in a plane perpendicular to the plane of incidence is referred to as *s-polarised*. For any beam it is possible to resolve the electric vector into its *s* and *p* components, and when these components are of the same frequency but different phase and amplitude the beam is said to be *elliptically polarised*. This name arises from the

fact that at any point in the beam the electric vector describes an ellipse with time. The state of this elliptical polarisation is defined by two parameters, ψ and Δ ; $\tan \psi$ is the ratio of the amplitudes of the p and s components of the electric vector and Δ is the phase difference between these components. Upon reflection at a surface, the values of ψ and Δ change, and these changes can be related to the optical properties of the interfaces. Ellipsometry involves measuring the values of ψ and Δ after reflection of an initially plane polarised beam. It is the principal technique used to determine the optical constants of clean surfaces, and is also widely used to investigate the properties of thin surface films.

Fig. 10.9 is a block diagram of a basic manual ellipsometer. The incident light beam is plane polarised, and the compensator and analyser are adjusted to obtain zero light intensity at the detector. From the settings of the polariser, analyser and compensator the values of ψ and Δ are obtained. This nulling procedure typically takes several minutes, and clearly such an ellipsometer is unsuitable for time resolved studies. Recently a number of designs for automatic instruments operating under computer control have been proposed, some of which enable measurements to be made in less than 20 ms and also permit wavelength scanning. These developments are fully discussed in a recent review [14]. The major drawback with these ellipsometers is their expense, and as yet there are very few installed around the world and still fewer being used for electrochemical applications.

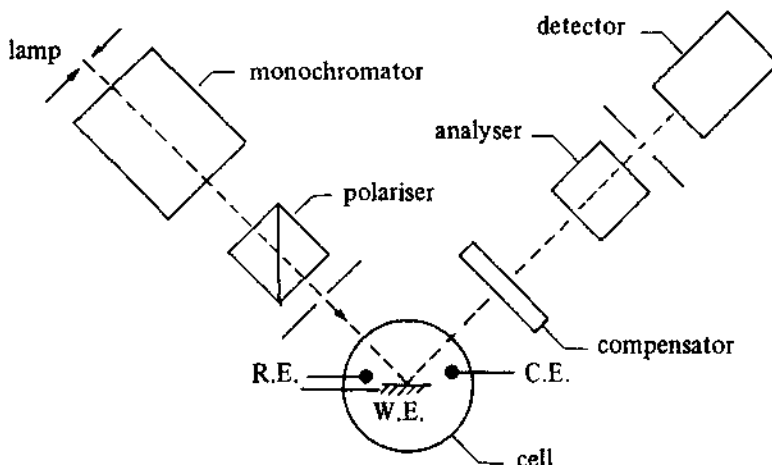


Fig. 10.9 – Schematic diagram of an ellipsometer.

The design of the electrochemical cell for ellipsometry is a fairly simple matter; apart from the normal electrochemical requirements, the only constraints are that the cell incorporates entrance and exit windows for the light beam that are of optical grade materials of high transmittance. A design that has been particularly successful is that of a hollow quartz cylinder, with the electrode mounted at the centre, as this permits easy variation of the angle of incidence.

Having obtained values of Δ and ψ for the electrode/solution interface of interest, or more commonly detected changes as the electrode potential is varied, the next step is to relate these values to the properties of the interface. As with all reflection techniques, this is usually done in terms of a three layer model consisting of bulk substrate/interfacial region/bulk solution as shown in Fig. 10.10. Assuming the optical constants of the substrate and solution and the film thickness are known, it is possible to obtain unique values of the effective optical constants of the interphase from Δ and ψ [15]. The optical characteristics of any phase are simply defined by $\hat{\epsilon}$, the magnetic permeability (usually equal to unity) and either the wavelength dependent complex dielectric constant defined by Equation (10.11)

$$\hat{\epsilon} = \epsilon' - i\epsilon'' \quad (10.11)$$

or alternatively the complex refractive index defined by Equation (10.12)

$$\hat{n} = n - ik \quad (10.12)$$

where n and k are related to ϵ' and ϵ'' as shown in Equations (10.13) and (10.14)

$$\epsilon' = \frac{n^2 - k^2}{\mu} \quad (10.13)$$

$$\epsilon'' = \frac{2nk}{\mu}. \quad (10.14)$$

This approach has proved remarkably successful in electrochemical studies of surface films despite the model being unrealistic; typically the surface film will not have a uniform dielectric constant, and it is also likely to be anisotropic. Efforts are currently being made to model the interface at a microscopic level but major developments seem some way off.

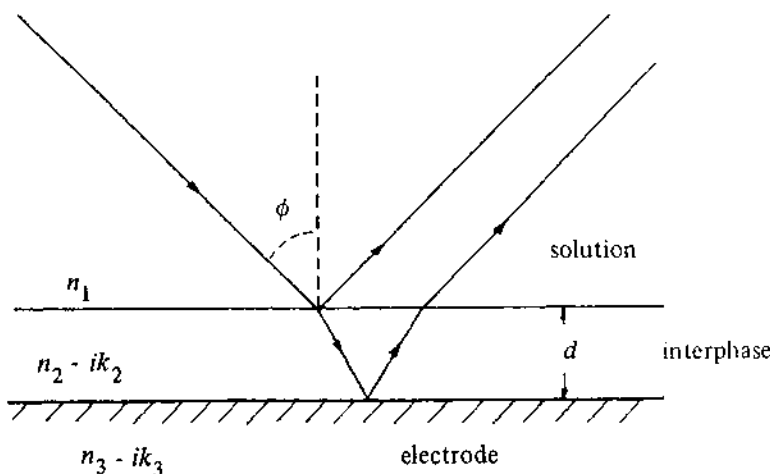


Fig. 10.10 -- The three layer optical model for the electrode/electrolyte interface.

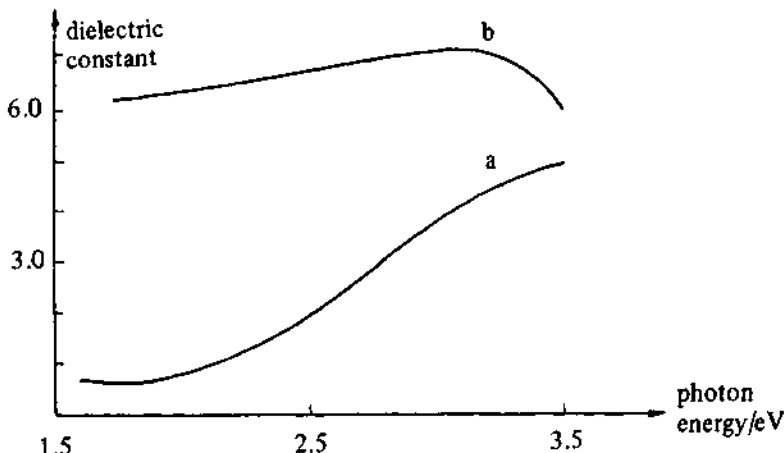


Fig. 10.11 - A plot of the frequency dependence of the optical constants of a passive film formed on iron in a borate buffer, pH 8, at 1.35 V vs NHE. These values were determined by ellipsometry at 1.25 V using an angle of incidence of 68° . (a) ϵ' , (b) ϵ'' . Reproduced with permission from C. T. Chen & B. D. Cahan, *J. Electrochem. Soc.*, 129, (1982), 17.

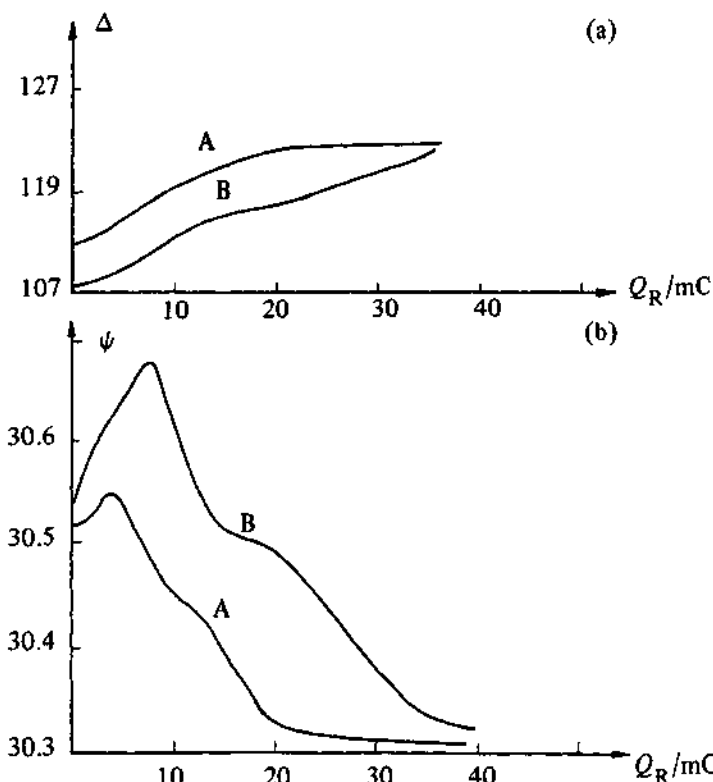


Fig. 10.12 - Plots showing the dependence of (a) Δ and (b) ψ on the charge passed during the reduction of passive iron oxides. The passive films were formed for 300 s at (A) 0.75 V and (B) 1.35 V and then reduced at -0.25 V vs NHE. The wavelength was 460 nm and the angle of incidence 68° . Reproduced with permission from C. T. Chen & B. D. Cahan, *J. Electrochem. Soc.*, 129, (1982), 17.

As was stated earlier, ellipsometry is best suited to the study of thin surface films, and the major area of application has been in corrosion studies, particularly the formation of passive layers. To indicate the type of information that can be obtained, we will consider a recent investigation of the corrosion of iron carried out by Chen & Cahan [16]. Fig. 10.11, for example, shows a plot of the wavelength dependence of the values of the real and imaginary parts of the dielectric constant of a thin passivating oxide film on iron determined *in situ*. By comparison with the values for known materials, it was concluded that the passivating layer consisted of Fe(III) species. Fig. 10.12, on the other hand, shows optical transients for the potentiostatic removal of the passivating layer. From the dependence of Δ and ψ on the charge passed it can clearly be seen that there are two reduction processes; the first corresponding to one third of total charge, and the second two thirds. It was therefore concluded that the ferric layer was first reduced to a ferrous one prior to reduction to the metal.

The above study represents the current 'state of the art' in the ellipsometry of electrochemical systems and, in particular, is one of very few that have used wavelength scanning. Most reported investigations have been at fixed wavelength, and these range from the study of oxide film formation on noble metals to studies of adsorption. Many examples of this type of work are presented in the proceedings of the International Conference on Ellipsometry [17, 18].

10.1.3.2 Specular reflectance spectroscopy

Whilst ellipsometry is undoubtedly the technique to use to obtain accurate optical constants for surfaces and surface films, it suffers from being both expensive and slow, and consequently has only been of limited use to electrochemists. As a result of these difficulties, several techniques based on simply monitoring of the reflectivity of an interface have been developed. Whilst in theory these are less informative, in practice they have proved much more useful. The major advantages are lower cost and greater speed, making them ideal for kinetic studies.

The principle of the reflectance spectroscopy technique is to shine a monochromatic light beam, usually polarised in a plane parallel or perpendicular to the plane of incidence, at an electrode surface at a known angle of incidence and to record the intensity of the reflected beam as a function of either wavelength, potential or time. The data obtained are then compared to model calculations made using the same three layer model as is used in ellipsometry, i.e. bulk electrode/interfacial region/bulk solution. These calculations are based on the Fresnel equations [19] and assume that all phases are isotropic.

For most systems of electrochemical interest, only very small changes in reflectivity are predicted, and these would be very difficult to detect and quantify directly. To overcome this problem several different approaches have been used to enhance the sensitivity of reflectance measurements. As a result, several distinct experimental techniques have been developed.

Probably the simplest way of increasing the sensitivity is to increase the number of reflections. This is done by using two, electrically linked working electrodes mounted parallel to one another as shown in Fig. 10.13, and bouncing

the light beam between them. In a recent design [20] the electrodes were mounted only 120 µm apart, and with 300 reflections in the cell, absorbance changes as low as 5×10^{-5} absorbance units per reflection were detectable. Such a cell is satisfactory for studying solution free species (with the usual limitations of a thin layer design), but since all polarisation information is lost after only a few reflections it is not suited to studying surfaces. An alternative way of enhancing the sensitivity to solution free species is to use an extremely glancing angle of incidence thereby increasing the path length. This enhancement (as compared to normal incidence) reaches a factor in excess of 100 for angles of incidence greater than 89°, and therefore this technique has a sensitivity comparable to that of the multiple reflection technique.

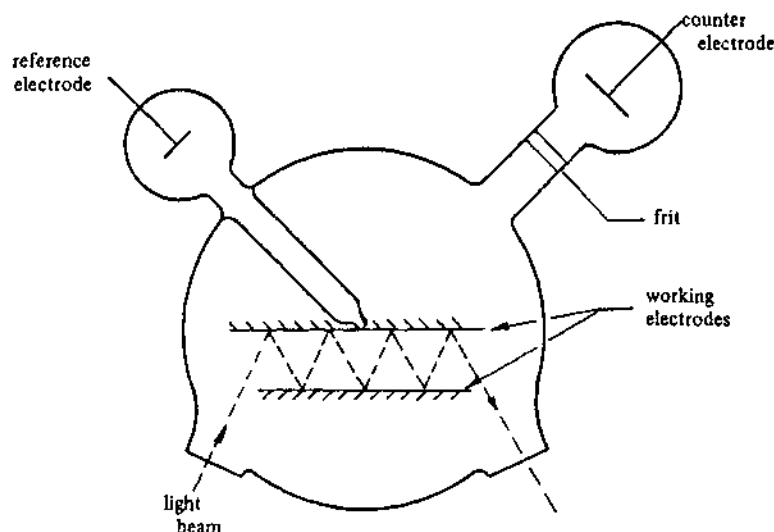


Fig. 10.13 – Cell for multiple reflectance experiments.

Both the above techniques still require absolute reflectivity measurements to be made if quantitative results are to be obtained (chopping the light beam and using phase sensitive detection aids these determinations). Such measurements are notoriously difficult to make, and therefore multiple reflection and glancing incidence are both best suited to qualitative investigations of solution free species. The optical equipment required is essentially identical to that used for OTE studies, and data treatment is also similar.

By far the most successful reflectance spectroscopic technique relies, not on measuring absolute reflectivities, but rather on detecting changes in reflectivity as the potential is modulated. A block diagram of a typical apparatus is given in Fig. 10.14. It consists of a highly stabilized intense light source (frequently an Hg or Hg/Xe arc), monochromator, polariser, cell, and photodetector with appropriate focusing and collimating lenses. Cell and electrode design requirements are identical to those for ellipsometry and, again, the cylindrical cell has proved

particularly effective. The electrode potential is periodically modulated, usually with a square waveform, though sinusoidal ones have also been used, and the resultant small changes in reflectivity are detected using the lock-in amplifier. With a well designed system, changes as small as one part in 10^6 can be detected, and this is roughly equivalent to the formation of 1% of a typical adsorbed monolayer. For studies of solution free species fairly low modulation frequencies are used, typically less than 100s^{-1} . However, to minimise noise it is always a good idea to avoid values close to the line frequency and its harmonics. For surface processes, higher frequencies are possible. However, it is essential to ascertain whether the results are frequency dependent. Such a dependence implies the presence of a slow kinetic step, and it is sometimes possible to obtain kinetic parameters relating to the slow step. Indeed, with the advent of frequency response analysers it is possible to record both in-phase and quadrature reflectance changes as the frequency is swept. The results can then be presented in the same way as impedance data (see Chapter 8).

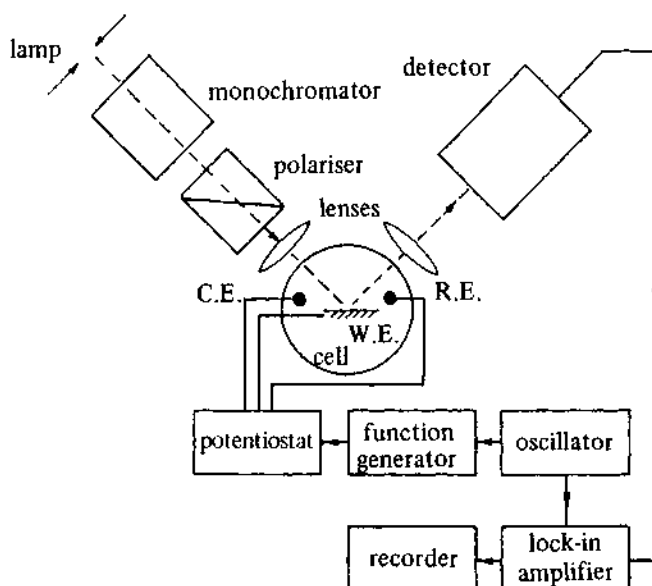


Fig. 10.14 - Schematic diagram of the apparatus for modulated specular reflectance spectroscopy.

Having obtained the reflectance change data, it is necessary to normalise them by dividing the reflectivity change by the steady state reflectivity, and consequently the results are presented as $\Delta R/R$ values. This normalisation is achieved in practice either by dividing the lock-in amplifier output by the photodetector output using a ratiometer or, when a photomultiplier is used, the high tension supply can be adjusted to give constant output using a feedback circuit (this

should be slow enough not to respond to the reflectivity changes caused by potential modulation). Using these techniques, $\Delta R/R$ values can therefore be recorded as either the bias potential, pulse height, or wavelength are slowly swept. For example, if an adsorption process is being studied the wavelength and pulse height might be fixed and $\Delta R/R$ values measured as the bias potential is slowly swept through a range encompassing the adsorption (or desorption). Alternatively, if it is desired to obtain the absorption spectrum of a reaction product the potential limits of the pulse would be fixed at values (a) where the electrode process of interest occurs at a diffusion controlled rate, and (b) where the reverse reaction occurs, and $\Delta R/R$ values would be recorded as the wavelength is swept. For kinetic studies the wavelength is fixed and the reflectance-time transient is recorded using a signal averager in place of the lock-in amplifier. One of the great advantages of potential modulation reflectance spectroscopy is that it is equally well suited to studies of solution free species and studies of surface processes, a feature not shared by other optical techniques.

Data obtained for solution free species are analysed in a manner identical to that used in OTE investigations except that in calculating the total absorbance due to a coloured species, allowance must be made for the increased path length through the diffusion layer. Thus the value given in Equation (10.2) has to be increased by the factor $2/\cos\phi$, where ϕ , the angle of incidence, is usually chosen to be about 45° as this minimises contributions to the reflectivity change from double layer effects. One additional, useful feature in reflectance studies is that data can be obtained for both s and p polarized light; for a purely solution free process $\Delta R/R$ should be independent of the polarisation state, whereas if surface effects, such as adsorption, are present the values will differ. Such a differentiation is not possible at an OTE.

Data analysis for surface processes is rather more complex, and as was stated earlier, relies on the use of the three layer model and the application of the Fresnel equations. The form of these equations is such that it is very difficult to see how changes in the optical properties of a particular component of the system will affect the reflectivity. Thus, while they are perfectly suitable for computer calculations, it is common to use the approximate equations first presented by McIntyre & Aspnes [21]. They showed that the reflectance changes on the formation of a surface phase (i.e. on going from a two layer system, bulk electrode/bulk solution, to a three layer one) are given by

$$\left(\frac{\Delta R}{R}\right)_s = \frac{8\pi d n_1 \cos\phi}{\lambda} \operatorname{Im}\left(\frac{(\hat{\epsilon}_2 - \hat{\epsilon}_3)}{(\epsilon_1 - \hat{\epsilon}_3)}\right) \quad (10.15)$$

$$\left(\frac{\Delta R}{R}\right)_p = \frac{8\pi d n_1 \cos\phi}{\lambda} \operatorname{Im}\left(\frac{(\hat{\epsilon}_2 - \hat{\epsilon}_3)}{(\epsilon_1 - \hat{\epsilon}_3)} \frac{1 - (\epsilon_1/\hat{\epsilon}_2\hat{\epsilon}_3)(\hat{\epsilon}_2 + \hat{\epsilon}_3)\sin^2\theta}{1 - (1/\hat{\epsilon}_3)(\epsilon_1 + \hat{\epsilon}_3)\sin^2\theta}\right) \quad (10.16)$$

where $\hat{\epsilon}_n$ is the complex dielectric constant of phase n , n_1 is the refractive index of the transparent incident phase, and $\operatorname{Im}(x)$ refers to the imaginary part of x . Using these relationships it was shown [22] that at 45° $(\Delta R/R)_s$ and $(\Delta R/R)_p$ are both very small when the interphase is transparent, and that

$$\left(\frac{\Delta R}{R}\right)_p = 2 \left(\frac{\Delta R}{R}\right)_s \quad (10.17)$$

for an absorbing interphase. This relationship has proved to be a very useful diagnostic tool.

The major areas of application of reflectance spectroscopy have been the elucidation of reaction mechanisms, double layer studies, investigations of underpotential deposition (UPD), and studies of the electroreflectance effect (ER). This range is too large for an in depth discussion to be given here. Instead, two examples of the type of information that can be obtained will be described (a third system, hydrogen adsorption on platinum, has been discussed in Chapter 7). Those readers interested in more details are referred to a recent review [1], and the literature cited therein.

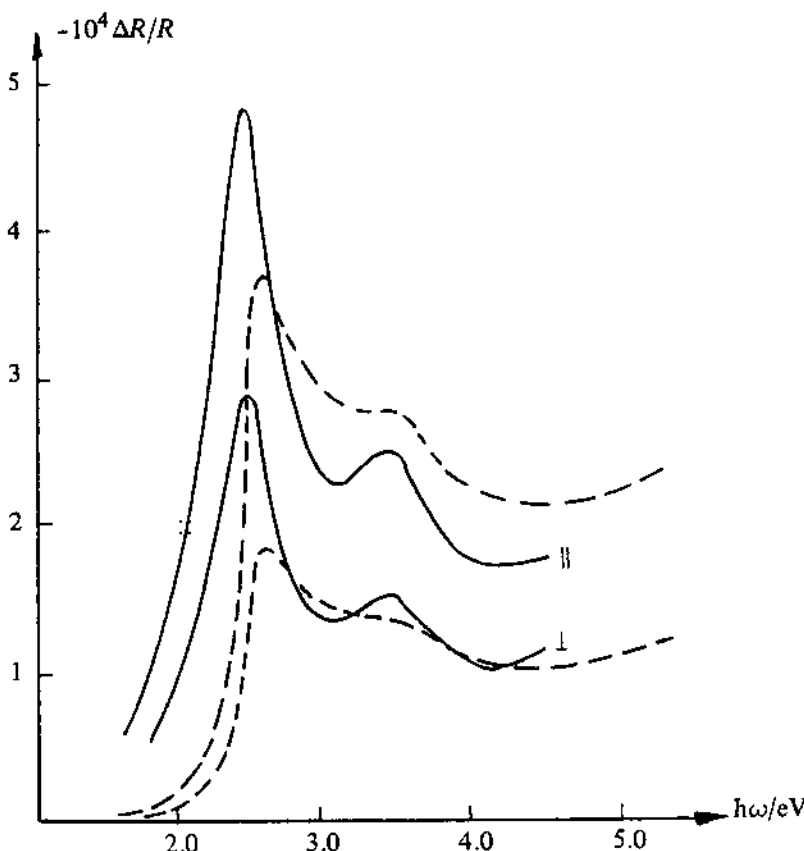


Fig. 10.15 – Electorelectance spectra for a gold electrode in HClO_4 (1 mol dm^{-3}) $\phi = 45^\circ$, potential pulsed between $+0.4 \text{ V}$ and $+1.6 \text{ V}$ vs NHE, charge modulation $1.91 \mu\text{C cm}^{-2}$ and modulation frequency 270 Hz . Experimental curves are solid lines, and theoretical ones are broken lines. Reproduced with permission from J. D. McIntyre, *Symp. Faraday Soc.*, 4, (1970) 99.

The first example concerns the ER effect, an effect which is always present in optical studies of electrode surfaces but which was first recognised using reflectance spectroscopy. It arises from the fact that, even in the absence of any surface reaction, there is a layer at the electrode surface (typically less than 0.1 nm thick) that does not have the same optical properties as the bulk electrode, and that the optical properties of this layer are potential dependent. There are now several theories to account for the ER effect; the simplest, and one that accounts fairly well for the behaviour observed at noble metal electrodes, is due to McIntyre & Aspnes [23]. It assumes that the optical properties of the metal can be split into two contributions, one from bound electrons and the other from free electrons. Whilst the bound electron contribution is assumed to be independent of the electrode potential, the free electron contribution changes with the surface charge density, and thus the potential. For normal incidence it is shown that

$$\frac{\Delta R}{R} = \frac{8\pi n_1}{\lambda} \frac{C_{dl}\Delta E}{N} \text{Im} \left(\frac{\hat{\epsilon}_{3f} - 1}{\hat{\epsilon}_3 - \epsilon_1} \right) \quad (10.18)$$

where C_{dl} is the double layer capacity, ΔE is the amplitude of the potential modulation, N is the bulk electron density, and $\hat{\epsilon}_{3f}$ is the free electron contribution to the bulk metal's optical constants (similar expressions can be developed for non-normal incidence when the polarisation state becomes important). Fig. 10.15 shows a comparison between the experimental ER effect for gold and the spectrum calculated using McIntyre & Aspnes' theory [24]. The fit is quite good. It has subsequently been shown for noble metals that bound electron contributions only become important at high surface charge densities whilst for some other metals, e.g. lead and indium, bound electron effects dominate.

The second example involves the underpotential deposition of Cu on platinum single crystals [25]. Fig. 10.16 shows how the $\Delta R/R$ values at normal incidence on (100), (111), and (110) faces vary as a function of copper coverage. On the (100) face current-potential data shows that the first half monolayer forms over a narrow potential range (implying weak ad-atom/ad-atom interactions), whilst the second half forms over a much wider range. The optical results show a change in slope of $\Delta R/R$ vs θ at $\theta = 0.5$. This slope is a measure of the ad-atom/ad-atom interaction, and thus these optical results support the conclusions drawn from the current-potential data. It is suggested that the first half monolayer forms a 2×2 structure, whilst monolayer coverage corresponds to a 1×1 epitaxial layer formed by filling in the gaps. On the (111) face the electrochemical data show that only $2/3$ of a monolayer is formed. The optical data show that there is a kink in the $\Delta R/R$ vs θ plot at $\theta = 1/3$, and this is taken to imply a reconstruction of the adsorbed layer. The most interesting results are on the (110) face where straight electrochemical data show there to be two well defined half monolayer processes. However, from the optical results when the electric vector is parallel to the (110) face the slope of $\Delta R/R$ vs θ is constant; only when the electric vector is perpendicular to this direction is there a change in slope at $\theta = 0.5$. This suggests that adsorption occurs preferentially along (110), and at all coverages the adsorbate is densely packed in this direction. It is suggested that for $\theta < 0.5$

only every second substrate groove in the (110) direction is full, but as θ exceeds 0.5 the rows in between become occupied. This study is one of the most detailed of a UPD system and clearly shows that optical experiments can reveal information not obtainable from simple electrochemical experiments.

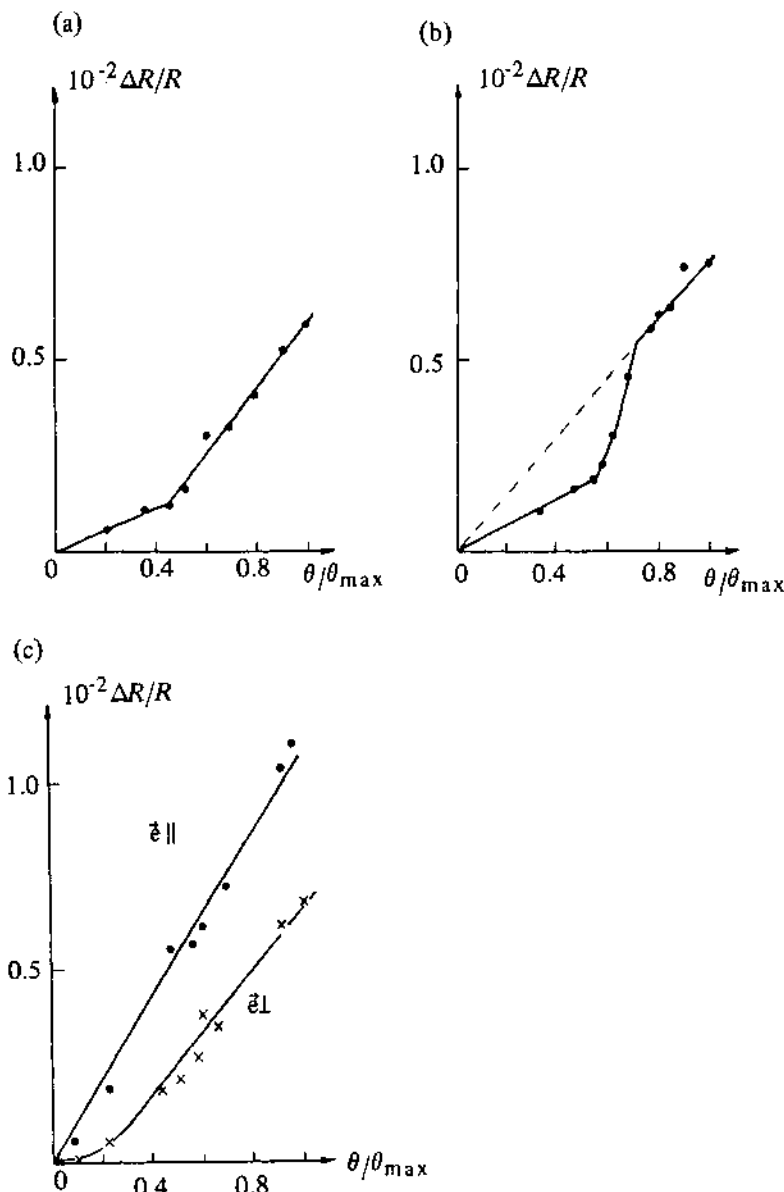


Fig. 10.16 -- Plots showing the dependence of $\Delta R/R$ on coverage of Cu adatoms on a Pt single crystal. The measurements were made at normal incidence at a wavelength of 450 nm on (a)(100), (b)(111) and (c)(110) surfaces. Reproduced with permission from D. M. Kolb, R. Kötz, & K. Yamamoto, *Surf. Sci.*, 87, (1979), 20.

10.1.3.3 Attenuated internal reflectance spectroscopy

The reflectance techniques discussed so far have all utilised external reflection of the light beam to monitor surfaces and species near a surface. There is, however, an alternative way of doing this type of experiment based on the use of an OTE. If we take an OTE cell and instead of directing the light beam normally through it, direct the beam through the OTE at an angle, then, as the angle of incidence at the electrode/solution interface is increased, a value (the critical angle) is reached at which the beam no longer passes through the cell but instead is totally internally reflected, and re-emerges back through the OTE. Though this beam is reflected at the electrode/solution interface, it in fact penetrates the solution to a distance up to a few hundred nanometers (the exact depth is a function of the wavelength and the optical properties of the system), and if the solution phase is absorbing, the emergent beam is attenuated. Thus by measuring the intensity of the internally reflected beam the absorbance of the thin layer next to the electrode can be monitored [26]. Since the penetration depth of the light beam is comparable to, or less than, the thickness of the diffusion layer at the electrode surface, this is quite a good technique for monitoring the concentrations of coloured species near, or on, an electrode. Thin evaporated metal films are the most suitable type of OTE for these experiments as the thickness of doped SnO_2 required to give adequate conductivity is comparable to the wavelength of light; hence there are problems with interference effects. By using multiple internal reflection, effective path lengths up to $2.5\mu\text{m}$ can be achieved, and hence a high sensitivity is possible.

The types of experiment that are performed and the data analysis are essentially the same as were discussed in connection with transmission experiments. Both solution free and surface species have been studied, and indeed, some of the first studies of the ER effect were made in this mode. However, internal reflectance spectroscopy has not proved to be particularly popular as other techniques are equally effective and are often easier to implement.

10.1.4 Photothermal and photoacoustic spectroscopies

One problem that is encountered when trying to investigate technologically important systems, e.g. fuel cell electrodes, using optical techniques, is that the electrode is generally not highly reflecting and smooth, e.g. it may be a sintered powder. This precludes the application of any of the techniques discussed so far. Two techniques, which take advantage of the temperature rise in a system when it absorbs radiation, have been developed for the study of such systems. These techniques are photothermal and photoacoustic spectroscopy, and though neither has been widely applied; especially photoacoustic spectroscopy appears to be quite promising.

In photothermal spectroscopy, a sensitive fast response thermistor is attached to the back of the test electrode with silver epoxy (to achieve a good thermal contact), whilst an identical thermistor is placed in the bulk of the solution [27]. These thermistors are then configured as two branches of a balanced Wheatstone bridge and the electrode is illuminated with a chopped monochromatic light beam. The small periodic changes in the electrode temperature are then detected

as an imbalance in the bridge using a phase sensitive detector. Thus a ΔT vs λ plot represents the absorption spectrum of the electrode surface. Unfortunately the sensitivity of this technique is not all that high (~ 100 monolayers of a strongly coloured adsorbate). Better results have, however, been obtained using photo-acoustic spectroscopy. Here the temperature changes are not detected directly but, instead, the resultant small dimensional changes in the electrode are monitored. A piezoelectric ceramic detector is bonded to the test electrode which is again illuminated by a chopped beam. Phase sensitive detection is then used to detect the output of the piezocrystal. The only example of the application of this technique is in a study of electrochromic materials [28] (used in display devices), and Fig. 10.17 shows a typical result for a heptylviologen film on a platinum electrode as the potential is swept. The colouring and bleaching can clearly be seen. This was only a preliminary study, but it suggests that it might be possible to achieve monolayer sensitivity, with μs time response.

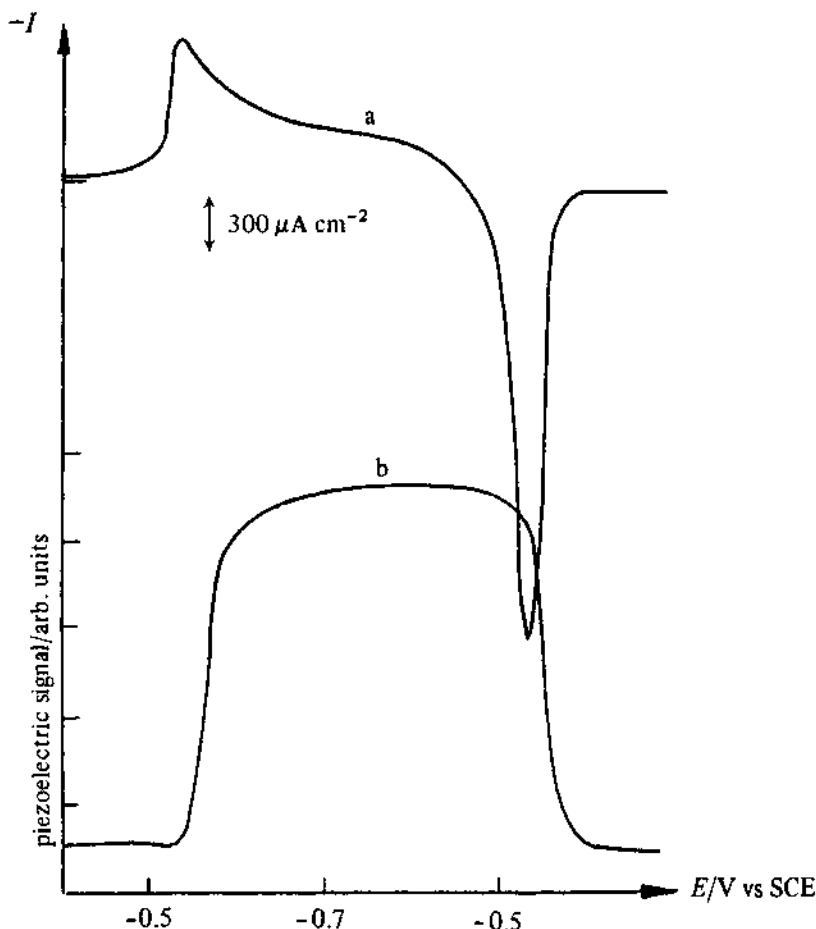


Fig. 10.17 – Simultaneous (a) cyclic voltammogram and (b) piezoelectric signal for the reduction of the heptylviologen dication on a Pt electrode. Scan rate 20 mV s^{-1} , $\lambda = 550 \text{ nm}$, chopping frequency 96 Hz . Reproduced with permission from R. E. Malpas & A. J. Bard, *Anal. Chem.*, 52, (1980), 109.

10.2 VIBRATIONAL SPECTROSCOPY

Whilst UV-visible techniques have proved extremely useful, they unfortunately lack molecular specificity. This means that they are not suitable for identifying adsorbates or studying adsorbate orientation and local environment. This type of information is best provided by vibrational spectroscopy, and therefore a considerable effort has been expended in developing vibrational spectroscopies that can be used *in situ* in an electrochemical cell. This effort is beginning to pay off, and techniques based on both infrared spectroscopy and Raman scattering spectroscopy are being increasingly used.

10.2.1 Infrared spectroscopy

Ever since the first reports of optical studies of electrochemical systems, efforts have been made to obtain infrared spectra of reaction intermediates and adsorbates. The earliest studies were based on total internal reflection using an n-type germanium electrode (transparent to IR radiation), and OTTLE systems using gold minigrids sandwiched between NaCl plates. These were not particularly successful, however, and it is only recently that these configurations have again been used, this time for Fourier Transform spectroscopy [29, 30]. Undoubtedly the most successful technique has been potential modulated external reflectance IR spectroscopy [31].

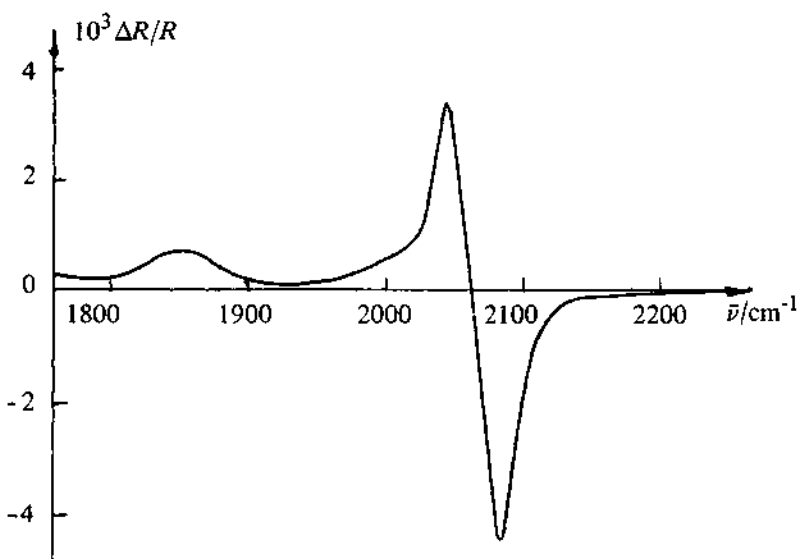


Fig. 10.18 IR spectrum of the adsorbed intermediate during methanol oxidation. Solution CH_3OH (0.5 mol dm^{-3}) in H_2SO_4 (1 mol dm^{-3}). Potential modulation between 50 mV and 450 mV. Reproduced with permission from A. Bewick, K. Kunimatsu, B. S. Pons, & J. W. Russell, *J. Electroanal. Chem.*, **160**, (1984), 47.

The experimental configuration is fairly similar to that described for UV-visible studies, except of course glass optics can no longer be used, silica or silicon being suitable replacements, and the source and detector also have to be changed. The changes in IR reflectivity caused by an adsorbate are very small indeed and frequently it is necessary to signal average the lock-in amplifier output, as the wavelength or potential are swept. Despite this a number of interesting results have been reported and it has even proved possible to obtain data in aqueous solution close to water absorption bands. This was achieved by pushing the electrode hard against the window of the cell, trapping a thin electrolyte layer. This layer is sufficiently thick that the surface electrochemistry is not significantly perturbed, but thin enough that not all the incident radiation is absorbed. One of the major areas of study using this technique has been the investigation of the electrocatalytic oxidation of small organic fuels [32]. As an example of this type of study Fig. 10.18 shows a spectrum obtained for the oxidation of methanol on platinum which clearly indicates that the species that poisons the catalysis is a bridge bonded CO species. More recently reflectance mode Fourier Transform IR spectroscopy has begun to be used [33], and it can be anticipated that this technique will increase in popularity.

10.2.2 Laser Raman vibrational spectroscopy

Infrared spectroscopy suffers from two major problems, absorption by the solvent, and, at low energies (less than 200 cm^{-1}), absorption by the window material. This latter point is particularly important as this is the region where metal adsorbate stretching frequencies are anticipated. One way of overcoming these difficulties is to obtain vibrational spectra using Raman scattering techniques, as then only visible radiation is involved.

Raman scattering cross-sections are very low, and if we consider a typical adsorbate, where there will be about $10^{15}\text{ molecules cm}^{-2}$ at monolayer coverage, or an electroactive species in the diffusion layer where the number of molecules is similar, it is clear that even with an optimised system the Raman scattering by the species of interest will be exceedingly difficult to detect. Fortunately it is possible to enhance the Raman scattering cross-sections. The first technique for achieving this enhancement is known as *resonance Raman scattering* (RRS) and is largely used for studying species in solution, whilst the second technique, *surface enhanced Raman scattering* (SERS), has been developed for studying surfaces and adsorbates.

The design of the spectrometer and counting system used for both RRS and SERS experiments is conventional with photodiode array detection becoming increasingly popular. The design of the cell requires some care, and a typical configuration is shown in Fig. 10.19. It consists of a glass cell with a single optical flat window. The removable working electrode is mounted close, and parallel, to the window, whilst the counter and reference electrodes, and gas purging facilities, are mounted elsewhere out of the light path. It is difficult to mount the counter electrode and Luggin capillary to ensure that there is no potential variation across the electrode, but the arrangement shown in Fig. 10.19 has proved effective. A useful type of working electrode consists of a rod sealed

into a glass, Teflon, or Kel-F sheath to expose only the circular cross-section (the use of epoxy resins should be avoided as much as possible as these frequently fluoresce strongly). The electrode is usually mounted about 1–2 mm from the cell window but can be moved closer if scattering by the solvent is a problem, though this can lead to local heating. The possibility of the reflected laser beam entering the collection optics is avoided by having the laser beam incident at an angle of about 45° to the electrode and collecting the scattered radiation perpendicular to the electrode.

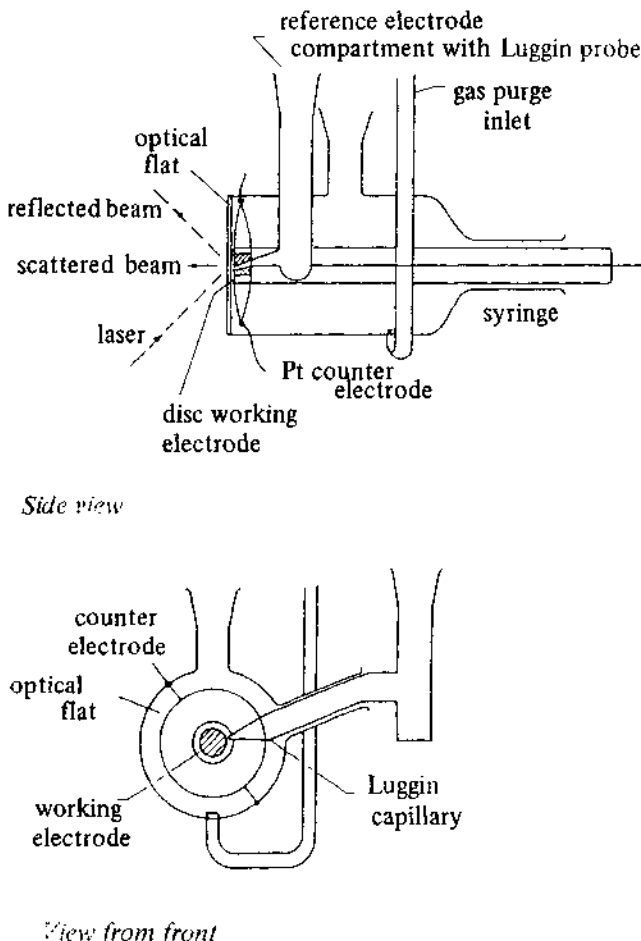


Fig. 10.19 – Cell for *in situ* Raman spectroscopy of electrode surfaces.

10.2.2.1 Resonance Raman scattering

Though scattering cross-sections for normal spontaneous Raman scattering are very small, they are increased by a factor of up to 10^6 if the frequency of the laser overlaps with an electronic transition in the sample. In order for the

enhancement to occur to a significant extent, the extinction coefficient of the sample should be in excess of $10^3 \text{ dm}^3 \text{ mol}^{-1} \text{ cm}^{-1}$ at the laser frequency, and therefore the sample should be fairly strongly coloured. The cross-sections of all vibrations are not enhanced to the same extent, those most closely associated with the electronic transition being enhanced most, and therefore some care has to be taken in interpretation as a resonance Raman spectrum will not necessarily resemble the normal one.

The bulk of applications of RRS to electrochemistry have been undertaken by Van Duyne and his co-workers and have been connected with the study of electrogenerated cation and anion radicals. This work is discussed in a review by Van Duyne [34]. Whilst no kinetic determination have been made using RRS, the capability is obviously there as it has been shown that transient data can be obtained on a ms timescale, although with all the systems studied the data fitted a model of simple diffusion control. The great advantage of Raman transients over optical transients in the UV-visible region of the spectrum is that peaks in a Raman spectrum are usually very narrow and therefore interference from other species in solution is unlikely.

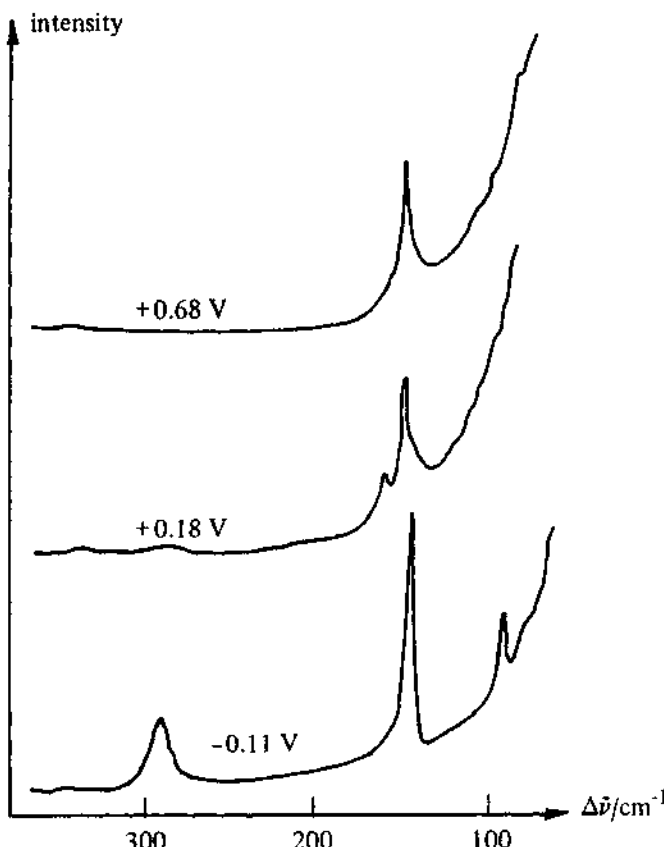


Fig. 10.20 – *In situ* Raman spectra of lead surfaces held for 18 hours in 0.1 mol dm^{-3} chloride solution, pH 7. The potentials (vs NHE) are shown on the figure. Reproduced with permission from R. J. Thibau, C. W. Brown, A. Z. Goldfarb, & R. H. Heiderbach, *J. Electrochem. Soc.*, 127, (1980), 1702.

RRS is not restricted to solution species, and Fig. 10.20 shows Raman spectra for the oxide film formed at pH 7 in chloride solution on Pb after 18 hours at various potentials, showing that as the potential changes from -0.11 V to $+0.68\text{ V}$ the film changes from an orthorhombic form of PbO to the thermodynamically favoured tetragonal form [35]. One difficulty in using the RRS technique at a surface is that the necessary absorption of the laser beam may lead to surface heating and consequently damage to the surface. Laser power should therefore be kept to the minimum required to obtain the spectrum, and if possible independent monitoring of the surface, e.g. by double layer capacitance measurements, should be performed to determine if the laser is affecting the surface properties.

10.2.2.2 Surface enhanced Raman scattering

When the first Raman spectroscopic study of an adsorbate on an electrode surface was undertaken [36], it was found that spectra could not be obtained from a smooth surface. It was therefore decided to increase the surface area, and hence the number of scatterers present, by roughening the electrode. The system studied was pyridine adsorption on silver, from a 0.1 mol dm^{-3} KCl solution, and the roughening was achieved by repeatedly sweeping the electrode potential from $+0.2\text{ V}$ vs SCE, where AgCl is formed, to -0.3 V where this film is reduced back to silver. Following this treatment, very intense spectra of adsorbed pyridine were obtained. It was soon recognised that the intensity of the spectra could not be accounted for simply by the surface area increase (enhancements by factors in excess of 10^6 have been reported), and that an enhancement mechanism, later to become known as *surface enhanced Raman scattering* (SERS) was in operation.

Since SERS spectra were first reported, the bulk of the research effort has been directed towards explaining the enhancement mechanism, though as yet without total success. On the basis of current evidence, it appears as though there are in fact two enhancement mechanisms in operation. The first of these is that the rough surface enables the laser beam to excite surface plasmons in the electrode surface which then couple with an adsorbate, thereby increasing its scattering cross-section, whilst the second effect is the presence of metal adatom and adatom clusters at the electrode surface. These adatoms, stabilised by adsorbed anions, are formed during the reductive part of the roughening cycle and may act to enhance the coupling of the excited surface plasmon to the adsorbate. A full discussion of these points is beyond the scope of this chapter, but full details of current theories for SERS are discussed elsewhere [37].

Despite the lack of an adequate theory for SERS, a very wide range of adsorption systems have been studied, with in excess of fifty papers having been published on the pyridine/silver system alone. Silver is by far the most commonly used substrate, though gold and copper have also been fairly widely used, with only occasional reports of the use of other metals. The roughening technique is basically the same for all metals, i.e. repeated cycling, or pulsing, into a potential region where the metal is oxidised, preferably to form an insoluble surface film, followed by a period at a potential where the oxidation

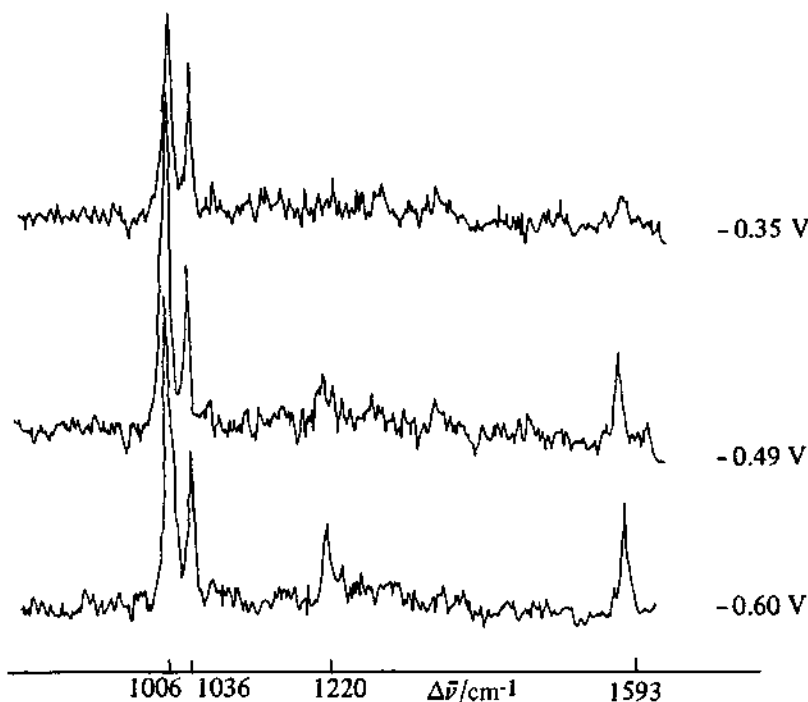


Fig. 10.21 – Spectra for pyridine adsorbed on a roughened silver electrode at the potentials shown. Spectra were acquired for 3 s as the potential was slowly scanned.

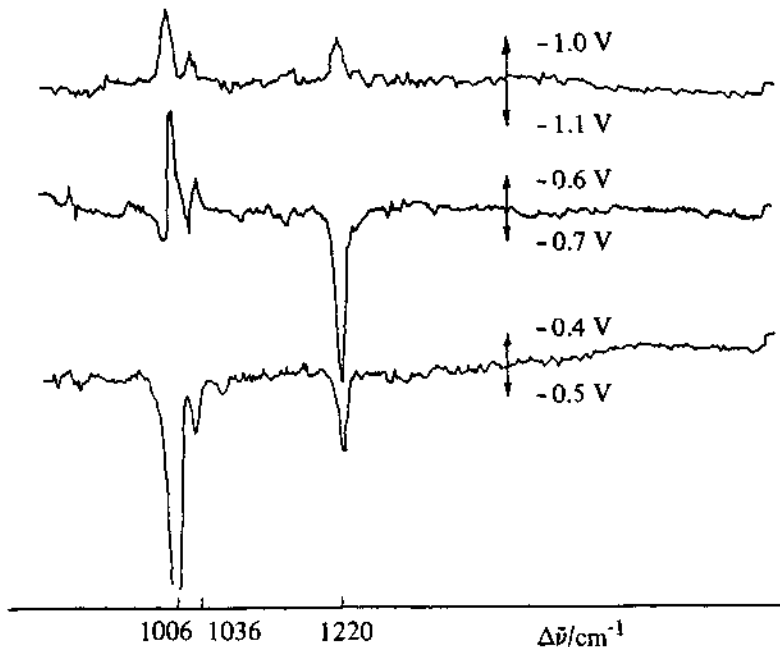


Fig. 10.22 – Potential difference spectra for pyridine adsorbed on roughened Ag after prolonged H_2 evolution. The spectra were acquired for 32 s at each potential and then subtracted.

product is reduced back to the metal. If the electrolyte system being used is such that a surface film is not formed but rather the electrode dissolves, e.g. a F^- solution, some roughening will still occur using the above procedure but better results will probably be obtained if the roughening is carried out in another cell containing for example Cl^- ions, followed by a thorough rinsing before transfer. The same argument applies to work in non-aqueous solvents where roughening in an aqueous Cl^- solution prior to transfer to the non-aqueous solution is recommended. SERS spectra have also been obtained from electrode surfaces that have only been roughened mechanically.

Many of the publications on SERS have been little more than a presentation of the spectra, and it is only recently that detailed investigations have begun to appear. Some of the more detailed studies, particularly of pyridine, halide, cyanide, and water adsorption on silver, have been reviewed recently [38]. As an example of the current capabilities of the SERS technique, Fig. 10.21 shows a series of 'snapshot' Raman spectra of pyridine adsorbed on silver. These spectra were obtained using a photodiode array detector which can acquire a complete spectrum in a few ms. Each of the spectra shown in Fig. 10.21 were acquired in 3 s as the electrode potential was slowly swept. The changes seen can be associated with features on a double layer capacitance plot obtained simultaneously, and can be attributed to orientational changes [39]. The use of the photodiode array opens up the possibility of time resolved spectroscopy and significantly increases the sensitivity of the Raman spectrometer, as well as permitting different types of data presentation. Fig. 10.22, for example, shows difference spectra (i.e. spectra obtained at one potential less than obtained at another) for the same system as studied for Fig. 10.21. These spectra were, however, obtained after prolonged evolution of hydrogen on the electrode, a procedure that is thought to remove adatoms. It can be seen that well defined difference spectra can be obtained at potentials where by comparison with Fig. 10.21, no clear features can be identified on the straight spectra. This is because the subtraction procedure differentiates against the bulk of the background scattering.

With increasing sensitivity of detectors, the detection of unenhanced surface Raman scattering becomes a possibility, and if this is achieved a wide range of effects can be investigated. In particular the determination of adsorbate orientation from depolarisation ratios and the angular dependence of the Raman signal will be possible. Currently, such measurements only serve as a means of investigating the enhancement mechanism.

10.3 ELECTRON SPIN RESONANCE SPECTROSCOPY

E.s.r. spectroscopy is, of course, widely used in chemistry to study species with unpaired electrons, and electrochemical oxidation or reduction have frequently been used to prepare species for such investigations. Indeed, many spectrometer manufacturers market electrochemical cells to be used with their instruments. These cells are generally of the two electrode type, and their use is therefore not recommended. In fact, spectra obtained using these cells have frequently

been misinterpreted; for example, an esr spectrum, in fact due to ClO_2 formed by the oxidation of ClO_4^- -base electrolytes, had been assigned to various organic and organometallic radical intermediates [40]. With careful cell design, however, reliable spectra can be obtained and transient data can be used to study reaction kinetics. The major application by electrochemists has, of course, been in the study of radical and radical ion intermediates, but transition metal species with unpaired spins are also amenable to study.

The spectrometers used for electrochemical e.s.r. experiments are totally conventional, but cell design presents considerable problems. If all that is required is the spectrum of a long lived reaction product, then it is probably simplest to use *ex situ* generation, i.e. the species of interest is generated by bulk electrolysis and is then drawn off under an inert atmosphere into a sample tube for analysis. A variation on this technique that enables all but the fastest kinetic systems to be studied has been developed by Albery and co-workers [41]. It involves using a flow system in which the electrolyte flows continuously through a capillary tube in the e.s.r. cavity (usually from bottom to top to prevent problems with bubbles). An annular ring working electrode is fitted flush with the walls inside this tube just below the e.s.r. cavity (secondary and reference electrodes being placed elsewhere), and therefore any radical species formed at the electrode rapidly pass into the cavity and are detected. The transport equations describing this system have been solved and kinetic studies can be made in a manner analogous to the ring disc electrode; the spectrometer functions like the ring. Thus the e.s.r. signal at fixed field and potential is monitored as a function of flow rate, and the data are analysed to obtain rate constants. Both first and second order reactions involving electrogenerated radicals have been studied in this way [42].

For most studies, *in situ* generation has, however, been used and this presents a number of cell design problems. The best e.s.r. spectra are obtained in solvents of low dielectric loss, but a high dielectric constant is favoured for good electrochemical behaviour. This means that it is usually necessary to use a cell of low volume, but this in turn limits the number of free spins present for detection. To overcome this difficulty it is desirable to have a large electrode surface area, but it is then often difficult to avoid iR_u drop problems. The presence of the electrode in the cavity will modify the resonant properties of the cavity, thus introducing problems of variable sensitivity. Finally, rigorous deoxygenation is essential. Several designs for cells have appeared in the literature, and the best are probably that of Goldberg & Bard [43], for use in a rectangular cavity, and that of Allendoerfer *et al.* [44], for use in a cylindrical one. The former consists of a platinum gauze working electrode, tungsten secondary, and silver wire reference, and the cell thickness can be adjusted to give optimum results for solvents of different dielectric constant. The cylindrical cavity design consists of a helical wire working electrode of 22 cm^2 area around a central secondary electrode. It shows good electrochemical behaviour and has the advantage that, like a thin layer cell, the contents of the cell can be completely electrolysed in 30 s. In both these cells the working and secondary electrodes are not separated, and therefore it must be remembered that it is possible that the product of the working electrode reaction may reach the secondary and react there, and also

that the secondary electrode reaction may produce a product with an e.s.r. spectrum.

The procedure followed during an e.s.r. study of an electrode reaction is essentially identical to that used in an O.T.E. study. Firstly the spectrum of the reaction intermediate, or product, is obtained by applying a fixed potential, usually corresponding to diffusion control, and sweeping the magnetic field. E.s.r. spectroscopy is capable of detecting radicals at about the 10^{-8} mol dm $^{-3}$ level, i.e. it is very sensitive. It is therefore important to ascertain that the e.s.r. signal strength observed is about what would be expected given the experimental conditions, and that the spectrum obtained is not due to some minor species. Having obtained a spectrum, transient data can be obtained by fixing the field at a value corresponding to the maximum in the spectrum and monitoring the e.s.r. signal in response to a potentiostatic or galvanostatic step. As with optical techniques, it is usually necessary to signal average transient data to obtain an acceptable signal-to-noise ratio. Assuming that the sensitivity throughout the cavity is uniform, the e.s.r. intensity is a direct measure of the concentration of unpaired species, and hence of the radical species under study. The analysis of transient e.s.r. data is therefore identical to the analysis of optical transient data, the experimental results being fitted to results of an analytical calculation or a simulation. Perhaps in view of the iR_0 drop problems encountered with

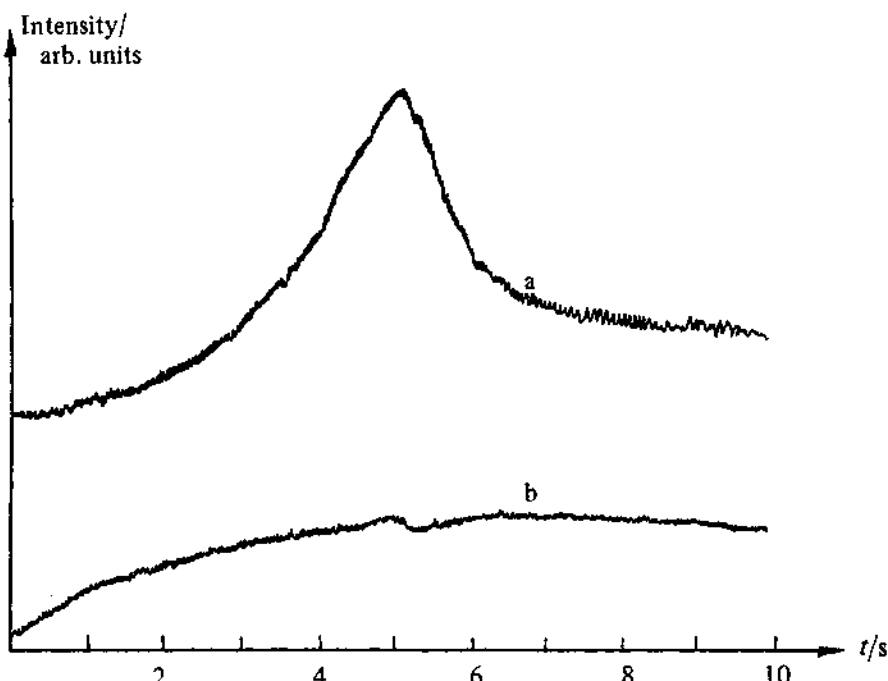


Fig. 10.23 – Intensity–time transients for the esr signals due to (a) SO_2^- and (b) S_2O_4^- formed during the reduction of SO_2 (4 mmol dm^{-3}) in $\text{DMF}/\text{Et}_4\text{NClO}_4$ (0.1 mol dm^{-3}). Reproduced with permission from E. C. Laman, C. L. Gardner, & D. T. Fouchard, *J. Phys. Chem.*, **86**, (1982), 3130.

in situ e.s.r. cells, there appears to have been a preference for galvanostatic measurements rather than potentiostatic ones, and Fig. 10.23 shows a typical example [45], the transient for the formation of SO_2^- and S_2O_4^- during the reduction of SO_2 in DMF.

There is one further e.s.r. technique, spin trapping, which has been developed fairly recently to aid in the identification of radical intermediates that are too short lived to be identified by e.s.r. directly [46]. The electrochemical experiment is carried out *in situ* in the normal way, but a spin trapping agent is also added to the system. This reacts with any electrogenerated radicals to form a more stable radical which is characteristic of the initial radical and can be identified by e.s.r. The most widely used spin traps are nitrones which react to give stable nitroxide radicals. These nitroxides are electroinactive over a wide potential range (+1.2 V to up to -1.0 V vs SCE) [47] and can therefore be used in many studies.

10.4 OTHER *IN SITU* TECHNIQUES

The techniques already discussed account for the vast majority of *in situ* spectroelectrochemical studies. There are, however, a few others, namely, surface conductance, *in situ* photoemission, photocurrent spectroscopy, *in situ* mass spectrometry, surface plasmon spectroscopy, Mössbauer spectroscopy, and *in situ* X-ray diffraction that at least deserve to be mentioned.

10.4.1 Surface plasmon spectroscopy

Surface plasmons are longitudinal electromagnetic waves that propagate at the interface between a metal and a dielectric and are characterised by electric and magnetic fields that decay exponentially on either side of the interface. As we have seen in connection with SERS, they can be excited by resonant optical absorption at a rough surface, but in view of the difficulties associated with roughening in a reproducible way this approach is not generally used to study them. Instead advantage is taken of the fact that they can also be excited at a smooth surface if the beam is incident in the internal reflection mode. The excitation of surface plasmons manifests itself as a sharp minimum in the reflectivity-angle of incidence curve. The shape of this curve is very sensitive to the optical constants of the components of the interface, and hence it can be used to study interfacial structure. Surface plasmon spectroscopy has been used largely to study double layer effects and adsorption, and this application has been discussed by Otto [48]. The equipment requirements are similar to those for other UV-visible optical techniques except that a laser source is usually used and it is also necessary to be able to sweep the angle of incidence accurately.

10.4.2 Surface conductance

Surface conductance is not a spectroscopic technique at all but is included here as it is in many ways complementary to optical studies, and the theoretical treatment has much in common with reflectance theory. Experimentally the conductivity of a thin film electrode (typically 5–50 nm) is measured as a function of an electrochemical variable such as potential (in fact modulation

techniques are often used as conductivity changes are small). The conductivity of the film is a function of the concentration and mean free path of the electrons, and this latter parameter is greatly affected by the presence of adsorbates and surface films. Conductivity measurements are therefore a useful probe of such processes. Typical studies are those of Anderson and Hansen [49, 50] in which comparison was made to simultaneous internal reflectance measurements. Fig. 10.24 shows how the normalised conductivity of a thin gold electrode varies in an iodide solution as the potential is swept.

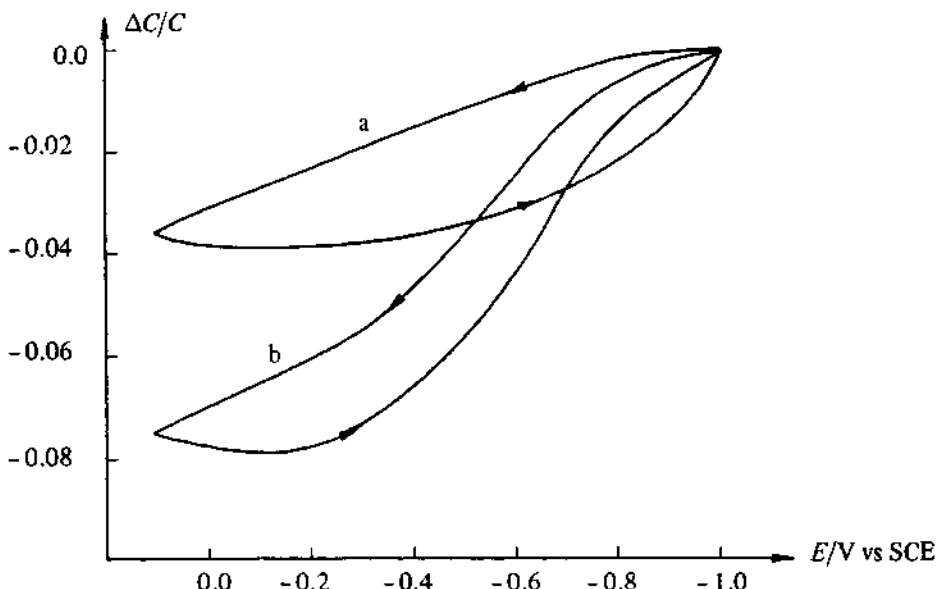


Fig. 10.24 – The potential dependence of $\Delta C/C$ obtained for a thin film gold electrode in NaI (10 mmol dm^{-3}) at sweep rates of (a) 20 V s^{-1} , (b) 0.2 V s^{-1} . Data taken from W. J. Anderson & W. N. Hansen, *J. Electrochem. Soc.*, **121**, (1974), 1570.

10.4.3 Photoemission into an electrolyte

In the conventional photoemission experiment carried out under high vacuum, the surface is illuminated and detailed information about its structure is obtained from an analysis of the angle and/or energy resolved photoemission current. At an electrode/electrolyte interface, photoemitted electrons cannot be detected directly. Upon emission they are rapidly solvated and are then trapped by electron scavengers, such as protons, deliberately added to the solution. The resulting reduced species then diffuse back to the electrode where they react and are detected as a current. As a consequence of the interaction of the emitted electrons with the solvent, all information on their direction of travel and energy is lost. Similar information can, however, be obtained from determining how the

photoemission current varies with incident energy, angle of incidence, or polarisation state. In this way, some progress has been made in the study of surface and evanescent states at noble metal electrodes, whilst the extension of the technique to the study of double layer properties and adsorption appears promising [51].

The photoemission experiment is fairly simple to perform. A chopped, monochromatic, plane polarised light beam is shone on the electrode at a defined angle, and the photoemission current is measured using phase sensitive detection. The currents are very small, therefore only a two electrode system is required, and this is anyway preferable as it is electrically less noisy. The photon energy is restricted to the transparent region of the solvent (less than 7 eV), and the optics should be designed to permit as much of this region as possible to be investigated.

10.4.4 Photocurrent spectroscopy

The illumination of semiconductor electrodes can give rise to a photocurrent due to the interband excitation of electrons. Although semiconductor photoelectrochemistry lies outside the scope of this chapter (an excellent review has been published by Morrison [57]), photocurrent spectroscopy has found more general application as an in-situ technique for the characterisation of surface films formed on metal electrodes such as Fe [58] and Pb [59] during corrosion. Quantitative analysis of photocurrent spectra can be used to identify semiconductor surface phases and to characterise their thickness and electronic properties.

10.4.5 Mass spectrometry

Mass spectrometry is, of course, widely used to identify and quantify the products of bulk electrolysis *ex situ*. The significant advance made by Bruckenstein & Rao Gadde [52] was to interface an electrochemical cell directly to the spectrometer by connecting a porous platinum electrode to the inlet port of the spectrometer. Gaseous products such as O₂ then passed through the electrode and could be detected as the electrode reaction proceeded. This technique does not appear to have been widely used since its development, but has recently again been used in the study of fuel cell reactions [53].

10.4.6 Mössbauer spectroscopy

Mössbauer spectroscopy involves the investigation of the resonant absorption of γ -rays by certain nuclei, and the conditions required for resonance provide information about the electronic environment of the absorbing nucleus. As far as electrochemical studies are concerned, it is ⁵⁷Fe that has been almost exclusively studied. The major experimental difficulty is that for a satisfactory spectrum to be obtained the sample must contain at least 100 mg of natural Fe per cm² of geometric area, but at the same time the sample must be fairly thin or all the γ -rays will be absorbed or scattered. It is therefore usually necessary to enrich the sample with ⁵⁷Fe. The major application of Mössbauer spectro-

scopy in electrochemistry has been in the area of corrosion studies, and Fig. 10.25 shows an example of the spectrum obtained *in situ* from an anodized Fe sample enriched with ^{57}Fe . The major features in the spectrum arise from the Fe substrate, but features due to the oxide can be identified, and it was concluded that the passivating film contained Fe^{III} oxides in both an amorphous and a polymeric form [54].

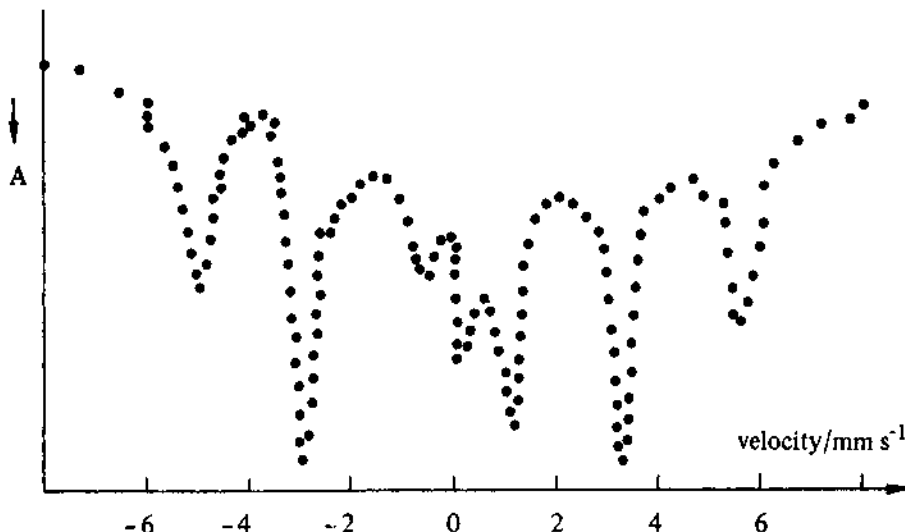


Fig. 10.25 – Mössbauer spectrum for a ^{57}Fe film passivated at 0.6 V vs NHE. The plot shows the characteristic Fe spectrum with two additional peaks in the centre due to the passive film. Reproduced with permission from W. E. O'Grady, *J. Electrochem. Soc.*, 127, (1980), 555.

10.4.7 *In situ* X-ray diffraction

This is one of the most recent techniques to have been used *in situ* in an electrochemical cell [55], and it shows promise of being able to provide the sort of information obtained in UHV studies by the application of LEED. Apart from the use of position sensitive detection, the apparatus is conventional, though it is likely that synchrotron sources, with their high flux, will be useful. Cells have to be designed to minimise absorption of the X-ray beam and therefore are of the thin layer type with polyester film windows.

10.5 EX SITU STUDIES

No detailed discussion will be given here of the application of UHV spectroscopic and scattering surface sensitive techniques to electrode systems. Of course, any of the wide range of such techniques may be applied to electrode surfaces, either prior to introduction to an electrolyte or after removal from a cell, but it must always be remembered that considerable restructuring can occur during

transfer between the electrochemical cell and the UHV system; the bulk of the solution side of the interface is inevitably lost during this procedure. Some fairly sophisticated procedures have been developed to help minimise this restructuring [56], but it still remains a problem. The most successful techniques have probably been X-ray photoelectron spectroscopy and Auger spectroscopy. The application of LEED has not been as successful, as it is so sensitive to surface contamination.

REFERENCES

- [1] J. Robinson in D. Pletcher (Ed) *Electrochemistry (Specialist Periodical Report)* The Royal Society of Chemistry, London, 1984, Vol. 9, page 101.
- [2] 1st and 2nd International Conferences on Non-traditional Approaches to the Study of Solid/Electrolyte Interfaces, *Surf. Sci.*, **101** (1980) *J. Electroanal. Chem.*, **150** (1983).
- [3] W. Von Benken & T. Kuwana, *Anal. Chem.*, **42** (1970) 1114.
- [4] E. Steckhan & D. A. Yates, *Ber. Bunsenges Phys. Chem.*, **81** (1977) 369.
- [5] J. W. Strojek, G. A. Gruver, & T. Kuwana, *Anal. Chem.*, **41** (1969) 481.
- [6] R. K. Rhodes & K. M. Kadish, *Anal. Chem.*, **53** (1981) 1539.
- [7] T. Kuwana, & N. Winograd in 'Electroanalytical chemistry' ed A. J. Bard, Marcel Dekker, New York, 1974, page 1.
- [8] M. K. Hanafey, R. L. Scott, T. H. Ridgway, & C. N. Reilley, *Anal. Chem.*, **50** (1978) 116.
- [9] H. N. Blount & T. Kuwana, *J. Electroanal. Chem.*, **27** (1970) 464.
- [10] H. N. Blount, *J. Electroanal. Chem.*, **42** (1973) 271.
- [11] A. Bewick, J. M. Mellor, & B. S. Pons, *Electrochim. Acta*, **23** (1978) 77.
- [12] R. W. Murray, W. R. Heinemann, & G. W. O'Dom, *Anal. Chem.*, **39** (1967) 1666.
- [13] D. F. Rohrbach, E. Deutsch, & W. R. Heineman in G. Manantov (Ed) *Characterisation of non aqueous solvents* Plenum, New York 1978.
- [14] P. S. Hauge, *Surf. Sci.*, **96** (1980) 108.
- [15] R. H. Müller in R. H. Müller (Ed) *Adv. in Electrochem. and Electrochem. Eng.* Wiley-Interscience, New York 1973, Vol. 9, p. 167.
- [16] C. T. Chen & B. D. Cahan, *J. Electrochem. Soc.*, **129** (1982) 17.
- [17] N. H. Bashara & R. M. A. Azzan (Eds) *Surf. Sci.*, **56** (1976).
- [18] R. H. Muller, R. M. A. Azzan, & D. E. Aspnes (Eds) *Surf. Sci.*, **96** (1984).
- [19] J. D. E. McIntyre in R. H. Müller (Ed) *Adv. in Electrochem. and Electrochem. Eng.* Wiley-Interscience, New York 1973, Vol. 9, p. 61.
- [20] C. E. Baumgartner, G. T. Marks, D. A. Aikens, & H. H. Richtol, *Anal. Chem.*, **52** (1980) 267.
- [21] J. D. E. McIntyre & D. E. Aspnes, *Surf. Sci.*, **24** (1971) 417.
- [22] J. D. E. McIntyre, *Surf. Sci.*, **37** (1973) 658.
- [23] J. D. E. McIntyre & D. E. Aspnes, *Bull. Am. Phys. Soc.*, **15** (1970) 366.
- [24] J. D. E. McIntyre, *Symp. Faraday Soc.*, **4** (1970) 99.
- [25] D. M. Kolb, R. Kotz, & K. Yamamoto, *Surf. Sci.*, **87** (1979) 20.
- [26] W. N. Hansen in R. H. Müller (Ed) *Adv. in Electrochem. and Electrochem. Eng.* Wiley-Interscience, New York, 1973, Vol. 9, p. 1.

- [27] G. H. Brilmyer & A. J. Bard, *Anal. Chem.*, **52** (1980) 685.
- [28] R. E. Malpas & A. J. Bard, *Anal. Chem.*, **52** (1980) 109.
- [29] H. Neugebauer, G. Nauer, N. Brinda-Konopik, & G. Gidaly, *J. Electroanal. Chem.*, **122** (1981) 381.
- [30] D. L. Dubois & J. A. Turner, *J. Amer. Chem. Soc.*, **104** (1982) 4989.
- [31] S. Bewick, K. Kunimatsu, & B. S. Pons, *Electrochim. Acta*, **25** (1980) 465.
- [32] B. Beden, A. Bewick, K. Kunimatsu, & C. Lamy, *J. Electroanal. Chem.*, **142** (1982) 345.
- [33] T. Davidson, B. S. Pons, A. Bewick, & P. P. Schmidt, *J. Electroanal. Chem.*, **125** (1981) 237.
- [34] R. P. Van Duyne in C. Bradley Moore (Ed) 'Chemical and biological applications of lasers' Academic Press, (1979) Vol. 4, p. 101.
- [35] R. J. Thibeau, C. W. Brown, A. Z. Goldfarb, & R. H. Heidersbach, *J. Electrochem. Soc.*, **127** (1980) 1702.
- [36] M. Fleischmann, P. J. Hendra, & A. J. McQuillan, *Chem. Phys. Lett.*, **26** (1974) 163.
- [37] R. K. Chang & T. E. Furtak (Eds) *Surface enhanced Raman scattering*, Plenum Press, New York, (1982).
- [38] M. Fleischmann & I. R. Hill in Ref. [37] page 275.
- [39] M. Fleischmann, P. R. Graves, & J. Robinson, *J. Electroanal. Chem.*, **182** (1985) 73.
- [40] M. C. R. Symons & M. M. Maguire, *J. Chem. Res. (S)* (1981) 330.
- [41] W. J. Albery, B. A. Coles, & A. M. Couper, *J. Electroanal. Chem.*, **65** (1975) 901.
- [42] W. J. Albery, R. G. Compton, A. T. Chadwick, B. A. Coles, & J. A. Lenkait, *J. Chem. Soc. Faraday Trans. 1*, **76** (1980) 1391.
- [43] I. B. Goldberg & A. J. Bard, *J. Phys. Chem.*, **75** (1971) 3281.
- [44] R. D. Allendoerfer, G. A. Martinchek, & S. Bruckenstein, *Anal. Chem.*, **47** (1975) 890.
- [45] F. C. Laman, C. L. Gardner, & D. T. Fouchard, *J. Phys. Chem.*, **86** (1982) 3130.
- [46] A. J. Bard, J. C. Gilbert, & R. D. Goodin, *J. Amer. Chem. Soc.*, **96** (1974) 620.
- [47] G. L. McIntire, H. N. Blount, H. J. Stronks, R. V. Shetty, & E. G. Janzen, *J. Phys. Chem.*, **84** (1980) 916.
- [48] A. Otto, *Surface Sci.*, **101** (1980) 99.
- [49] W. J. Anderson & W. N. Hansen, *J. Electroanal. Chem.*, **43** (1973) 329.
- [50] W. J. Anderson & W. N. Hansen, *J. Electrochem. Soc.*, **121** (1974) 1570.
- [51] T. E. Furtak & K. L. Kleiwer, *Comments on Solid State Phys.*, **10** (1982) 103.
- [52] S. Bruckenstein & R. Rao Gadde, *J. Am. Chem. Soc.*, **93** (1971) 793.
- [53] O. Wolter & J. Heitbaum, *Ber. Bunsen. Phys. Chem.*, **88** (1984) 2 and 6.
- [54] W. E. O'Grady, *J. Electrochem. Soc.*, **127** (1980) 555.
- [55] M. Fleischmann, P. Graves, I. R. Hill, A. Oliver, & J. Robinson, *J. Electroanal. Chem.*, **150** (1983) 33.
- [56] P. N. Ross, *Surface Sci.*, **102** (1981) 463.

- [57] S. R. Morrison, *Electrochemistry of semiconductor and oxidised metal electrodes* Plenum Press, (1980).
- [58] L. M. Abrantes & L. M. Peter, *J. Electroanal. Chem.*, **150** (1983) 593.
- [59] J. S. Buchanan, N. P. Freestone & L. M. Peter, *J. Electroanal. Chem.*, **182** (1985) 383.

11

The design of electrochemical experiments

Experiments for the study of electrode reactions can be categorised into three major types:

(i) *Equilibrium techniques.* In such experiments, the measurement is made with the electrode reaction at equilibrium or perturbed only slightly from equilibrium by the application of a small amplitude a.c. signal. The more common techniques are potentiometry, amperometry, differential capacitance, measurement of surface tension and impedance. Included in such methods are measurements on reversible electrochemical cells which have been used to determine thermodynamic properties, e.g. solubility products, activity coefficients, and equilibrium potentials.

(ii) *Steady state techniques.* In these methods the system is not necessarily at equilibrium, but the response to an applied perturbation is only measured after it has become independent of time. In practice it is commonly advantageous to use a cell with well defined convective stirring to control the mass transport. Typical techniques are voltammetry, polarography, coulometry, and rotating electrodes.

(iii) *Transient techniques.* In these methods the system is perturbed from its equilibrium or steady state condition and electrochemical information is obtained from the relaxation in the time domain to the new steady state condition. Double potential step, chronoamperometry, chronocoulometry, and chronopotentiometry are typical examples of transient techniques.

In all experiments, precise control or measurement of potential, charge and/or current is an essential requirement of the experiment. In addition, modern electrochemical investigation is often supplemented with *in situ* spectroscopic techniques as an independent probe to monitor changes that occur at the electrode surface; this introduces further design criteria. Consequently an electrochemical experiment rapidly becomes complex, and it is the aim of this chapter to examine some of the limitations of electrochemical equipment and to outline the precautions that must necessarily be taken to obtain quantitative data and to avoid erroneous results or incorrect conclusions. Features of cell design will be discussed initially, followed by a section on instrumentation.

11.1 THE DESIGN OF ELECTROCHEMICAL CELLS

The electrochemical cell consists primarily of the electrodes and the electrolyte, together with a container. Commonly a glass frit, separator, or membrane may be incorporated to isolate the anolyte from the catholyte. Three electrodes are commonly employed: a working electrode which defines the interface under study, a reference electrode which maintains a constant reference potential, and a counter (or secondary) electrode which supplies the current. The cell must be designed so that the experimental data are determined by the properties of the reaction at the working electrode. The cell components are discussed in detail below.

11.1.1 Working electrodes

Designs of working electrodes are diverse. Most commonly in experiments to study mechanism and kinetics in the laboratory, the working electrode is a small sphere, small disc, or a short wire, but it could also be metal foil, a single crystal of semiconductor or metal, an evaporated thin film, or a powder as pressed discs or pellets. An essential feature is that the electrode should not react chemically with the solvent or solution components. The useful working range is difficult to define as it may be limited by a number of different processes such as oxide or complex formation, hydrogen or oxygen evolution, or solvent decomposition, as well as depending on the reactants and products of the system being studied. In principle, the electrodes can be large or small, but there are commonly experimental reasons why the electrode area should be relatively small ($<0.25\text{ cm}^2$). Moreover it should preferably be smooth, as the geometry and mass transport are then better defined. It is desirable to have an even current and potential distribution and hence for the cell to be designed so that all points on the working electrode surface are geometrically equivalent with respect to the secondary electrode. This requirement is, for example, effectively met by a small bead or wire electrode surrounded by a larger cylindrical counter electrode.

An important class of working electrode is mercury and amalgam electrodes which, being liquid, have reproducible homogeneous surfaces and are relatively easy to prepare and maintain clean. The large hydrogen overvoltage on these electrodes allows a considerable working range at negative potentials. The hanging mercury drop electrode uses a piston arrangement operated by a micrometer screw to extrude into the electrolyte a drop of mercury of known

surface area. Another arrangement is the dropping mercury electrode described in Chapter 5. This continually presents a clean electrode surface to the electrolyte and has been used extensively in polarography. Hg drop electrodes sometimes give problems at very negative potentials since changes in surface tension can lead to solution creeping up inside the capillary bore, thereby increasing the effective area of the electrode. In extreme cases, drop formation is unstable, and mercury flows as a fine spray. In practice, this condition can be minimised by drawing dimethyldichorosilane vapour into the capillary bore prior to use, thus creating a non-wetting surface. Large mercury pools are often used as cathodes in constant potential electrolysis as they can be continually agitated either mechanically or by bubbling inert gas.

A wide range of solid materials are used as electrodes. Commonly the electrode material is predetermined by the nature of the study (e.g. the corrosion of steel), but the most common 'inert' solid electrodes are lead, vitreous carbon, gold, and platinum. In order to obtain consistent results with solid electrodes it is important to establish a satisfactory electrode pretreatment procedure which ensures a reproducible state of oxidation, surface morphology, and freedom from adsorbed impurities. Electrodes are polished on cloth pads impregnated with diamond particles down to $1\mu\text{m}$ and then with alumina of fixed grain size down to $0.05\mu\text{m}$. Care should be taken with the diamond abrasives, as they often contain dyes for easy recognition of the grain sizes, and these may be electro-active. Similarly, small particles of alumina may affect the kinetics of a reaction under study owing to the adsorption of reactant at the alumina surface. Particles of polishing abrasive may be efficiently removed by placing the electrode briefly in an ultrasonic bath. Often the electrode will be chemically etched to produce a smoother surface. These etches are usually strong oxidising solutions and work by producing a high oxidation state of the material that dissolves in the aqueous phase. Chemical etches can also be used to visualise dislocations and grain boundaries and to identify crystal planes. Finally the electrodes may be electrochemically polished or pretreated. For example, platinum is often cycled between the oxygen evolution and hydrogen adsorption regions to oxidise surface impurities. A particularly convenient way of mounting solid electrodes that readily permits polishing and other pretreatments, is to seal a rod of the material into an inert tube, such that only a circular cross-section of the metal is exposed. Some materials can be sealed into a glass tube simply by heating the tube whilst applying a vacuum. More frequently the seal to the glass will have to be made with epoxy resin. Plastics such as 'Teflon' and 'Kel-F' can also be used, and in these cases the seal is usually made by shrink fitting. Indulux glass electrodes consisting of a thin glass slide coated with transparent, conducting SnO_2 is useful for *in situ* transmission and photocurrent spectroscopy.

11.1.2 Counter electrodes

The purpose of the counter electrode is to supply the current required by the working electrode without in any way limiting the measured response of the cell. It is essential that the electrode process is decomposition of the electrolyte medium or oxidation/reduction of a component of the electrolyte so that current flows

readily without the need for a large overpotential. In some cases, it can be arranged that the counter electrode reaction is the reverse of the working electrode reaction so that the composition of the electrolyte is unaltered. This latter arrangement would be ideal for a photovoltaic cell or the study of kinetics, even if fatal for an electrosynthetic process. The products of the counter electrode reaction should always be considered, since they must not interfere with the reaction being studied. This is a particularly difficult problem in aprotic media where the counter electrode reaction often leads to decomposition of the solvent and a complex mixture of species in solution; at least, the decomposition of water causes only gas evolution and a pH change. In practice, such interference is perhaps best minimised by isolating the anolyte and catholyte with a frit or ion exchange membrane. Ionic conduction is maintained, but the mixing of the respective solutions is prevented. An alternative approach is to seek an electrode reaction which leads only to non-contaminating products, e.g. an insoluble solid on the electrode surface or an innocuous metal ion in solution.

As noted above, the counter electrode should not impose any characteristics on the measured data, and in consequence it should have a large area compared to the working electrode. Moreover, as also noted above, its shape and position are important since these determine whether the working electrode is an equipotential surface, and consequently it is preferable to avoid a separator in the cell. This requires the choice of clean counter electrode chemistry.

11.1.3 Reference electrodes

The role of the reference electrode is to provide a fixed potential which does not vary during the experiment (e.g. it should be independent of current density). In most cases, it will be necessary to relate the potential of the reference electrode to other scales, for example to the normal hydrogen electrode, the agreed standard for thermodynamic calculations.

In potentiostatic experiments the potential between the working electrode and reference electrode is controlled by a potentiostat, and as the reference half cell maintains a fixed potential, any change in applied potential to the cell appears directly across the working electrode–solution interface. The reference electrode serves the dual purpose of providing a thermodynamic reference and also isolates the working electrode as the system under study. In practice, however, any measuring device must draw current to perform the measurement, so a good reference electrode should be able to maintain a constant potential even if a few microamperes are passed through its surface. This criterion will be satisfied if the exchange current density is high and hence the reaction is totally reversible. Experimentally, this can be assessed with a micropolarisation test (Figs. 11.1(a) and (b)). A three electrode system is set up with the reference electrode under test as the working electrode, and current–potential curves are recorded in the linear $I-\eta$ region. The curves indicate the error in the reference potential when current is forced through the electrode, and any hysteresis is indicative of irreversibility. Thermodynamic equilibrium can be demonstrated

using a concentration cell and plotting the Nernst equation (Fig. 11.1(c)), although in practice difficulties arise from liquid junction potentials and non-ideal solution behaviour at high concentrations. When the current demanded by the experiment is only a few microamperes, the reference electrode can also act as the counter electrode, and measurements can be made with a two electrode cell. A further characteristic of a good cell, especially for the transient techniques, is that it should have a fast response time. This depends upon the time constant for the reference electrode circuit, and this can be lowered if the internal resistance of the electrode is reduced by eliminating ceramic frits, porous plugs, or ground glass joints from the design. This is particularly important when fast electrode processes are being studied as their presence degrades the high frequency response of the potentiostat. The glass electrode has an internal resistance of the order of $2 \times 10^8 \Omega$ and is quite unsuitable for transient measurements. Some of the problems associated with internal resistance will be expanded further in the section on instrumentation.

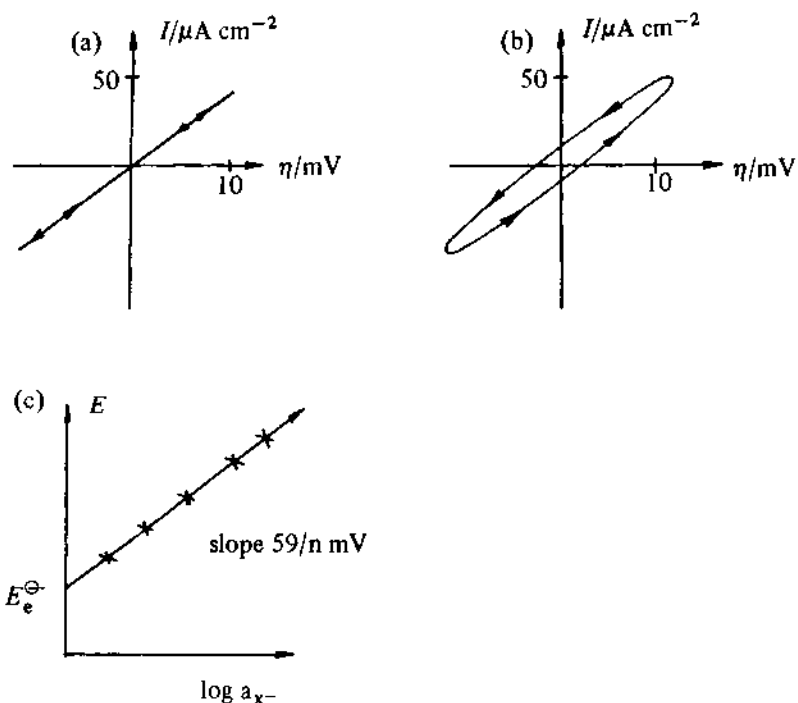


Fig. 11.1 — Tests for a reference electrode. (1) The micropolarisation tests: the reversibility of the reaction is examined in the linear $I-\eta$ region. Figs (a) and (b) show the response for a good and bad reference electrode respectively. (2) The dependence of potential on anion concentration. Fig. (c) shows the Nernst plot for a good reference electrode.

The theory and characteristics of a variety of reference electrode systems have been critically reviewed in an excellent text by Janz & Ives [1]. They fall broadly into two major groups, the fixed potential types (e.g. the calomel

electrode and silver–silver halide electrodes) and the indicator type (e.g. metal/metal ion electrodes, ion selective electrodes and the glass electrode). If possible, the reference electrode should be designed to be as similar as possible to the system under investigation. For example, in a study of the oxidation of ferro/ferricyanide at a platinum electrode, the reference electrode could be a platinum wire in the same solution. This provides a convenient zero for the potential scale and eliminates any errors due to cross-contamination. Often this arrangement is not possible, and it is necessary to use a reference electrode that is dissimilar to the working solution. The liquid junction which is formed can develop a potential gradient due to the diffusion of ions across the junction, and in practice these can be difficult to reproduce and are often unstable. It is possible to reduce the liquid junction potential to a low value by using an appropriate salt bridge between the working and reference solutions. Finally, care should be taken to ensure that reactants, products, and inert electrolytes do not falsify the potential of the reference electrode.

In practice the main requirement of a reference electrode is that it has a stable potential and that it is not substantially polarised during the experiment. Hence it is common to use the highly convenient aqueous calomel electrode in many experiments in all solvents. Even so, a very wide range of reference electrodes have been used in non-aqueous solvents. Where there is any doubt about the potential of the reference electrode, it is recommended to check the potential of a standard couple, e.g. ferrocene/ferrocinium ion, by cyclic voltammetry. This is also the easiest way to compare potential scales in different solvents; it is assumed that the potential of this couple, where both halves of the couple are poorly solvated, is independent of solvent [2].

Some common electrodes for aqueous systems are outlined below.

Mercury–mercurous chloride. This is probably the most widely used reference electrode. It is reversible to chloride ion and is usually made up in saturated aqueous potassium chloride solution, although 1 mol dm^{-3} and 0.1 mol dm^{-3} solutions are also common. In commercial electrodes, the solution is often retained with a porous plug or ceramic frit; saturated aqueous KCl, being very dense, easily leaks out. A separate compartment will therefore be necessary for the reference electrode if chloride ions must be kept out of the working solution. Calomel electrodes can easily be prepared by shaking clean dry mercury with the powdered mercurous chloride which forms a skin around the mercury. The chloride ion solution is then carefully poured on top to complete the electrode. Home-made calomel electrodes can have a very low resistance and high performance.

Mercury–mercurous sulphate. This electrode is prepared in the same way as the calomel, but the mercurous sulphate has to be specially prepared. It is a useful electrode for sulphate solutions but becomes unstable if the sulphate concentration falls below 0.1 mol dm^{-3} .

Mercury–mercuric oxide. This electrode is easy to prepare and is recommended for use in alkaline solutions.

Silver-silver halide. These electrodes give very stable potentials in halide solutions providing the halide concentration is not too high ($<1\text{ mol dm}^{-3}$), when the increasing solubility of the silver salt causes problems. They are available commercially but are also easily prepared in the laboratory.

All these reference electrodes are anion reversible, and their potentials are listed in Table 11.1. Occasionally a study requires cation reversible systems. This is particularly true for double layer studies where electrodes reversible to the cation are required to obtain the surface excess of the anion by thermodynamic arguments. If such an electrode is not available, a combination of hypothetical and reversible cell potentials often allows the potential scale to be transposed [3].

Table 11.1 – Potential of some typical reference electrodes in aqueous solutions at 298K.

Common name	Electrode	Potential/ V vs NHE
SCE	Hg/Hg ₂ Cl ₂ , sat KCl	+ 0.241
Calomel	Hg/Hg ₂ Cl ₂ , 1 mol dm ⁻³ KCl	+ 0.280
Mercurous sulphate	Hg/Hg ₂ SO ₄ , sat K ₂ SO ₄	+ 0.640
	Hg/Hg ₂ SO ₄ , 0.5 mol dm ⁻³ H ₂ SO ₄	+ 0.680
Mercurous oxide	Hg/HgO, 1 mol dm ⁻³ NaOH	+ 0.098
Silver chloride	Ag/AgCl, sat KCl	+ 0.197

A great deal of modern electrochemistry is carried out in non-aqueous solvent media, and often aqueous reference electrodes can be used at the expense of an unknown aqueous–non aqueous junction potential. The liquid junction potential can be estimated if the free energies of transfer for the ions are known. However, the use of single ionic parameters involves a non-thermodynamic assumption. Anyway, often the stringent removal of water from the system is a prime requirement, and then non-aqueous electrode systems have to be used. The non-aqueous silver and mercury salt electrodes work well in alcohols like methanol and ethanol, but in dimethylformamide and dimethylsulphoxide these salts are unstable, and an amalgam system is probably the best choice. Both cadmium and sodium amalgam in contact with the respective cations are satisfactory, and thallium amalgam in contact with thallic chloride solution has also been well studied. In acetonitrile, the calomel electrode is unstable, and the most frequently used reference electrodes are Ag/AgCl or Ag/Ag⁺. While the Ag/AgCl electrode can be used in acetonitrile, AgCl is soluble, and it requires special precautions. Silver in contact with silver nitrate or silver perchlorate is a satisfactory reference electrode, whilst even a Ag wire immersed in CH₃CN/electrolyte frequently provides a useful and practical system. A modified version of the calomel electrode using a second insoluble salt has been successful

in the solvents hexamethylphosphoramide (HMPA) [4], propylene carbonate [5], and acetonitrile [6]. In hexamethylphosphoramide [7] and propylene carbonate [8] the Ag/Ag^+ couple also works satisfactorily. For other non-aqueous solvent systems, a discussion of reference electrodes will be found in two reviews [9, 10].

As has been noted above, it is commonly necessary to compare potentials in different solvents, and this again requires a non-thermodynamic assumption. It may be shown from a simple thermodynamic cycle that the potential of a couple involving two solution soluble species depends on the free energies of solvation of the reduced and oxidised species and on the ionisation potential of the reduced species. Hence if it is possible to design a couple where the change in the free energy of solvation on oxidation/reduction is independent of solvent, the formal potential of this couple is independent of solvent and may be used to compare potential scales. The best choice is a couple where both oxidised and reduced species are ions surrounded tightly by large organic ligands so that solvent can only be involved in the second solvation shell. Ferrocene/ferrocinium ion is the couple which has usually been selected [2, 3]. Even if this argument is not thermodynamically sound, it allows some comparison of potential scales in different solvents. Moreover, it is often worthwhile to measure and report the potential of such a standard couple, since it acts as a marker for other workers to compare potentials in the same solvent. Certainly, it overcomes the problem that some reference electrodes used by some laboratories for studies in non-aqueous solvents have not proved reproducible when used by others.

Finally, it should be stressed that the reference electrode must be stable in the system being studied. For example, a Pt hydrogen electrode or indicator electrode cannot be used in solutions containing metal ions that would poison the platinum surface.

11.1.4 The electrolyte solution

The electrolyte solution is the medium between the electrodes in the cell, and it will consist of solvent and a high concentration of an ionised salt as well as the electroactive species; it may also contain other materials, complexing agents, buffers, etc. The supporting electrolyte is present (a) to increase the conductivity of the solution and hence to reduce the resistance between the working and counter electrodes (to avoid undue Joule heating, to help maintain a uniform current and potential distribution, and to reduce the power requirement on the potentiostat), and also to minimise the potential error due to the uncompensated solution resistance, iR_u , see section (11.1.6); (b) to minimise the variation of the ϕ_2 potential with applied potential and thereby to suppress the double layer effect on kinetics, see Fig. 5.10 and section 5.4; and (c) to effectively eliminate migration as a mode of mass transport for the electroactive species; transport numbers are proportional to concentration, and since the ions of the supporting electrolyte are present in large excess over the electroactive species, they will transport a large majority of the charge through the solution.

With appropriate precautions, electrochemical experiments are possible in almost any medium, and, indeed, experiments have been described in molten naphthalene, glasses, and *in vivo* in rats' brains! High quality data from most

of the experiments discussed in this book, however, will only be possible when the electrolyte has a reasonably low resistance. Hence, we are generally restricted to solvents with a dielectric constant above twenty and able to dissolve electrolytes. Such requirements are not, however, very restrictive, and Table 11.2 lists some widely used media.

Table 11.2 – Common solvents and media for electrochemical experiments.

1. Water

Aqueous solutions of many salts and/or complexing agents at various pH.
Buffered and unbuffered media.

2. Other protonic solvents

e.g. acetic acid, ethanol, methanol, liquid HF.

3. Aprotic solvents

e.g. acetonitrile, dimethylformamide, dimethylsulphoxide, sulphur dioxide, ammonia, propylene carbonate, tetrahydrofuran. Many studies use as electrolytes $R_4N^+X^-$, $R = CH_3, C_2H_5$ or C_4H_9 , $X = ClO_4^-, BF_4^-, PF_6^-$, or halide ion. Media difficult to buffer.

4. Mixed solvents

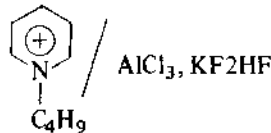
Particularly mixtures of water with ethanol, acetonitrile, etc. Again, these media may be buffered or unbuffered, contain many electrolytes, etc.

5. Molten salts

e.g. $NaCl$, $KCl/NaCl$ /LiCl eutectics etc.

6. Low temperature molten salts

e.g.



Electrode reactions can be extremely sensitive to impurities in the solution; for example, organic species are often strongly adsorbed even at $10^{-4} \text{ mol dm}^{-3}$ bulk concentration from aqueous solutions. Hence salts should be of the highest available purity and/or recrystallised, solvents should be carefully purified, and solutions must be carefully deoxygenated. Water is normally triply distilled (from dilute $KMnO_4$, then H_3PO_4 with a final distillation) prior to electrochemical experiments, while it is not uncommon for aqueous electrolytes to be pre-electrolysed in order to further remove impurities. Organic solvents must also be purified, always by distillation (at atmospheric or reduced pressure), and commonly only after chemical treatment. Such treatment for electrochemistry often includes refluxing with strong oxidising or reducing agents. For example, two purifications of acetonitrile use $KMnO_4/Na_2CO_3$ and NaH .

In non-aqueous solvents, a ubiquitous impurity is water. This is initially removed by distillation from a dehydrating agent, e.g. molecular sieves, BaO or CaH₂, but it is often better to dry the solvent/electrolyte combination immediately prior to the experiment. Possible methods include refluxing in a Soxhlet extractor or passing the solution through a column of activated alumina or molecular sieves; the use of molecular sieves or alumina within the cell has also been recommended, but all methods with such materials should be applied cautiously because of their high area and the possibilities for adsorption and/or ion exchange. In principle, residual water may be determined by glc or by Karl-Fischer titration [11]. Two reviews [12, 13] have discussed the purification and drying of non-aqueous solvents in some detail.

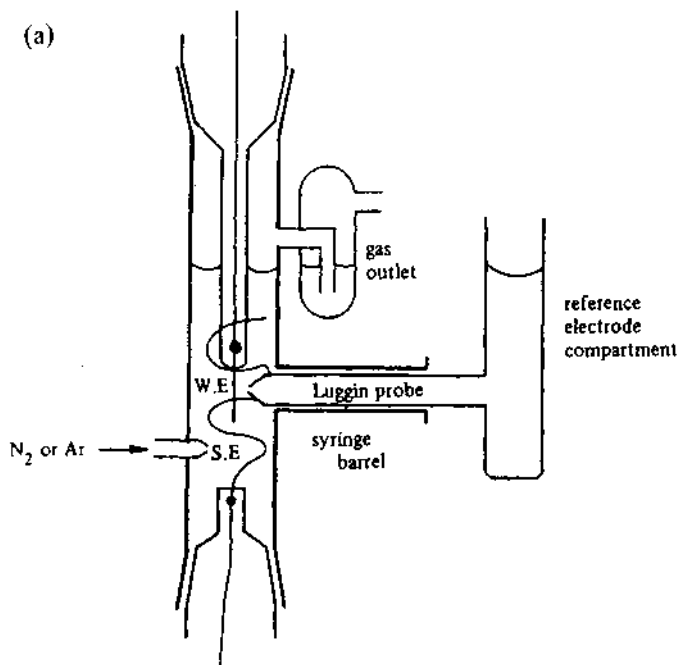
Probably the most common other impurity is dissolved oxygen which is always reduced, in protonic media through peroxide to hydroxide ion, and in aprotic solvents to superoxide and peroxide ion. It is common practice to remove dissolved oxygen by purging the solution with a fine stream of oxygen-free nitrogen; organic solvents require longer purge times than aqueous solutions. Often the nitrogen needs to be oxygen scrubbed before use. One way to achieve this is to pass the gas through a column of finely divided copper heated to 200°C. The copper oxide formed from the oxygen in the nitrogen may be reduced back to copper by passing hydrogen gas through the system, again at 200°C. A second method that is chemically less clean involves bubbling nitrogen through a mixture of concentrated sulphuric acid, V₂(SO₄)₂ and granular amalgamated zinc or of chromic chloride, hydrochloric acid, and amalgamated zinc. The lower oxidation states are produced *in situ* and reduce any oxygen impurity. A disadvantage is the need for anti-splash and drying trains to prevent acid being carried over into the electrochemical cell. It is important that the nitrogen is presaturated with solvent vapour before entering the cell to avoid concentration changes by evaporation. Argon and helium, although more expensive, are more thorough scrubbers of trace oxygen.

In aqueous solution a very wide range of electrolytes may be used. Electrochemical studies in non-aqueous solvents [12, 13] are, however, very dependent on the use of tetraalkylammonium salts, the large cation making many such salts soluble in organic media. Indeed, it was the development of simple methods of preparation of (C₄H₉)₄N⁺ClO₄⁻ and similar salts which led to the widespread development of non-aqueous electrochemistry (note R₄N⁺X⁻, X = ClO₄⁻, BF₄⁻ or PF₆⁻ are made simply by precipitation on mixing aqueous solutions of R₄NHSO₄ and NaX).

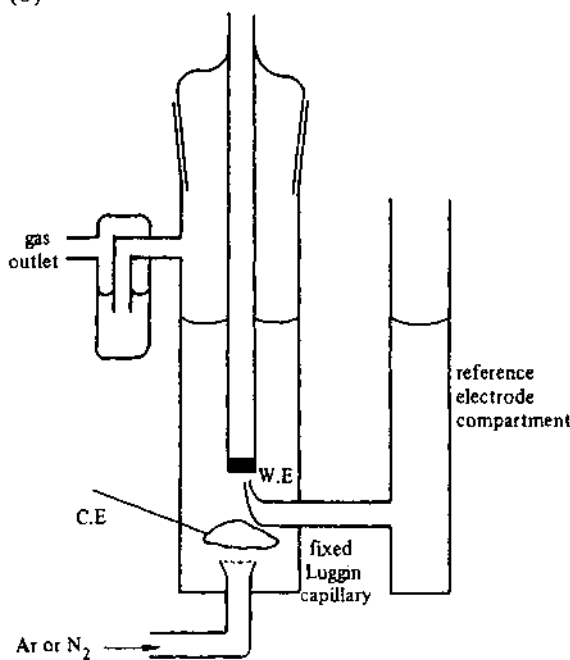
11.1.5 Cells

Typical designs for cells are illustrated in Fig. 11.2 and 5.12. Cells are usually constructed in glass or occasionally quartz, but for work in corrosive media and molten salt electrolytes there are a whole range of polymer materials that can be used. The cell should have a frit for entry of an inert gas to deoxygenate the solution and may have separate anolyte and catholyte compartments. The compartments may be isolated using permeable glass (Vycor), ceramic materials, ion exchange membranes, or diaphragms of sintered glass. It is advan-

(a)



(b)



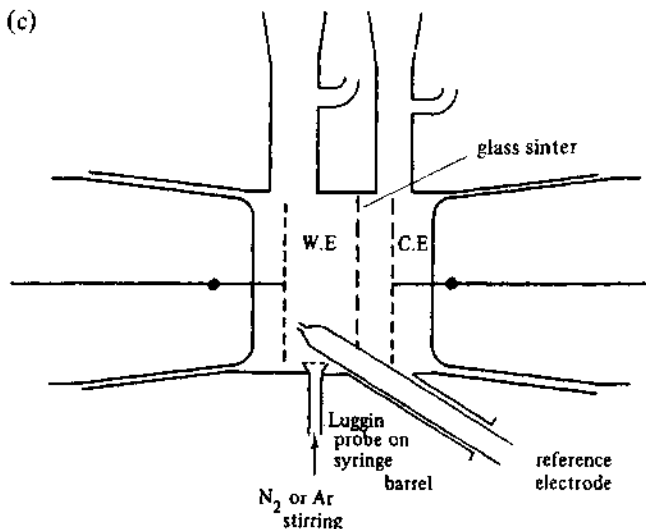


Fig. 11.2 – Some typical laboratory cells. (a) and (b) are cells for kinetic studies and (c) a cell for controlled potential electrolysis.

tageous to have the working and counter electrodes close together as this minimises the cell resistance and maximises the current which may be driven through the cell by the potentiostat. Furthermore, the working and counter electrodes should be arranged so that the current distribution over the whole of the working electrode is uniform. This will be achieved if all points on the surface of the electrode are equivalent with respect to the counter electrode. Good arrangements are a plane parallel configuration with the back of the working electrode shielded from the solution, or a small bead electrode at the centre of a cylindrical counter electrode (Fig. 5.12). An approximation to the latter configuration is a sphere surrounded by a spiral of wire. The geometrical arrangement of the electrodes should match the requirements of the experiment being performed. An experiment in simple linear diffusion would be best performed with a parallel plate configuration. These design features become particularly important in high resistance solutions. Care should also be taken with capacitance measurements to ensure that geometrical capacitances are not inadvertently produced in the cell design. This can only be checked by making measurements on the same system in a variety of cell designs and comparing the results. Care should be taken with stirring, and in systems using forced convection (rotating electrodes) it is a prerequisite that the cell dimensions are sufficient to maintain the desired hydrodynamic conditions.

The reference compartment often contains a solution sealed tap that can be used in the closed position to create a junction between dissimilar solutions. In Southampton, we recommend mounting the reference electrode with a Luggin

capillary consisting of a tapered glass probe on a movable syringe barrel that enables the potential to be sampled close to the working electrode and the gap between the Luggin tip and the working electrode to be adjusted easily.

The cell should contain no corners or crevices that may be difficult to clean. Glassware can be cleaned by immersion in strong oxidising solutions like aqua regia, permanganic, or chromic acids. However, these solutions attack platinum but a 1:1 nitric acid/sulphuric acid mixture does not. It is often a good idea to store a cell in either a nitric acid/sulphuric acid mixture or, alternatively, a completely rinsable detergent solution such as 'Decon'. The glasswear should be washed free of acid using distilled water and steamed to complete the cleaning process. Grease should never be used in the cell.

Wherever possible, electrochemical experiments should be carried out at constant temperature by immersing the cell in a thermostat bath. This minimises the density differences which lead to natural convection. Moreover it must be remembered that diffusion coefficients increase by 1–2% per degree increase in temperature, while the temperature variation of rate constants may be up to 10% per degree.

11.1.6 The Luggin capillary

The Luggin capillary is a device for minimising errors in the potential due to the uncompensated solution resistance, R_u . The origin of the resistance is shown in Fig. 11.3. The reference potential is monitored at the tip of the Luggin capillary which is placed in the potential gradient generated by the current flowing between the counter and the working electrodes. The capillary behaves in effect like the contact on the slide wire of a potentiometer, and as the potentiostat maintains a constant potential between the Luggin tip and the working electrode, then the actual potential across the interface is in error by an amount.

$$V_{iR} = iR_u \quad (11.1)$$

where i is the cell current and R_u is the resistance of the solution between the electrode and the probe tip. In principle, the capillary can be moved very close to the working electrode, but as the probe is an insulator it screens the field at the electrode, altering the current distribution and potential profile in the region where the potential is being measured. The uncompensated resistance tends to increase the potential error, whereas screening has the opposite effect. It has been shown by plotting equipotential surfaces that the best compromise is reached if the capillary is placed $2d$ away from the electrode where d is the outside diameter of the Luggin probe [14]. However, in this configuration for a planar electrode, the potential that is sampled actually corresponds to an equipotential surface that is positioned $5d/3$ away from the electrode [15]. This arises because the probe distorts the equipotential lines close to it. The dependence of the iR_u drop on distance of the Luggin capillary from the electrode can be calculated for some simple geometries if it is assumed that the specific conductivity, κ , is constant (Table 11.3).

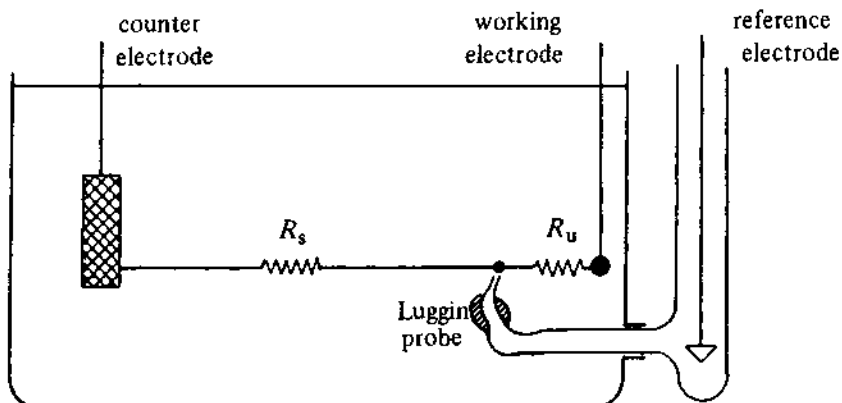


Fig. 11.3 – Schematic diagram of cell showing the principle of the Luggin probe. R_s is the solution resistance between counter electrode and the tip of the probe, and R_u the uncompensated resistance between the Luggin tip and the working electrode surface.

Table 11.3 – Theoretical equations for the iR drop for simple geometry types. Values have been calculated for the probe placed $5/3d$ away from the electrode; $\kappa = 0.02\Omega^{-1}\text{ cm}^{-1}$; $r_o = 4 \times 10^{-3}\text{ cm}$; $d = 0.02\text{ cm}$; and $i = 20\text{ mA cm}^{-2}$.

Geometry		Equation	V_{iR}/mV
Planar		$V_{iR} = \frac{i\delta}{\kappa}$	33
Cylindrical		$V_{iR} = \frac{ir_o}{\kappa} \left[\ln 1 + \frac{\delta}{r_o} \right]$	24
Spherical		$V_{iR} = \frac{i\delta}{\kappa} \left[\frac{r_o}{r_o + \delta} \right]$	18

The correction for the iR_u drop depends not only on the diameter of the Luggin capillary but also on the electrode geometry. The corrections for spherical electrodes are smaller than for cylindrical wires, and planar geometry is worst of all. Furthermore, with spherical geometry the value of R_u falls very rapidly with distance and then becomes almost constant, so that the distance between the electrode and the capillary tip is not critical. For the best results small spherical electrodes should be combined with small capillaries. In all cases V_{iR} is proportional to the current density, so the correction will be the dominant effect in

transients at short times when large instantaneous currents flow. If the Luggin probe is too close to the electrode then the observed transient following a potential step will display severe ringing (i.e. the current will oscillate). As the probe is moved away the oscillations will cease, but the transient will still be distorted at short times and should not be analysed in this region. Other sources of errors at short times are double layer charging, with time constant $R_u C_{dl}$, and stray capacitances to ground. These can be minimised by careful design to reduce the resistance of the reference electrode by avoiding glass taps, porous plugs and lead resistance, and by maintaining highly conducting electrolyte solutions within the capillary. Stray capacitance between electrolyte inside and outside the capillary and between the reference solution and counter electrode can be reduced by having a thick walled probe. The best design for the Luggin probe [16] is one that has a narrow capillary with thin walls at its tip to prevent shielding, but has thick walls in the main body and widens rapidly away from the tip to reduce resistance. Any resistance in the working electrode itself due to the formation of resistive films, poorly conducting electrodes, or non-ohmic contacts, will also appear as an uncompensated resistance. These can only be reduced by electronic compensation.

11.2 INSTRUMENTATION

The electrochemist's armoury is based on electronic apparatus designed to control/measure the charge passed (coulostat/integrator), current (galvanostat/current follower) and potential (potentiostat/high impedance voltmeter) in an electrochemical cell. It may also contain instruments for signal averaging and for separating small signal responses from electronic noise. This apparatus may be linked to a digital computer which controls the course of the experiment, acquires the data, and processes the information often into hard copy tabular or graphical form. The control and measurement equipment relies on the properties of the operational amplifier which, although complex electronically, can be regarded as a three terminal black box (Fig. 11.4(a)) with four useful properties.

- Two terminals are inputs and are referred to as the *inverting* (−) and *non-inverting* inputs (+). They have infinite input impedance, which means they can accept an input voltage without drawing current into the device through the voltage source.
- The third terminal is the output, and this has zero impedance so that the output voltage remains constant irrespective of the current drawn by the load.
- The amplifier is essentially an inverting differential amplifier with infinite gain, A , so that:

$$E_{\text{out}} = -A(E_- - E_+) , \quad (11.2)$$

and any voltage difference at the inputs drives the output to $\pm\infty$.

- The amplifier is able to follow changes in input voltage with infinite speed.

Many of the limitations and design criteria associated with real devices arise because of the failure of the operational amplifier to meet fully these ideal properties.

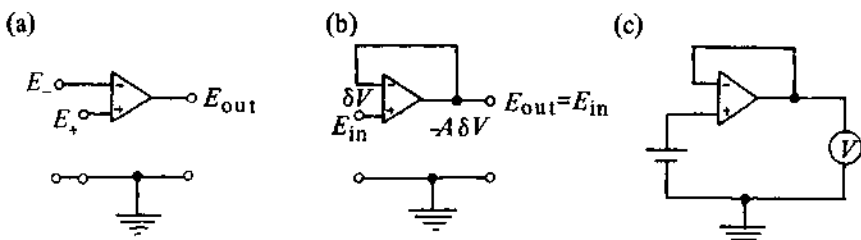
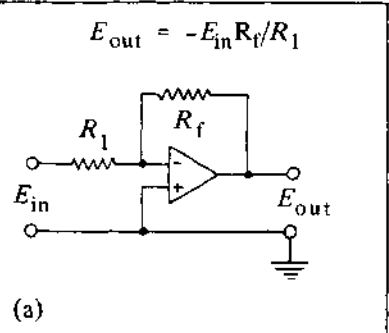
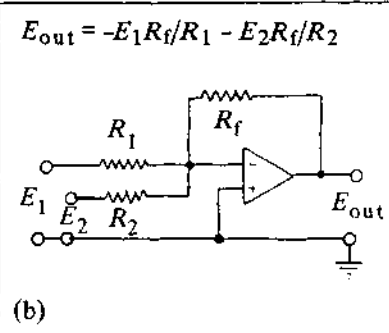
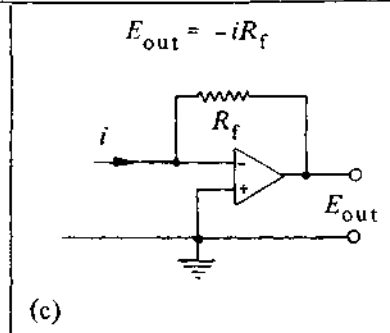
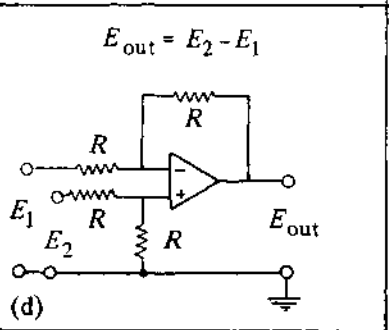
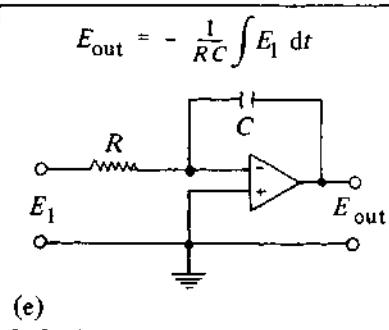
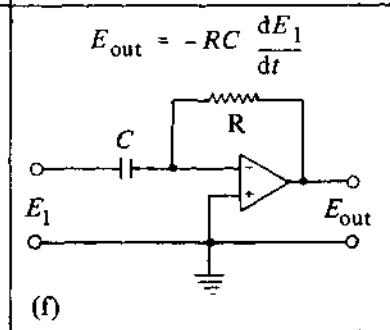


Fig. 11.4 – The operational amplifier: (a) the open loop configuration, (b) the principle of negative feedback, (c) the voltage follower as used to measure the voltage, V , of a standard cell.

To use the operational amplifier as a control device it is necessary to introduce the principle of negative feedback where part of the output voltage is fed to the inverting input of the amplifier, as shown in Fig. 11.4(b). In this configuration the amplifier operates to maintain the potential difference between the inputs at zero. Any error that appears across these inputs ($+\delta V$) is amplified to give an output $-A\delta V$ that acts to reduce the error $+\delta V$ back to zero. This simple configuration is an extremely useful circuit known as the *voltage follower* because within the limits imposed by the sensitivity of the real device, the output voltage follows exactly the input voltage. Furthermore, the input impedance of the device is infinite and the output impedance is zero. This means that the circuit can measure potential at its input without drawing current from the voltage source, and display the result on a measuring device which draws current. An arrangement is shown in Fig 11.4(c) for measuring the potential of a Western Standard cell. In real devices the input bias current is not strictly zero but typically has a value of the order of 10^{-7} - 10^{-10} A. This is acceptable for most applications, but problems arise with the measurement of pH using the glass electrode which has a resistance of the order of 10^9 Ω; in order to measure potentials to within 1mV the measuring device should not draw currents in excess of 10^{-12} A. This special requirement is met only in devices called *electrometer amplifiers* that have field effect transistors as inputs and impedances in the range 10^{12} - 10^{14} Ω.

Other useful circuits can be derived by including other circuit elements in the input and feedback loops, and some examples are collected together in Table 11.4. The derivation of the equations describing the behaviour of the circuits can be found in many texts [17-24], whilst the use and problems associated with some of these circuits will be discussed in the remaining part of this chapter. The current follower and differential amplifier find applications in the measurement of cell current; the integrator enables the charge to be electronically measured and also forms the basis of a linear ramp generator; the differentiator finds limited use as it tends to degrade the signal-to-noise ratio.

Table 11.4 – Various configurations for operational amplifier circuits: (a) inverting amplifier, (b) summing inverting amplifier, (c) current follower, (d) differential amplifier, (e) integrator, (f) differentiator.

$E_{\text{out}} = -E_{\text{in}} R_f / R_1$ 	$E_{\text{out}} = -E_1 R_f / R_1 - E_2 R_f / R_2$ 	$E_{\text{out}} = -i R_f$ 
$E_{\text{out}} = E_2 - E_1$ 	$E_{\text{out}} = - \frac{1}{R C} \int E_1 dt$ 	$E_{\text{out}} = -R C \frac{dE_1}{dt}$ 

11.2.1 The potentiostat

The potentiostat is a device for controlling the potential between the working electrode and the reference electrode at a fixed and selected potential (commonly we also wish to programme this potential with time). There are several possible configurations, but the simplest, which is of little practical use but outlines the principles, is shown in Fig. 11.5 where the cell has been approximated by a very simple equivalent circuit of a solution resistance in series with a double layer capacitance. It can be seen that the device is simply a voltage follower maintaining the output voltage between RE and WE at the programming potential E_1 . The working electrode, which is at ground potential, has a potential $-E_1$ relative to the reference electrode, so that the input voltage is inverted in the cell. Also in this arrangement there is no device for measuring the current through the cell, and the potentiostat is unable to apply more than a single potential profile at any one time. A better design is indicated in Fig. 11.6. Neglecting amplifiers

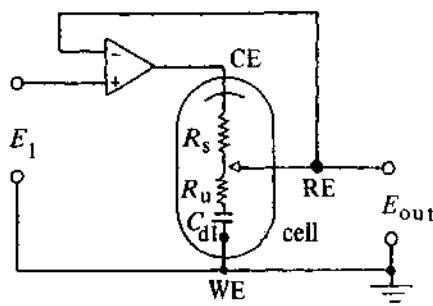


Fig. 11.5 – Simple potentiostat for maintaining a constant potential between a reference electrode, RE, and working electrode, WE; R_s is the solution resistance between the reference electrode probe and the counter electrode, CE; R_u the uncompensated resistance between the Luggin tip and the working electrode; and C_{dl} the double layer capacitance of the working electrode.

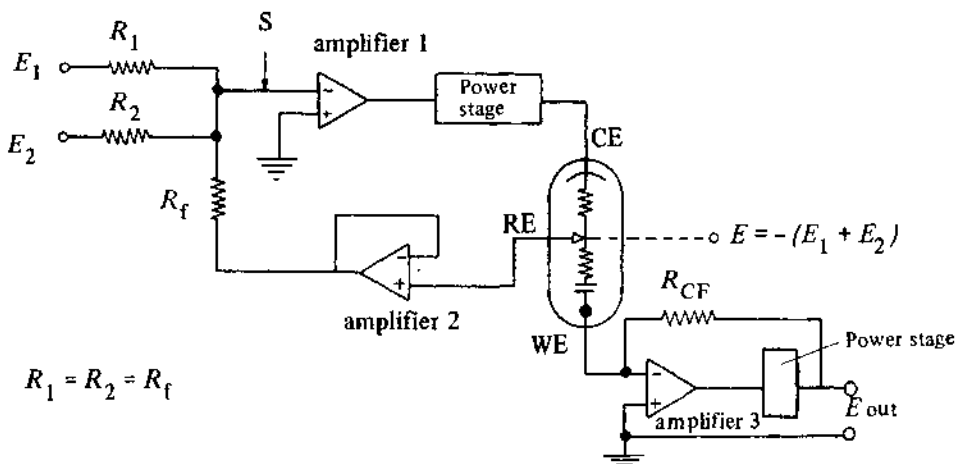


Fig. 11.6 – Potentiostat operating in the summing configuration.

2 and 3 for the moment it can be seen by comparison with the current circuit in Table 11.4(b) that amplifier 1 is the control amplifier in the inverting adder configuration. The circuit works to keep the summing point, S, at virtual ground so that programmable potentials E_1 and E_2 are inverted, summed, and controlled between the reference electrode and ground. The potential of the working electrode is maintained at virtual ground by amplifier 3, so the potential of the working electrode relative to the reference electrode is $+(E_1 + E_2)$, and there is no sign inversion in this kind of potentiostat. In an electrochemical system the feedback loop contains the reference electrode, and the input current drawn by the potentiostat must not be sufficient to polarise this electrode. This is achieved by including a voltage follower (Amplifier 2) in the feedback loop as an impedance matching unit, and the drain on the reference electrode is now due solely to the input impedance, and input bias current, of the operational amplifier. Generally, commercial reference electrodes have ceramic plugs in their design so reference electrode resistances can easily reach a value of $1\text{M}\Omega$. Typically, real bipolar operational amplifier input bias currents are of the order of 10^{-7} A , which would falsify the potential by 0.1 V. It is therefore important that amplifier 2 should be of the FET type previously mentioned. The high impedance between the reference electrode and the non-inverting input makes this part of the circuit extremely sensitive to mains hum and noise pickup, and this cannot be separated from the signal. To minimise this, the leads to the reference electrode should be shielded and the voltage follower placed as close to the electrode as possible. The power stage in the feedback loop serves to boost the current that can be drawn from the potentiostat, as the control amplifier will not itself deliver much current. Amplifier 3 forms the basis of a current follower circuit to determine and display as a voltage the current flowing through the cell. The output, E_{out} , is given simply by the product iR_{CF} . All the cell current is drawn through the feedback resistor, so if the control circuit contains a power stage, then i_{out} must also be boosted, although the current follower amplifier does not necessarily have to supply large power but only enough voltage to drive a recorder or oscilloscope. The operational amplifier should be chosen to have an extremely low input bias current as this is the main source of error in the measurements, especially for low currents. The current follower is, in general, a low frequency device as it suffers instability at higher frequencies. There are two factors to consider: firstly, the current follower is an active device in the feedback loop of the control amplifier, and careful ground arrangements are necessary; secondly, the input impedance of a real operational amplifier has stray capacitance and inductance across its inputs, and these can give rise to phase shifts which can bring about oscillations.

An alternative arrangement for current measurement is to place a resistor in the feedback loop of the control amplifier and measure the voltage across it using a differential amplifier, Fig. 11.7. The voltage followers act as impedance converters and also prevent shunting of cell current to ground. If these are FET operational amplifiers, then R_f may be as large as $1\text{M}\Omega$. The potential developed across R_f is measured by the differential amplifier (see Table 11.2(d)) and the current is given by E_{out}/R_f when $R_1 = R_2 = R_3 = R_4$. However, care should be taken with the choice of R_f so that the potentiostat's output voltage limits are not exceeded. For an

ideal differential amplifier E_{out} depends only on $(E_1 - E_2)$ and is independent of the absolute value of the input potential with respect to ground. In a real amplifier, the output voltage is given by

$$E_{\text{out}} = A_{\text{cm}} E_{\text{cm}} + A_o (E_- - E_+) \quad (11.3)$$

where A_{cm} is the common mode gain which is the ratio between the output voltage and the voltage E_{cm} with respect to ground of each input when $(E_- - E_+) = 0$. The common mode gain is reflected in a manufacturer's specification called the *common mode rejection ratio* (CMRR), M .

$$\text{CMRR} = M = \frac{A_{\text{cm}}}{A_o} . \quad (11.4)$$

A potential E_{in} at the inputs with respect to ground will cause an error in $(E_- - E_+)$ equivalent to E_{in}/M , so an amplifier with high CMRR should be chosen for this device.

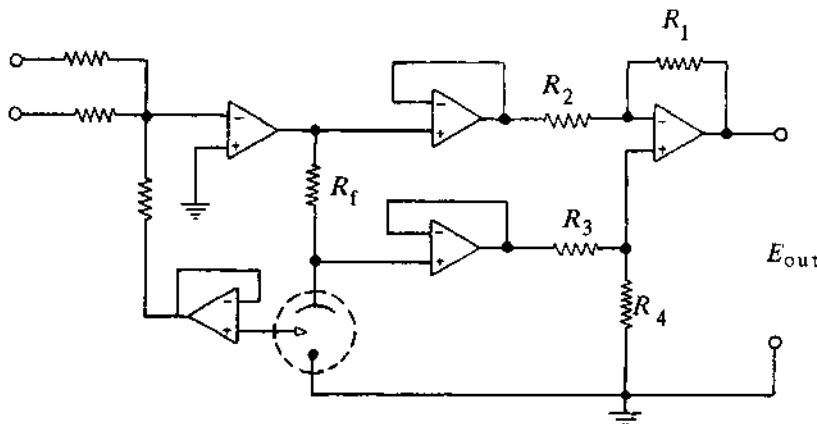


Fig. 11.7 ~ Current measurement using a differential amplifier configuration.

11.2.2 The performance of potentiostats

The following characteristics should be considered when designing or purchasing a potentiostat [24-29].

(a) Output drive

The output current provided by the control amplifier should exceed the maximum current in the experiment under study, and the output voltage should be high enough to drive this current through the cell. The maximum output voltage is usually limited by the value of the power supply rail to the device. If the output current is not sufficient for the purpose intended, a current amplifier can be used to boost the output up to three orders of magnitude. Non-steady state methods demand large currents at short times to charge the double layer capaci-

tance. For example, to charge $10\mu\text{F}$ by 1V in 10^{-5} seconds would require a current of 1A and an output of 100V for a cell resistance of 100Ω . If the counter and working electrode can be kept close together this will reduce the load seen by the output of the control amplifier and reduce the voltage required to drive current through the cell.

(b) Static accuracy

The accuracy of the operational amplifier is given by Equation (11.3) which can be rearranged in the form

$$\delta V = \frac{E_{\text{out}}}{A_o} + \frac{E_1}{M} + \text{drift} + \text{noise} \quad (11.5)$$

where E_1 is the input reference potential. For $\pm 1\text{mV}$ accuracy both M and A_o should be of the order of 10^4 - 10^5 or larger, and a thermal drift of $100\mu\text{V}/^\circ\text{C}$ is likely to be appropriate. The static error signal often referred to as the *input offset voltage* can be balanced out with a small potentiometer included in the design of the operational amplifier. This is, however, limited by the drift of the offset voltage with time, which can be up to $1\text{mV}/\text{day}$. A special type of device called a *chopper stabilised amplifier* is one in which the offset voltage is controlled and can be stabilised to $0.1\mu\text{V}/\text{day}$.

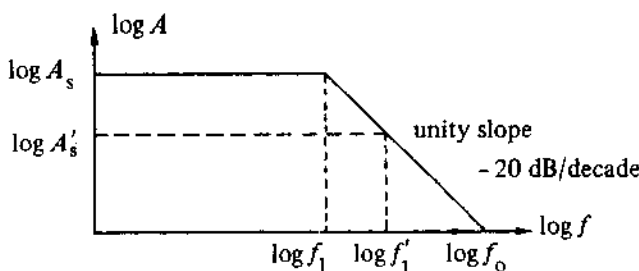


Fig. 11.8 – Bode plot showing the frequency dependence of the gain for a typical operational amplifier. f_1 is the roll-off frequency, f_0 the frequency at unity gain. For $A_s \gg A'_s$, then $f_1 \ll f'_1$.

(c) The response time and instability of potentiostats

In previous considerations of operational amplifier analysis, we have assumed that the device was ideal in the sense that it can respond instantly to any change in response at the inputs. This is equivalent to assuming that the open loop gain is independent of frequency. The characteristic dependence of open loop gain for a real operational amplifier is shown in Fig. 11.8. The roll-off frequency determines the time constant for the potentiostat, τ_1 , through the relationship

$$\tau_1 = \frac{1}{2\pi f_1} \quad (11.6)$$

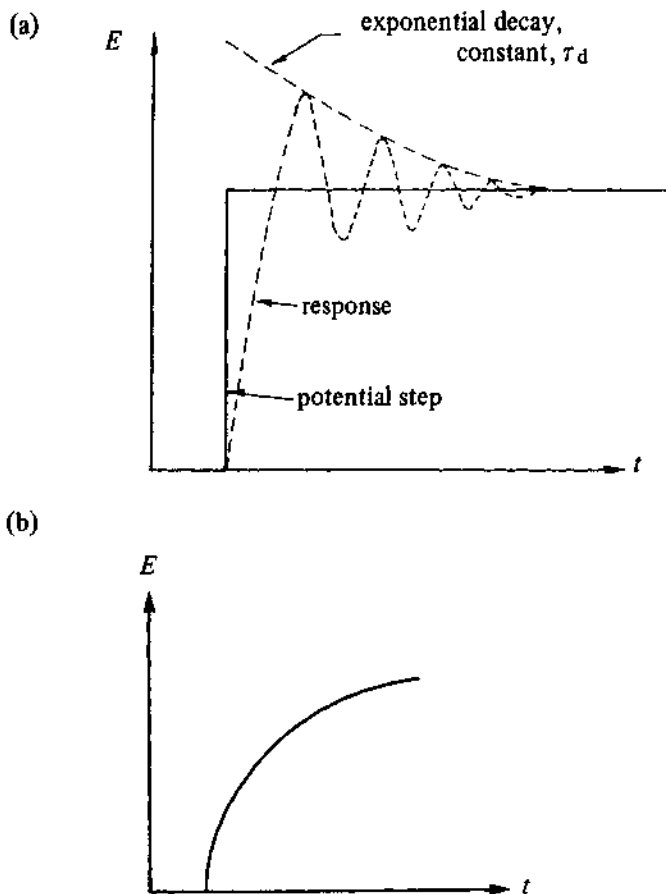


Fig. 11.9 – Response of the working electrode to a potential step (a) due to the response time of the cell, (b) when there is an uncompensated resistance. τ_d is the time constant for the combined cell and potentiostat.

where

$$\tau_1 = \frac{f_0}{A_s} \quad (11.7)$$

and A_s is the static gain. From these equations it can be seen that τ_1 can be minimised by using a fast amplifier with a high f_0 or by decreasing the gain. As a large open loop gain is required for good accuracy, a compromise must be reached between high accuracy and fast response. However, the cell itself will have a time constant τ_2 given in the simplest case by $R_e C_{dl}$, where R_e is the electrolyte resistance between the counter electrode and the working electrode and C_{dl} is the double layer capacitance. Any attempt to minimise R_e by avoiding frits, porous plugs, or increasing the conductivity of electrolyte or decreasing electrode separation will be beneficial. C_{dl} can be reduced by using

spherical electrodes of a small area. The response time constant for the combined potentiostat and cell, τ_d , depends on many factors, but if τ_1 and τ_2 differ by at least an order of magnitude then τ_d will be determined entirely by the larger of the two time constants. It may be possible to effectively eliminate the potentiostat time constant and, by careful cell design, to minimise τ_2 . The response of the combination in the absence of any iR_u drop will be the damped oscillation shown in Fig. 11.9(a), and the damping time constant is a good measure of the response time of the system. Clearly the time for the oscillation to decay to the steady value imposes a lower limit upon the analysis of the electrochemical data. If any uncompensated resistance is present in the cell then the response will be aperiodic as shown in Fig. 11.9(b) as the cell current and hence the product iR_u is also a function of time. Furthermore, there is an additional error $i_{cell}R_u$ in the potential of the working electrode.

The stability of the control circuit relies on negative feedback to the inverting input. If the response of the potentiostat or the impedance of the cell elements in the feedback loop introduce phase shifts in excess of 180° , then the signal that is fed back no longer limits the gain but reinforces the output and the potential becomes unstable or oscillates. The control amplifier introduces a 90° phase shift for frequencies higher than the roll-off frequency, and an extra 90° can easily be generated in an electrochemical cell. A typical equivalent circuit is shown in Fig. 11.10. While little can be done to reduce phase shifts in the cell, any reduction in the time constant $R_{ref}C_{ref}$ will be an advantage. All the precautions described in the section on the Luggin probe are applicable to reducing R_{ref} . C_{ref} may be due to excessive capacitance to ground, especially if leads to the cell have grounded shields and are unduly long. A better arrangement uses a driven shield maintained at the reference potential as shown in Fig. 11.11. Noise pickup can often also be reduced by placing the cell in a Faraday cage or even a grounded Al box.

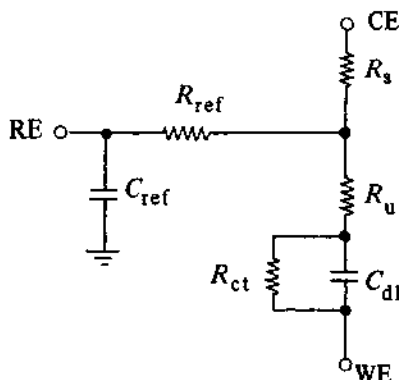


Fig. 11.10 – Equivalent circuit for an electrochemical cell. R_{ref} is the resistance of the reference electrode, and C_{ref} represents parasitic loss to ground in the leads. R_s and R_u are the solution and uncompensated resistances respectively, C_{dl} the double layer capacitance of the working electrode, and R_{ct} the charge transfer resistance.

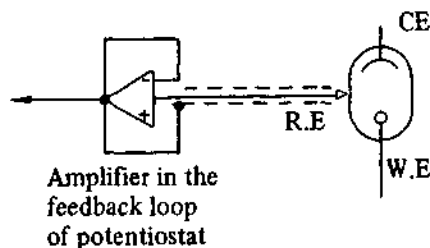


Fig. 11.11 – Principle of a driven shield to minimise excessive capacitance to ground in the reference electrode lead.

11.2.3 Uncompensated resistance measurement and correction

The majority of commercially available potentiostats have a facility for electronically compensating for the ohmic drop due to the solution resistance between the Luggin capillary and the electrode. The Luggin probe is placed far enough away into the solution to prevent shielding of the electrode, and part of the output signal from the current follower is fed back into the potentiostat to compensate for the resistance between the Luggin tip and the electrode. A typical circuit is shown in Fig. 11.12.

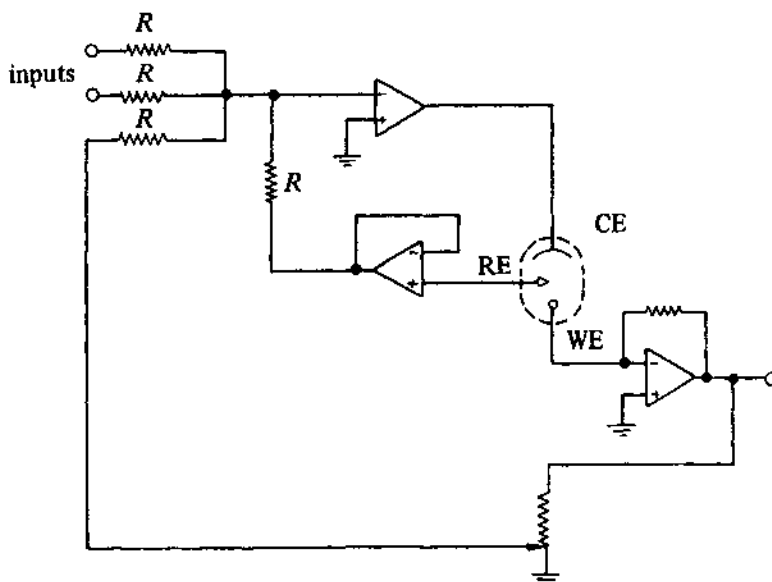


Fig. 11.12 – Potentiostat employing positive feedback to correct for uncompensated solution resistance.

In practice it is difficult to know exactly how much positive feedback to apply, and the usual approach is to set the potential in a region where the electrode reaction does not occur and then to increase the feedback resistance until the potentiostat oscillates. A potentiostat, however, appears to require some uncompensated resistance for stability, and so the compensation is then reduced to roughly 90% of the critical value. Clearly, it is assumed that the uncompensated resistance is constant, and this may be in error if resistive films are formed or if high currents flow and change the solution composition. An alternative approach to this rather empirical rule of thumb is to measure the uncompensated resistance and then impose the necessary correction.

The a.c. techniques described in Chapter 8 allow the solution resistance to be determined from the high frequency intercept of the impedance semi-circle on the real axis. A second real time method is the current interruption technique [30, 31]. When the current through the electrochemical cell is interrupted suddenly, the potential of the working electrode does not immediately return to its steady state value but decays in a complex manner determined by the discharge of the double layer capacitance through the faradaic process. However, any potential drop that is purely ohmic in character will be reduced to zero at the moment of current interruption, and this allows the uncompensated resistance to be measured from the potential time transient, Fig. 11.13. High speed current interruption can be accomplished using a boosted operational amplifier circuit in which a switching pulse is introduced into the booster [30], or by using a very short break time relay with mercury wetted contacts. Periodic current interruption with a short duration pulse ($\approx 10-100\mu s$) allows constant monitoring of the solution resistance without undue perturbation of the electrode process being studied. In principle, the resistance can now be compensated directly by positive feedback, but, practically, there may be problems as the cell and amplifiers introduce phase shifts that may cause a time lag between applying compensation and establishing the control, and the transients will be distorted by overshoot and ringing. It is generally accepted that positive feedback techniques should be used only when all other reasonable steps to minimise R_u have been attempted, and then it should be used only with the utmost care. Several critical reviews on the art of iR_u compensation are available [32-38].

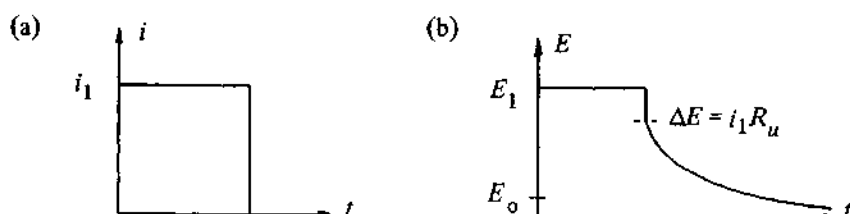


Fig. 11.13 – Measurement of the uncompensated resistance using the current interruption technique: (a) i - t function applied, (b) E - t response.

11.2.4 Galvanostats

The simplest way to obtain a constant current is to apply a voltage from a low output impedance voltage source across a large resistor in series with the cell, as shown in Fig. 11.14. The current will be given by the ratio E_{in}/R (provided resistance R is very large compared with the impedance of the cell). Several operational amplifier circuits are also available for galvanostats. Two of the simplest are shown in Fig. 11.15. The circuit arrangement is that of the voltage follower with the cell in the feedback loop, and the current is determined by the ratio E_{in}/R . Configuration 11.15(a) has the advantage that the working electrode is at virtual ground, so the reference potential, E_{ref} , can be monitored using a voltage follower. However, the output impedance of the voltage source, E_{in} , must be able to supply the required current into the feedback loop. In configuration 11.15(b) the current is supplied by the output of the operational amplifier, but the working electrode is not at virtual ground, so E_{ref} has to be monitored with a differential voltmeter. Most potentiostats can be converted to a galvanostat by inserting a standard resistor R between the working and reference inputs of the instrument and then connecting the working electrode to the reference electrode input and the counter electrode in the normal configuration. This is shown in Fig. 11.16 for the simple potentiostat of Fig. 11.5. The modification to the summing potentiostat of Fig. 11.6 is totally analogous. The current is given by the ratio of E_{in}/R . A drawback associated with this arrangement is the need for a differential amplifier to record the working electrode potential. The circuit is identical to Fig. 11.15(b).

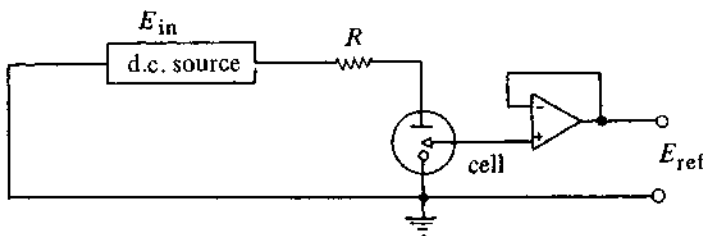


Fig. 11.14 – Early galvanostat circuit.

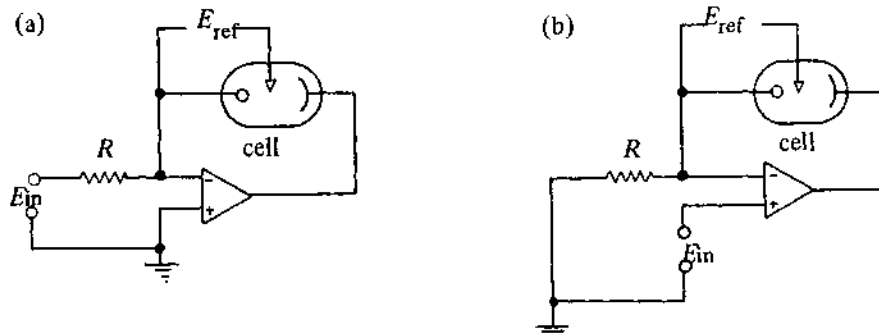


Fig. 11.15 – Two galvanostat circuits employing operational amplifiers.

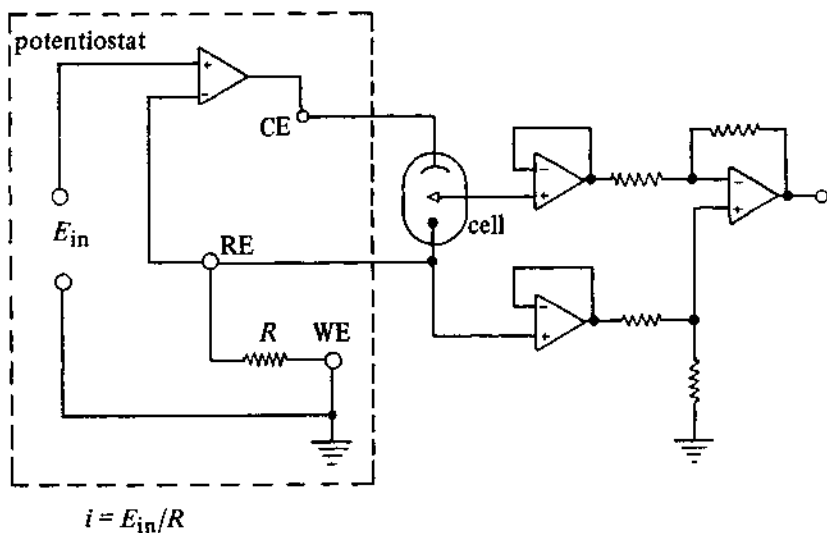


Fig. 11.16 – Conversion of a potentiostat into a galvanostat.

11.2.5 Computer automation of electrochemical experiments

Throughout the earlier chapters, we have tried to indicate the increasing role that mini- and microcomputers are playing in the control of electrochemical experiments, in data acquisition, as well as in data processing. Indeed, as we have seen, several new techniques have been developed recently that rely heavily on these capabilities (e.g. convolution cyclic voltammetry).

Minicomputers were first used for on-line control of electrochemical experiments in the early 1970s [39–41], and on reading these early papers it will be seen that considerable expertise in both analog and digital electronics was required to interface the computer with the electrochemical cell. This remained the case until fairly recently. Now it is possible to purchase ‘off the shelf’, at reasonable cost, very satisfactory interface units for several of the more popular home/business microcomputers, as well as for many minicomputers. Support software is also often available. Typical interface units comprise analog to digital converters (ADCs), digital to analog converters (DACs), a real time timer, and digital input/output ports, and they either connect directly with the microcomputer bus or alternatively do so via a user port or an IEEE-488 bus. This latter bus system is now available on a wide range of microcomputer systems. It permits the connection of the computer to an extensive and increasing range of electrical instruments, such as oscilloscopes and recorders, which it is then able to control and interrogate.

The application of on-line computers to electrochemistry developed rather slowly, owing to the early problems associated with the interfacing and, perhaps more significantly, to the high costs. Both of these obstacles have been largely overcome. It is now possible to purchase a microcomputer based system capable

of controlling a wide range of experiments, acquiring and processing the data, and displaying the results on both a screen and in hard copy form, at a comparable cost to a conventional analogue system (e.g. high quality oscilloscope or recorder). When considering the purchase of new equipment, such a route should therefore always be considered. The microcomputer based system is particularly well suited to situations where many experiments of the same type will be undertaken with only slight changes in the experimental conditions, e.g. in corrosion studies. It is less well suited to the initial investigation of an unknown system, e.g. by cyclic voltammetry, where the ability to change rapidly the conditions, e.g. sweep limits, during the experiment is desirable.

Thus far, all microcomputer based electrochemical experiments have used a conventional potentiostat (or galvanostat) as the control device, with the computer based instrumentation taking over the roles of the function generator and the recording device. The links between the digital world of the computer and the analog world of the potentiostat and cell are made via ADCs and DACs, whilst digital inputs and outputs on the computer can be used to open and close switches and to sense changes such as the fall of a DME. Timing is achieved either with a hardware timer or, alternatively, in software, by counting machine cycles.

It is the DAC that enables the microcomputer to be used as a function generator; its role is to convert a binary number into a proportional analog voltage. Thus by successively converting a series of binary numbers, any desired waveform can in theory be generated. The major limitation is the resolution of the DAC. Two factors affect this: the output voltage range and the number of bits that are converted. Output ranges of 1V, 5V and 10V are common, and both unipolar and bipolar devices are available. It is also often possible to change ranges by altering links on the terminals of the device. For electrochemical purposes a bipolar 5V DAC is probably the best all round choice, i.e. one that spans the range -5 V to $+5\text{ V}$. The cost of DACs increases as the number of bits converted increases, and a good compromise is therefore a 12-bit device. The settling time of DACs is very short and does not normally need to be considered. A 12-bit, $\pm 5\text{ V}$ device will have a resolution of 2.4 mV , which will be satisfactory for most purposes. There can, however, be a difficulty when trying to generate smoothly varying functions, e.g. a voltage ramp for cyclic voltammetry, as the computer generated signal will consist of 2.4 mV steps. To remove these steps, the signal can be smoothed with a low pass filter, but a better approach to generating ramps is probably to feed the output of the DAC to an integrator (see Table 11.4). Thus a fixed output from the DAC gives a constant sweep rate, and by changing the DAC output polarity the sweep is reversed.

The ADC is used to convert the cell response to machine interpretable, digital form. Again, these devices are available in different input ranges which should be matched as closely as possible to the output range of the sensing device, e.g. current follower. Devices are available that can convert a voltage with 16-bit resolution in less than $1\mu\text{s}$. These, however, are very expensive, and generally 12-bit precision will be sufficient provided the input range is well chosen. The price of an ADC also increases with increasing conversion rate. A device capable of sampling at 20 kHz should be adequate for nearly all experi-

ments, but slower (or cheaper) ADCs can be used if only quasi-steady state measurements are to be made. Since the A to D conversion takes a finite time it is usual to place sample and hold circuitry between the signal source and the ADC, whilst a multiplexer is also often incorporated to enable signals from several sources to be processed by the same converter. Commercially available interfaces usually have both these features.

As was stated earlier, the timing and synchronising of the various functions of the interface can be achieved by either of two approaches, software or hardware. The former approach simply involves inserting loops of a known number of machine cycles into a machine code program so that a known time elapses between I/O operations. The no-operation instruction, if available, is particularly useful in this respect. This approach is rather clumsy, however, and the use of timers, particularly in the interrupt mode, is preferable. The timer is loaded with a number, and it then counts down on pulses from either the processor clock or a dedicated external clock. On reaching zero, the timer interrupts the processor, and the appropriate interrupt service routine, e.g. to read data from an ADC, can be called and the timer restarted.

It is almost impossible to give advice on the purchase of microcomputers, since advances are occurring so rapidly, 8- and 16-bit machines are currently the norm, but these will undoubtedly be replaced by 32-bit ones in the next few years. Probably the best advice that can be given is to choose a machine for which a wide range of laboratory interface devices is available, preferably from more than one manufacturer, as this implies that it should be well suited to this type of application, and suitable software might be available. The temptation to buy the latest machine should be resisted, as this will probably result in considerable effort being expended on designing interfaces as these will not yet be available commercially. One useful feature if extensive data manipulation is envisaged is the ability to connect the microcomputer directly to a mainframe computer and to pass files between the two. Some form of mass storage will be required, and for all but the most trivial applications, floppy disc drives will prove much more convenient than tape cassettes. A high resolution graphics display is essential, and a digital plotter will also probably be needed though data can be output to an *X-Y* recorder via a pair of DACs. For some applications a screen dump routine to a printer can be used.

The details of 'computerising' any electrochemical experiment are inevitably dependent on the computer system being used, and therefore no specific examples will be discussed here. Several examples are, however, available in the literature [42-44].

11.3 SOME FINAL TIPS ON EXPERIMENTATION

There are always times in experimental science when experiments do not proceed as anticipated, owing, for example, to a malfunction of the instrumentation. Electrochemistry is no exception to this rule, and, indeed, many practitioners, particularly students, regard it as especially prone to this type of difficulty, although recent improvements in instrumentation have undoubtedly made life easier. In this final section we seek to pass on some hints and advice, based on

many years of experience of dealing with experimental problems. Some suggestions have been made earlier in this book, but it was felt that it would be useful to collect them together here. Problems usually fit into one of two categories: (i) where the behaviour observed is basically correct, but the cell response is noisy, (ii) where either no response is observed or where the response is incorrect or erratic. We will deal with the latter problem first.

As when trouble shooting any system, the first step is to attempt to locate the source of the problem. In electrochemistry this usually means testing the instrumentation on a dummy cell. The simplest dummy cell consists of a 100Ω resistor connected between the working and reference terminals of the potentiostat and a $1k\Omega$ resistor (both resistors should have a power rating of at least 1 watt) between the reference and secondary terminals. The applied voltages are then all set at zero and the dummy cell is switched in. No current should flow, but on applying a voltage, a current (determined by Ohm's law applied to the 100Ω resistor) should be observed. The correct behaviour of recorders and oscilloscopes can also be checked with the dummy cell by applying suitable voltage ramps and observing the output current. It is our experience that apparent faults in the instrumentation are more usually due to faults in the interconnecting cables.

Assuming that the instrumentation functions correctly (as is usually the case), the cell and wiring must be checked. Electrical connections often cause problems and, in particular, those made to electrodes using crocodile (alligator) clips. These clips corrode very easily, and this can lead to high resistance contacts and hence poor behaviour. Internal connections to electrodes, e.g. copper wire soldered to platinum, also often break (all contacts are readily checked by measuring the resistance of that part of the system with a DVM). If the connections all appear to be satisfactory, then the reference electrode/Luggin capillary must be suspected. Frequent problems here are blocked frits in commercial reference electrodes, air bubbles in Luggin capillaries, and dry ground glass taps where they are used to form a liquid junction (particularly with non-aqueous solvents). Other possible faults are blocked frits separating cell compartments and electrodes incompletely sealed into their shroud, thus exposing the side of the electrode, and other metals, to the electrolyte solution. If the problem still cannot be located it can be helpful to observe the current on an oscilloscope, as this will reveal any high frequency oscillations. These can be due to too much positive feedback if using iR_o compensation, the Luggin capillary being too close to the working electrode, or, with some potentiostats, to too little resistance between the working and secondary electrodes (particularly in concentrated aqueous solutions). If this latter explanation is the cause, it can be eliminated by incorporating a $1k\Omega$ resistor between the secondary electrode and the potentiostat to reduce the open loop gain of the potentiostat.

Noise is a common problem in electrochemistry, and it usually arises from 50/60 Hz mains frequency pickup. Whilst its effects can be minimised by filtering (either with an appropriate notch filter or a capacitor across the terminals of the X-Y recorder), it is certainly preferable to try to remove the problem. As already stated, all connections between the cell and the potentiostat should be as

short as possible, and the resistance of the reference electrode/Luggin capillary should be as low as possible. Noise is greatly reduced by placing the cell in a Faraday cage, an earthed screen of perforated paramagnetic material. Indeed, placing the cell inside any earthed metal box usually brings about a dramatic improvement in noise performance.

REFERENCES

- [1] G. J. Janz & D. J. G. Ives, *Reference electrodes*, Academic Press, (1961).
- [2] G. Gritzner & J. Kuta, *Electrochim. Acta*, **29** (1984) 869.
- [3] H. Schneider & H. Strehlow, *J. Electroanal. Chem.*, **12** (1966) 530.
- [4] M. D. Mackey & R. Peat, *J. Electroanal. Chem.*, **137** (1982) 321.
- [5] I. Piljac & R. T. Iwamoto, *J. Electroanal. Chem.*, **23** (1969) 484.
- [6] O. Bravo, Thesis, University of Kansas, 1967.
- [7] R. Parsons & E. de Valera, *Nouv. J. Chim.*, **2** (1978) 111.
- [8] E. Kirowa-Eisner & E. Gileadi, *J. Electroanal. Chem.*, **25** (1970) 481.
- [9] C. K. Mann, *Electroanal. Chem.*, **3** (1969) 58.
- [10] J. N. Butler, *Advances in Electrochem. and Electrochem. Eng.*, Vol VII, (Eds) C. W. Tobias & P. Delahay (1970).
- [11] J. Bizot, *Bull. Soc. Chim., France* (1967) 151.
- [12] H. Lund in *Organic electrochemistry*, Eds. M. M. Baizer & H. Lund, Marcel Dekker, 1983.
- [13] A. J. Fry & W. E. Britton in *Laboratory techniques in electroanalytical chemistry*, Eds. P. T. Kissinger and W. R. Heineman, Marcel Dekker, 1984.
- [14] S. Barnartt, *J. Electrochem. Soc.*, **99** (1952) 549.
- [15] S. Barnartt, *J. Electrochem. Soc.*, **108** (1961) 102.
- [16] A. Bewick, M. Fleischmann & M. Liler, *Electrochim. Acta*, **1** (1959) 83.
- [17] J. I. Smith, *Modern operational circuit design*, Wiley (1971).
- [18] Operational Amplifier Symposium, *Anal. Chem.*, **35**, 1770 (1963).
- [19] J. G. Graeme, G. E. Toby, & L. Heulsman, *Operational amplifiers, design and applications*, McGraw-Hill, 1971.
- [20] G. B. Clayton, *Operational amplifiers*, Butterworths, London, 1971.
- [21] G. B. Clayton, *Experiments with operational amplifiers*, Butterworth, London, 1975.
- [22] G. B. Clayton, *Linear integrated circuit applications*, MacMillan, London, 1975.
- [23] J. S. Mattson, H. B. Mark, & H. MacDonald (Eds), *Instrumentation*, Vol. 2, Marcel Dekker, Chapter 6.
- [24] R. Greef, *J. Physics E. Sci. Instrum.*, **11**, 1978, 1.
- [25] J. Schoen & K. E. Staubach, *Regelungstechnik*, **2** (1954) 159.
- [26] M. Breiter & F. G. Will, *Z. Elektrochem.*, **61** (1957) 1177.
- [27] H. Gerischer & K. E. Staubach, *Z. Elektrochem.*, **61** (1957) 789.
- [28] A. Bewick & M. Fleischmann, *Electrochim. Acta*, **8** (1963) 89.
- [29] J. A. Harrar & C. L. Pomenoski, *Anal. Chem.*, **45** (1973) 57.
- [30] J. D. E. McIntyre & W. F. Peck, *J. Electrochem. Soc.*, **117** (1970) 747.
- [31] D. Britz & W. A. Brocke, *J. Electroanal. Chem.*, **58** (1975) 301.
- [32] W. B. Holbrook & G. L. Booman, *Anal. Chem.*, **37** (1965) 795.

- [33] E. R. Brown, T. G. McCord, D. E. Smith, & D. D. DeFord, *Anal. Chem.*, **38** (1966) 1119.
- [34] A. Bewick, *Electrochim. Acta*, **13** (1968) 825.
- [35] D. Britz, *J. Electroanal. Chem.*, **88** (1978) 309.
- [36] D. Garreau & J. M. Saveant, *J. Electroanal. Chem.*, **86** (1978) 63.
- [37] C. Gabrielli, M. Ksouri, & R. Wiart, *Electrochim. Acta*, **22** (1977) 255.
- [38] D. E. Smith, *Crit. Rev. Anal. Chem.*, **2** (1971) 247.
- [39] R. A. Osteryoung in Computers in Chemistry and Instrumentation, Ed. J. S. Mattson, H. B. Mark and H. C. Macdonald, Vol. 2, p. 353, Marcel Dekker, (1972).
- [40] D. E. Smith, *ibid*, p. 369.
- [41] S. P. Perone, *ibid*, p. 423.
- [42] O. R. Brown, *Electrochim Acta*, **27**, (1982), 33.
- [43] D. E. Smith, *Anal. Chem.*, **48** (1976) 221A.
- [44] J. A. Harrison and C. E. Small, *Electrochim. Acta*, **25** (1980) 447.

APPENDIX

Mathematical methods for the development of a theory for electrochemical experiments

Throughout this book we have sought to show that the general form of the response to any electrochemical experiment can be deduced by qualitative arguments based on an understanding of the nature of electrode reactions. On the other hand, the quantitative determination of kinetic constants from experimental data is always based on a theoretical calculation of the nature of the response as a function of kinetic and experimental parameters and a comparison of these calculated (or computer simulated) responses with the experimental data. Hence it is essential to design laboratory experiments so that they may be described by a set of mathematical equations which are capable of solution. Indeed, even when, as is usually the case, one chooses not to do the mathematics oneself, but instead goes to the literature to seek the appropriate equation or dimensionless plot, it is still necessary to be confident that the experiment is carried out in such a way that it matches the system treated by the theory in the literature.

The purpose of this appendix is to outline the mathematical techniques used in the development of the theoretical basis of electrochemical methods, i.e. the equations and dimensionless plots discussed in earlier pages. The methods are illustrated by a number of examples when complete solutions are presented so that the reader can see, in detail, each step in the method.

The first stage is always to describe the experiment by a set of partial differential equations, initial and boundary conditions which will reflect (i) the mass transport processes of the electroactive species, intermediates and products, (ii) the nature of any coupled chemical reactions, (iii) the initial concentrations of each species in the electrolyte, and (iv) the changes in concentration at the electrode surface induced by the particular electrochemical experiment. There-

fore the first necessity is to be able to describe the mass transport processes in an exact way. Systems where migration and convection are important as well as diffusion (always present in electrochemical systems because of the concentration differences induced by the electrode reaction) are frequently not describable with precision, and certainly lead to complex mathematics. Hence this chapter will largely deal with unstirred solutions containing excess base electrolyte so that only diffusion need be considered. Moreover, in the first part we shall limit discussion to experiments which may be modelled by linear diffusion to a plane electrode (i.e. a one-dimensional model) since this greatly simplifies the equations which need to be solved. Later, spherical and cylindrical geometries will be briefly considered. In all cases the algebra is reduced by the assumption that $D = D_O = D_R$.

The second stage is to find a solution to the set of equations. Three basic approaches are possible: (a) a complete analytical solution, (b) a partial analytical solution which is completed by a numerical method such as numerical integration, (c) a computer solution either based on a simulation of the experiment or a numerical solution of the set of equations. The first approach is always to be preferred since it leads to an exact equation relating experimental measurables to kinetic parameters. Its range of applicability is, however, limited to relatively simple experiments, and as the experiment becomes more complex it is necessary to deal with time dependent boundary conditions, coupled partial differential equations, and perhaps non-linear equations. Then the computer techniques must be employed, and these generally lead to dimensionless plots.

It should be noted that complete solutions of the equations, the concentration profiles for each species in the system, $c_i = f(x, t)$, are seldom required in electrochemistry. Generally we only require to solve for the flux of electroactive species at the surface which is proportional to $(\partial c_i / \partial x)_{x=0}$, or a ratio of concentrations at the surface $(c_O^g / c_R^g)_{x=0}$, as a function of time. This allows some short cuts, see below.

A.1 ANALYTICAL METHODS

A.1.1 Linear diffusion to a plane electrode

You will remember that in this model, we assume that the electrode is completely flat and of infinite dimensions so that it is only necessary to consider concentration differences and hence diffusion in the direction perpendicular to the surface. Migration and convection are avoided by using a base electrolyte and a still solution. While laboratory electrodes are commonly spherical or cylindrical or a flat electrode of rather small size, each of these fortunately approximates to the model on a timescale of below 10 s.

A.1.1.1 Steady state experiments

Steady state experiments may be described by a set of ordinary differential equations and their boundary conditions. The solutions are relatively straightforward and require only elementary calculus. The techniques are illustrated by two examples.

Example 1: *The calculation of the steady state, diffusion controlled current for the simple electron transfer reaction*



where O and R are both stable and the solution initially contains only O.

The starting point is to consider the way the concentrations of O and R at a point, distance x from the electrode but within the diffusion layer, vary with time. This is given by Fick's 2nd law, i.e.

$$\frac{\partial c_O}{\partial t} = D \frac{\partial^2 c_O}{\partial x^2} \quad (\text{A.2})$$

and

$$\frac{\partial c_R}{\partial t} = D \frac{\partial^2 c_R}{\partial x^2}. \quad (\text{A.3})$$

But, clearly, if we are concerned only with the steady state situation $\partial c_O/\partial t = \partial c_R/\partial t = 0$, and the two equations we need to solve are

$$\frac{\partial^2 c_O}{\partial x^2} = 0 \quad (\text{A.4})$$

and

$$\frac{\partial^2 c_R}{\partial x^2} = 0 \quad (\text{A.5})$$

with the boundary conditions

$$(i) \text{ at } x = 0, c_O = 0 \quad (\text{A.6})$$

Since the electrode reaction is under diffusion control, all the electroactive species reaching the surface is reduced.

$$(ii) \text{ at } x = 0, -\left(\frac{\partial c_O}{\partial x}\right)_{x=0} = \left(\frac{\partial c_R}{\partial x}\right)_{x=0} \quad (\text{A.7})$$

This boundary condition is true for all electrode reactions, and reflects the fact that the fluxes of reactant and products at the surface are always equal but of opposite sign. It should be noted that we can also equate the flux of O and R at $x = 0$ with the flux of electrons, i.e.

$$\frac{I}{nF} = -D \left(\frac{\partial c_O}{\partial x}\right)_{x=0} = D \left(\frac{\partial c_R}{\partial x}\right)_{x=0} \quad (\text{A.8})$$

and these are always the equations we use to calculate the current from the concentration profiles for species in solution.

$$(iii) \text{ at } x = \infty, c_R = 0 \text{ and } c_O = c_O^\infty \quad (\text{A.9})$$

since a long way from the surface the solution is unchanged by the electrode reaction.

Since the boundary conditions for the species R at $x = 0$ are only known in terms of O, a good start to the solution is to add Equations (A.4) and (A.5) and to group the boundary conditions (A.7) and (A.9) appropriately. That is

$$\frac{d^2(c_O + c_R)}{dx^2} = 0, \quad (\text{A.10})$$

with the modified boundary conditions, at $x = 0$, $d(c_O + c_R)/dx = 0$ and at $x = \infty, c_O + c_R = c_O^\infty$. Then simple integration of (A.10) using these boundary conditions to find the integration constants leads to

$$c_O + c_R = c_O^\infty \quad (\text{A.11})$$

at all x . This result can be seen to be chemical sense since the only chemical change involves the interconversion of O and R.

Thus the boundary conditions at $x = 0$, Equations (A.6) and (A.7), may in this case be simplified to

$$\text{at } x = 0, c_O = 0 \quad \text{and} \quad c_R = c_O^\infty. \quad (\text{A.12})$$

Simple integration of Equations (A.4) or (A.5) and substitution of the boundary conditions (A.12) and (A.9) shows that as stated in Chapter 1, the solutions of the equations are indeterminate. It can be shown by solving the time dependent equations (see later) and letting $t \rightarrow \infty$ that the only steady state solution is $c_O = 0$ and $I = 0$. This is because with the model used, there are no steady concentration profiles until all the species O is removed from solution. In practice we know that a steady state current is easily obtained, and the experimental situation is readily predicted if we define a boundary layer, thickness δ , and we assume that outside this layer the concentrations of O and R are maintained constant by convection, either natural or forced. The boundary conditions to (A.4) and (A.5) are then

$$\text{at } x = 0, c_O = 0 \quad \text{and} \quad c_R = c_O^\infty \quad (\text{A.13})$$

and

$$\text{at } x = \delta, c_O = c_O^\infty \quad \text{and} \quad c_R = 0. \quad (\text{A.14})$$

Integration of (A.4) and (A.5) and substitution of the boundary conditions to obtain the constants of integration leads to

$$c_O = \frac{c_O^\infty}{\delta} x \quad (\text{A.15})$$

and

$$c_R = -\frac{c_O^\infty}{\delta}x + c_O^\infty , \quad (A.16)$$

and we can see that this steady state Nernst diffusion layer model leads to linear concentration profiles. The current density is given by

$$I = -nFD \left(\frac{dc_O}{dx} \right)_{x=0} = -\frac{nFDc_O^\infty}{\delta} . \quad (A.17)$$

It must be remembered that while this model is applicable to all experimental situations because of natural convection, it is only under particular circumstances, e.g. the rotating disc electrode, that δ is a known or calculable quantity.

Example 2: *The calculation of the steady state limiting current (also known as the catalytic current) for the system*



where S is an electroinactive species present in large excess and k is a pseudo-first order rate constant. Initially the solution medium contains only O , concentration c_O^∞ .

Again we commence by considering the way in which the concentrations of O and R at a point, distance x from the electrode, vary as a function of time. In this system, changes will occur both because of diffusion and because of the homogeneous chemical reaction. The equations describing the system are

$$\frac{\partial c_O}{\partial t} = D \frac{\partial^2 c_O}{\partial x^2} + kc_R \quad (A.20)$$

$$\frac{\partial c_R}{\partial t} = D \frac{\partial^2 c_R}{\partial x^2} - kc_R , \quad (A.21)$$

where the first term on the right-hand side represents the changes due to diffusion, and the second the changes due to the chemical reaction (A.19). Since we are interested in a steady state current it is only necessary to solve the equations

$$D \frac{\partial^2 c_O}{\partial x^2} + kc_R = 0 \quad (A.22)$$

$$D \frac{\partial^2 c_R}{\partial x^2} - kc_R = 0 , \quad (A.23)$$

with the appropriate boundary conditions, which for the experiment described are

$$\text{at } x = \infty, c_O = c_O^\infty, c_R = 0 \quad (\text{A.24})$$

$$\text{at } x = 0, c_O = 0, c_R = c_O^\infty. \quad (\text{A.25})$$

The Equations (A.24) again simply describe the solution prepared for the experiment. The most general boundary conditions at $x = 0$, would be $c_O = 0$ (since we wish to calculate the limiting current) and

$$D\left(\frac{dc_O}{dx}\right)_{x=0} = -D\left(\frac{dc_R}{dx}\right)_{x=0}.$$

The simplified boundary condition may be used, however, since the electrode reaction and the homogeneous chemical reaction again only lead to interconversion between O and R. Hence chemical intuition confirms that for all x ,

$$c_O + c_R = c_O^\infty, \quad (\text{A.26})$$

and therefore at the surface $c_R = c_O^\infty$. Moreover, because of (A.26) a complete solution for $c_O(x)$, $c_R(x)$ and the current may be obtained by solving only (A.23).

A table of standard integrals would confirm that equation (A.23) has the general solution

$$c_R = M \exp\left(\frac{k}{D}\right)^{1/2} x + N \exp -\left(\frac{k}{D}\right)^{1/2} x, \quad (\text{A.27})$$

and again, using the boundary condition at $x = \infty$, one finds $M = 0$ (otherwise $c_R \rightarrow \infty$ as $x \rightarrow \infty$), and from the boundary conditions at $x = 0$, clearly $N = c_O^\infty$. Hence

$$c_R = c_O^\infty \exp -\left(\frac{k}{D}\right)^{1/2} x. \quad (\text{A.28})$$

This is the steady state concentration profile for the species R, and its counterpart for the species O may be found by combining it with (A.26), i.e.

$$c_O = c_O^\infty \left(1 - \exp -\left(\frac{k}{D}\right)^{1/2} x\right). \quad (\text{A.29})$$

The current density is given by

$$I = -nFD\left(\frac{dc_O}{dx}\right)_{x=0} \quad (\text{A.30})$$

so that

$$I_L = -nFD^{1/2}k^{1/2}c_O^\infty , \quad (A.31)$$

and it may be seen that the steady state current depends on the rate of the homogeneous chemical reaction (A.19); provided reaction (A.19) is rapid, the limiting current will be larger than the diffusion controlled current for (A.18) uncomplicated by a following chemical reaction, effectively since the electroactive species is regenerated by the chemical reaction. Hence the term 'catalytic current'.

It is worthwhile to note that Equations (A.22) and (A.23) have genuine steady state solutions without the need to introduce a boundary layer. This is because the chemical reaction (A.19) causes the formation of a steady state kinetic layer. Only within this boundary layer is R present in solution, and the concentration of O perturbed from its initial concentration. The thickness of the kinetic layer depends on k ; the larger k the thinner the layer. Certainly for high values of k , the kinetic layer will lie well within the normal steady state diffusion layer defined by natural convection. The time required to reach the steady state (from the kinetic layer) also depends inversely on k .

A.1.1.2 Non-steady state experiments

Most electrochemical experiments in the laboratory make use of the principle of non-steady state diffusion. Certainly this is the case for cyclic voltammetry, potential step, a.c. methods, and spectroelectrochemical techniques, and hence we must develop the techniques to solve the partial differential equations which describe non-steady state diffusion.

The methods generally used are based on Laplace Transformations. The Laplace Transform of a quantity y is written $L\{y\}$ or \bar{y} and is defined by the equation

$$\bar{y} = \int_0^\infty y \exp(-st) dt \quad (A.32)$$

where s is the variable of the transformation. Whereas y is a function of time and position, \bar{y} is a function of s and position. We shall be particularly concerned with the transformation of concentration terms, e.g. c to \bar{c} , and typically we shall wish to transform an equation such as

$$\frac{\partial c_O}{\partial t} = D \frac{\partial^2 c_O}{\partial x^2} - kc_O \quad (A.33)$$

in which each of the terms is readily transformed.

Since

$$L\left(\frac{\partial c_O}{\partial t}\right) = \int_0^\infty \frac{\partial c_O}{\partial t} \cdot \exp(-st) dt$$

$$\begin{aligned}
 &= \left[c_O \exp(-st) \right]_0^\infty + \int_0^\infty s \cdot c_O \exp(-st) dt \\
 &= -(c_O)_{t=0} + s\bar{c}_O
 \end{aligned} \tag{A.34}$$

and

$$L\left(\frac{\partial^2 c_O}{\partial x^2}\right) = \frac{d^2 \bar{c}_O}{dx^2}. \tag{A.35}$$

The partial differential equation (A.33) therefore transforms term by term to give the ordinary differential equation

$$\bar{s}\bar{c}_O - (c_O)_{t=0} = D \frac{d^2 \bar{c}_O}{dx^2} - k\bar{c}_O. \tag{A.36}$$

The problem of finding a solution of (A.33) is therefore reduced to solving (A.36), using the transforms of all the boundary conditions, and inverting the solution of (A.36) back to the variables t and x . Many problems may be tackled in this way by using a table of transforms of functions (see Table A.1). The entire procedure may be summarised into the following stages:

- (i) Write down the partial differential equations, initial, and boundary conditions which describe the system and experiment.
- (ii) Laplace Transform the partial differential equation and the boundary conditions; the initial conditions will be used in the transform process.
- (iii) Solve the resulting ordinary differential equations with the transformed boundary condition.
- (iv) Invert the solution, again using tables of transforms.

If the inverse of a transform cannot be found in a table it can be derived by applying the Convolution Theorem

$$L^{-1}\{f_1(s)f_2(s)\} = \int_0^t f_1(\tau)f_2(t-\tau)d\tau = \int_0^t f_1(t-\tau)f_2(\tau)d\tau. \tag{A.37}$$

For example,

$$L^{-1}\left\{\frac{1}{s^{1/2}(s-1)}\right\} = \int_0^t \frac{1}{\pi^{1/2}\tau^{1/2}} \exp(t-\tau)d\tau \tag{A.38}$$

using transforms X and XIV in Table A.1. Making the substitution $y^2 = \tau$ in Equation (A.38) and noting that $2ydy = d\tau$ we obtain

$$\begin{aligned}
 L^{-1}\left\{\frac{1}{s^{1/2}(s-1)}\right\} &= \exp t \int_0^{t^{1/2}} \frac{2}{\pi^{1/2}} \exp(-y^2) dy \\
 &= \exp(t) \operatorname{erf}(t^{1/2})
 \end{aligned} \tag{A.39}$$

Table A.1 – Laplace transforms used in examples

No.	Function	Transform
I	c_O	\bar{c}_O
II	$\frac{d^n c_O}{dx^n}$	$\frac{d^n \bar{c}_O}{dx^n}$
III	$\frac{\partial c_O}{\partial t}$	$s\bar{c}_O - (c_O)_{t=0}$
IV	$t^n f(t)$	$(-1)^n f^n(s)$
V	$\int_0^t f(\tau) d\tau$	$\frac{1}{s} f(s)$
VI	$\int_0^t f_1(\tau) f_2(t-\tau) d\tau$	$f_1(s) f_2(s)$
	$= \int_0^t f_2(\tau) f_1(t-\tau) d\tau$	
VII	$f(t-\alpha)$ for $t > 0$ 0 for $t < 0$	$\exp(-\alpha s) f(s)$
VIII	1	$\frac{1}{s}$
IX	t^n (n integer > 1)	$n! s^{-(1+n)}$
X	$(\pi t)^{-1/2}$	$s^{-1/2}$
XI	$\frac{1}{\pi^{1/2} t^{1/2}} \exp -\frac{\alpha^2}{4t}$	$\frac{1}{s^{1/2}} \exp -\alpha s^{1/2}$
XII	$\operatorname{erfc} \frac{\alpha}{2t^{1/2}}$	$\frac{1}{s} \exp -\alpha s^{1/2}$
	where $\operatorname{erfc} z = 1 - \operatorname{erf} z$	
	$= 1 - \frac{2}{\pi^{1/2}} \int_0^z \exp(-y^2) dy$	
XIII	$2 \left(\frac{t}{\pi} \right)^{1/2} \exp \left(-\frac{\alpha^2}{4t} \right) - \alpha \operatorname{erfc} \left(\frac{\alpha}{2t^{1/2}} \right)$	$\frac{1}{s^{3/2}} \exp -\alpha s^{1/2}$

Table A.1 — continued.

No.	Function	Transform
XIV	$\exp(-\alpha t)$	$\frac{1}{s + \alpha}$
XV	$\alpha^{-1/2} \exp(\alpha t) \operatorname{erf}(\alpha t)^{1/2}$	$\frac{1}{s^{1/2}(s - \alpha)}$
XVI	$\exp(\alpha t) f(t)$	$f(s - \alpha)$
XVII	$\exp \alpha^2 t \operatorname{erfc} \alpha t^{1/2}$	$\frac{1}{s^{1/2}(s^{1/2} + \alpha)}$
XVIII	$\sin \alpha t$	$\frac{\alpha}{s^2 + \alpha^2}$

A further useful property of Laplace Transforms is that of converting functions with discontinuities in t -space into continuous functions in s -space. Let us consider the function

$$\begin{aligned} g(t) &= f(t - \alpha) && \text{for } t > \alpha \\ &= 0 && \text{for } t < \alpha . \end{aligned} \quad (\text{A.40})$$

$$\begin{aligned} \mathcal{L}\{g(t)\} &= \int_0^\infty g(t) e^{-st} dt = \int_0^\alpha g(t) e^{-st} dt + \int_\alpha^\infty g(t) e^{-st} dt \\ &= \int_0^\alpha 0 e^{-st} dt + \int_\alpha^\infty f(t - \alpha) e^{-st} dt \\ &= \int_0^\infty f(t - \alpha) e^{-st} dt . \end{aligned} \quad (\text{A.41})$$

Substituting $x = t - \alpha$ into (A.41) we obtain

$$\begin{aligned} \mathcal{L}\{g(t)\} &= \int_0^\infty f(x) e^{-s(x+\alpha)} dx = e^{-\alpha s} \int_0^\infty f(x) e^{-sx} dx \\ &= e^{-\alpha s} f(s) . \end{aligned} \quad (\text{A.42})$$

Here we have in fact derived a rule known as the *Shift theorem*:

$$\begin{aligned} L^{-1}\{\exp(-\alpha s)f(s)\} &= 0 & 0 < t < \alpha \\ &= f(t-\alpha) & t > \alpha . \end{aligned} \quad (A.43)$$

Even using the Convolution and Shift Theorems, however, the Laplace transform of the required solution to a problem may sometimes be of a form which cannot be inverted directly. Possible approaches to the solution of such difficult inversion include

- (i) a series solution obtained either by expanding the transform of the solution using series expansions or by resolving the transform into partial fractions and then inverting the expanded form, term by term;
- (ii) the use of the *Residue Theorem* (see texts at the end of the appendix);
- (iii) numerical inversion.

An alternative to (iii) is to Laplace transform directly the experimental data (e.g. by using analogue computer elements) and to compare this data with the theoretical expression in the *s*-space.

The use of the Laplace transformation is now illustrated by some examples chosen to show various simple methods of obtaining an inversion of the transform of the solution. The experiments associated with this theory are discussed earlier in the book.

Example 3: *Calculation of the I-t transient in response to a potential step from a potential where the rate of the electrode process*



is negligible to a value where it is diffusion controlled. Again the initial solution contains only O.

Changes in concentration of O and R within the boundary layer caused by the electrode reaction will only arise by diffusion. Hence the partial differential equations we need to solve are simply Fick's 2nd law. Moreover, we can specify the initial conditions and the boundary conditions for O at both $x = 0$ ($c_O = 0$ since the reduction is diffusion controlled) and $x = \infty$ in an exact manner. Therefore, we can calculate the *I-t* response by solving a single set of equations describing the behaviour of O. These are

$$\frac{\partial c_O}{\partial t} = D \frac{\partial^2 c_O}{\partial x^2} \quad (A.45)$$

with the initial condition

$$c_O = \bar{c}_O \quad (A.46)$$

at all x , and the boundary conditions, at

$$x = 0, \quad c_O = 0$$

and at

$$x = \infty, \quad c_O = c_O^\infty.$$

Laplace transforming Equation (A.45) and the boundary conditions (A.47), see above, we obtain

$$s\bar{c}_O - c_O^\infty = D \frac{d^2 \bar{c}_O}{dx^2}. \quad (\text{A.48})$$

With at

$$x = 0, \quad \bar{c}_O = 0$$

and at

$$x = \infty, \quad \bar{c}_O = \frac{c_O^\infty}{s},$$

since

$$\mathcal{L}\{\text{const}\} = \frac{\text{const}}{s} \quad (\text{A.49})$$

The solution of (A.48) consists of the *Complementary Function* (see table of integrals in a standard text)

$$A \exp\left(\frac{s}{D}\right)^{1/2} x + B \exp -\left(\frac{s}{D}\right)^{1/2} x$$

and the *Particular Integral* c_O^∞/s , that is,

$$\bar{c}_O = A \exp\left(\frac{s}{D}\right)^{1/2} x + B \exp -\left(\frac{s}{D}\right)^{1/2} x + \frac{c_O^\infty}{s}. \quad (\text{A.50})$$

Using the transformed boundary conditions (A.49) one can find that $A = 0$ and $B = -c_O^\infty/s$, therefore

$$\bar{c}_O = \frac{c_O^\infty}{s} \left(1 - \exp -\left(\frac{s}{D}\right)^{1/2} x\right). \quad (\text{A.51})$$

Using the transform Table A.1 (VIII and XIII) we can invert this expression, i.e. to

$$c_O = c_O^\infty \left(1 - \operatorname{erfc} \frac{x}{2(Dt)^{1/2}}\right) = c_O^\infty \operatorname{erf} \frac{x}{2D^{1/2} t^{1/2}}. \quad (\text{A.52})$$

To obtain the current density, we differentiate (A.52):

$$\frac{\partial c_O}{\partial x} = \frac{c_O^\infty}{(Dt)^{1/2}} \exp - \left(\frac{x^2}{4Dt} \right). \quad (\text{A.53})$$

Whence

$$I = -nFD \left(\frac{\partial c_O}{\partial x} \right)_{x=0} = -\frac{nFD^{1/2} c_O^\infty}{\pi^{1/2} t^{1/2}}. \quad (\text{A.54})$$

Equation (A.54) can also be derived by differentiating (A.51), and noting that

$$\bar{I} = -nFD \left(\frac{dc_O}{dx} \right)_{x=0} = -\frac{nFD^{1/2} c_O^\infty}{s^{1/2}} \quad (\text{A.55})$$

which may then be inverted using standard transform X (Table A.1).

Note that Equation (A.54) states that at potentials where the electrode reaction is diffusion controlled, the $I-t$ transient can be replotted to give a linear plot of I versus $t^{-1/2}$ which passes through the origin.

Example 4: Calculation of the $I-t$ transient in response to a potential step experiment from a potential where no current for the electrode reaction



is observed to a value where reduction of O takes place, but the reaction is not diffusion controlled. Again, the solutions prepared for the experiment contain O but no R although both O and R are stable.

The mathematics now become more complex because we cannot specify the boundary condition at $x = 0$, in terms of O alone. All the equations describing the situation at the electrode surface contain concentrations of both O and R. As a result, it is necessary to solve the pair of equations

$$\frac{\partial c_O}{\partial t} = D \frac{\partial^2 c_O}{\partial x^2} \quad (\text{A.57})$$

and

$$\frac{\partial c_R}{\partial t} = D \frac{\partial^2 c_R}{\partial x^2}, \quad (\text{A.58})$$

with the boundary conditions

$$(i) \text{ at } x = 0, -D \left(\frac{\partial c_O}{\partial x} \right)_{x=0} = D \left(\frac{\partial c_R}{\partial x} \right)_{x=0} \quad (\text{A.59})$$

and

$$-D \left(\frac{\partial c_O}{\partial x} \right)_{x=0} = \tilde{k}(c_R)_{x=0} - \tilde{k}(c_O)_{x=0} . \quad (\text{A.60})$$

The second equation arises because both the left-hand side and the right-hand side are equal to the flux of electrons I/nF . $(c_O)_{x=0}$ and $(c_R)_{x=0}$ are the time dependent concentrations of O and R at the electrode surface, and \tilde{k} and \tilde{k} are the potential dependent rate constants for electron transfer, and

$$(ii) \quad \text{at } x = \infty, c_O = c_O^\infty \quad \text{and} \quad c_R = 0 . \quad (\text{A.61})$$

The initial conditions are

$$c_O = c_O^\infty \quad \text{and} \quad c_R = 0 \quad \text{at} \quad t = 0 \quad \text{for all } x \quad (\text{A.62})$$

Laplace transforming Equations (A.57) to (A.61) we obtain

$$s\bar{c}_O - c_O^\infty = D \frac{d^2 \bar{c}_O}{dx^2} \quad (\text{A.63})$$

and

$$s\bar{c}_R - 0 = D \frac{d^2 \bar{c}_R}{dx^2} \quad (\text{A.64})$$

with at

$$x = 0, -D \left(\frac{d\bar{c}_O}{dx} \right)_{x=0} = D \left(\frac{d\bar{c}_R}{dx} \right)_{x=0} = \tilde{k}(\bar{c}_R)_{x=0} - \tilde{k}(\bar{c}_O)_{x=0} \quad (\text{A.65})$$

and at

$$x = \infty, \bar{c}_O = \frac{c_O^\infty}{s} \quad \text{and} \quad \bar{c}_R = 0 . \quad (\text{A.66})$$

Equations (A.63) and (A.64) have the solutions (the sum of a particular integral and a complementary function)

$$\bar{c}_O = M \exp \left(\frac{s}{D} \right)^{1/2} x + N \exp - \left(\frac{s}{D} \right)^{1/2} x + \frac{c_O^\infty}{s} \quad (\text{A.67})$$

$$\bar{c}_R = P \exp \left(\frac{s}{D} \right)^{1/2} x + Q \exp - \left(\frac{s}{D} \right)^{1/2} x + 0 \quad (\text{A.68})$$

Since the values of \bar{c}_O and \bar{c}_R are not infinite at $x = \infty$, (A.66) $M = P = 0$.

Also, using $D(d\bar{c}_O/dx)_{x=0} = -D(d\bar{c}_R/dx)_{x=0}$ one finds $N = -Q$. Therefore Equations (A.67) and (A.68) may be reduced to

$$\bar{c}_O = N \exp - \left(\frac{s}{D} \right)^{1/2} x + \frac{c_O^\infty}{s} \quad (\text{A.69})$$

and

$$\bar{c}_R = -N \exp -\left(\frac{s}{D}\right)^{1/2} x . \quad (A.70)$$

Finally, to determine N we need to use the final part of the boundary conditions, that is,

$$\text{at } x = 0, -D \left(\frac{d\bar{c}_O}{dx} \right)_{x=0} = \vec{k} (\bar{c}_R)_{x=0} - \vec{k} (\bar{c}_O)_{x=0} .$$

Substituting (A.69) and (A.70) into this expression, one finds

$$D \left(\frac{s}{D} \right)^{1/2} N = -\vec{k} N - \vec{k} \left(N + \frac{c_O^\infty}{s} \right)$$

or

$$N = \frac{-\vec{k} c_O^\infty}{D^{1/2} s \left(s^{1/2} + \frac{\vec{k} + \vec{k}}{D^{1/2}} \right)} . \quad (A.71)$$

Hence the complete solution of (A.63) is

$$\bar{c}_O = \frac{-\vec{k} c_O^\infty \exp -\left(\frac{s}{D}\right)^{1/2} x}{D^{1/2} s \left(s^{1/2} + \frac{\vec{k} + \vec{k}}{D^{1/2}} \right)} + \frac{c_O^\infty}{s} . \quad (A.72)$$

For determining \bar{I} we require $(d\bar{c}_O/dx)_{x=0}$. Hence

$$\frac{d\bar{c}_O}{dx} = \frac{\vec{k} c_O^\infty}{D^{1/2} s \left(s^{1/2} + \frac{\vec{k} + \vec{k}}{D^{1/2}} \right)} \left(\frac{s}{D} \right)^{1/2} \cdot \exp -\left(\frac{s}{D}\right)^{1/2} x$$

and

$$\left(\frac{d\bar{c}_O}{dx} \right)_{x=0} = \frac{\vec{k} c_O^\infty}{D} \frac{1}{s^{1/2} \left(s^{1/2} + \frac{\vec{k} + \vec{k}}{D^{1/2}} \right)} \quad (A.73)$$

$$\bar{I} = \frac{-nF\vec{k} c_O^\infty}{s^{1/2} \left(s^{1/2} + \frac{\vec{k} + \vec{k}}{D^{1/2}} \right)} . \quad (A.74)$$

Again the inverse of (A.74) is available in tables, e.g. Table A.1, No. XVII

$$I = -nF\vec{k}c_O^\infty \exp \frac{(\vec{k} + \vec{\bar{k}})^2 t}{D} \operatorname{erfc} \frac{(\vec{k} + \vec{\bar{k}})t^{1/2}}{D^{1/2}} \quad (\text{A.75})$$

and this is the expression for the $I-t$ transient over the whole timescale.

Since $\exp y^2 \operatorname{erfc} y = 1 - 2y/\pi^{1/2}$ for small values of the argument y and $1/\pi^{1/2}y$ for large values of y , Equation (A.75) has two limiting forms

(i) At short times, the argument y will be small and

$$I = -nF\vec{k}c_O^\infty \left(1 - \frac{2(\vec{k} + \vec{\bar{k}})}{\pi^{1/2} D^{1/2}} \cdot t^{1/2} \right), \quad (\text{A.76})$$

and a plot of $I-t^{1/2}$ is linear with an intercept at $t = 0$, which allows \vec{k} to be determined.

(ii) At long times, the argument y will be large

$$I = \frac{-nF\vec{k}c_O^\infty D^{1/2}}{\pi^{1/2}(\vec{k} + \vec{\bar{k}})} \cdot t^{-1/2}, \quad (\text{A.77})$$

and a plot of $I-t^{-1/2}$ is now linear and should pass through the origin. Note that at potentials where $\vec{k} \gg \vec{\bar{k}}$ Equation (A.77) reduces to

$$I = \frac{-nFc_O^\infty D^{1/2} t^{-1/2}}{\pi^{1/2}},$$

the normal equation for a diffusion controlled transient.

Although these limiting forms have been commonly used, the best analyses for experimental data are those which use the current over the complete time regime. Chronocoulometry and chronoamperometry analysed by the method of Delahay and Oka are good examples of such procedures (see Chapter 2).

Example 5: Calculation of the impedance at the equilibrium potential for the electrode reaction



when the initial solution contains equal concentrations of O and R.

Any electrode/solution interface may be characterised by an impedance which is frequently determined by imposing an a.c. current and measuring the potential response, or alternatively applying an a.c. voltage and measuring the current response. The interpretation of this impedance in terms of kinetic parameters requires the assumption of an equivalent circuit whose components will model the mechanism of the electrode reaction (see Chapter 8). The simple electrode reaction, (A.78), may be characterised by a two component, series

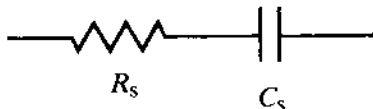


Fig. A.1 – Simple, two component circuit equivalent to electron transfer process.

circuit (Fig. A.1), where R_s is called the *polarisation resistance* and C_s the *pseudo capacitance*. If an alternating current, with frequency ω and small amplitude ΔI , is passed through the circuit, the total potential across the elements is given by

$$E = E_c + IR_s + \frac{1}{C_s} \int I dt , \quad (\text{A.79})$$

where E_c is the potential in the absence of any a.c. perturbation; in the example discussed here $E_c = E_e^\ominus$ because of the choice of the solution, $c_O^\infty = c_R^\infty = c^\infty$ and the absence of any net electrode reaction.

Differentiating Equation (A.79), one obtains

$$\frac{dE}{dt} = R_s \frac{dI}{dt} + \frac{I}{C_s} \quad (\text{A.80})$$

and substituting

$$I = \Delta I \sin \omega t , \quad (\text{A.81})$$

$$\frac{dE}{dt} = \omega \Delta I R_s \cos \omega t + \frac{\Delta I}{C_s} \sin \omega t . \quad (\text{A.82})$$

Now to interpret R_s and C_s in terms of electrochemical parameters, it is necessary to consider the nature of the electrochemical experiment and hence to derive an expression for dE/dt which contains the desired constants. Firstly, it is necessary to note that the potential response to an imposed a.c. current will be a function of the a.c. current, and the concentrations of O and R at the surface, i.e.

$$E = f[I, (c_O)_{x=0}, (c_R)_{x=0}] . \quad (\text{A.83})$$

Hence by the normal rules of differentiation

$$\frac{dE}{dt} = \frac{\partial E}{\partial I} \cdot \frac{dI}{dt} + \frac{\partial E}{\partial (c_O)_{x=0}} \cdot \frac{d(c_O)_{x=0}}{dt} + \frac{\partial E}{\partial (c_R)_{x=0}} \cdot \frac{d(c_R)_{x=0}}{dt} , \quad (\text{A.84})$$

and one must derive the various derivatives.

The terms $d(c_O)_{x=0}/dt$ and $d(c_R)_{x=0}/dt$ may be found by a procedure similar to that used in Examples 3 and 4. In fact, since O and R are both stable in solution, we know that $c_O + c_R = 2c^\infty$ at all x . Hence we need only solve the equation

$$\frac{\partial c_O}{\partial t} = D \frac{\partial^2 c_O}{\partial x^2} \quad (\text{A.85})$$

with the boundary conditions at

$$x = \infty, \quad c = c^\infty, \quad (\text{A.86})$$

and at

$$x = 0, \quad I = \Delta I \sin \omega t = -nFD \left(\frac{\partial c_O}{\partial x} \right)_{x=0} \quad (\text{A.87})$$

Laplace transforming Equations (A.85) to (A.87) leads to

$$s\bar{c}_O - c^\infty = D \frac{d^2 \bar{c}_O}{dx^2} \quad (\text{A.88})$$

with boundary conditions:

$$\text{at } x = \infty, \quad \bar{c}_O = \frac{c^\infty}{s} \quad (\text{A.89})$$

$$\text{at } x = 0, \quad D \left(\frac{d\bar{c}_O}{dx} \right)_{x=0} = -\frac{\Delta I}{nF} \cdot \frac{\omega}{s^2 + \omega^2} \quad (\text{A.90})$$

using transform XVIII. Again, (A.88) has the solution (complementary function + particular integral)

$$\bar{c}_O = M \exp \left(\frac{s}{D} \right)^{1/2} x + N \exp - \left(\frac{s}{D} \right)^{1/2} x + \frac{c^\infty}{s}. \quad (\text{A.91})$$

Moreover, as always we know that \bar{c}_O is not infinite at $x = \infty$, and hence M must be zero. N is determined by substitution of (A.90) in (A.91) so that the complete solution of (A.88) is

$$\bar{c}_O = \frac{\Delta I}{nFD^{1/2}} \frac{\omega}{s^{1/2}(s^2 + \omega^2)} \exp - \left(\frac{s}{D} \right)^{1/2} x + \frac{c^\infty}{s}. \quad (\text{A.92})$$

But we only require the information at $x = 0$, so

$$(\bar{c}_O)_{x=0} = \frac{\Delta I}{nFD^{1/2}} \frac{\omega}{s^{1/2}(s^2 + \omega^2)} + \frac{c^\infty}{s}, \quad (\text{A.93})$$

and inversion of this expression requires transforms X and XVII in Table A.1 and also the use of the convolution theorem

$$(c_O)_{x=0} = c^\infty + \frac{\Delta I}{nFD^{1/2}} \int_0^t \frac{1}{\pi^{1/2} \tau^{1/2}} \sin \omega(t-\tau) d\tau . \quad (\text{A.94})$$

Since $\sin(\alpha - \beta) = \sin \alpha \cos \beta - \sin \beta \cos \alpha$

$$(c_O)_{x=0} = c^\infty + \frac{\Delta I}{nFD^{1/2} \pi^{1/2}} \left[\sin \omega t \int_0^t \frac{\cos \omega \tau}{\tau^{1/2}} d\tau - \cos \omega t \int_0^t \frac{\sin \omega \tau}{\tau^{1/2}} d\tau \right] . \quad (\text{A.95})$$

Again these integrations may be simplified because we shall only measure the response when we have allowed the system to reach a steady state (although cyclic) response. Hence we can let $t \rightarrow \infty$, and since

$$\int_0^\infty \frac{\sin \omega \tau}{\tau^{1/2}} d\tau = \int_0^\infty \frac{\cos \omega \tau}{\tau^{1/2}} d\tau = \left(\frac{\pi}{2\omega} \right)^{1/2} \quad (\text{A.96})$$

$$(c_O)_{x=0} = c^\infty + \frac{\Delta I}{nFD^{1/2}(2\omega)^{1/2}} [\sin \omega t - \cos \omega t] \quad (\text{A.97})$$

Also since

$$(c_O)_{x=0} + (c_R)_{x=0} = 2c^\infty$$

$$(c_R)_{x=0} = c^\infty - \frac{\Delta I}{nFD^{1/2}(2\omega)^{1/2}} [\sin \omega t - \cos \omega t] , \quad (\text{A.98})$$

and therefore we can obtain the two required derivatives

$$\frac{d(c_O)_{x=0}}{dt} = \frac{\Delta I}{nF} \left(\frac{\omega}{2D} \right)^{1/2} (\sin \omega t + \cos \omega t) \quad (\text{A.99})$$

$$\frac{d(c_R)_{x=0}}{dt} = -\frac{\Delta I}{nF} \left(\frac{\omega}{2D} \right)^{1/2} (\sin \omega t + \cos \omega t) . \quad (\text{A.100})$$

We still need to calculate $\partial E / \partial I$, $\partial E / \partial (c_O)_{x=0}$ and $\partial E / \partial (c_R)_{x=0}$. These come from the Butler-Volmer equation, here conveniently written in the form

$$I = \frac{I_0}{c^\infty} \left[(c_R)_{x=0} \exp \frac{\alpha nF}{RT} \eta - (c_O)_{x=0} \exp -\frac{\alpha nF}{RT} \eta \right] \quad (\text{A.101})$$

where we are assuming $\alpha_A = \alpha_C = \alpha$. Rearranging this equation, we have

$$(c_O)_{x=0} = (c_R)_{x=0} \exp \frac{2\alpha nF}{RT} \eta - \frac{c^\infty I}{I_0} \exp \frac{\alpha nF}{RT} \eta \quad (\text{A.102})$$

and

$$\begin{aligned}\frac{\partial(c_O)_{x=0}}{\partial E} &= \frac{\partial(c_O)_{x=0}}{\partial\eta} \\ &= \frac{2\alpha nF}{RT}(c_R)_{x=0} \exp \frac{2\alpha nF}{RT}\eta - \frac{\alpha nF}{RT} \frac{c^\infty I}{I_0} \exp \frac{\alpha nF}{RT}\eta\end{aligned}\quad (\text{A.103})$$

This equation may be simplified considerably; under conditions where the perturbation from E_e is very small, i.e. η is very small (a) it is possible to use the linear approximation to the Butler-Volmer equation, $I = I_0(nF/RT)\eta$, (b) the exponential term may be expanded as a series, $\exp x = 1 + x + \dots$, and here and elsewhere all terms containing η^2 and higher powers may be ignored, (c) the surface concentration of R remains close to c_R^∞ , and we may consider $(c_R)_{x=0} = c^\infty$. Then

$$\frac{\partial(c_O)_{x=0}}{\partial E} = \frac{nFc^\infty}{RT} \left(1 + \frac{\alpha nF}{RT} \eta \right). \quad (\text{A.104})$$

Similarly

$$\frac{\partial(c_R)_{x=0}}{\partial E} = -\frac{nFc^\infty}{RT} \left(1 - \frac{\alpha nF}{RT} \eta \right). \quad (\text{A.105})$$

Now we are close to a solution. Substituting (A.99), (A.100), (A.104), and (A.105) into (A.84) one obtains

$$\begin{aligned}\frac{dE}{dt} &= \frac{RT}{I_0 nF} \omega \Delta I \cos \omega t \\ &+ \frac{RT}{nFc^\infty} \left[\frac{1}{1 + \frac{\alpha nF}{RT} \eta} + \frac{1}{1 - \frac{\alpha nF}{RT} \eta} \right] \frac{\Delta I}{nF} \left(\frac{\omega}{2D} \right)^{1/2} (\sin \omega t + \cos \omega t) \\ &\simeq \frac{RT}{I_0 nF} \omega \Delta I \cos \omega t + \frac{2RT\Delta I}{n^2 F^2 c^\infty} \left(\frac{\omega}{2D} \right)^{1/2} (\sin \omega t + \cos \omega t),\end{aligned}\quad (\text{A.106})$$

since again $1 > (\alpha^2 n^2 F^2 / R^2 T^2) \eta^2$ for values of η used in such experiments. Finally, comparing (A.82) with (A.106) we can see that

$$R_s = \frac{RT}{I_0 nF} + \frac{RT}{n^2 F^2 c^\infty} \left(\frac{2}{\omega D} \right)^{1/2} \quad (\text{A.107})$$

$$C_s = \frac{n^2 F^2 c^\infty}{RT} \left(\frac{D}{2\omega} \right)^{1/2} \quad (\text{A.108})$$

It can be seen that a plot of R_s vs $1/\omega^{1/2}$ should be linear, and that the intercept may be used to estimate a value for the exchange current density. Also it may be seen that the polarisation resistance is made up of a frequency independent and a frequency dependent term. Hence it is frequently broken into two circuit components (Fig. A.2).

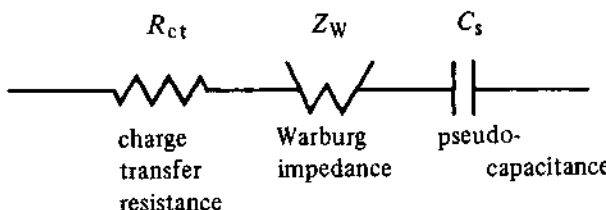


Fig. A.2 – Equivalent circuit for the polarisation resistance.

Example 6: *The calculation of the I-t response in a thin layer cell bounded by two electrodes acting as working and counter electrodes (the reference electrode is external to the thin layer). The potential of the working electrode is stepped from the equilibrium potential to that for the diffusion controlled reduction $O + ne^- \rightarrow R$ and the solution contains excess R so that only the reverse reaction occurs at the counter electrode. O and R are both stable.*

This simple thin layer cell has a uniform potential over all the surface of the working electrode, but clearly cannot be used for coulometric type experiments. As always when both O and R are stable, we know that at all x , $c_O + c_R = \text{constant}$, determined by the solutions prepared for the experiment. Moreover, we again need to solve the differential equation

$$\frac{\partial c_O}{\partial t} = D \frac{\partial^2 c_O}{\partial x^2} \quad (\text{A.109})$$

with the initial condition

$$c_O = c \quad \text{for } 0 < x < l, \quad (\text{A.110})$$

where l is the interelectrode gap. The boundary conditions are

$$(i) \quad \text{at } x = 0, c_O = 0. \quad (\text{A.111})$$

since the electrode is at a potential where the reaction is diffusion controlled

$$(ii) \quad \left(\frac{\partial c_O}{\partial x} \right)_{x=0} = \left(\frac{\partial c_O}{\partial x} \right)_{x=l}. \quad (\text{A.112})$$

since the currents at the two electrodes are equal but opposite in sign.

Laplace transforming equations (A.109) to (A.112) we obtain

$$s\bar{c}_O - c = D \frac{d^2\bar{c}_O}{dx^2} \quad (\text{A.113})$$

with at

$$x = 0, \bar{c}_O = 0 \quad (\text{A.114})$$

and

$$\left(\frac{d\bar{c}_O}{dx} \right)_{x=0} = \left(\frac{d\bar{c}_O}{dx} \right)_{x=l}. \quad (\text{A.115})$$

Equation (A.113) again has the solution (sum of particular integral + complementary function)

$$\bar{c}_O = A \exp\left(\frac{s}{D}\right)^{1/2} x + B \exp -\left(\frac{s}{D}\right)^{1/2} x + \frac{c}{s}, \quad (\text{A.116})$$

and A and B are determined using (A.114) and (A.115). It follows that

$$\bar{c}_O = \frac{c \exp -\left(\frac{s}{D}\right)^{1/2} (l-x)}{s \left(1 - \exp -\left(\frac{s}{D}\right)^{1/2} l\right)} - \frac{c \exp -\left(\frac{s}{D}\right)^{1/2} x}{s \left(1 - \exp -\left(\frac{s}{D}\right)^{1/2} l\right)} + \frac{c}{s} \quad (\text{A.117})$$

and

$$\left(\frac{d\bar{c}_O}{dx} \right)_{x=0} = \frac{c}{D^{1/2} s^{1/2}} \cdot \frac{1 + \exp -\left(\frac{s}{D}\right)^{1/2} l}{1 - \exp -\left(\frac{s}{D}\right)^{1/2} l}. \quad (\text{A.118})$$

The inverse of this expression does not appear in the tables of transforms. For large values of s (i.e. short times) the term $[1 - \exp - (s/D)^{1/2} l]^{-1}$ may, however, be expanded by the binomial theorem

$$\begin{aligned} \left. \frac{d\bar{c}_O}{dx} \right|_{x=0} &= \frac{c}{D^{1/2} s^{1/2}} \left(1 + \exp -\left(\frac{s}{D}\right)^{1/2} l \right) \left(1 + \exp -\left(\frac{s}{D}\right)^{1/2} l + \exp - 2\left(\frac{s}{D}\right)^{1/2} l \dots \right) \\ &= \frac{c}{D^{1/2} s^{1/2}} \left(1 + 2 \exp -\left(\frac{s}{D}\right)^{1/2} l + \exp - 2\left(\frac{s}{D}\right)^{1/2} l \dots \right) \\ &= \frac{c}{D^{1/2} s^{1/2}} \left(1 + 2 \sum_{n=1}^{\infty} \exp \left(-nl \left(\frac{s}{D} \right)^{1/2} \right) \right). \end{aligned} \quad (\text{A.119})$$

This expression may be inverted using the transforms X and XI. The series is inverted term by term. Thus

$$\left(\frac{\partial c_O}{\partial x}\right)_{x=0} = \frac{c}{D^{1/2} \pi^{1/2} t^{1/2}} \left(1 + 2 \sum_{n=1}^{\infty} \exp -\frac{n^2 l^2}{4Dt}\right). \quad (\text{A.120})$$

Solutions of this kind are useful only for large values of s and hence short times (s, t is equal to one).

To obtain a solution for long times, i.e. small s , we can rewrite Equation (A.118) in the form (i.e. multiply top and bottom by $\exp \frac{1}{2}(s/D)^{1/2}l$):

$$\begin{aligned} \left(\frac{d\bar{c}_O}{dx}\right)_{x=0} &= \frac{c}{D^{1/2} s^{1/2}} \left(\frac{\exp \frac{1}{2} \left(\frac{s}{D}\right)^{1/2} l + \exp -\frac{1}{2} \left(\frac{s}{D}\right)^{1/2} l}{\exp \frac{1}{2} \left(\frac{s}{D}\right)^{1/2} l - \exp -\frac{1}{2} \left(\frac{s}{D}\right)^{1/2} l} \right) \\ &= \frac{c}{D^{1/2} s^{1/2}} \frac{\cosh \frac{1}{2} l \left(\frac{s}{D}\right)^{1/2}}{\sinh \frac{1}{2} l \left(\frac{s}{D}\right)^{1/2}} \\ &= \frac{c}{D^{1/2} s^{1/2}} \frac{1 + \frac{1}{8} \left(\frac{s}{D}\right) l^2}{\frac{1}{2} \left(\frac{s}{D}\right)^{1/2} l + \frac{1}{48} \left(\frac{s}{D}\right)^{3/2} l^3} \dots \dots \dots \\ &= \frac{2c}{sl \left(1 + \frac{1}{24} \left(\frac{s}{D}\right) l^2\right)} + \frac{cl}{4D \left(1 + \frac{1}{24} \left(\frac{s}{D}\right) l^2\right)}. \end{aligned} \quad (\text{A.121})$$

Resolving the first term into partial fractions, (A.121) becomes

$$\begin{aligned} \left(\frac{d\bar{c}_O}{dx}\right)_{x=0} &= \frac{2c}{sl} - \frac{cl}{12D \left(1 + \frac{1}{24} \left(\frac{s}{D}\right) l^2\right)} + \frac{cl}{4D \left(1 + \frac{1}{24} \left(\frac{s}{D}\right) l^2\right)} \\ &= \frac{2c}{sl} + \frac{cl}{6D \left(1 + \frac{1}{24} \left(\frac{s}{D}\right) l^2\right)} \\ &= \frac{2c}{sl} + \frac{4c}{l \left(\frac{24D}{l^2} + s\right)} \end{aligned} \quad (\text{A.122})$$

and the final expression is readily inverted using transforms VII and XIV.

$$\left(\frac{\partial c_O}{\partial x}\right)_{x=0} = \frac{2c}{l} + \frac{4c}{l} \exp\left(\frac{-24D.l}{l^2}\right), \quad (\text{A.123})$$

and the current at long and short times is then found from (A.120) and (A.123) respectively by multiplying the expression for $(\partial c_O/\partial x)_{x=0}$ by nFD . Fig. A.3 shows the development of the concentration profiles in the thin layer cell for this experiment. The steady state current (let $t \rightarrow \infty$ in (A.123)) is simply $2nFDc/l$, and it may be noted that the concentration profile is linear.

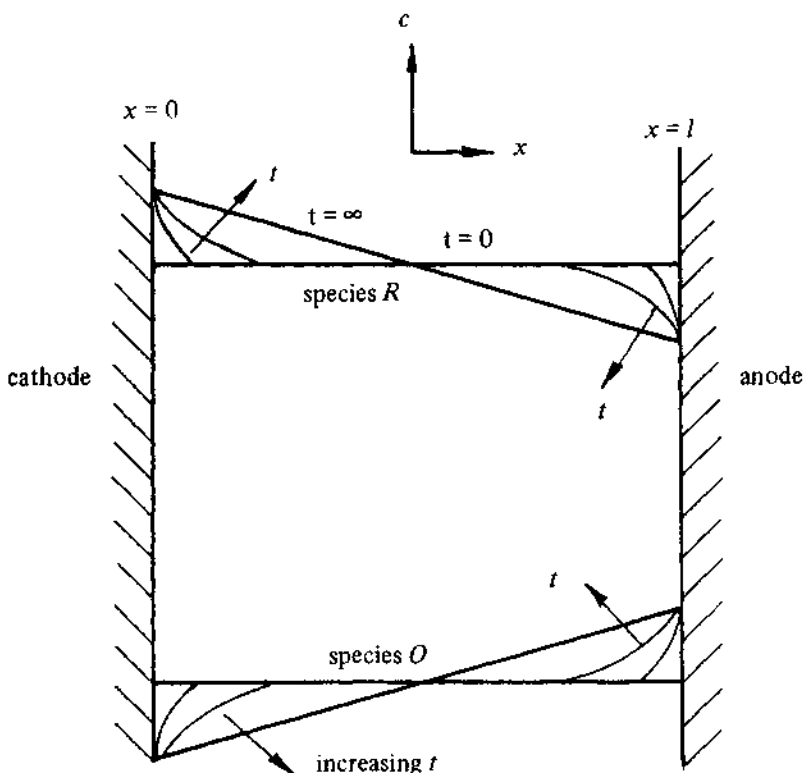


Fig. A.3 – Development of concentration profiles in a thin layer cell bounded by two electrodes. Initially $c_R = 6c_O$.

A.1.2 Diffusion to other electrode geometries

So far, we have only considered situations where the mass transport conditions may be described by linear diffusion to a plane electrode. It is now appropriate to consider diffusion to a spherical (i.e. drop) and cylindrical (i.e. wire) electrodes. In order to understand these geometries, however, it is necessary to be clear how Fick's second law is derived for the case of linear diffusion to a plane electrode – the first law is just a commonsense statement that the flux of a species in any direction is proportional to the concentration difference across any plane in space.

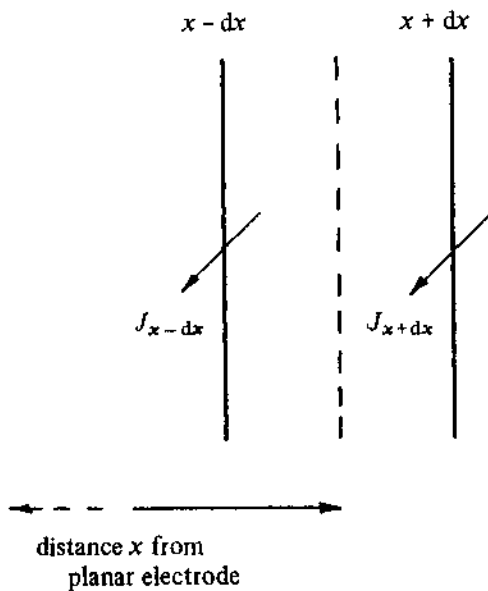


Fig. A.4 – Linear diffusion to a plane electrode.

Figure A.4 illustrates the situation at a plane, distance x , from the electrode. The accumulation of material at this distance from the electrode is derived by considering a very thin volume of solution bounded by planes at $x + dx$ and $x - dx$. The species will both diffuse into the volume through the plane at $x - dx$ and out through the plane at $x + dx$. The flux at $x - dx$ is calculated by noting

$$\begin{aligned} J_{x-dx} &= J_x - \frac{\partial J_x}{\partial x} dx \\ &= -D \frac{\partial c}{\partial x} + D \frac{\partial^2 c}{\partial x^2} \cdot dx \end{aligned} \quad (\text{A.124})$$

by substitution of Fick's first law. Similarly,

$$\begin{aligned} J_{x+dx} &= J_x + \frac{\partial J_x}{\partial x} dx \\ &= -D \frac{\partial c}{\partial x} - D \frac{\partial^2 c}{\partial x^2} \cdot dx . \end{aligned} \quad (\text{A.125})$$

The net accumulation of species is $J_{x-dx} - J_{x+dx}$, but it is also $2dx(\partial c/\partial t)$ where $2dx$ is the volume of the element/unit area. Hence

$$2dx \frac{\partial c}{\partial t} = J_{x-dx} - J_{x+dx}$$

$$= 2D \frac{\partial^2 c}{\partial x^2} dx$$

that is,

$$\frac{\partial c}{\partial r} = D \frac{\partial^2 c}{\partial x^2}. \quad (\text{A.126})$$

A.1.2.1 Spherical diffusion

A sphere is totally symmetrical, and hence diffusion to its surface may be considered in terms of a single dimension, the distance from the centre of the sphere, r . Fick's second law for spherical diffusion may be derived by a similar argument to that above. One considers the accumulation of a species in a volume of solution bounded by two spheres distance $r - dr$ and $r + dr$ from the centre of the electrode, see Fig. A.5. In this case one considers diffusion in and out of the volume element at $r - dr$ and $r + dr$ respectively, and the accumulation of material is given by

$$\text{Net accumulation} = A_{r-dr} J_{r-dr} - A_{r+dr} J_{r+dr} \quad (\text{A.127})$$

where A_{r-dr} and A_{r+dr} are the areas through which diffusion is occurring. Now

$$\begin{aligned} J_{r-dr} &= J_r - \frac{\partial J_r}{\partial r} dr \\ &= -D \frac{\partial c}{\partial r} + D \frac{\partial^2 c}{\partial r^2} dr \end{aligned} \quad (\text{A.128})$$

and

$$J_{r+dr} = -D \frac{\partial c}{\partial r} - D \frac{\partial^2 c}{\partial r^2} . dr. \quad (\text{A.129})$$

$$\begin{aligned} \text{Net accumulation} &= 4\pi(r-dr)^2 \left(-D \frac{\partial c}{\partial r} + D \frac{\partial^2 c}{\partial r^2} . dr \right) \\ &\quad - 4\pi(r+dr)^2 \left(-D \frac{\partial c}{\partial r} - D \frac{\partial^2 c}{\partial r^2} . dr \right) \\ &= 4\pi r^2 D \frac{\partial^2 c}{\partial r^2} dr - 4\pi r^2 D \frac{\partial c}{\partial r} + 8\pi r dr D \frac{\partial c}{\partial r} \\ &\quad + 4\pi r^2 D \frac{\partial^2 c}{\partial r^2} dr + 4\pi r^2 D \frac{\partial c}{\partial r} + 8\pi r dr D \frac{\partial c}{\partial r} \\ &= 8\pi r^2 D \frac{\partial^2 c}{\partial r^2} dr + 16\pi r dr D \frac{\partial c}{\partial r} \end{aligned} \quad (\text{A.130})$$

where throughout all terms in dr^2 and dr^3 are considered negligible. But again the net accumulation is also given by

$$\begin{aligned} \text{Net accumulation} &= V_{\text{element}} \frac{\partial c}{\partial t} \\ &= \frac{4}{3}\pi[(r+dr)^3 - (r-dr)^3] \frac{\partial c}{\partial t} \\ &\approx 8\pi r^2 dr \frac{\partial c}{\partial t} \end{aligned} \quad (\text{A.131})$$

if terms in dr^2 and dr^3 are neglected as insignificant. Equating (A.130) and (A.131) leads to

$$\frac{\partial c}{\partial t} = D \frac{\partial^2 c}{\partial r^2} + \frac{2D}{r} \frac{\partial c}{\partial r}, \quad (\text{A.132})$$

and it can be seen that Fick's second law has an additional term. The boundary conditions are known at $r = r_o$ (the electrode surface) and at $r = \infty$ (where the electrode reaction will not have changed the initial solution).

Equation (A.132) may be simplified by the substitution

$$z = r(c^\infty - c) \quad \text{or} \quad c = c^\infty - \frac{z}{r}. \quad (\text{A.133})$$

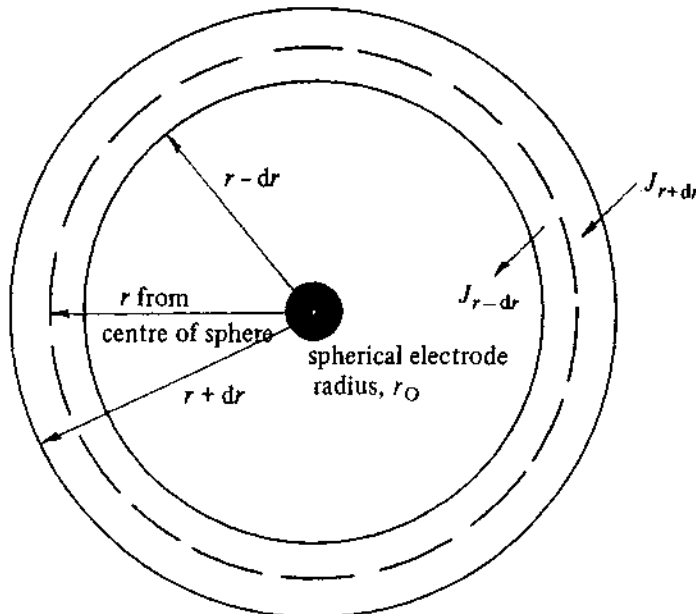


Fig. A.5 – Diffusion to a spherical electrode.

Since

$$\frac{\partial c}{\partial t} = -\frac{1}{r} \frac{\partial z}{\partial t}$$

$$\frac{\partial c}{\partial r} = -\frac{1}{r} \frac{\partial z}{\partial r} + \frac{z}{r^2}$$

and

$$\frac{\partial^2 c}{\partial r^2} = -\frac{1}{r} \frac{\partial^2 z}{\partial r^2} + \frac{1}{r^2} \frac{\partial z}{\partial r} + \frac{1}{r^2} \frac{\partial z}{\partial r} - \frac{2z}{r^3}$$

Equation (A.132) reduces to

$$\frac{\partial z}{\partial t} = D \frac{\partial^2 z}{\partial r^2}. \quad (\text{A.134})$$

In fact the same simplification could be obtained by the substitution $z = rc$, but in electrochemical problems (A.133) is better because it simplifies the boundary condition at $r = \infty$.

Example 7: Calculation of the $I-t$ response to a potential step from a value where $I = 0$ to that where the reaction $\text{O} + e^- \rightarrow \text{R}$ is diffusion controlled at a spherical electrode. The initial solution contains only O.

It is necessary to solve the equation

$$\frac{\partial c_O}{\partial t} = D \frac{\partial^2 c_O}{\partial r^2} + \frac{2D}{r} \frac{\partial c_O}{\partial r} \quad (\text{A.135})$$

with the initial condition,

$$\text{for } t = 0 \text{ and } r > r_O, c_O = c_O^\infty, \quad (\text{A.136})$$

and the boundary conditions

$$\text{at } r = r_O, c_O = 0 \quad (\text{A.137})$$

and

$$\text{at } r = \infty, c_O = c_O^\infty. \quad (\text{A.138})$$

Now making the substitution $z = r(c_O^\infty - c_O)$ leads to

$$\frac{\partial z}{\partial t} = D \frac{\partial^2 z}{\partial r^2} \quad (\text{A.139})$$

with

$$\text{for } t = 0, z = 0 \quad (\text{A.140})$$

and

$$\text{for } t > 0, \text{ at } r = r_O, z = r_O c_O^\infty \quad (\text{A.141})$$

and

$$\text{at } t = \infty, z = 0. \quad (\text{A.142})$$

Laplace transforming Equation (A.139) gives

$$s\bar{z} = D \frac{d^2\bar{z}}{dr^2}, \quad (\text{A.143})$$

and equations (A.141) and (A.142),

$$\text{at } r = r_O, \bar{z} = \frac{r_O c_O^\infty}{s}, \quad (\text{A.144})$$

and

$$\text{at } r = \infty, \bar{z} = 0 \quad (\text{A.145})$$

(A.143) has the solution

$$\bar{z} = M \exp\left(\frac{s}{D}\right)^{1/2} r + N \exp -\left(\frac{s}{D}\right)^{1/2} r \quad (\text{A.146})$$

since the particular integral is $\bar{z} = 0$. Moreover, since $\bar{z} = 0$ at $r = \infty$, $M = 0$. N is found from (A.144):

$$N = \frac{r_O c_O^\infty}{s} \exp\left(\frac{s}{D}\right)^{1/2} r_O,$$

and hence

$$\bar{z} = \frac{r_O c_O^\infty}{s} \exp\left(\frac{s}{D}\right)^{1/2} (r_O - r). \quad (\text{A.147})$$

Using transform XII in Table Table A.1, this equation may be inverted to

$$z = r_O c_O^\infty \operatorname{erfc} \frac{(r_O - r)}{2D^{1/2} t^{1/2}} \quad (\text{A.148})$$

and

$$\begin{aligned} c_O &= c_O^\infty - \frac{z}{r} \\ &= c_O^\infty \left(1 - \frac{r_O}{r} \operatorname{erfc} \frac{(r_O - r)}{2D^{1/2} t^{1/2}}\right) \end{aligned}$$

$$= c_O^\infty \left(1 - \frac{r_O}{r} + \frac{r_O}{r} \operatorname{erf} \frac{(r_O - r)}{2D^{1/2} t^{1/2}} \right).$$

Therefore

$$\frac{\partial c_O}{\partial r} = c_O^\infty \left(\frac{r_O}{r^2} - \frac{r_O}{r^2} \operatorname{erf} \frac{(r_O - r)}{2D^{1/2} t^{1/2}} + \frac{r_O}{r} \cdot \frac{1}{(\pi D t)^{1/2}} \exp - \frac{(r - r_O)^2}{4Dt} \right) \quad (\text{A.149})$$

We only need $(\partial c_O / \partial r)_{r=r_O}$ and thus by putting $r = r_O$ in (A.149)

$$\left(\frac{\partial c_O}{\partial r} \right)_{r=r_O} = \frac{c_O^\infty}{r_O} + \frac{c_O^\infty}{(\pi D t)^{1/2}} \quad (\text{A.150})$$

and

$$\begin{aligned} I &= -nFD \left(\frac{\partial c_O}{\partial r} \right)_{r=r_O} \\ &= -\frac{nFDc_O^\infty}{r_O} - \frac{nFD^{1/2}c_O^\infty}{\pi^{1/2}t^{1/2}}. \end{aligned} \quad (\text{A.151})$$

It can be seen that, unlike the case of a planar electrode, the current for a spherical electrode contains two terms, a time dependent and a steady state term. It should be noted

- (i) that equation (A.151) predicts a steady state current density,

$$-\frac{nFDc_O^\infty}{r_O}$$

even in the absence of natural convection;

- (ii) in a typical experiment where say $D = 10^{-5} \text{ cm}^2 \text{ s}^{-1}$ and $r_O = 0.1 \text{ cm}$, the steady state current density is only about 5% of the transient response after 1 s, and this is the reason why for many experiments a spherical electrode approximates to a plane electrode;
- (iii) (A.151) is also the basis of a microelectrode experiment. If an electrode with radius $1 \mu\text{m}$ behaves as a sphere, the steady state current is equivalent to the transient response at 0.3 ms. As a result, quite rapid kinetics can be studied in the steady state (cf. the rotating disc electrode).

A.1.2.2 Cylindrical diffusion

An argument exactly analogous to that for a spherical electrode, but now considering the accumulation of material in a volume of solution bounded by cylinders at $r - dr$ and $r + dr$, leads to the basic equation for cylindrical diffusion (i.e. diffusion to a wire of infinite length), that is,

$$\frac{\partial c}{\partial t} = D \frac{\partial^2 c}{\partial r^2} + \frac{D}{r} \frac{\partial c}{\partial r} . \quad (\text{A.152})$$

This form of equation cannot be solved by similar substitution methods. But if we transform the equation, assuming for simplicity that at $t = 0, c = 0$, we obtain

$$\frac{d^2 \bar{c}}{dr^2} + \frac{1}{r} \frac{dc}{dr} - \frac{s}{D} \bar{c} = 0 . \quad (\text{A.153})$$

Now, substituting $x = (s/D)^{1/2} r$ leads to

$$\frac{d^2 \bar{c}}{dx^2} + \frac{1}{x} \frac{dc}{dx} - \bar{c} = 0 , \quad (\text{A.154})$$

which is a well known differential equation whose solutions are known in terms of Bessel functions of zero order. Bessel functions are an example of a special function, and they have a defined algebra and calculus.

A.2 COMPUTATIONAL METHODS

While it has already been stressed that complete analytical solutions are elegant and lead to a result in the most useful form, i.e. precise equations relating experimental parameters to kinetic constants, we have seen that the mathematics can be tough even for relatively simple experiments. Not surprisingly, therefore, there is a range of experiments of interest to electrochemists where this approach does not succeed. This is where the computer can come to our assistance.

Indeed, there are several ways in which the computer can aid the electrochemist. In the earliest procedures, the approach was to take the analytical solution as far as possible and complete the process by a numerical method. For example, it was common to convert the set of partial differential equations into a set of integral equations which were then solved by numerical integration. Such approaches lead to either dimensionless plots or equations containing numerical factors. Later methods are based on the application of one of the many procedures of numerical analysis (e.g. finite difference) to the solution of the original set of partial differential equations describing the experiment. A further approach, which is conceptually quite different from the finite difference method although it leads to similar programmes, is based on a simulation of the experiment. A model is set up which reflects the behaviour of the electrode reaction including diffusion, adsorption, electron transfer, and coupled chemistry, and this model is simulated in a computer programme. Such simulations are particularly attractive for complex experiments since the difficulty of programming is almost independent of the nature of the experiment; for example, time dependent boundary conditions at the electrode surface, complex reaction sequences such as ece processes, multi-order chemical reactions, and convection, can all be handled. All such computer methods can be made to lead to dimensionless plots.

All the above methods realistically require main-frame or minicomputers, but microcomputers are also having an impact on electrochemical experiments. They can take the tedium out the treatment of experimental data and, properly used, provide a much more critical test of the fit between experiment and theory. Moreover they make available new methods of data treatment, e.g. convolution cyclic voltammetry, and impedance analysis.

The influence of microcomputers on electrochemical techniques is, we hope, illustrated in the earlier chapters. Here we wish to discuss the simplest of the digital simulation procedures, that popularised by Feldberg [1-3]. Its only drawback is that it can be excessive in its use of computer time; faster but more complicated procedures are then discussed briefly.

A.2.1 Digital simulation

The major use of digital simulation is to obtain kinetic parameters for systems where the theoretical equations cannot be developed analytically, e.g. those involving second, or higher order, coupled homogeneous reactions and complex reaction sequences. The basic philosophy is to simulate the behaviour of the differential equations describing the system and, by adjusting rate parameters in the simulation, obtain the best fit to the experimental data. Computing time is saved by setting up the simulations in terms of dimensionless parameters, thus enabling one simulation to serve for a variety of experimental conditions. There is, however, a second, and perhaps overlooked, use for simulations; namely as an educational aid. It can be very helpful to set up simulations for both simple and complex reaction schemes and to see, by graphical output to a terminal, how for example the concentration profiles of reactants, products, and intermediates evolve with time after the application of a potential step.

Before proceeding to discuss specific simulation methods, a comment about the accuracy of simulations is probably in order. There are two distinct sources of error; firstly the simulation only provides an approximate solution to the differential equations, and in certain circumstances, e.g. through an inappropriate choice of parameters, this approximation may be poor; secondly there may be a mistake in the coding of the program. One of the difficulties in this respect is that inevitably, in most cases, the system of differential equations being simulated cannot be solved in closed analytical form. There is therefore no direct way to check whether the simulated result is a good approximation or not. A number of checks can, however, be performed in order to reduce the risk of errors, and the desirability of using these cannot be overemphasised. Some of these checks are specific to the technique being used, but there are two that are universally applicable. The first is to adjust the values of rate constants, e.g. set homogeneous rate constants to zero, such that the simulated system corresponds to one for which an analytical solution exists and compare the simulated and analytical results. The second check is to always follow the concentrations of all the species involved to ensure that matter is neither created nor destroyed, and to check that concentration profiles look realistic. Both of these checks are good at showing up coding errors or errors in the algorithm used. The detection of errors due to an unsuitable choice of simulation con-

ditions is more difficult and comes largely with experience, though there are technique dependent checks, and these are discussed later.

A.2.1.1 *The explicit finite difference method*

Since Feldberg first introduced it to electrochemists in the 1960s [1-3], the explicit finite difference method for providing approximate solutions to partial differential equations has undoubtedly become the most widely applied simulation technique amongst the electrochemical community. Its great virtue is that it is simple to understand and to implement, even for those who are not conversant with numerical techniques, and whilst there are better methods (i.e. faster or more accurate), many systems can be very successfully simulated using this simple approach. It is only in special circumstances, e.g. in the presence of very fast coupled homogeneous reactions, that other methods may necessarily have to be used. When considering undertaking simulations for the first time this technique is undoubtedly the first that should be tackled.

The basic principle behind all finite difference techniques for solving differential equations is to replace all the derivatives by appropriate difference-quotient approximations. The differential equations are thus replaced by a set of difference equations which, after the incorporation of the appropriate boundary conditions, can be solved. The solutions obtained for these difference equations are analytical, and therefore, provided that the difference equations are a good approximation to the differential ones, they will represent good approximate solutions to the differential equations.

As we have seen earlier, the mass transport in the majority of simple electrochemical systems approximates to one-dimensional mass transport to a semi-infinite planar electrode, and it is the simulation of such systems that will be discussed here. The extension to cylindrical and spherical geometries is fairly straightforward, but systems such as the finite disc, or the ring disc electrode, where two-dimensional mass transport has to be considered, are more difficult to handle.

To see how a set of partial differential equations describing an electrochemical system is converted into the equivalent set of difference equations we have first to construct a model to describe the mass transport in the system. The basic concepts of this model are,

- (i) space and time may be divided into small discrete units;
- (ii) on small distance and time scales the various parts of an electrode process, i.e. diffusion, convection, electron transfer, and chemical reaction, can be dealt with separately and consecutively.

We will start by discussing a system where we only have to consider diffusion, and will see later how the other features such as chemical reactions are incorporated.

A.2.1.1.1 *Diffusion*

In our model the solution phase near the electrode is divided into a series of volume elements of thickness Δx , as shown in Fig. A.6. Each of these elements has the same cross-sectional area as the electrode. They are labelled from 1 to N ,

and it is assumed that they are thin enough that the concentration of any species can be considered homogeneous within the box. From Fick's law we know that at any point in the solution the flux of any species is given by

$$J = -AD \frac{\partial c}{\partial x} . \quad (\text{A.155})$$

Thus the flux (J_I) at the boundary between boxes I and $I-1$ in Fig. A.6 is given by

$$J_I = -AD \left(\frac{\partial c}{\partial x} \right)_I \quad (\text{A.156})$$

The finite difference approximation to this expression is

$$J_I \approx -AD \frac{(c_I - c_{I-1})}{\Delta x} \quad (\text{A.157})$$

where c_I is the concentration in box I . This approximation improves as the value of Δx is reduced. In the same way the flux at the boundary between boxes I and $I+1$ is given by

$$J_2 \approx -AD \frac{(c_{I+1} - c_I)}{\Delta x} , \quad (\text{A.158})$$

and therefore the total flux, J , into box I is given by

$$J = J_1 - J_2 = \frac{AD}{\Delta x} (c_{I-1} - 2c_I + c_{I+1}) . \quad (\text{A.159})$$

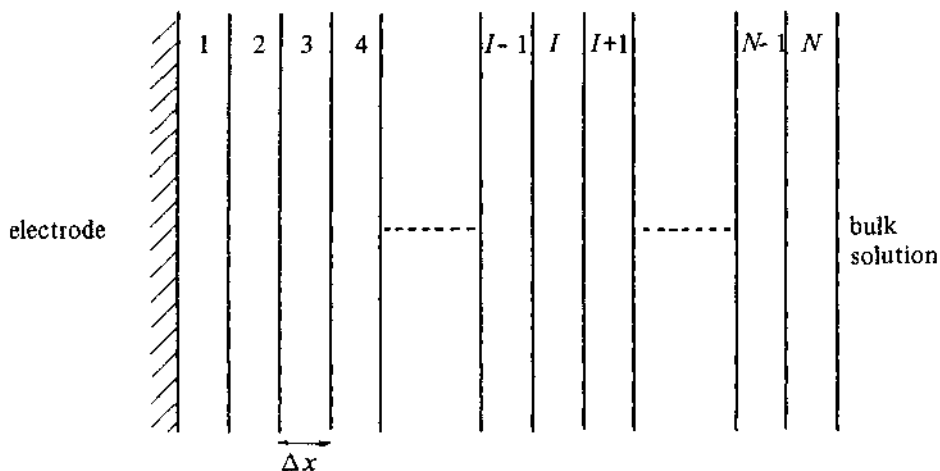


Fig. A.6 -- Schematic diagram of the space grid used in the simulation of systems involving one dimensional mass transport to a semi-infinite planar electrode.

As stated earlier, time is also divided into small discrete units, Δt , and therefore in each unit of time the amount of material, n , added to box I is

$$n = J \cdot \Delta t . \quad (\text{A.160})$$

Since the volume of this box is simply given by $A \cdot \Delta x$, the change in concentration of box I in each unit of time is

$$\Delta c_I = \frac{n}{A \cdot \Delta x} = D \frac{\Delta t}{\Delta x^2} (c_{I-1} - 2c_I + c_{I+1}) , \quad (\text{A.161})$$

and therefore

$$c_I(t + \Delta t) = c_I(t) + D_M (c_{I-1}(t) - 2c_I(t) + c_{I+1}(t)) \quad (\text{A.162})$$

where D_M , the model diffusion coefficient, is given by

$$D_M = D \frac{\Delta t}{\Delta x^2} . \quad (\text{A.163})$$

Equation (A.162) is the explicit finite difference approximation to Fick's 2nd law, and it describes how the concentration of any species in boxes 2 to $N-1$ changes with time. The expressions for boxes 1 and N require a knowledge of the boundary conditions. Box N is the simplest to deal with, since we just set the concentration of the 'imaginary' box $N+1$ to the bulk concentration, c^∞ , and therefore

$$c_N(t + \Delta t) = c_N(t) + D_M (c_{N-1}(t) - 2c_N(t) + c^\infty) . \quad (\text{A.164})$$

The first box is a little more difficult to handle since it is bounded on the left-hand side by the electrode. As before, the flux at the boundary between the first and second boxes, J_2 , is given by

$$J_2 \approx -AD \frac{(c_2 - c_1)}{\Delta x} , \quad (\text{A.165})$$

but that at the boundary with the electrode, J_1 , is now given by

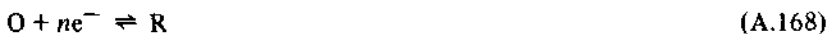
$$J_1 \approx -AD \frac{(c_1 - c_0)}{\frac{1}{2} \Delta x} \quad (\text{A.166})$$

where c_0 is the surface concentration. The term in the denominator is now $\frac{1}{2} \Delta x$ since c_1 is assumed to be the concentration at the centre of the first box, and this is separated from the electrode surface by the distance $\frac{1}{2} \Delta x$. Therefore, following the same arguments as before,

$$c_1(t + \Delta t) = c_1(t) + D_M (2c_0(t) - 3c_1(t) + c_2(t)) . \quad (\text{A.167})$$

By using Equations (A.162), (A.164), and (A.167) iteratively it is then possible

to find the concentration in any box at any time provided c_0 is known. This is obtained from the boundary conditions. We will consider here the example of simulating a potential step experiment in the diffusion controlled region for the reaction



for which the electrode surface boundary conditions are

$$t > 0, \quad x = 0$$

$$c_{\text{O}} = 0 \quad \text{and} \quad \left(\frac{\partial c_{\text{O}}}{\partial x} \right) = - \left(\frac{\partial c_{\text{R}}}{\partial x} \right). \quad (\text{A.169})$$

Other examples will be considered later. For species O the finite difference expression in the first box therefore becomes

$$c_{\text{O},1}(t + \Delta t) = c_{\text{O},1}(t) + D_M(-3c_{\text{O},1}(t) + c_{\text{O},2}(t)). \quad (\text{A.170})$$

For R we have to equate the fluxes for O and R, and in finite difference terms this boundary condition becomes

$$\frac{(c_{\text{O},1} - c_{\text{O},0})}{\frac{1}{2}\Delta x} = - \frac{(c_{\text{R},1} - c_{\text{R},0})}{\frac{1}{2}\Delta x} \quad (\text{A.171})$$

and hence with $c_{\text{O},0}$ equal to zero[†]

$$c_{\text{R},0} = c_{\text{O},1} + c_{\text{R},1}, \quad (\text{A.172})$$

and therefore for species R

$$c_{\text{R},1}(t + \Delta t) = c_{\text{R},1}(t) + D_M(2c_{\text{O},1}(t) - c_{\text{R},1}(t) + c_{\text{R},2}(t)). \quad (\text{A.173})$$

We are now in a position to commence our simulation, but as stated earlier we must first convert the simulation to a dimensionless form. We have already taken one step in this direction by introducing the model diffusion coefficient D_M . We now have to fix suitable values for Δx and Δt . Clearly it would be useful if we could set these values independently, but unfortunately this is not possible. It can be shown that stable solutions to the finite difference expressions are only obtained for values of D_M less than 0.5, and since D_M is equal to $D \cdot \Delta t / \Delta x^2$ the values of Δt and Δx are linked. Specifically, if Δx is decreased, Δt also has to be reduced, and for any given length of experiment the number of iterations has to be increased. In view of the Δx^2 term this, of course, leads to a sharply increased computation time. One of the major problems in designing a simulation is to choose all the parameters so that they are physically meaningful and so that there is a useful correlation between them and the constants of the real system.

[†] The first subscript refers to species (O), the second to space (0), i.e. the number of the box.

For convenience in programming it is useful to start by fixing the total number of iterations, L , and this might typically be in the range 10^2 to 10^4 . Then, if the duration of our experiment is t_c seconds,

$$\Delta t = \frac{t_c}{L} . \quad (\text{A.174})$$

For any given value of Δt we will obtain a better simulation as we reduce Δx , and therefore D_M should be as large as possible. It is usual therefore, to fix the value of D_M close to its maximum value, say 0.45, and then from Equation (A.163) Δx is given by

$$\Delta x = \left(\frac{D \Delta t}{D_M} \right)^{1/2} \quad (\text{A.175})$$

or substituting for Δt

$$\Delta x = \left(\frac{Dt_c}{D_M L} \right)^{1/2} . \quad (\text{A.176})$$

Thus for the simulation of any given experiment the choice of L , the number of iterations, fixes both the values of Δt and Δx . With these fixed, we can now determine how many boxes are required. The volume of solution affected by the electrode reaction is a function of time. In an experiment lasting t_c seconds it is generally considered necessary to take into account concentration changes up to a distance $6(Dt_c)^{1/2}$ from the electrode, and thus N , the number of boxes required, is given by

$$N = \frac{6D^{1/2}t_c^{1/2}}{\Delta x} , \quad (\text{A.177})$$

or substituting for Δx from equation (A.176),

$$N = 6(D_M L)^{1/2} . \quad (\text{A.178})$$

The choice of L therefore fixes all the parameters of the simulation. This simulation can, however, be used for experiments of any length and with any value of the real diffusion coefficient. The correspondence of the model variables Δt and Δx to the real ones are made through Equations (A.174) and (A.176).

We frequently require simulations of experiments with a range of reactant starting concentrations, and it would be helpful if we did not need a separate simulation for each. To achieve this we do not work in real concentrations but instead normalise all values with respect to the starting concentration of one of the reactants, and the simulation is carried out in terms of these fractional concentrations. Thus

$$\xi c_I(t) = c_I(t)/c^\infty , \quad (\text{A.179})$$

and therefore Equation (A.162) can be rewritten as

$$\xi c_I(t + \Delta t) = \xi c_I(t) + D_M(\xi c_{I-1}(t) - 2\xi c_I(t) + \xi c_{I+1}(t)) \quad (\text{A.180})$$

with similar expressions for the first and last boxes.

We are now almost in a position to write a simulation program. But, at present, all we determine are approximations to the concentrations of species present, whereas in the actual conventional experiment, what we measure is the current density. Therefore we require an expression for the simulated current. We know that in terms of real variables

$$I = -nFD\left(\frac{\partial c_O}{\partial x}\right)_{x=0} . \quad (\text{A.181})$$

In terms of our model variables and in the finite difference approximation this becomes

$$I = -\frac{nFDc_O^\infty(\xi c_{O,1} - \xi c_{O,0})}{\frac{1}{2}\Delta x} \quad (\text{A.182})$$

or, substituting for Δx

$$I = -\frac{2nFD^{1/2}D_M^{1/2}L^{1/2}}{t_c^{1/2}}c_O^\infty(\xi c_{O,1} - \xi c_{O,0}) . \quad (\text{A.183})$$

By rearranging model variables to the right and experimental ones on the left we obtain

$$Z = -\frac{I t_c^{1/2}}{nFD^{1/2}c_O^\infty} = 2D_M^{1/2}L^{1/2}(\xi c_{O,1} - \xi c_{O,0}) \quad (\text{A.184})$$

where Z is known as the *dimensionless current*. It only remains to determine what time this corresponds to, and at the end of the k th iteration this is given by

$$t = k\Delta t \quad (\text{A.185})$$

or

$$t = \frac{kt_c}{L} . \quad (\text{A.186})$$

It is therefore a simple matter to compare the simulated current density directly with the experimentally obtained value.

The above algorithm for simulating a simple electrochemical reaction can therefore be implemented by the following steps:

- Step 1 Set values for the number of iterations and the model diffusion coefficient.
- Step 2 Initialise the fractional concentrations in all boxes to the bulk values.

- Step 3 Using the finite difference equations determine a new set of fractional concentrations.
- Step 4 Calculate the current.
- Step 5 Replace old fractional concentrations by the new ones.
- Step 6 Are all the iterations complete? If not, go back to step 3.
- Step 7 Output data.

A program, written in FORTRAN, for the simulation of a simple potential step experiment in the diffusion controlled region is included at the end of this Appendix. Translation to other languages should prove easy. This program also compares the simulated value of Z with the corresponding analytical value obtained from the Cottrell equation. For the k th iterations this is given by

$$Z_c \approx \left(\frac{L}{\pi k} \right)^{1/2}. \quad (\text{A.187})$$

Figure A.7 shows how the ratio Z/Z_c varies with the number of iterations. It can be seen that initially the simulated value of Z oscillates around the analytical value, but it quickly settles down and after 100 iterations the error is about 0.2%.

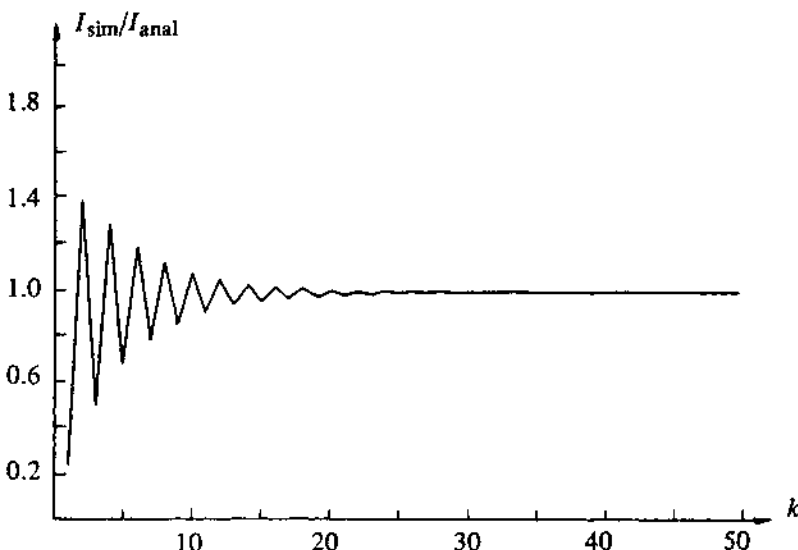
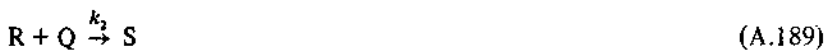


Fig. A.7 – A plot to show how the simulated current approaches the analytical value as the number of iterations increase. The ratio of the simulated to analytical current for a diffusion controlled pulse experiment for a reversible system is plotted as a function of the iteration number, k . A value of 0.45 was used for model diffusion coefficient, D_M .

A.2.1.1.2 Homogeneous reactions

It was stated earlier that one of the principles of the explicit finite difference method was that all the various parts of the electrochemical process can be treated sequentially. Thus for systems involving homogeneous reactions each iteration involves first a diffusional part as described above and then a kinetic part. To see what form this kinetic part takes let us consider the ece process described below:



where Q is not electroactive. The simulation will include a diffusional part for each of the species O , R , Q , S , Z , but there will also have to be a kinetic segment for R , Q , and S since the concentrations of these species are affected by the chemical reaction. The rate of reaction, q_I , in any box, I , is given by

$$q_I = k_2 c_{R,I} c_{Q,I}, \quad (A.191)$$

and hence the amount of R lost from box I in the period Δt is given by

$$\Delta c_{R,I} = -\frac{k_2 c_{R,I} c_{Q,I}}{\Delta t} \quad (A.192)$$

or, converting to the dimensionless form

$$\Delta \xi c_{R,I} = -\frac{k_2 t_c c_O^\infty \xi c_{R,I} \cdot \xi c_{Q,I}}{L}, \quad (A.193)$$

or

$$\Delta \xi c_{R,I} = -k_m \xi c_{R,I} \xi c_{Q,I} \quad (A.194)$$

where

$$k_m = \frac{k_2 t_c c_O^\infty}{L} \quad (A.195)$$

is the dimensionless model rate constant (for first order reactions the model rate constant is simply $k_m = k_2 t_c / L$). Thus the fractional concentrations of R calculated at the end of the diffusional segment are adjusted by the amount $\Delta \xi c_R$. Similar expressions can be derived for Q and S .

In practice, the range of values of k_m that may be used with a particular space grid is limited; to have a realistic simulation the chemical reaction must occur in several boxes, e.g. if an intermediate reacts very rapidly so that it all disappears within the first box, the simulation will not work. Conversely a significant amount of reaction must occur before the species diffuses out of the solution layer being considered. Ideally $(D\tau_{1/2})^{1/2}$ ($\tau_{1/2}$ is the half life of the

intermediate) should be about $6(Dt)^{1/2}/2$. The model rate constant should certainly not exceed 0.1. These limitations mean that fast reactions require a fine space grid and hence a fine time grid also. This can lead to computer store and time problems, and sometimes other simulation techniques are better (see later).

The simulation of reactions where electroinactive species are present introduces a new type of boundary condition. For such systems we know that the concentration gradient at the surface equals zero, i.e.

$$\xi c_{Q,1} = \xi c_{Q,0} , \quad (\text{A.196})$$

and therefore the finite difference diffusion equation in the first box for such a species becomes

$$\xi c_{Q,1}(t + \Delta t) = \xi c_{Q,1}(t) + D_M(\xi c_{Q,2}(t) - \xi c_{Q,1}(t)) . \quad (\text{A.197})$$

A FORTRAN program for the simulation of a potential step experiment with a system such as that described by Equations (A.188)–(A.190) is given at the end of this Appendix.

A.2.1.1.3 Sweep voltammetry

Thus far we have only considered potential step experiments, and these only in the potential region where the electron transfer step occurs at a diffusion limited rate. The major part of any simulation for any technique is the same as that already outlined, but the boundary conditions, and hence the finite difference expressions for the first box, do vary. As an example of a different type of experiment we will now consider sweep voltammetry. Here the boundary conditions are a function of time, and for a reversible system can be derived from the Nernst equation

$$\frac{c_{O,0}}{c_{R,0}} = \exp \frac{nF}{RT} \eta \quad (\text{A.198})$$

where for a linear sweep experiment, η , the overpotential is given by

$$\eta = \eta_i + \Delta\eta k \quad (\text{A.199})$$

where η_i is the overpotential at $t = 0$ (i.e. at the start of the simulation), $\Delta\eta$ is the increment added at each iteration, and k is the iteration number. The potential can be normalised by dividing by RT/F , and therefore in terms of model variables Equation (A.198) becomes

$$\frac{\xi c_{O,0}}{\xi c_{R,0}} = \exp n.E_m \quad (\text{A.200})$$

where

$$E_m = E_{m,i} + \Delta E_m \cdot k . \quad (\text{A.201})$$

The value of ΔE_m is determined from the sweep rate, the characteristic time, and the number of iterations. In the case of pulse experiments, t_c was shown to be the total length of the experiment, and this is also a convenient choice here. Therefore

$$t_c = (E_f - E_i)/\nu \quad (\text{A.202})$$

and hence

$$\Delta E_m = (E_{m,f} - E_{m,i})/L \quad (\text{A.203})$$

To determine the surface boundary conditions we use Equation (A.200) and the fact that at the electrode surface

$$\left(\frac{\partial c_O}{\partial x} \right)_{x=0} = - \left(\frac{\partial c_R}{\partial x} \right)_{x=0} \quad (\text{A.204})$$

From these equations it can be shown that

$$c_{R,0} = \exp(n \cdot E_m) \cdot \xi c_{O,0} = \frac{(\xi c_{R,1} + \xi c_{O,1})}{1 + \exp(n \cdot E_m)} \quad (\text{A.205})$$

Thus at the end of each iteration the value of E_m is calculated and hence $\xi c_{R,0}$ and $\xi c_{O,0}$. Using these values, the finite difference expressions for the first box are solved and the current calculated as before.

The procedure for a cyclic voltammetry experiment is essentially the same with t_c again corresponding to the time required to sweep from E_i to E_f ($2L$ iterations are therefore required for a complete cycle). An example of a FORTRAN program for the simulation of a cyclic voltammetry experiment with a reversible system is given at the end of the appendix.

A.2.1.1.4 Convection -- The rotating disc electrode

Like homogeneous kinetics, convection is most easily handled separately from diffusion. Thus in simulating the behaviour of a rotating disc electrode, at the end of each iteration the concentration profile determined by the diffusional segment is adjusted to allow for the convective flow normal to the disc. This adjustment is made analytically.

It was shown in Chapter 4 that the fluid velocity normal to the electrode is given by

$$\frac{dx}{dt} = V_x = -0.51 \omega^{3/2} \nu^{-1/2} x^2 \quad (\text{A.206})$$

where ν is the kinematic viscosity and ω the rotation rate. This equation may be integrated to find the distance travelled in the time element Δt , i.e.

$$\frac{1}{x_2} - \frac{1}{x_1} = 0.51 \omega^{3/2} \nu^{-1/2} \Delta t \quad (\text{A.207})$$

where x_1 and x_2 are the positions before and after the time element Δt . In terms of our space elements therefore

$$x_1 = (I - \frac{1}{2}) \Delta x \quad (\text{A.208})$$

and

$$x_2 = (I' - \frac{1}{2}) \Delta x , \quad (\text{A.209})$$

and hence

$$I' = \frac{(I - \frac{1}{2})}{1 + k_m(I - \frac{1}{2})} + \frac{1}{2} \quad (\text{A.210})$$

where I is the box number before convection and I' that after it, and where

$$k_m = 0.51 \omega^{3/2} \nu^{-1/2} \Delta x \Delta t . \quad (\text{A.211})$$

Thus the effect of convection can be allowed for by replacing the contents of box I' with those of box I on each iteration. In order that k_m is dimensionless, t_c is defined as

$$t_c = (0.51 \omega^{3/2} \nu^{-1/2} D^{1/2})^{-2/3} , \quad (\text{A.212})$$

and therefore

$$k_m = D_M^{-1/2} L^{-3/2} . \quad (\text{A.213})$$

Since it is usually the steady state behaviour that is required in an RDE simulation, the simulation is run until the concentration profiles and current do not change with further iterations.

As we have seen, the various parts of an electrode process can be treated sequentially in a finite difference simulation, and it is possible to write a program to cover most eventualities. A flow diagram for such a program is shown in Fig. A.8. However, since programming is relatively straightforward it is usual to write a program for each new system and to include only the required parts.

A.2.1.2 More advanced simulation techniques

Simulations of the type described above commonly require computers which are both fast and have a large store, and, indeed, there are experiments which may only be simulated by using this method if extravagant use is made of the computer. This is particularly the case when dealing with systems: (a) involving fast chemical reactions; the kinetic layer can then lie well within the diffusion layer, and a successful simulation requires the whole diffusion layer to be broken up into large number of very small boxes and consequently a large number of

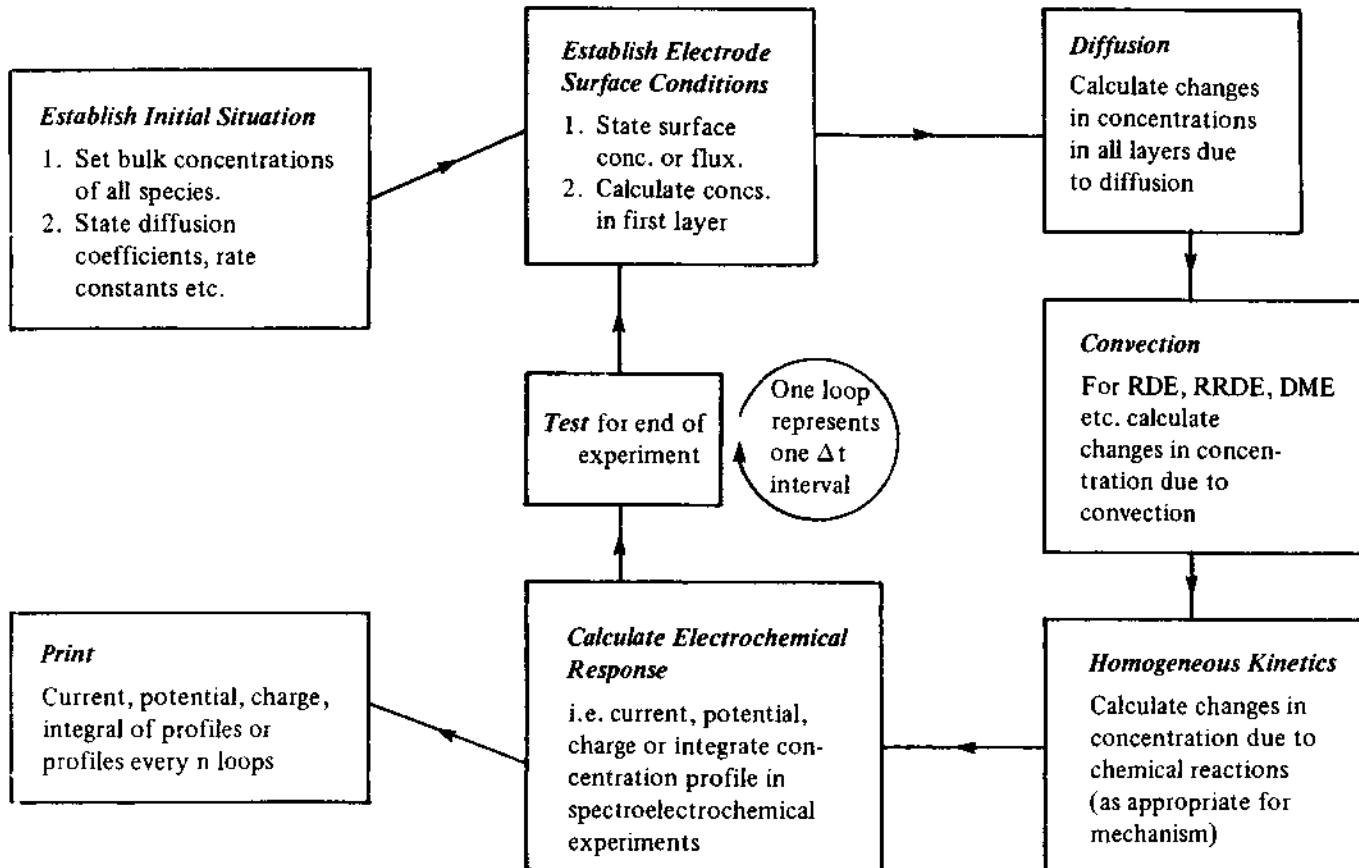


Fig. A.8 – Flow chart for the simulation of laboratory electrochemical experiments.

iterations; (b) where it is necessary to use a two-dimensional space grid to describe the mass transport conditions, e.g. rotating ring disc and microelectrode systems.

Several solutions to the first problem have been proposed. In the simulation techniques described above, the equations describing diffusion have effectively been solved explicitly. It has been shown that the diffusion equations may also be solved implicitly [4]; such solutions have the advantage that the stability criterion $D\Delta t/\Delta x^2 < 0.5$ no longer applies. This modification does reduce computation times to some extent, but its success is limited. A more general procedure involves the use of non-uniform space elements [5]. The idea is to construct a space grid where the space elements are small within the kinetic layer close to the electrode surface but where they increase in magnitude rapidly away from this region. It was suggested that the optimum space grid is one where the boxes increase in size smoothly as a function of the distance from the electrode surface. More recently a different technique known as *orthogonal collocation* has been used to simulate electrochemical systems, and particularly those involving homogeneous reactions [6]. It is undoubtedly faster than finite difference methods, but is conceptually more difficult, and the programming is more involved, although only very few statements need to be changed on going from one mechanism to another. Another alternative approach was developed by Ruzić & Feldberg [7]; the form of the kinetic layer is estimated analytically using a steady state approximation, and the homogeneous reaction is taken into account by combining the steady state approximation into the expressions for the surface fluxes. All these approaches are able to reduce considerably the computation time and possibly also the store requirement.

The technique used to simulate systems involving two-dimensional mass transport are similar to those outlined above, but are, of course, more complex. The ring-disc electrode has been simulated by finite difference methods using the techniques of Prater & Bard [8], whilst the finite disc electrode has been simulated both by the finite difference method [9, 10] and by orthogonal collocation [11].

REFERENCES

- [1] S. W. Feldberg in *Electroanal. Chem.*, Ed. A. J. Bard, Volume 3, (1969) 199.
- [2] S. W. Feldberg in *Electrochemistry - calculations, simulations and instrumentation*, Eds. J. S. Mattson, H. H. Mark, & H. C. MacDonald, Marcel Dekker, New York, 1972.
- [3] D. Britz, *Digital simulation in electrochemistry*, Springer Verlag, Berlin, 1981.
- [4] N. Winograd, *J. Electroanal. Chem.*, **43** (1973) 1.
- [5] T. Joslin & D. Pletcher, *J. Electroanal. Chem.*, **49** (1974) 171.
- [6] B. S. Pons in *Electroanal. Chem.*, Ed. A. J. Bard, **13** (1984) 115.
- [7] I. Ruzić and S. W. Feldberg, *J. Electroanal. Chem.*, **50** (1974) 153.
- [8] K. B. Prater & A. J. Bard, *J. Electrochem. Soc.*, **117** (1970) 207 and 335.

- [9] J. Heinze, *J. Electroanal. Chem.*, **124** (1981) 73.
- [10] D. Shoup & A. Szabo, *J. Electroanal. Chem.*, **140** (1983) 237.
- [11] B. Speiser & S. Pons, *Can. J. Chem.*, **60** (1982) 1352.

Further reading for analytical solutions

- (1) *Handbook for tables of mathematics*, The Chemical Rubber Co., 1964.
- (2) *Theory and problems of Laplace transforms*, M. R. Spiegel, Schaum's Outline Series, McGraw-Hill, 1966.
- (3) *The mathematics of chemistry and physics*, H. Margenau & G. M. Murphy, Van Nostrand Reinhold, 1943.
- (4) *Mathematics of diffusion*, J. Crank, Oxford University Press, 1956.

A.2.3 Model programs

A.2.3.1 Potential step experiment – reversible system

We shall consider the system



with only A initially present.

DIMENSION FANEW (150), FAOLD (150), FBNEW (150), FBOLD (150),
RAT (100)

DM = 0.45

L = 100

C INITIALIZE CONCENTRATIONS

DO 10 J = 1, 150

FAOLD(J) = 1.

FBOLD(J) = 0.

10 CONTINUE

DO 20 I = 1, L

JMAX = IFIX (4.2*SQRT(FLOAT(I))) + 1

C DIFFUSION SEGMENT

DO 30 J = 2, JMAX

FANEW(J) = FAOLD(J)+DM*(FAOLD(J-1)-2.*FAOLD(J)+FAOLD(J+1))

FBNEW(J) = FBOLD(J)+DM*(FBOLD(J-1)-2.*FBOLD(J)+FBOLD(J+1))

30 CONTINUE

C FIRST BOX

FANEW(1)=FAOLD(1)+DM*(-3.*FAOLD(1)+FAOLD(2))

FBNEW(1)=FBOLD(1)+DM*(2.*FAOLD(1)-FBOLD(1)+FBOLD(2))

```

C   CALCULATE CURRENT
Z = SQRT(FLOAT(L)*DM)*FANEW(1)*2.
C   CALCULATE TIME
T = FLOAT(I)/FLOAT(L)
CUR = 1./SQRT(3.1415*T))
C   CALCULATE RATIO OF SIMULATED TO COTTRELL CURRENT
RAT(I) = Z/CUR
C   RESET CONCENTRATION ARRAYS
DO 40 J = 1, JMAX
FAOLD(J) = FANEW(J)
FBOLD(J) = FBNEW(J)
40  CONTINUE
20  CONTINUE

C   OUTPUT DATA
DO 50 I = 1, L
WRITE(6,100) I, RAT(I)
50  CONTINUE
100 FORMAT (I5, F10.5)
STOP
END

```

A.2.3.2 Potential step experiment – ECE system

Consider the reaction scheme .



Where only A and C are initially present in equal concentration, B, D, and E are absent, and all electron transfers occur at a diffusion controlled rate.

DIMENSION FAOLD(150), FANEW(150), FBOLD(150), FBNEW(150),
FCOLD(150), FCNEW(150), FDOLD(150), FDNEW(150), FEOLD(150),
FENEW(150), NAPP(100)

```
C SET CONSTANTS
DM = 0.45
L = 100
RATE = 0.02
C INITIALIZE CONCENTRATIONS
DO 10 J = 1, 150
FAOLD(J) = 1.
FBOLD(J) = 0.
FCOLD(J) = 1.
FDOLD(J) = 0.
FEOLD(J) = 0.
10 CONTINUE
DO 20 I = 1, L
JMAX = IFIX(4.2*SQRT(FLOAT(I))) + 1
C DIFFUSION SEGMENT
DO 30 J = 2, MAX
FANEW(J) = FAOLD(J)+DM*(FAOLD(J-1)-2.*FAOLD(J)+FAOLD(J+1))
FBNEW(J)=FBOLD(J)+DM*(FBOLD(J-1)-2.*FBOLD(J)+FBOLD(J+1))
FCNEW(J)=FCOLD(J)+DM*(FCOLD(J-1)-2.*FCOLD(J)+FCOLD(J+1))
FDNEW(J) = FDOLD(J)+DM*(FDOLD(J-1)-2.*FDOLD(J)+FDOLD(J+1))
FENEW(J) = FEOLD(J)+DM*(FEOLD(J-1)-2.*FEOLD(J)+FEOLD(J+1))
30 CONTINUE
C FIRST BOX
FANEW(1)=FAOLD(1)+DM*(-3.*FAOLD(1)+FAOLD(2))
FBNEW(1)=FBOLD(1)+DM*(2.*FAOLD(1)-FBOLD(1)+FBOLD(2))
FCNEW(1)=FCOLD(1)+DM*(FCOLD(2)-FCOLD(1))
FDNEW(1)=FDOLD(1)+DM*(-3.*FDOLD(1)+FDOLD(2))
FENEW(1)=FEOLD(1)+DM*(2.*FDOLD(1)-FEOLD(1)+FEOLD(2))
C KINETIC SEGMENT
DO 40 J=1, JMAX
REACT = RATE*FBNEW(J)*FCNEW(J)
FBNEW(J) = RBNEW(J)-REACT
FCNEW(J) = FCNEW(J)-REACT
FDNEW(J)=FDNEW(J)+REACT
40 CONTINUE
```

C CALCULATE CURRENT

$ZA = 2.*\text{SQRT}(\text{FLOAT}(L)*DM)*\text{FANEW}(1)$

$ZD = 2.*\text{SQRT}(\text{FLOAT}(L)*DM)*\text{FDNEW}(1)$

$Z = ZA+ZD$

$T = \text{FLOAT}(I)/\text{FLOAT}(L)$

$ZCOTT = 1./(\text{SQRT}(3.1415*T))$

C APPARENT NO. OF ELECTRONS

$NAPP(I) = Z/ZCOTT$

C RESET CONCENTRATIONS

DO 50 J=1, JMAX

$FAOLD(J) = \text{FANEW}(J)$

$FBOLD(J) = \text{FBNEW}(J)$

$FCOLD(J) = \text{FCNEW}(J)$

$FDOLD(J) = \text{FDNEW}(J)$

$FEOLD(J) = \text{FENEW}(J)$

50 CONTINUE

C OUTPUT DATA

DO 60 I=1, L

WRITE(6, 100) I, NAPP

60 CONTINUE

100 FORMAT (I5, F10.5)

STOP

END

A.2.3.3 Cyclic voltammetry – reversible system

Consider the system described by equation (A.214)

DIMENSION FANEW(150), FAOLD(150), FBNEW(150), FBOLD(150),
 $Z(200)$

DM = 0.45

L = 100

C SET POTENTIAL LIMITS

EI = 10.

EF = -10.

```
C THEREFORE POTENTIAL INCREMENT
    DELTAE = (EF-EI)/FLOAT(L)
C INITIALIZE POTENTIAL
    EMOD = EI
C INITIALIZE CONCENTRATIONS
    DO 10 J = 1, 150
        FAOLD(J) = 1.
        FBOLD(J) = 0.
10 CONTINUE
C TOTAL NO. OF INCREMENTS IS 2*L
    LTWO = 2*L
    DO 20 I = 1, LTWO
        JMAX = IFIX(4.2*SQRT(FLOAT(I)))+1
C DIFFUSION SEGMENT
    DO 30 J=2, JMAX
        FANEW(J)=FAOLD(J)+DM*(FAOLD(J-1)-2.*FAOLD(J)+FAOLD(J+1))
        FBNEW(J)=FBOLD(J)+DM*(FBOLD(J-1)-2.*FBOLD(J)+FBOLD(J+1))
30 CONTINUE
C CALCULATE SURFACE CONCENTRATIONS
C FIRST INCREMENT POTENTIAL
    EMOD = EMOD + DELTAE
    RATIO = EXP(EMOD)
    FBSURF = (FBOLD(1)+FAOLD(1))/(1.+RATIO)
    FASURF = RATIO*FBSURF
C FIRST BOX
    FANEW(1)=FAOLD(2)+DM*(2.*FASURF-3.*FAOLD(1)+FAOLD(2))
    FBNEW(1)=FBOLD(1)+DM*(2.*FBSURF-3.*FBOLD(1)+FBOLD(2))
C CALCULATE CURRENT
    FACT = 2.*SQRT(DM*FLOAT(L))/(1.+ RATIO)
    Z(I) = FACT*(FANEW(1)-RATIO*FBNEW(1))
C RESET CONCENTRATIONS
    DO 40 J = 1, JMAX
        FAOLD(J) = FANEW(J)
        FBOLD(J) = FBNEW(J)
40 CONTINUE
```

```
C TEST FOR CHANGE IN SWEEP DIRECTION
IF(I.EQ.L) DELTAE = -DELTAE
20 CONTINUE
C OUTPUT DATA
DELTAE = - DELTAE
EMOD = EI
DO 50 I = 1, LTWO
EMOD = EMOD + DELTAE
WRITE(6,100) EMOD,Z(I)
IF(I.EQ.L) DELTAE = -DELTAE
50 CONTINUE
100 FORMAT (2F10.5)
STOP
END
```

Index

A

- a.c. cyclic voltammetry, 218, 273
- a.c. polarography, 270
- a.c. techniques, 251, 403
 - applications
 - adsorption, 275
 - analysis, 270
 - anodic dissolution of metals, 276
 - capacitance measurement, 268
 - electron transfer kinetics, 263, 403
 - porous electrodes, 274
 - rotating disc electrode, 274
 - experimental considerations, 257
 - graphical presentation of results
 - Argand diagram, 265, 278
 - Bode plot, 278
 - Kramers-Kronig analysis, 280
 - impedance measurement by
 - Wheatstone Bridge, 258
 - analogue analysers, 259
 - Fourier transform techniques, 262
 - sine wave correlation, 261
 - a.c. theory, 251
 - a.c. voltammetry, 218, 269
 - adatoms
 - catalysis by, 245
 - deposition of, 284, 291
 - role in electrocrystallisation, 291, 295
 - admittance, 256
 - adsorption, 21, 38, 67, 158, 160, 207
 - catalysis, 231, 235
 - ions, 160
 - isotherms, 38, 166

organic molecules, 158

- study by
 - capacitance, 157, 171
 - chronoamperometry, 67
 - chronocoulometry, 57
 - cyclic voltammetry, 207
 - impedance, 275
 - RRDE, 146
 - spectroelectrochemical techniques, 340
 - surface tension, 158, 174
- anode reactions, 16
- anodic dissolution of metals, 129, 133
- anodic films, 276, 313
- Argand diagram, 265, 278
- attenuated internal reflectance spectroscopy, 338

B

- Bode plot, 278
- Butler Volmer equation, 24, 43, 81

C

- capacitance, 157, 162, 171, 268
- catalytic current, 197, 392
- catalytic mechanism (ec'), 197, 392
- cathodic reactions, 16
- cation radical reactions, 230, 322, 339
- cells, 123, 174, 357, 365
- ce mechanism
 - chronoamperometry, 61
 - RDE, 133
 - cyclic voltammetry, 190

- charged interfaces, 153
 charge transfer resistance, 85, 264, 267, 408
 chemical potential, 79
 chlorocyanobenzene reduction, 203
 chronoamperometry, 49
 study of
 adsorption, 67
 diffusion, 29, 51, 398, 415
 electron transfer, 53, 400
 following chemical reactions, 61
 phase growth, 57, 299, 304
 chronocoulometry, 55
 study of
 adsorption, 57
 electron transfer, 55
 chronopotentiometry, 73, 314
 collection efficiency (RRDE), 138
 computer automation of experiments, 219,
 261, 382, 418
 computer simulations, 419
 concentration profiles, 29, 51, 181
 controlled potential electrolysis, 44
 convection, 26, 32, 47, 113, 274, 429
 convolution cyclic voltammetry, 219
 corrosion, 145, 276
 Cottrell equation, 31, 50, 400, 425
 coulometry, 44
 counter electrode, 358
 coupled chemical reactions, 20, 37, 59, 189,
 213, 392
 ce mechanism, 59, 61, 133, 190
 disp 1 mechanism, 60
 disp 2 mechanism, 60
 ec mechanism, 59, 64, 143, 193
 ec' mechanism, 60, 197, 392
 ece mechanism, 60, 63, 134, 198, 427
 cyclic voltammetry, 179
 a.c. cyclic voltammetry, 218, 273
 adsorption, 206
 catalytic mechanism, 197
 ce mechanism, 190
 complex mechanisms, 213
 convolution cyclic voltammetry, 218
 derivative cyclic voltammetry, 218
 double layer charging effects, 225
 ec mechanism, 193
 ece mechanism, 198
 examples of preliminary studies, 200
 experimental parameters, 179
 iR drop effects, 225
 irreversible electron transfer, 185
 metal deposition, 210
 microelectrodes, 217
 passivation, 212
 peak shape, 181
 reaction order approach, 216
 redox catalysis, 221
 reversible electron transfer, 180, 428
- D**
- derivative cyclic voltammetry, 218
 design of electrocatalysts, 232, 246
 design of experiments, 356
 diethylfumarate, 143, 201
 diethylmaleate, 143, 201
 differential capacity
 definition, 157
 measurement, 171, 268
 differential pulse polarography, 70
 diffusion, 26, 389
 diffusion coefficient
 definition, 28
 measurement by
 chronoamperometry, 50, 398
 chronocoulometry, 55
 chronopotentiometry, 74
 cyclic voltammetry, 183, 186
 impedance, 264, 407
 RDE, 124
 diffusion layer, 33, 121, 420
 double layer, 142
 double layer charging current, 52, 225, 370
 double layer effect on kinetics, 168
 double potential step experiments, 65
- E**
- ec mechanism, 59
 cyclic voltammetry, 193
 double potential step, 64
 RRDE, 143
 ec' mechanism, 60, 392
 cyclic voltammetry, 197
 ece mechanism, 60, 427
 chronoamperometry, 63
 cyclic voltammetry, 198
 RDE, 134
 electrical double layer, 149
 electrical double layer structure, 169
 electrocapillary curves, 156
 electrocatalysis, 229
 electrochemical cells, 123, 174, 318, 325,
 332, 342, 365
 electrocrystallisation, 283
 thermodynamics, 287
 kinetics, 294
 electrode geometry, 357, 411
 electrode materials, 232, 248, 357
 electrodeposition, 311
 electrode reactions, 16
 electrolytes, 363
 electron transfer, 20, 22, 76, 87
 energy diagrams, 94
 energy surfaces, 87
 semi-conductors, 104
 electron transfer equilibrium, 23, 77
 electron transfer kinetics, 24, 77, 102
 influence of double layer, 168
 study by
 chronoamperometry, 53, 400
 chronocoulometry, 57
 cyclic voltammetry, 187
 impedance, 263, 403
 RDE, 128
 electropolating, 311

- electroreflectance effect, 336
 ellipsometry, 327
 energy diagrams for electron transfer, 97
 energy of activation for electron transfer, 88
 energy surface for electron transfer, 87
 equilibrium potential, 23
e.s.r. in situ, 346
 exchange current density
 definition, 23, 80, 169
 determination
 impedance, 264, 403
 steady state, 25, 43, 85
 influence on $I-\eta$ characteristic, 82, 86
 experimental problems, 52, 123, 225, 356, 384
 experimental tips, 384
ex situ techniques, 352
- F**
- Faraday's law, 18, 46
 Fermi level, 98
 Fick's laws, 28, 411
 fluctuating energy model for electron transfer, 96
 free energy of cell reaction, 18
 fuel cell reactions, 244
- G**
- Galvani potential, 79
 galvanostat, 381
 Gibb's model for interphase, 154
 Gouy-Chapman model of double layer, 150
 Gouy-Chapman-Stern model of double layer, 151
 Grahame's model of double layer, 152
 growth of nuclei, 298, 303
 Guggenheim model of interphase, 154
- H**
- Helmholtz double layer, 150
 homogeneous chemical reactions, 20, 37, 39, 189, 213
 ce mechanism, 59, 61, 133, 190
 disp 1 mechanism, 60
 disp 2 mechanism, 60
 ec mechanism, 59, 64, 143, 193
 ec' mechanism, 60, 197, 392
 ece mechanism, 60, 63, 134, 198, 427
 homogeneous electron transfer, 102
 homogeneous nucleation, 285
 homogeneous redox catalysis, 221
 hydrogen adsorption, 209, 235
 hydrogen evolution, 233
 hydrodimerisation of activated olefins, 214
 hydrodynamics, 115
 hydrodynamically modulated RDE, 135
- I**
- ideally polarised electrode, 149, 269
 $I-E$ characteristic, 24, 34, 83
 impedance, 255, 257, 263, 403
- instrumentation, 258, 370
 internal reflectance spectroscopy, 338
 inversion techniques, 398
iR compensation, 379
iR drop, 19, 225, 368, 379
 irreversible electrode reaction, 37, 77
 study by
 chronoamperometry, 53, 400
 chronocoulometry, 57
 cyclic voltammetry, 187
 impedance, 263, 403
 RDE, 128
 isomerisation of anion radicals, 143, 201
- K**
- Kramers-Kronig analysis, 280
- L**
- Laplace transformation, 394
 laser Raman spectroscopy, 341
 linear approximation to Butler Volmer equation, 25, 83, 264
 linear diffusion to a plane electrode, 27, 389
 linear potential sweep techniques, 178
 Lippmann equation, 156
 Luggin capillary, 368
- M**
- mass spectroscopy *in situ*, 351
 mass transport, 20, 26, 47, 115, 389, 411, 420
 mathematics for electrochemistry, 388
 metal corrosion, 127, 133, 145, 212, 276, 331
 metal deposition, 211, 311
 microelectrodes, 48, 217, 417
 migration, 26
 monolayer deposition, 298, 336
 Mossbauer spectroscopy, 351
- N**
- Nernst diffusion layer, 33, 121
 Nernst equation, 23, 79
 p-nitrosophenol reduction, 199
 normal pulse polarography, 68
 nosylate ester reduction, 205
 nucleation, 285
- O**
- operational amplifiers, 370
 optically transparent electrodes (OTE), 318
 optically transparent thin layer cells (OTTLE), 324
 overpotential, 24, 81
 oxygen evolution, 242
 oxygen reduction, 127, 139, 242
- P**
- passivation, 212, 276
 phase angle, 255
 phase formation, 21, 40, 67, 211, 283

photoacoustic spectroscopy, 338
 photocurrent spectroscopy, 351
 photoemission, 350
 photothermal spectroscopy, 338
 porous electrodes, 274
 potentiostat, 19, 373
 design, 373
 performance, 375
 selection, 375
 potential step techniques, 29, 49, 398, 415
 potential sweep techniques, 179
 pseudocapacitance, 264, 404
 pulse polarography
 differential, 70
 normal, 68
 square wave, 72

R

Raman spectroscopy *in situ*, 341
 Randle's circuit, 267
 rapid scanning spectrometer, 319
 rate constant for electron transfer
 definition, 26, 80
 determination
 chronoamperometry, 53, 400
 chronocoulometry, 57
 RDE, 128
 reactance, 254
 reaction coordinate, 87
 redox catalysis, 221
 reference electrodes, 359
 reflection techniques – *in situ* spectroscopy, 327
 resonance Raman spectroscopy, 342
 reversible electrode potential, 23
 reversible electron transfer
 definition, 37
 study by
 cyclic voltammetry, 180
 RDE, 125
 rotating disc electrode, 113
 ce mechanism, 133
 ece mechanism, 133
 electrode design 114
 electron transfer kinetics, 125
 experimental factors, 123
 hydrodynamics, 116
 hydrodynamically modulated RDE, 135
 irreversible reactions, 126
 mass transfer control, 124
 Nernst diffusion layer approximation, 121
 reversible electron transfer process, 125
 rotating ring-disc electrode, 136
 adsorption on disc, 146
 collection efficiency, 138
 corrosion, 145
 electrode design, 136
 homogeneous chemical reactions, 144
 oxygen reduction, 139
 shielding experiments, 145

S

selection of catalysts, 232, 246
 semi-conductor electrodes, 99, 104, 351
 SERS, 344
 shielding experiments (RRDE), 145
 single crystal electrodes, 232, 336, 358
 solvents, 364
 spectroelectrochemical techniques, 317
 specular reflectance spectroscopy, 331
 spherical diffusion, 413
 square wave voltammetry, 72
 standard rate constant
 definition, 26, 80, 103
 determination of by
 chronoamperometry, 53
 chronocoulometry, 57
 cyclic voltammetry, 187
 impedance, 264
 RDE, 128
 standard electrode potential, 23, 80
 steady state experiments, 43, 389
 ce mechanism, 44, 392
 electron transfer kinetics, 25, 43
 structure of the double layer, 149
 surface conductance, 349
 surface diffusion, 295
 surface excess, 155, 158, 160, 206
 surface plasmon spectroscopy, 349
 surface pressure, 158
 surface roughness, 231
 surface tension,
 definition, 153
 measurement, 174

T

Tafel equation, 24, 43, 85, 129, 229
 theory of electrochemical experiments, 388
 thick deposits, 311
 thin layer cells, 45, 324, 408
 three dimensional phase growth, 303
 tosyl ester reduction, 225
 transfer coefficient
 definition, 24, 80
 determination
 chronoamperometry, 55
 cyclic voltammetry, 187
 impedance, 81, 85, 264
 RDE, 125
 steady state, 25, 81, 85
 effect on $I-\eta$ curves, 83, 86
 influence of double layer, 170
 potential variation, 90
 trouble shooting electrochemical experiments, 384
 two dimensional phase growth, 298

U

underpotential deposition of metals, 146, 336
 UV-visible spectroscopy *in situ*, 240, 318

V

vibrational spectroscopy *in situ*, 240, 340

W

Warburg impedance, 265, 408

working electrode, 357

X

X-ray diffraction *in situ*, 352